Optimising the Use of Spent Oil Shale

HELEN JANE FOSTER

Optimising the Use of Spent Oil Shale

Helen Jane Foster

Thesis submitted in partial fulfilment of the requirements for the degree of Doctor of Philosophy at Durham University

Department of Earth Sciences

Durham University

August 2014

Helen Jane Foster

Optimising the use of spent oil shale

Abstract

Worldwide deposits of oil shales are thought to represent ~3 trillion barrels of oil. Jordanian oil shale deposits are extensive and high quality, and could represent 100 billion barrels of oil, leading to much interest in the development of deposits. The exploitation of oil shales has raised a number of environmental concerns including: land use, water consumption, gaseous emissions and spent oil shale disposal.

To understand the environmental impact of spent oil shale, a study was conducted in Lothian, Scotland, providing a unique opportunity to examine the weathering process on aged deposits. Sequential extraction studies were conducted to determine the partitioning of trace elements within spent oil shale, soil and vegetation, with results demonstrating the stability of spent oil shale deposits.

The sequestration of CO_2 within spent oil shale has the potential to reduce CO_2 emissions associated with the retorting of oil shale. Jordanian spent oil shale was found to sequester up to 5 wt % CO_2, on reacting under supercritical conditions, which is 68 % of the theoretical carbonation. Results show that the duration of reaction; gas temperature; CO_2 pressure; and the interactions between these factors significantly affect the extent of carbonation.

The magnitude of the CO_2 sequestration achieved was sufficient that it could lower CO_2 emissions by up to 29 kg CO_2/bbl, thereby bringing the emissions from oil shale processing in line with those from conventional oil extraction methods. Modification of the processing conditions was also considered: to reduce CO_2 emissions, maximise oil recovery, and produce valuable by-products. Pyrolysis at 500 °C, combustion at 750 °C, and accelerated carbonation methods, may offer the greatest benefits for the processing of Jordanian oil shale.

Declaration

I declare that the content of this thesis is my own, except where reference is made to previously published work. I declare that this thesis presented for the degree of Doctor of Philosophy at Durham University, has not been previously submitted to this or any other university.

Acknowledgements

Firstly, I would like to thank my two supervisors for their continued support throughout my time in Durham as a PhD student. To Fred Worrall, for his reassurance and encouragement through challenging times, and for always being on hand to offer advice and guidance in the right direction. To Jon Gluyas, for offering exciting ideas and insight into the oil industry, while adding another dimension to the research project.

Secondly, I would like to thank Jordan Energy and Mining, and in particular John Fraser and Chris Morgan, who provided the resources and funding for the PhD, while enabling travel to international conferences where I was able to present my research in a stimulating and engaging environment. Also to the JEML office in Amman, who were incredibly hospitable when we visited. Furthermore, thanks go to Daniel Melo and Steven Odut at UMATAC, and Roy Jackson and Mohammad Amer at Monash University, who provided captivating discussion at JIOSS and endeavoured to provide samples to allow for the completion of Chapter 7.

Throughout my (almost) 4 years in the Earth Sciences department, I have received amazing levels of support from fellow PhD students, postdoctoral researchers, academics and other members of staff, who I would like to give my thanks to. In particular, members of the Carbon, Waste and Water research group: Suzie, Ian, Cat, Simon and Bill, who unreservedly offered help and entertainment during long hours at work. Also, to Chris Ottley, for providing guidance and time using ICP-MS; to Andrew Tuxworth for being on hand with advice and help with D9 issues; while thanks also go to John Booth at Scimed for continued assistance with the maintenance of critical lab equipment. Thanks also to Nick Marsh at Leicester University for the XRF analysis, and to Pablo Cubillas at Durham, for the provision of samples of carbonate.

Special thanks go to Hui Huang, Suzane Qassim, Rachel Bezard and Claire Nattrass, of whom I could not imagine taking this on without. To Hui, for being the best housemate I could have asked for, and for always being there, through the good times and the bad, we finally made it! To Suzie, for the dancing, and the long discussions, while of course not forgetting the provision of snacks to help us through the evenings and weekends. To Rachel: for her inspiring and absolute dedication to work; and to Claire, for not actually moving permanently to Edinburgh.

Final thanks go to my family. To my parents and to my sister Alice, for helping me reach the end. Thank you for your unwavering support and helping me accomplish, what only a few years ago, was just an idea and a blank piece of paper.

Contents

List of Figures

List of Tables

Chapter 1: Introduction

1.1 Introduction

Oil shale, a vast unconventional fossil fuel resource found worldwide, is to be mined and processed from the Al Lajjun deposit in Jordan by the company Jordan Energy and Mining Limited (JEML). This previously unexploited resource containing a high concentration of organic matter will be able to provide oil for a country which has very limited conventional oil reserves, whilst doing so at a reasonable price.

Oil shale will be retorted, to produce oil, by pyrolysing the oil shale at temperatures > 500 °C. There are concerns with the mining and retorting of oil shale however, including environmental concerns, geological constraints, water usage, waste disposal and social and economic considerations. The environmental concerns include: the production of waste, of unknown environmental stability, which is referred to as spent oil shale; the production of large amounts of CO_2; and the use of water, which is of particular concern in Jordan due to water scarcity and common over-extraction of aquifers.

The environmental issues associated with the processing of oil shale are discussed in this thesis, with suggestions on methods to tackle and minimise the negative impact of oil shale use. The environmental mobility of heavy metals within spent oil shale was investigated and this was followed by a proposal for reducing CO_2 emissions. A simple and effective mechanism, replicating natural weathering processes and making use of the reactive spent oil shale, could significantly reduce emissions by locking CO_2 permanently away in the form of stable carbonate minerals.

1.2 Aims and objectives

The principle objective of this research thesis is to explore the viability of using spent oil shale to limit the impact of oil shale processing. The aims for this project were therefore to:

1. Characterise the composition of Jordanian oil shale, and compare this to other global oil shale deposits. This was done by:
    - Investigating the influence of depositional setting on mineralogy.
    - Assessing as to whether deposits contain any economically viable by-products which could be obtained alongside oil.

2. Characterise the composition of spent oil shale, specifically observing any structural and chemical changes occurring after retorting and combustion methods.

3. Investigate the environmental stability of spent oil shale deposits, to determine if any course of action is required to stabilise waste materials which will be predominantly used as mine backfill in Jordan. This has been investigated by:
   - Studying a natural analogue in the form of Scottish spent oil shale deposits, known locally as 'bings', which were deposited as waste mine heaps more than 50 years ago. An investigation was conducted to determine the speciation of trace metals of concern, in relation to the stability of mineral phases.
   - Compare and discuss these results with respect to Jordanian spent oil shale.

4. Investigate the CO_2 sequestration potential of spent oil shale. This was done by:
   - Using the results from the characterisation study to determine how much theoretical carbonation can be achieved.
   - Reacting spent oil shale samples at high pressures and temperatures to actively sequester CO_2 by forming carbonate minerals, and to quantitatively determine the amount of CO_2 sequestered.
   - Optimisation of carbonation experiments, by conducting a factorial design and analysing the results statistically to determine the significance of multiple pre-determined factors, on the extent of carbonation.

5. Examine the optimum conditions for oil shale processing, with regards to the retorting temperature, combustion temperature and degree of carbonation. Suggestion of appropriate retorting designs is provided, based on different outcomes of the study.

Exploration of the literature is provided in the introductions to each chapter, and further background information is provided in Section 1.3 to put this research into context.

1.3 Background

1.3.1 Introduction

Demand for energy and fuels are ever on the rise and with sustained high oil prices, the ongoing discovery and production of oil from conventional and unconventional resources can be ensured. Unconventional resources are vast, yet have undergone limited exploitation in comparison to conventional resources due to high costs and environmental considerations.

The underlying theme to this research thesis is the commercial development of unconventional resources which minimise their impact on the environment. The mitigation of CO_2 emissions in particular, is an issue as global warming is considered a threat to society. Methods for mitigation of CO_2 emissions include carbon capture and storage (CCS) techniques, which aim to store CO_2 in the subsurface, yet issues of potential groundwater contamination and CO_2 leakage have delayed the initiation of many projects. An alternative method is the permanent storage of CO_2 by the formation of carbonate minerals, mimicking natural weathering reactions that continually occur on the surface of the Earth. This is the method studied in this thesis.

1.3.2 Energy demand

Demand for energy is expected to continue increasing worldwide, as global population increases, yet this is coupled with a dwindling supply of cheap energy resources, alongside growing concerns for the future of the planet if anthropogenic emissions are not mitigated, with the possibility of irreversible and irrevocable climate change. Governments are continually updating their policies on energy security and climate change, with targets to meet mounting energy demands whilst cutting down on harmful emissions.

To fulfil demand, countries must ensure that the supply of energy is secure, by investing in infrastructure for the development of new and existing sources. For the alleviation of climate change, cleaner technologies are required, which means: using more renewables, updating old power plants, retrofitting for CCS technologies, as well as ensuring that regulatory frameworks are in place to enable sustainable development (Dehen, 2010; Gadonneix, 2010). Improvements in the efficiency of fuel and electricity usage are also necessary, and advancements have been previously shown, for example old coal power plants operate at ~33 % efficiency compared with ~44 % of new operating power plants (Kearney, 2010).

Contributing factors to the recent variation in energy demand and supply include: the increasing price of oil, the rise of renewable and 'smart' grid technologies, concerns with CO_2 emissions and combating climate change, political and economic problems, the shale gas boom, as well as natural or accidental disasters such as the Fukushima and Deepwater Horizon events (WEC, 2013). Outlook reports about the future of energy markets are prepared by various governmental or private organisations, to analyse different projected energy scenarios. They are comprised of estimated forecasts, which are based on current economies, technological improvements, and policy changes, as well as taking into account current data from oil fields and known reserves (IEA, 2010; Jackson, 2009)

Renewable technologies and unconventional resources are expected to contribute more to the energy mix in the future, yet these come at a higher price. To reduce the impact of this on the economy, the promotion of more efficient and connected energy markets is essential (IEA, 2013). Additionally, fossil fuels are projected to still produce the majority of global energy in the near future, contributing to 76 % of the total energy demand in 2035 (EIA, 2013; IEA, 2013). Figure 1.1 shows the projections for different energy sources, which are all expected to increase steadily over the next twenty to thirty years. This correlates with predictions for energy consumption, which is estimated to increase by 1.75 to 1.87 %/year by 2035 to 2040 (EIA, 2013; Kearney, 2010), 50 % greater than projected a few years previous to this (EIA, 2010). Demand is increasing significantly with population and economic growth, especially true of non-OECD (Organisation for Economic Co-operation and Development) countries projected to account for more than 90 % of the growth in energy demand, such as China and India where imports are continually increasing. Energy markets are shifting, resulting in concerns with energy security. As a result, many countries are aiming to supply their own energy, for example the United States (US) is preparing to supply all of their own energy by 2035 (IEA, 2013).

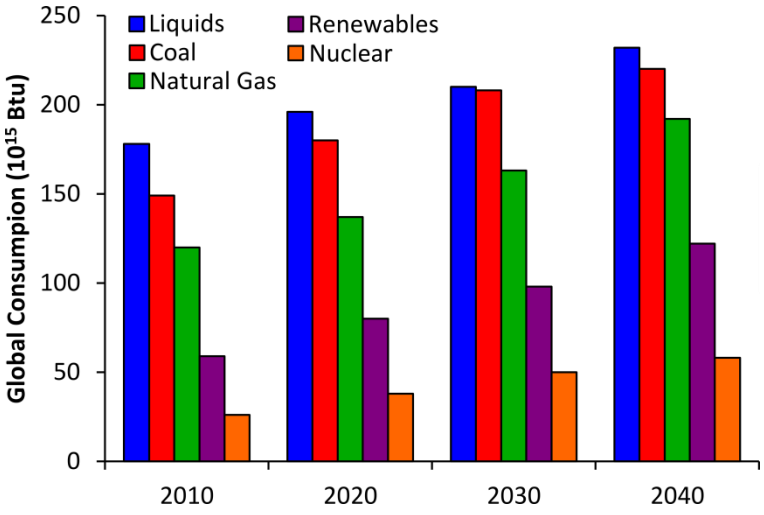

Figure 1.1 - *Present and future projection of global energy consumption from different sources (liquids, coal, natural gas, renewables and nuclear), where Btu = British thermal unit. Adapted from EIA (2013).*

1.3.3 Oil

Oil production is driven by various factors, which include: the price of oil and industry costs, progressions in exploration and development, geopolitics, and technological improvements (EIA, 2013). With increasing demand for energy resources, the market for oil in particular is strong in the agriculture, industrial and transportation sectors (Figure 1.2).

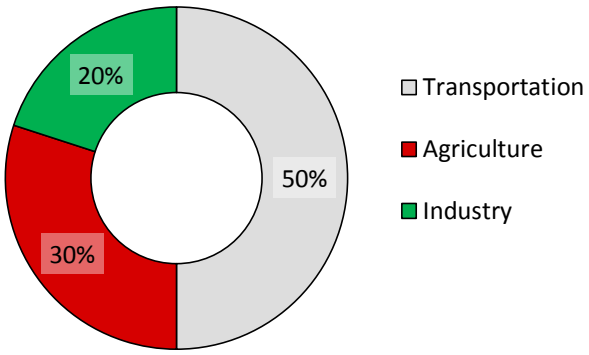

Figure 1.2 - *Proportion of global oil usage. Adapted from Ellis (2011).*

High oil prices have been retained recently, due to conflict in the Middle East, where countries produce the majority of global oil supply; and also throughout the endurance of a global recession. Fluctuations in past prices make it difficult to predict future prices, and therefore usage. For example in 2008 oil prices were at a record high of > $120 per barrel of oil (bbl), an increase of $100/bbl from 10 years previous (Siirde, 2008). A year later in 2009, oil prices dropped to just $70-80/bbl (Jackson, 2009), before averaging a spot price for Brent Crude oil of $110/bbl since 2011 (IEA, 2013). Oil prices are expected to remain fairly steady in the short-term, however in the long-term prices are projected to rise to ~$165/bbl by 2040, with an upper and lower limit of $237/bbl and $75/bbl, respectively (Figure 1.3; EIA, 2013). These future high prices are subject to many uncertainties, influenced by economic growth and industry costs, with additional pressure being put on: the addition of carbon taxes, reduction in energy and fuel consumption, and an increase in energy efficiency (EIA, 2013).

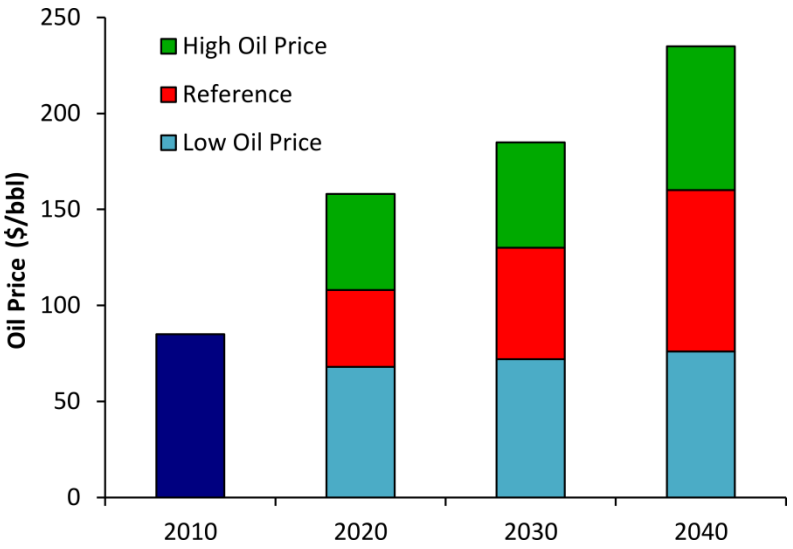

Figure 1.3 - *Current and projected global oil prices. Adapted from EIA (2013).*

Oil consumption is set to increase, rising from 87 to 115 mbd (million barrels per day) by 2040 with high demand expected in the transportation and industrial sectors (EIA, 2013). Oil usage has increased by 32 % since 1991, yet the extent of proven reserves that have been discovered has risen by 60 %, with 12 billion barrels (bbbl) of oil currently discovered each year, enabling continued production (WEC, 2013; Jackson, 2009). Total crude oil reserves have been proven as 1.67 trillion barrels (tbbl), as of January 2013 (BP, 2013), yet according to the World Energy Council (WEC), it will take 60 years to consume only half of the world's potential resources. However, due to the unequal distribution of these, there is more risk involved, and short-term variability in trading and pricing (WEC, 2013). Additionally, in the long term, conventional supplies are projected to fall by 17.5 % of total oil, due to future declining output from existing oil fields. To meet the increasing rate of consumption, there are three main new sources to consider: enhanced oil recovery from existing fields; oil recovery from ultra-deepwater fields, and light tight oil, which are harder to access; and also oil shale and other unconventional sources. These all come at a higher price, but will ensure future demand is still met (IEA, 2013).

1.3.4 Unconventional oil

Unconventional oil resources include: oil shale, biofuels, oil sands, extra heavy oil and coal/gas-to-liquid techniques. They are known for their difficulty and costliness in the extraction and processing of oil, yet the economic value of these resources is significant, and as the price of crude oil has increased in recent years, exploitation and development of oil from these sources becomes more viable, while future projections of oil production include the assessment of unconventional resources (Figure 1.4).

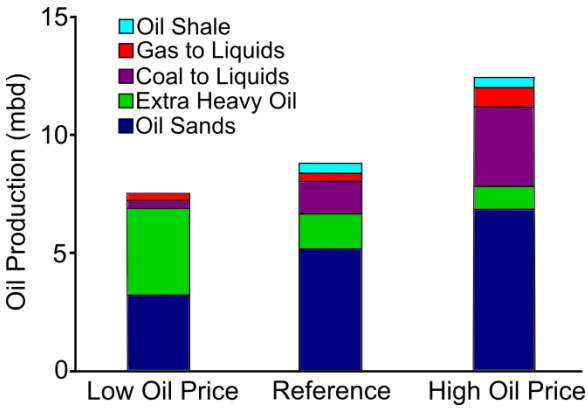

Figure 1.4 - *Predicted contribution, in 2035, from unconventional resources for 3 different oil price scenarios. Oil production is reported in million barrels per day (mbd). Adapted from EIA (2010).*

Unconventional resources are vast, with current estimates reaching 5.87 tbbl of total global oil reserves, almost 4 times greater than the value for recoverable crude oil alone (IEA, 2013). Figure 1.4 shows large contributions from oil sand and heavy oil; two of the world's largest unconventional resources include Canadian tar sands and Venezuelan heavy oil, which hold 168 bbbl and 220 bbbl of oil respectively (BP, 2013). Nevertheless, the limited use of unconventional resources is partially due to the association with environmental problems; mainly greater CO_2 emissions and water usage. This supplements difficulties encountered with production. These are issues that can be addressed, but technologies need to be improved to reduce their impact. Overall unconventional liquid production is predicted to increase by ~5 %/year, to account for 12 % of total liquid production in 2035 (EIA, 2010), and in predictions by the World Energy Council (2013), oil shale is projected to contribute towards more than a third of growth in unconventional oil by 2030.

1.3.5 Oil shale

Oil shale is an unconventional fossil fuel resource, which has up until recently, remained untouched in most areas of the world. Oil shale is defined as a sedimentary rock with a high concentration of organic matter, typically 5 to 25 percentage weight (wt %), in the form of kerogen, which has the ability to provide shale oil or gas after retorting, when oil shale is heated to temperatures exceeding 500 °C. Alternatively oil shale can be used directly as a fuel (Boggs, 2009). It has been defined by Russell (1990) to consist of:

'Wide variety of laminated, solidified mixtures of argillaceous sediments and organic matter having the common property of yielding oil upon destructive distillation, yet being but slightly susceptible to the action of solvents.' (Russell, 1990)

Oil shale is formed as a sedimentary rock by low-energy deposition occurring in marine or lake settings, alongside the burial of organic matter in anaerobic/reducing environments. This is followed by the conversion of organic matter into kerogen by diagenesis (Boggs, 2009). Oil shale can be regarded as an immature source rock; if buried at greater depths (and therefore higher pressures and temperatures) the classification may change to a gas or oil producing source rock. For example, the Green River formation, an oil shale deposit in the US, is thought to also act as a source rock for oil in the Red Wash field in Utah (Dyni, 2006).

The wide range of depositional environments means that oil shale deposits vary considerably in their mineralogy and oil content. Oil shales can be classified from the depositional environment which provides the greatest diversity between deposits, before being further separated based upon how the organic matter was formed. The classification by Hutton (1987) is as follows: terrestrial deposition (deposits known as cannel coal); lacustrine deposition (lamosite or torbanite types); and marine deposition (marinite, tasmanite and kukersite types). Additionally, oil shales can be classified by their mineralogy: being carbonate-rich or silica-rich (Reinsalu et al., 2007), with the sedimentary rock type varying from silcia-rich mudstones to carbonate-rich marlstones.

Oil shale has been used since ancient times, but came into more common usage in the 19th century. In France and Scotland, oil shale was used in early production operations to provide: kerosene and lamp oil, paraffin wax, fuel oil, lubricating oil and grease, naphtha, illuminating gas, and ammonium sulphate. It wasn't until the early 1900s that oil shale was used for the production of fuels for transportation (WEC, 2010). Worldwide, production declined from 1980 onwards, mainly due to the cost of production being far out of reach of conventional oil sources which were more economically viable (Figure 1.5). Now production is on the rise again with recent increases in oil prices, and improvements in processing technologies.

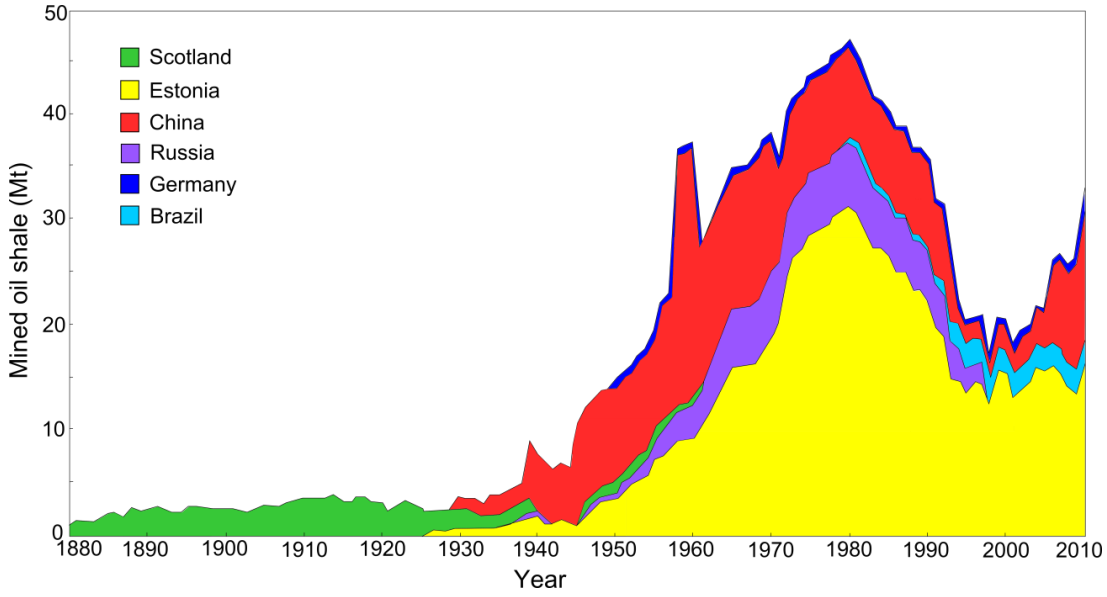

Figure 1.5 - *History of oil shale usage, where Mt = Megatonnes. Adapted from Allix et al., (2010); Dyni, (2006).*

Oil resources from oil shale make up more than double the world's conventional oil reserves, with 2.5 to 3.2 tbbl proven worldwide (Dyni, 2006). An upper estimate of 4.8 tbbl has also been given (WEC, 2010; Jackson, 2009), however, the economical recoverable fraction of this is much less (SER, 2013). Oil shale resources are known deposits of oil shale that may not be currently commercially viable for exploitation. Oil shale reserves provide a lower estimate than resources, as these are defined as deposits currently being developed for oil recovery (EASAC, 2007). Oil shale deposits are globally distributed, far and wide, with > 600 deposits known, in > 50 countries, with the US accounting for > 3/4 of global resources (WEC, 2013; Russell, 1990).

Table 1.1 - *Top five global oil shale resources in 2011 (WEC, 2013).*

Country	Resources (bbbl)
USA	3,707
China	354
Russia	248
Congo	100
Brazil	82

Many factors control whether deposits are viable to use, including but not limited to: the cost of mining/processing; environmental considerations; waste disposal; water usage; and current/future oil prices. By-products in oil shale can increase the economic value to deposits, such as those containing high concentrations of heavy metals, uranium, vanadium, zinc, alumina, phosphate, sodium carbonate minerals, ammonium sulphate, and sulphur (WEC, 2010). Also, spent oil shale can be used in the cement industries or in construction, rather than primarily as mine backfill (Motlep et al., 2010). However, general public perception is very poor and there are environmental issues associated with oil shale processing. These include the production of potentially harmful emissions and greenhouse gases; the pollution of nearby water reserves; and difficulties with disposal of waste shale. These problems must be tackled if unconventional oil production is able to compete with conventional practices.

Due to the high costs previously associated with unconventional oil shale extraction, only a small number of deposits are under current exploitation, which include, but are not limited to: deposits in Estonia (since 1924), China (since 1930), and Brazil (since 1981) (Liive, 2010; Aleksandrov, 2009). Estonia predominantly use the oil shale for direct power production, with 80 % of mined oil shale being used for this purpose, however elsewhere the production of shale oil is dominant using retorting technologies (EASAC, 2007).

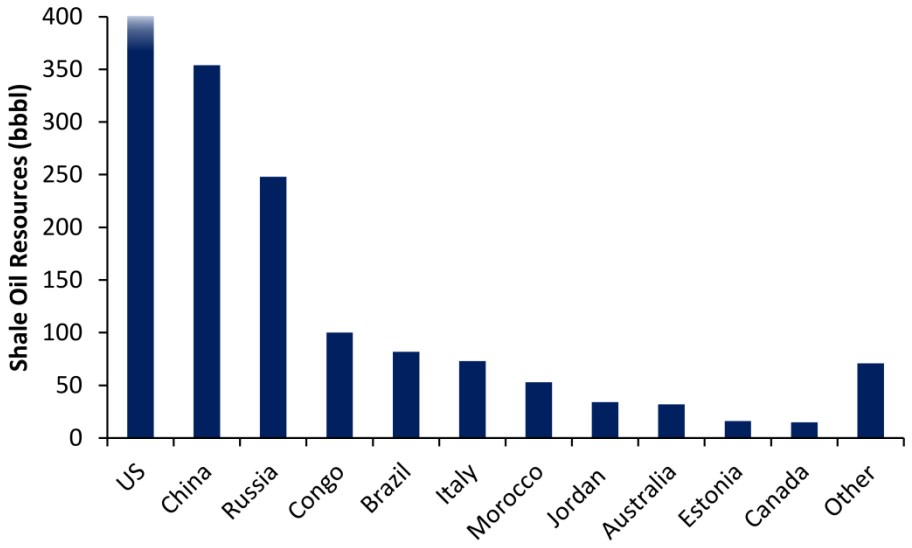

Figure 1.6 - *Shale oil resources from global deposits. Produced from data from WEC, 2013; Dyni, 2006.*

1.3.6 Jordanian oil shale

Unlike its neighbouring countries in the Middle East, Jordan contains limited oil reserves and the country currently imports 100,000 bbl per day. This leaves Jordan dependent on neighbouring countries, such as Iraq, where oil is imported by road which can be very expensive (Alali et al., 2006). Yet, significant oil shale deposits can be found in Jordan, which remain unexploited.

Jordan contains the 8th largest oil shale deposits, based on resource data from the WEC (2013) and Dyni (2006), as shown in Figure 1.6. However, some estimates place resources at > 100 bbbl (JEML, 2009), ranking it 4th globally. These resources have potential to boost the economy, by bringing jobs, as well as political and financial stability (Jaber et al., 1997a). The Ministry of Energy and Mineral Resources in Jordan predicts that 11 % of the energy supply will be provided by indigenous oil shale resources by 2015 and 14 % by 2020 (WEC, 2010). For Jordanian oil shale, a country with limited freshwater reserves, the use of water is of great concern. Shortages and water pollution are common problems due to over-extraction of non-renewable aquifers, and a low annual precipitation rate of < 300 mm (Jaber et al., 1997c). The CO_2 emissions from oil shale processing by the Alberta Tacuik Process (ATP) are also considered to be very high, being one of the reasons operations at the Stuart deposit in Australia (also using ATP technology) was shut down in 2004, following protests by Greenpeace and due to other economic considerations (EASAC, 2007; Fischer, 2005).

1.3.7 Global warming

Climate change and global warming is a topic of considerable debate. The extent and consequences of anthropogenic emissions are therefore introduced before focusing on the styles and methods of mitigation.

Carbon is distributed between the geosphere, biosphere, hydrosphere and atmosphere, where a complex cycle exists to transfer carbon between these systems. The concentration of CO_2 emissions in the atmosphere, as well as other greenhouse gases, has a direct effect on the global temperature, by acting to absorb infrared radiation (Pachauri and Reisinger, 2007). Current CO_2 levels in the atmosphere are 398 parts per million (ppm) (as of February 2014, Tans, 2014), compared with ~280 ppm only 250 years ago. The rise in concentration of CO_2 in the atmosphere is predominantly attributed to anthropogenic burning of fossil fuels and human activities, ultimately resulting in an increase of global temperature. Global warming

thereby causes climate change, with effects on biological, chemical and physical natural systems (Pachauri and Reisinger, 2007).

The critical level, for CO_2 concentration in the atmosphere, is predicted to be 450 ppm (IEA, 2010), with the potential for devastating consequences if left to spiral out of control beyond this. This has led to targets being put into place for the reduction of CO_2 emissions. However, global co-operation and an increase in public awareness are paramount to tackle the mitigation of emissions directly and effectively. Increased confidence, comprehensible regulations and trading standards, and increased funding in research and development, will bolster progression in this sector (Metz, 2007).

The energy industry accounts for up to two thirds of global CO_2 emissions, which are currently producing levels of 31 billion tonnes CO_2 per year, projected to increase to > 37 billion by 2035, due to a lasting reliance on fossil fuels (EIA, 2013; IEA, 2013; Gadonneix, 2010). To minimise the large amount of CO_2 emissions produced from power plants, increased focus is being put on renewable power, but as the majority (> 85 %) of current energy supply is from fossil fuels, demand cannot be met purely by the use of alternative power in the short-term.

Carbon dioxide emissions associated with electricity production, from fossil fuels to renewables, is compared in Figure 1.7, illustrating the difference between non-renewable fuels and other sources of power. The processing of unconventional resources are known for producing even greater CO_2 emissions. For example, oil sands produce CO_2 emissions ~5-15 % higher than those associated with conventional oil (EIA, 2013). The increasing interest in unconventional resources, and continued use of oil, means that techniques to minimise the production of CO_2 is necessary to remain competitive on the global market. Consequently, techniques to capture harmful emissions from these power plants and reduce CO_2 emissions are one of the top priorities in cutting emissions in the interim (Schrag, 2007).

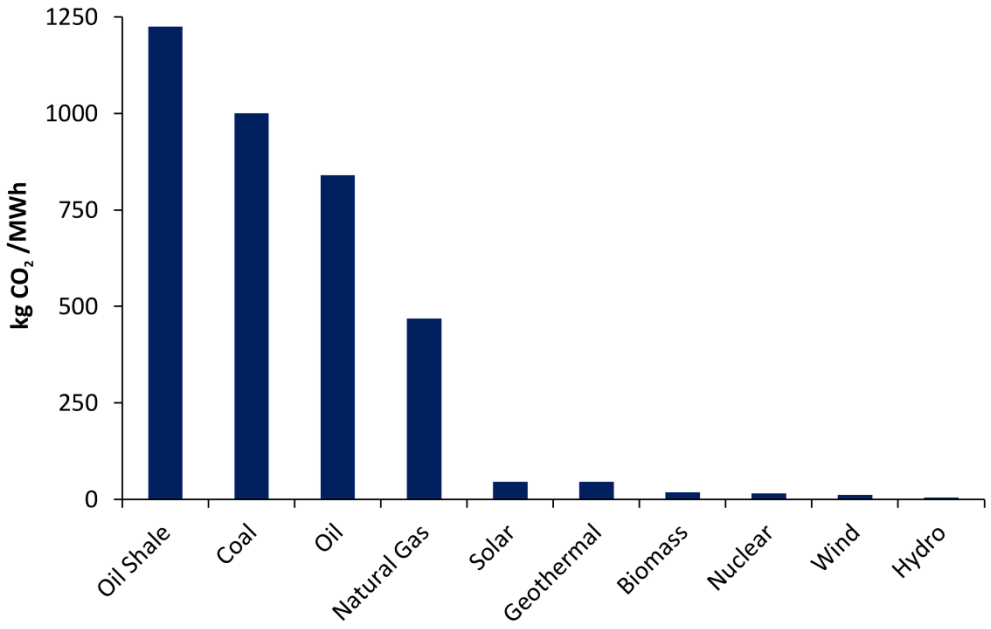

Figure 1.7 - *Lifecycle CO_2 emissions from electricity production, MWh = Megawatt hour. Adapted from EASAC (2007); Moomaw et al., (2011).*

1.3.8 Mitigating anthropogenic emissions

Obtainable mitigation methods can be split into three broad categories, all with an aim to reduce the utilisation and production of CO_2 emissions from carbon-rich fossil fuels, whether this is by: reduction in energy usage and increase in energy efficiency; the transfer of power production to nuclear or renewable technologies; or by the storage of CO_2 emissions produced by the burning of fossil fuels. It is likely that a combination of all the above methods will be required in tackling the rise in CO_2 emissions. A reduction in energy usage is unlikely, based upon predicted energy usage projections, discussed at the beginning of this chapter. Increasing the efficiency of energy production and usage, as well as the utilisation of nuclear and renewable technologies requires further research and development, as well as investment, and in the short term it is unlikely that we can meet our energy demands using these technologies alone (based on the current rate of development of new renewable and nuclear technologies). This means a bridging solution is required, to keep the emissions from increasing out of control.

Carbon capture and storage (CCS) techniques are gathering increasing interest and support, as a tool to bring down emissions from fossil-fuel powered plants. CCS involves the capturing of carbon at source, then transporting this to geological storage basins (such as saline aquifers, or depleted oil reservoirs) where the CO_2 is injected underground into porous rocks, with the

intention of permanent storage, with the rock able to hold the carbon for up to a few millennia (until the natural carbon cycle will be able to absorb the excess CO_2). As a short-term 'bridging' solution to reducing CO_2 emissions; CCS may produce cost benefits that will allow progression in mitigation against climate change. Alternative suggestions to the mitigation of emissions are geoengineering techniques, whereby a reduction of CO_2 emissions is approached by extensive methods to modify radiation or remove CO_2 from the atmosphere (Wigley, 2006). For example, ocean liming combats acidification of waters, and subsequently attracts the drawdown of CO_2 from the atmosphere (Renforth et al., 2013).

1.3.8.1 Carbon capture and storage

Current progress in CCS includes involvement on a multi-national level. The G8 intends to develop multiple industrial-scale projects by 2020, and the US, India and China have all promised to cut their emissions accordingly (Kearney, 2010; McKee, 2010). However, based on future projections by the IEA (2013), it is expected that only 1 % of fossil fuel plants will implement CCS technologies (IEA, 2013). If CCS is implemented, it has the potential to reduce CO_2 levels by 33 % by 2050, according to the Intergovernmental Panel on Climate Change (IPCC). This is a significant contribution to the government's 80 % reduction targets, and if the 2050 targets are to be met in an economical way, the use of CCS could account for a 60 % reduction in overall cost (Metz, 2005).

There are several CCS projects underway; with the largest (and oldest) project storing 1 Mt CO_2 per year since 1996, at the Sleipner gas hydrocarbon field, where CO_2 is separated out of the natural gas, before being pumped into the shallower Utsira geological formation (Korbol et al., 1995). Extensional forms of CCS include Enhanced Coal-Bed Methane (ECBM) and Enhanced Oil Recovery (EOR), which is being used in Weyburn, Canada, where the storage of anthropogenic CO_2 also aids with the recovery of oil and gas (Preston et al., 2005; White et al., 2005).

The use of CCS is associated with high costs, which can be as much as 70 % of the overall costs of a project (Metz, 2005). Other challenges include ensuring that CO_2 will be stored permanently, due to the possibility of leakage, via natural fractures or injection wells. Also, the migration of CO_2 into groundwater is suspected to leach pollutants into drinking water. The storage and confinement must therefore be controlled and optimised, by considering: careful site selection, risk assessments, and modelling/monitoring. Geochemical modelling, alongside constant monitoring, investigates the behaviour and interactions of CO_2, while ensuring there is no leakage or contamination to the surrounding environment (Gaus et al., 2005).

CCS can be divided into three steps. The first is carbon capture, the second is transport, and the third is storage:

1. Capture

There are three dominant pathways for carbon capture: Post-combustion capture, pre-combustion capture and oxy-combustion capture. The CO_2 is commonly scrubbed from the flue-gas using post-combustion methods, which allows operating power plants to be retrofitted with this design, although large amounts of energy (30 % of production) is required for operation (Gibbins et al., 2008; Schrag, 2007). Pre-combustion capture is less energy intensive, but new gasification plants are required to incorporate the technology. Alternatively, oxy-combustion can be used, where fuel is burned in pure O_2 rather than air. However, this is also an energy intensive process (Figueroa et al., 2008).

2. Transport

After separation, CO_2 is dehydrated and compressed, ready for transportation as a supercritical fluid. With the correct infrastructure in place, CO_2 can be conveyed by ship or pipeline, ready for injection at site (Gibbins et al., 2008).

3. Storage

Requirements for storage basins include: high porosity and permeability to allow for movement into the pore spaces; appropriate reservoir depth so that CO_2 may be stored as a supercritical fluid; sufficient capacity to store significant amounts; and trapping mechanisms where the reservoir is sealed with an impermeable rock (Metz, 2005). Current worldwide storage capacities are estimated at 2000 Gt of CO_2 (Metz, 2005), whereas in Europe, a conservative value of 116 Gt of CO_2 is thought to be available for storage (Vangkilde Pedersen et al., 2009).

After CO_2 is injected into suitable reservoirs, it is then trapped by several mechanisms, which can cause CO_2 to be retained over significant time periods (Figure 1.8; Hepple et al., 2005). First of all it accumulates beneath the cap rock, which prevents upwards migration by sealing the reservoir (structural trapping). Immobilisation of CO_2 occurs within pores, due to the capillary forces preventing movement (residual trapping). Dissolution into pore water or brine occurs, which is dependent on the pressure, temperature and salinity of the fluids, which lowers the buoyancy of the fluid (solubility trapping). Finally, there is the process of mineralisation, which is dependent on the pH and minerals present in the system. As the dissolution of minerals is necessary for carbonation to occur, this process could take tens to thousands of years to be a dominant process (Benson et al., 2008). Possible sites for storing

CO_2 are depicted in Figure 1.9. These sites include: depleted hydrocarbon fields; saline aquifers; oilfields using enhanced oil recovery (EOR); and coal seams, using enhanced coal-bed methane recovery (ECBM) (Energy Institute, 2010).

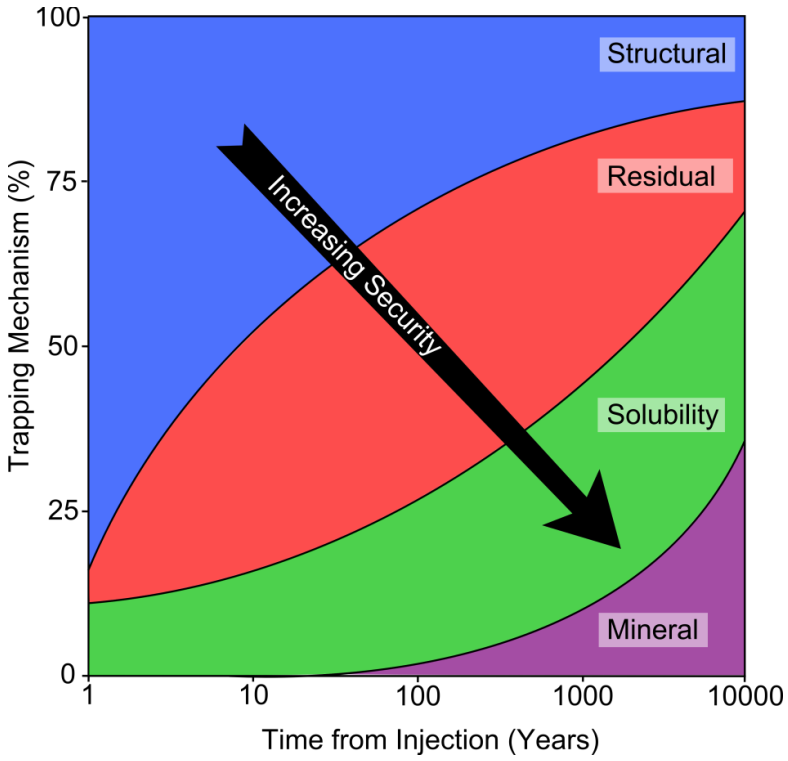

Figure 1.8 - *Trapping Mechanisms, based on Metz (2005).*

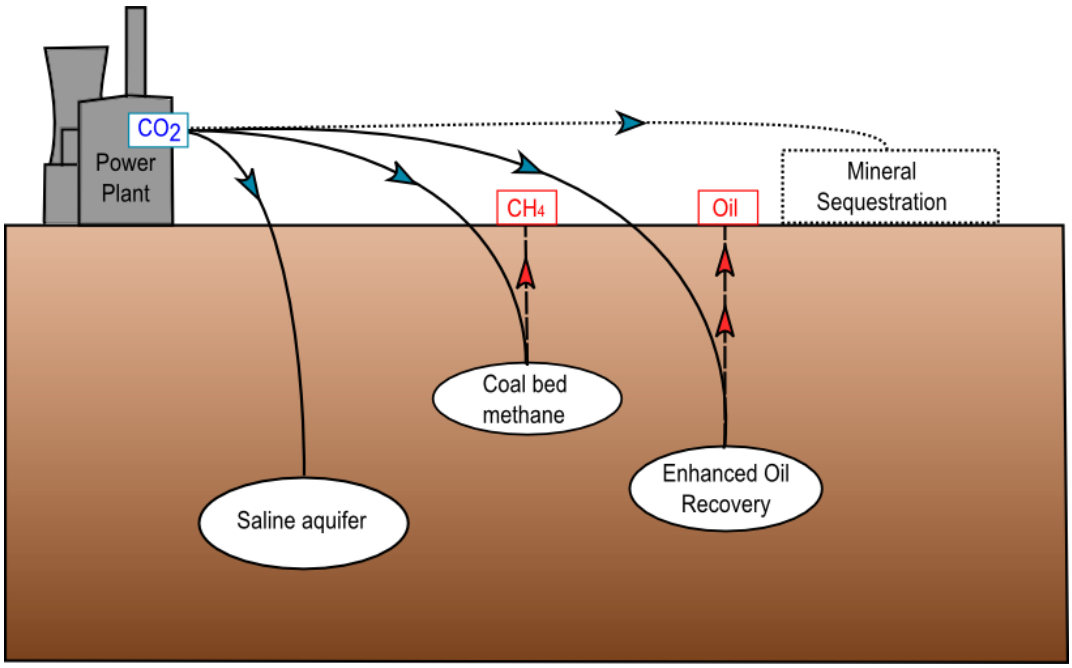

Figure 1.9 – *Geological storage of CO_2.*

1.3.8.2 Mineralisation

An alternative mechanism for the capture and storage of CO_2 is by chemical reactions, sometimes referred to as Carbon Capture and Storage by Mineralisation (CCSM). This still acts to capture carbon, but instead of storing in a geological reservoir, the first three trapping mechanisms (structural, residual, and solubility) are bypassed, and mineralisation reactions are the focus. CO_2 can be reacted with divalent cations, principally from the dissolution of oxide or silicate minerals, to produce thermodynamically stable carbonate minerals. These techniques may be considered in particular in areas where conventional CCS basins are not found and large amounts of CO_2 emissions are being produced, such as certain areas of India and China (Benson et al., 2008).

Substantial research on mineral carbonation began in the 1990s by investigating the acceleration of natural silicate weathering (Lackner et al., 1995; Seifritz, 1990). Research has since progressed to the use of waste materials, such as mining waste or industrial processing waste, as sources for mineralisation. Waste materials are often ideal for CO_2 sequestration reactions because: there is no extra cost associated with the production of these materials; they are usually situated close to CO_2 emission points; they tend to be reactive with respect to CO_2, containing large amounts of Ca/Mg-containing minerals; and they would otherwise be released in the environment (Gunning et al., 2010; Huijgen et al., 2005). Little research has been undertaken on spent oil shale, yet material is likely to be suitable for the sequestration of CO_2 because of the alkaline nature of the material and high concentrations of Ca and Mg containing minerals. The mechanisms and possible feedstock materials for these carbonation reactions are discussed in more detail in Chapter 5.

1.4 Thesis structure

The thesis follows a structure with multiple results chapters followed by a conclusive synthesis chapter. Each chapter will include: introduction, methodology, results, discussion, and conclusion sections. The basis for the work completed, and the links between chapters and sections are discussed throughout. The aims and content for each chapter have been briefly outlined below:

Chapter 1

Chapter 1 includes an introduction and background study, in the context of the research theme on aspects of: energy demand, oil prices and usage, unconventional resources and oil

shale, global warming and methods of mitigation of CO_2 emissions including CCS techniques. An outline of the aims, objectives and thesis structure is provided.

Chapter 2

A characterisation study of oil shales from 15 global locations has been completed. Information on the chemistry and mineralogy of deposits was obtained by analytical testing of point samples, in the laboratory in Durham. Results are collated, to compare and contrast different oil shales, and are seen to be dependent on their depositional environment and organic content. The economic potential, besides oil recovery, is discussed, as well as consideration of the retorting technologies and exploitation.

Chapter 3

Further detailed characterisation of Jordanian oil shale by microscopy and thermal analytical techniques are used, to gain more understanding into the compositional and structural properties of the oil shale. Jordanian spent oil shale was also analysed, providing a basis for future environmental and CO_2 sequestration studies.

Chapter 4

An investigation into the environmental stability of spent oil shale was conducted by the use of an existing analogue. Scottish oil shale deposits were sampled, and environmentally assessed by the use of a sequential extraction study. This was used to identify the mineral phase that dangerous heavy metals are associated with, and whether heavy metals within these phases are readily released into the environment. A discussion of the environmental mobility with respect to Jordanian spent oil shale deposits is also added.

Chapter 5

Chapter 5 is the first chapter investigating CO_2 sequestration within spent oil shale. A thorough literature review is presented, and the feasibility of CO_2 sequestration within Jordanian material is discussed. The limitations of methods, for calculating the theoretical carbonation, and actual carbonation, were considered, and CO_2 mitigation values are reported.

Chapter 6

Further work on the optimisation of CO_2 sequestration experiments is the basis of Chapter 6. The choice of a factorial design was achieved to feasibly implement the experiments and

analysis, whilst testing all crucial factors. The importance of each factor and interaction effects were tested by the use of 'analysis of variance' (ANOVA) statistical methods.

Chapter 7

The foundation of Chapter 7 is to find the right conditions to support: appropriate calcination to use spent oil shale in the cement industry and for providing energy in the retorting process; sufficient oil recovery; sufficient 'free' Ca to achieve carbonation. A final partial factorial design and analysis of variance was used in the determination of optimum conditions for processing of oil shale.

Chapter 8

This final chapter discusses the overall conclusions in relation to the main research question, and investigates in more detail the economic considerations of optimising processing conditions coupled with CO_2 sequestration techniques, as well as discussing options for future work along with the major limitations of the completed study.

Chapter 2: The characterisation of oil shales from global deposits

2.1 Introduction

The aim of this chapter was to characterise and compare oil shale samples from around the world, investigating their structure composition and mineralogy, using a combination of X-ray fluorescence (XRF), X-ray diffraction (XRD) and inductively coupled plasma mass spectrometry (ICP-MS). This study estimated the variability in oil shale composition worldwide and characterised oil shales to determine if there were any minerals or trace elements which could be economically exploited; finally assessing whether the mineralogy is likely to be detrimental or beneficial to oil recovery. Chapter 3 will go onto discuss the characteristics of Jordanian Oil Shale, specifically oil shale from the Al Lajjun deposit, in more detail. Methods will be proposed to limit the impact of processing mechanisms in Chapters 7 and 8 and further discussion on whether or not these proposals can be implemented on a global scale as a standard procedure for all types of oil shale will be provided.

The characterisation study was completed on oil shales from: Scotland, Estonia, Morocco, Israel, Jordan, Mongolia, China, Thailand, Australia, Canada, and the United States; totalling 15 samples. Characterisation of the mineralogy of oil shales has been attempted by researchers (Kumar et al., 2013; Wang et al., 2009; Bhargava et al., 2005) however, no full, comprehensive study, of this scale, has been published to date.

2.2 Background

Oil shale, as described in Chapter 1, is a sedimentary rock with a large amount of insoluble kerogen, which requires heat to obtain oil. The predominantly amorphous organic matter in oil shale is in the form of kerogen (~80 % of total organic matter) and bitumen (Boggs, 2009). The oil yield is commonly determined by the Fischer Assay (FA) technique, which was developed as a standard lab procedure for calculating oil yield by Stanfield and Frost in 1949, and distils oil and gas vapours as they are removed from the oil shale by retorting (Stanfield, 1949). The use of this alongside the calorific value of oil shale can indicate how viable it is as a source, for example, oil shales in Jordan have high oil yield and calorific values of ~10 wt % and 6 MJ/kg, respectively (Jaber et al., 1997a). The use of thermal analysis was first suggested as an alternative for the complex Fischer Assay process by Rajeshwar (1981). Differential scanning calorimetry (DSC) with thermogravimetric analysis (TGA) measures the energy change

produced when heating oil shales, and acts to measure the percentage weight of organic matter. Thermal analysis is therefore a rapid and effective way of determining the amount of organic matter that is present (Rajeshwar et al., 1981). Thermal methods can also be used to identify the presence of inorganic components which may be decomposed at high temperatures. The principle mineral phases of oil shale are quartz (SiO_2) and calcite ($CaCO_3$) that can be detected and semi-quantified alongside other minerals using X-ray diffraction (XRD) and X-ray fluorescence (XRF) methods (Bhargava et al., 2005).

The kerogen within oil shale is insoluble in organic solvents and requires heat to form extractable hydrocarbons. The majority of oil shale is processed in this way, in a process known as retorting, where crude oil is produced as a distillation product, leaving residual carbon within the spent oil shale. To be suitable for retorting, the proportion of organic matter within the oil shale must be > 5 %, so that there is a resultant net gain in energy (Jaber et al., 1997a). Retorting may be done *in-situ*, if the deposits are deep underground or external retorting can be accomplished after surface-mining of deposits. *In-situ* processing most commonly involves fracturing a formation, before heating the oil shale to initiate pyrolysis and subsequently obtaining oil via production wells, such as is currently being developed in the Shell ICP (*In-situ* conversion process), illustrated in Figure 2.1.

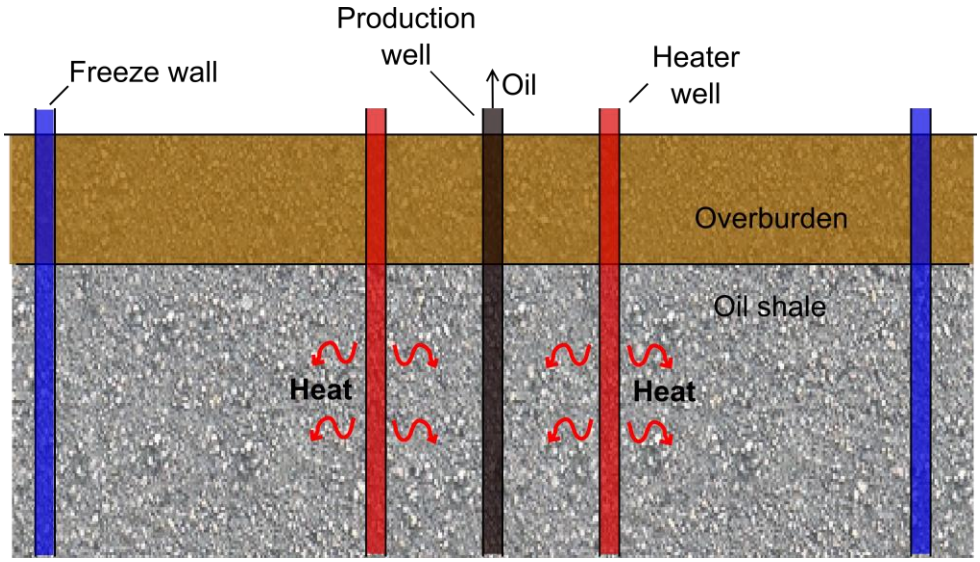

Figure 2.1 – *Illustration of the ICP in-situ retorting process developed by Shell, adapted from Brandt (2008). Oil is obtained by heating the oil shale unit, and collecting oil through production wells. Freeze walls are used to prevent the contamination of groundwater.*

Ex-situ processing involves mining and crushing of oil shale, which is then heated directly (by the use of hot combustion gases), or indirectly (by mixing hot solids with fresh material or by external processes) (Russell, 1990). An example of external processing is the Alberta Tacuik Process (ATP), explained in more detail in Chapter 3. The process retorts oil shale in an atmosphere void of oxygen, at temperatures up to 500 °C, to produce oil and hydrocarbons gases. The remaining solids are then combusted at higher temperatures, burning the residual carbon to produce heat for the retorting of oil shale, before the spent solids are cooled and removed. *Ex-situ* processing holds advantages over *in-situ* processing. The lower costs, ease of oil shale extraction and the pre-existence of mining and retorting technologies consequently results in more widespread occurrences of surface retorting. Environmental concerns over groundwater contamination by *in-situ* retorting must also be considered (WEC, 2013). Though, for oil shale to be feasible for surface extraction and external retorting, the oil shale and deposits must meet several criteria. It must have a low stripping ratio (thin overburden) to be economical for surface mining. The reserves must be large, containing a high concentration of oil and low moisture content to be suitable for retorting. Deposits must be accessible to good roads or transport routes, as well as being situated distanced away from populated areas. The abundance of groundwater is also of value, to be used during retorting (Alali et al., 2006).

Oil shale can also be used directly as a low-grade fuel, rather than for production of shale oil. There are a few production technologies in place focused on the complete combustion of oil shale, to produce electricity rather than extract oil. These include: pulverised combustion (PC) operating in Estonia, fluidised bed combustion (FBC) which reduces the amount of sulphur emitted, and circulated fluidized bed (CFB), operating in China, Estonia and Israel (Kashirskii et al., 2007; Alali et al., 2006).

2.2.1 Global oil shales

Information on the oil shale deposits, which were used to provide samples for this study, is given in Table 2.1 and locations are shown in Figure 2.2.

Oil shales deposited in a marine setting and characterised in this study include oil shales from Estonia, Jordan, Israel, Morocco and Saskatchewan. The oldest deposits are the Ordovician kukersites, deposited in a shallow subtidal environment, occupying 50,000 km^2 in northern Estonia (Dyni, 2006). The oil shales have been extensively mined for the past 90 years (Aleksandrov, 2009), and are able to yield > 180 litres per metric tonne (l/t) of oil, reaching 500 l/t in the richest layers with total deposits containing an estimated 3.9 billion barrels (bbbl) of oil (Dyni, 2006; Russell, 1990).

Figure 2.2 - *Location of the 15 oil shales used in this study.*

The marinite oil shales of Jordan, Israel and Morocco are similar with respect to their petrology and depositional history. All were deposited in shallow marine environments less than 72 million years ago, in the Maastrichtian, Cretaceous period. In Morocco 53.4 bbbl of oil can be found in the two largest deposits: Tarfaya and Timahdit (Dyni, 2006; Kolonic et al., 2002). Oil shale deposits in Jordan and Israel both overly phosphorite formations and deposits are estimated to contain 1.26 bbbl and 0.82 bbbl in Mishor Rotem, Israel and Al Lajjun, Jordan, respectively (Minster, 2013; Shawabkeh, 1991). The Israeli oil shale contains up to 26 % organic matter in the Ghareb formation, similar to Jordanian material which contains up to 30 % (Russell, 1990). The Saskatchewan, Boyne and Favel marinites were deposited in the Upper Cretaceous period also, but differ from the other marinites studied as they contain a lower concentration of carbonate minerals due to deposition occurring in a 'muddy sea' rather than a shallow marine basin. Large, low yielding (up to 60 l/t) resources could produce an estimated 1.25 bbbl (Macauley, 1981).

Oil shales deposited in a lacustrine environment include those from: Scotland, Australia, Asia (Mongolia, China, Thailand) and Northern America (New Brunswick and the U.S.). Scottish oil shales were deposited in a tropical lagoonal setting over 320 million years ago, in the Mississippian, Carboniferous period (Carruthers et al., 1912). The Lothian silicate rich deposits are located within nine oil shale seams, with the potential to provide 50 million barrels (mbbl) of oil from remaining resources which are viable for extraction. The varied fossil content and chemical composition across the oil shale seams indicates an alternation of fresh and brackish

water over the course of sedimentation (Russell, 1990). Also deposited in the Carboniferous period was oil shale found in the Albert formation in New Brunswick, Canada. The lamosites yield up to 94 l/t, with resources estimated at 270 mbbl (Macauley, 1981).

Asian deposits vary in age from Cretaceous to Neogene. Mongolian oil shales contain up to 30 % organic matter, and were deposited in the Early Cretaceous in tropical-subtropical freshwater lakes, with the majority of accumulation in the East Gobi basin where resources are thought to exceed 170 bbbl of oil (Johnson et al., 2003; Yamamoto, 1998). The oil shales are commonly associated with coal measures, similar to the Chinese oil shale deposits of Eocene age at Harbin and Fushun as well as the deposits in Thailand. China contains large resources of oil shale (> 400 billion tonnes), with high concentrations of clay and rare earth elements (REE) (Russell, 1990). The Yilan area of the Heilongjiang Province (Harbin) yields an average of 5 % oil from lacustrine oil shales from the Dalianhe formation (Chen, 2007). Oil shales from the Liaoning Province, Jijuntun formation, is able to produce higher yields of ~7-8 % oil, from the Fushun deposit with estimated resources totalling 127 mbbl (Dyni, 2006). Oil shale resources in Thailand were deposited over the whole of the country, in shallow seas, large lakes, and lagoonal environments (Russell, 1990). The lamosite oil shale from the Mae Sot basin was deposited in lacustrine-fluvial lacustrine environments in the Miocene period and is one of the more extensively studied deposits, containing a large proportion of organic content averaging 10–24 % (Suwannathong, 2007). The Mao Sot basin is estimated to contain 6.4 bbbl of oil, with compositional similarities to oil shale found in the Green River (GR) Formation (Dyni, 2006).

The GR formation in the U.S. extends into three states: Colorado, Wyoming and Utah, covering over 4 million hectares and containing ~70 % of global oil shale resources. The oil shales were formed in two large lakes: Lake Uinta (now the Uinta and Piceance basin) and Lake Gosiute (Green River and Washakie basin) over ten million years in the Eocene period (Dyni, 2006; Russell, 1990). Despite deposition in separate lakes, the oil shales are similar in composition. The Mahogony zone contains the richest oil shale seams, producing oil yields of up to 100 l/t, and can be found in: the Uinta basin, Utah (1.3 tbbl); the Piceance basin, Colorado (1.5 tbbl); and the Green River basin; Wyoming (1.4 tbbl) (Johnson, Pantea et al. 2010; Johnson et al. 2010). Often compared to the GR oil shales are those from the Stuart deposit in Eastern Queensland, Australia and also of Tertiary age. They are thick lamosites, accumulating in grabens and deposited in freshwater lakes associated with coal forming swamps, where resources are estimated at 3 bbbl of oil (Dyni, 2006).

Table 2.1 – *Location, resources and oil yield from the sampled oil shale deposits, where l/t = litres per metric tonne. *Resource estimates from (Dyni, 2006) unless otherwise indicated, where values are calculated or found from references therein. Reliability of resource estimates varies, as many countries contain limited or no published data on oil shale deposits.*

	Country	Deposits	Age	Deposition	Resources 10^9 bbl*	Oil Yield
Africa	Morocco	Tarfaya & Timahdt	Cretaceous	Marinite	53.4	50 – 60 l/t
Asia	Israel	Mishor Rotem	Cretaceous	Marinite	1.26 (Minster, 2013)	60 – 71 l/t
	Jordon	Al Lajjun	Cretaceous	Marinite	0.82	100 l/t (Russell, 1990)
	Morocco	Gobi	Jurassic	Lacustrine	0.3 - 170	-
	Thailand	Mae Sot	Tertiary	Lamosite	6.4	-
	China	Fushun Harbin	Tertiary	Laucstrine	> 0.13	-
Australasia	Australia	Stuart	Tertiary	Lamosite	3	> 50 l/t
Europe	Estonia	Estonian	Ordovician	Marine kukersite	3.9	> 180 l/t
	Scotland	Lothian	Carboniferous	Lacustrine	0.05 (Russell, 1990)	< 100 l/t
N America	Utah, US Wyoming, US Colorado, US	Green River	Tertiary	Lacustrine	1,466	< 125 l/t
	New Brunswick, Canada	Albert	Carboniferous	Lamosite	0.27	< 94 l/t
	Saskatchewan, Canada	Boyne & Favel	Cretaceous	Marinate	1.25	< 60 l/t (Macauley, 1981)

2.2.2 Oil shale processing requirements

Prior to the processing of oil shale, it is important to gain an understanding of the mineralogy, as materials can (Patterson, 1994):

- be a source of trace metals of potential economical use or environmental concern;
- alter the amount of heat required during the retorting process;
- affect the types of gaseous emissions that are produced;
- influence the degree of oil coking (excessive decomposition of oil into undesirable reaction products) that occurs during combustion.

Many minerals start to decompose at temperatures of 400-600 °C encountered during retorting. Some of these decomposition reactions can be endothermic, such as the decomposition of clay and carbonate minerals and result in heat energy being removed from the retorting process to enable this reaction to proceed (Sohns et al., 1951). Following mineral decomposition, the gaseous products and new mineral phases allow for further reactions to proceed. For example, CaO can react with SO_2 to produce $CaSO_4$. Additionally, minerals can adsorb organic matter or gases, for example clay minerals are able to catalyse oil formation by acting as Lewis acids, which are able to break down kerogen (Hu et al., 2014; Johns, 1979). Mineral effects on oil conversion rates during retorting were investigated using GR oil shale and shown to be catalysed by alkaline earth metal cations, which are chemically bonded in carbonate minerals (Karabakan et al., 1998).

The mobilisation of elements, both during and after retorting, is an area of concern when considering oil shale processing conditions and is dependent on the mineralogy (Hill, 2006). Gaseous emissions produced during retorting may include sulphur oxides, nitrous oxides, carbon monoxide, carbon dioxide and ozone precursors; which may contribute to acid rain and global warming. Also, particulate matter released may negatively impact human health if inhaled (Saether, 2004). Additionally; arsenic, mercury, cadmium and selenium, elements which are toxic at high concentrations, may also be released in gaseous emissions during retorting (EASAC, 2007). Waste liquids produced during oil processing and upgrading may contain organic contaminants, whilst spent oil shale deposits may lead to the production of alkaline water. This could lead to contamination of groundwater, if toxic elements are released from the solid material (Saether, 2004).

Metals or trace elements at sufficient concentration and able to be simply extracted from mineral phases could be of benefit if economically viable for extraction alongside the oil.

Examples of elements that have been investigated include exploiting sulphur from pyrite, and vanadium and molybdenum from clays (Patterson, 1994). Others include: heavy metals, uranium, zinc, alumina, phosphate, sodium carbonate minerals, and ammonium sulphate (WEC, 2010). Fu (2010) suggested extracting REEs from oil shale; to be applicable REEs must be in phases that are susceptible to leaching, and not in the refractory phase such as is in oil shales from the GR formation (Birdwell, 2012).

Therefore, this chapter aims to characterise and investigate inter-deposit variation using a range of global oil shale samples. By determining the mineralogy and trace elemental enrichment, oil shales can be assessed and ranked by their: influence on retorting, by-product exploitation, and environmental impacts.

2.3 Methodology

2.3.1 Samples

Oil shale samples, of particle size <2 cm and sample size 50 g, were provided by Jordan Energy and Mining Ltd, with the exception of the Lothian Oil Shale which was collected from an oil shale seam below the Forth Bridge in South Queensferry, Scotland. Table 2.1 and Figure 2.1 list the location and deposits of all the sampled oil shales that were obtained as point samples and therefore are not representative of the heterogeneity within oil shale deposits. Samples were firstly ground into a fine powder (< 0.5 mm) using an agate pestle and mortar, and were then stored in polypropylene vials and in a silica desiccator to prevent hydration of the samples. Powdered oil shale samples were then analysed to determine the mineralogy and the major and trace elemental compositions. The analytical methodology is discussed in more detail in Appendix A.

2.3.2 Analysis

Inductively coupled plasma mass spectrometry (ICP-MS) was used to determine the concentration of trace metals and rare earth elements (REEs), typically < 0.1 wt % concentration range, within digested rock samples. Sample solutions were injected into the ICP analyser, where they were ionised, before passing through a mass spectrometer, and values converted into concentrations, in mg/l, based on the calibration curves. A standard method was used in the preparation and analysis of oil shales (Ottley et al., 2003), as detailed in Appendix A.

X-ray fluorescence (XRF) was used to determine the major elemental composition of oil shale samples, where major elemental concentrations are typically > 0.1 wt %. XRF was conducted using the PANalytical Axios Advanced XRF Spectrometer, in the Department of Geology, University of Leicester, and was used to calculate major elemental concentrations, in wt%, using fused glass beads for the analysis.

X-ray diffraction (XRD) provided detailed information on the structure of crystals, and was used to identify mineralogical composition within oil shales. Data was collected on a Bruker D8 Advance, and the mineralogy of samples was determined by using search and match techniques of known mineral reflections using Diffrac Suite EVA software, coupled with spectra downloaded from the ICDS database (ICSD, 2014).

The confirmation of the identity of mineral phases detected by XRD was accomplished by the presence of more than two 'important' reflections that diffracted X-rays at the correct angle and with the correct relative intensity. When only one or two reflections were present, the use of XRF analysis was required to propose that the mineral was present, as well as the absence of any overlapping peaks caused by different mineral phases. If only one weak reflection was assigned to a specific mineral, and it was likely that the overlap of other mineral phases could also occur, then the presence was not confirmed. However, the presence may have been suggested based on knowledge of the deposits from the literature, and from experience in analysing multiple samples of differing composition. Mineral reflections were identified on the XRD patterns throughout the chapter, and other mineral phases were tabulated and divided into dominant, sub-dominant, accessory and minor phases. Because of the nature of the analysis and the low concentration of clay minerals, clay minerals were not quantified further by separation techniques.

Qualitative mineralogical analysis by XRD was semi-quantified by the use of XRF. This combined method was used to identify mineral phases by using XRD, estimate the proportion of these mineral phases by correlating back to XRF results, and also to provide indication to the presence of trace phases which may not be detectable from XRD: due to either a low detection limit, or the presence of amorphous phases. Oil shale contains a high percentage of organic matter, mainly in the form of kerogen which is amorphous and does not diffract X-rays (Abed et al., 2009), and this is therefore likely to cause broad peaks in the diffraction pattern. Clay minerals are difficult to identify from XRD, however interpretation of the different types present has been attempted. The main identification methods included: using the (*00l*) reflections, typically identified at low 2θ angles and representing the distance along the z-axis

(or distances between the layered structures). Further differentiation was accomplished by using the (*060)* reflection, found at higher 2θ angles (Moore et al., 1997).

2.4 Results

2.4.1 Mineralogy and major elemental trends

The relative proportions of major elemental oxides, in percentage weight (wt %), as determined by XRF, illustrated the variance in oil shale deposits from around the world (Table 2.2 and Figure 2.3) and samples were grouped based on their chemical composition. Errors on the major elemental concentrations were not calculated as only one sample was used for each deposit, however errors associated with XRF analysis are commonly low, and have been shown to be < 2 % for the analysis of sediment cores (Weltje et al., 2008).

Table 2.2 - *XRF data for oil shales, separated into groups based on their chemical composition (marine, muddy marine, lacustrine, and saline lacustrine) showing the concentration (wt %) of major elements.*

Sample	SiO_2	TiO_2	Al_2O	Fe_2O	MnO	MgO	CaO	Na_2	K_2O	P_2O_5	SO_3	LOI	Total	Si/Al
Marine														
Estonia	23.62	0.19	4.25	1.72	0.011	1.28	24.62	0.27	0.997	2.535	3.518	36.58	99.59	3.13
Morocco	13.53	0.13	2.35	1.18	0.008	0.52	32.55	0.23	0.309	0.250	4.106	43.99	99.15	4.02
Israel	8.32	0.15	3.24	1.53	0.009	0.50	37.63	0.18	0.178	1.590	3.694	41.46	98.47	1.79
Jordan	23.33	0.12	2.64	1.23	0.006	1.30	24.88	0.20	0.394	3.040	4.699	37.51	99.36	6.16
Muddy marine														
Saskatchewan	34.41	0.41	10.79	4.24	0.033	0.93	15.92	0.86	1.987	0.286	5.366	25.04	100.2	2.22
Lacustrine														
Lothian	65.21	1.13	17.22	1.86	0.015	0.97	0.46	0.20	3.002	0.138	0.098	10.34	100.6	2.64
Mongolia	46.27	0.44	11.43	4.71	0.195	2.30	7.53	0.75	2.145	0.368	1.447	22.94	100.5	2.82
Harbin	41.44	0.34	10.36	3.65	0.033	0.29	0.26	0.06	0.583	0.044	0.000	43.75	100.8	2.79
Fushun	47.78	1.11	17.88	7.63	0.090	1.08	0.67	0.73	0.950	0.249	0.069	22.43	100.6	1.86
Australia	45.42	0.47	11.65	5.59	0.118	1.46	2.85	0.48	1.340	0.194	0.417	30.70	100.7	2.72
Saline														
Thailand	31.69	0.31	10.04	3.57	0.052	5.68	12.72	2.85	2.592	0.126	0.456	30.52	100.6	2.2
New Brunswick	41.37	0.51	11.28	4.93	0.087	3.18	9.19	1.18	1.645	0.257	2.330	24.63	100.6	2.56
Wyoming	44.69	0.35	9.12	3.49	0.050	4.46	9.44	1.18	4.053	0.110	0.729	22.78	100.4	3.42
Colorado	28.08	0.20	5.41	2.23	0.030	7.05	14.71	1.25	1.923	0.681	0.759	38.14	100.4	3.62
Utah	25.72	0.19	5.07	2.36	0.033	5.55	14.94	2.31	1.139	0.147	1.840	41.25	100.5	3.54

Lacustrine samples (for example Lothian and Chinese oil shales) have the highest concentrations of silica, mainly in the form of quartz. Alumina concentration was found to decrease proportionally with decreasing silica concentration (Table 2.2), indicating the presence of common aluminosilicate minerals such as clay and feldspars. Conversely, the

concentration of silica was indicated to be inversely proportional to the calcium content, because marine deposits contain larger concentrations of carbonate minerals. This indicates variability in the rock types, and a shift from silicate-hosted shales and mudstones, to carbonate-hosted marine-type marlstones. The loss on ignition (LOI) accounts for gases, such as H_2O, CO_2 and hydrocarbons, which are released on the decomposition of samples. Larger values of LOI could be caused by an increase in CO_2 emissions, attributed to higher concentrations of CaO and therefore carbonate minerals.

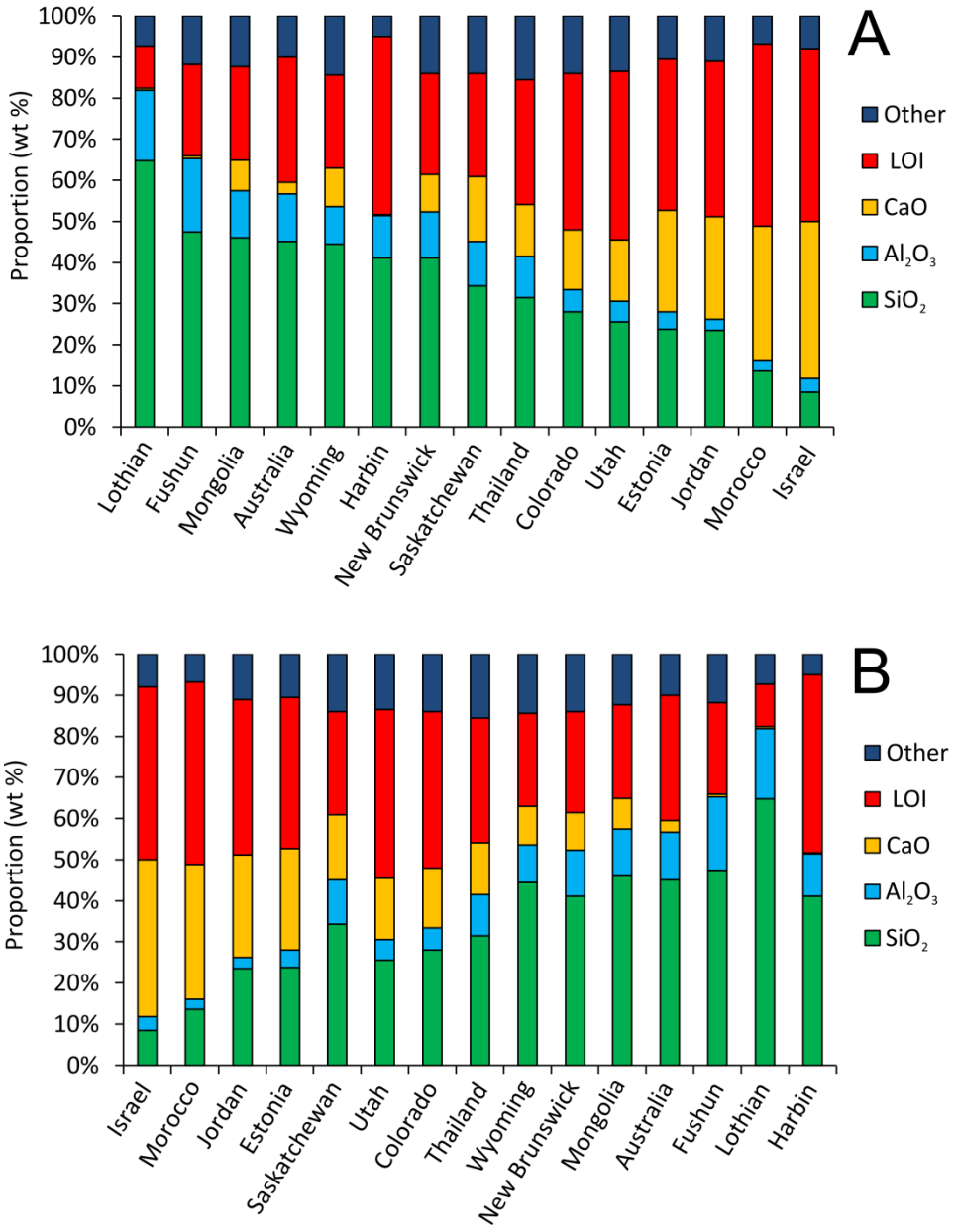

Figure 2.3 - *Proportion of dominant elemental phases within oil shales in order of decreasing silica content (A) and decreasing calcium content (B), where LOI = loss on ignition.*

The relationships between different major elements are illustrated in Figure 2.4. Most elements did not show a strong relationship (based on the regression R^2 values), however the correlation between Ti and Al was shown to be positive, with strong correlations between different groups of oil shale that were similar in mineralogy (R^2=0.99, 0.83 and 0.87 for lacustrine, saline lacustrine and marine, respectively). This same relationship was found between Ti and Fe as well (not shown in figure), indicating the possible association of Ti with aluminosilicates and Fe-oxides. The correlation between Ca and Mg showed two different trends: firstly, a positive relationship between Mg and Ca, which could be due to increasing dolomite concentrations (R^2=0.93). Secondly: increased Ca, independent of Mg. This occurred in marine oil shales, indicating high concentrations of calcite lacking in dolomite minerals. Increasing silica with alumina, indicated the presence of clay minerals, with greater concentrations of aluminosilicates deposited in a lacustrine environment.

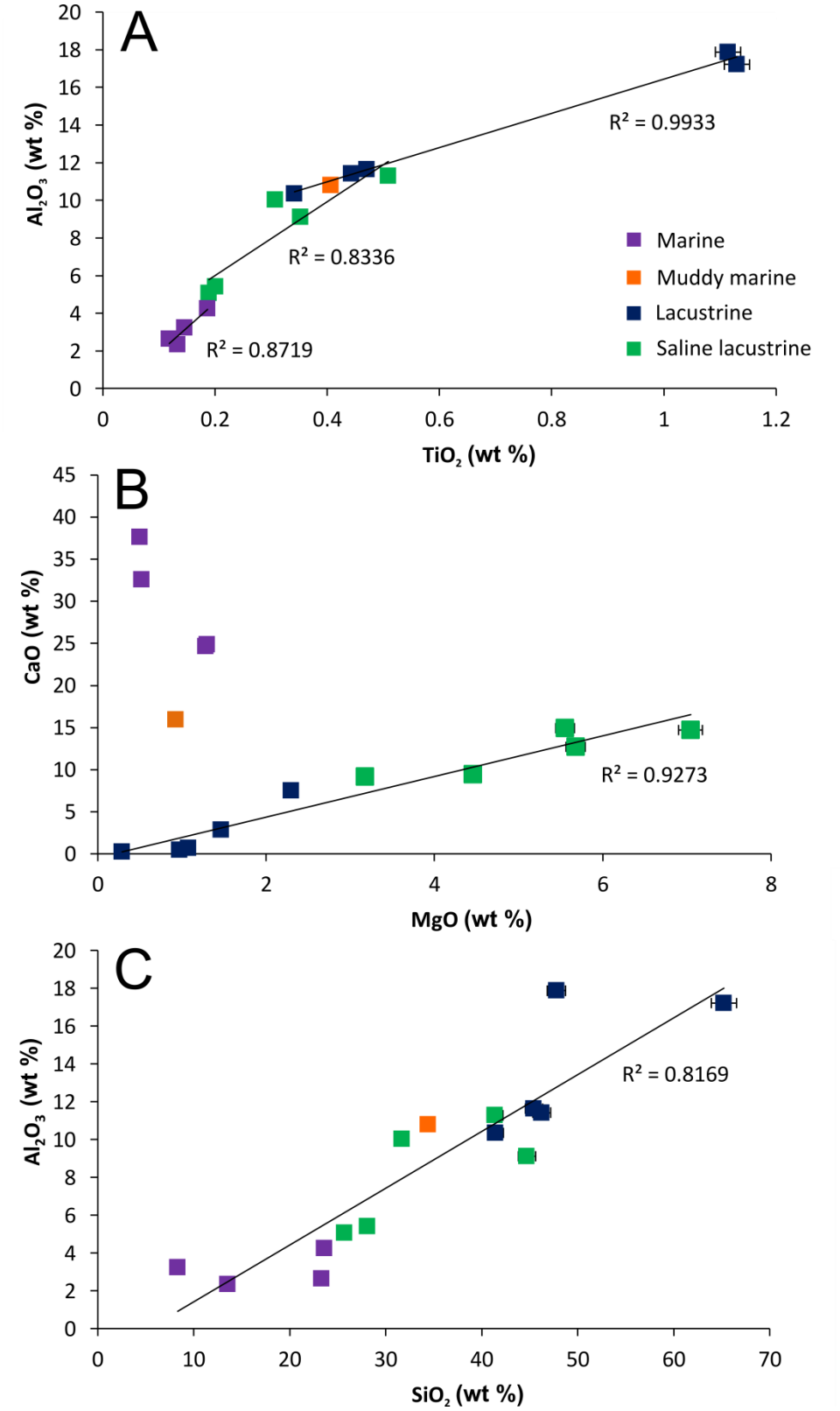

Figure 2.4 - *Major elemental relationships between titanium and aluminium (A), calcium and magnesium (B), and silicon and aluminium (C). Errors (2 %) are indicated as horizontal and vertical bars, except when smaller than the square data points.*

Oil shales were divided into groups based on chemical similarities and depositional environment, which were: marine, muddy marine, lacustrine and saline lacustrine. Further work was achieved by investigating the mineralogy using XRD analysis. X-ray fluorescence gave useful information on the relative mineral groups and major elemental composition of the samples, yet XRD can be used to determine or exclude precise mineral forms. The detection limit was first determined by using the relative intensities of minerals identified by XRD, and comparing this with quantitative elemental concentrations provided by XRF analysis. Results showed that elements found at concentrations > 1 wt %, could be detected as minerals by XRD. Of course, if the element exists in multiple mineral forms within the sample, there is the possibility it may not be detected by XRD. One example that caused difficulties was Fe-containing minerals, where mineral identifying reflections commonly overlap in XRD patterns, and are also often found at low concentrations within oil shales. Quantitative X-ray diffraction by Rietveld refinement was not used in this study, due to difficulties in analysing samples of varied composition, and large errors associated with the quantitative analysis.

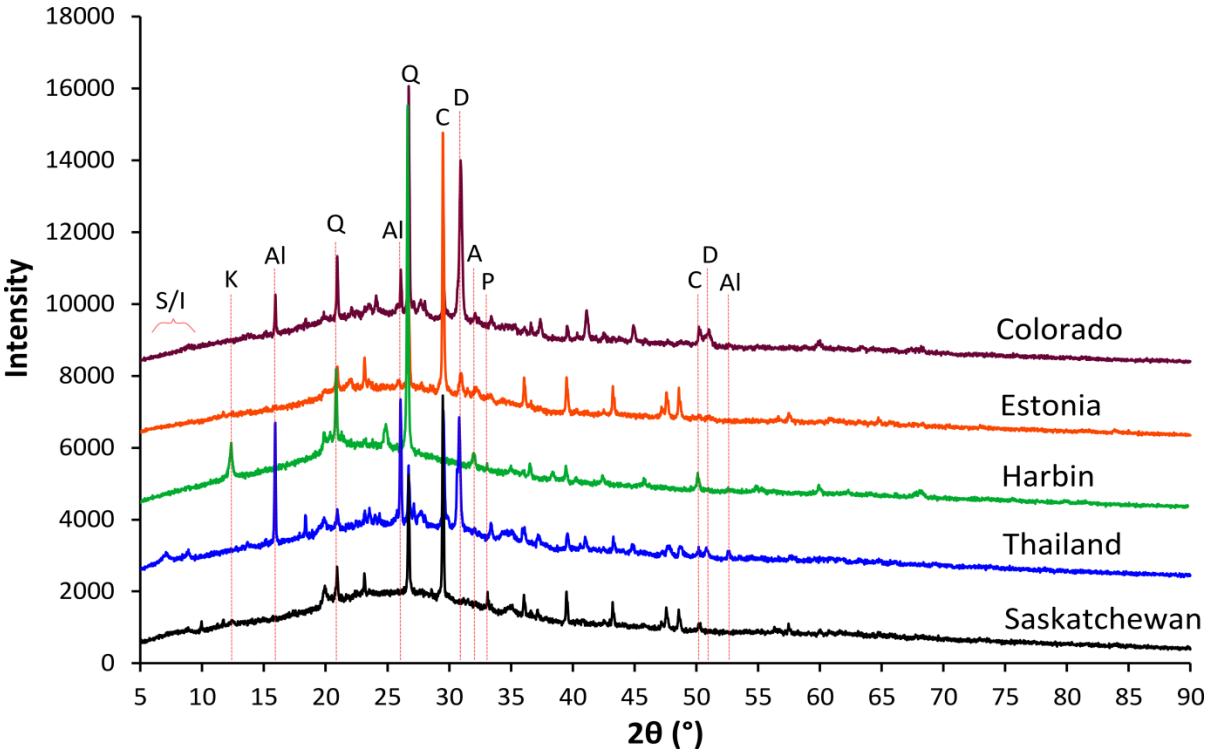

Figure 2.5 - *X-ray diffraction patterns for oil shales from Colorado, US; Estonia; Harbin, China; Thailand; and Saskatchewan, Canada. Minerals identified include quartz (Q), calcite (C), dolomite (D), apatite (A), kaolinite (K), pyrite (P), analcime (Al) and smectite/illite (S/I).*

The XRD patterns in Figure 2.5 are representative of the different oil shales studied, showing a range of ages, depositional environments, locations, and dominant mineral compositions. To summarise the variances: Colorado oil shale was deposited in a saline lake and consisted of high concentrations of dolomite [$MgCa(CO_3)_2$] and analcime [$NaAlSi_2O_6.H_2O$] as a consequence; Estonian marine oil shales were found to be carbonate rich, yet the marine oil shale from Saskatchewan was unique in that it also contained a significant proportion of pyrite [FeS_2], formed most likely under reducing conditions at deposition (muddy marine deposition). Thailand oil shale showed the most mixed mineralogy of all deposits studied, with relatively high concentrations of quartz [SiO_2], calcite [$CaCO_3$], dolomite, analcime and clay minerals; then the remaining lacustrine oil shale from China was shown to be dominated by quartz and clay minerals enriched in rare earth elements (REEs). The formulae of minerals identified by XRD in this study can be found in Appendix B, along with individual oil shale XRD patterns, in Appendix C.

Table 2.3 contains the detailed semi-quantitative mineralogical composition of oil shales. These results will be discussed by identifying similarities between oil shales in relation to their depositional history and oil shale type, as well as identifying any strong characteristics which could impact the retorting process and economic potential of deposits.

Table 2.3 - *Mineralogy of oil shales as determined by XRF and XRD. xxxx = dominant mineral, xxx =sub-dominant > 20 %, xx = accessory 5-20 %, x =minor < 5 %, t = trace.*

	Quartz	Cristobalite	Calcite	Dolomite	Siderite	Dawsonite	Clay	*Smectite*	*Illite*	*Illite/Smectite*	*Muscovite*	*Kaolinite*	*Chlorite*	Analcime	Feldspar	*Plagioclase*	*K-feldspar*	Apatite	Gypsum	Anhydrite	Pyrite	Fe-oxide
Lothian	**xxxx**			*x*			*xxx/xx*		*x*	*x*	*?*	*x*			*x*		*x*					*x*
Estonia	xxx		**xxxx**	*xx*			*x*								*x*		*x*	*xx*			*t*	
Morocco	xx		**xxxx**				*x*					*x*			*x*							
Israel	xx		**xxxx**				*x*								*t*			*x/xx*				
Jordan	xxx	x	**xxxx**	*xx*			*x*	*x*				*x*			*x*			*xx*			*t*	x
Mongolia	**xxxx**		xx	*x*	*x*		*x*	*x*	*x*			*x*			*x*	*x*	*x*			*x*	*t*	
Harbin	**xxxx**				*x*		*x*					*xx*									*t*	
Fushun	**xxxx**		x		*x*		*xxx*	*xx*				*xx*			*x*		*x*				*t*	
Thailand	xxx		xxx	*xxx*	*x*		*xx*	*x*	*x*				*x*	***xxx***	*x*		*x*					
Australia	**xxxx**		xx/x	*x*	*x*		*xx*	*x*	*x*	*x*	*?*	*x*			*x*	*x*	*t*		*x*		*x*	
Saskatchewan	xxx		xxx		*x*		*xx*	*x*	*x*	*x*		*x*			*x*						*xx*	
New Brunswick	**xxxx**		xx	*xx*	*x*		*xx*		x	*x*	*?*				*xx*	*x*	*x*					*x*
Wyoming	**xxxx**		xx	*xxx*	*x*	*x*	*x*		*x*	*x*				*xx*	*xx*	*x*	*xx*					*x*
Colorado	**xxxx**		xx	*xxx*	*x*	*x*	*x*		*x*	*x*			*x*	*xx*	*xx*	*x*	*x*					*x*
Utah	**xxxx**		xx	*xxx*	*x*	*x*	*x*		*x*	*x*			*x*		*Xx*	*xx*	*x*			*x*		*x*

The deposits in Northern Africa and the Middle East (Jordan, Israel and Morocco) were found to be similar in their mineralogical composition as all were deposited in a marine environment. Jordanian and Israeli oil shales matched very closely in their mineralogy, containing high concentrations of calcite and quartz. Both oil shales overlie phosphate formations, explaining the presence of apatite minerals. Also identified in both deposits were small amounts of dolomite, as well as low concentrations of clay and feldspar. The feldspar reflections were very minor and could not be separated further. Iron-containing minerals were also difficult to distinguish, due to the overlap of primary identification reflections at 33° 2θ for minerals such as goethite, hematite and pyrite (Song et al., 2009; Legodi et al., 2007). As the Fe_2O_3 concentration was commonly < 2 wt % for most oil shale deposits, it was especially difficult to assign minerals to this commonly encountered reflection. Goethite, commonly associated with Jordanian oil shale (Alali et al., 2006) could be present and is formed from the weathering of Fe-containing minerals, possibly indicating the previous occurrence of pyrite minerals (Vassilev et al., 1996), minerals which are normally dominant in marine deposits (Potter et al., 1980). The absence of apatite was noticeable in Moroccan oil shale, however the mineralogy was otherwise similar to deposits in Jordan, Israel and Estonia, with Estonian deposits shown to contain calcite, quartz, dolomite, K-feldspar, apatite, pyrite and clay minerals. The high concentration of sulphur and organic matter within all these marine deposits indicated anoxic conditions at deposition, as the organic material was prevented from decomposition (Shirav et al., 1988). Carbonates were present at high concentrations in the marine sediments, with the four marinites (Jordan, Israel, Estonia and Morocco) containing the highest concentrations of calcium (Figure 2.3).

Saskatchewan oil shale, another marine deposit, also contained a high concentration of sulphur, similar to the marine deposits of the Middle East and Europe. The majority of sulphur was identified as pyrite and not present as sulphate anions, indicating the low redox conditions present at the time of deposition. This is unlike the shallow marine deposits in Jordan, which typically contained only trace amounts of pyrite, with most of the sulphur associated with organic matter (Al-Otoom et al., 2005). In addition to pyrite minerals, Saskatchewan oil shale contained calcite, quartz, clay minerals (kaolinite and mixed illite-smectite) as well as smaller amounts of feldspar and siderite. Minor amounts of jarosite were also identified from the XRD pattern, with reflections at 17.5° and 31.2° 2θ corresponding to this Fe-containing sulphate mineral which is a common product of pyrite weathering (Vassilev et al., 1996).

Mongolian oil shale can be grouped with deposits from China for analysis, as they are all lacustrine sediments, containing quartz as the dominant phase. The Mongolian oil shale also contained calcite, with minor quantities of dolomite, siderite, clay (smectite, illite, kaolinite), feldspars and anhydrite. In contrast, oil shale from Harbin and Fushun had a much greater clay contribution, with both deposits containing large amounts of nacrite (a monoclinic kaolinite, as signified by reflections at 20.5° and 21.2° 2θ). No calcite, but small amounts of siderite were identified in Harbin oil shale, while Fushun also indicated the presence of smectite and K-feldspar, along with minor calcite and siderite. The lack of Ca and Mg carbonates within the Chinese deposits is only shared with one other oil shale deposit – the Lothian oil shale. This oil shale was characterised by its large concentration of SiO_2 (> 65 wt %) predominantly in the form of quartz, K-feldspar and clay minerals, such as mixed illite-smectite, kaolinite and illite. Trace amounts of dolomite, ankerite and magnetite were also detected. The high concentration of authigenic clay minerals within lacustrine oil shale deposits in particular may be a result of silicate mineral hydrolysis (Smith, 1983). Authigenic kaolinite may be replaced by smectite minerals, which then transform to illite. Mixtures of smectite and illite layers within clay minerals are common, and may be detected using XRD based on broad and asymmetric reflections at low values of 2θ (< 10° 2θ).

The composition of oil shale from New Brunswick was found to consist of quartz, calcite, dolomite, clays and feldspar. Clay minerals included illite-smectite and both types of feldspar (plagioclase and K-feldspar) were present. Reflections corresponding to illite or muscovite crystal structures were also detected, as well as reflections for siderite yet the peak was shifted slightly in the XRD pattern, possibly due to the presence of other divalent cations within the mineral structure. The shifted siderite peak also occurred in Australian oil shales as well, and high concentrations of Fe_2O_3 (> 4.9 wt %) were detected in both samples. Internal standards were not used in XRD analysis, but could be used alongside FTIR analysis to further clarify the mineralogy of Fe-containing minerals. Fe was also in the form of pyrite in the Australian oil shale, but within New Brunswick oil shale traces of hematite were identified instead. Australian oil shale mainly consisted of quartz and calcite, alongside minor proportions of feldspars (predominantly plagioclase), gypsum, clays (smectite, illite/ muscovite, illite-smectite, kaolinite) and very small concentrations of dolomite. Generally oil shales lack authigenic sulphate minerals as they are reduced to other mineral forms, yet in this case evaporites were established due to secondary development (Lindner, 1983). A small amount of chlorite was identified, a mineral also found in GR deposits, possibly existing as a diagenetic clay product from deposits that are Mg-rich (Potter et al., 1980).

Oil shale from Thailand was also deposited in a lacustrine environment, however the minerals identified were rather varied being unique in relation to other oil shale deposits. Dominant minerals included quartz, calcite, dolomite, and analcime. Other minerals included clays (smectite, illite, chlorite), K-feldspar, siderite, with the possibility of trace anhydrite and serpentine, with the latter indicated by reflections at ~60.3° 2θ (Moore et al., 1997). Analcime, an alteration product, was also picked up as a dominant phase within the Wyoming and Colorado oil shales from the GR Formation, however was absent from the Utah oil shale also belonging to the same formation. The three deposits, although similar, do vary in composition due to differences in stratigraphy within the basins, and intra-deposit variation.

All of the GR oil shales contained high concentrations of quartz and dolomite, the latter being formed by the transformation of illite minerals (Smith, 1983). The high concentration of Mg within carbonates of GR and Thailand oil shales is typical of saline lakes (Vassilev et al., 1996). The presence of siderite and dawsonite also indicate particularly saline conditions during deposition (Dyni, 2006). Calcite and mixed layer clays were also present, common authigenic minerals, while the concentration and type of detrital feldspar varied among the samples. Plagioclase is more stable to weathering, and was dominant in the Utah oil shale, which also contained chlorite and anhydrite, possibly as products of diagenesis. Wyoming oil shale, in contrast, contained more K-feldspar and high concentrations of analcime. The Colorado oil shale contained chlorite and analcime, as well as smaller concentrations of both types of feldspar.

The variation between oil shale samples from numerous different deposits has been shown to be large, with multiple controls on the types of mineral products formed under different depositional conditions, and whether minerals are biogenic, authigenic or detrital. In addition, variation is likely to occur within deposits due to heterogeneity, which was not accounted for in this characterisation study due to the analysis of single point samples. Results from trace elemental analysis will now be discussed to further investigate occurrences of enrichment and identify relationships between elements and oil shale samples.

2.4.2 Trace elemental trends

The principle aim of trace elemental analysis was to gain insight into the economic significance of oil shale deposits, alongside their organic content, with regards to trace elements that are normally found at low concentrations within crustal rocks. The concentration of a suite of geologically significant elements was conducted, and a partial table of results is presented in Table 2.4, for the elements that were found to be enriched within multiple oil shale samples.

The remaining results were tabulated and are presented in Appendix D for reference. The concentrations of the elements were normalised to upper continental crust (UCC) compositions (McLennan, 2001; Taylor et al., 1995), and also average shale composites, such as the North American Shale Composite (NASC) (McLennan, 2001; McLennan, 1989; Taylor et al., 1985; Gromet et al., 1984), and Post-Archean Australian Shales (PAAS) (McLennan, 2001; Barth et al., 2000; McLennan, 1989; Taylor et al., 1985).

Table 2.4 – *Trace elemental concentrations in mg/kg, measured by ICP-MS. Literature concentrations are included for UCC, NASC, and PAAS as specified in the chapter text. bdl = below detection limit.*

	Lothian	Estonia	Morocco	Israel	Jordan	Mongolia	Harbin	Fushun	Thailand
V	100.20	152.20	549.10	66.30	161.70	71.29	44.13	116.90	73.95
Cr	83.52	370.45	52.99	242.10	420.41	bdl	bdl	86.46	bdl
Cu	22.34	78.40	57.72	66.85	83.59	22.85	15.19	45.01	50.38
Zn	132.20	354.10	281.10	195.90	543.13	90.46	33.99	77.43	49.33
Sr	371.40	825.00	856.00	1214.00	768.28	425.00	119.80	122.10	264.20
Cs	5.67	1.49	1.21	0.70	0.63	7.89	2.43	4.74	16.77
Pb	19.36	7.23	8.53	4.88	4.30	34.52	26.68	16.80	55.06
U	3.84	24.44	7.89	15.06	21.57	7.10	2.51	1.90	18.56
Sr/Ba	0.67	6.24	7.35	27.27	14.17	1.44	0.90	0.31	0.98

	Australia	Saskatchewan	New Brunswick	Wyoming	Colorado	Utah	UCC	NASC	PAAS
V	77.92	529.70	90.70	99.48	72.00	83.50	107	130	140
Cr	13.39	40.69	11.25	9.25	bdl	bdl	83	125	100
Cu	33.28	66.50	38.71	44.01	33.92	36.45	25	-	50
Zn	68.77	184.30	50.98	53.24	47.17	34.01	71	-	85
Sr	184.40	235.90	613.40	533.30	792.80	754.20	350	142	200
Cs	4.84	5.07	5.59	6.20	3.30	3.47	4.60	5.16	6.00
Pb	11.96	17.24	16.35	20.10	22.39	24.40	17.00	-	20.00
U	2.18	19.84	3.85	4.55	8.34	4.37	2.80	2.66	3.10
Sr/Ba	0.73	0.41	1.65	1.08	2.11	2.06	0.64	0.22	0.31

Trace elements were plotted with each other and major elements to identify relationships between elements and rock fractions, to indicate mineral phases of enrichment therefore showing whether they may be beneficial or detrimental to oil recovery and further exploitation beyond oil alone. With increasing Al_2O_3 content, the elements La, Ga, and Nb, showed a

positive trend (Figure 2.6, R^2=0.77, 0.98, 0.8 respectively). This indicates the association of REE and other trace elements associated with aluminosilicates and clay minerals. A positive correlation was shown between Cs with Pb and Rb (R^2=0.78 and 0.81), elements of similar ionic charge and size which can be associated with each other in mineral structures. Other positive trends were identified, and further separated into the oil shale groups, including: increasing Sr with Ca, a common substitute in carbonate minerals; increasing Zn with S, suggesting association with pyrite (Dale et al., 1984); and increasing Co with Fe, both transition elements which may be associated with each other. The Ni data was poor due to contamination within the instrument and large errors associated with the data. Therefore data was not used, but it has been suggested that Ni is commonly incorporated within clay minerals (Shirav et al., 1988).

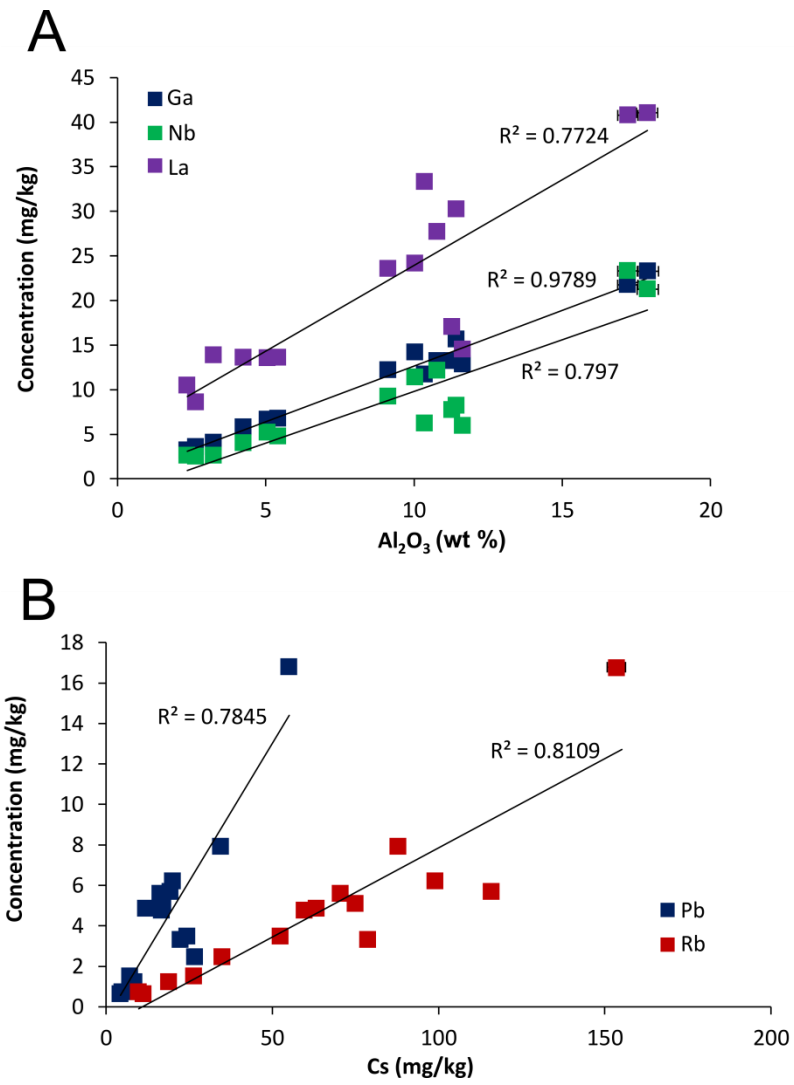

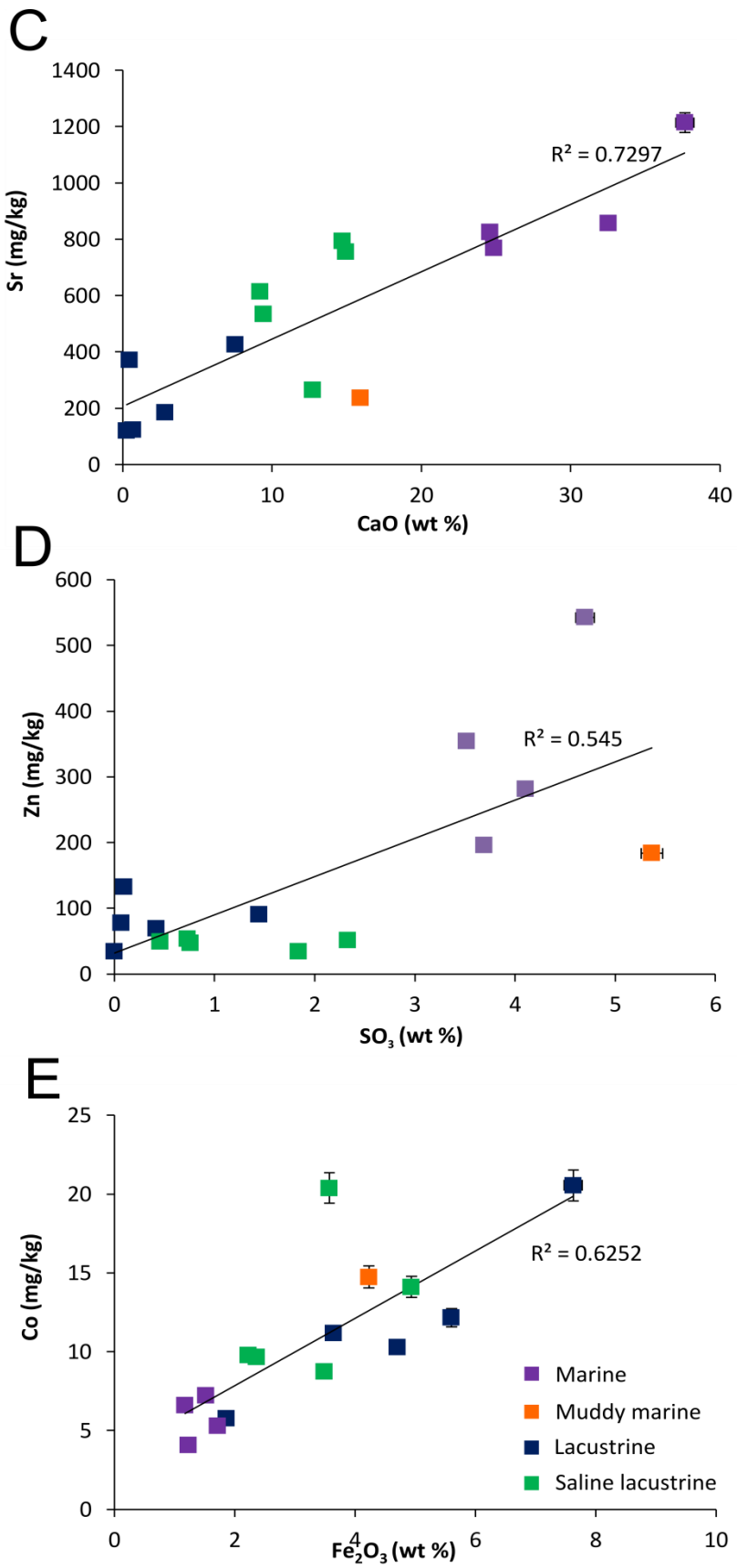

Figure 2.6 – *Relationship between trace and major elements within oil shales: Ga, Nb and La vs Al (A), Pb, Rb vs Cs (B), Sr vs Ca (C), Zn vs S (D), and Co vs Fe (E). Errors (2 % for major elements and from Table D.1 in Appendix D for trace elements) are indicated as horizontal and vertical bars, except when smaller than the square data points.*

As can be seen in Figure 2.7, not all trace elements analysed within Jordanian oil shale were enriched compared with the UCC, PAAS, and NASC. The concentration of elements within UCC is lower than the shale composites, with the exception of Sr which is normally more depleted in shale samples, explaining why enrichment was greater for oil shale normalised to the UCC.

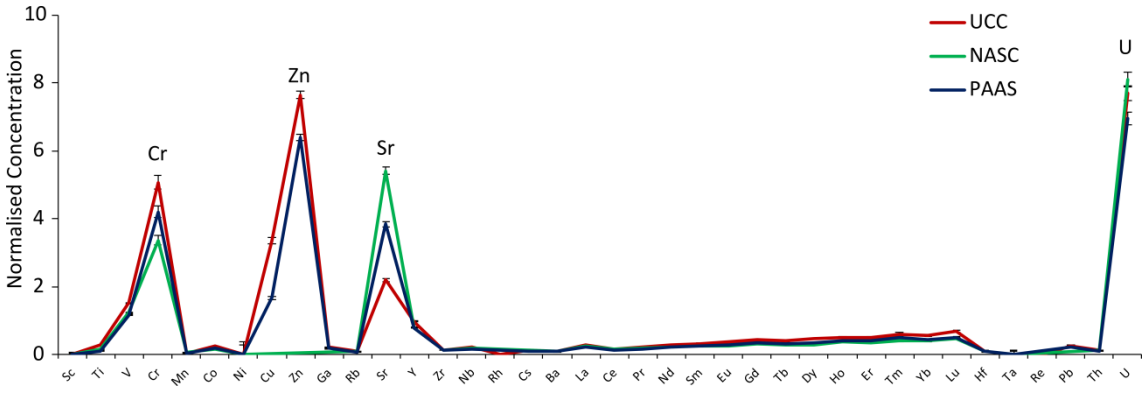

Figure 2.7 – *Enrichment of trace elements in Jordanian oil shale relative to Upper Continental Crust (UCC), North American Shale Composite (NASC) and Post Archean Australian Shale (PAAS).*

Trace elements enriched within the oil shales are of interest to study further and were identified from their UCC normalised values in multiple oil shales. These elements are: V, Cr, Ni, Cu, Zn, Sr, Cs, Pb, U and REEs, and data are shown in Tables 2.4 and 2.5. There was great variation between the oil shales analysed and no noticeable correlation with rock forming major elements.

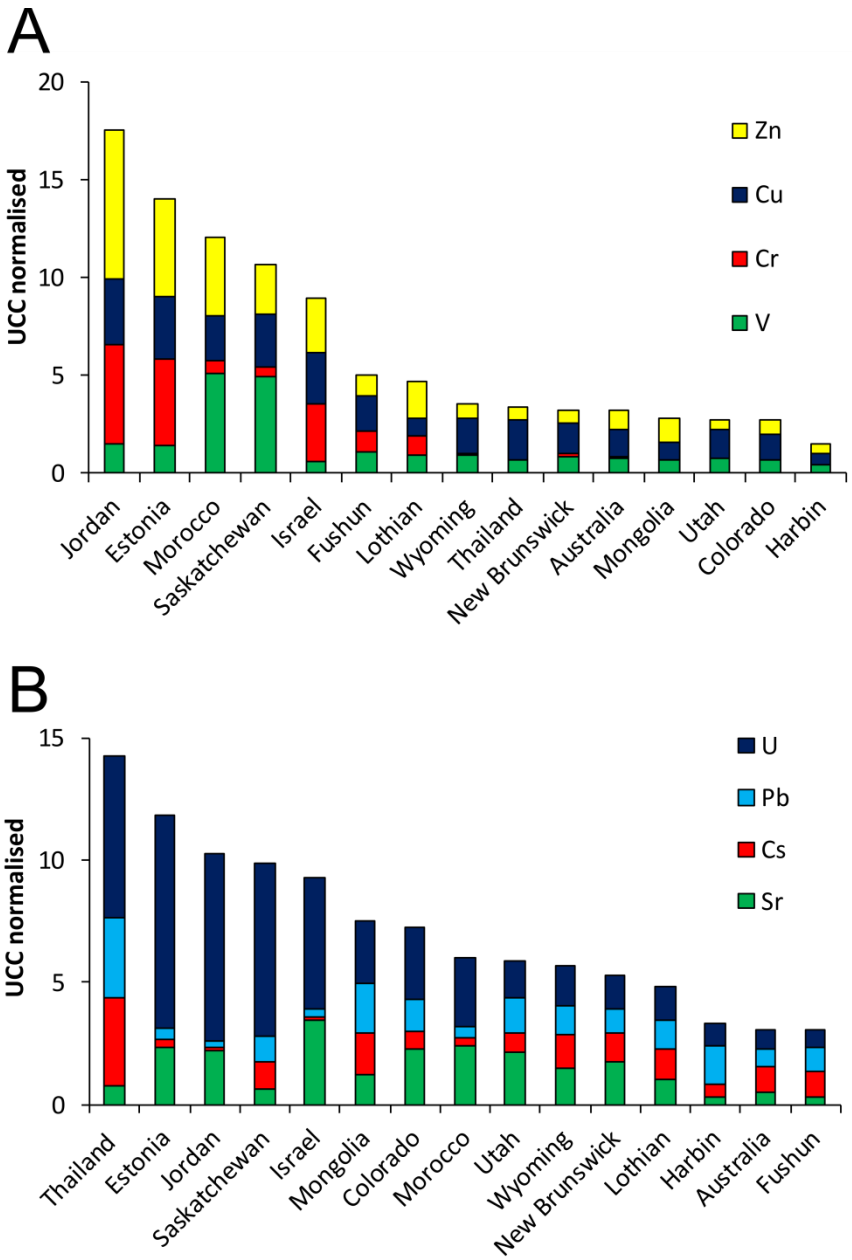

Figure 2.8 - *Proportion of UCC normalised trace elements: zinc, copper, chromium and vanadium (A); and uranium, lead, caesium and strontium (B), in order of decreasing concentration.*

The total enrichment of trace elements was especially strong in marine oil shales, with high concentrations of Cr, Zn, Cu and U in Jordanian, Estonian, and Israeli deposits (Figure 2.8 A). However, in contrast to this, lacustrine samples (eg. Harbin) showed lower concentrations of these elements. This suggests the depositional history affects the source and accumulation of these elements. For the elements Pb and Cs, these were observed to be at high concentrations within oil shale from Thailand, Mongolia and other lake deposits, yet were considerably depleted in marine oil shales. An exception to this was found in the marine oil shale from Saskatchewan which was not depleted in Pb and Cs, however the mineralogy was identified to be similar to that of lacustrine deposits with high concentrations of clay and pyrite. Pb is a chalcophile element likely to be associated with pyrite (Albarède, 2003), and the mineralogy in this case may be a controlling factor for higher concentrations of Pb. In addition, Cs has a high affinity for clay minerals, and is commonly adsorbed to illite and smectite clay minerals (Cornell, 1993). Conversely, although U enrichment is prevalent in marine deposits, it is also a widespread occurrence amongst lacustrine oil shales. This is due to the reducing conditions that occur during oil shale deposition, as this encourages the precipitation of U-oxide, thus becoming concentrated within the sediments. Additionally, uranium is commonly found at high concentrations of ~60–180 mg/kg within phosphorite deposits, potentially explaining the high concentration within the Israel and Jordan oil shales (Jaber et al., 1997b). As well as U, other metals such as V, Zn, Cu, Cr, Pb and Ni are able to become enriched under reducing conditions, prevalent at times of oil shale deposition (Saether, 2004). Other elements such as Mn become more mobile in alkaline conditions, and Mn was found to be depleted in all samples with the exception of oil shale from Israel and Utah, oil shales that showed only limited enrichment in other elements analysed.

The trends between oil shales containing enriched elements (V, Cr, Cu, Zn, Sr, Cs, Pb, U) can be visualised more easily, especially at the lower concentrations, in Figure 2.9. The oil shales which showed the greatest enrichment in transition metals (Jordan, Morocco, Estonia, Israel, Thailand, Saskatchewan) included five marinites and the UCC normalised concentrations are shown in Figure 2.9 A. Moroccan and Saskatchewan oil shales were especially enriched in V and Zn, yet were depleted in Cr, whilst Estonian, Jordanian and Israeli oil shales all showed enrichment in both Cr and Zn. Most other oil shales were depleted in Zn, with the exception of the Lothian oil shale. The zig zag pattern observed in Figures 2.9 B & C indicates that oil shales that were less enriched in trace metals had relatively higher concentrations of Cu and Sr. They include oil shales from Wyoming, Colorado, Utah, New Brunswick.

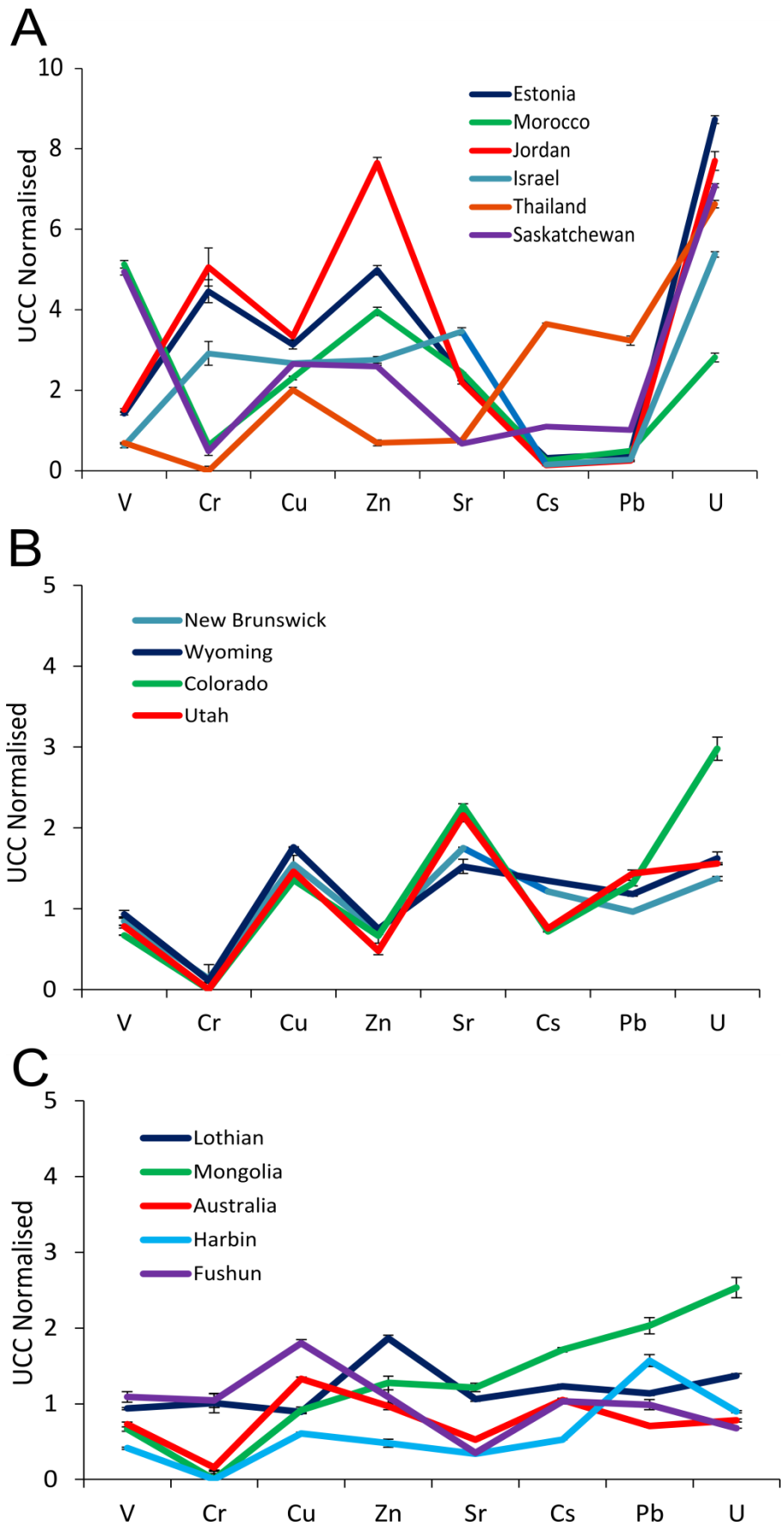

Figure 2.9 – *Trace elements normalised to UCC for all the oil shales studied, divided into three graphs based on values of enrichment.*

Geochemical characteristics, in addition to the enrichment of elements, can be used to gain more insight into the depositional environment of oil shale deposits. For example, the Sr/Ba ratio can be used to distinguish between fresh and saltwater deposition (Chen, 2007). The Sr/Ba ratios (Table 2.4) for all marine deposits were > 5, and were < 1 for lacustrine sediments, with the exception of marine Saskatchewan and lacustrine GR, Mongolian and New Brunswick oil shales. The differences are likely to be due to the conditions present at deposition, with saline conditions at deposition for the lacustrine sediments and the 'muddy' conditions that gave rise to the Boyne formation in Saskatchewan.

Rare Earth Element (REE) concentrations were compared between oil shales. These elements are useful to study as they are detected at high levels of precision by ICP-MS and do not significantly fractionate during sedimentary and diagenetic processes, as they tend to be transported within particulate matter only being mobilised by mechanical processes. They are therefore useful to identify sedimentation mechanisms and the significance of mineralogy on REE patterns (Taylor et al., 1985). Rare earth elements were detected at low concentrations within the oil shales and the concentrations were chondrite normalised (McDonough et al., 1995), before being plotted in order of increasing atomic mass and compared with UCC, NASC and PAAS concentrations.

Table 2.5 – *Rare earth element concentrations in mg/kg, for oil shales measured by ICP-MS. Literature concentrations are included for UCC, NASC, PAAS and chondrites, as specified in the chapter text.*

	Lothian	Estonia	Morocco	Israel	Jordan	Mongolia	Harbin	Fushun	Thailand	Australia
La	40.74	13.57	10.47	13.86	8.58	30.22	33.29	41.04	24.14	14.50
Ce	82.92	19.09	12.59	14.26	10.63	60.12	68.24	78.01	43.88	29.59
Pr	8.70	2.46	1.67	2.32	1.49	6.27	7.03	8.27	4.52	3.42
Nd	37.94	11.66	7.81	11.59	7.21	27.55	29.99	36.28	18.86	16.36
Sm	6.65	2.26	1.44	2.28	1.39	4.92	5.22	6.34	3.46	3.49
Eu	1.42	0.51	0.35	0.54	0.33	0.91	0.95	1.58	0.61	0.82
Gd	6.01	2.51	1.69	2.79	1.63	4.87	5.23	6.26	3.47	3.52
Tb	0.77	0.37	0.25	0.43	0.25	0.67	0.70	0.78	0.48	0.54
Dy	4.16	2.42	1.60	2.89	1.64	3.68	3.87	4.12	2.50	3.18
Ho	0.86	0.56	0.36	0.70	0.39	0.73	0.75	0.76	0.46	0.66
Er	2.52	1.66	1.04	2.06	1.19	2.04	2.11	2.06	1.26	1.87
Tm	0.44	0.29	0.17	0.35	0.20	0.35	0.36	0.33	0.22	0.33
Yb	2.77	1.70	0.97	2.10	1.24	2.18	2.23	1.91	1.25	1.95
Lu	0.45	0.31	0.16	0.36	0.22	0.36	0.35	0.30	0.20	0.31
Gd/Yb	2.17	1.48	1.74	1.33	1.31	2.23	2.35	3.28	2.78	1.81

	Saskatch-ewan	New Brunswick	Wyoming	Colorado	Utah	UCC	NASC	PAAS	Chondrite
La	27.72	17.02	23.55	13.62	13.55	30.00	32.00	38.20	0.24
Ce	47.60	35.19	44.00	25.42	26.79	64	73	80	0.61
Pr	5.59	3.92	4.78	2.74	2.82	7.10	7.90	8.90	0.09
Nd	25.15	18.14	20.46	11.87	11.94	26.00	33.00	33.90	0.46
Sm	4.67	3.59	3.51	2.04	2.11	4.50	5.70	5.60	0.15
Eu	1.06	0.86	0.82	0.53	0.53	0.88	1.24	1.10	0.06
Gd	4.90	3.57	3.54	2.04	2.14	3.80	5.20	4.70	0.20
Tb	0.68	0.53	0.46	0.28	0.29	0.64	0.85	0.77	0.04
Dy	3.87	3.08	2.39	1.62	1.54	3.50	5.80	4.68	0.25
Ho	0.80	0.62	0.45	0.37	0.31	0.80	1.04	1.00	0.05
Er	2.21	1.73	1.20	1.18	0.83	2.30	3.40	2.90	0.16
Tm	0.38	0.30	0.20	0.22	0.14	0.33	0.50	0.40	0.02
Yb	2.23	1.82	1.11	1.45	0.84	2.20	3.06	2.80	0.16
Lu	0.36	0.30	0.19	0.24	0.14	0.32	0.46	0.43	0.02
Gd/Yb	2.20	1.96	3.19	1.41	2.55	1.73	1.70	1.68	1.25

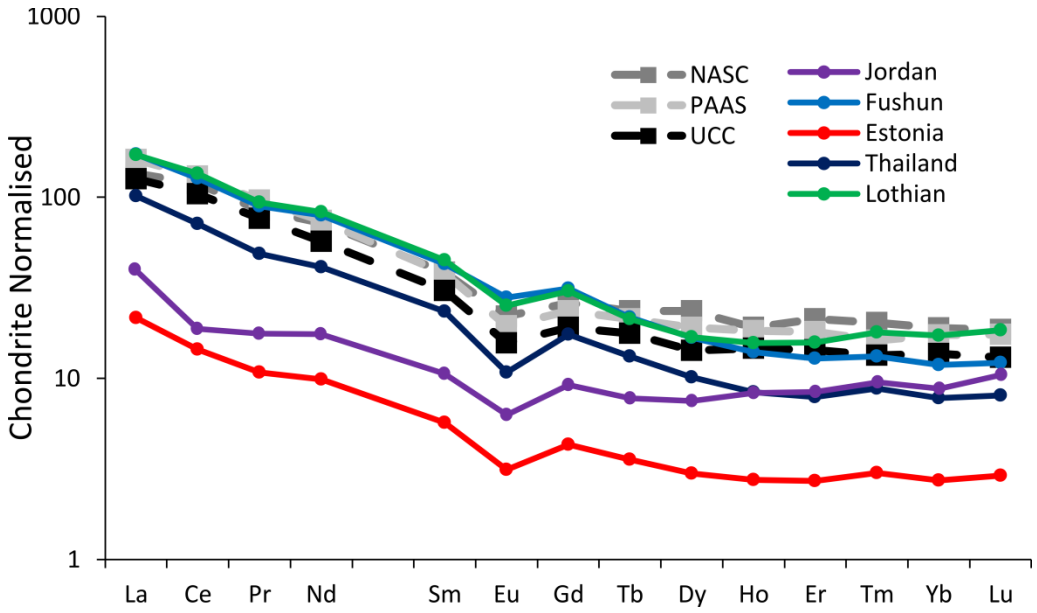

Figure 2.10 – *Chondrite normalised rare earth elemental (REE) concentrations for oil shales from Jordan; Fushun, China; Estonia; Thailand; and Lothian, Scotland.*

A representative selection of oil shales is given in Figure 2.10, which showed the concentration of REEs in comparison to other UCC and sedimentary standards. Depletion is common, due to dilution of REE-containing minerals during sedimentation. The REE patterns were all relatively uniform and parallel to the UCC, NASC and PAAS and showed no significant deviations from this curve. The Eu anomaly is common with oil shales and other rocks due to the integration of Eu within plagioclase minerals during rock forming processes. The Ce anomaly is less prevalent, yet is common in sedimentary marine deposits, and occurred in all the marinites studied (Jordan, Estonia, Israel, Saskatchewan, Morocco) (Lipin et al., 1989).

Clay rich oil shales showed the most enrichment in REEs, such as Lothian and Fushun deposits, and the lowest concentrations were found in clay poor samples, typical of the marinites (Table 2.5). The ratio of Gd/Yb (LREE/HREE) also varied across the sample set. Higher ratios occurred in lacustrine oil shales from Fushun, Thailand, and Wyoming, and lower ratios occurred in oil shales depleted in REE relative to shale standards, typical of marinites such as Jordanian and Moroccan oil shales.

2.5 Discussion

Minerals found within oil shales can be beneficial or detrimental to oil recovery and the environmental stability of waste deposits. Prospective processing improvements include: reducing gaseous/particulate emissions, improving the efficiency of oil shale processing,

producing spent oil shale which can be recycled, as well as preventing the leaching of trace elements which may be at high concentration within this alkaline material. As global oil shale deposits varied considerably and had different chemical compositions, the properties are therefore different and methods for the processing of oil shale and its waste are not the same. This leads to the requirement that each deposit be considered for development individually, taking into account the geology, chemistry, potential oil yield, and how the oil shale may be processed and whether it may pose problems environmentally (Siirde, 2008). This also includes whether any by-products can be extracted, and reducing CO_2 and other gaseous emissions.

The apparent lack of correlation of trace metals with rock forming major elements is due to multiple factors controlling their enrichment, including: the organic content and type of organic matter; the depositional environment and sedimentation rate; and the source of concentrated metals (Leventhal, 1991). It is likely that V, Cr, Cu, Zn, Pb, Ni and U become enriched within organic and clay fractions, accumulating within sediments due to slow deposition rates and reducing conditions prevalent at times of oil shale deposition , but further work would be required to confirm this, and the extraction of organic matter and analysis of clay separates may be an area of interest for future work (Abed et al., 2009; Lewan et al., 1982). In particular V, Ni and Co commonly form organometallic compounds (Dale et al., 1984), and Cr and Zn are also associated with organic matter (Shirav et al., 1988). These elements that are originally bound to organic matter, can be retained in sediments after diagenesis, being incorporated into clay minerals (Breit et al., 1991). Lacustrine oil shales showed depletion in Cr and Zn and greater REE and Cs enrichment, signifying greater association with clay fractions. However, within marine deposits, Cr, Zn, Cu and U are commonly enriched (Figure 2.9), where conditions favour the accumulation of redox sensitive elements (Leventhal, 1991). The precipitation of heavy metals from sea water, with additional input from an exogenic metal source, could lead to the enrichment in these marine environments (Fleurance et al., 2013). Even with heavy metal enrichment in marine environments, most concentrations are not high enough for economical exploitation. The elements V, Cr, and Zn, found at concentrations of ~0.05 wt % may be suitable for extraction as by-products alongside oil, for example, commercial vanadium deposits are often in the range of 0.2–2 wt % V (Navarro et al., 2007; Moskalyk et al., 2003). Although U was found to be enriched compared with UCC concentrations, concentrations were only < 0.003 wt % and for REE to be economical for extraction the concentration of REEs must be at least 0.4 wt %, which was not attained in the depleted oil shale samples (Lipin et al., 1989).

Marinite oil shales and lacustrine oil shales deposited in saline conditions (eg. GR) contained high concentrations of carbonate minerals, in the form of calcite and dolomite (Table 2.3). High concentrations of carbonate minerals can be disadvantageous in terms of retorting as they decompose endothermically, affecting the heat balance in the reaction by requiring more heat overall to complete the pyrolysis of organic matter in oil shales (Sohns et al., 1951). Additionally, carbonate rich deposits will produce large amounts of CO_2 gaseous emissions during thermal processing due to the decomposition of these carbonate minerals at temperatures from 500 °C. To minimise the amount of CO_2 produced, oil shale must be retorted at lower temperatures whilst still generating sufficient oil yields. For example, whilst normally oil shale is retorted between 425 to 525 °C, retorting between 355 to 425 °C can still achieve oil recovery > 86 % (Fei et al., 2012).

It is predicted that high-temperature processing of GR oil shale (rich in calcite and dolomite) could release 1.5 to 5 times more CO_2 than conventional oil production (Sundquist, 1980). Nevertheless, high concentrations of calcite may be beneficial, due to the formation of calcium silicate and calcium sulphate minerals by the reaction of the reactive oxide with SiO_2 and SO_2 respectively. These calcium silicates are able to fix trace elements, released from organic matter, clays and other minerals on heating (Shirav et al., 1988); yet their formation is limited by their reaction and coating of mineral surfaces (Thompson et al., 1983).

$$CaO + MgO + SiO_2 \rightarrow CaMg\text{-}silicate + CO_2 \qquad \text{Eq. 2.1}$$

Clays were found at high concentrations within lacustrine oil shales in China, Thailand, Australia and Canada (Table 2.3). Clay mineral decomposition, like carbonate decomposition, is also endothermic, yet the presence of these silicates may catalyse retorting (Jeong et al., 1983) as clay minerals act as Lewis acids, promoting the formation of hydrocarbons from kerogen, that could allow for retorting at lower temperatures (Hu et al., 2014). Additionally, when clays decompose they produce water, for example:

$$Al_2Si_2O_5(OH)_4 \rightarrow Al_2Si_2O_7 + 2H_2O \qquad \text{Eq. 2.2}$$

This water may go on to react with pyrite, such as was found in high concentrations in the Saskatchewan and Australian deposits, to produce SO_2 in the following reaction:

$$FeS_2 + 2H_2O \rightarrow 3FeS + 2H_2S + SO_2 \qquad \text{Eq. 2.3}$$

Sulphur is also released from the organic matter, and so long as calcite is present, calcium sulphate minerals will form and prevent the formation of dangerous sulphur oxide gaseous emissions (Bhargava et al., 2005).

The interaction and effect of the complex structure of oil shales lead to many different controls on oil production and control of the waste material (Table 2.6), some of which are not discussed here, being related to the organic geochemistry and intricate processing details not necessary for this level of analysis. Instead, simple mechanisms primarily controlled by the chemistry of the rock fraction are discussed.

The oil shales studied range in composition from clay rich shales and mudstones, to carbonate rich marlstones, dependent on the depositional environment (Figure 2.3 and Figure 2.5). To accomplish catalysed oil recovery and limit CO_2 emissions, oil shales rich in clay minerals such as the Scottish or Chinese deposits, could be used. However heat requirements are high for processing, and dangerous heavy metals or trace elements which become enriched within the spent oil shale may be easily leached into the environment, however with certain oil shales such as Harbin oil shale, enrichment was not very high. On the other hand, oil shale which is able to reduce SO_2 emissions and retain trace elements of environmental concern within the residual fraction can be achieved with oil shales rich in carbonates, such as marinites, or saline lacustrine deposits. More CO_2 is produced, and the heat requirements are also high, but elements from Group 2 of the periodic table found within the GR formation, could catalyse pyrolysis reactions.

Table 2.6 – *Summary of beneficial chemical properties required for oil shale processing.*

Benefits	Material	Example
Oil recovery	Clay rich and carbonate poor	Lothian, Fushun, Harbin
Reducing CO_2 emissions	Carbonate poor	Lothian, Fushun, Harbin
Reducing SO_2 emissions	Carbonate rich	Jordan, Estonia, Israel
Heat requirements	Carbonate and clay poor	Mongolia
Retaining trace elements within spent oil shale	Carbonate rich or depleted in heavy metals	GR, Thailand

Whilst the variation between separate deposits is significant, variation also exists within deposits, for example intra-deposit variation has been identified by comparing oil shales from the GR formation. This is a factor that has not been assessed further in this study, and future work is required to identify the heterogeneity within individual deposits to produce more

accurate proposals with regards to the exploitation of enriched elements and the impact of oil shale composition on processing conditions, as the results presented in this chapter may underestimate or overestimate average compositions. The mineralogical composition that has an effect on the processing is less effected by small variations within deposits, but nevertheless care must be taken in the interpretation of results.

2.6 Conclusion

Inter-deposit variation between oil shales from Europe, Australasia, Asia, Africa and North America was determined by the use of XRD, XRF and ICP-MS and the sampled oil shales were divided into four groups according to their chemical composition:

Group 1: Marine deposits consisted of oil shales from Estonia, Jordan, Israel and Morocco. These were all calcite rich, and contained high concentrations of trace elements such as Cr, Zn, Cu, and U, possibly being incorporated into the organic matter that accumulated under reducing conditions (Fleurance et al., 2013).

Group 2: Saskatchewan oil shale was formed in a 'muddy' marine setting, consequently leading to a different composition, with a greater clay contribution, compared with other marine oil shales. The oil shale was enriched in Pb and pyrite minerals, the highest concentration detected amongst all the analysed oil shales.

Group 3: Lacustrine oil shales that were rich in clay minerals and depleted in carbonates included: Lothian, Mongolia, Chinese and Australian oil shales. These oil shales were more enriched in Cs and also showed the greatest REE concentrations out of the oil shales studied, being incorporated into the aluminosilicate minerals.

Group 4: Lacustrine oil shales deposited under saline conditions, in the GR formation, New-Brunswick and Thailand, showed higher proportions of dolomite and analcime minerals. Trace element enrichment in Cu and Sr was common amongst all samples, and deposits also showed more HREE enrichment than others analysed.

Intra-deposit variation means that further assessment of individual basins is required in order to attain a comprehensive picture of the chemical composition, to identify the economic benefits and impacts on processing. Nevertheless, the economic potential for the extraction of trace metals as by-products is likely to be low, with the exception of marine deposits from Groups 1 and 2, where high concentrations of redox sensitive heavy metals such as V, Zn, Cr and U could be viable for further exploitation. Oil shales lacking in carbonates, yet rich in clay

minerals, such as those in Group 3, could hold advantages over other oil shales in terms of oil recovery, heat requirements and CO_2 emissions. Alternatively, oil shales from Group 4 and Group 1 that are rich in carbonate minerals could reduce SO_2 emissions during processing and may produce spent oil shale that is environmentally stable.

The mining and processing of Jordanian oil shale, falling into this latter category, also raises concerns over the production of excessive CO_2 emissions, retorting conditions and heavy metal enrichment with the spent oil shale that may become environmental mobile. These issues will be tackled in subsequent chapters of the thesis, but first the characterisation of oil shale and spent oil shale will be investigated in more detail in Chapter 3.

Chapter 3: The impact of processing on the characteristics of Jordanian oil shale

3.1 Introduction

Significant resources of oil shale are contained within the Al Lajjun deposit in Jordan, with estimates placing oil content between 600 to 800 million barrels (mbbl), yielding 100 litres per tonne (l/t) (Bsieso, 2003; Shawabkeh, 1991; Russell, 1990). These resources are advantageous for exploitation with a high concentration of organic matter, suitability towards surface mining, and location near good roads and away from populated areas (Alali et al., 2006). However, concerns with the retorting of Jordanian oil shale include the production of CO_2 emissions, heat requirements and the enrichment of heavy metals within oil shale, as were identified in Chapter 2.

To prepare a method for minimising the future impact of oil shale processing in Jordan requires an investigation into the mechanisms that take place during the retorting of oil shale, and the characteristics of the spent oil shale that is produced as a result of this high temperature treatment. Further characterisation of the Jordanian oil shale has been completed in this chapter, adding to the knowledge of the mineralogy and trace elemental composition provided in Chapter 2 by investigating the structure and thermal properties of the material, with the use of optical microscopy (OM), scanning electron microscopy (SEM) and thermogravimetric analysis (TGA). In addition, details of the mineralogical and chemical changes during retorting were obtained by comparing the composition of oil shale and spent oil shale. The suitability of spent oil shale to act as an agent for reducing CO_2 emissions, while also remaining an environmentally stable material with respect to trace elements of enrichment were determined as potential areas for further investigation.

3.1.1 Background

The Hashemite Kingdom of Jordan is situated in the Middle-East, bordering Israel (and the West Bank) to the west, Syria to the north, while to the east lie Iraq and Saudi Arabia. It has an area of ~90,000 km^2, less than half the area of the UK (~240,000 km^2). In the west of the country, alongside the Dead Sea, is the Jordan valley, which is ~330 m below sea level with a warm and temperate climate. However, the most populated areas lie in the mountainous region to the east of the Dead Sea, at elevations between 1000-1500 m above sea-level. The remaining two thirds of the country is desert.

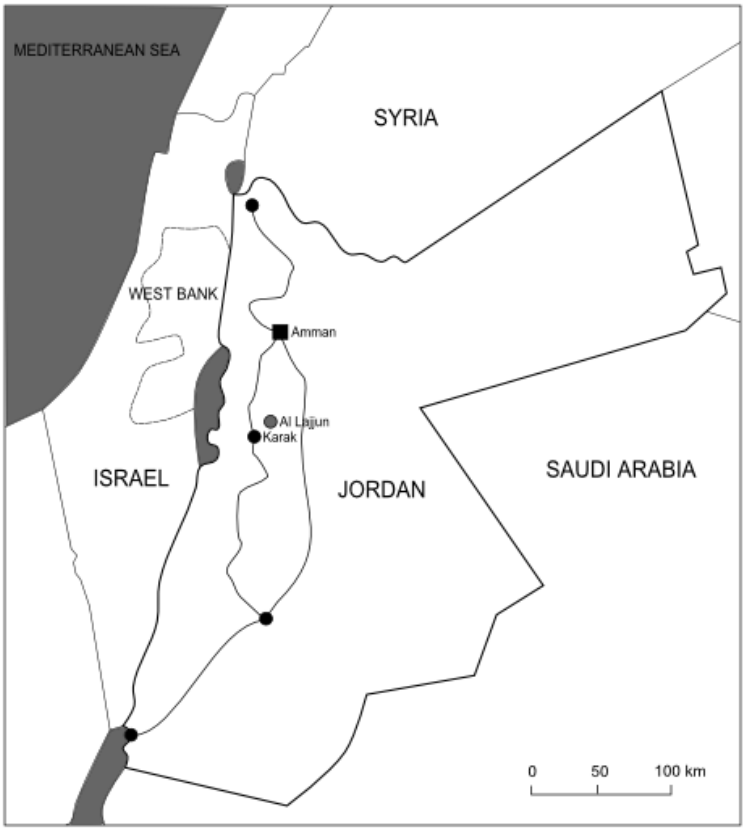

Figure 3.1 – *Map of Jordan showing the location of the Al Lajjun deposit, modified from Dyni (2006).*

Sixty percent of the country contains oil shale deposits, with ~90 % of these deposits available for open-cast mining and total resources placed at 34 billion barrels of oil (bbbl) (WEC, 2013). Jordanian oil shale deposits consist of mostly marine marlstone found primarily in central and north-western areas of Jordan, yet the sequence is also found in Israel and is postulated to extend into Syria (Russell, 1990). Oil shale was formed in the Cretaceous period, in a shallow marine environment, where deposition was initiated by the transgression of the Tethys Ocean in the north and uplift of the Arabian-Nubian shield in the south (Alali et al., 2006). Upwelling currents rich in nutrients facilitated the production of organic matter and phosphorites in the underlying formation (Pufahl et al., 2003). The deposition and accumulation of the organic matter would have occurred in an anoxic environment, allowing for the preservation of high concentrations of organic matter (Fleurance et al., 2013). Significant oil shale deposits in Jordan are situated in Wadi Maghar, Wadi Thamad, Attarat Um Ghudran, Juref Ed-Drawish, Al Lajjun, Sultani, Khan Ez Zaib and Siwaga (Dyni, 2006). Enafit and the Jordan Oil Shale Company (a subsidiary of Royal Dutch Shell) are investigating deeper sources in the north of the country at Yarmouk, near Irbid, with aims to use *in-situ* processing methods (Jaber, 2008). Other companies operating in Jordan include Total, Petrobras, BP and Exxon Mobil.

The oil shale from Al Lajjun has been studied in this thesis, the location of which is shown in Figure 3.1. The Al Lajjun deposit is situated in central Jordan, in the Adir area, ~110 km south of Amman, and 20 km ENE of Al Karak (Russell, 1990). The Al Lajjun deposit was discovered in the 1960s by the German Geological Mission, with more exploration followed up by the Jordanian Natural Resources Authority (NRA). Oil shale is found in the Muwaqqar Chalk-Marl (MCM) formation, an organic rich marlstone that is rich in calcite and quartz, deposited above the Al Hisa Phosphorite (AHP) formation, both of Upper Cretaceous (Maastrichtian) age (Ibrahim et al., 2007; Shawabkeh, 1991).

The Al Lajjun deposit has properties that make it ideal for surface mining and subsequent retorting and an evaluation by the NRA has shown it is suitable for producing 50,000 barrels per day (bpd) for 25 years by this method (Alali et al., 2006). The deposits are extensive containing ~600 mbbl that are thick and near the surface, and the deposit has a low stripping ratio (Table 3.1). The oil shale is of high grade, containing low moisture content with a high concentration of organic matter and subsequently a high oil yield, but oil shale also has a large amount of sulphur that could be detrimental to processing. In addition to the rich organic properties, oil shale deposits are located away from populated areas and near good roads (Figure 3.2).

Table 3.1 - *Properties of the Al Lajjun oil shale deposit (Bsieso, 2003; Shawabkeh, 1991).*

Area	10 km x 2 km
Thickness	25-30 m
Overburden	30 m
Oil Shale	1.3 Gt
Organic matter	22-30 wt %
Av. Oil content	10.5 wt %
Av. Sulphur	3.9 wt %
Av. Moisture	2-3 wt %
Stripping ratio	1.2:1

Figure 3.2 - *Photos showing a mined area of the Al Lajjun deposit and the surrounding sparsely populated area.*

Jordan Energy and Mining Ltd (JEML) will mine and process oil shale from the areas shown in Figure 3.4 (next page), a significant proportion of the Al Lajjun oil shale deposit. JEML will use the Alberta Tacuik Process (ATP) to retort oil shale; a horizontal retort which has lower production and equipment demands compared with other retorting technologies, yet able to produce oil to a very high efficiency of recovery (Bsieso, 2003). Other advantages include the powering of turbines by waste gases and the minimal water that is required compared with other retorting technologies. Four pilot plants have been successful; including the use of the ATP process on the Stuart oil shale deposits in Australia, while in Jordan the ATP process will be scaled up for use at the Al Lajjun deposit.

The ATP retorting schematic is shown in Figure 3.3, highlighting the different stages of the process (Brandt, 2009). Firstly oil shale is crushed into pieces < 2 cm, before being fed into the reactor where it is preheated at temperatures up to 250 °C in order to remove moisture. In the adjacent reaction zone, oil shale is held at temperatures 500-550 °C. Kerogen decomposes producing hydrocarbon vapours, gaseous emissions and coke. The solid material is heated further at 700-750 °C, burning any residual carbon and using the heat from the solids to heat oil shale entering the pre-heat zone. Finally, spent oil shale is cooled and removed for use as mine-backfill, while the hydrocarbon vapours are used to produce shale oil and naphtha by external refinery processes. The majority of the heat in this process is self-contained, meaning that with the exception of start-up fuels, limited external power resources are required.

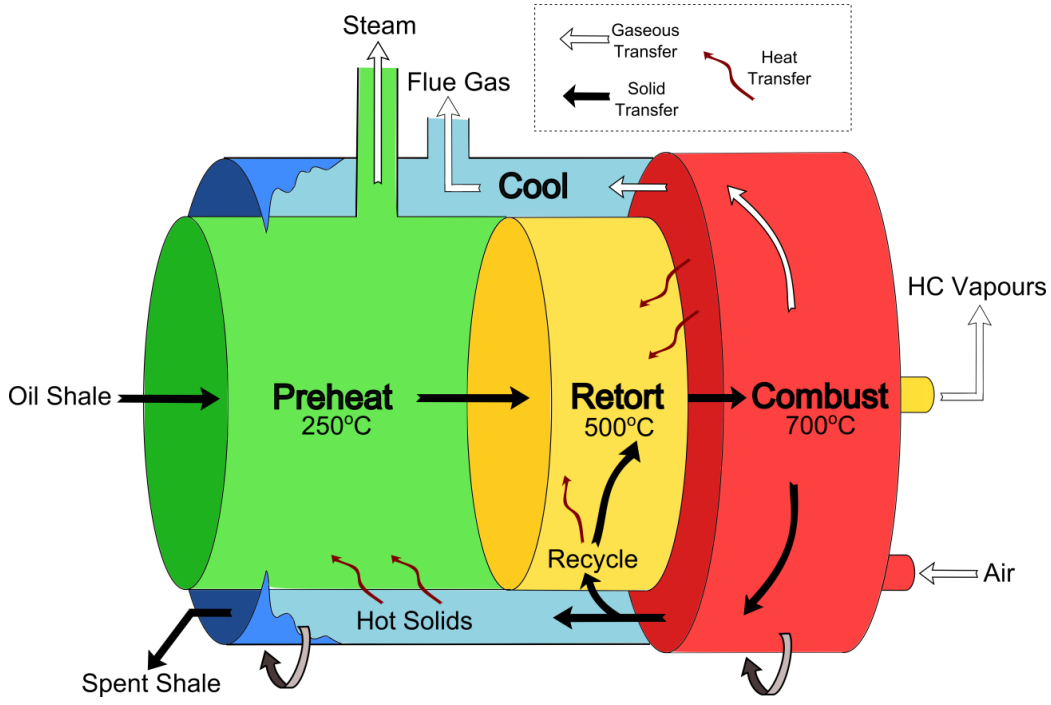

Figure 3.3 – *The ATP design for retorting oil shale, adapted from JEML (2012) and Brandt (2009).*

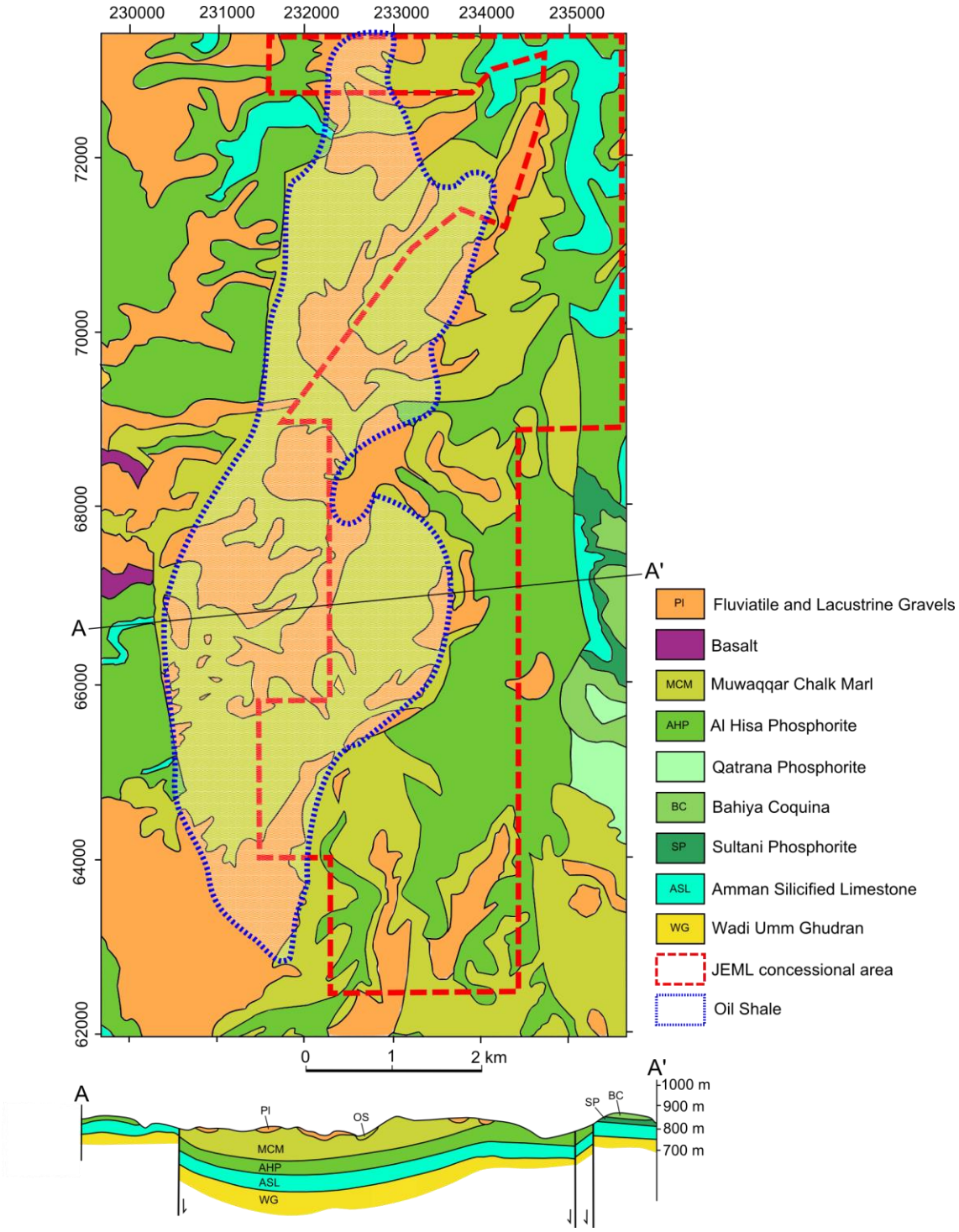

Figure 3.4 – *Geological map of the Adir area, modified from information provided by JEML; Alali et al., (2006); and Shawabkeh (1991). The oil shale deposit is marked out in blue dashes and the JEML concessional area for mining is marked out in red dashes. A cross-section from A to A', showing the stratigraphy, is also shown.*

The lifetime for mining Jordanian oil shale from the Al Lajjun deposit is estimated at 30 years, with a start-up capacity of 4,000 bpd, increasing to 15,000 bpd and finally ramping up to 60,000 bpd by 2024. Water will be used from a brackish aquifer, with a guaranteed supply of 2.5 Mm^3/year, meaning JEML will not be depleting Jordanian freshwater reserves. Projections from feasibility and economic studies performed by JEML, indicate that the construction of the oil shale processing facility is likely to take 3 to 4 years, and when operating will cost $128 million/year, with revenue of $514 million/year producing 5.7 mbbl/year. With prices above $60 to $70 /bbl, the project will be able to make reasonable returns. By-products can also add value to the oil shale, with opportunities available for JEML to exploit the sulphur, estimated at 120,000 t/year; and to export excess power, estimated at 30-40 MW to the Jordanian grid. Additionally, there is potential for spent oil shale to be used as a by-product rather than as mine backfill.

Spent oil shale differs in composition from the oil shale it originates from due to the removal of organic matter and the decomposition and oxidation of existing minerals during the combustion process. These new minerals are often basic phases, produced when acidic gases are removed by combustion (such as SO_2 and CO_2) (Saether, 2004). Because of the basic nature of spent oil shale, it could also be added to cement or used in construction materials and can even be used in the treatment of acidic soils, by acting as a neutralising agent, however the material must be environmentally stable with respect to the leaching of toxic metals (Hanni, 1996). As well as this, spent oil shale has been used to remove pollutants from wastewater, for example, spent oil shale from the Al Lajjun deposit was used to adsorb Pb^{2+} from wastewater, reducing the concentration by up to 94 % (Ibrahim et al., 2007); while the extraction of carbon from retorted oil shale to produce activated carbon has also been identified as a potential use for the material (Trikkel et al., 2008).

3.2 Methodology

3.2.1 Samples

Crushed Jordanian oil shale (J-OS) and spent oil shale (J-SOS) samples (> 1 kg) were provided by Jordan Energy and Mining Ltd, alongside a cored sample of oil shale. Spent oil shale was produced from a test-run of the ATP (Alberta Tacuik Process) batch retort, undertaken by UMATAC industrial processes (Calgary, Canada), and is independent to the J-OS sample received from JEML. Crushed samples were ground into a fine powder using an agate pestle and mortar, for further analytical analysis. A thin section was also prepared from the oil shale

core for microscopic analysis. The analytical methods are described in more detail in Appendix A.

3.2.2 Analysis

The analysis by X-ray fluorescence (XRF), X-ray diffraction (XRD) and inductively coupled plasma mass spectrometry (ICP-MS) was introduced in Chapter 2. Additionally, thermogravimetric analysis and microscopy techniques were used to provide a more detailed characterisation of the Jordanian material used throughout the research thesis.

Thermogravimetric analysis (TGA) provided information on the organic and inorganic matter within J-OS. Samples were heated using a high mass TGA 1200 iSeries analyser and the weight loss was recorded. Weight loss at characteristic temperatures can be attributed to specific minerals or organic material, for example calcite decomposes between 600-900 °C, and portlandite between 300-500 °C, however more than one mineral is likely to decompose within the same temperature window so it cannot be used alone to identify minerals. The types of weight loss that commonly occur are indicated in Table 3.2.

Table 3.2 – *Typical temperature range for mineral decomposition by thermogravimetric analysis (Wang et al., 2009; Todor, 1976).*

Temperature range	Attributed to:
< 250 °C	Moisture, crystallization and interlayer water
200-600 °C	Dehydroxylation of clay minerals
	Decomposition of kerogen
	Oxidation of pyrite
600-950 °C	Decomposition of major carbonate minerals (eg. calcite, dolomite)

Optical microscopy (OM) and scanning electron microscopy (SEM) and micro-analysis techniques were used on J-OS samples to fully characterise the structural and chemical properties for future studies. The detailed methodology for TGA, OM and SEM techniques is described in more detail in Appendix A.

3.3 Results

The chemical and mineralogical composition of oil shale samples was determined by X-ray fluorescence (XRF) and X-ray diffraction (XRD), as discussed in Chapter 2. These techniques were used alongside other analytical methods providing detailed information on the inorganic and organic structure of oil shale.

3.3.1 Oil shale

Oil shale from the Al Lajjun deposit is dark-grey to black in colour indicating the high organic content within the sedimentary rock. The surface however appears bluish grey due to weathering (Figure 3.5).

Figure 3.5 - *Photo showing the cross section of a piece of oil shale from the Al Lajjun deposit, Jordan.*

3.3.2 Microscopy

The oil shale was studied by scanning electron microscopy (SEM) and optical microscopy (OM) to identify structural components of the oil shale and to ascertain information related to the mineralogy, the organic matter and the environment of deposition and formation. By using optical microscopy, the grey microcrystalline material was identified to be calcite, which was distributed relatively homogenously along with other minerals and organic matter across the laminated section (Figure 3.6). The brown/dark brown argillaceous and organic rich material was interstratified amongst the carbonate, along with small quartz grains. Calcite filled fossil foraminifera were also identified in the section, with average particle sizes between 25–100 µm.

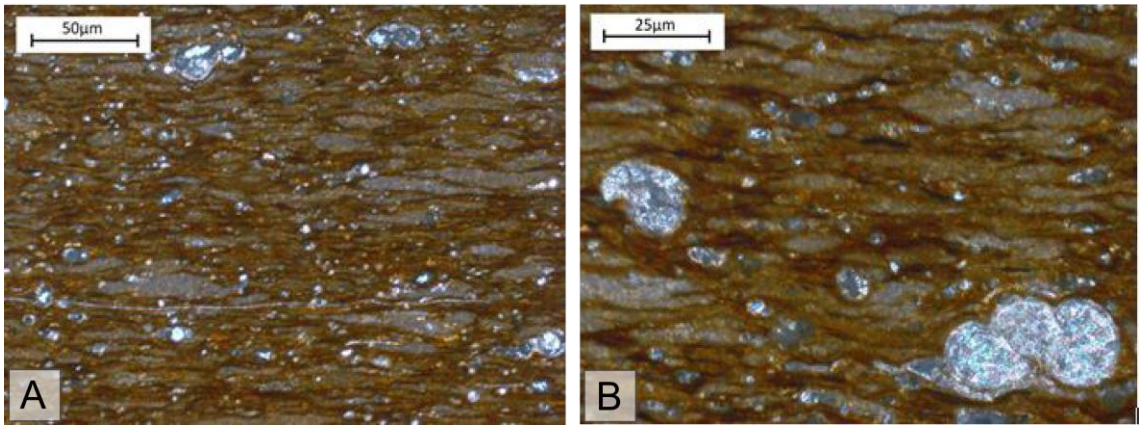

Figure 3.6 – *J-OS under A) 5x magnification and B) 10x magnification.*

Key features identified using SEM include platy clay minerals, as seen in the top of Figure 3.7A as well as abundant microfossils which appeared as particle coatings, or separate structures amongst the fine-grained matrix. Figure 3.7B shows the outline of a larger foraminifera particle, partially replaced by calcite. Energy dispersive spectroscopy indicated a high concentration of Si, Ca and S, confirming the presence of quartz, calcite and organic matter respectively.

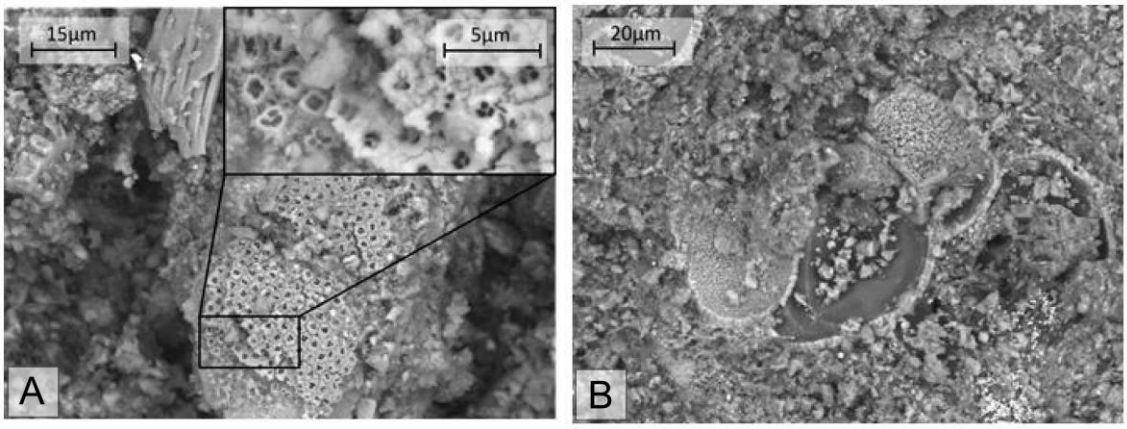

Figure 3.7 – *Scanning electron microscope images of Jordanian oil shale particles.*

3.3.3 Thermogravimetric analysis

Thermogravimetric analysis (TGA) was used to investigate the mineralogy and composition of the oil shale and spent oil shale. The TGA weight loss profiles showed weight loss above 600 °C for both samples, confirming the presence of carbonate in both samples (Figure 3.8). The oil shale contains organic matter, which decomposed at temperatures from 300 °C, peaking at 460 °C and contributing to 17.5 wt % loss from the oil shale, in agreement with literature values provided in Section 3.2.2. The TGA results are tabulated in Table 3.3, showing the weight loss regions of J-OS and J-SOS, as well as showing the proportion of total weight loss.

Table 3.3 – *Weight loss from thermogravimetric analysis, presented at 200 °C intervals, with the fraction of total observed weight loss.*

	0 – 200 °C	–400 °C	-600 °C	-800 °C	-1000 °C	Total
J-OS (wt %)	1.59	2.73	14.75	4.93	15.49	39.48
Fraction	0.04	0.07	0.37	0.12	0.39	1
J-SOS (wt %)	1.28	2.48	2.49	4.39	8.85	19.49
Fraction	0.07	0.13	0.13	0.23	0.45	1

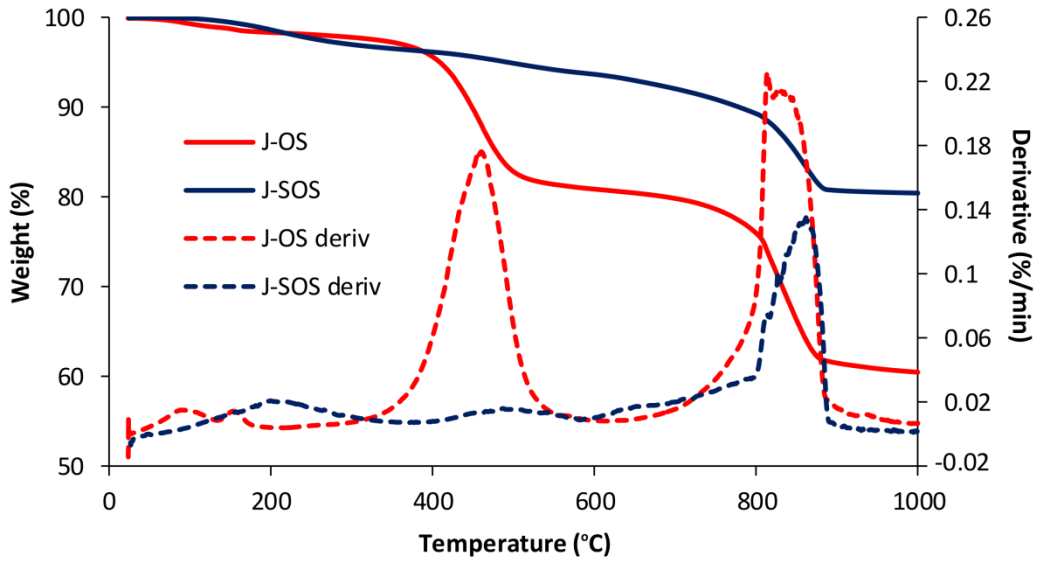

Figure 3.8 – *Thermogravimetric weight loss profile (solid line) and derivative (dashed line) for oil shale (red) and spent oil shale (blue).*

In addition to organic matter decomposition between 400-600 °C, a small proportion of water is lost at temperatures < 200 °C and carbonate minerals decompose in both oil shale and spent oil shale at temperatures > 600 °C. The total carbonate mineral content was determined based on the decomposition of calcite and dolomite at temperatures > 600 °C, as identified from Figure 3.8. After correcting for organic matter, the amount of CO_2 within the remaining carbonate mineral fraction of oil shale was calculated to be 24.7 wt %, compared with only 13.2 wt % within spent oil shale. The loss of CO_2 from the decomposition of carbonate minerals was calculated to be 10.9 wt % CO_2 from oil shale.

3.3.4 X-ray diffraction

The mineralogy of J-OS was established by X-ray diffraction (XRD) analysis, which showed the oil shale to be rich in quartz and calcite, as well as containing smaller amounts of dolomite and

apatite. Minor concentrations of feldspar, clay and cristobalite were also found to be present. After retorting and combustion at temperatures up to 700 °C, the composition of the oil shale was altered (Figure 3.9), based on multiple analysis of large mixed samples (> 1 kg) received from JEML and independently processed. Chapter 5 includes analysis of oil shale combusted at Durham and therefore a direct comparison of the mineralogical changes occurring during heating (Section 5.3). Quartz remained present, however the calcite and dolomite content decreased. Ca-oxides and hydroxides were difficult to detect, and if present were only minor phases, suggesting that the decomposed calcite and dolomite minerals would have gone on to react with silica to form high temperature phases, such as Ca-silicates or amorphous phases. The biggest change observed was the appearance of reflections at 9° 2θ and 14.8° 2θ, identified in this case as ettringite (a hydrated Ca-Al-sulphate-hydroxide mineral) formed during weathering processes. Also identified within the spent oil shale were minor amounts of Fe-oxides, whilst a lack of feldspar and clay minerals indicated the decomposition of these minerals at temperatures up to 700 °C and the formation of high temperature silicates.

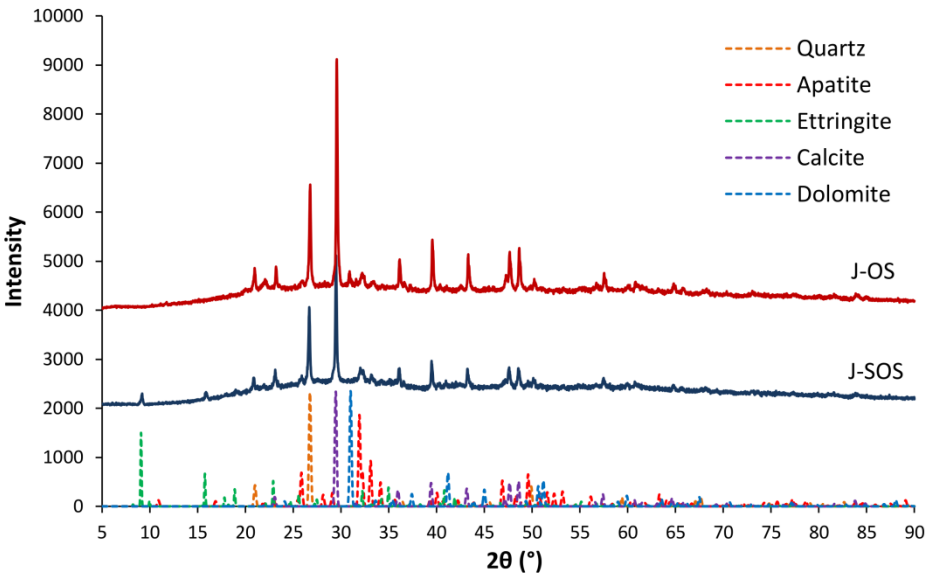

Figure 3.9 – *X-ray diffraction patterns of J-OS and J-SOS with mineral matches from the ICSD database shown by the dashed patterns, with quartz, apatite, ettringite, calcite and dolomite included (ICSD, 2014).*

3.3.5 Elemental composition

Jordanian oil shale was indicated to be mainly depleted in trace elements, with the exception of U, Zn and Cr enrichment in comparison to upper continental crust (UCC) concentrations, as discussed in Chapter 2. Concentrations for these metals were 21 mg/kg, 497 mg/kg and 388 mg/kg, respectively, with standard error determined to be < 2 % for these elements. In

comparison with J-SOS, there was greater enrichment in trace metals compared with the unreacted material (Table 3.4). Trace elements were found to be ~15-20 % more concentrated within this spent material, which was expected due to the loss of organic matter, leading to a concentration effect for the remaining minerals and elements (Figure 3.10) and concentration was also observed for major elements. The exceptions to this were: Mn, not shown in Figure 3.10 due to difficulties in detection using ICP-MS analysis; and Ba which was depleted in spent oil shale.

Table 3.4 – *Major and trace elemental concentrations, recorded as wt % and mg/kg respectively. Errors were < 2 % for major elements and < 5 % for trace elements.*

	J-OS	J-SOS			J-OS	J-SOS	
SiO_2	23.33	32.61	wt %	**Nb**	2.17	2.51	mg/kg
TiO_2	0.12	0.16	wt %	**Cs**	0.59	0.72	mg/kg
Al_2O_3	2.64	3.59	wt %	**Ba**	53.79	50.05	mg/kg
Fe_2O_3	1.23	1.94	wt %	**La**	9.40	10.81	mg/kg
MgO	1.30	1.93	wt %	**Ce**	11.79	13.74	mg/kg
CaO	24.88	31.52	wt %	**Pr**	1.92	2.21	mg/kg
Na_2O	0.20	0.25	wt %	**Nd**	7.67	8.88	mg/kg
K_2O	0.394	0.533	wt %	**Sm**	1.49	1.69	mg/kg
P_2O_5	3.040	3.486	wt %	**Eu**	0.38	0.42	mg/kg
SO_3	4.699	4.365	wt %	**Gd**	1.75	2.01	mg/kg
Sc	3.47	4.29	mg/kg	**Tb**	0.26	0.31	mg/kg
Ti	685.31	824.17	mg/kg	**Dy**	1.66	1.91	mg/kg
V	167.15	199.99	mg/kg	**Ho**	0.41	0.46	mg/kg
Cr	387.48	444.20	mg/kg	**Er**	1.20	1.35	mg/kg
Co	2.18	2.58	mg/kg	**Tm**	0.20	0.22	mg/kg
Ni	168.19	193.99	mg/kg	**Yb**	1.22	1.38	mg/kg
Cu	84.08	95.03	mg/kg	**Lu**	0.23	0.25	mg/kg
Zn	497.30	592.08	mg/kg	**Hf**	0.55	0.63	mg/kg
Ga	3.33	4.18	mg/kg	**Ta**	0.14	0.16	mg/kg
Rb	11.49	14.14	mg/kg	**Pb**	3.94	4.67	mg/kg
Sr	761.70	894.20	mg/kg	**Th**	1.35	1.62	mg/kg
Y	21.71	25.16	mg/kg	**U**	20.77	24.08	mg/kg
Zr	25.72	30.80	mg/kg				

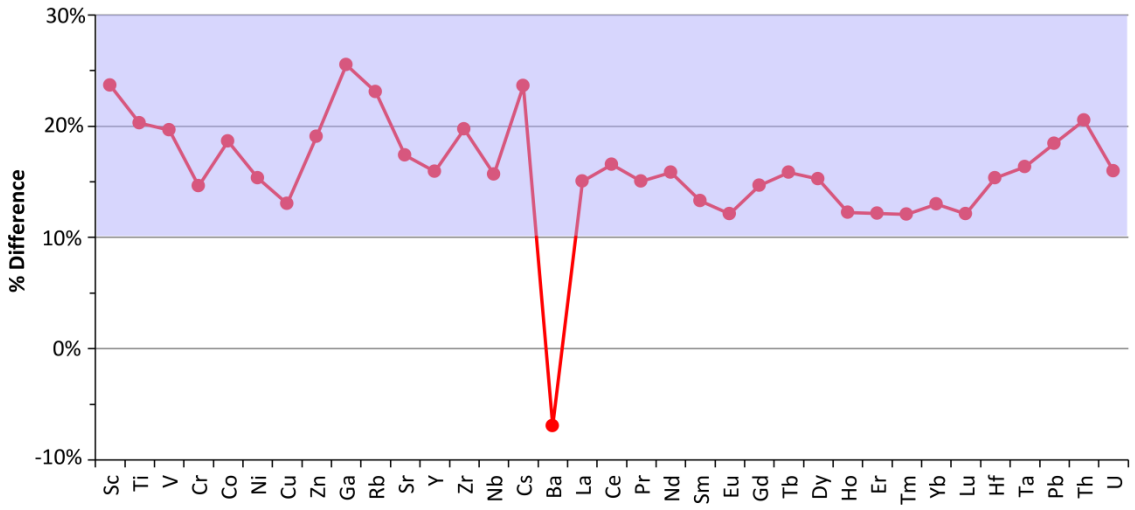

Figure 3.10 – *Percentage difference of trace elements contained within J-SOS compared with J-OS, with the 10–30 % enrichment zone highlighted.*

3.4 Discussion

Results from microscopy techniques indicate the predominance of calcite, quartz, and clay minerals in J-OS (Figure 3.6 and Figure 3.7), along with the presence of microfossils and organic matter, with mineral phases evenly interdispersed throughout the sample. The abundance of microfossils and foraminifera confirms that the oil shale was formed in a marine environment, likely in a shallow basin with limited oxygen or partially reducing conditions that is required for the preservation of organic matter that was found at high concentrations up to 20 wt % from TGA analysis (Figure 3.8). This confirms the suitability of Jordanian oil shale for retorting, with the ability to yield large proportions of oil.

High concentrations of sulphur were detected in Jordanian oil shale. This was not identified in large amounts within the mineral matter by the use of XRD (Figure 3.9), instead being likely to be incorporated within the organic matter. Al-Otoom (2005) identified the sulphur within the organic component by the use of EDS-SEM, which shares similarities with oil shale from the Volga basin in Russia, material that is rich in calcite and clay minerals, with a high concentration of sulphur that is attributed to the organic matter (Kashirskii et al., 2007). The sulphur that is present at concentrations of ~1.9 % in the organic matter of J-OS (calculated from values in Table 3.4), is readily oxidised on combustion and it is likely that this will occur during retorting, producing sulphate anions which are able to react with divalent cations, such as Ca that was detected at high concentrations. The Ca-sulphate reaction product were detected within J-SOS by XRD (Figure 3.9) and identified as the mineral ettringite, a readily

hydrated crystal form of calcium sulphate also found within weathered Estonian spent oil shale (Motlep et al., 2010). The decomposition of clay and carbonate minerals during retorting will result in the formation of other crystalline or non-crystalline phases that are difficult to identify using XRD when present at low concentrations or when amorphous phases are unable to diffract X-rays. However, probable phases present in the J-SOS high temperature product include secondary minerals such as oxyhydroxides and silicate minerals, as well as amorphous phases (Vassilev et al., 1996).

Major and trace element concentrations within J-OS were determined by XRF and ICP-MS (Table 3.4) based on sampling from one area of the Al Lajjun deposit and therefore the results do not indicate the variation and heterogeneity that can exist within deposits. Although the mineralogy detected by XRD is in agreement with other sources (Ibrahim et al., 2007; Al-Otoom et al., 2005; Shawabkeh, 1991), the proportion of these dominant phases can vary, as well as the trace minerals that may be present. Regarding trace elements, the analysis of five shales from Jordan, where similar trace elemental enrichment occurs, Fleurance et al. (2013) determined great variability in heavy metal concentrations. For example, elements in order of increasing concentration were analysed, where Cr = 300-500 mg/kg; Sr = 400-700 mg/kg; V = 300-1000 mg/kg; U = 100-5900 mg/kg; Zn = 400-9000 mg/kg (Fleurance et al., 2013). Whilst, the concentration of U and V detected in J-OS in this study was lower than the range recorded by Fleurance (2013), all of these elements were enriched within the J-OS compared with UCC concentrations. Of particular note, is the finding of unique minerals elsewhere in Jordan: hashemite, a sulphate mineral containing Ba and Cr [$Ba(Cr,S)O_4$] has been characterised (Hauff et al., 1983); as well as Cr-smectite that was identified within phosphatic marls, where Cr^{3+} substitutes for Al^{3+} in the clay crystal structure (Khoury et al., 2014).

In addition to the enrichment of trace elements within J-OS, J-SOS was more concentrated in major elements and trace metals compared with the unreacted material. The concentration of trace elements within spent oil shale indicates that these species are associated with minerals in the spent oil shale and will not be released into the environment by retorting, either in gaseous emissions or by immediate leaching from the spent oil shale. The exception to this was Ba, which was not detected at high concentrations in the spent oil shale in this study (Figure 3.10), where concentrations decreased by < 5 mg/kg. Assuming that the ICP-MS instrument was performing correctly and that the Ba concentration decreased significantly during retorting, Ba must therefore be released at some point during the retorting process. Ba has been documented to be released into the air as particulate emissions, by various industrial processes (Choudhury, 2001), and a study on trace elements released by the processing of oil

shale, showed Ba (along with Mn and Sr) to be depleted within the retorted material (Essington, 1989). Alternatively the heterogeneity of material could explain the difference in composition.

It is likely that the majority of heavy metals are associated with clay minerals and organic matter but when these source minerals are decomposed on retorting it is postulated that high temperature silicates may retain these trace elements, such as Cr and Zn, leading to enhanced concentrations and reduced mobility within spent oil shale (Abed et al., 2009; Shirav et al., 1988). Certain metals, such as Cr, Zn and U, that become more concentrated within the spent oil shale could potentially be recovered, if deemed to be economically viable, which would depend on the cost of extraction and the ease of constructing these technologies to do so. The formation of environmentally stable spent oil shale is a key concern, therefore Chapter 4 will describe further work carried out to determine phases that enrich heavy metals and the effect of retorting and weathering on the release of these dangerous metal species into the environment.

Possibilities for the use of spent oil shale as a by-product include: the cement industry, road construction, and soil conditioning (Alali et al., 2006). The use of spent oil shale in the cement industry is controlled by its composition, with detrimental effects caused by high phosphate levels within J-SOS, detected at 3.5 wt %, thereby reducing how much spent oil shale can be used as an additive (Bsieso, 2003). High concentrations of sulphur can also pose problematic with retorting, raising the cost of refining due to the corrosive nature of sulphur rich organic material and expensive desulphurisation methods have to be implemented to ensure the oil products are sulphur free (Jaber, 2008). Nevertheless, the formation of calcium sulphate minerals within the spent oil shale indicates that a lot of sulphur can be retained within the residual solid material, and will not be released into the atmosphere.

The loss of > 10 wt % CO_2 by the decomposition of carbonate minerals during retorting represents only part of the total CO_2 emissions released from oil shale retorting, the rest coming from the combustion of organic matter. The newly formed secondary minerals, within the alkaline spent oil shale, could be suitable for carbonation reactions, and the use of J-SOS as a source material for CO_2 sequestration will be explored in more detail in Chapter 5, to identify the feasibility and extent of CO_2 sequestration on a laboratory scale.

3.5 Conclusions

The use of OM, SEM, TGA, ICP-MS, XRF and XRD enabled a mineralogical and chemical characterisation study to be completed on Jordanian oil shale (J-OS) and the residual spent oil shale (J-SOS) produced by retorting of oil shale by the ATP process. J-OS has been identified as a material rich in organic matter, being deposited in anoxic conditions which suppressed the degradation of organics. Retorting J-OS will yield large amounts of oil, with the total organic matter calculated to be between 15-20 wt % of the oil shale. Further combustion of oil shale at temperatures reaching 700 °C also results in mineralogical and structural changes within the solid material, where carbonate, clay and feldspar minerals decompose resulting in the formation of high temperature secondary phases, based on multiple analyses of Jordanian oil shale and Jordanian spent oil shale. Carbonate content in particular in particular is reduced by almost 50 %, producing 10.9 wt % CO_2 and lime that goes on to form the weathered ettringite mineral, and other calcium-rich phases. The use of J-SOS in the production of cement is likely to be limited to only 10 % of production, due to high concentrations of P and S, despite its high Ca content. Alternatively, this reactive alkaline material could be used as a way to mitigate CO_2 emissions, by the sequestration of CO_2 within carbonate minerals, due to the large amounts of CO_2 released into the atmosphere from the combustion of organic matter and the decomposition of carbonate minerals, and will be approached from Chapter 5 onwards. In addition, changes to the mineralogy of oil shale as it is directly combusted is investigated in more detail in Chapter 5.

With the majority of J-SOS destined for mine-backfill, the stability of this material with respect to the enriched trace elements is a key concern and will be discussed in Chapter 4. Trace metals were concentrated within J-SOS, by 15-20 % compared with the J-OS, due to the loss of organic matter and concentration effect due to retention within residual phases. The recovery of heavy metals of enrichment compared to UCC may be achieved before they are sequestered within high temperature residual phases on combustion, alongside oil recovery, yet this would require further assessment.

In this chapter, the use of spent oil shale as a by-product alongside oil recovery in Jordan has been identified as a potential pathway to minimise the impact of the retorting process, ultimately leading to the formation of a material that is environmentally stable and that is able to reduce CO_2 emissions produced from retorting.

Chapter 4: The environmental stability of Lothian spent oil shale

4.1 Introduction

Environmental issues are associated with each stage of the production of oil from oil shale, including: mining, which can release organic matter and dust particles, produce noise pollution, and can lead to contamination of groundwater and surrounding sediments; retorting, which produces emissions such as H_2S, NO_x, SO_2, trace metals, and particulate matter; and the waste disposal of process waters and residual solid material, that contain high concentrations of heavy metals (Jaber et al., 1997b). The resultant solid material that is formed after retorting of mined oil shale is referred to as spent oil shale and is commonly dumped in spoil heaps after processing. Existing knowledge about the effects of mining and oil processing allows for controls to be put into place to minimise the environmental impact of oil shale retorting. However, less is known about the characteristics of spent oil shale and how it acts when exposed to the natural environment. In countries such as Estonia, the vast quantities (> 280 million tonnes) of this alkaline waste, has raised concerns over the release of toxic metals into the environment (Motlep et al., 2010; Veski, 2005), however to date it is unknown if the spent oil shale has led to contamination in the surrounding groundwater, soil and sediments.

It is important to monitor the speciation, and mobility of trace metals in the environment, as the leaching of metals from solid materials, such as sediments or waste, into groundwater supplies could have detrimental impacts on plant, animal and human health. Trace elements are associated with various different rock phases; being adsorbed to organic matter or mineral phases by complexation mechanisms, co-precipitation reactions or ion-exchange mechanisms (Filgueiras et al., 2002). For redox sensitive trace elements, including transition metals and heavy metals, their speciation and mobility is dependent on the environmental conditions. Therefore the association of elements with specific rock fractions is a significant factor in determining whether elements may be readily leached into the environment. This is especially true in waste materials that have undergone chemical or thermal processing that can alter the chemical and physical properties of the solid material, and therefore the partitioning of elements within the solid phases. Secondary minerals formed during high temperature processing and weathering reactions include common rock forming minerals: silicates, oxides, sulphates, carbonates, and amorphous phases (Vassilev et al., 1996) and spent oil shale in

particular contain a large abundance of high temperature oxide and silicate phases. Trace elements are often concentrated within stable complexes in alkaline material such as spent oil shale, yet a change in environmental conditions could release these elements (Harber et al., 2001), potentially resulting in contamination of groundwater and danger to the environment. Therefore, in order to ensure that dangerous or toxic metals are not leached into the environment, mobility studies are commonly performed on waste materials (Filgueiras et al., 2002).

At the Al Lajjun deposit in Jordan, the company Jordan Energy and Mining plan to use the majority of spent oil shale as mine backfill, yet a small amount may be suitable for use in the cement industry. The spent oil shale in Jordan will be encased using overburden, and the aquifer below the oil shale formation is protected by the phosphorite formation inbetween. Nevertheless, a large amount of spent oil shale deposited in the environment may have cause for concern, even depite the low precipitation that occurs (Jaber et al., 1997c); especially as the retorting of oil shale is shown to increase the concentration of trace metals within the spent material, by the removal of organic matter and retaining trace elements within mineral fractions (see Chapter 3). In Jordan, oil shale has yet to be commercially processed to produce oil and spent oil shale, and therefore the chemical analysis of spent oil shale has been conducted as part of feasibility studies. In Jordan, leachate studies were completed in 2010 on spent oil shale produced by the retorting of Al Lajjun oil shale by the Alberta Tacuik Process (ATP). The conclusions of this study showed that by using water to leach elements from oil shale and spent oil shale samples, no metals were detected above Jordanian Drinking Water Standards, with the exception of Al from spent oil shale, and Ni from oil shale; however, an elevated pH was found in the leachates (JEML, 2012). Additionally, no heavy metals were detected on column leaching of Al Lajjun oil shale under acidic conditions in a separate study (Ibrahim et al., 2007).

There are limitations to these previous studies, including: a lack of consideration for the weathering processes on spent oil shale, how this may affect waste stability over the course of many years, and whether this may lead to a change in the partitioning of these elements. Jordanian spent oil shale was weathered over the course of several months before being analysed, and large weathered deposits do not currently exist in Jordan. However, in West Lothian, Scotland, multiple waste deposits of different ages, and therefore varying weathering exposure, (known locally as ‘bings’) exist as a result of the extensive oil shale mining industry that ran until the 1960s. The enrichment of trace metals within the Lothian spent oil shale compared with upper continental crust (UCC), coupled with the extensive weathering of bings

that has occurred for over sixty years, make these deposits interesting to study. Jordanian material is rich in calcite; yet Lothian material is instead enriched in clay and silica minerals. Despite the difference in mineralogy and chemical composition, the processing of both Lothian and Jordanian oil shale results in the formation of high temperature silicate minerals that are postulated to adsorb and stabilise trace elements on retorting and combustion (Shirav et al., 1988), leading to spent oil shale that is more environmentally stable with respect to the release of trace metals. The variation between global oil shale deposits is large, but nevertheless, through retorting mechanisms, oil shale undergoes similar thermal processing and structural changes. Although Estonian oil shale is similar in composition to Jordanian oil shale, and large deposits do exist; the post-processing methods vary considerably, with spent oil shale removed and deposited as slurry, which is postulated to have a large control on the composition and stability of spent oil shale (Motlep et al., 2007). By conducting mobility studies on the longstanding spent oil shale deposits in Scotland, information may be gained on the stability of these post-industrial spoil heaps, therefore acting as an analogue for future studies on Jordanian spent oil shale.

4.1.1 Scottish oil shale industry

The Scottish oil shale industry began in the 1850s, when James Young (often referred to as James 'Paraffin' Young), a Glaswegian chemist, developed techniques to extract oil from coal at Bathgate. He then turned his attention to the retorting of oil shale, initially processing 50 kg per day using horizontal retorts, until the development of the vertical Pumpherston retort (named after the oil shale mining village in Scotland) (Carruthers et al., 1912). This process was an improvement on previous retorts, able to produce high yields of oil and ammonia at high levels of efficiency. At peak production in 1913, oil shale was used to produce 27 million barrels of oil as well as: motor spirit, naphtha, light diesoleum, paraffin wax, candles, ammonium sulphate, paraffin coke, industrial oil, motor oil, and lamp oil (Harvie, 2010; Scottish Oils, 1938). Furthermore, spent oil shale was used in the construction of bricks, roads, and other building works (Harvie, 2011). The oil shale industry in Scotland started to decline in the 1920s, and the final mine was closed in 1963 at Westwood due to competition from conventional oil imports (Harvie, 2005).

Oil shale in West Lothian, Scotland, can be found between South Queensferry in the north, to Cobbinshaw in the south, and in total the oil shale encompasses an area of ~200 km^2, from previous extensive mining operations and studies in the late 1800s and early 1900s. (Harvie, 2011). Oil shale was deposited in the Carboniferous period, in the Dinantian oil shale group.

Basin subsidence probably controlled sedimentation in the tropical, lagoonal environment (Parnell, 1988; Scanlon et al., 1980) and oil shales occur in association with coal deposits, formed from the surrounding swamp environment (Harvie, 2010).

Reminders of Scotland's extensive oil shale industry occur in the form of multiple post-industrial spoil heaps, known as bings, that remain in the West Lothian and can reach up to 95 m in height in the otherwise relatively flat topography (Harvie, 2005). The bings have naturally weathered over the past 50 to 100 years and have a characteristic red colour due to the oxidation of iron-containing minerals. Initially there were 27 bings in the Lothian at the closure of all oil shale mines, however only 19 were reported to be remaining in 2005 due to their dismantlement for use in construction. The bings are an important fixture to the Scottish Lothian landscape, considered socially, ecologically and historically important, with protected status associated with 4 of the sites (Harvie, 2005). The unique environment provided by the bings has allowed for animal and a wide diversity of plant species to inhabit many of the sites (Mackenzie, 1996) and reclamation at 8 of the sites has stabilised the steep slopes and promoted plant growth. In total 350 species of plant have been documented in these bing environments. The museum of the Scottish oil shale industry in Millfield, contains an extensive collection of archive material regarding the shale industry, promoting the use of bings for educational and recreational use. Furthermore, the West Lothian county logo even includes a picture of the Five Sisters bing, a landmark which stands out in the surrounding area near Livingston (Figure 4.1).

Figure 4.1 - *West Lothian county logo. The five peaks correspond to the five spoil heaps at the 'five sisters' bing (Westlothian council, 2014).*

4.1.2 Environmental mobility studies

Sequential extraction studies are commonly used to identify the speciation of heavy metals within sediments, and therefore identify methods to limit the release of dangerous elements

into the environment (Belazi et al., 1995). A sequential extraction procedure is used to breakdown materials, such as rocks, in 'sequential' phases. Each fraction, in order of increasing stability, is dissolved separately and the concentration of elements within each of these separate solid fractions can be determined. This can be used to track the mobility of trace metals under natural environmental conditions, as the mobility of elements within solid material, such as rocks, will decrease as the stability of fractions increases. For example, trace metals that are loosely bound to solid material and easily exchanged by rainwater, are considered mobile in normal weathering conditions, and trace metals will be readily released into the environment. Any metals bound to the crystal structure of residual minerals are of little threat to the environment, as they are not expected to be released under normal conditions, or over a significant time span. They are considered immobile and safe to the environment.

Spent oil shale deposits in Lothian, Scotland may act as an analogue for Jordanian spent oil shale by determining if the conditions at the spoil heaps may increase the mobility of heavy metals. Although the composition of the two oil shales prior to retorting and combustion are quite different, both deposits of spent oil shale contain high concentrations of high temperature silicate minerals. Weather conditions in Jordan are typically warmer and dryer than in Lothian, with average precipitation < 300 mm compared with < 800 mm in Lothian. Average temperatures range from 3-15 °C in Lothian, compared with 8-27 °C in Karak, Jordan; however freezing temperatures and snowfall are not uncommon in the winter months (Climatemps, 2014). The difference in weathering conditions could result in greater hydration and chemical weathering in Lothian, compared to greater freeze-thaw physical weathering in Jordan, and the effects of these are explored in more detail in Section 4.4.3.1. Despite climate and compositional differences, the bings in the Lothian have been left to weather for > 50 years, and could provide indication to whether spent oil shale is a stable material.

The various spent oil shale deposits from West Lothian represent deposits of varying age and composition. They do not occur alone, and are often associated with overburden, soil and vegetation. Overburden is rock that is associated with oil shale deposits, being removed at the same time as the mining of oil shale. Overburden is subsequently replaced into the mine alongside the spent oil shale waste and is commonly darker in colour than spent oil shale, as minerals have not been retorted and decomposed. Trace elements that are mobile in spent oil shale or overburden may be transferred to the soil; either through mechanical weathering in soil formation processes, or by the release of elements into pore-waters. Then, dissolved elements within the soil may flow through surface or pore-waters, or be transferred into

vegetative species (Ure et al., 2002). By extending the sequential extraction procedure for samples of spent oil shale, overburden, soil and vegetation; the concentration, speciation and relationship of elements within each of these sample types can be determined, and therefore the mobility of elements in these 'bing' environments can be established.

Analysis of the elemental composition of spent oil shale, overburden, soil and vegetation by inductively coupled plasma mass spectrometry (ICP-MS) was conducted, in addition to analysis of sequential extracts where samples were separated into: exchangeable, acid soluble, reducible, oxidisable, and residual fractions (Tessier et al., 1979). A sequential extraction study, used alongside whole rock analysis and mineralogical studies can act to gain insight into the changes in mobility of trace elements, and how this may be related to weathering or processing conditions.

4.2 Methodology

Oil shale was obtained from an exposed oil shale seam in South Queensferry, beneath the Forth Bridge. Locations and access points of spoil heaps to be sampled in the West Lothian were found by using detailed ordnance survey maps of the area. Samples of spent oil shale, soil and vegetation were obtained from five chosen spoil heaps and a soil sample was also collected from a non-bing setting (Figure 4.2). The full list of samples collected is given in Table 4.1 and the sites are described in Section 4.2.1. Rock, soil and vegetation samples were dried in an oven at 105 °C, for 24 hours to remove any moisture, then samples were ground into a fine powder using an agate pestle and mortar, before being stored in a drying cabinet ready for sequential extraction and analysis (Section 4.2.2). More details regarding the sample preparation and analysis are provided in Appendix A.

Vegetation, soil samples, and where possible additional overburden, were taken from the surface of the spoil heaps, whereas spent oil shale was taken from 5-10 cm below the surface. Samples were collected from different locations and positions (top plateau or slope) of each site (Figure 4.3), so as to take into consideration the different transport pathways into the mobility study. Samples were not taken further from the site, due to a restriction on the number of samples that could be processed.

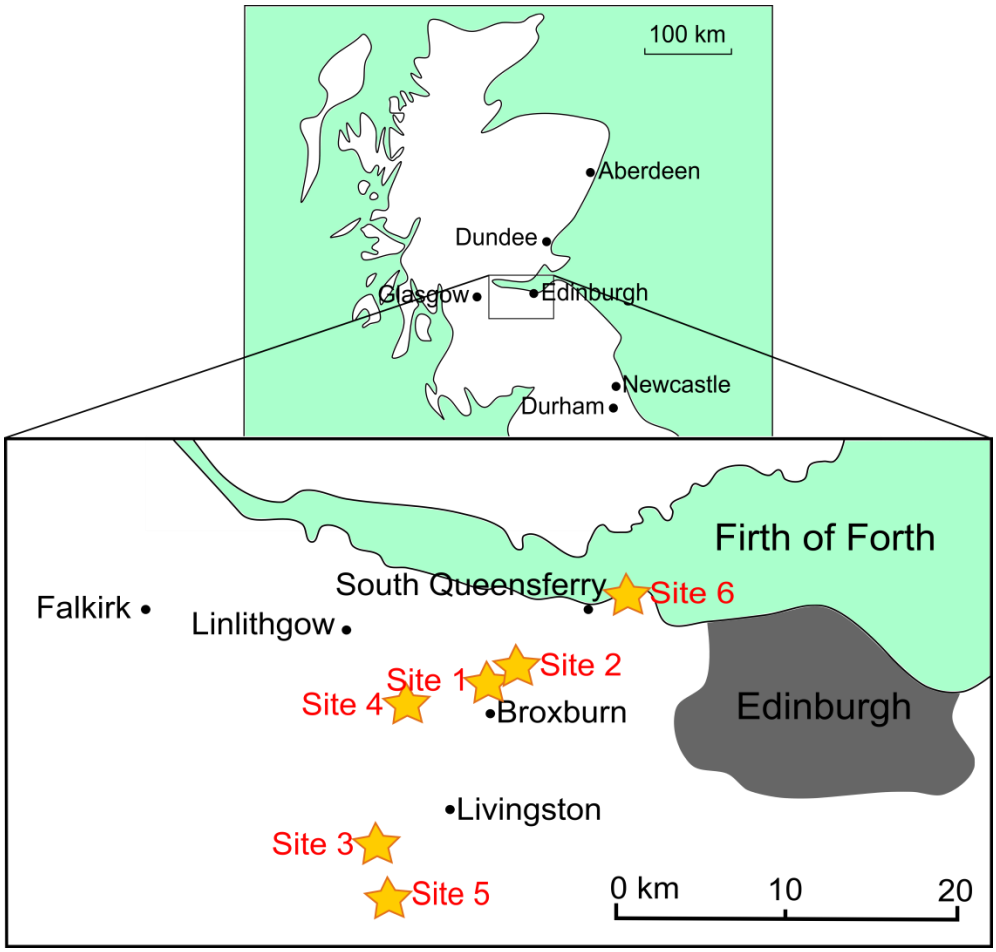

Figure 4.2 – *Oil shale and spent oil shale site locations in West Lothian, Scotland.*

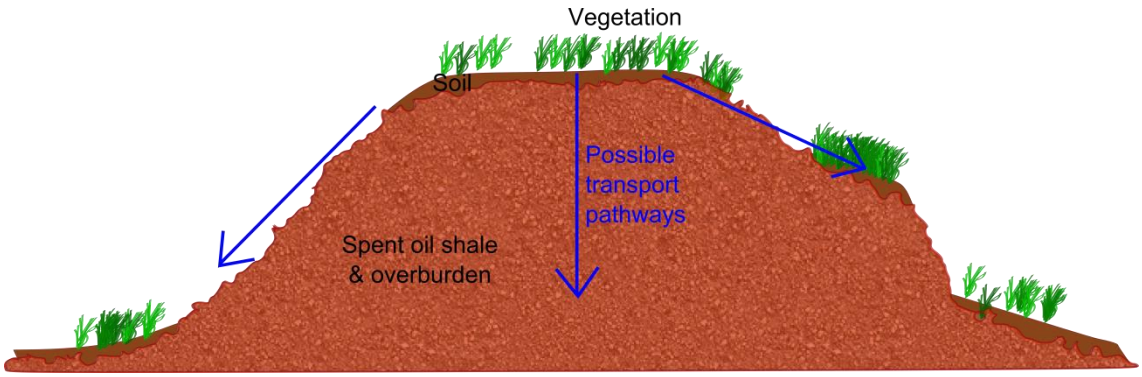

Figure 4.3 – *Schematic showing the possible transport pathways of mobile elements through the spent oil shale deposits, with samples taken from the top plateau, and from the slope.*

4.2.1 Description of sites

Site 1 - Greendykes:

The Greendykes bing at Broxburn was the largest spoil heap sampled (Figure 4.4C). Samples were obtained from the plateau to the northwest of the deposit, and included: red coloured spent oil shale pieces, no larger than 10 cm (Figure 4.4A); welded shale which was a large clump of red and black rock (Figure 4.4B); overburden which was typically grey in colour compared with the red spent oil shale; top soil; bottom soil; and vegetation, in the form of grass. The southeast slope of the Broxburn bing was also sampled, removing spent oil shale, overburden, soil and vegetation.

Site 2 - Niddry:

The Niddry site is located close to the Greendykes bing at Broxburn, yet is currently being excavated for use in road building and construction (Figure 4.4E). The western slope was sampled: spent oil shale and vegetation were taken (Figure 4.4D), and the plateau on the eastern side was sampled, removing spent oil shale, soil and vegetation.

Site 3 – Five sisters:

The Five sisters bing is another massive spent oil shale site, with five ascending peaks radiating out from each other. Samples of spent oil shale and vegetation were collected from the plateau at the summit of the middle peak; and spent oil shale, soil and vegetation was collected 10 m from the bottom of the steepest slope (Figure 4.4F).

Site 4 – Seafield:

Another reclaimed site is located at Seafield, where spent oil shale, overburden, soil and vegetation were sampled from the slope at this spoil heap now converted for recreational use. The red spent oil shale and grey overburden were interdispersed and the area was covered in more grass and vegetation compared with the other deposits (Figure 4.4G).

Site 5 – Hermand:

The final spent oil shale site was the oldest and smallest of all deposits sampled. A cross section of the deposit can be seen in Figure 4.4H, showing the heterogeneity of deposits. Samples of the red spent oil shale and the lighter coloured grey material were taken, along with black overburden, soil and vegetation.

Site 6 – South Queensferry:

Oil shale was sampled from an exposed oil shale seam, found below the Forth Bridge in South Queensferry. Other samples of oil shale directly related to the spent oil shale within the bings was not able to be obtained.

Site 7 – Soil control:

Top soil was collected from a grass field located nearby the Greendykes bing at Broxburn, ~200 m from the slope of the Western side of the bing.

Table 4.1 - *Site location, according to locality and grid reference; age of deposits; and number of samples collected. SOS = spent oil shale, OB = overburden.*

Site	Site Name	Location	Age (yrs)	Grid Ref	Rock		Soil		Veg
					SOS	OB	Top	Bottom	
1A	Greendykes	Broxburn	89	08473 73907	2	1	1	1	1
1B				08655 73428	1	1	1	1	1
2A	Niddry	Winch-burgh	53	09576 74537	1	-	-	-	1
2B				09984 74731	1	-	1	-	1
3A	Five Sisters	West Calder (North)	52	00922 63846	1	-	-	-	1
3B				00668 64133	1	-	1	-	1
4	Seafield	Seafield	92	00475 66640	1	1	1	-	1
5	Hermand	West Calder (South)	119	02886 62476	2	1	1	-	1
6	-	South Q'ferry	Oil shale	13793 78393	-	-	-	-	-
7	-	Broxburn	Control	08249 73827	-	-	1	-	-

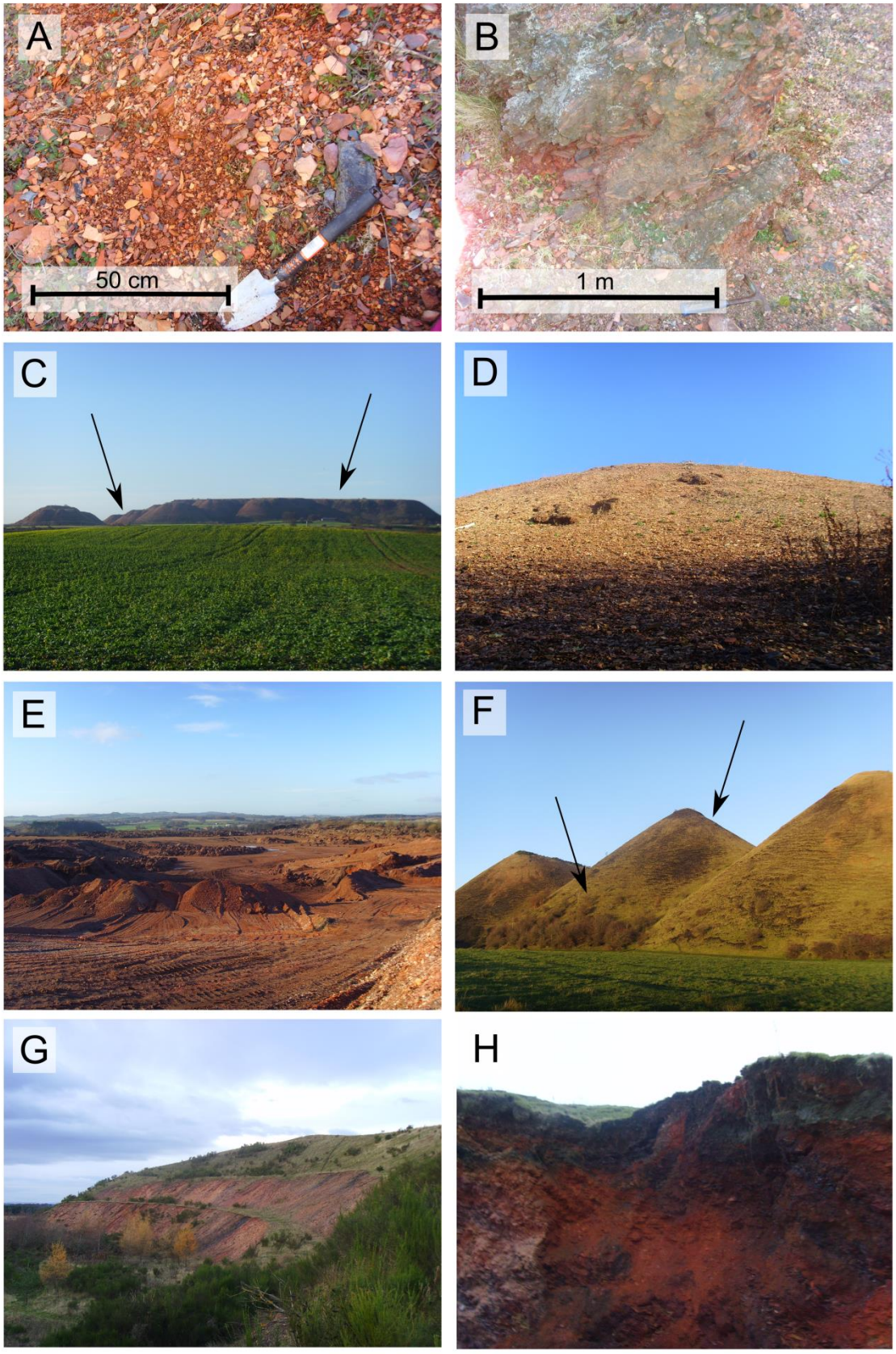

Figure 4.4 - *A) Spent oil shale and B) welded shale from Greendykes bing. C) Locations sampled at Greendykes bing, D) western slope sampled at Niddry, and E) excavation from the plateau at Niddry. F) Locations sampled at the Five sisters bing, G) vegetation covered Seafield bing, and H) variation at the Hermand spoil heap.*

4.2.2 Sequential extraction

The sequential extraction method adopted in this thesis is based upon a sequential extraction procedure by Tessier et al. (1979), that divides the rock or soil sample into five separate fractions, with modifications based upon the BCR procedure (Rauret et al., 1999). Additional alterations and improvements were made during experimental work and the method was extended for use on the analysis of rock, soil and vegetation samples (Tessier et al., 1979). Rock fractions were separated according to how they may be broken down by a change in environmental conditions and were named after the principle material or adsorption process that governs the fraction. They include: exchangeable phases, carbonates, Fe-Mn oxides, organic matter and residual material. Each phase may be fractionated using different reagents, summarised in Table 4.2 and reagents progressively increased in strength, beginning with salt solutions; progressing to acids, reducing agents, and oxidising agents; and finally using strong acids (Filgueiras et al., 2002).

Table 4.2 – *Rock fractions in order of increasing stability.*

Step	Rock Fraction	Reagent	Details
1	Exchangeable	**NaOAc (pH 7)**	Metals bound by weak adsorption interactions are released by a simple salt solution.
2	Carbonates	**NaOAC/HOAc (pH 5)**	Metals bound to carbonates are released by a change in pH.
3	Fe-Mn oxides	**$Na_2S_2O_4$/Na-cit/H-cit**	Metals are released in anoxic conditions.
4	Organic matter	**H_2O_2/HNO_3 (pH ~2) + NH_4OAc**	Metals are released by oxidising agents.
5	Residual	**HF/HNO_3**	Metal ions are bound within crystal structure of remaining minerals. Metals here are of little threat to the environment.

The collected samples of rock, soil (both 2.5 g) and vegetation (0.5 g) were transferred into vessels suitable for centrifugation, alongside blanks and duplicates. Three different types of blank solution were used in the sequential extraction procedure. Reagent blanks were used to determine the contribution of trace elements from the reagents used, vessel blanks showed the contamination from the sample vials, and procedural blanks indicated the accumulated contamination and errors involved in the sequential extraction procedure (Rauret et al., 1999). Each sample was subjected to 5 sequential extractions. The first 4 sequential extraction steps followed the general method depicted in Figure 4.5 for steps A to E:

A: The 20 ml of reagent solution was added to pre-weighed solid samples.

B: Samples were reacted for a pre-specified duration, and where necessary this included agitation and heating to aid with extraction.

C: Vials were centrifuged at 4000 rpm, and then 15 ml of reagent solution was decanted and retained for analysis.

D: Samples were then washed and centrifuged twice by the addition of 15 ml H_2O and then repeating steps B and C.

E: Solid samples were dried in an oven at 105 °C and weighed, before repeating steps A - E using a different reagent solution.

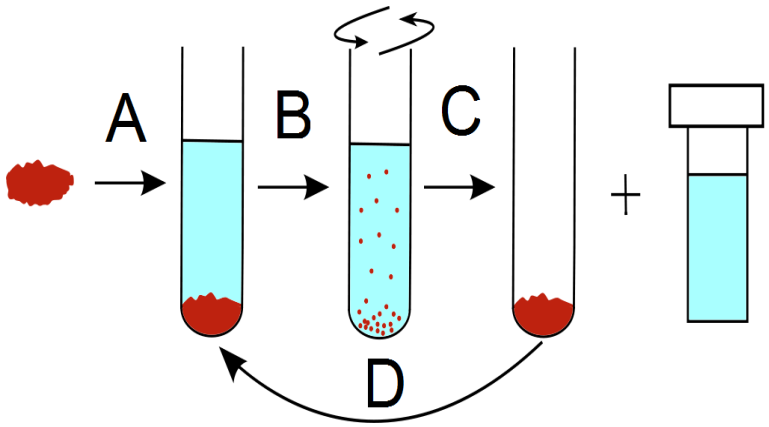

Figure 4.5 – *General reaction procedure for steps A-D of the sequential extraction. See text for explanation of steps A-E.*

The reaction mechanisms of reagents used to chemically react with each specific fraction is complex, and is not only dependent on the strength of the reagents, but also upon the duration, heating steps and whether any re-adsorption may occur directly after dissolution (Zakir et al., 2006). The detailed extraction procedure for each fraction is outlined below, along with the choice and action of reagents in each step of the sequential extraction process:

Fraction 1 - Exchangeable: The reagent sodium acetate was used to remove readily exchangeable metals bound by weak electrostatic reactions (Filgueiras et al., 2002). The reagent does not have an effect on silicates, sulphides, organic matter, or Fe-Mn oxides, yet may cause slight dissolution of calcite. Any elements partitioned in the exchangeable phase are easily desorbed, and move from the solid to the liquid phase, whereas elements bound in other more stable phases are retained in the solid.

A 1 M solution of NaOAc, pH 8.2, was prepared, added to the pre-weighed samples and the solution was agitated for one hour before: centrifugation, decanting, washing and drying steps.

Fraction 2 - Carbonates: The use of acidified sodium acetate enabled the complete dissolution of carbonate minerals, causing the release of any metals bound to them. Tessier et al. (1979) found there to be no effect on the solubility of Fe-Mn oxides when used for up to 5 hours, however there is likely to be dissolution of specifically adsorbed exchangeable ions that are not released in fraction 1 (Ure et al., 2002). The use of acetic acid also prevents dissolution of apatite, compared with other reagents (Muhammad et al., 2011).

The dissolution of carbonates used 1 M NaOAc, at pH 5 (attained by addition of HOAc) and samples were agitated for 5 hours, followed by centrifugation, decanting, washing and drying.

Fraction 3 - Fe-Mn oxides: Iron and manganese oxides are unstable in anoxic conditions at low pH, so the introduction of a reducing agent, such as sodium dithionite with a sodium citrate buffer, acts to decompose the oxides and prevent the re-precipitation of other mineral phases, releasing any trace metals bound to them; by adsorption, complexes or as co-precipitates (Filgueiras et al., 2002). Tessier et al. (1979) chose to use hydroxylamine hydrochloride and acetic acid in this step as dithionite can precipitate trace metals in the form of sulphides, yet hydroxylamine hydrochloride may also react with organic matter present (Ure et al., 2002).

Metals bound to Fe-Mn oxides were extracted using a mixture of a 1 L solution of 0.3 M, 0.175 M and 0.025 M, $Na_2S_2O_4$, Na-cit, and H-cit respectively, which was added to samples for 12 hour reaction, with occasional agitation (5 minutes using shaker plate every 3-4 hours). Samples were then centrifuged, decanted, washed and dried.

Fraction 4 - Organic matter: Trace elements may have bioaccumulated within organic matter, or be bound to organic material by complexation mechanisms. The use of an oxidising agent like hydrogen peroxide with nitric acid degrades the organic matter releasing these metals with very little degradation of silicates (Filgueiras et al., 2002). Additionally, sulphide minerals are also extracted. Ammonium acetate must be used in conjunction with hydrogen peroxide in order to extract the metals into solution to prevent readsorption. This step must occur after the dissolution of Fe-Mn oxides, otherwise oxalate ions can react with this mineral phase (Ure et al., 2002).

The organic matter was treated using 3.75 ml of 0.02 M HNO_3, followed by 6.25 ml of H_2O_2 (pH 2) and the solution was agitated for one hour. A further 3.75 ml of H_2O_2 was added and heated at 85 °C for 3 hours, with occasional agitation. The solutions were cooled and 6.25 ml of

NH_4OAc was immediately added and agitated for 1 hour. Solutions were then centrifuged, decanted, washed and dried.

Fraction 5 - Residual: Any trace elements remaining, which have not been released in previous fractions, were finally removed in the final dissolution step. The residual matter is dissolved in the final step, using strong acids to break down crystal structures of stable minerals, such as silicates, refractory organics and remaining sulphides.

The method used for the final step differs from the general reaction scheme and does not use a mixture of hydrofluoric acid and perchloric acid, as used by Tessier et al. (1979). Instead, a small sample of each residual solid that was dried after previous extraction methods, were added to Teflon vials along with international reference materials, and new blanks and duplicates were used. These samples were then dissolved using the standard method described in Chapter 2 and Appendix A, resulting in a solution diluted to 50 ml (Ottley et al., 2003).

Whole rock: In addition to the analysis of elemental concentrations within five separate fractions after sequential extraction, the 'whole rock' elemental concentration within samples and international reference materials was also determined, using the same method as for fraction 5.

In total, 34 solid samples of rock, soil and vegetation, were subjected to 5 extractions, as trace elements were extracted from the exchangeable to the residual fraction of the rock. Additionally, a total dissolution step was also completed to provide 'whole rock' elemental concentrations. This resulted in the formation of 204 primary solutions containing extracts for further analysis, and 100 µl of HNO_3 (68 %) was added to each decanted supernatant solution in order to maintain the ion concentration in solution prior to analysis, and prevent microbial activity (Horowitz et al., 1994).

4.2.3 Analysis of sequential extracts

Elements were chosen for analysis to represent a range of major and trace elements, and included rare earth elements, redox sensitive elements, and heavy metals. Studies included elements considered in previous leachate analysis: Sc, T, V, Cr, Mn, Fe, Co, Ni, Cu, Zn, Rb, Sr, Ba, Pb and U, of which regulations are in place within Jordanian drinking water. Out of these elements, Cr, Cu, Ni, Pb, and Zn are commonly associated with dangers to health and the environment (Zakir et al., 2006). The full suite of elements analysed was: Mg, Al, K, Ca, Sc, Ti, V, Cr, Mn, Fe, Co, Ni, Cu, Zn, Ga, Rb, Sr, Y, Zr, Nb, Cs, Ba, La, Ce, Pr, Nd, Sm, Eu, Gd, Tb, Dy, Ho, Er,

Tm, Yb, Lu, Hf, Ta, Pb, Th, U. Data were collected using a Perkin Elmer Sciex 6000 inductively coupled plasma mass spectrometer (ICP-MS). The use of: external standards, internal standards, sample duplicates, replicates, and blanks, were used as checks during the quantitative analysis (Gill, 1997). Details of sample and standard preparation for both residual, whole rock, and other extracts is detailed in Appendix A. For the extracts from fractions 1 to 4 (exchangeable, carbonate, Fe-Mn oxides, and organic), concentrations of elements within solution was lower, and therefore international reference materials could not be used as standards. Instead, external standards were prepared by diluting stock solutions containing elements of interest. Due to low concentrations in solutions used for analysis, the detection limit for each element in each sample was determined by calculating the standard error for samples and blanks (Eq. 4.1), where σ = standard deviation, in mg/l; and sample = sample concentration, in mg/l.

$$Detection\ limit = Sample - Sample\ 3\ \sigma - Blank\ 3\ \sigma \quad \text{Eq. 4.1}$$

To ensure that the concentrations of standard and sample solutions were suitable for analysis, samples and standards were diluted to reduce matrix effects, caused by high concentrations of total dissolved solids (TDS) in reagent solutions. Matrix effects can result in signal drift throughout analysis as well as the suppression of elemental counts. In particular, reagents that contain sodium ions must be diluted to at least 500 µg/ml prior to analysis. Total dilution was 1/4027 for fractions 1, 2 and 4, and 1/8053 for fraction 3, for the complete sequential extraction and analysis steps. Results of solution elemental concentrations were then converted into concentrations (mg/kg) within the rock and are tabulated in Appendix E.

4.2.4 X-ray analysis

X-Ray diffraction (XRD) and X-Ray Fluorescence (XRF) data were collected as detailed in Chapter 2 and Appendix A.

4.3 Results

4.3.1 Mineralogical analysis

The mineralogical composition was determined by use of X-ray diffraction (XRD) to identify why differences were observed in enrichment and trace elemental partitioning between the spent oil shale, soils and overburden. X-ray diffraction was used to identify differences in mineralogy that may be caused by thermal processing and chemical reactions due to

weathering processes, and 4 samples representing different sites (sites 1, 3 and 5), and sample types (spent oil shale and overburden) were analysed.

Spent oil shale from site 1 showed the presence of quartz and mullite, as well as amorphous phases and hematite, however, spent oil shale sampled from the plateau at site 3 contained a high concentration of magnetite, with quartz, carbonate and clay peaks also detected (Figure 4.6). A high concentration of magnetite within this waste material may be the reason for the strong background interference, caused by the interaction with Fe and CuKα radiation (Sumner, 2000). Analysis of overburden from stie 1 and grey spent oil shale at site 5 indicated structural similarities between the two samples. Clay minerals and quartz were detected in both. Additionally, feldspar minerals were detected in overburden and hematite within SOS.

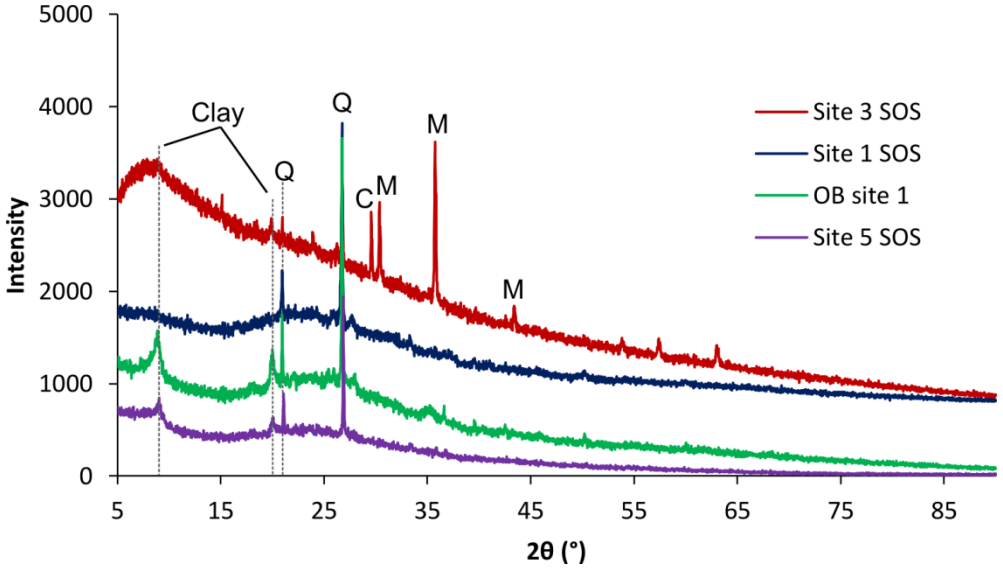

Figure 4.6 - *XRD patterns for spent oil shale and overburden from site 1, spent oil shale from the plateau at site 3 and grey shale from site 5. Minerals labelled include Q = quartz, C = calcite and M = magnetite.*

4.3.2 Whole rock analysis

X-ray fluorescence (XRF) and inductively coupled plasma mass spectrometry (ICP-MS) were used to determine concentrations of major and trace elements within soil, vegetation and solid waste associated with spent oil shale deposits in West Lothian, Scotland. Additionally, the elemental concentration within separate phases was assessed by separating each sample into five sequential extracts which were also analysed by ICP-MS techniques. Calibration curves were tested and verified for use, based on blanks and standard solutions, confirming the suitability of results for further analysis. Elemental concentrations for each of the samples and fractions are tabulated in Appendix E.

The major elemental composition of spent oil shale samples from site 5 were very similar, as were the overburden and spent oil shale from site 1 (Figure 4.7). Samples from site 3 showed different compositions, with spent oil shale sampled from the plateau very different in composition to the other spent oil shales analysed. Instead the composition of spent oil shale from site 3 contained a very high percentage of Fe, and less Al and Si. This indicates that instead of the formation of Al-rich clay minerals, Fe-containing phases were dominant in the form of magnetite from XRD analysis (Figure 4.6), that may be from an external source rather than a common constituent of spent oil shale.

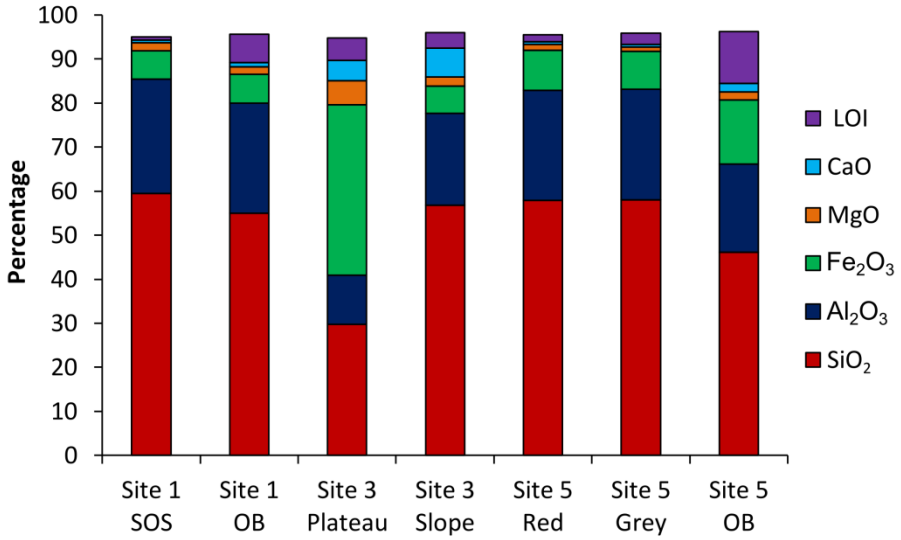

Figure 4.7 - *XRF major elemental concentrations for rock samples from site 1, 3 and 5, where LOI = loss on ignition.*

4.3.3 Errors associated with ICP-MS analysis

Limitations with the use of ICP-MS to analyse sequential extracts, included: the difficulties in analysing elements of low concentration, and the incapacity to analyse > 200 samples in one single run and same sensitivity of detection. Low elemental concentrations, often below the detection limit, were observed in extracts from vegetation, soil and spent oil shale, in particular in fractions 1 to 4 (Appendix E). Also, due to the large number of samples, analysis by ICP-MS was conducted in batches. Each fraction from 1 to 4 were analysed in separate runs, while for extracts from whole rock and fraction 5 analysis was split into 3 analytical runs. The suitability of ICP-MS to evaluate the chosen elemental suite and set of extracts was therefore examined based on the errors associated with analysis. Replicates, samples that were repeated during analysis; and duplicates, that were samples that encountered the same sequential extraction and sample preparation procedure, were both used to calculate the error.

Using replicates of spent oil shale from the same analytical run, the error associated with the analysis of each element by ICP-MS, based on 2σ of cumulative fractions, was calculated to average 3.3 % of the recorded concentration, compared with 1.9 % for whole rock data. In addition, extracts from the first 4 fractions, of the replicated spent oil shale, correlated well despite low concentrations, with high R^2 values, as shown in Table 4.3. In addition, replicates of the extracts from residual and whole rock solutions that were analysed in separate batches were found to correlate well.

Table 4.3 - *Correlation values for replicates and duplicate samples of spent oil shale from site 1.*

Rock fraction	R^2 of replicates	Analytical run	R^2 of duplicates	Analytical Run
1	0.9179	Same	0.9087	Same
2	0.986	Same	0.9938	Same
3	1	Same	0.9995	Same
4	0.9996	Same	0.9816	Same
5	0.999	Different	0.9998	Same
WR	0.999	Different	0.9999	Same

However, despite replicates that were analysed in separate analytical runs correlating well, replicates showed up to 20 % differing concentration in whole rocks and residual extract samples (Figure 4.8); mainly found for elements of lower atomic mass, which can be difficult to analyse accurately by ICP-MS (Gill, 1997).

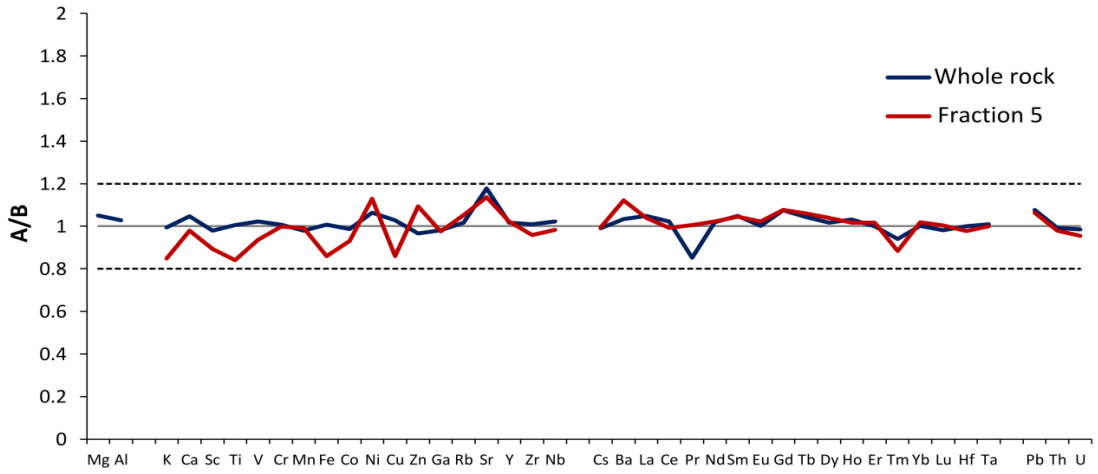

Figure 4.8 – *Error from the comparison of 2 separate runs (A and B) from the analysis of whole rock and residual (fraction 5) extracts by ICP-MS. Dashed lines indicate 20 % difference between the 2 extract concentrations.*

The sum of the elements analysed in each sequential extract should equal the total whole rock concentration of that element (Σ Fraction 1 → Fraction 5 = Whole rock); however, the value for the sum of elements within all five extracts was found to be greater than the whole rock concentration. This effect was also greater on samples with lower concentrations, such as soil samples, as indicated by the ratio of soil to spent oil shale samples from site 1 (Figure 4.9). Overall elemental concentrations were greater overall within spent oil shale compared with soil (green line, Figure 4.9), with the exception of Zn and Pb. Because of the lower concentration of elements within the soil sample, the difference was greater between the concentration of elements from the sum of extracts, and the whole rock concentration, but generally did not differ by more than 50 % in total. The exceptions to this were for elements of lower mass such as Mg, Al, K, Ca, as well as Mn and Cu, in addition to the rare earth element Tm. However, for the elements Ca and Mn in particular, the trend was the opposite for spent oil shale, with greater concentrations indicated within the whole rock compared with the sum of the extracts.

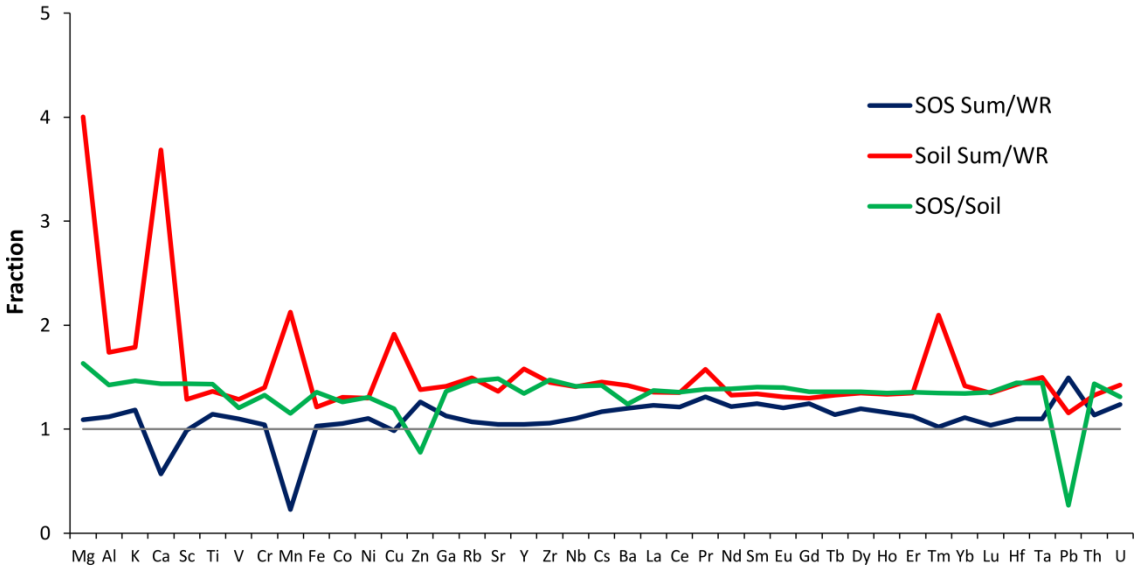

Figure 4.9 - *Comparison of the sum of five extracts with the whole rock (WR) concentration, for spent oil shale (SOS) and soil from site 1, as well as a comparison between spent oil shale and soil whole rock concentrations. The grey line indicates a normalisation factor of 1.*

Due to inherent problems with analysing lighter elements, in particular for extracts of a lower concentration range, these were removed from sample and site comparisons and a reduced set of elements was used that included: Sc, Ti, V, Cr, Mn, Fe, Co, Ni, Cu, Zn, Rb, Sr, Y, Ba, La, Ce, Pr, Nd, Sm, Eu, Gd, Tb, Dy, Ho, Er, Tm, Yb, Lu, Pb, U. In addition, due to low concentrations

within vegetation samples, analysis was based on their overall whole rock concentration and not on their extracts.

4.3.4 Enrichment

Whole rock samples from site 1, including spent oil shale, welded shale, overburden and soils, were enriched in elements on comparison with the Lothian oil shale (Figure 4.10). The difference in concentration between rock and soil sample types was low, with an order of magnitude no greater than 2 for elements, with the exception of Mn, Ni and Pb. However, concentrations of elements within vegetation were very low compared with the higher concentrations from the soil and spent oil shale.

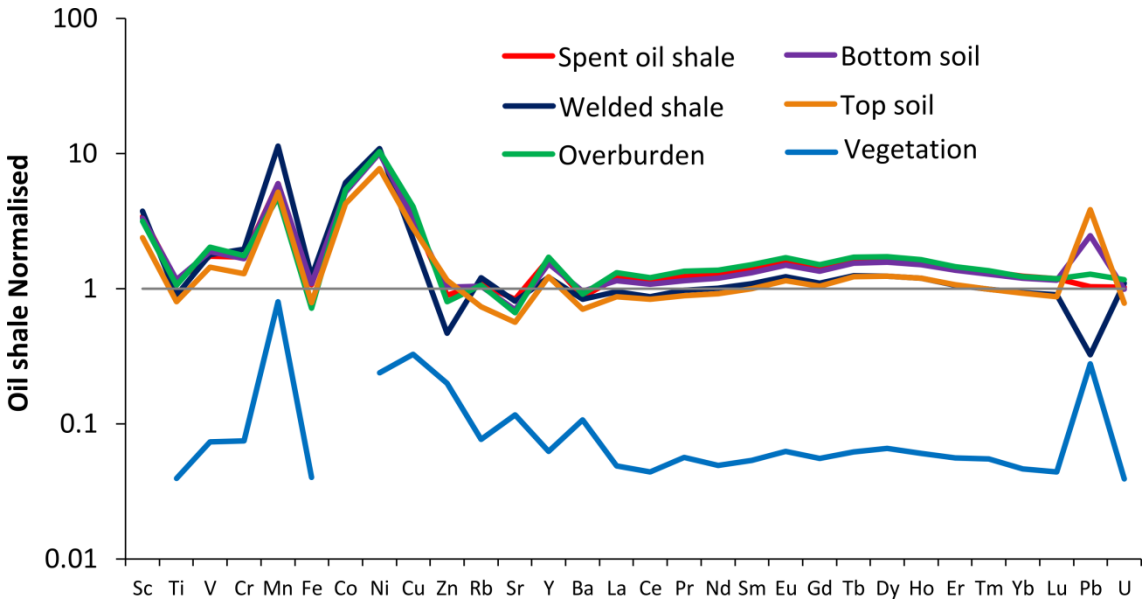

Figure 4.10 – *Oil shale normalised elemental plots, for samples from site 1, including spent oil shale, welded shale, overburden, soil and vegetation. The grey line indicates a normalisation factor of 1.*

Spent oil shale and bottom soil from site 1, were found to contain the majority of trace elements within the residual matter, based on the full elemental suite tested, with only very low concentrations of elements within other phases (Figure 4.11). Spent oil shale was determined to contain 86 % of elements concentrated within fraction 5, however, the soil showed less partitioning within the residual fraction (72 %), despite a similar overall enrichment of elements compared to the spent oil shale.

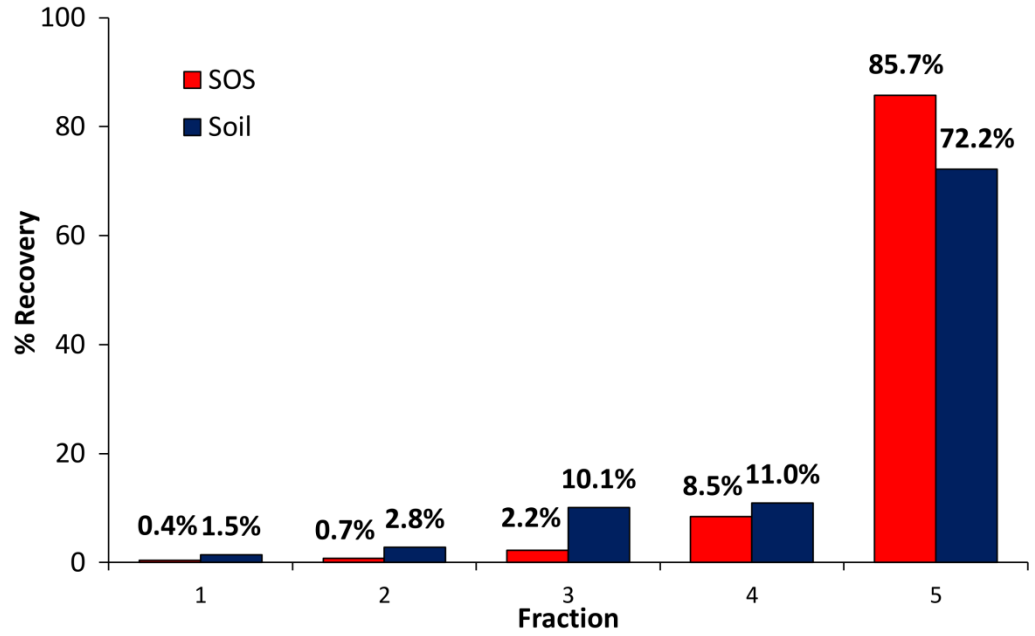

Figure 4.11 – *Partitioning of elements within different rock fractions for spent oil shale and bottom soil from site 1.*

On comparison of the soil from site 1, with a control soil, there was greater partitioning within residual matter when the soil was associated with spent oil shale (Figure 4.12).

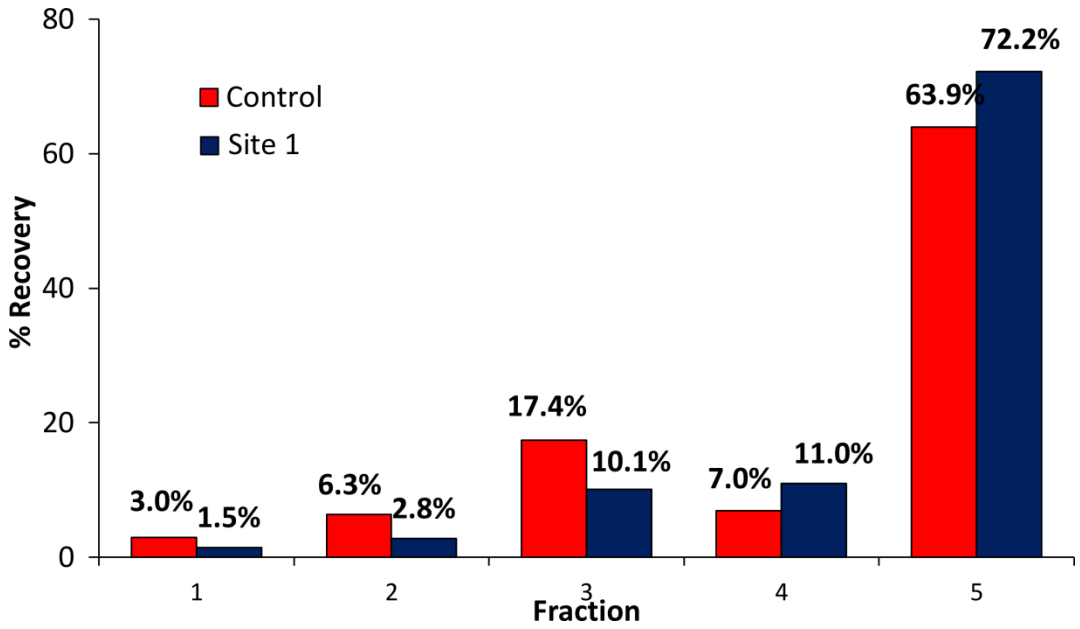

Figure 4.12 - *Partitioning of elements within different rock fractions for soil from site 1, compared with a control soil sample.*

A greater proportion of elements were found in more mobile phases within the control soil sample, with greater partitioning in fractions 1, 2 and 3. This was not the case for soil from site 1, however, where greater concentrations of elements were partitioned within fractions 4 and 5. Taking into account the whole rock elemental concentrations, soil samples from site 1 were enriched compared with the control soil (Figure 4.13), with a greater enrichment factor than when compared with the oil shale. Exceptions of depletion within control soil was observed for the elements Pb, Ni, and Mn, which were greater in concentration in the control soil sample, explaining the greater concentration of these elements when soil samples were compared with the oil shale.

Additionally, a difference in the concentration and partitioning of elements, between top and bottom soil samples, was observed, with greater enrichment in bottom soil compared with the top soil (Figure 4.13). Partitioning of elements in residual phases was similar between the two samples; however, in fraction 2 more Fe was found in top soil, in fraction 3 more Pb was in top soil and more Zn in bottom soil, while in fraction 4 more Zn was in the top soil.

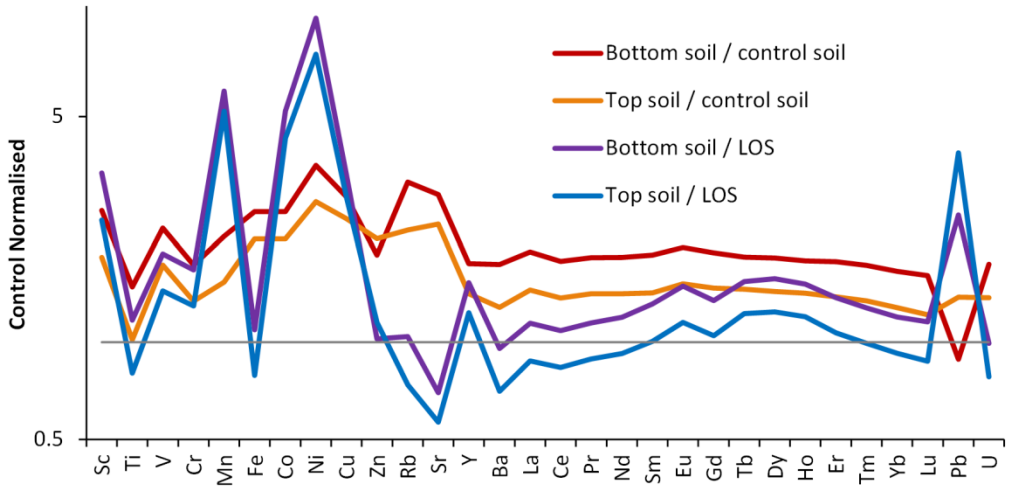

Figure 4.13 – *Normalisation of top and bottom soil from site 1 to control soil and Lothian oil shale. The grey line indicates a normalisation factor of 1.*

4.3.5 Variability

In the previous results section, only samples from the Greendykes bing (site 1) were considered. To compare and contrast the differences observed in concentrations and partitioning of elements within fractions of spent oil shale and soil, samples from all sites were used in the analysis.

Consideration of the maximum and minimum whole rock concentrations for rock (SOS, overburden), soil and vegetation samples from all sites, displayed the variation between sites and samples, shown in Figure 4.14. Vegetation samples showed the largest range, but also the lowest concentrations, whereas the spent oil shale and soil were more enriched in trace elements and similar in concentration.

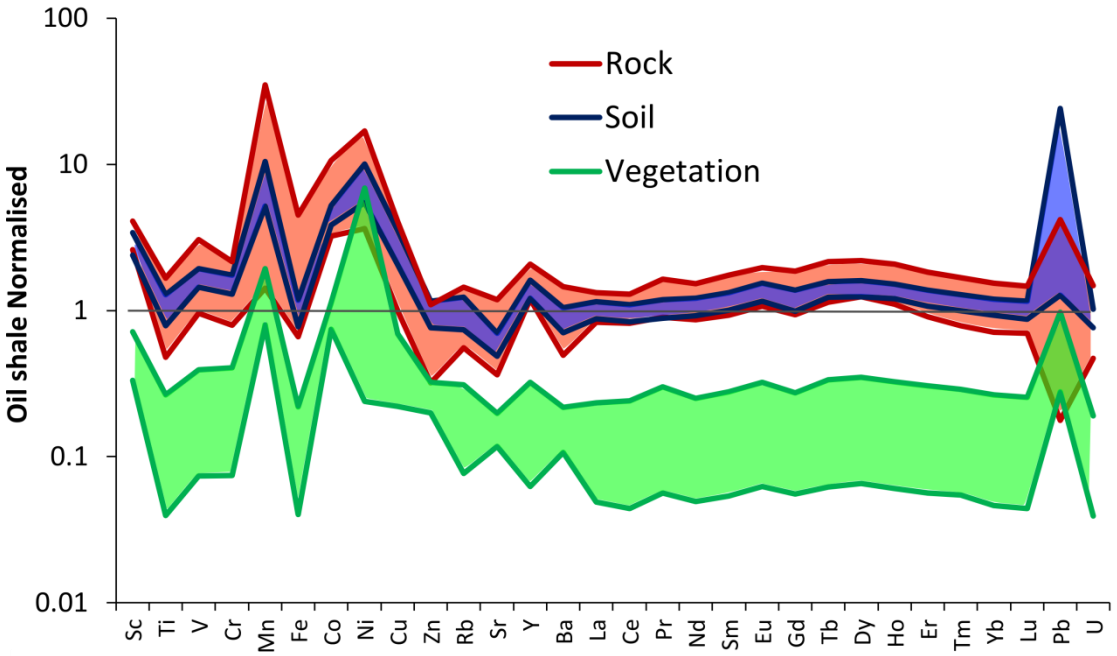

Figure 4.14 - *Range of elemental concentrations, normalised to oil shale, for rock, soil and vegetation samples from all sites, based on whole rock data.*

The sites which showed the highest concentration of trace elements within spent oil shale were sites 2 and 5, the youngest and oldest sites, respectively. The lowest concentrations were found within samples of overburden, as well as within spent oil shale from site 3. Within soil samples, the greatest concentrations of trace elements were found at site 1 (bottom soil) and site 5, while major elements (Mg, Al, K, Ca) were found at high concentrations in soil from site 3. Lowest concentrations were detected within site 1 (top soil) and redox elements at site 2. Within vegetation, lowest concentrations were detected from site 1, whereas the highest concentrations were found at site 3. Further investigation of these samples identified which phase the elements were associated with and can be illustrated in Figure 4.15 and Table 4.4, focusing on the redox sensitive elements without including the rare earth elements.

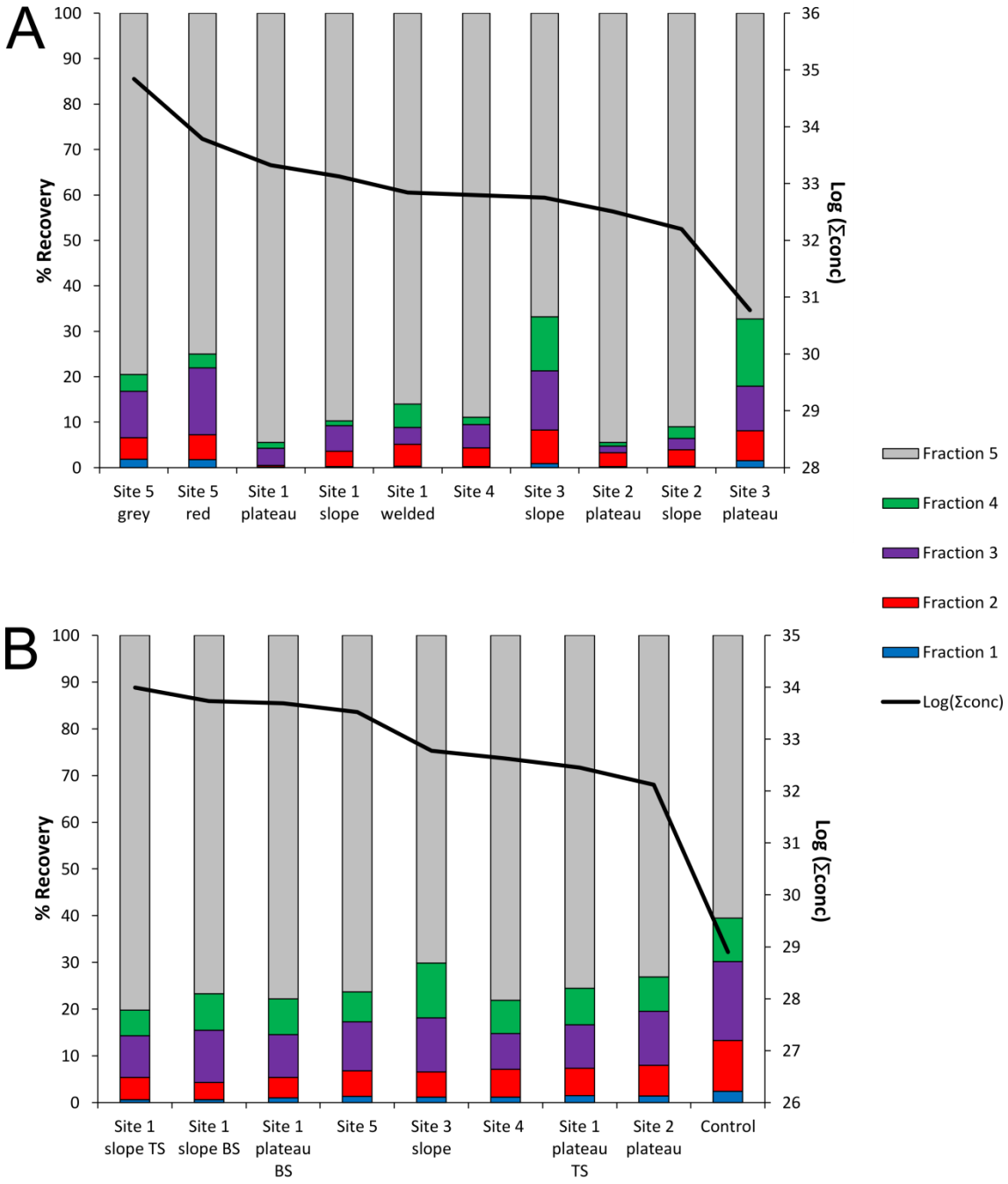

Figure 4.15 - *A) Partitioning of elements within fractions 1–5, for spent oil shale samples of decreasing overall elemental concentration. B) Partitioning of elements within fractions 1–5 for soil samples of decreasing overall elemental concentration, where TS = top soil and BS = bottom soil.*

From Figure 4.15B, soil samples showed similar partitioning of elements within fractions. However, it should be noted, there was an increase in the concentration of elements within residual phases, compared with the depleted control that contained a greater proportion of elements associated with oxide and carbonate minerals. In contrast, Figure 4.15A showed the variability in phase partitioning of elements across the rock samples studied in the Lothian. The

results are summarised in Table 4.4. Site 5 contained the highest concentration of trace metals and also greater associations of these elements with non-residual fractions. This is the same for site 3, however, samples contained lower concentrations of trace elements overall. For sites 1, 2 and 4; < 5 % trace elements were found within mobile fractions, mainly in the form of Cu and Sr within carbonate minerals.

Table 4.4 – *Proportion of trace elements within rock fractions of spent oil shale for the five sampled sites.*

	Site 1	Site 2	Site 3	Site 4	Site 5
Residual	92.1 %	92.8 %	67.0 %	88.9 %	77.3 %
Other	5.9 %	3.7 %	24.8 %	6.8 %	15.8 %
Mobile	2.0 %	3.6 %	8.2 %	4.3 %	6.9 %

4.3.6 Site specific results

A detailed investigation of elemental partitioning at sites 1, 3 and 5 was completed, so that a more detailed picture could be formed of the processes occurring during weathering of spent oil shale, and the movement of trace metals through rock fractions, and from spent oil shale to soil to vegetation species. Site 1 was chosen to look at the variety of samples (including welded shale, overburden, top soil and bottom soil) that showed high elemental concentrations within the residual matter. Large proportions of elements were partitioned within non-residual fractions in samples from sites 3 and 5, yet differences in age and overall elemental enrichment were apparent. Therefore these sites were chosen for further study, alongside samples from site 1.

Site 1:

The greatest proportion of samples was obtained from site 1. As well as spent oil shale, soil and vegetation, they also include samples of welded shale and overburden. Similar to site 2 and site 4, samples of spent oil shale from these sites contained the lowest concentration of trace elements in non-residual phases, regardless of slope position and the location of samples. A similar range of elemental concentrations were discovered in soil samples compared to the spent oil shale, yet they were associated with more non-residual fractions, similar to overburden and control soil partitioning. Nonetheless, soils indicated a preference for immobile fractions, such as organic matter, sulphides and oxides that incorporate the elements V, Mn, Fe, Co, Ni, Cu, Sr, Ba and Pb within these fractions (Figure 4.16C).

Overburden showed greater enrichment of elements within fraction 3 and 4, compared with the spent oil shale, indicating a greater proportion of elements within organic matter, carbonates, and clay mineral phases, as detected by XRD analysis (Figure 4.6). Common elements of high concentration detected in mobile fractions included: Sr, a common substitute in carbonate minerals (Reeder et al., 1983); and elements such as Fe, Mn, Cu, Zn that are enriched within fractions released by a change in redox conditions. Additionally, elements were found to be associated with organic matter, for example Pb.

Site 3:

Spent oil shale and soil samples from site 3 indicated greater preference for mobile fractions compared with site 1 (Figure 4.17). In particular, spent oil shale was shown to contain high proportions (> 10 %) of: Cu and Sr in fraction 2; Sc, V, Mn, Fe, Co and U in fraction 3; and Zn, Sr, Ba, Pb, U in fraction 4. Soil on the other hand contained the majority of transition elements within the oxidisable fraction (fraction 4), in addition to Sr, Ba, Pb and U. Fraction 3 also contained higher proportions of Mn, Fe, Co and Zn.

Site 5:

Compared with site 3, the spent oil shale from site 5 contained fewer elements within mobile fractions and a greater proportion in the residual matter. The exceptions were Mn and Fe in oxide minerals and Cu in carbonates. The composition of grey and red spent oil shale samples were seen to be very similar in composition, despite their differing colouring, with both containing high concentrations of elements within the same phases, with similar mineral compositions as identified by XRD and XRF analysis (Figure 4.6 and Figure 4.7). The soil contained lower concentrations of trace elements than SOS at site 5, but one of the most enriched soil samples overall and elements were partitioned in similar phases to the rock samples.

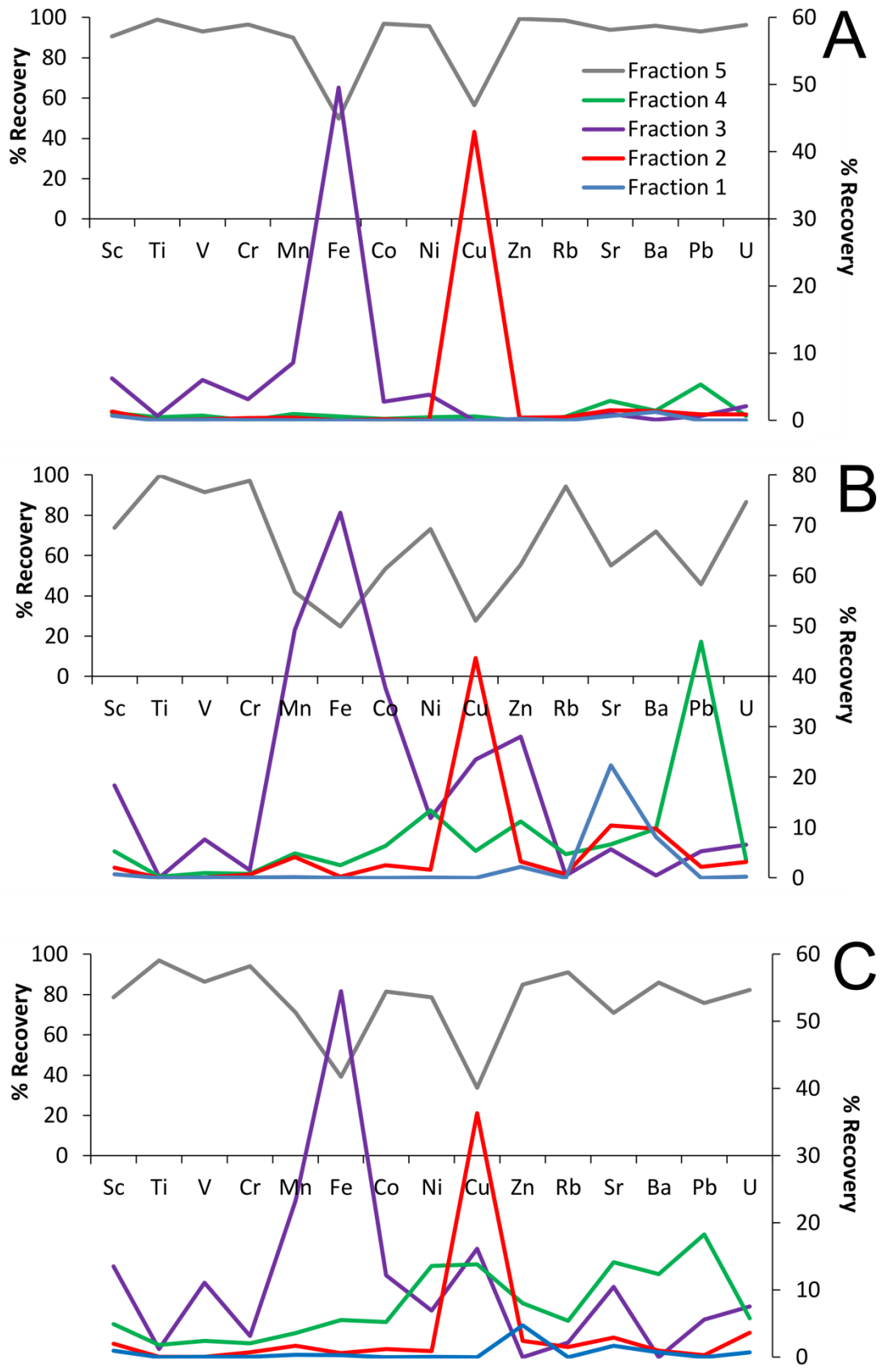

Figure 4.16 - *Proportion of trace elements within fractions 1–5, in A) spent oil shale B) overburden and C) soil from site 1.*

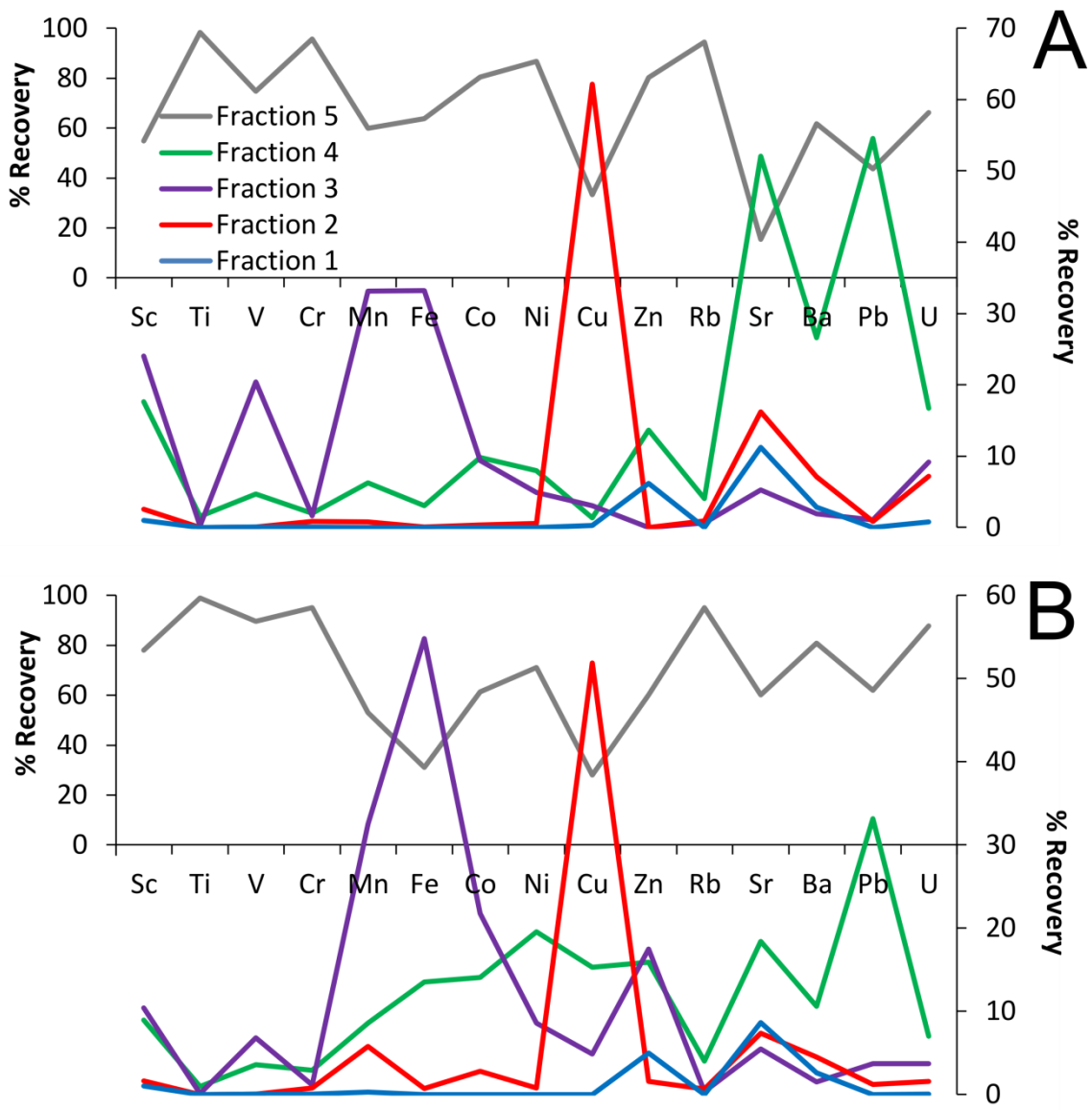

Figure 4.17 - *Proportion of trace elements within fractions 1–5, in a) spent oil shale b) soil from site 3.*

4.3.7 Rare earth elements

Rare Earth Elements (REE), although not very mobile in the environment, may provide indication of the physical processes occurring during weathering of waste deposits, by indicating whether these elements are transferred to clay or amorphous mineral phases. The speciation of REEs was similar in all soils analysed, with an accumulation of REE within the reducible and oxidisable phases, and the remaining majority associated with residual matter. However, although the sampled soils show similarities, this is in contrast to the control soil sample, which contains a greater proportion of REE within the oxide fraction and also a lower concentration overall. The differences are illustrated in Figure 4.18.

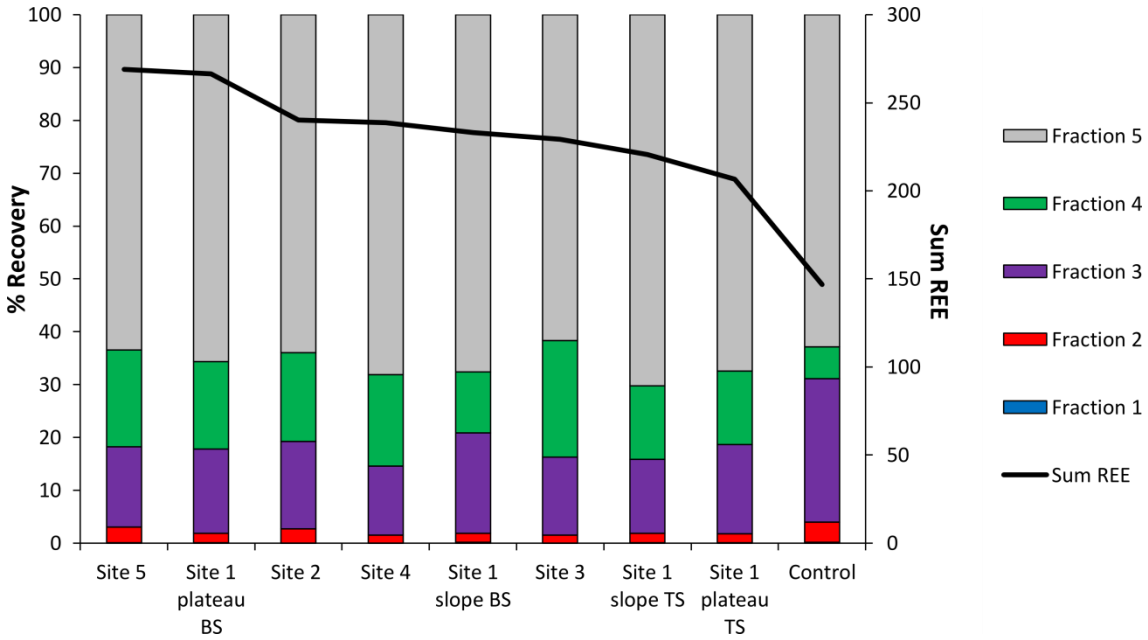

Figure 4.18 - *Partitioning of REE within fractions 1–5, for soil samples of decreasing REE concentration.*

Within spent oil shale there was seen to be greater variation in phase association of REE, which may be due to differences in mineralogy of the samples. Samples from site 2, in particular, show considerable variation (Figure 4.19) indicating that the slope position and location of spent oil shale on the bing may play a part in determining the fate of REE.

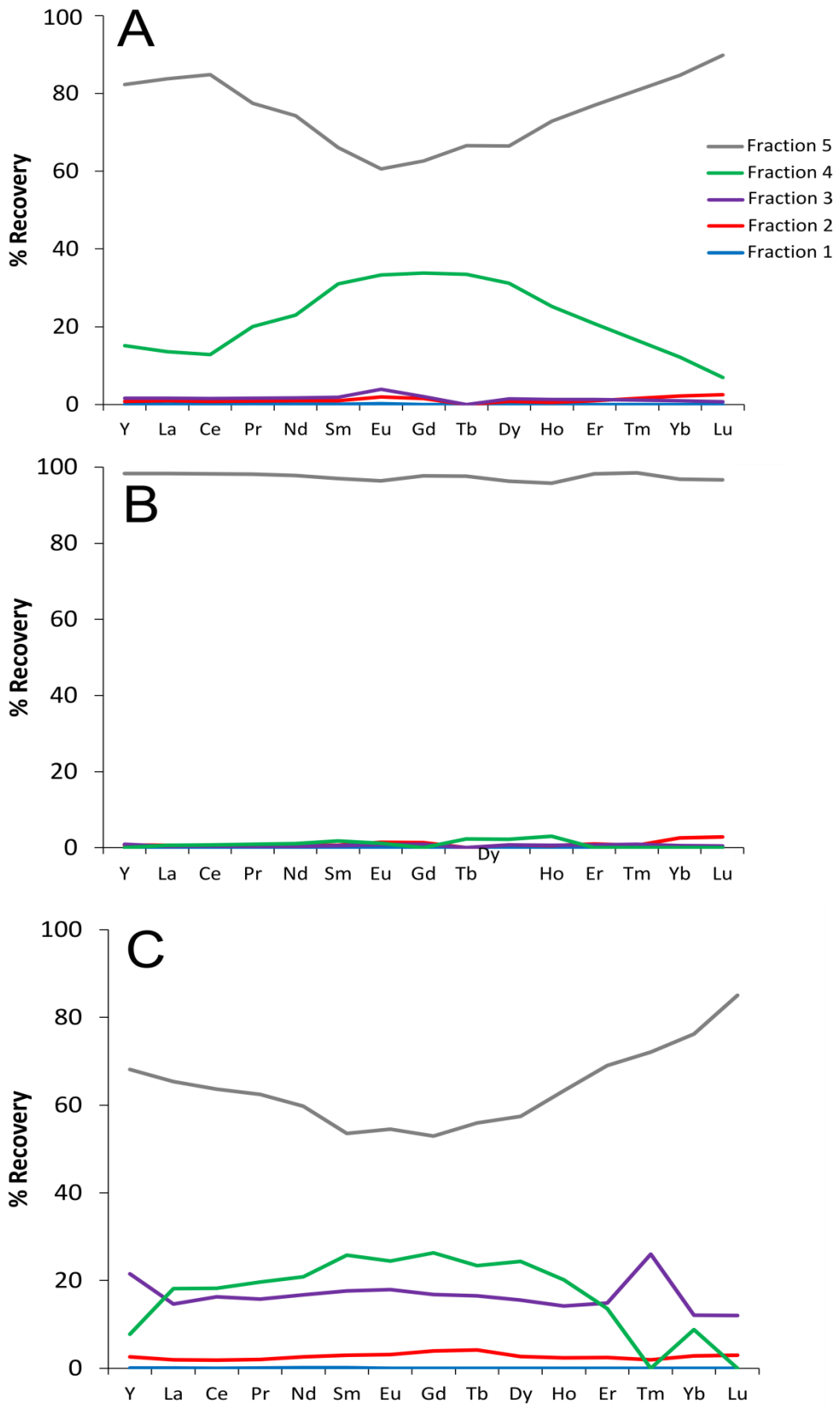

Figure 4.19 - *REE partitioning at site 2 for: A) spent oil shale from the slope; B) spent oil shale from the plateau; C) soil from the plateau.*

Partitioning occurred in all fractions of grey spent oil shale from site 5, and spent oil shale from the slope at site 3. However, the red sample of spent oil shale from site 5, was similar to spent oil shale from other sites, with the majority of REE contained within the residual phase and ~10-20 % within oxidisable matter. The heterogeneity of REE distribution within rock samples from site 5 is unlike the redox elements studied above which show the same partitioning within the rock. The differences between samples from site 3 and site 5 is illustrated in Figure 4.20.

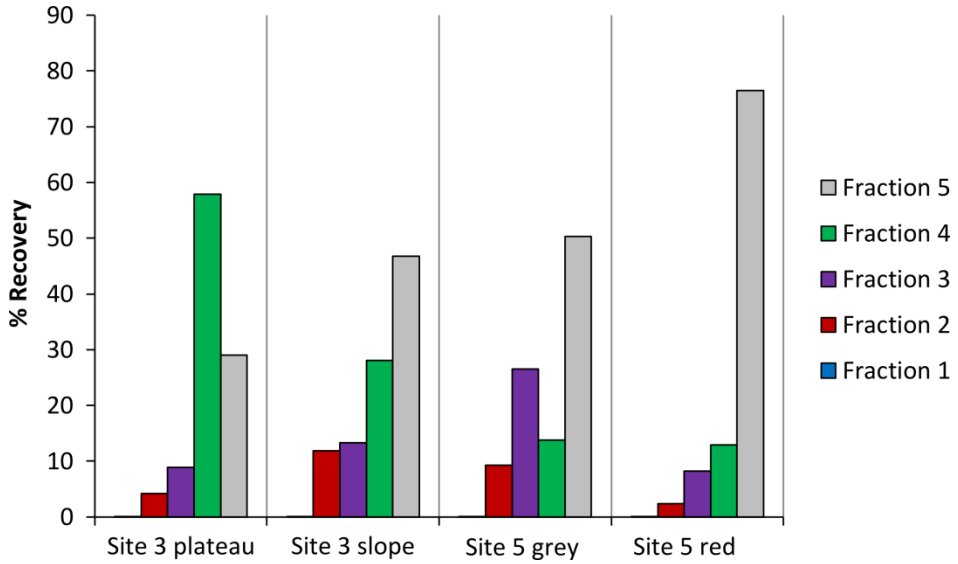

Figure 4.20 – *Distribution of total REE within fractions 1-5, of spent oil shale from site 5 and site 3.*

4.4 Discussion

4.4.1 Errors

The detection and analysis of major and trace elemental concentrations, within samples that underwent sequential extractions, was conducted by ICP-MS analysis. Errors and sample discrepancies were identified and reduced by the use of: external and internal standards, reagent and procedural blanks, and replicates and duplicates. However, difficulties arose due to the necessity to analyse samples in batches, low sample concentrations, and errors associated with the detection of elements of low mass.

Errors associated with ICP-MS analysis were low, up to 3.3 %, as calculated by the analysis of replicates from cumulative fractions. However, differences between the concentrations of elements in duplicate samples were shown to be larger than 4 %, and for some elements close to 50 %, for the whole sequential extraction procedure (Figure 4.9). The analysis of duplicates indicates that the majority of error originates from systematic errors within the sequential

extraction procedure, as well as the heterogeneity of samples. In addition, both random and systematic errors were able to propagate due to accumulation during: each extraction step, sample preparation procedures, and detection methods using ICP-MS. Considering an upper estimate of 50 % for error associated with the technique, this can be compared to a similar value of +/- 10 % for each fraction as identified in a study by Tessier (Tessier et al., 1979).

Larger errors were especially apparent in soils, where elements were detected at lower concentrations overall and with partitioning more propotionate through the separate fractions. Exceptions to the elemental enrichment of spent oil shale compared with soil was observed for Zn and Pb (Figure 4.9), which were more concentrated within soil samples perhaps due to an association with organic matter (Lewan et al., 1982). Elements were difficult to detect in extracts from vegetation samples, therefore only results from the overall (whole rock) concentration was used for further analysis. Elements below the detection limit, were assumed to have a concentration close to zero, and were especially dominant within the exchangeable and carbonate fractions of samples (Table E.2 – E.5, Appendix E).

Large errors were associated with the analysis of the lighter elements ($m/z < 80$), being difficult to analyse accurately by ICP-MS due to the: ease of contamination during sample preparation; matrix effects and interference with the instrument, from gases or polyatomic species; and low concentrations of elements within extracts (Gill, 1997). Therefore, lighter elements were removed from sample and site comparisons. Techniques such as atomic absorption (AA) and inductively coupled plasma optical emission spectroscopy (ICP-OES) are preferred for analysing these lighter elements. However, AA is time consuming and requires large sample sizes for the analysis of each element. This was not practical due to the large number of low concentration extracts produced by the sequential extraction procedure. Furthermore, ICP-OES could not be used, as was initially planned, due to recurring problems with the instrument. The full elemental suite was therefore not used for further analysis, and instead elements were chosen, based on instrument detections and errors. The reduced list of elements mainly consisted of redox sensitive elements, such as heavy metals and transition metals, as well as rare earth elements that are commonly associated with aluminosilicate minerals that are decomposed during retorting (Lipin et al., 1989).

Based on the results from the error analysis, the use of ICP-MS was restricted to qualitative analysis. Duplicates of each sample, along with a reduction in the amount of analytical runs, could improve the accuracy and reliability of ICP-MS to use as a quantitative technique to analyse sequential extracts in future work. However, due to strong correlations between

replicates (Table 4.3), ICP-MS was used as a comparative tool; to investigate differences in concentrations between samples and fractions where qualitative analysis was suitable.

4.4.2 Enrichment

Samples of spent oil shale, overburden and soil from site 1 each showed slight enrichment of trace elements when compared with Lothian oil shale (Figure 4.10). As described in Chapter 3, enrichment of trace elements commonly occurs during retorting, as the organic matter is removed and trace elements reside in the remaining residual fraction (Shirav et al., 1988). There were some exceptions to this rule, for example elements such as Zn, Sr, Ba and Pb. However, these exceptions were mainly found in soil samples or welded shale, which are likely to be mineralogically different to the waste material. In addition, oil shale associated with each bing was not sampled, therefore direct comparisons cannot be made between the oil shale and spent oil shale at each site, which are of a slightly different composition (Figure 4.15).

Differences in the concentrations of elements within top and bottom soil, from site 1, were highlighted, showing greater enrichment of elements within bottom soil. Soil samples were formed from the addition of topsoil from external sources, and the breakdown of spent oil shale (Harvie, 2005). Greater concentrations of Fe, Pb, and Zn, found in exchangeable phases within top soil (Figure 4.16), are likely a result of the addition of soil on the top of bings for reclamation purposes. Also, a greater incorporation of spent oil shale, that has mechanically weathered, within bottom soil is similarly likely, leading to higher concentrations of elements in the bottom soil compared with the top soil. The breakdown of spent oil shale to form soil is also the reason why more elements reside in the residual fraction of soil formed at spoil heaps, compared with the control sample, that contains lower concentrations of trace metals within more exchangeable phases (Figure 4.12).

The concentration of trace metals within vegetation was lower than that of the soil and spent oil shale (Figure 4.10), and therefore they were analysed based on their overall concentration rather than the concentration within extracts; however, the concentration was seen to vary between sites, with depletion ranging from 2 to 20 times that of oil shale normalisation values (0.005 to 0.5). This shows similarities with results from studies on levels of Cu, Pb, Zn, and Cr within mangroves in China. The mangroves showed a depletion compared with sediments, of 5 to 7 for Cu and Zn, and higher values of 17 and 27 times more depletion for Pb and Cr (Qiu et al., 2011).

The pattern of enrichment was similar for solid samples (overburden, spent oil shale and soil) from the same system (i.e. the same site), indicating the principal controls on elemental concentration were coming from both the oil shale used in retorting and the spent oil shale produced. In particular, spikes of enrichment compared with oil shale from the elements Ni and Mn, as well as variability in Pb enrichment (Figure 4.13), can be explained by the presence of these elements at high concentrations within soil, being associated amongst oxide and organic fractions. Whilst spent oil shale is enriched in trace elements compared to oil shale samples, the enrichment effect within spent oil shale may be diluted due to the addition of overburden and soil alongside the spent oil shale, or elements may be less concentrated due to their release into the environment. The latter, however, is not likely to be the case based on the following discussion.

4.4.3 Controls on environmental mobility

Metal mobility in the environment, was assessed by the use of a sequential extraction procedure, in which the fraction of the rock to which elements were associated with, was linked with the reagent used to extract the elements. As the strength of the reagent increased, so the susceptibility to release in the environment decreased. Metals associated with the exchangeable and carbonate rock fraction are considered mobile in the environment, whereas elements associated with the organic, oxide and residual fraction are considered immobile (Tessier et al., 1979). These latter fractions also encompass sulphide and clay minerals, which are degraded when a change in redox conditions occurs. Controls on the mobility of trace elements, and therefore partitioning within rock fractions, is the subject of further discussion.

4.4.3.1 Weathering & heterogeneity

A change in colour of the spent oil shale, from bluish grey to red, indicates that weathering has occurred at all the bing sites and the colour change itself occurs due to the oxidation of iron containing minerals within the spent oil shale, with Fe_2O_3 concetnrations > 5 wt %, and weak reflections due to hematite identified in XRD spent oil shale patterns (Figure 4.6 and Figure 4.7) (Harvie, 2005). Weathering, both physical and chemical, is postulated to impact the composition of spent oil shale, by altering the mineralogy and structure, so that it has the potential to leach elements that are of danger to the environment (Tuttle et al., 2009), such as heavy metals Cr, Cu, Pb and Zn (Zakir et al., 2006).

Chemical weathering results in the hydration and natural carbonation of existing minerals in the spent oil shale, leading to the formation of alteration products and secondary minerals.

Enhancement of these hydration reactions occurs in Estonia, as a result of the deposition of spent oil shale as slurry (Motlep et al., 2007), while in Jordan, natural weathering results in the formation of ettringite, a hydrated sulphate mineral (Myneni et al., 1998). In Estonia, the mineralogy of the waste deposits varies with depth, with the presence of smectite and calcite near the surface, and amorphous material at greater depth. The varied mineralogy indicates the heterogeneity of deposits, likely to be caused from weathering processes dominant near the surface (Motlep et al., 2010). At brownfield sites however, reaction products were found at lower concentrations near the surface, indicating the dependence of mineral composition on the draining mechanism (Renforth et al., 2009), and fly ash with low permeability showed that trace elements had little impact on the composition of leachates (Mayes et al., 2006). The Lothian material, being processed and deposited in a similar way to the Estonia spent oil shale, is likely to share similarities with the weathering reactions that occur. However, the spent oil shale heaps, in Scotland, are reported to be porous (Harvie, 2005), which increases as organic matter is lost due to retorting (Rajeshwar et al., 1979), and therefore the drainage mechanisms may be dominant factors in affecting the extent of weathering in material (see Figure 4.3 for likely transport pathways). However, limitations with the sampling study meant that samples at great depth could not be obtained, and instead, samples from the plateau and slope were taken, at 5-10 cm depth. Weathering reactions in Lothian, are likely to consist of physical and chemical weathering. The physical breakdown of material, due to erosion, and the incorporation into soil, is encountered at the bing sites. Also, chemical weathering, by the formation of hydrated and oxidised mineral products, has occurred. In particular, the presence of hematite within spent oil shale and clay minerals within overburden, may be formed due to weathering reactions (Figure 4.6).

In spent oil shale, elements predominantly reside with the residual fraction, likely to consist of mullite, quartz and high-temperature amorphous phases that are stable to leaching and weathering processes. However, the difference in elemental partitioning within spent oil shale may be related to the slope position, as samples of spent oil shale from site 2 showed greater partitioning of elements within fractions 3 and 4 when taken from the slope compared with the plateau (Figure 4.15). Elemental enrichment was similar for samples of spent oil shale from the slope and plateau, indicating that fractionation and leaching has not occurred at one position of the bing compared to another, suggesting that the dominant control on elemental partitioning is the mineralogy. Spent oil shale sampled from the slope at site 2 showed greater partitioning of redox elements within fractions 3 and 4, while ~10 % of rare earth elements were associated with fraction 4, compared with ~100 % in fraction 5 sampled from the plateau

(Figure 4.19). Soil, sampled from the plateau, was similar in composition and partitioning of elements to soil samples from other sites, and REE were adsorbed to minerals in fractions 3 and 4 (Figure 4.19). The differences observed in the spent oil shale from the plateau compared to the slope, therefore indicate a lack of mineral matter that commonly adsorbs REE, such as clays. This may be due to the heterogeneity of spent oil shale deposits. Alternatively, clay minerals may result as a weathering product within spent oil shale that is still able to retain trace elements, or within clays and organic matter that may be present due to mixing of spent oil shale with overburden, the unprocessed rock. Nevertheless, elements residing in fractions 3 and 4 are relatively stable, only releasing bound elements by a change in redox conditions (Filgueiras et al., 2002), and enrichment between the 2 samples is similar.

As mentioned previously, the increased rare earth element (REE) and redox elemental content within residual matter of soils, compared with the control, is due to physical weathering processes and the breakdown of spent oil shale, leading to formation of soil in bing environments that has a large spent oil shale component, for example bottom soil sampled from the plateau at Greendykes. The partitioning of elements within the residual matter of soil indicates that there is limited release of trace elements during the soil formation process, and any remaining elements not associated with residual matter, are associated with fractions 3 and 4 that are also considered immobile. Alternatively, it is possible that mobile species may be leached and transported through bings (Figure 4.3), resulting in lower concentrations of elements in fractions 1 and 2. However, variability of the concentration of elements within vegetation (Figure 4.14) indicates that that some elements may be released from the spent oil shale and absorbed by vegetative species. The proportion of elements that are released and absorbed by vegetation is likely to be minor though, based upon the enrichment factor and partitioning of elements within residual and immobile fractions in soil and spent oil shale deposits (Figure 4.11).

The largest enrichment of trace elements was found in spent oil shale from sites 1 and 5 (Figure 4.15); deposits that are more than 80 years old. The lowest enrichment of trace elements was found in the youngest samples, from sites 2 and 3. If the leaching of elements was primarily weathering controlled, the expectation would be for weathering (and therefore leaching) to increase with age. However, the age of the deposits is given from when the mine closed, and therefore samples may be older than indicated. It is also suggested, that the majority of breakdown of the spent oil shale in Scotland occurs within the first twenty years after deposition. All of the sampled bings are > 50 years old, which would mean all sites underwent significant weathering and mineralogical alterations (Mackenzie, 1996).

There was variation in both the enrichment of trace elements, and the partitioning of elements, between sites. It is therefore likely that there are more dominant contrals than weathering on the distribution and mobility of elements within spent oil shale which are the subject of future discussion. In addition to weathering mechanisms and the age of deposits, these include: the rock source and depositional environment, and the processing mechanism for the retorting of oil shale.

4.4.3.2 Processing

The mechanism for the movement of trace elements of environmental significance within oil shale as it is processed consists of multiple steps:

1) Firstly, oil shale that is retorted at high temperatures releases elements adsorbed to organic matter and other minerals that are decomposed within the retorting temperature range.

2) Secondly, combustion leads to the decomposition and release of elements from more mineral phases, such as carbonate and clay minerals (Motlep et al., 2007).

3) Secondary (and often metastable) minerals are then formed as a result of reactions between the reactive decomposition products at high temperatures (Trindade et al., 2009), and these new minerals may adsorb trace elements that were previously released during retorting (Mayes et al., 2006).

The redistribution of elements is dependent on the stability of the secondary mineral phases, as well as the sorption mechanisms on the mineral surface (Tuttle et al., 2009). Trace elements may become incorporated or adsorbed to the new minerals, being especially scavenged by reducible and oxidisable rock fractions (Tessier et al., 1979). In addition, the alkalinity of material dictates the amount of adsorption of elements from solution onto clay, oxides and organic matter (Ure et al., 2002). Furthermore, new minerals formed at high temperatures may be susceptible to hydration mechanisms that occur after the removal and transportation of the solid material to the spoil heap (Saether, 2004), however, re-distribution of elements into pore waters may be limited based on values of enrichment and partitioning within residual and immobile rock fractions.

The chemical composition of Lothian spent oil shale was similar to the overburden from the same site (Figure 4.7), except for the increase in organic matter within the unprocessed overburden. The major elemental composition remained unchanged after retorting, but the

partitioning of elements differed due to the breakdown and formation of new mineral phases. Crystalline clay minerals were detected in the overburden, but mullite and other high temperature amorphous aluminosilicate phases were detected within the spent oil shale that were formed at high temperatures (Figure 4.6) (Trindade et al., 2009). The difference in mineralogy and processing explains the difference in the partitioning of elements between the spent oil shale and overburden (Figure 4.16). When samples of oil shale are retorted, elements are released from decomposed phases, such as clays, oxides or organic matter (fractions 3 to 4), and then primarily bind to the newly formed silicate phases within the residual fraction (Shirav et al., 1988).

The heterogeneity of deposits was further demonstrated by the mixing of spent oil shale, and likely overburden (reported as grey spent oil shale), from site 5. The rock samples from site 5, although different in colour, showed the same chemical composition but differing REE partitioning (Figure 4.20). The mineralogy of the grey shale was found to be similar to that from overburden from site 1 (Figure 4.6), or welded shale, which is material that forms when the retorting process fails (Harvie, 2005). The lack of organic matter signifies that either the sample was overburden containing no organic matter, or the sample did undergo retorting at very low temperatures. Processing that occurs at lower temperatures may remove the oil, yet leaving the same mineralogy and therefore the partitioning of elements remains within the original rock phases (Vassilev et al., 1996). The greater partitioning of rare earth elements within fraction 3 of the grey shale could be due to concentration within clay minerals (Figure 4.20). Clay minerals are decomposed between 200-600 °C (Bhargava et al., 2005), therefore, it is likely that the grey shale is unprocessed overburden. Also, red spent oil shale contained the majority of REE within fraction 5 due to removal of clay minerals, and concentration of elements within residual matter. The partitioning of REE was also illustrated by the analysis of soil samples associated with spent oil shale (Figure 4.18). Control soil, contained REE within fraction 3, likely associated with clay minerals. However, REE within soils from the bings were concentrated within fraction 4, indicating the release and readsorption of REE to secondary phases, such as silicate minerals.

While the partitioning of elements within non-residual fractions was dominant within samples of overburden and soils, which naturally incorporate trace elements into minerals such as clays and oxides, the partitioning of elements within non-residual fractions was also dominant in spent oil shale at site 3 (Figure 4.15 and Figure 4.17). This was in contrast to other sites, which mostly showed enrichment of trace elements within residual immobile fractions, and therefore

spent oil shale from site 3 may suggest an environment where elements are readily released from waste material.

The chemical composition of spent oil shale from the plateau at site 3 was determined to be Fe-rich, with high concentrations of amorphous material and magnetite, differing in both the chemical structure and the partitioning of elements, compared with spent oil shale samples from other sites (Figure 4.6 and Figure 4.7). The addition of metals such as iron, into spent oil shale waste, can occur by contamination during processing, with retorting equipment commonly made from iron (Carruthers et al., 1912). However, in this case the high concentrations of iron oxide (40 wt %) suggest a material source, for example, contamination of bing sites with industrial waste such as blast furnace slag. Because the spent oil shale contains less aluminosilicate minerals, the trace elemental concentration was diluted compared with other spent oil shale samples studied (Harber et al., 2001). In particular, the depletion of REE from the residual fraction shows the association of REE within fraction 4 (Figure 4.20), and minerals that require a change in redox conditions to release the trace elements. The presence of rare earth elements within fraction 4 may indicate the occurrence of iron oxides within this phase that were not fully extracted using dithionite in fraction 3; or within residual amorphous silicates that are readily extracted by peroxide.

Despite the significant differences in the chemical and mineralogical composition of the waste material from the plateau at site 3, similarities do exist with the spent oil shale taken from the slope (Figure 4.20), showing partitioning of REE and redox elements within multiple fractions. Redox elements were partitioned in fractions 2, 3, 4 and 5, and the distribution of elements was more similar to samples of overburden or soils that have not been processed at high temperatures. The release of more trace elements, due to greater amounts of mineral decomposition may lead to the association of higher concentrations of trace elements within amorphous matter. These elements may then be relocated to the newly formed oxide and aluminosilicates. Nonetheless, the partitioning of elements within non-residual fractions; the presence of carbonate minerals; and the lower enrichment of trace elements at site 3 all indicate increased mobility of trace elements at this site, and further work would be required to confirm the composition and mobility of trace elements at this site due to the large contribution of magnetite within spent oil shale that may be from a separate external source (Figure 4.6). The greater concentration of elements within vegetation at site 3 suggests the uptake of metals from groundwater and the exchangeable fraction of soils or rock (Filgueiras et al., 2002). The slight concentration of elements within vegetation may be beneficial and could be the reason for the diversity of vegetation species found at the bing sites (Harvie,

2005; Zhang et al., 2001), however, may also be explained by discrepancies with elemental analysis.

4.4.4 Implications for Jordanian oil shale

The mobilisation of trace elements in the environment is related to: the concentration of trace elements within spent oil shale and soil; their mobility and solubility; and environmental conditions (Kashem et al., 2007). In this study: weathering reactions, processing mechanisms, and the compositional characteristics, were identified as controls on the partitioning and mobility of elements in spent oil shale.

Chemical weathering in Lothian was not identified to be a primary control on the distribution of elements, with weathering mineral products minimal in the spent oil shale (Figure 4.6), and the majority of elemental partitioning within residual fractions of spent oil shale and associated soil (Figure 4.15). However, weathering processes that occur in Lothian are likely to be different to those that occur in Jordan. With a precipitation rate of more than double that in Jordan, and colder temperatures, chemical weathering and hydration reactions is a dominant process in the bing environment. In Jordan, where temperature extremes range from freezing to > 30 °C, may cause physical mechanisms to play a part in the weathering of spent oil shale deposits, such as expansion/contraction and freeze-thaw. As Jordanian spent oil shale will be deposited as mine backfill, with an overburden layer above, deposits will be less exposed and in particular aeolian transport is likely to be limited.

The processing methods to produce Lothian and Jordanian spent oil shale were very similar, by heating oil shale to temperatures > 700 °C, by retorting and combustion methods. Any elements released from the organic matter, or from minerals decomposed during high-temperature processing (such as clay minerals, carbonates and feldspar) will be adsorbed by new mineral products, such as aluminosilicates or Ca-silicates. Minerals already present in the spent oil shale that were not broken down during retorting, will not release any trace elements associated with them. It is therefore likely that elements are partitioned within residual matter after retorting, with weathering of little influence on these stable minerals.

In Lothian, spent oil shale from sites 3 and 5, showed greater partitioning of elements within other immobile fractions, yet up to 10 % may be associated with mobile fractions, predominantly carbonate minerals (Figure 4.17). Restrictions to the elements that calcite incorporates is dependent on the size of the cation, with smaller elements such as Fe, Mn, Zn,

and Cu, commonly associated and explaining the higher concentration of these elements within the carbonate rock fraction (Reeder et al., 1983).

Despite some association with mobile fractions, spent oil shale may therefore by partially controlled by the solubility of these mineral phases, which is increased in acidic pore solution conditions. The pH of the bings is slightly acidic, at values of ~4-5, due to chemical weathering processes (Harvie, 2005). However, Jordanian material is different in composition to the Lothian material, and is highly alkaline due to the high concentrations of Ca and Mg in carbonate minerals. The solubility of alkaline minerals is lower, and therefore trace elements are less mobile within alkaline substances (Essington, 1991). Estonian spent oil shale is also highly alkaline and rich in carbonate minerals, and studies suggest it may take up to 500 years to naturally neutralise alkaline deposits (Motlep et al., 2010), while leaching studies indicate that the Estonia semicoke meets EU regulations (Orupold et al., 2008). Other research indicates that most metals remain in spent oil shale after retorting, such as deposits from the Green River formation (Shendrikar et al., 1978), and retorted oil shale from Brazil has been used to remove heavy metals from wastewater by adsorption on mineral active sites (Pimentel et al., 2010).

Lothian spent oil shale from sites 1, 2 and 4, despite being deposited for different lengths of time, and undergoing different methods of processing, showed enrichment of redox elements compared to Lothian oil shale, in addition to partitioning of elements within the residual fraction of the rock (Table 4.4), indicating that these elements are immobile in the environment. The effect of processing conditions on the partitioning of elements and the resultant composition of spent oil shale therefore needs to be considered when estimating the mobility of trace elements within Jordanian spent oil shale. Initial studies suggest that Jordanian spent oil shale may be naturally more stable to environmental conditions than Lothian material, however further work would be required to confirm this.

Limitations of this sequential extraction study on the Lothian spent oil were mainly in the sampling and analytical procedures, where the latter was previously discussed based on the restrictions of using ICP-MS. Improvements to the sampling method could include sampling at depth, and with an increased number of sampling points per site, to take into account any heterogeneity and further interpret the weathering mechanisms in the bing environment in Scotland. Greater controls on the sequential extraction procedure to reduce systematic errors, and the use of more specific reagents, may also be of use in pinpointing the exact mineral phases that adsorb trace elements.

Further chapters investigate the capacity of spent oil shale to sequester CO_2 by accelerated carbonation reactions. The reduction of the CO_2 emissions produced by the retorting of oil shale emissions is the principal objective of the thesis, however the carbonation of spent oil shale can act to reduce trace metal mobility, by increasing the proportion of metals within residual phases (Essington, 1989), and therefore could link in with the results provided in this chapter.

4.5 Conclusions

In this study the mobility and concentration of elements has been studied within samples of spent oil shale, soil and vegetation from Lothian bings, using qualitative analysis of sequential extracts by ICP-MS. Elements partitioned within exchangeable and acid soluble fractions are considered mobile, whereas, elements only released by strong acids or reducing or oxidising agents are considered immobile, as aggressive conditions would be required to release elements from these phases, that may be bound by co-precipitation mechanisms within oxides, or isomorphous substitution within clay minerals (Krol et al., 1986).

Results show that 84 % of elements analysed within spent oil shale samples were concentrated at > 100 % of Lothian oil shale concentration levels. The high levels of concentration compared to the sampled Lothian oil shale, indicate that samples do not undergo leaching of elements, instead retaining the elements within the waste material, and this was confirmed by the analysis of rock fractions from spoil heaps at Broxburn, Winchburgh, West Calder and Seafield. However, oil shale used for the comparison was not directly associated with individual spent oil shale deposits. Considering the elements of environmental significance, such as redox elements and heavy metals, these were mainly found within residual fractions of the rock, or otherwise associated with reducible and oxidisable fractions of rock, including phases such as Fe-Mn oxides or sulphides, which can act as scavengers for trace metals (Tessier et al., 1979). On average 95 % of these trace elements were partitioned within immobile phases within all the samples of spent oil shale analysed. At 3 of the 5 sites, < 5 % of trace elements were located within mobile fractions, < 10 % within reducible or oxidising fractions, with the remaining > 85 % in the residual fraction. For elements partitioned within spent oil shale at the remaining sites, at the Five sisters and Hermand, > 65 % and > 75 % of trace elements were partitioned within residual fractions, respectively and < 10 % within mobile fractions. The remaining < 25 % of trace elements were associated with the reducible/oxidising fractions.

This variation in the partitioning of elements within spent oil shale at different sites is due to the composition of spent oil shale, which can vary as a result of the processing mechanism and source rock variation, and was especially apparent at site 3 and site 5. Indeed, the heterogeneous nature of the spoil heaps extends to the mixing of overburden with the spent oil shale, with elements partitioned within non-residual matter.

Incorporation of soil and vegetation occurred as part of reclamation efforts, in efforts to restore the bing habitats into nature reserves and recreational habitats (Harvie, 2005). However, soils and vegetation also established naturally, and analysis of soils showed a strong contribution of material from the physical breakdown of overburden and spent oil shale, without considerable release of trace elements, with over 97 % of trace elements showing enrichment in soil samples associated with the bings, compared with a control soil.

The mobility of trace elements within Jordanian spent oil shale has been explored previously by the use of leaching studies (Ibrahim et al., 2007), yet did not take into consideration weathering and the heterogeneity of deposits and processing mechanisms (Ibrahim et al., 2007). By considering the concentration and phase association of trace elements within spent oil shale from five different sites in Lothian, Scotland, it was concluded that elements are relatively immobile with respect to natural weathering conditions.

Despite compositional differences between the Lothian and Jordanian oil shale, retorting and combustion processes led to the formation of high temperature crystalline and amorphous silicates, such as mullite (Lothian) and gehlenite (Jordan – Chapter 7), that reside in the residual fraction of the rock. The newly formed silicate minerals are stable with respect to weathering processes, and in addition, chemical weathering was not determined to be a dominant control on the mobility of elements within the Lothian spent oil shale. Due to the greater alkalinity of Jordanian spent oil shale and similarities in resultant mineralogical compositions as a result of high temperature processing, it is predicted that spent oil shale will be stable with respect to the environment. However, future work using sequential extractions on weathered Jordanian spent oil shale is recommended to ensure the stability of this material in the long term.

Chapter 5: Sequestration of CO_2 within Jordanian spent oil shale

5.1 Introduction

The processing of Jordanian oil shale to produce 15,000 barrels of oil per day, has raised concerns over the large amounts of CO_2 produced from the combustion and degradation of organic matter, as well as the decomposition of existing carbonate minerals. CO_2 sequestration by mineralisation has been suggested to be an effective and alternative mechanism for the reduction of CO_2 emissions, by locking away CO_2 in the form of thermodynamically stable carbonate minerals. Many silicate-rich materials may act as a feedstock for carbonation reactions, yet it is postulated that waste materials in particular are more reactive towards the capture of CO_2, due to their alkaline nature and concentrated divalent metal content (Mazzotti, 2005).

In this chapter, Jordanian spent oil shale (J-SOS) has been investigated as a source material for reaction with CO_2. If successful this would enable the use of spent oil shale as a by-product rather than a waste product, by forming a permanent and unreactive carbonate product. Estonian spent oil shale has already been identified as a potential reactant for CO_2 sequestration (Uibu et al., 2009), however as noted in Chapter 2, oil shales vary significantly in their chemistry, mineralogy and physical properties, based on depositional occurrence and conditions. Therefore, to ensure that J-SOS is a suitable feedstock for sequestration procedures, the material was first characterised by X-ray fluorescence (XRF), X-ray diffraction (XRD) and thermogravimetric analysis (TGA) methods as detailed in Chapter 3. The theoretical carbonation was calculated based on these results and accelerated carbonation was achieved by reacting spent oil shale with water and CO_2, at high temperatures and pressures, before the extent of carbonation was calculated.

An in-depth literature review of the progression within carbonate mineralisation research is presented, before moving onto the characterisation study and results of carbonation within spent oil shale.

5.1.1 Carbon capture and storage (CCS)

A brief introduction to the mitigation of anthropogenic emissions was provided in Chapter 1, with a discussion about the options available to reduce CO_2 emission rates, so that global greenhouse gas targets may be met within the next few decades. Carbon capture and storage

in particular is currently receiving increasing levels of attention and funding, yet CO_2 storage within geological reservoirs is not yet established, with concerns about leakage and reservoir stability, and requirements for ongoing, expensive monitoring techniques (Gaus et al., 2005; Metz et al., 2005). When CO_2 is pumped into geological reservoirs underground, preferably at depths of more than 800 m, it exists as a supercritical fluid when pressures and temperatures exceed the critical point at 72.9 bar and 31.1 °C (Benson et al., 2008). Initially, the CO_2 is physically trapped, but over time CO_2 can dissolve in the pore water and react with minerals to form secondary carbonate phases, as has been observed in both experimental and numerical modelling at elevated pressures and temperatures relevant to reservoir conditions (Bateman et al., 2011; Busch et al., 2008; Xu et al., 2005). Over time, the CO_2 is preferentially sequestered by Mg- and Fe-containing minerals (such as siderite, ankerite and magnesite), as well as aragonite [$CaCO_3$], a polymorph of calcite, which in comparison is not stable at very high pressures (e.g. 200 bar). Additionally, CO_2 is able to adsorb to clay minerals and organic matter within shale rocks, acting as another trapping mechanism (Busch et al., 2008; Xu et al., 2005).

An alternative form of carbon storage techniques are accelerated mineralisation reactions, storing CO_2 permanently as thermodynamically stable carbonate minerals. To achieve successful carbonation, there are a few requirements. The first is a material that is rich in Ca- or Mg-containing minerals, in the form of oxides, hydroxides or silicates. A material that is rich in Ca, but in the form of $CaCO_3$ or minerals that are more stable to dissolution (eg. $CaSO_4$) will not react with CO_2. Secondly, water is required for the reaction to proceed, as water acts as a solvent for CO_2 and for the dissolution of metal ions. There is a fine balance between the amount of water and promotion/inhibition of carbonation: too much water causes the diffusion of CO_2 to active surfaces to be reduced; yet too little prevents complete dissolution of mineral phases for carbonate ions to react with (Assima et al., 2013a; Miller et al., 2013).

Accelerated carbonation processes copy the natural mechanisms of silicate weathering that occur on a global scale as part of the carbon cycle, where the rate of silicate dissolution governs the subsequent carbonation reaction. Carbonate rocks contain 40,000 times more carbon than that in the atmosphere, with 79.99 % of global carbon incorporated within carbonate minerals, indicating the suitability of carbonation reactions as a tool to mitigate rising CO_2 levels (Oelkers et al., 2008). Accelerated carbonation may be divided into *in-situ* or *ex-situ* processes. *Ex-situ* carbonation focuses on industrial or accelerated carbonation reactions at the surface, whereas *in-situ* carbonation takes place deep underground within geological reservoirs (Hovelmann et al., 2012a). *In-situ* carbonation has similarities to CCS

techniques, yet accelerates the formation of carbonate minerals by bypassing other trapping mechanisms. CarbFix is an organisation developing methods for *in-situ* carbonation within basaltic rocks in Iceland, involving the testing of CO_2 injection as a miscible single phase, into the rocks. This enables solubility trapping of CO_2, facilitating mineral carbonation by reaction of CO_2 with metal cations leached from the igneous rocks (Aradottir et al., 2011; Benson et al., 2008). Current predictions of *in-situ* carbonation reach ~10 % of reactive material. It is a self-limiting process due to the decrease in porosity as carbonation progresses (Gislason et al., 2010). To increase carbonation repeated, fracturing of the rock is likely to be necessary; however, this endangers the economic feasibility of the *in-situ* process (Hovelmann et al., 2012a).

5.1.2 Mechanism

The mechanism of carbonation can be pictured simply as an acid-base neutralisation reaction, for example the basic Mg/Ca oxide and hydroxide minerals readily react with carbonate ions, formed from the dissolution of carbonic acid (Shriver et al., 2009). This results in the production of a carbonate precipitate and water, expressed for Ca-hydroxide in Eq. 5.1.

$$Ca(OH)_2 + H_2CO_3 \rightarrow CaCO_3 + 2H_2O \qquad \text{Eq. 5.1}$$

Several steps can be discerned by looking at this reaction in more detail. Firstly, gaseous CO_2 dissolves into water, causing a drop in pH and formation of carbonic acid, that dissociates into bicarbonate and carbonate ions, as indicated in the Bjerrum plot (Figure 5.1 and Eq. 5.2, 5.3, 5.4). The amount of CO_2 that dissolves in water is dependent on both the pressure and temperature, where the concentration of H_2CO_3 is proportional to the partial pressure of CO_2, according to Henry's law (Shriver, 2009).

$$CO_{2(g)} \rightleftharpoons CO_{2(aq)} \qquad \text{Eq. 5.2}$$

$$CO_{2(aq)} + H_2O_{(l)} \rightleftharpoons H_2CO_{3(aq)} \qquad \text{Eq. 5.3}$$

$$H_2CO_{3(aq)} \rightleftharpoons H^+_{(aq)} + HCO_3{}^-_{(aq)} \qquad \text{Eq. 5.4}$$

$$HCO_3{}^-_{(aq)} \rightleftharpoons H^+_{(aq)} + CO_3{}^{2-}_{(aq)} \qquad \text{Eq. 5.5}$$

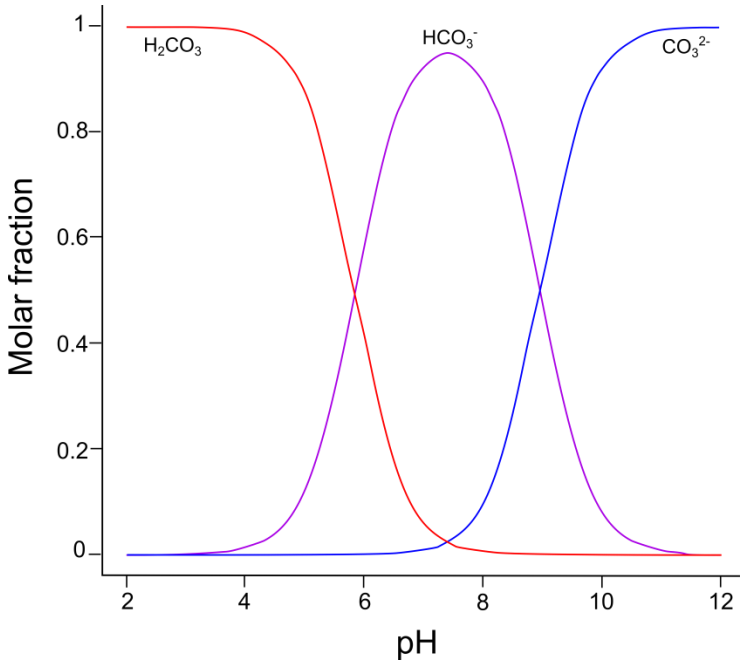

Figure 5.1 - *Bjerrum plot showing pH dependence of H_2CO_3 - HCO_3^- - CO_3^{2-} system.*

The drop in pH results in the dissolution of basic oxide, hydroxide, and silicate minerals, consuming protons and producing more alkaline conditions (Eq. 5.6; Schramke, 1992).

$$Ca(OH)_2 + 2H^+ \rightleftharpoons Ca^{2+} + 2H_2O \qquad \text{Eq. 5.6}$$

The divalent cations in solution readily react with carbonate anions that now exceed the solubility product, resulting in the formation of carbonate minerals (Eq. 5.7) and reducing the pH. In alkaline conditions, equilibrium is kept towards the formation of carbonate minerals with high concentrations of CO_3^{2-} (Dietzel et al., 1992) that are insoluble at pH > 9 (Uibu et al., 2009).

$$Ca^{2+} + {CO_3}^{2-} \rightleftharpoons CaCO_3 \qquad \text{Eq. 5.7}$$

Oxides/hydroxides

Lime (CaO) and portlandite ($Ca(OH)_2$), are reactive towards carbonation and do not require pre-treatment, and 88 % carbonation of portlandite occurs with water and CO_2, in atmospheric conditions (Morales-Florez et al., 2011). CaO, is one of the principle materials of focus for CO_2 sequestration reactions, and is already in use in other applications, such as the Bayer process to produce alumina (Xu et al., 1998). Magnesium ions (Mg^{2+}) have a greater energy of dehydration, compared to Ca^{2+} (Mingos, 1998). Therefore, MgO is less reactive to carbonation in aqueous conditions, and magnesite and dolomite rarely form at ambient temperatures (Saldi et al., 2009). However, this also means that the mineral's Mg ions form are stronger and

more stable, a preferential property for permanent sequestration. Also greater amounts of CO_2 are able to be sequestered using the same weight of Mg compared to Ca (0.9 tonnes of MgO are required, compared to 1.3 tonnes of CaO to sequester one tonne of CO_2) (Huijgen, 2003).

Basic oxide and hydroxide minerals are rare in nature, because they are naturally very reactive (Jacobs and Hitch, 2011); however, the mechanism of carbonation also extends to the more available silicate minerals, so long as they produce divalent cations on dissolution, preferably Mg or Ca (Lackner, 2002). Other cations such as the alkali metals will produce carbonates that are more soluble, whereas transition metals, such as Fe, tend to occur at concentrations too low to be viable for carbonation (Lackner et al., 1995).

5.1.3 Thermodynamics and kinetics

The thermodynamics for the carbonation reaction is favourable for oxide, hydroxide and silicate minerals, at standard pressure and temperature (Lackner et al., 1995). Due to the exothermic nature of the reaction, heat is produced as the reaction proceeds. The Gibb's free energy (ΔG^{θ}) data for oxide and silicate minerals is provided in Table 5.1, showing the greater preference for carbonation of oxide minerals compared to the silicates, due to the relative stability of the reaction products compared to the reactants. Values for the stability of reaction products can be compared to the combustion of carbon, that has a Gibb's free energy of ΔG^{θ} = -394 kJ/mol (Prigiobbe et al., 2009; Lackner et al., 1995). The reverse calcination reaction is endothermic, and therefore requires heat to proceed, reiterating the stability of the newly formed carbonate minerals (Stanmore et al., 2005).

Table 5.1 - *Gibb's free energy data for the reaction of CO_2 with different minerals (Lackner et al., 1995).*

Mineral	Forward reaction	Gibbs free energy, ΔG^{θ}
Lime	$CaO + CO_2 \rightarrow CaCO_3$	-179 kJ/mol
Periclase	$MgO + CO_2 \rightarrow MgCO_3$	-118 kJ/mol
Olivine	$Mg_2SiO_4 + 2CO_2 \rightarrow 2MgCO_3 + SiO_2$	-89 kJ/mol
Wollastonite	$CaSiO_3 + CO_2 \rightarrow CaCO_3 + SiO_2$	-90 kJ/mol
Serpentine	$Mg_3Si_2O_5(OH)_4 + 3CO_2 \rightarrow 2MgCO_3 + 2SiO_2 + H_2O$	-64 kJ/mol

However, despite the favourable thermodynamics, reaction kinetics for carbonation are notoriously slow with reactions occurring very slowly in nature; therefore a large proportion of related research is investigating methods of optimisation to identify conditions that are

feasible on an industrial and economical time scale, so that CO_2 may be stored efficiently and effectively (Gerdemann et al., 2007; Thiery et al., 2007; Seifritz, 1990; O'Connor, 1999). These include: increasing the pressure and temperature, varying the water content, and increasing the surface area, as discussed further in Chapter 6.

5.1.4 Silicates

The CO_2 sequestration by the energetically favourable transformation of silicate minerals into stable carbonate minerals, by accelerating natural weathering processes that occur on geological time-scales, was first proposed by correspondence by Seifritz (1990). Further considerations and viability analysis was carried out by Lackner et al. (1995) based on the knowledge of abundant igneous mineral reserves, coupled with a need to reduce CO_2 emissions. It is estimated that 65 x 10^6 tonnes of CO_2 could be sequestered per year by placing ground silicate-containing rocks on agricultural land and forested areas, however this is realistically estimated to be < 0.1 % of anthropogenic emissions with current procedures and technologies (Hartmann et al., 2008).

Carbonation of silicates can be achieved by direct or indirect methods, where slow rates are encountered due to the rate-limiting silicate dissolution step (Prigiobbe et al., 2009). Direct aqueous sequestration involves high temperatures and pressures to increase the rate of reaction, whereas indirect methods use extractants to dissolve the metal cations, before carbonation in a separate step. Initial experiments used HCl as an extractant with serpentine, producing brucite that could then be carbonated; however pre-treatment steps are also required, to increase the reactivity of the silicate feedstock (Lackner et al., 1997). Mechanical or thermal pre-treatment techniques are commonly used; where the surface area of solids is increased by grinding to a fine particle size, or solids are heated to temperatures > 600 °C, removing water and increasing the porosity of material (Gerdemann et al., 2007). Increasing the surface area has been shown to increase the conversion rate from 10 % to 90 % within olivine, when carbonated for 24 hours, at 185 °C and 115 bar (O'Connor, 1999). Carbonation of thermally treated serpentine has been achieved at 185 °C and 115 bar also, however in this case $NaCl/Na_2CO_3$ was also used to speed up the reaction by promoting the leaching of metal cations from silicates (Jo et al., 2012; Alexander et al., 2007). Wollastonite is more reactive than olivine or serpentine, and therefore sequesters CO_2 at lower temperatures and pressures. For example, 82 % carbonation was achieved at 80 °C, 86 bar, for 6 hours (Tai et al., 2006), and 72 % outside of supercritical conditions at 200 °C, 40 bar, for 1 hour (Huijgen et al., 2006). The pre-treatment of silicates uses considerable amounts of energy, and thermal treatment at

600 °C alone could add up to $100/tonne of CO_2 sequestered, lowering the economic feasibility of sequestration within silicate feedstock (Jacobs and Hitch, 2011).

5.1.5 Industrial material carbonation

High costs associated with silicate carbonation, mining and transport have led to suggestions of the utilisation of industrial processing wastes or mining tailings (Kelly et al., 2011). Although the volume of reactive material is much less, industrial wastes are readily available and offer greater potential for carbonation. They are commonly more reactive towards mineralisation due to their alkaline nature and divalent cation concentration, hence pre-treatment, indirect mechanisms and intensive reaction conditions are not required to achieve sufficient levels of carbonation (Table 5.2; Bobicki et al., 2012). In addition, mining is not required, and waste materials are usually located close to CO_2 emission sources, resulting in lower costs for sequestration of CO_2 (Huijgen et al., 2005).

Natural sequestration has been suggested by the use of artificial soils, such as disused industrial land modified by the addition of Ca-rich waste materials (Renforth et al., 2009). These sites can contain Ca-silicate minerals and portlandite, at high pH, which are able to react with organic carbon derived from plants, to form carbonate minerals, which if implemented on a global scale could yield a maximum sequestration of 290 Mt C/year, mitigating the amount of natural emissions from the soil as part of the natural carbon cycle (Renforth et al., 2009; Kuzyakov et al., 2000).

Due to the greater stability of $MgCO_3$ in comparison to $CaCO_3$, and their greater abundance within mine wastes, $MgCO_3$ has been the object of experimental investigations of mine tailings in Canada, using enhanced carbonation techniques, by reacting ultramafic mine tailings with CO_2 at atmospheric temperature and pressure (Harrison et al., 2013; Power et al., 2013; Jacobs and Hitch, 2011). Metastable Mg-carbonate minerals, such as dypingite, nesquehonite and hydromagnesite, are commonly precipitated by accelerated carbonation processes, being kinetically favoured over magnesite formation (Surface et al., 2013; Hovelmann et al., 2012b; Zhao et al., 2010). However, due to the thermodynamic instability, over time they will convert to magnesite (Prigiobbe et al., 2009). In addition, magnesite will form from serpentine minerals in hydrothermal conditions, and has been observed to form at low temperatures using supercritical conditions (Klein et al., 2013; Felmy et al., 2012).

A wide variety of waste materials have been considered for sequestration of CO_2, including: asbestos tailings, bauxite, biomass ash, blast furnace slag, cement kiln dust, clinical waste

incineration ash, coal fly ash, municipal solid incineration fly ash/bottom ash, nickel tailings, oil shale ash, paper sludge incineration ash, phosphogypsum, pulverised fuel ash, red mud, sewage sludge ash, steel slag, steel wastewater sludge, waste cement and wood ash (Bobicki et al., 2012; Sanna et al., 2012; Cardenas-Escudero et al., 2011; Gunning et al., 2010). Reported conditions for the carbonation of waste materials are given in Table 5.2, showing the variety of conditions used to achieve CO_2 sequestration and the difference in the amount of carbonation that can be achieved. A high extent of carbonation may be achieved using steel slag, waste cement and cement bypass dust, paper sludge incineration ash and coal fly ash, however, steel slag and waste cement requires grinding, papersludge incinerator ash is only available in small quantities, and coal fly ash has a low overall CO_2 sequestration capacity. Oil shale ash on the other hand has a high CO_2 sequestration capacity and does not need grinding (Bobicki et al., 2012). Results from two comprehensive studies of the carbonation of various wastes places the potential for CO_2 sequestration in the UK from 200,000 tonnes of CO_2 (Gunning et al., 2010), up to 1 Mtonne CO_2/year (Sanna et al., 2012).

Other considerations to take into account for the process of carbonation are the use of large amounts of energy. Therefore, cost analysis will be required for each individual industrial carbonation process, as it is dependent on: the volume of waste; the location of the carbonation plant in relation to the emissions point; the chemical composition of the material and the level of pre-treatment required; the technology used for carbonation; the amount of water needed; the storage site; the suitability of material for use in other industries as a by-product; and the CO_2 emissions credits that can be gained by reduction in emissions (Sanna et al., 2012). Even if the potential for CO_2 sequestration is low, other benefits that can occur as a result of the carbonation of waste materials in particular are the decrease in potential for leaching of potentially harmful metals, and the improvement of physical properties if to be used in industry, for example in construction (Gunning et al., 2010).

Table 5.2 - *Experimental conditions and CO_2 sequestered using different waste materials. Optimum conditions are reported, providing the greatest extent of carbonation observed. The extent of carbonation was calculated using Ca and Mg data only. RH = relative humidity, achieved using NaCl.*

Type	P	T	Duration	Water	Other	Ca and Mg, wt %	wt % CO_2	Extent	Reference
Steel slag	19 bar	100 °C	30 mins	1:2	< 38 µm	CaO = 31.7 MgO = 6	15.5 %	58 %	Huijgen et al., 2005
Papersludge incineration ash	2 bar	room	72 hrs	paste	RH 75 %	CaO = 67.4 MgO = 2.1	26 %	64 %	Gunning et al., 2010
Cement bypass dust						CaO = 66.3 MgO = 1.1	25 %	63 %	
MSWI fly ash						CaO = 32.1 MgO = 3.4	7 %	26 %	
Waste cement	4 bar	room	48 mins	0.5	80 µm	CaO = 25.2 MgO = 0.3	16.5 %	98 %	Teramura et al., 2000
MSWI fly ash	3 bar	room	3 hrs	0.3	RH 75 %	CaO = 36.27 MgO = 0.28	7-10 %	< 39 %	Li et al., 2007
MSWI bottom ash	17 bar	room	3.5 hrs	0.2	< 4 mm	CaO = 16.3 MgO =2.6	2.9 %	19 %	Rendek et al., 2006
Coal fly ash	10 bar	30 °C	18 hrs	1:10		CaO = 4.1	2.6 %	83 %	Montes-Hernandez et al., 2009
Spent oil shale	atm	room	1 hr	1:10	15 % $CO_{2(g)}$	CaO = 47.59 MgO = 13.65	15.51 %	35 %	Uibu et al., 2009

5.1.6 Approach

Estonian spent oil shale has been used in experimental CO_2 sequestration by Uibu et al. (2009). The spent oil shale was obtained from pulverised firing (PF) or circulating fluidised bed combustion (CFBC), as oil shale in Estonia is used primarily for electricity production, rather than the extraction of oil by retorting. The experiments were carried out at room temperature and pressure, using flue gas with 10–15 % CO_2, and a solid:water ratio of 1:10 (Table 5.2). The CO_2 reacted with Ca- and Mg-oxides, hydroxides and silicates, present at high concentrations within Estonian spent oil shale. Carbonation was achieved and was greater for Ca-containing minerals compared to Mg-containing minerals. The carbonation also appeared to be more dependent on the porosity of the material. The extent of carbonation in CFBC was greater than PF, owing to reduced porosity within PF caused by sintering. The research sequestered 290 kg CO_2/tonne of rock, by passing flue gas through the aqueous mixture. This is compared to just 22 kg CO_2/tonne for natural weathering – which only occurs within the top few cms of deposits, due to slow diffusion of CO_2 through sediments (Uibu et al., 2011; Motlep et al., 2010; Uibu et al., 2009).

This present research aims to suggest a method which utilises the Jordanian spent oil shale to permanently sequester CO_2. This would not only reduce CO_2 emissions significantly, but also uses a material which would otherwise be deposited as mine-backfill. Carbonation reactions were carried out using supercritical CO_2 (high pressures and temperatures) which may increase the extent of carbonation, by increasing CO_2 access to active surfaces and increasing dissolution rates. In addition, particle size is considered less important under supercritical conditions due to beneficial properties of the fluids, where the fluid is dense like a liquid, but has gaseous properties (Das, 1989). Using the ATP process, oil shale is crushed to particle size 6-8 mm (Brandt, 2009) and then retorted. The use of supercritical CO_2 negates the need for further energy-intensive pre-processing treatments, such as crushing, grinding or chemical activation. Water is required for the carbonation process, and further implications of the reaction conditions are considered in future chapters, where carbonation by supercritical conditions is compared to subcritical conditions. The amount of carbonation achieved was analysed using quantitative thermogravimetric analysis and the extent of carbonation with respect to the calculated theoretical carbonation was determined.

5.2 Methodology

Crushed samples of Jordanian Oil Shale (J-OS) and Jordanian Spent Oil Shale (J-SOS), of size fraction < 2 cm, were provided by Jordan Energy and Mining Ltd (JEML). The J-OS was mined from the Al-Lajjun deposit, and J-SOS was produced from a test-run of the ATP (Alberta Tacuik Process) batch retort, undertaken by UMATAC industrial processes (Calgary, AB, Canada) in 2009. Samples of Jordanian oil shale (J-OS) were heated in a furnace at 500 °C and 700 °C, producing the combusted samples (J-OS 500) and (J-OS 700) respectively.

5.2.1 Characterisation

X-ray fluorescence (XRF), X-ray diffraction (XRD) and thermogravimetric analysis (TGA) were carried out as detailed in Chapters 2 and 3 and Appendix A. TGA was used for quantitative analysis of the amount of carbonate minerals within spent oil shale and carbonated spent oil shale, and therefore the samples were heated at a slower rate of 10 °C/min compared to 20 °C/min as used for analysis in Chapter 3.

The schematic in Figure 5.2 shows the relationship between the samples used to analyse the change in carbonate content by thermogravimetric analysis (TGA).

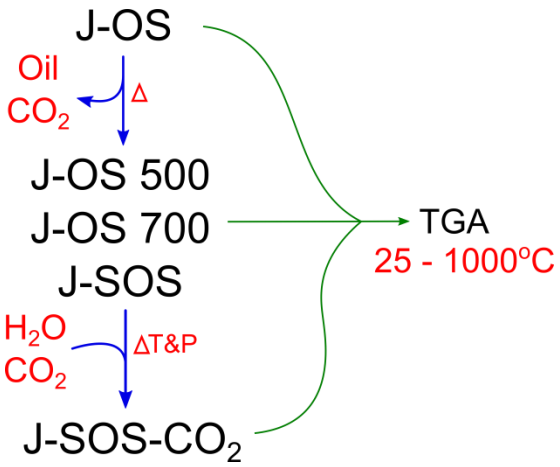

Figure 5.2 – *Schematic showing the relationship between samples and processes.*

Thermogravimetric analysis (TGA) is an accurate, sensitive, and reproducible analytical method that has been used in this study to determine the concentration of carbonate minerals, within samples of J-SOS and J-SOS-CO_2. The decomposition of the carbonate minerals, calcite [$CaCO_3$] and dolomite [$CaMg(CO_3)_2$], occurs by the following reactions, at temperatures from 600 °C, resulting in a solid residue of CaO and MgO, and emitting gaseous CO_2:

$$CaCO_{3(s)} \xrightarrow{\Delta} CaO_{(s)} + CO_{2(g)} \quad \text{Eq. 5.8}$$

$$CaMg(CO_3)_2 \xrightarrow{\Delta} CaCO_3 + MgO + CO_2 \xrightarrow{\Delta} CaO_{(s)} + CO_{2(g)} \quad \text{Eq. 5.9}$$

Assuming that no other minerals are contributing to the weight loss > 600 °C, or that their contribution is negligible, then the amount of carbonate can be calculated based on the weight loss and the stoichiometry of the decomposition reaction, using the molecular weight (M_r) of each of the compounds. Each mole of CO_2 reacts with one mole of $M^{II}O$ (CaO or MgO), so that the percentage weight (wt %) of CO_2 added by carbonation is equal to the wt % of CO_2 lost in the TGA at temperatures > 600 °C.

Errors

While TGA is an analytical tool commonly associated with quantification techniques, it is necessary to determine any error that may be caused by the instrument, sample heterogeneity, or processing; to identify whether the technique is suitable, in this instance for quantitative analysis of carbonate minerals within spent oil shale.

To minimise errors, the same analytical parameters were used in each thermogravimetric analysis, chosen based on an understanding of the: chemical and physical properties of the solid sample, the high accuracy of measurement required, and the operating conditions within the instrument itself. Important factors that can especially influence the weight loss curve for spent oil shale decomposition, include, but are not limited to: the heating rate; the furnace atmosphere; and the sample mass/particle size (Brown, 2001). Firstly, a heating rate which was sensitive to changes in mass whilst retaining a sufficient turnaround time for the large number of samples analysed was necessary. Additionally, it was observed that the onset of decomposition decreases as the heating rate is lowered, therefore reiterating the importance of analysing samples using the same conditions to be comparable (Villain et al., 2007). Secondly, an inert, dynamic atmosphere was also required, to remove gases from the furnace, so that reactions between the sample and the evolved gases did not occur. Furthermore, the sample mass and particle size were shown to influence the extent of decomposition and the degree of evolved gases; hence, these were kept as constant as possible to reduce the sources of error (Rajeshwar, 1983). It was also important to take into account the heterogeneity of spent oil shale; therefore a high mass thermogravimetric analyser was used, capable of heating samples up to 400 mg. This reduces error from heterogeneity; however it must be acknowledged that the error is not completely removed.

To calculate the error associated with thermogravimetric analysis, three procedural replicates were used for each experiment, and analytical replicates were used to calculate instrumental and sample error, using calcium oxalate and spent oil shale, respectively. The mean (μ), variance, and standard deviation (σ) were calculated for the weight loss associated with carbonate decomposition, and then the coefficient of variance (CV) was calculated using Equation 5.10, which was used to express the experimental error with 95 % confidence:

$$CV = \frac{2\sigma}{\mu} \qquad \text{Eq. 5.10}$$

The instrumental error was determined by using calcium oxalate [CaC_2O_4], a common standard. This was chosen because of its homogenous composition and well defined weight loss regions, including a weight loss step due to carbonate decomposition. The same experimental conditions were used as in the sample analysis (heating rate of 10 °C/min, N_2 purge gas, 25-1000 °C). The sample error was identified by repeating the analysis of J-SOS, to test for the effect of heterogeneity.

The processing error was determined by the use of J-SOS that underwent carbonation and analysis using the same conditions (Table 5.3), to investigate the cumulative experimental error that can be caused by experimental variation, such as: weighing and transferring of samples; the addition and distribution of water; the distribution of heat to samples within the pressure vessel; any slight variations in the measurement of processing conditions used (temperature, pressure, duration); and time spent ramping up and depressurising. These factors could all could play a part in the variability of carbonation accomplished.

Table 5.3 - *Method used for the calculation of instrumental, sample and processing error. A, B, and C are separate experimental runs, operated under the same conditions.*

Error	Sample	TGA runs
Instrumental	Ca-oxalate	x 3
Sample	J-SOS	x 3
Processing	J-SOS-CO_2 A	x 1
	J-SOS-CO_2 B	x 1
	J-SOS-CO_2 C	x 1

5.2.2 Carbonation

Initial experiments were conducted by measuring 2 g of unground J-SOS of particle size < 2 cm followed by the addition of 0.4 ml deionised water and sealing in a pressure vessel at 100 bar and 60 °C for 6 hours. In subsequent experiments, samples were prepared by grinding to a fine particle size (< 1 mm) using an agate pestle and mortar, before varying amounts of deionised water (0-10 ml) were added to the 1 g samples. These were held for 24 hours, at 100 bar and 80 °C. High pressures and temperatures were obtained using the 4760 Parr 5L external pressure vessel and temperature controller, connected to a Thar CO_2 delivery system (Figure 5.3). Samples were recovered and dried at 105 °C to remove any water, before analysis by TGA. Carbonated samples are referred to as J-SOS-CO_2, and the conditions for formation of carbonated spent oil shale are provided in Table 5.4.

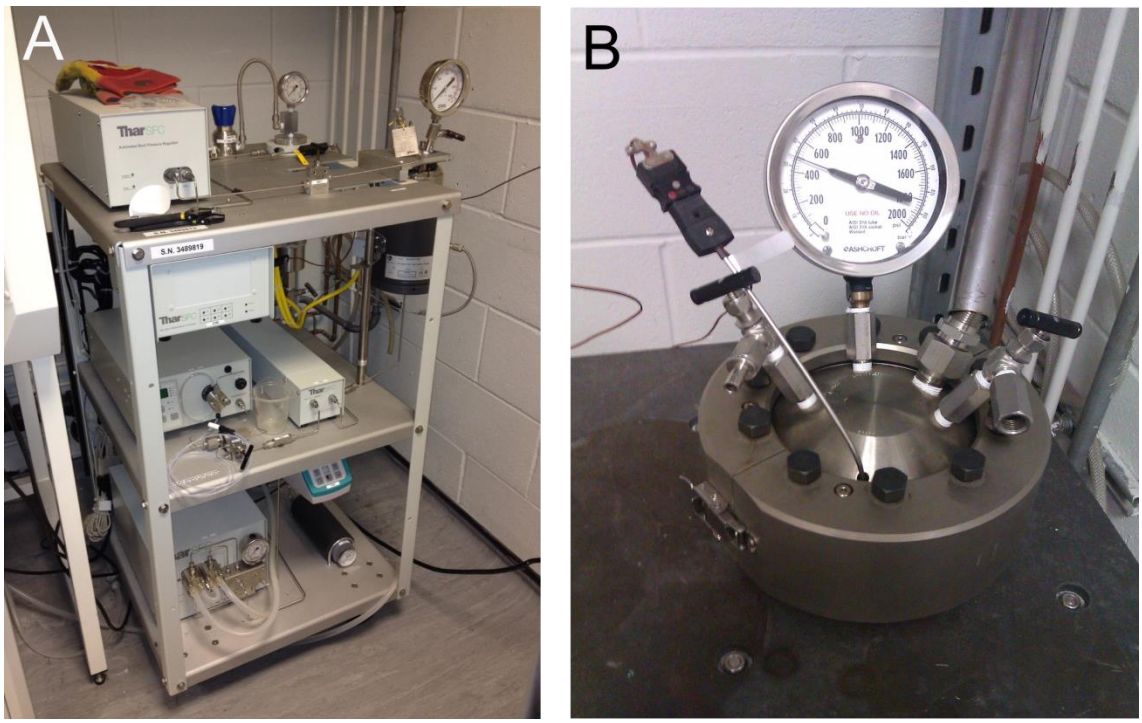

Figure 5.3 – *CO_2 delivery rig (A) and 5 L high pressure vessel (B) used in the carbonation studies.*

Table 5.4 - *Experimental parameters used in the carbonation of J-SOS.*

Sample Name	Particle Size	Mass	Pressure	Temperature	Duration	Water
J-SOS-dry	Unground	50 g	80 bar	40 °C	6 hrs	0 ml
J-SOS-wet	Unground	50 g	77.5 bar	40 °C	6 hrs	20 ml
J-SOS-CO_2-1	Unground	2 g	96.5 bar	60 °C	24 hrs	0.4 ml
J-SOS-CO_2-2						
J-SOS-CO_2-3						
J-SOS-CO_2-A-0.1	Ground	1 g	100 bar	80 °C	24 hrs	0.1 ml
J-SOS-CO_2-B-0.1						
J-SOS-CO_2-A-0.2	Ground	1 g	100 bar	80 °C	24 hrs	0.2 ml
J-SOS-CO_2-B-0.2						
J-SOS-CO_2-A-0.3	Ground	1 g	100 bar	80 °C	24 hrs	0.3 ml
J-SOS-CO_2-B-0.3						
J-SOS-CO_2-A-0.4	Ground	1 g	100 bar	80 °C	24 hrs	0.4 ml
J-SOS-CO_2-B-0.4						
J-SOS-CO_2-A-0.5	Ground	1 g	100 bar	80 °C	24 hrs	0.5 ml
J-SOS-CO_2-B-0.5						
J-SOS-CO_2-A-0.6	Ground	1 g	100 bar	80 °C	24 hrs	0.6 ml
J-SOS-CO_2-B-0.6						
J-SOS-CO_2-A-0.7	Ground	1 g	100 bar	80 °C	24 hrs	0.7 ml
J-SOS-CO_2-B-0.7						
J-SOS-CO_2-A-0.8	Ground	1 g	100 bar	80 °C	24 hrs	0.8 ml
J-SOS-CO_2-B-0.8						
J-SOS-CO_2-A-0.9	Ground	1 g	100 bar	80 °C	24 hrs	0.9 ml
J-SOS-CO_2-B-0.9						
J-SOS-CO_2-A-1	Ground	1 g	100 bar	80 °C	24 hrs	1 ml
J-SOS-CO_2-B-1						
J-SOS-CO_2-C-1						
J-SOS-CO_2-D-1						
J-SOS-CO_2-C-2	Ground	1 g	100 bar	80 °C	24 hrs	2 ml
J-SOS-CO_2-D-2						
J-SOS-CO_2-C-3	Ground	1 g	100 bar	80 °C	24 hrs	3 ml
J-SOS-CO_2-D-3						
J-SOS-CO_2-C-4	Ground	1 g	100 bar	80 °C	24 hrs	4 ml
J-SOS-CO_2-D-4						
J-SOS-CO_2-C-5	Ground	1 g	100 bar	80 °C	24 hrs	5 ml
J-SOS-CO_2-C-6	Ground	1 g	100 bar	80 °C	24 hrs	6 ml
J-SOS-CO_2-D-7	Ground	1 g	100 bar	80 °C	24 hrs	7 ml
J-SOS-CO_2-C-8	Ground	1 g	100 bar	80 °C	24 hrs	8 ml
J-SOS-CO_2-D-8						
J-SOS-CO_2-C-9	Ground	1 g	100 bar	80 °C	24 hrs	9 ml
J-SOS-CO_2-D-9						
J-SOS-CO_2-C-10	Ground	1 g	100 bar	80 °C	24 hrs	10 ml
J-SOS-CO_2-D-10						

5.2.3 Theoretical carbonation

Two methods were used to determine the theoretical carbonation of spent oil shale, the choice of which will be discussed further in Section 5.4.

Method 1 – Divalent cations

The theoretical carbonation was calculated using the concentration of divalent cations present within the material that may be available for carbonation by the following method:

1. Using XRF data, the concentration of total divalent metal oxides ($M^{II}O$) was calculated, in wt %. Divalent cations included Mg and Ca.

$$MeO_T = MgO_T + CaO_T \quad \text{Eq. 5.11}$$

2. The concentration of $M^{II}O$ was converted into sequestered CO_2 (% CO_2), in wt %, based on the molar quantities of CO_2 consumed in the carbonation reaction (Eq. 5.8, 5.9)

$$(\%\, CO_2)_T = \left(CaO_T * \frac{M_w CO_2}{M_w CaO}\right) + \left(MgO_T * \frac{M_w CO_2}{M_w MgO}\right) \quad \text{Eq. 5.12}$$

The terms used in the equation are explained in Table 5.5.

Table 5.5 - *Terms used in Equations 5.11 to 5.14.*

$M^{II}O_T$	Total concentration of divalent metal oxide
$M^{II}O_A$	Concentration of metal oxide available for CO_2 sequestration
% CO_2	Sequestration potential of J-SOS for CO_2

This method assumes that all the divalent cations are available for reaction with CO_2 and therefore a more accurate calculation is provided in method 2.

Method 2 – Corrected

The method for calculating the theoretical carbonation was modified based on knowledge of the mineralogy and concentration of divalent cations present (Gunning et al., 2010). The concentration of $CaCO_3$, $CaSO_4$ and $Ca_5(PO_4)_3(F,OH)$ within J-SOS was incorporated into the calculation:

1. Using XRF, the concentration of total CaO and MgO was calculated, in wt %.

2. Using TGA, the concentration of $CaCO_3$ was determined using the weight loss between 600-950 °C, before it was then converted into concentration of CaO, in wt %.

3. Using XRF, the concentration of $CaSO_4$ and $Ca_5(PO_4)_3(F,OH)$ were calculated assuming that all the sulphur and phosphate ions present react with available Ca-ions, and converted into concentration of CaO, in wt %.

4. The concentration of available CaO was calculated, in wt % and the total concentration of available metal oxides was determined.

$$MeO_A = MgO_T + \left[CaO_T - \left(CO_2 * \frac{M_w CaO}{M_w CO_2}\right) - \left(SO_3 * \frac{M_w CaO}{M_w SO_3}\right) - \left(P_2O_5 * \frac{10 M_w CaO}{3 M_w P_2O_5}\right)\right]$$

Eq. 5.13

5. The concentration of $M^{II}O$ was converted into sequestered CO_2 (% CO_2)

$$(\%\, CO_2)_T = CaO_A * \frac{M_w CO_2}{M_w CaO} + MgO_T * \frac{M_w CO_2}{M_w MgO}$$

Eq. 5.14

5.2.4 Extent of carbonation

Comparison of the experimental amount of CO_2 sequestered, to the calculated theoretical sequestration, was achieved to determine the extent of carbonation. Firstly, the experimental CO_2 sequestration value was calculated, based on the weight loss of carbonate minerals between 600-950 °C.

$$\Delta\%\, CO_2 = wt\ \%\ J\text{-}SOS_{600-950\,°C} - wt\ \%\ J\text{-}SOS\text{-}CO_{2\ 600-950\,°C}$$

Eq. 5.15

The extra CO_2 produced during thermogravimetric analysis of J-SOS-CO_2, was attributed to a gain in $CaCO_3$ or $MgCO_3$, assuming that no other minerals decompose within this temperature range. The extent of carbonation was then calculated based on methods by Huijgen and Uibu but with extra modifications specifically for carbonating spent oil shale and the analytical process used (Uibu et al., 2009; Huijgen et al., 2005):

1. The theoretical carbonation potential of J-SOS was calculated based on the concentration of available divalent cations.

2. The carbonation achieved by experimental techniques was determined by measuring the difference in carbonate content between J-SOS and J-SOS-CO_2, in Δ% CO_2 (Equation 5.15).

3. The Δ% CO_2 was corrected by accounting for the mass change from fresh to carbonated spent oil shale. Assuming that the only gain in weight was due to CO_2, the unreacted material has a mass of 100 %, while the reacted material has a mass of (100 + CO_2) %, therefore this is used to accurately calculate the CO_2 within spent oil shale (Fernandez Bertos et al., 2004).

4. The extent of carbonation was calculated.

$$\% \, Extent = \left[\frac{\left(\frac{\Delta \% CO_2}{100 - \Delta \% CO_2} \right) * 100}{CaO_A * \frac{M_W CO_2}{M_W CaO} + MgO_A * \frac{M_W CO_2}{M_W MgO}} \right] * 100 \qquad \text{Eq. 5.16}$$

5.3 Results

Firstly, results from the characterisation study on Jordanian spent oil shale, by TGA, XRF and XRD, (Chapter 3) were provided in more detail so that the suitability of this material for CO_2 sequestration by carbonation could be confirmed. Secondly, compositional changes occurring within the material on carbonation are detailed, and the results of the carbonation study are used to calculate the extent of carbonation, in comparison to the theoretical carbonation.

5.3.1 Characterisation

The concentration of divalent cations, necessary for carbonation, was calculated using results from XRF analysis (Table 5.6). The concentration of CaO and MgO, in weight percentage (wt %) were determined to be 31.52 wt % and 1.93 wt % respectively. These concentrations can be expressed as 22.53 wt % Ca^{2+} and 1.16 wt % Mg^{2+} (or 5.62 mol/kg and 0.477 mol/kg respectively).

Table 5.6 - *Major elemental concentrations within J-SOS, in wt %, with errors estimated at < 2 wt % for the individual sample.*

SiO_2	32.61	**CaO**	31.52
TiO_2	0.16	**Na_2O**	0.25
Al_2O_3	3.59	**K_2O**	0.533
Fe_2O_3	1.94	**P_2O_5**	3.486
MnO	0.011	**SO_3**	4.365
MgO	1.93	**LOI**	19.05
		TOTAL	**99.43**

In addition to the major elemental composition, XRD methods were used to determine the mineralogy of spent oil shale, to be able to calculate the theoretical carbonation potential of spent oil shale more accurately (Figure 5.4). Major minerals present include calcite, quartz, ettringite and apatite, with lesser amounts of anhydrite and Fe-oxides. Other high temperature phases may be present, such as Ca/Mg-oxides and Ca-silicates, but these were difficult to distinguish from the XRD pattern.

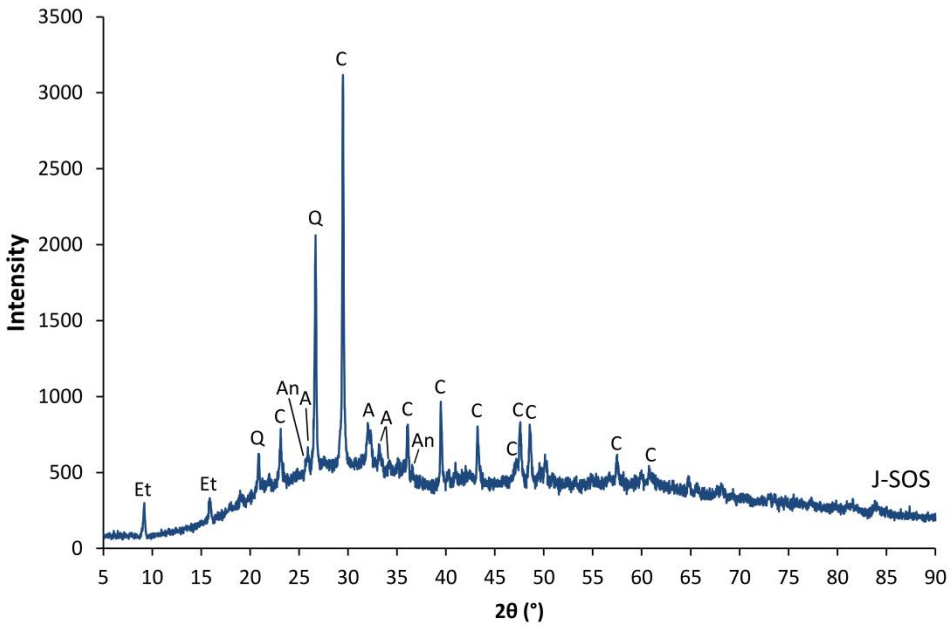

Figure 5.4 - *XRD pattern of J-SOS. Minerals identified included: C= calcite, Et = ettringite, An = anhydrite, A = apatite and Q = quartz.*

The weight loss due to carbonate mineral decomposition between 600-950 °C was identified from the thermogravimetric weight loss profile for J-SOS (Figure 5.5) and the concentration of CO_2 released was determined to be 13.14 wt % +/- 0.15 wt % based on replicates. The derivative of the curve provides the rate of change of decomposition, and a peak identified at ~800 °C clearly signifies the increase in weight loss due to breakdown of carbonate minerals.

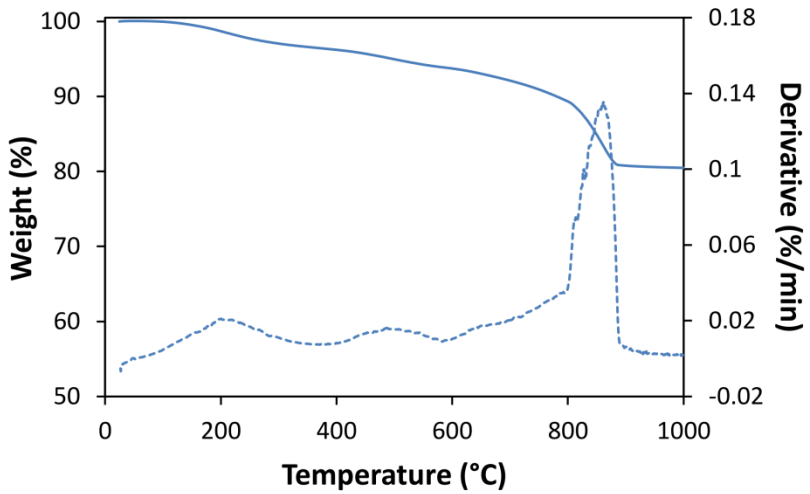

Figure 5.5 – *Thermogravimetric weight loss profile for J-SOS (solid line), including the derivative (dashed line).*

5.3.2 Theoretical carbonation

The theoretical carbonation was calculated based on the compositional analysis of J-SOS, while the amount of CO_2 sequestered experimentally was determined by TGA analysis of the carbonated product. From this data the extent of carbonation was calculated to provide an indication of the success of the carbonation reaction. XRF results confirm that the material has high concentrations of metal cations, with a theoretical CO_2 sequestration limit of 26.84 wt % CO_2 if able to react fully with Ca and Mg ions to form carbonate minerals. A corrected theoretical carbonation potential was calculated to be 7.70 wt % CO_2, with 29 % of the total $M^{II}O$ content available for carbonation, due to Ca taken up in the minerals calcite, apatite and ettringite.

5.3.3 Experimental carbonation

The compositional changes occurring after combustion and subsequent carbonation were monitored using XRD (Figure 5.6), and the greatest observed changes were: the appearance of reflections due to the formation of sulphate minerals; and decreasing calcite content as combustion temperature increases. Although no sulphur containing minerals were detected

within J-OS, three samples of combusted J-OS all show sulphate phases, indicating that the organic matter acts as a source for sulphur that is not removed in the retorting process. J-OS combusted at 500 °C and 700 °C showed increasing amounts of grossite [$CaAl_4O_7$] and anhydrite [$CaSO_4$]. However, within J-SOS the major sulphate phase was ettringite [$Ca_6Al_2(SO_3)_3(OH)_{12}.26H_2O$]. After carbonation, J-SOS-CO_2 showed a reflection corresponding to bassanite [$CaSO_4.0.5H_2O$], a partially hydrated sulphate mineral which is an indication that ettringite has decomposed to form this mineral of greater stability (Motlep et al., 2010).

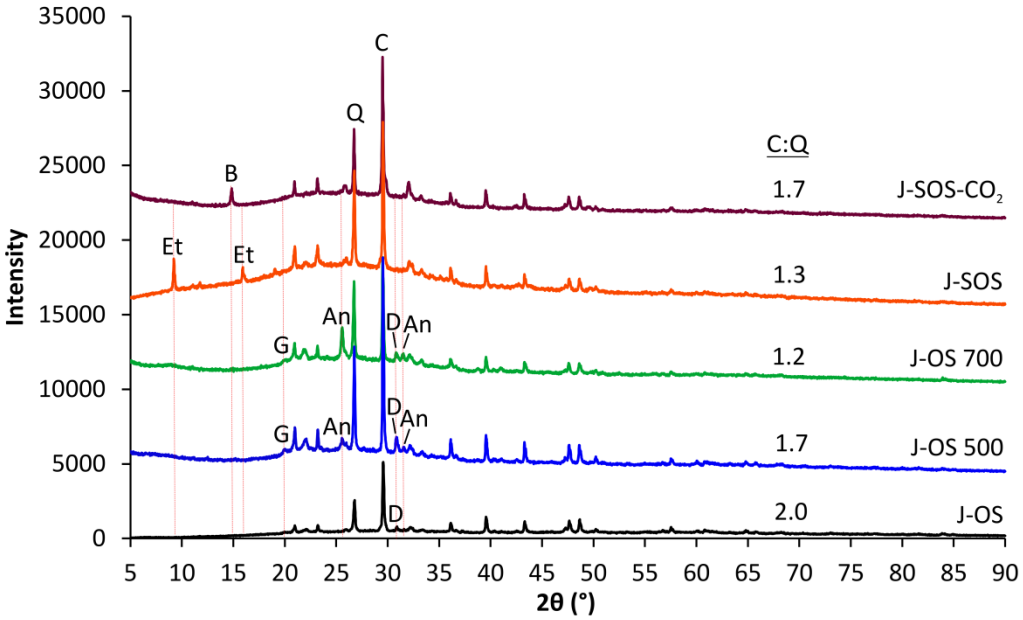

Figure 5.6 – *XRD patterns for J-OS, J-OS 500, J-OS 700, J-SOS and J-SOS-CO_2. The calcite:quartz (C:Q) ratio is labelled, as are dominant minerals, where C = calcite, Q= quartz, Et = ettringite, B= bassanite, D=dolomite, G= grossite, An = anhydrite.*

The calcite to quartz ratio from the intensities of major peak reflections are shown on Figure 5.6, a semi-quantitative comparison to gain insight into the amount of carbonate, in the form of calcite, that was decomposed by combustion and regained by carbonation. Calcite was present at higher concentrations within J-SOS-CO_2 than the un-carbonated samples, and the relationship between calcite content and combustion temperature showed decreasing calcite as combustion temperatures increase. More carbonate was found within J-SOS compared to J-OS 700, despite being processed at the same temperature. However, J-SOS was weathered, as indicated by the presence of ettringite, therefore the greater carbonate content could be due to a small amount of natural carbonation, or the difference may be due to heterogeneity or error associated with analysis. As well as calcite decomposition, dolomite concentrations also decreased as the combustion temperature increased, with dolomite mostly absent within J-

SOS. Limitations with the use of reflection peak intensities, is the large associated error caused by preferential orientation of minerals within the powdered samples. In addition, sensitivities to the instrument and other minerals can result in differing peak intensities (Gill, 1997).

Quantitative TGA analysis was used to expand upon the qualitative XRD results that indicate the relative proportions of carbonate minerals within the samples of J-SOS and J-SOS-CO_2. The amount of CO_2 within J-SOS-CO_2 was determined to be 16.88 wt % +/- 0.05 wt %, based on sample repeats. By comparison of the weight loss curves for the combusted and recarbonated material, the amount of sequestered CO_2 was 3.7 wt % CO_2 +/- 0.2 wt % CO_2, confirming successful carbonation, and the TGA weight loss curve shown (Figure 5.7; Table 5.7) is indicative of all carbonation experiments performed in this initial study.

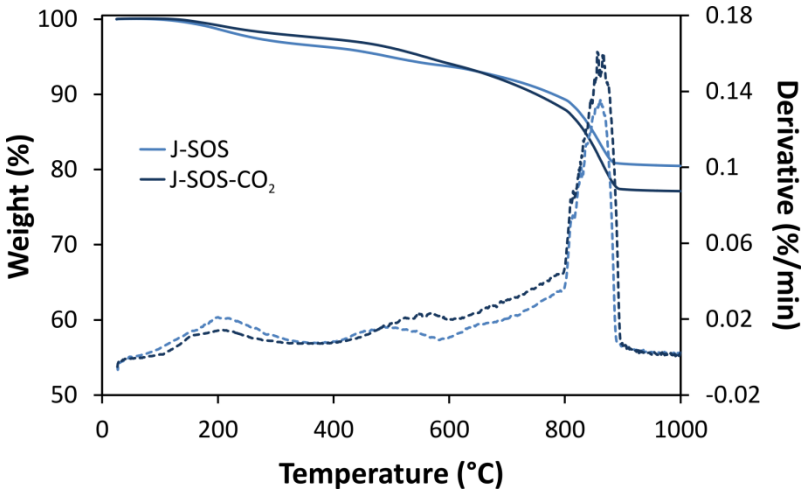

Figure 5.7 – *Weight loss curves for J-SOS-dry and J-SOS-CO_2-1, with the derivative curve shown as a dashed line.*

Table 5.7 – *Weight loss from thermogravimetric analysis, presented at 200 °C intervals, with the fraction of total observed weight loss.*

	0 – 200 °C	-400 °C	-600 °C	-800 °C	-1000 °C	Total
J-SOS-dry (wt %)	1.276	2.481	2.491	4.394	8.85	19.492
Fraction	0.06	0.13	0.13	0.23	0.45	1
J-SOS-CO_2-1 (wt %)	0.824	1.852	3.246	6.112	10.856	22.890
Fraction	0.04	0.08	0.14	0.27	0.47	1

Further experimental carbonation reactions were conducted at supercritical conditions using higher temperatures and pressures, but varying the water content. The results showed an increase in CO_2 content within carbonate minerals, ranging from 2.96 to 4.2 wt % CO_2. The average % CO_2 sequestered was 3.42 wt %, which correlates to 46 % of the theoretical carbonation (Table 5.9, next page). Replicate experiments were used to calculate the processing error and the coefficient of variance averaged 2.99 % (based on 2 sd) (Table 5.8). The error was calculated to average +/- 0.98 wt % CO_2 of the ΔCO_2 value, or 29 % of the total carbonation.

Table 5.8 – *Standard deviation and coefficient of variance for instrument, sample and processing error of the calculated carbonate content.*

Type	Standard deviation (σ)	CV (%)
Instrument	0.0712	0.48 %
Sample	0.183	2.11 %
Processing	0.051 – 0.741	0.5 – 6.9 %

On plotting the data for J-SOS-CO_2 A vs B and for J-SOS-CO_2 B vs C, no significant trends were observed on altering water content due to large errors associated with the carbonation (Figure 5.8), but is a factor that will be studied in more detail in Chapter 6.

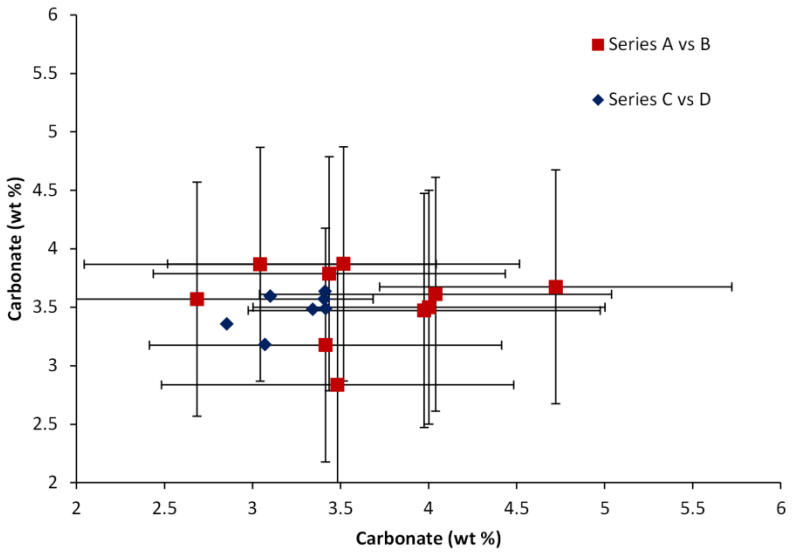

Figure 5.8 – *Carbonate content (wt %) of J-SOS-CO_2 A vs. B; and J-SOS-CO_2 C vs D.*

Table 5.9 – *For each experiment with differing water content: the coefficient of variance was calculated with 95 % confidence, the amount of CO_2 sequestered, and the calculated extent of carbonation.*

Samples	Water content	CV (2sd)	CO_2 seq (wt %)	Extent (%)
J-SOS-CO_2-A-0.1 **J-SOS-CO_2-B-0.1**	0.1 ml	2.87	3.83	51.6
J-SOS-CO_2-A-0.2 **J-SOS-CO_2-B-0.2**	0.2 ml	4.47	3.16	42.4
J-SOS-CO_2-A-0.3 **J-SOS-CO_2-B-0.3**	0.3 ml	1.63	3.30	44.4
J-SOS-CO_2-A-0.4 **J-SOS-CO_2-B-0.4**	0.4 ml	5.63	3.46	46.5
J-SOS-CO_2-A-0.5 **J-SOS-CO_2-B-0.5**	0.5 ml	6.14	3.13	41.9
J-SOS-CO_2-A-0.6 **J-SOS-CO_2-B-0.6**	0.6 ml	3.38	3.72	50.2
J-SOS-CO_2-A-0.7 **J-SOS-CO_2-B-0.7**	0.7 ml	3.37	3.75	50.6
J-SOS-CO_2-A-0.8 **J-SOS-CO_2-B-0.8**	0.8 ml	6.90	4.20	56.9
J-SOS-CO_2-A-0.9 **J-SOS-CO_2-B-0.9**	0.9 ml	2.38	3.61	48.6
J-SOS-CO_2-C-1 **J-SOS-CO_2-D-1**	1 ml	0.50	3.45	46.4
J-SOS-CO_2-C-2 **J-SOS-CO_2-D-2**	2 ml	3.48	3.11	41.6
J-SOS-CO_2-C-3 **J-SOS-CO_2-D-3**	3 ml	0.75	3.12	41.9
J-SOS-CO_2-C-4 **J-SOS-CO_2-D-4**	4 ml	0.94	3.41	45.9
J-SOS-CO_2-C-5	5 ml	-	3.17	42.5
J-SOS-CO_2-C-6	6 ml	-	3.34	44.9
J-SOS-CO_2-D-7	7 ml	-	2.96	39.6
J-SOS-CO_2-C-8 **J-SOS-CO_2-D-8**	8 ml	1.51	3.52	47.4
J-SOS-CO_2-C-9 **J-SOS-CO_2-D-9**	9 ml	1.11	3.49	46.9
J-SOS-CO_2-C-10 **J-SOS-CO_2-D-10**	10 ml	3.38	3.35	45.0

5.4 Discussion

5.4.1 Theoretical carbonation

Method 1

The presence of divalent metal cations, in particular Ca and Mg, is necessary for carbonation to occur and the concentration of Ca and Mg (Table 5.6) was used to calculate the potential for CO_2 sequestration (Method 1) (Huijgen et al., 2005). The calculated theoretical carbonation potential of spent oil shale was greatly overestimated, using Eq. 5.11 and 5.12, due to the assumption that all the cations present are available for reaction; therefore the concentration alone was not sufficient to determine if waste materials are viable for CO_2 sequestration and the mineralogy was also considered by the analysis of J-SOS by XRD for a more accurate calculation of the theoretical carbonation.

Although J-SOS contained high concentrations of Ca, it is likely that the majority of this was in the form of calcite, ettringite or anhydrite, and apatite, with lesser amounts of Ca-oxides and Ca-silicates, minerals reactive towards carbonation, which have been difficult to distinguish from the XRD pattern (Figure 5.4). Apatite, was present in both the oil shale and spent oil shale, however, Ca-sulphate minerals were detected only in spent oil shale, and are inhibitive towards carbonation (Figure 5.6).

Difficulties in identifying oxides and silicates by XRD is possibly due to the amorphous nature of these newly formed high temperature phases, contributing towards the presence of increased background intensity between 20-35° 2θ from the XRD pattern (Oskierski et al., 2013; Yoffe et al., 2002). Further work using Fourier transform infrared (FTIR) spectroscopy is used in Chapter 7, to aid with the identification of amorphous silicate and carbonate minerals. The lack of CaO or $Ca(OH)_2$ is unexpected and unlike that of Estonian combusted oil shale which contains a large proportion of CaO and $Ca(OH)_2$, due to the decomposition of calcite minerals during the retorting/combustion process, at temperatures up to 800 °C (Uibu et al., 2009), however researchers have also struggled to detect lime or portlandite within samples of Estonian semi-coke (Motlep et al., 2007). In addition, reflections from MgO cannot be detected using XRD despite the decomposition of dolomite minerals, perhaps due to its low concentration or presence as amorphous phases. Because of the difficulty in identifying high temperature phases by XRD, the method for calculating the theoretical carbonation was based on assumptions that Ca and Mg were available for reaction, if they were not in the form of carbonate, sulphate or phosphate minerals.

Decomposition of organic matter and primary minerals, such as clays, feldspar and carbonates, by the retorting and combustion of oil shale, result in the formation of high temperature secondary mineral phases, including silicates, aluminates and sulphates (Stanmore et al., 2005). Due to the high concentration of carbonate minerals that decompose at temperatures > 600 °C, combustion at ~700 °C results in the release of CO_2 and formation of reactive CaO that proceeds to form secondary minerals (Kuusik et al., 2005). An example of reaction schemes involving calcite decomposition are as follows:

1) The formation of Ca-silicates:

$$Ca\text{-}carbonate + silica \rightarrow Ca\text{-}silicate + carbon\ dioxide \quad \text{Eq. 5.17}$$

$$CaCO_3 + SiO_2 \rightarrow CaSiO_3 + CO_2 \quad \text{Eq. 5.18}$$

2) The formation of Ca-aluminates:

$$Al\text{-}silicate + CaCO_3 \rightarrow Ca\text{-}aluminate + Ca_xSi_yO_z + 2CO_2 \quad \text{Eq. 5.19}$$

$$Eg.\ 2Al_2Si_2O_5(OH)_4 + 3CaCO_3 + 2O_2 \rightarrow CaAl_4O_7 + 2CaSiO_3 + 3CO_2 + 4H_2O \quad \text{Eq. 5.20}$$

3) The formation of Ca-sulphates:

$$Ca\text{-}carbonate + sulphur \rightarrow Ca\text{-}sulphate + carbon\ dioxide \quad \text{Eq. 5.21}$$

$$CaCO_3 + S + 1.5O_2 \rightarrow CaSO_4 + CO_2 \quad \text{Eq. 5.22}$$

The formation of Ca-aluminates and Ca-silicates incorporates Ca into phases that are susceptible to carbonation, albeit more difficult to react than Ca-oxide and hydroxide minerals. The carbonation of Ca-aluminates is not as extensively researched as silicates, but are suitable for reaction with CO_2 nonetheless (Fernández-Carrasco et al., 2008).

Method 2

Many researchers claim to use the Steinour formula, or a modified version of this, to produce a more accurate prediction of the theoretical carbonation, based on concentrations of Ca, Mg, Na and K ions (Sanna et al., 2012; Kelly et al., 2011; Gunning et al., 2010; Fernandez Bertos et al., 2004). However, there are variations in the formulas used, with a lack of consistency clearly apparent. Detailed explanations of the constants used are required, as there are some discrepancies, detailed in Table 5.10 that may not be explained alone by the use of different starting materials. The values used by Sanna et al. (2012) appear to be correct; however the conversion values for Na and K used by other authors are different to those expected (Kelly et

al., 2011; Gunning et al., 2010; Fernandez Bertos et al., 2004). The corrected conversion values based on molar equations is provided in Table 5.11 and was used in Method 2 for the calculation of theoretical carbonation within spent oil shale in this study, using Eq. 5.13 and 5.14.

Table 5.10 – *Reported conversion values used in Steinour formula.*

Author	Ca	Mg	Na	K
Gunning et al., 2010	0.785(CaO-0.7SO_3)	-	1.09Na_2O	0.93K_2O
Fernandez Bertos et al., 2004	0.785(CaO-0.7SO_3)	-	1.09Na_2O	0.93K_2O
Kelly et al., 2011	0.785(CaO-0.7SO_3)	1.091MgO	2.09Na_2O	0.93K_2O
Sanna et al., 2012	0.785(CaO-0.56$CaCO_3$-0.7SO_3)	1.091MgO	0.71Na_2O	0.468(K_2O-0.632KCl)

Table 5.11 – *Corrected conversion values.*

$CaCO_3$ → CaO	0.56
$CaSO_4$ → CaO	0.7
CaO → CO_2	0.79
MgO → CO_2	1.09
Na_2O → CO_2	0.71
K_2O → CO_2	0.47
2KCl → K_2O	0.63

The method for calculating the theoretical carbonation within spent oil shale was corrected to account for the formation of secondary mineral phases, similar to methods observed above (Sanna et al., 2012). In addition, Na_2O and K_2O were not used in the calculation of the theoretical carbonation, as the concentrations of these compounds were very low (< 1 wt % combined), and therefore likely to be negligible towards sequestration of CO_2. The limitations and conservative nature of using the corrected Method 2 were assessed, and the viability of this method is discussed below.

Because of the difficulty in identifying high temperature phases by XRD, the method for calculating the theoretical carbonation was based on assumptions that Ca and Mg are fully available for reaction, except when in the form of phosphate, carbonate and sulphate

minerals. Firstly, it was assumed that the total Ca content is associated with carbonate, sulphate, phosphate, silicate, aluminate, oxide and hydroxide minerals (Equation 5.23).

Total Ca = Ca-carbonate + Ca-sulphate + Ca-phosphate + Ca-silicate + Ca-aluminate + Ca-oxide/hydroxide Eq. 5.23

Secondly, the assumption was made that all the weight loss above 600 °C during TGA is from the decomposition of carbonate minerals. Also it is assumed that all phosphate present is in the form of apatite, which remains in the spent oil shale after retorting and combustion of J-OS, while any sulphur in the system is postulated to react with free Ca from the decomposition of carbonate minerals, removing Ca in the form of sulphate minerals. The remaining Ca and Mg was then assumed to be in the form of oxide, hydroxide, silicate or aluminate minerals that are reactive towards carbonation (Lackner et al., 1995), leading to the quantification of reactive Ca minerals (Equation 5.24).

Reactive Ca = Ca-silicate + Ca-oxide/hydroxide Eq. 5.24

Reactive Ca= Total Ca – Ca-Carbonate (TGA) – Ca-sulphate (XRF) – Ca-phosphate (XRF) Eq. 5.25

5.4.2 Experimental observations

On analysis of XRD patterns of combusted, weathered and carbonated samples of Jordanian oil shale (Figure 5.6), compositional changes were identified. Sulphate minerals were not detected within oil shale, yet were present in spent oil shale (J-OS 500/700), weathered spent oil shale (J-SOS) and carbonated spent oil shale (J-SOS-CO_2) as anhydrite, ettringite and bassanite, respectively. Sulphur is likely to be present within organic matter which is then able to act as an inhibitor to carbonation by preferentially reacting with free Ca to form sulphate minerals, such as anhydrite or gypsum (Schramke, 1992). It is likely that during storage of the sample, the weathering of thermal decomposition products (from decomposed calcium carbonates, clay minerals and organic matter), results in the formation of ettringite, a hydrated aluminosulphate mineral, that is commonly formed in systems containing high concentrations of Ca and SO_4 (Motlep et al., 2007; Dietzel et al., 1992). Ettringite is stable in alkaline environments (Myneni et al., 1998), yet can react with CO_2 leading to the formation of gypsum and alumina (Fernandez Bertos et al., 2004). Heating can result in the formation of bassanite, a partially hydrated sulphate (Hall et al., 1996) that was observed within carbonated spent oil

shale. As well as carbonation, weathering mechanisms can also include hydration, precipitation, dissolution, and redox reactions (Li et al., 2007).

The decrease in calcite and dolomite content as samples were combusted was predicted, due to the decomposition of these minerals at temperatures from 500 °C. The amount of calcite re-precipitated on carbonation was detected to be similar to the amount of calcite within the oil shale combusted at the lower temperature of 500 °C (Figure 5.6). Slightly higher concentrations of calcite within weathered material compared to J-OS 700 may be due to natural weathering processes (Gunning et al., 2010). However, due to the non-quantitative nature of the XRD reflection intensities, the small differences between J-SOS and J-OS 700, as well as between J-SOS-CO_2 and J-OS 500, may be due to large errors and sample heterogeneity (Assima et al., 2013b). Additionally, amorphous carbonate minerals may not be detected using XRD methods. Instead, thermogravimetric methods were used to quantitatively determine the amount of carbonate minerals formed during supercritical reactions (Figure 5.5, Figure 5.7 and Table 5.7), while assumptions and drawbacks of the use of TGA analysis as a quantitative technique were considered.

The only additives to J-SOS before carbonation at high temperatures and pressures, was CO_2 and H_2O, and due to the nature of the retorting and combustion process, organic matter and other minerals unstable at temperatures < 700 °C decomposed. Any water incorporated within mineral structures, before or during carbonation as interlayer or structural water, is likely to decompose at temperatures below 600 °C; therefore it is assumed that these mineral phases will not overlap with the temperature region assigned to carbonate decomposition (Bhargava et al., 2005). Hydrated phases include: sulphate minerals, such as gypsum and bassanite that lose crystalline water between 100-300 °C, and ettringite at < 100 °C (Anthony et al., 2000); and hydroxide minerals such as portlandite and brucite that decompose at 400-500 °C (Todor, 1976). Additionally, minerals formed due to reaction with water are likely to be present within J-SOS and J-SOS-CO_2 at similar (and low) concentrations, therefore the two samples can be compared when taking this into account for the calculation of carbonate content. Also, samples were dried before analysis by TGA, so that moisture released at temperatures < 105 °C, would not have a large effect on the quantitative assessment of carbonate content. Therefore, the percentage value for loss of water was not accounted for in calculations, such as those used by Gunning et al., (2010).

Other mineral phases identified by XRD include oxides and silica that are stable up to temperatures > 1000 °C, as well as phosphates and dehydrated sulphates that do not cause a

change in mass during carbonation. Other silicate decomposition is regarded as insignificant at temperatures within the carbonate decomposition range (Jeong et al., 1983), therefore it is assumed that the weight loss between 600-950 °C is exclusively due to the decomposition of carbonate minerals, and other mineral contribution is negligible. Also, carbonate minerals may decompose outside of the 600-950 °C window, for example magnesite is known to decompose at lower temperatures, as low as 450 °C (Todor, 1976). The formation of amorphous, or disordered carbonate minerals could result in a mineral structure that is less stable and more susceptible to decomposition at lower temperatures (Kalinkin et al., 2004), however, from the nature of the TGA curve and mineral identification using XRD, it is likely that calcite is predominant within samples of J-SOS-CO_2.

Based upon the assumptions and limitations, we arrive at a theoretical carbonation value which is both conservative and highly dependent on the nature of mineral phases within J-SOS, as well as a calculated % CO_2 value that may overestimate or underestimate carbonate precipitation depending on the carbonate mineral structure, and other mineral phases present. It is probable that the extent of carbonation (Eq. 5.16), that compares the experimental to theoretical values, provides a value that is lower than actually accomplished due to the underestimation of carbonate minerals.

The results from carbonation show that up to 4.2 wt % of CO_2 may be sequestered, when reacting spent oil shale for 24 hours at 100 bar, 80 °C and with 80 % water (Table 5.9). No CO_2 was sequestered when reacted at the same conditions without water, as observed in other studies (Miller et al., 2013), and greater amounts of carbonation were achieved when accelerated reactions were used compared to natural carbonation (Cultrone et al., 2005). A large proportion of calcite is converted into anhydrite on combustion (Eq. 5.22), therefore inhibiting the amount of CO_2 sequestration that can occur; a process that has been observed previously within Jordanian spent oil shale (Al-Otoom et al., 2005). This inhibition was accounted for within the calculation of the theoretical carbonation, so the low value (< 50 %) for the extent of carbonation may be due to pore blockage preventing the movement of CO_2, or newly precipitated calcium carbonate or silicates on the surface of reactant particles (Chen et al., 2006; Xu et al., 1998). However, the use of supercritical CO_2 fluids should overcome the reduction in porosity, because there is no surface tension the fluids are able to access fine pores (Fernandez Bertos et al., 2004). The extent of carbonation is high at > 80 %, within Portland cement, which is a material reactive towards carbonation due to high concentrations of CaO. This suggests that there is potential for further carbonation of the spent oil shale (Gunning et al., 2010), with limitations due to evaporation of capillary water at atmospheric

pressure, and reduction in CO_2 solubility (Cultrone et al., 2005). The pH of spent oil shale was not identified as a limiting factor in carbonation, and previous work using CO_2 at pressures of < 5 bar, with 20 % water, decreased the pH of spent oil shale from pH 12 to ~pH 9 (Reddy et al., 1994), allowing for the presence of carbonate ions in solution according to the Bjerrum plot (Figure 5.1).

The error caused by sample heterogeneity (Table 5.8) was found to vary by more than 4x than that of the Ca-oxalate standard, which shows that use of a high mass TGA does not remove all sources of error caused by heterogeneity, yet other sources of error were reduced as much as possible by using appropriate heating rates, sample mass and particle size, and a flowing inert gas (Rajeshwar, 1983). The processing error for experimental and analytical components of the carbonation process was identified by repeating experimental runs, with the error ranging from 0.5-6.9 %, and an average of 2.99 % CV (Table 5.8). Because of the large uncertainty associated with the gain in CO_2 by carbonation, an understanding of the mechanisms that affect the amount of CO_2 sequestered is difficult to ascertain. Varying the water content did not produce results with a clear trend. Given the results found in this chapter a more systematic approach was required and a factorial experimental design, to test different factors was the approach taken in Chapter 6, with analysis undertaken using ANOVA techniques, to identify processes that can be used to optimise the carbonation process.

It is likely that there is ~60 wt % of carbonate minerals present, based on TGA data from J-SOS and J-OS (corrected for organic matter), which will decompose by combustion at temperatures up to 700 °C, thereby significantly contributing to the CO_2 emissions as a result (Chapter 3: Table 3.3, Figure 3.8). The combustion of carbonate minerals is considered beneficial, as it results in capture of sulphur emissions as Ca-sulphate minerals, and improves the characteristics of waste material to be as a by-product in construction. However, CO_2 sequestration using the remaining reactive calcium containing minerals could reduce emissions by 20 kg CO_2/bbl, assuming 46 % carbonation, and could offer JEML a reduction in CO_2 emissions by 7 %. Optimisation reactions and further work on the mechanisms of combustion, carbonation and material characteristics will be discussed in more detail in Chapter 7, while the costs and effectiveness of active sequestration by use of supercritical CO_2 is discussed further in Chapter 8.

5.5 Conclusions

Mineralisation reactions to sequester CO_2 within spent oil shale have been achieved by reactions for 24 hours using water and supercritical CO_2, with pressures of up to 100 bar and temperatures up to 80 °C. Sulphur present in the organic matter of oil shale inhibited CO_2 sequestration by forming calcium sulphate minerals and only divalent cations in the form of silicate, oxide or hydroxide minerals were susceptible to carbonation mechanisms. An average of 3.4 wt % of CO_2 was sequestered in the form of carbonate minerals, as detected by quantitative thermogravimetric analytical methods.

Newly formed carbonate minerals were thermodynamically stable, therefore offering a permanent storage option for CO_2, with the potential to reduce emissions from oil shale retorting. The CO_2 sequestered in the form of new carbonate minerals was calculated to reach 46 % of the theoretical carbonation, with the potential to increase this value through optimisation of the reaction conditions. Carbonation by active methods described in this chapter could reduce CO_2 emissions by up to 20 kg CO_2/bbl.

Chapter 6: Optimisation of CO_2 sequestration techniques

6.1 Introduction

The previous chapter showed that CO_2 sequestration was achieved within spent oil shale, when subjected to hydrous and supercritical conditions. The extent of carbonation reached 56.9 % of the theoretical value, when reacted at 100 bar, 80 °C, with 80 % water, for 24 hours (Chapter 5), leaving a large proportion of unreacted material that may be suitable for further carbonation, if subjected to the right conditions and processes. Therefore, this chapter aims to optimise the CO_2 sequestration potential of spent oil shale by systematically varying the reaction conditions.

Whilst the extent of research in the field of *ex-situ* mineralisation by carbonation is large, there is no single common method used by researchers, mostly due to the use of different starting materials and different objectives. Reaction conditions are dependent on the type of feedstock that is used, for example, igneous minerals, such as serpentine, will require harsh reaction conditions and pre-treatment to improve reactivity, whereas industrial by-products and alkaline wastes are naturally more reactive towards carbonation (Huijgen et al., 2005). Researchers have performed carbonation experiments to: improve reaction kinetics and identify rate-limiting pathways; determine the extent of carbonation; investigate chemical, physical and morphological changes; and identify the different types of carbonate minerals which can store CO_2, in a permanent state (Hovelmann et al., 2012; Thiery et al., 2007; Fernandez Bertos et al., 2004). The carbonation objective determines the reaction conditions used, for example, the reaction of serpentine to achieve maximum sequestration will likely involve different conditions to CO_2 sequestration within serpentine that achieves maximum cost benefit.

6.1.1 Background

As outlined in Chapter 5, the alkaline nature of spent oil shale, and the amount of available calcium determine how much carbonation is possible. Inhibitors, such as sulphate anions, act to reduce the amount of carbonate that can be precipitated; however there are additional factors that affect the kinetics and extent of reaction.

Carbonation reaction mechanisms focus on the movement of Ca^{2+} and CO_2. Firstly, CO_2 diffuses into the solid material, where it dissolves in the pore water. It is then able to form carbonic

acid that then dissociates to form bicarbonate and carbonate ions, resulting in a pH drop and dissolution of reactive Ca-containing minerals. The dissolution of Ca^{2+} is the second step, which involves the movement of Ca to the surface of the mineral, and the dissolution into solution. On contact of the reactive ions, Ca^{2+} and CO_3^{2-}, nucleation and precipitation of calcium carbonate minerals on the surface of solid particles results (Huijgen et al., 2005; Fernandez Bertos et al., 2004). The mechanism steps are interlinked, and vary with each other, for example, the dissolution of Ca is dependent on the pH of solution and therefore how much CO_2 has dissolved, while the concentration of carbonate anions in solution affects the rate of nucleation and precipitation of calcium carbonate (Cizer et al., 2012). The rate and extent of reaction are controlled predominantly by the diffusion of CO_2 to the active site, and the reactivity of CO_2. The latter is controlled by how much CO_2 there is available, the solubility of CO_2, the amount of dissolved Ca^{2+}, the duration of the experiment, the concentration of reactive Ca-minerals and the reactive surface area. The diffusion of CO_2 is controlled by the concentration of CO_2, and also depends on the water content and the permeability of the solid material (Fernandez Bertos et al., 2004). The factors described by these properties include: the pressure, temperature, water content, saturation time, and solid particle size, which are explored in more detail below.

Carbonation experiments have been reported to occur very quickly, with steel slag reaching 40 % conversion in only 2 minutes (Huijgen et al., 2005), suggesting that with sufficient concentration of reactive ions in solution, the precipitation of carbonate is not rate limiting. However, the rate of reaction has been reported to decrease over time using wollastonite, a reactive silicate mineral, which may be due to pore blocking, thereby reducing the amount of carbonate that can be formed overall (Huijgen et al., 2006). The conversion to carbonate minerals has been reported to increase within alkaline material, from 12 to 60 % (Huijgen et al., 2006). In addition, the effect of the particle size is governing, where an increase in the surface area leads to an increase in the reaction rate (Cultrone et al., 2005). Greater permeability can lead to an increase in the amount of CO_2 that can access reactive surfaces, and supercritical fluids can overcome the surface tension of water, to increase the amount of CO_2 in contact with solid surfaces (Domingo et al., 2006).

The water used in the carbonation experiment acts as a medium for the reaction to take place with the ideal water content differing based on the nature of the starting material used. For example, samples of municipal solid waste incineration ash (MSWI) reacted at room temperature and pressures up to 20 bar, require only 15 % water for carbonation to proceed (Rendek et al., 2006). Too much water results in less contact between CO_2 and the reactive

surface and can prevent diffusion of CO_2 into pores, yet too little prevents dissolution of ionic species and decreases the movement of ions in solution, therefore inhibiting the reaction (Thiery et al., 2007). Within cement, the amount of water required is also less than 20 % (Fernandez Bertos et al., 2004), yet for wollastonite, up to 100 % water is reported to be necessary for optimum carbonation (Miller et al., 2013).

The reaction of aqueous CO_2 to form carbonic acid, is considered rate determining, and can be controlled by the pressure and temperature (Fernandez Bertos et al., 2004). In addition, the pressure and temperature conditions interact with each other, leading to complex effects on the carbonation reaction. At low temperatures, typically < 200 °C, Ca^{2+} availability is reported to be the rate determining step within steel slag and other alkaline waste (Rendek et al., 2006; Huijgen et al., 2005). However, on increasing the temperature, the reaction rate for the dissolution of Ca-minerals increases, for example by heating wollastonite to 140 °C (Tai et al., 2006). The rate of the dissociation of carbonic acid also increases, as the temperature increases, yet the solubility of CO_2 decreases, leading to the availability of CO_2 to become rate determining, affecting the nucleation and growth of calcium carbonate (Huijgen et al., 2006). At lower temperatures, the interface tension is lower, so that CO_2 and water are more miscible (Domingo et al., 2006), and the availability of CO_2 can also be controlled by the pressure, where increasing pressure results in increasing CO_2 due to the solubility of CO_2 being related to the partial pressure of CO_2 (Diamond et al., 2003). Within MSWI, the pressure was found to be rate determining at room temperature and increasing pressures up to 20 bar. In addition temperature was also found to affect the extent of carbonation as well as the rate, where an increase in temperature led to less overall conversion (Li et al., 2007; Rendek et al., 2006), and a decrease in conversion with increasing temperature was also reported in fluidized bed combustion (FBC) ash (Anthony et al., 2000).

6.1.2 Factorial design

The use of a comprehensive and significant study to reveal the effects of multiple factors on the extent of carbonation that can be achieved, using reactive feedstock such as alkaline waste, has yet to be completed in this field of research. Screening experiments were completed in Chapter 5, indicating that ground samples of Jordanian spent oil shale can achieve high levels of carbonation when reacted under supercritical conditions, and with differing amounts of water. However, the effect of individual factors was not assessed.

This chapter takes the carbonation reaction forward, by analysing the optimum conditions for sequestration of CO_2, in terms of maximum sequestration and feasibility, by varying the

pressure, temperature, duration, and water content. A factorial design was used, so that carbonation experiments were undertaken using a method where all the factors can be manipulated intentionally, to be able to assess and understand their impact on the experimental response. A large number of experiments were required to test all combinations of variables and to investigate the effect of individual factors and their interactions, so as to enable a significant statistical technique to be used for analysis. Carbonation experiments were undertaken as described in Chapter 5, and quantitative thermogravimetric analysis (TGA) was used to determine the amount of carbonate formed in the accelerated carbonation reactions.

The use of a factorial design, quantitative thermogravimetric analysis and analysis of variance (ANOVA) enabled the validation of results obtained from the carbonation of J-SOS at high pressures and temperatures, so that the carbonation experiments may be optimised, accounting for the effect of each individual factor and random error associated with it.

6.2 Methodology

6.2.1 Designing an experiment

An experimental design begins with the identification of key factors that could play a part in the experimental response, defined as part of the experimental objective. Table 6.1 lists the factors already identified to be important to the carbonation of spent oil shale, and gives information as to how these measurable quantities were tested, the hypothetical response related to each variable, and the type of analysis used to identify the response.

Table 6.1 – *The expected response from factors used in the experimental design.*

Factor	Response	Measured by:	Analysis
Duration	Increase time to enable equilibrium to be reached.	Clock	TGA & XRD
Temperature	Increases the kinetics of dissolution, dissociation and diffusion and decrease CO_2 solubility, as temperature is increased	Thermocouple	TGA
Pressure	Increase the reactive surface area and the availability of CO_2 due to increased dissolution	Gauge	TGA
Grain size	Increase reactive surface area	Sieve	TGA
Water content	Too little water can be diffusion limiting, whereas too much affects the kinetics of the reaction.	Pipette	TGA

In addition to the identification of factors that play a role in the carbonation process, the number of factor levels was chosen, based upon the need to produce a statistically significant model to explain the data, with sufficient experimental power, using an achievable number of experimental runs to gain the results. An increase in samples and replicates leads to an increase in the resolution of the factorial design.

6.2.1.1 Two-level design

Initially, a 2-level design was produced, based on 4 factors: duration, temperature, pressure and water content (Table 6.2). Using 3 replicates for each experiment, a resultant design of 48 experiments was established.

Table 6.2 - *Factors tested in the 2-level design and the assigned values.*

	Factor	# of levels	level values
A	Pressure	2	70, 100 (bar)
B	Temp	2	40, 80 (°C)
C	Duration	2	1, 24 (hrs)
D	Water	2	10, 60 (%)

6.2.1.2 Full factorial design

Based on the results from the above design, the model was expanded into a full factorial multi-level design based on the same four factors, but with an increased number of levels for the temperature and the duration (Table 6.3). The expansion of the design was performed to increase the power and resolution, and thereby increase the sensitivity of the subsequent statistical analysis.

Table 6.3 – *Factors tested in the GLM model and the number of levels used.*

	Factor	# of levels	level values
A	Pressure	2	70, 100 (bar)
B	Temp	3	40, 60, 80 (°C)
C	Duration	5	0.5, 1, 2, 4, 24 (hrs)
D	Water	2	10, 60 (%)

6.2.2 Experimental

6.2.2.1 Quantitative TGA

Quantitative thermogravimetric analysis (TGA) was carried out as detailed in Chapter 5, to calculate the amount of carbonate within samples, as the experimental response in the factorial design (Table 6.1). Exceptions were the increased heating rate of 20 °C/min to increase the throughput capacity, ensuring that samples could be processed and analysed with no delays. In addition, weight loss attributed to carbonate decomposition was taken from 550-950 °C. Particle size was not used as a factor in the experimental design so that replicates could be used by TGA to account for any error due to heterogeneity and analysis. Therefore, to allow for a feasible factorial design, ground particles (< 1mm) were used, to increase the potential for carbonation by an increase in reactive surfaces.

6.2.2.2 Carbonation experiments

Samples of J-SOS (as used in experiments detailed in Chapter 5) were used throughout the carbonation experiments. Sample size of 1 g, < 1 mm particle size, were sealed in the 4760 Parr 5L external pressure vessel and temperature controller, connected to a Thar CO_2 delivery system. Reactions were carried out at varying durations (0.5 to 24 hrs), pressures (70 to 100 bar) and temperatures (40 to 80 °C), with combinations detailed in the experimental design. Six samples could be sealed in the reaction vessel, half with 10 % water added, and half with 60 % water. This enabled 3 repeats to be analysed using TGA, after being dried at 105 °C. Controls were achieved as above, by adding 10 % water to 3 samples of J-SOS, and 60 % water to 3 samples of J-SOS for one hour, however the hydrated solids were not added to the pressure vessel, instead being dried at 105 °C, before TGA analysis.

During this design process, uncontrollable variables were minimised as much as possible, to lessen associated error and strengthening the subsequent analysis. In addition to experimental replicates, variation within the reaction procedure was reduced by: analysing the samples the day after reaction at high pressure and temperature, to prevent further carbonation; using samples of constant size, for carbonation and analysis by high-mass TGA; the same conditions within the TGA were used; and the ramp-up and depressurisation durations were kept as constant as possible. In total, 32 experiments were performed (Table 6.4), with 3 replicates for each sample and 192 samples for analysis by TGA. In addition, 2 control experiments were completed, resulting in an extra 12 samples for analysis by TGA, leading to a total of 204 samples for analysis.

Table 6.4 – *Total number of carbonation experiments performed as part of the factorial design, with 30 different experimental conditions used.*

Samples A-F	Duration (hrs)	Temperature (°C)	Pressure (bar)	Water (%)
1 A	0.5	40	70	3 x 10, 3 x 60
1 B	,,	,,	,,	3 x 10, 3 x 60
2	0.5	40	100	3 x 10, 3 x 60
3	0.5	60	70	3 x 10, 3 x 60
4	0.5	60	100	3 x 10, 3 x 60
5	0.5	80	70	3 x 10, 3 x 60
6	0.5	80	100	3 x 10, 3 x 60
7	1	40	70	3 x 10, 3 x 60
8	1	40	100	3 x 10, 3 x 60
9	1	60	70	3 x 10, 3 x 60
10	1	60	100	3 x 10, 3 x 60
11	1	80	70	3 x 10, 3 x 60
12	1	80	100	3 x 10, 3 x 60
13	2	40	70	3 x 10, 3 x 60
14	2	40	100	3 x 10, 3 x 60
15	2	60	70	3 x 10, 3 x 60
16	2	60	100	3 x 10, 3 x 60
17	2	80	70	3 x 10, 3 x 60
18	2	80	100	3 x 10, 3 x 60
19	4	40	70	3 x 10, 3 x 60
20	4	40	100	3 x 10, 3 x 60
21	4	60	70	3 x 10, 3 x 60
22	4	60	100	3 x 10, 3 x 60
23	4	80	70	3 x 10, 3 x 60
24	4	80	100	3 x 10, 3 x 60
25	24	40	70	3 x 10, 3 x 60
26	24	40	100	3 x 10, 3 x 60
27	24	60	70	3 x 10, 3 x 60
28	24	60	100	3 x 10, 3 x 60
29 A	24	80	70	3 x 10, 3 x 60
29 B	,,	,,	,,	3 x 10, 3 x 60
30	24	80	100	3 x 10, 3 x 60

6.2.3 Statistical analysis

Minitab 14 was used in the statistical analysis of imported datasets. Initial data analysis was carried out visually and distributions were plotted. Statistical methods, specifically analysis of variance (ANOVA), were used to identify and confirm trends in datasets, by comparing the effect of multiple factors on a defined response, in this case the amount of carbonate. ANOVA was used to identify whether the amount of carbonation was caused by random error, or by significant changes as a result of changing one, or two, of the factor levels, and therefore was used to provide valid and objective conclusions, enabling conclusions to be made based on the effectiveness of the carbonation experiments.

The ANOVA was performed using a two–way model, followed by the use of a general linear model (GLM) later on which allowed for a flexible design with more levels. Insignificant factors ($P > 0.05$) were dropped out, one-by-one, until a model based on significant factors and their interactions was determined. ANOVA can distinguish differences in the response due to: random errors; errors due to the influence of factors; and interactions between factors if a full factorial design is used. The level of confidence used was 95 %, unless otherwise stated, where data is only accepted if $P < 0.05$, which is where 95 % of result can be explained by the tested hypothesis or model.

The R^2 output value shows how much of the data can be explained by the model produced, with the significant factors and interactions which play a role in the model. However, it does not give information on the contribution from individual factors and interactions, nor does it determine where the significant differences lie, between levels of individual factor effects. Tukey's *post-hoc* testing was carried out to determine where significant differences lie and the pairwise comparisons were indicated on main effects plots. Main effects and interaction plots were produced showing the influence of each factor in terms of their least squares means and the standard error associated with this. Main effects plots show the effect of each variable on the tested response within the model, while interaction plots show the effect of combined variables on the response. Additionally, the effect size (importance) from each individual factor and their interactions in the model, were accounted for by determining the amount of the original variance, which takes into account the variation from each individual factor, in relation to the total variation and error. This % variance can be expressed using the generalised omega squared value (ω^2) which was calculated using the following method (Equation 6.1), producing a value based on the variation within the dataset, both as a whole and for individual factors (Olejnik et al., 2003).

$$\%\ \omega_G{}^2 = \left[\frac{(SeqSS_a - d_{fa} * AdjMS_{error})}{(SeqSS_{total} + AdjMS_{error})}\right] * 100 \qquad \text{Eq. 6.1}$$

Where $SeqSS_a$ is the sequential sum of squares for factor a; $SeqSS_{total}$ is the total sequential sum of squares; d_{fa} is the degrees of freedom for factor a; and $AdjMS_{error}$ is the means squares of the error.

ANOVA will provide reliable results, but only if: samples are drawn independently, parent populations are normal, and populations share equal variances. Sample sets were analysed for normality using the Anderson-Darling test, tested for equal variances using Levene's test, and the independence (lack of systematic errors) of samples was ensured by data checks. If the data failed some of the above stipulations, steps were taken to achieve these conditions, without significant alteration of the dataset. The increase in normality and equal variances can be accomplished by: firstly the removal of outliers; and secondly the transformation of data. The latter was required in Section 6.3.2, being mentioned in the discussion of the analysis.

Outliers were identified and removed according to the following method, based on Chauvenet's criterion (Taylor, 1997). This method was only used once for each model, and is based on the number of 'extreme' measurements you would expect to see based on the number of data points in the analysis. Using the 99.7 % confidence level (3σ), outlying points were removed if the probability that points occurring outside of 3σ is < 0.5 samples. The following equation is used:

$$0.003 * N = Outliers \qquad \text{Eq. 6.2}$$

However, even if the data does not match these conditions, ANOVA can remain an accurate and sensitive technique, so long as the sample size is significantly large and errors are accounted for within the method for ANOVA and subsequent model.

6.3 Results

6.3.1 Optimisation

Initial analysis of the results indicated that the duration of the carbonation experiment is likely to play a major role in the amount of carbonation that can be achieved when reacting at high pressures and temperatures, with greater carbonation occurring when samples were reacted for 4 or 24 hours, compared to 2 hours or less (Figure 6.1). The effect of other factors was less obvious, therefore statistical analysis was required to determine whether the effect of a

change in temperature, pressure or water content significantly changed the amount of carbonate formed.

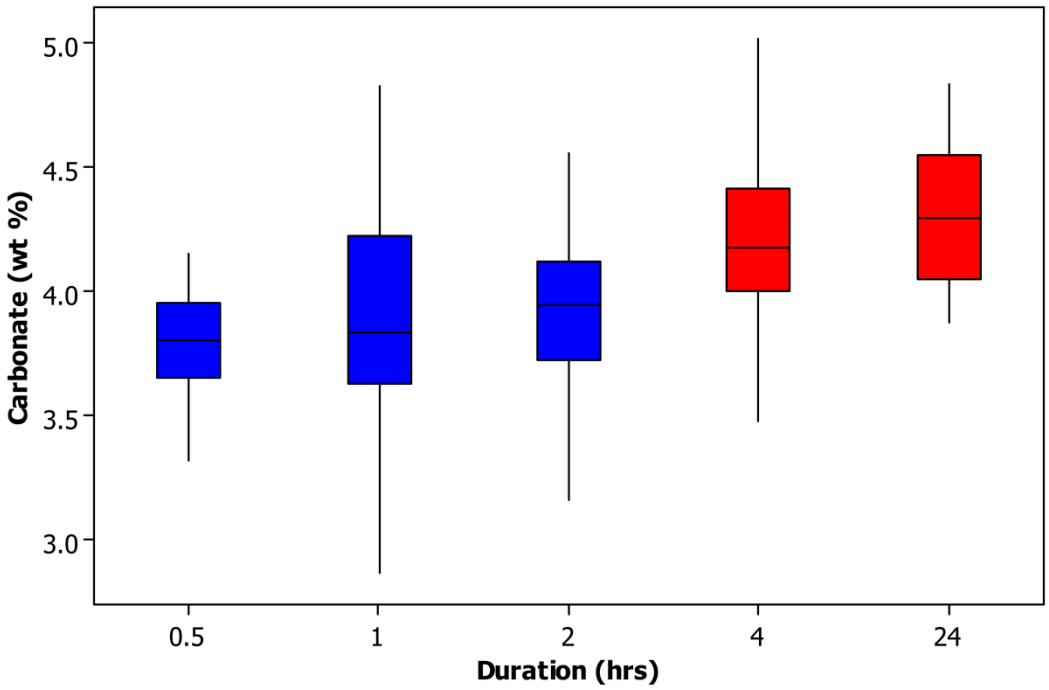

Figure 6.1 – *Box-and-whisker plot showing the maximum and minimum carbonate concentration (in wt %) of samples of spent oil shale carbonated from 0.5 to 24 hours.*

To test the statistical significance of different factors on the extent of carbonation, a factorial design was established, as noted previously, and results from both 2-level and full factorial design were obtained.

6.3.1.1 Two-level factorial design

A 2-level 4-factor design was used to produce a model based on 46 data points, after the removal of 2 outliers. With this design, a significant effect resulting in +/- 0.30 wt % CO_2 was determined with 80 % confidence, or +/- 0.39 wt % CO_2 with 95 % confidence. The mean was calculated to be 4.183 wt % CO_2 and the standard error of the mean = 0.053 wt % CO_2. Results were independent and results from the Anderson-Darling test indicated the data were normal, while Levene's test indicated equal variances. The resultant ANOVA 2-level model was produced to determine the effect of each factor on carbonation (Table 6.5).

Table 6.5 – *ANOVA model of 2-level design, showing for each factor and interaction the degrees of freedom (DF), the probability (significant if P < 0.05), and the % variance (ω^2).*

Source	DF	P	ω^2	Standardized Effect
Duration	1	0	19.76 %	+
Temp	1	0.002	2.94 %	-
Pressure	1	0.001	4.46 %	-
Water	1	0.008	3.84 %	+
Duration*Temp	1	0	22.87 %	+
Duration*Pressure	1	0	17.01 %	+
Duration*Water	1	***0.073***	0.93 %	**Not sig**
Temp*Pressure	1	***0.823***	0 %	**Not sig**
Duration*Temp*Pressure	1	0	10.70 %	-
R^2	86.03 %			
N	46			
S	0.150463			

The model explained 86 % of variance in the dataset, with the duration, temperature, pressure and water content all found to be significant factors. The duration was the most important of these, with a contribution of almost 20 %, more than four times greater than other factors that contribute < 5 %. Interaction effects also play a role, especially interactions with the duration. The factors and interactions in order of importance were: duration*temp, duration, duration*pressure, duration*temp*pressure, pressure, temp, and water. The significance of these is indicated on the Pareto chart (Figure 6.2) and the positive or negative effect on carbonation is displayed in Table 6.5 and Figure 6.3. The positive standardized effect for 2-way interactions means that an increase in the duration and temperature, or duration and pressure led to greater carbonation, however, due to the cumulative effect of the negative standardized effect of the pressure and temperature, the 3-way interaction is also negative. The ω^2 values suggest that main effects and interaction effects that incorporate the duration, contribute to 70 % of the dataset (or 85 % of the model) (Figure 6.4).

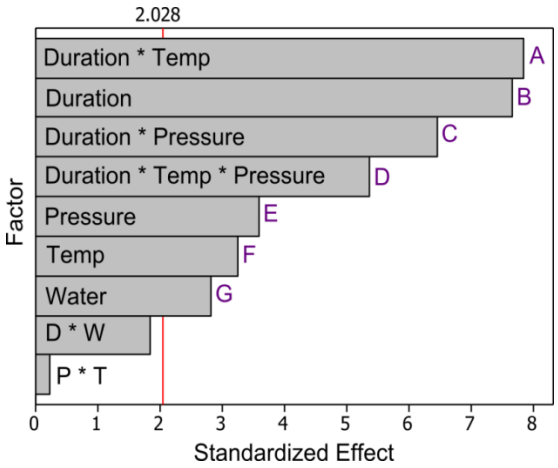

Figure 6.2 – *Pareto chart of the standardized effects.*

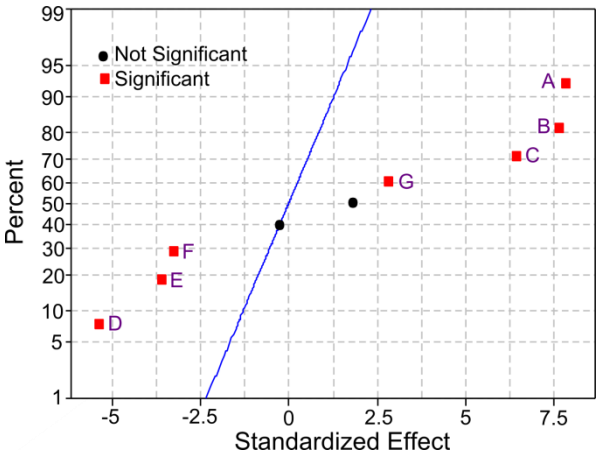

Figure 6.3 – *Normal probability plot of the standardized effects.*

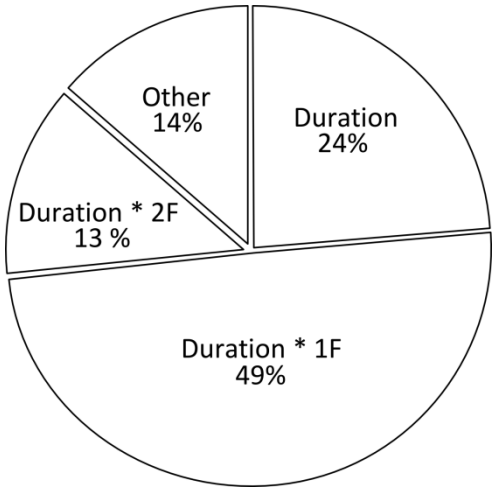

Figure 6.4 – *Pie chart of the main factor and interaction effects contributing to the ANOVA 2-level model.*

Post-hoc testing was included, to determine the result of the effect of each of the significant variables on carbonation. These differences are indicated in Table 6.6, and can also be observed on the main effects plot (Figure 6.5). They show that an increase in duration and water content led to an increase in carbonation, however an increase in temperature and pressure led to a decrease in carbonation.

Table 6.6 – *Post-hoc testing results for each main factor effect, placed in order of importance.*

	Conditions	P-value
Duration (hrs)	1 < 24	0.0000
Pressure (bar)	70 > 100	0.0010
Temperature (°C)	40 > 80	0.0025
Water (%)	10 < 60	0.0079

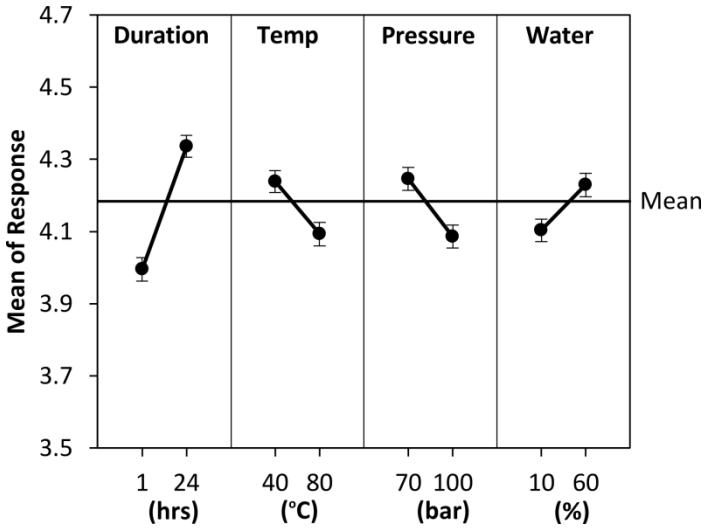

Figure 6.5 – *Main effects plot for the factors: duration, temperature, pressure and water content.*

Interaction effects between variables can influence the complex carbonation reaction, where the carbonation response is dependent on multiple factors, and the interaction plots are shown below, where parallel lines show no interactions, but non-parallel lines indicate interactions between the displayed factors. The interaction between the duration of the reaction and the temperature is similar to the interaction between the duration and pressure, and both interaction effects are plotted in Figure 6.6, showing the mean of each response.

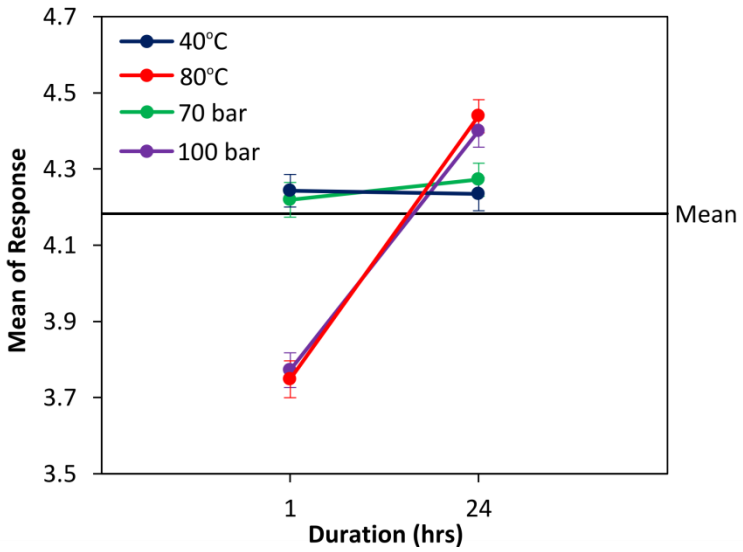

Figure 6.6 – *Interaction plot for duration*temp (blue and red) and duration*pressure (green and purple).*

An increase in the duration at low temperatures and pressures did not result in a change in carbonation, however, an increase in the duration at higher temperatures and pressures led to a significant change in total carbonation. Overall, lower temperatures and pressures resulted in more carbonation when reacted for one hour, compared to greater carbonation at higher temperatures and pressures when reacted for 24 hours.

Figure 6.7 shows the 3-way interaction effect for duration*temperature*pressure. A change in pressure at 80 °C, did not lead to a change in the carbonation effect when the duration was increased from 1 hour to 24 hours. However, an increase in pressure to 100 bar at 40 °C led to an increase in carbonation as the duration increased, compared to a decrease in carbonation at 70 bar.

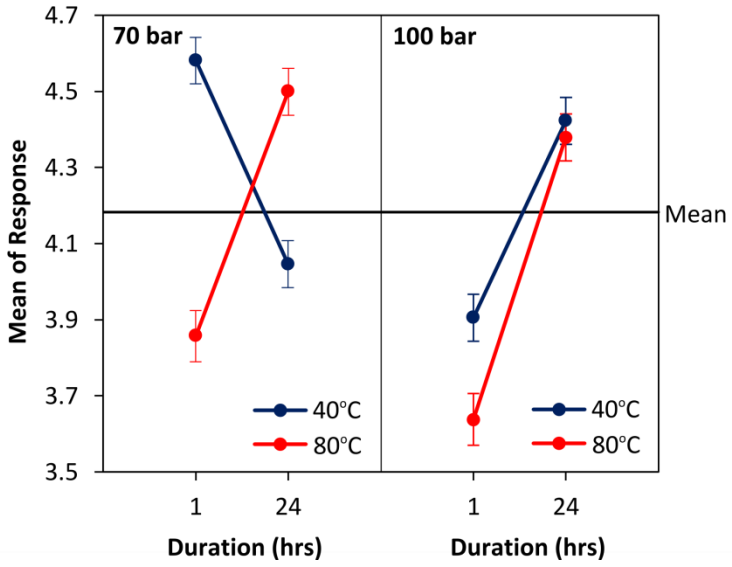

Figure 6.7 – *Interaction plot for duration*temperature*pressure.*

Overall, a combination of an increase in pressure, temperature, and water led to the lowest extent of carbonation when reacted for 1 hour, as shaded in orange on the cube plot (Figure 6.8). Other low carbonation values were achieved when reacted for the shortest duration, with varied pressure, temperature and water content with the exception of the reaction at 40 °C and 70 bar which achieved the greatest carbonation (shaded green). Alternatively, reactions at the longest duration and highest temperature and water content, also yielded higher carbonation results.

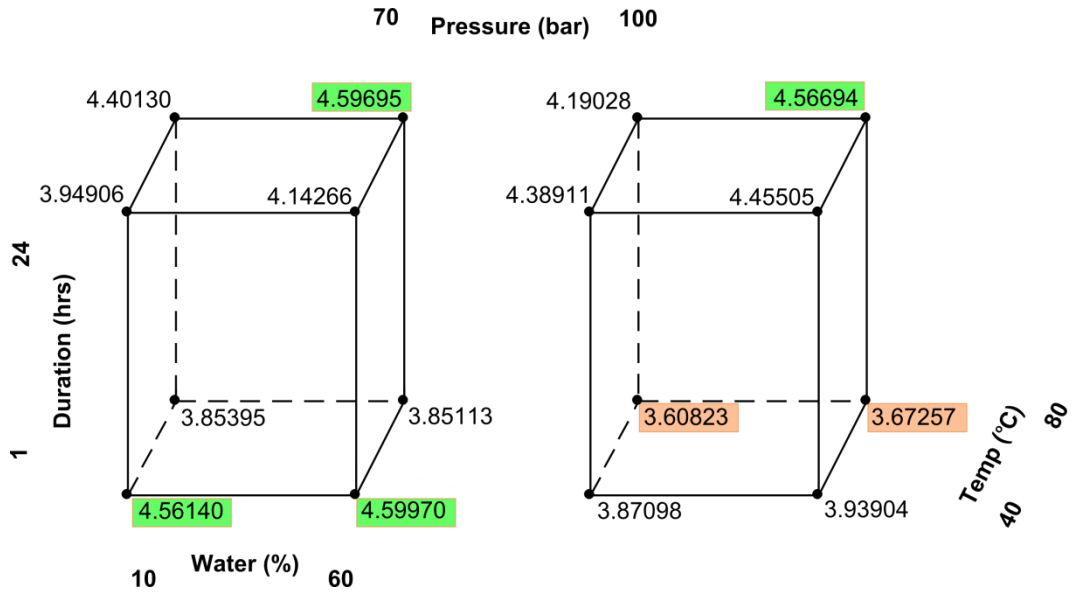

Figure 6.8 – *Cube plot for carbonation response based on each factor in the 2-level design.*

6.3.1.2 Full factorial design

A General Linear Model (GLM) using multiple levels of the 4 factors was produced by an extension of the factorial design, to improve the significance and reliability of ANOVA results from the 2-level design. The model was extended for the two most important factors from the 2-level design that was the duration, and the interaction of the duration with the temperature.

A model was produced based on 190 data points, after the removal of outliers, and the reduction of the model to focus on significant factors and interaction effects. The mean was calculated to be 4.0283 wt % CO_2 and the standard error of the mean = 0.029 wt % CO_2. The greatest response to carbonation was 5.02 wt % CO_2, that occurred when carbonated with 60 % water, for 4 hours, at 80 °C and 100 bar, however, the least carbonation occurred when the duration was reduced to 2 hours, with 60 % water at 70 bar and 60 °C. Results were independent and results from the Anderson-Darling test indicated that the data was normal, while Levene's test indicated equal variances. The resultant ANOVA GLM model was produced to determine the effect of each factor on carbonation (Table 6.7).

Table 6.7 - *ANOVA model for the GLM design, showing for each factor and interaction the degrees of freedom (DF), the probability (significant if P < 0.05), and the % variance (ω^2).*

Source	DF	P	ω^2
Duration	4	0	20.05 %
Temp	2	0.001	3.01 %
Pressure	1	0.118	0.5 %
Water	1	0.046	0.56 %
Duration*Temp	8	0	10.47 %
Duration*Pressure	4	0	4.25 %
Duration*Water	4	0	6.94 %
Temp*Pressure	2	0.001	2.37 %
Temp*Water	2	0.039	0.82 %
Duration*Temp*Pressure	8	0	5.06 %
Duration*Temp*Water	8	0.001	4.27 %
R^2	68.11 %		
N	190		
S	0.260568		

Results from the full factorial design explain 68.11 % of the variance in the dataset, compared to 86.03 % using the 2-level design. The effect of the duration and other factors interacting with the duration were significant and make up a large proportion of the model, similar to the 2-level design (Figure 6.9) contributing to 88 % of the model, however, temperature also largely contributed, accounting for 45 % of the produced model. More 2-way and 3-way interactions became significant using the improved model, and the pressure alone was not significant. A list of the factors and their interactions in decreasing order of importance were: duration, duration*temp, duration*water, duration*temp*pressure, duration*temp*water, duration*pressure, temp, temp*pressure, temp*water, and water.

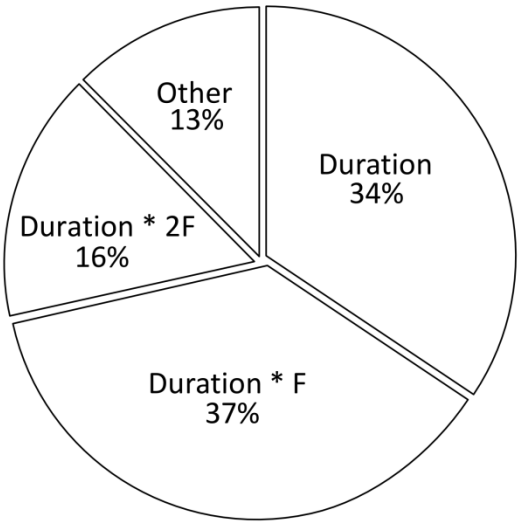

Figure 6.9 – *Pie chart of the main factor and interaction effects contributing to the ANOVA GLM model.*

The results from *post-hoc* testing are provided in Table 6.8. Results showed that an increase in duration and water content led to an increase in carbonation. The carbonation result from varying the temperature was more complex, where no significant difference was determined between carbonation at 40 °C and 80 °C, however the results from carbonating at the lowest and highest temperatures was significantly greater than carbonating at 60 °C. These main factor effects are displayed in Figure 6.10 to show the significant differences.

Table 6.8 – *Post-hoc testing results for each main factor effect, placed in order of importance, for the GLM model.*

	Conditions	**P-value**
Duration (hrs)	0.5, 1, 2 < 4, 24	All 0.0000
Temperature (°C)	40 > 60; 80 > 60	0.0202; 0.0007
Water (%)	10 < 60	0.046

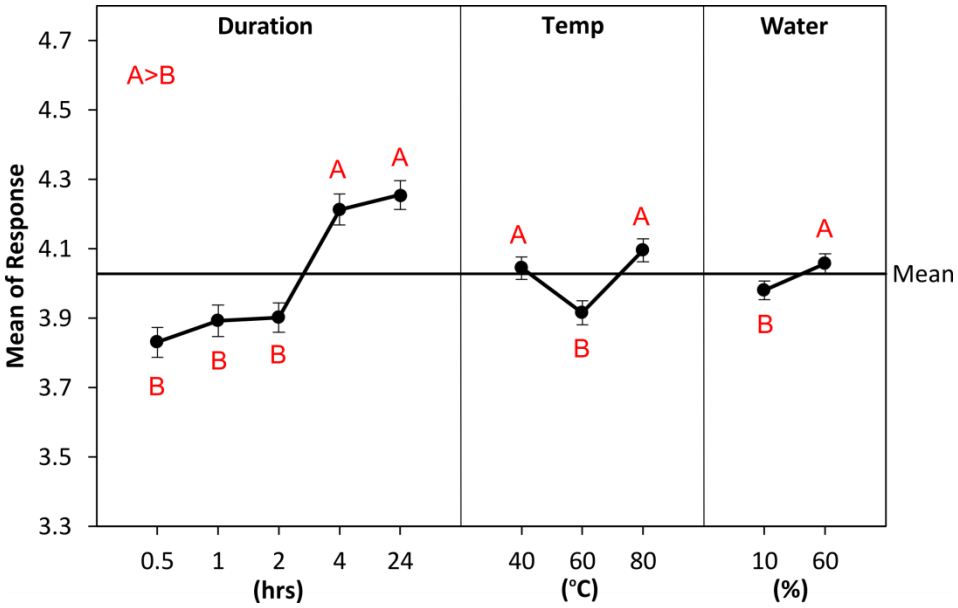

Figure 6.10 – *Main effects plot for the factors: duration, temperature and water content. The significant differences are shown by the labels A and B, where % CO_2 for A > B.*

The interaction effects were more complex for the extended factorial design compared to the 2-level design. Results from the interaction of duration separately with temperature, water and pressure are shown in Figure 6.11. Results indicated an increase in carbonation, from 2 to 24 hours, at 40 °C and 80 °C with no interaction between the temperature and the duration (Figure 6.11A). However increasing carbonation time from 30 minutes to 1 hour, caused carbonation to increase at 40 °C, yet decrease at the higher temperatures. Conversely, increasing carbonation from 1 hour to 2 hours, the carbonation decreased at 40 °C, yet increased at 80 °C. Overall, carbonation was greater at 80 °C, with the exception of the 1 hour experiment where the carbonation was significantly greater when performed at 40 °C. The same effect was noticed for the interaction with pressure and duration, with an increase in carbonation at the lower pressure going from 30 minutes to 1 hour, followed by a decrease in carbonation as the reaction was extended to 2 hours (Figure 6.11B). However, when comparing the carbonation reaction between 4 hours and 24 hours, greater carbonation was achieved at lower pressure within 24 hours, compared to higher pressures within 4 hours. The final interaction plot showed no interaction between water and duration between 30 minutes to 1 hour, where the greatest carbonation was achieved using 10 % water, however, as the reaction was extended from 2 to 4 hours, the carbonation increased significantly when using 60 % water, remaining constantly high up to 24 hours, compared to the lower carbonation results when using 10 % water at the higher durations (Figure 6.11C).

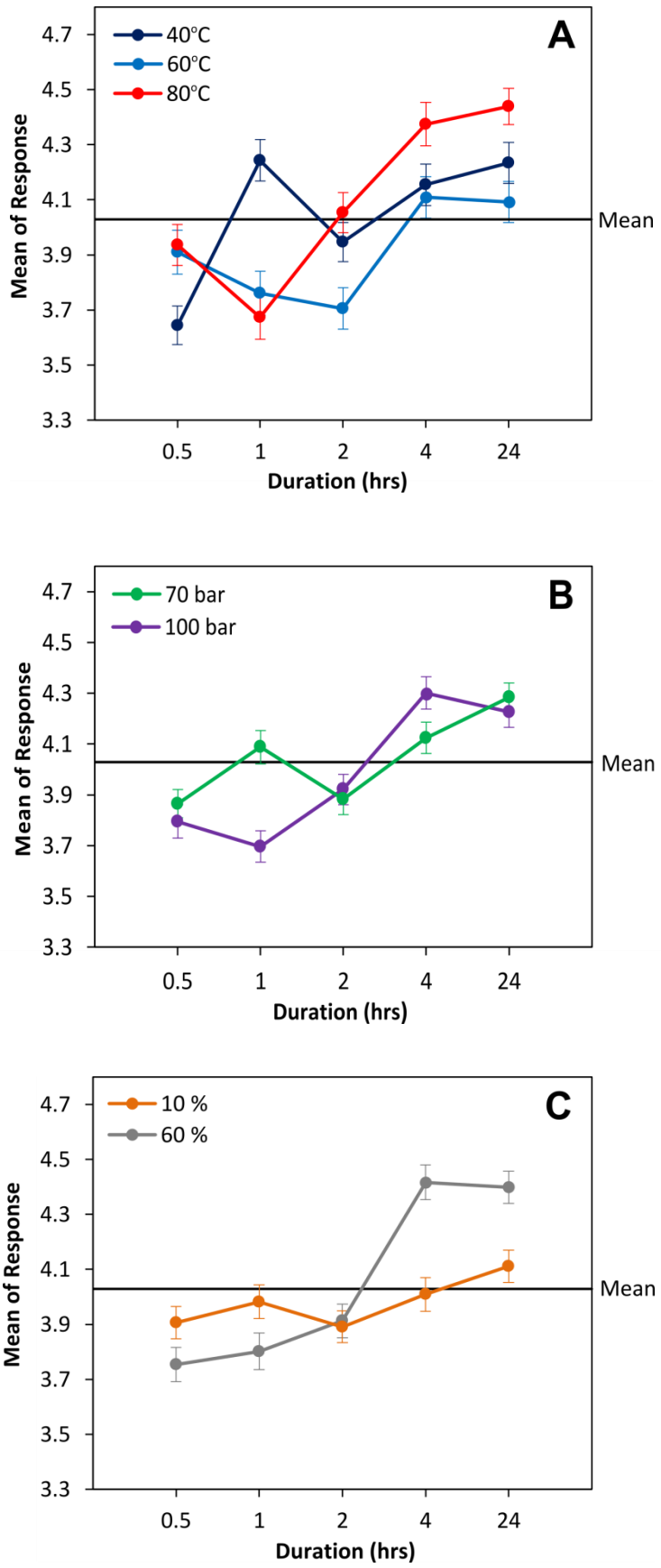

Figure 6.11 – *Interaction plots for A) duration*temp; B) duration*pressure; and C) duration*water content.*

Interactions between the temperature and pressure, and temperature and water contributed very little to the model, however small interaction effects can be observed between 60 °C and 80 °C, where an increase in carbonation occurred at the higher temperature and higher pressure, compared to the lower pressure (Figure 6.12). On the other hand, higher carbonation was also achieved at lower temperatures (40 °C and 60 °C) and lower pressures. For the interaction of temperature with water, an increase in carbonation was also observed when reacted at 80 °C with 60 % water, however the significance of this interaction was low, contributing to only 0.82 % of the model, with a P-value of 0.039.

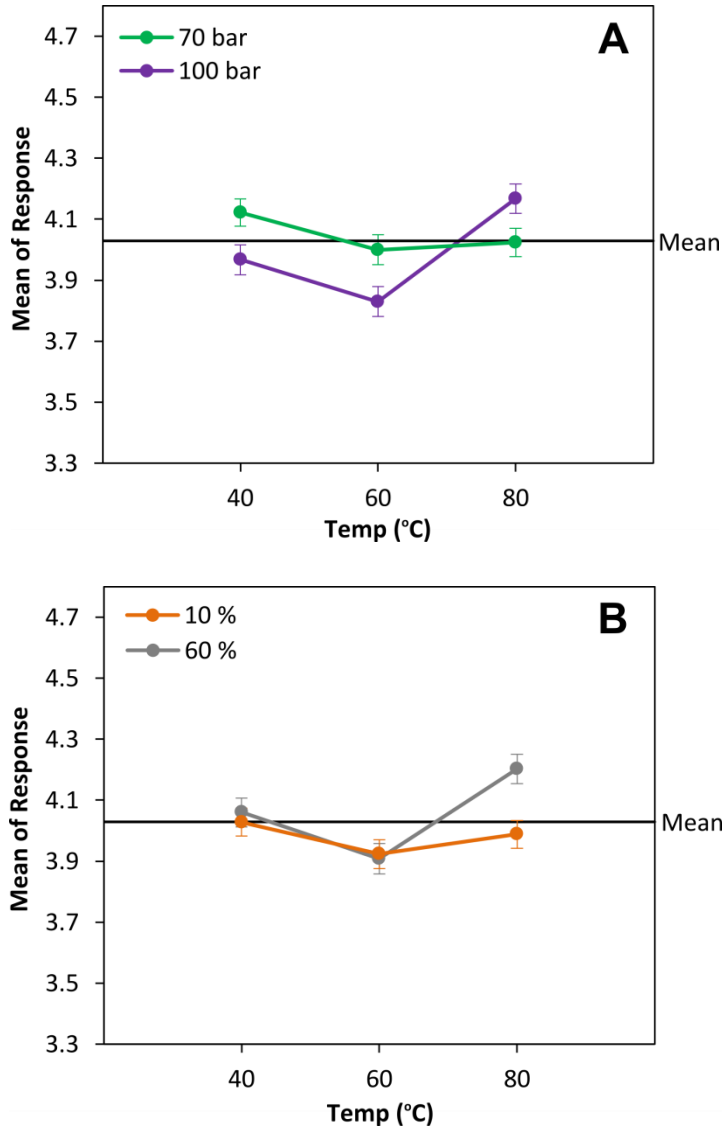

Figure 6.12 – *Interaction plots for A) temperature*pressure and B) temperature*water.*

The 3-way interactions are shown in Figures 6.13 and 6.14. Firstly, the interaction between the duration, temperature and pressure was analysed, which was found to be more complex than first observation in the 2-level design. On comparison of Figure 6.13: A and B, the carbonation effect at 60 °C and 80 °C at 100 bar, from 2 to 24 hours was similar to carbonation at 40 °C and 70 bar, where the greatest carbonation was observed at 4 hours. The converse was also true, where carbonation increased from 2 to 24 hours, at 40 °C and 100 bar, and also 60 and 80 °C, at 70 bar. At the lower durations, from 30 minutes to 1 hour, carbonation at 80 °C and 100 bar had the opposite effect to 40 °C and 70 bar, that showed an increase in carbonation at 1 hour. The same was also true for 40 °C and 100 bar, but was less exaggerated.

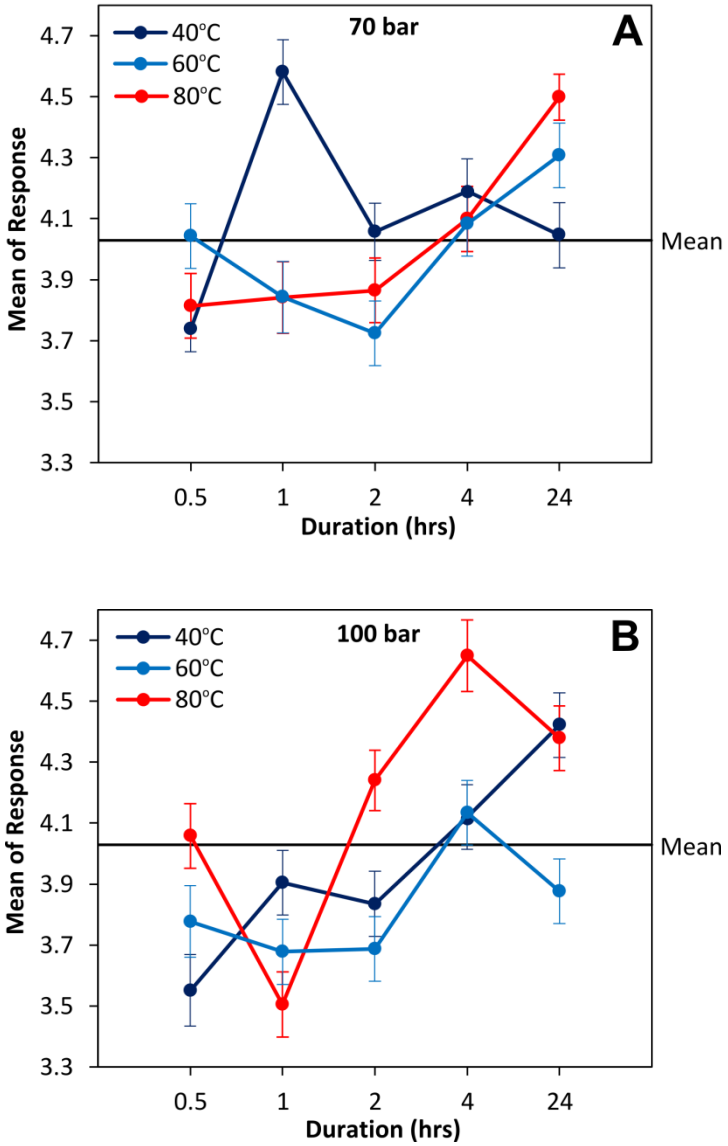

Figure 6.13 – *Interaction plots for duration*temperature*pressure.*

Interaction effects between the duration, temperature and water content are shown in Figure 6.14. No interaction was observed at 40 °C and varying water content, however at 80 °C, a greater increase in carbonation was observed with 60 % water, from 1 to 4 hours. The carbonation at 60 °C varied in a similar way to 80 °C with 60 % water, however with only 10 % water, no significant change in carbonation was observed as the reaction was extended from 30 minutes to 24 hours. The greatest carbonation overall was detected using 60 % water, and the sudden increase in carbonation as the duration increased was observed at different points of the reaction: firstly at 40 °C, then at 80 °C and finally at 60 °C.

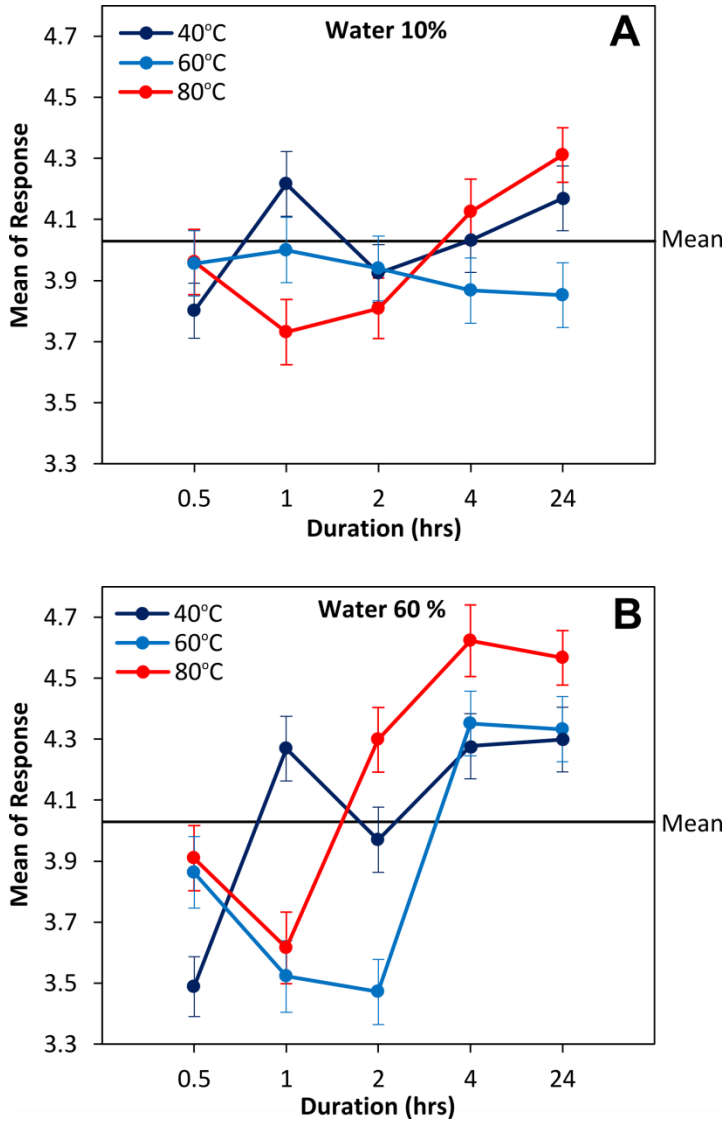

Figure 6.14 – *Interaction plot for duration*temperature*water.*

6.3.2 Further analysis

On analysis of the cumulative density function (CDF) for carbonation at different durations, the water content had a strong influence on the shape of the curves (Figure 6.15). Reaction with 10 % water did not show large variation in the shape of the density function, however, increasing the amount of water to 60 %, the initial starting value for new carbonate content increased between 2 to 4 hours.

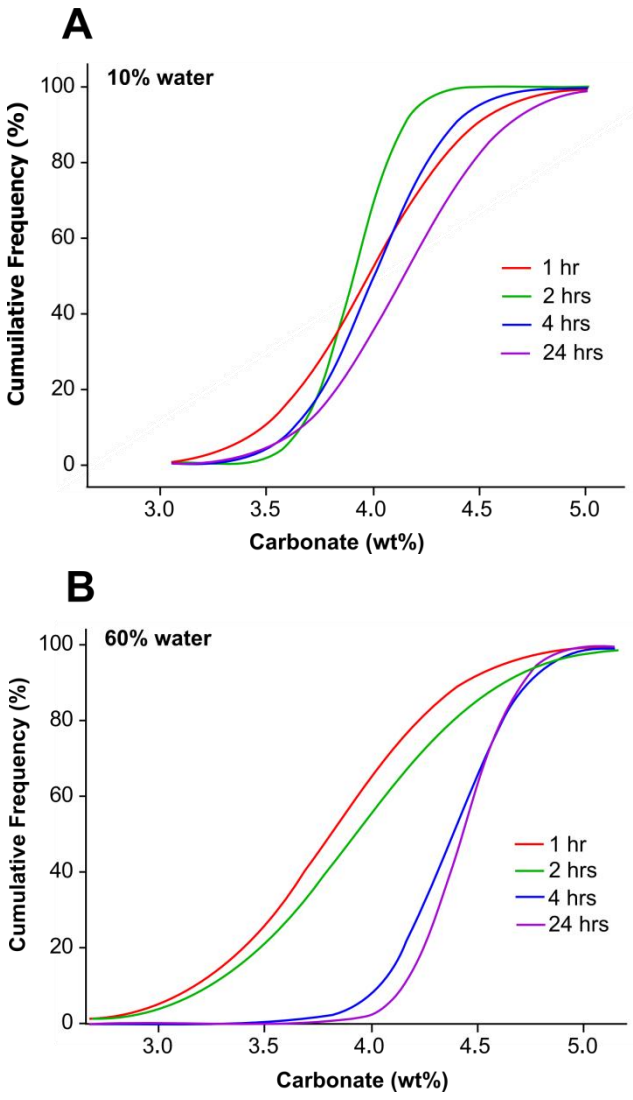

Figure 6.15 – *Cumulative frequency curve for carbonation with A) 10 % water and B) 60 % water.*

Due to the significance of the interaction between the duration and the water content, further investigation into the quantitative assessment of carbonate content using thermogravimetric analysis (TGA) was conducted. The weight loss due to carbonate content was taken to be from 550-950 °C, however, the extent of weight loss was not found to be constant within this carbonate decomposition zone, being split into phases which are dependent on their rate of decomposition, where phase 1 = 550-770 °C, and phase 2 = 770-950 °C, based on the division of a typical TGA weight loss curve and it's derivative (Figure 6.16).

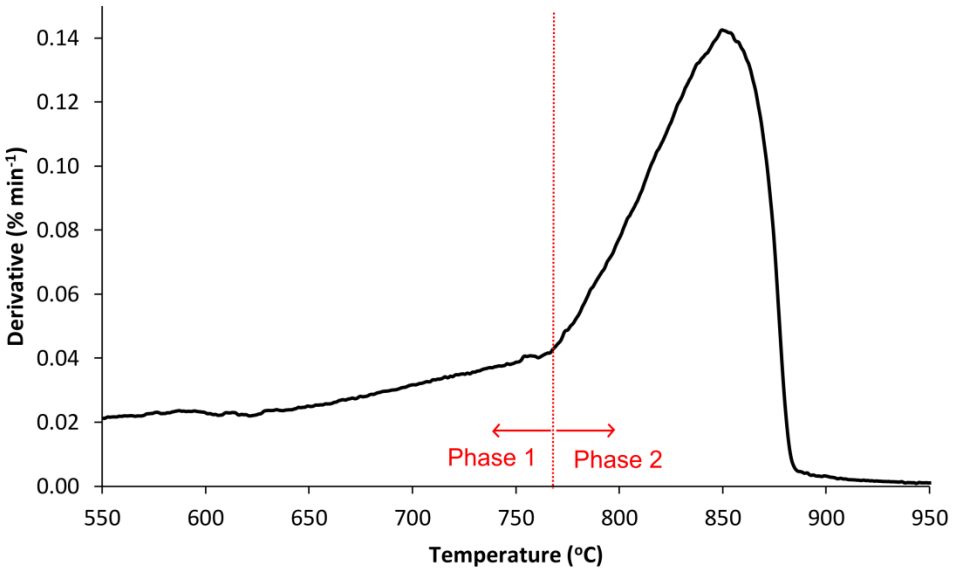

Figure 6.16 – *Derivative curve showing the rate of change for the weight loss from J-SOS-CO_2, carbonated for 30 minutes, at 60 °C, 70 bar with 60 % water.*

By looking at the relationship between water content and the percentage weight (wt %) of the new carbonate, for a series of samples (regardless of the conditions forced upon them), a cyclic trend was identified (Figure 6.17), where greater amounts of new carbonate were detected in phase 1, at low water conditions, and greater amounts of new carbonate in phase 2, at higher water contents. The two phases were inversely proportional, where high concentrations within phase 1 led to lower concentrations within phase 2, and the opposite was also true (Figure 6.18).

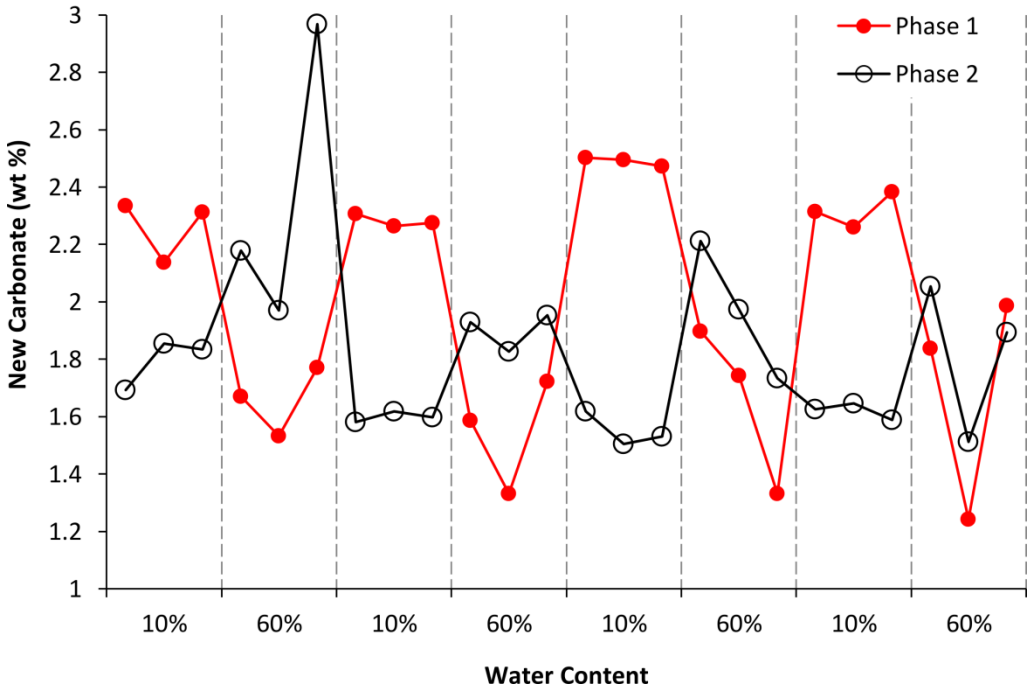

Figure 6.17 – *New carbonate content associated with phase 1 and phase 2, in wt %, for samples carbonated using 10 % and 60 % water.*

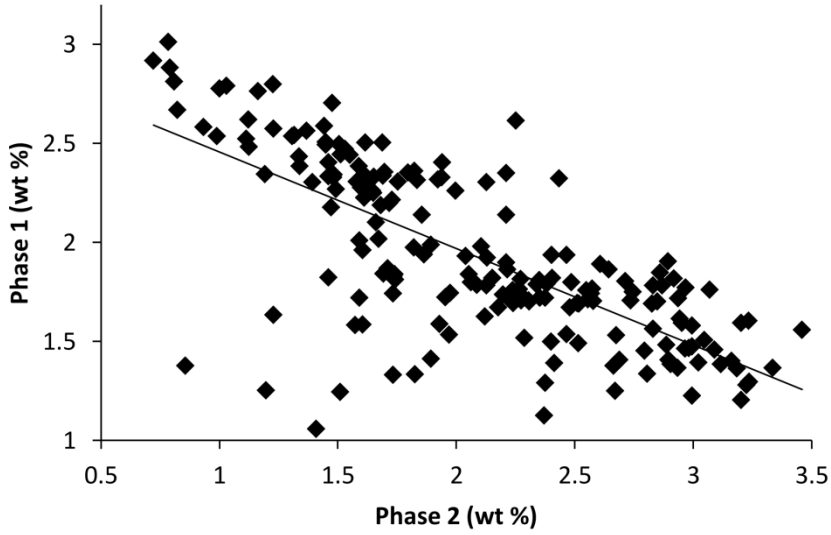

Figure 6.18 – *Scatterplot and linear regression between new carbonate in phase 1 (y-axis) versus new carbonate in phase 2 (x-axis).*

To analyse the data further, a model based on the ratio of phase 1 to phase 2 was established using ANOVA. The data was not normal and did not show homogenous variances, yet was improved when log transformed. Due to the robustness of the ANOVA technique, the model was used to look at the effect of main factors, however interaction effects were not analysed. Additional variables were added to the model: firstly the total carbonation value was used as a covariate, and the date analysed was added as a factor. The latter was used because the shape of the weight loss curve varied according to the date it was analysed, due to slight differences in the way the TGA recorded and measured the mass of each sample, yet this was not found to statistically affect the overall weight loss as a result of carbonation (Figure 6.19). To account for this, the variable was split into 2 numerical levels to be used as a factor in the model.

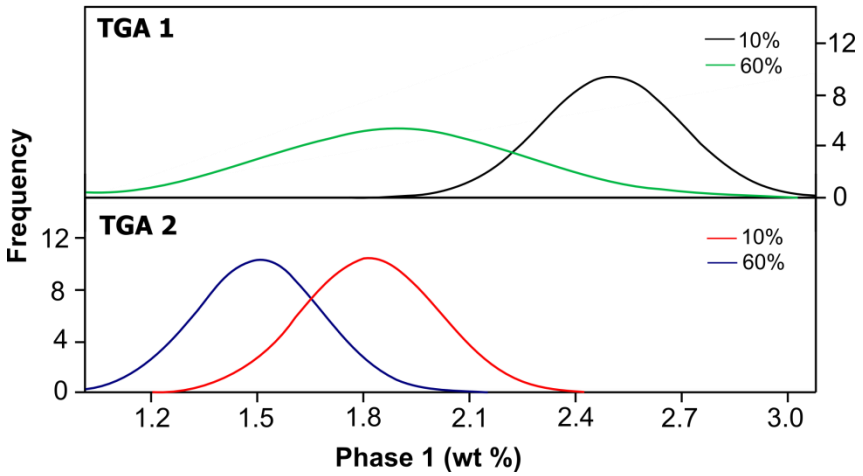

Figure 6.19 – *Histogram of phase 1 new carbonate content showing the comparison of TGA runs (1 and 2) and water content (10 % or 60 %).*

A General Linear Model (GLM) using multiple levels of the 5 factors and the covariate (Table 6.9) was produced based on 187 data points, after the removal of outliers, and the reduction of the model to focus on significant factors and interaction effects. The mean of the ratio of phase 1: phase 2 was calculated to be 0.95 after transformation. The resultant ANOVA GLM model for the response Log (Ph 1/Ph 2) was produced to determine the effect of each factor on carbonation (Table 6.10).

Table 6.9 – *Factors and covariates used in the GLM model and the number of levels tested.*

	Factor	# of levels	level values
A	Pressure	2	70, 100 (bar)
B	Temp	3	40, 60, 80 (°C)
C	Duration	5	0.5, 1, 2, 4, 24 (hrs)
D	Water	2	10, 60 (%)
E	TGA	2	1, 2 (type)
Covariate	Total new carbonate	-	-

Table 6.10 - *ANOVA model of the GLM design for LOG (Ph 1/Ph 2), showing for each factor and interaction the degrees of freedom (DF), the probability (significant if P < 0.05), and the % variance (ω^2).*

Source	DF	P	ω^2
Total new carbonate	1	0	26.56 %
Duration	4	0.001	13.82 %
Temp	2	0	16.27 %
Pressure	1	0	3.68 %
Water	1	0	19.20 %
TGA	1	0	6.82 %
Duration*Temp	8	0	2.71 %
Duration*Pressure	4	0	0.71 %
Duration*Water	4	0	1.97 %
Temp*Pressure	2	0	1.67 %
Temp*Water	2	0.147	0.01 %
Pressure*Water	1	0.184	0.04 %
Duration*Temp*Pressure	8	0	1.62 %
Duration*Pressure*Water	4	0.002	0.33 %
Temp*Pressure*Water	2	0.02	0.14 %
R^2	96.64 %		
N	187		
S	0.0478675		

The GLM ANOVA explained 96.64 % of the variance in the dataset, for the response of Log (Ph 1/Ph 2) using the assigned variables. A list of factors and their interactions in decreasing order of importance were: total new carbonate, water, temp, duration, TGA, pressure and duration*temp. All other interaction effects contributed to < 2 % of the model. The most important factors were the total carbonation, the pressure, water and duration, as opposed to interaction effects in models looking at the total carbonation response.

The results from *post-hoc* testing of the principal factors are provided in Table 6.11. Results showed that an increase in duration (from 4 to 24 hours), temperature and pressure led to an increase in carbonation within phase 1, whereas an increase in water content led to an increase in carbonation within phase 2. These main factor effects are displayed in Figure 6.20 to show the significant differences.

Table 6.11 – *Post-hoc testing results for each main factor effect, placed in order of importance for the GLM model.*

	Conditions	**P-value**
Water	10 > 60	0.0000
Temperature	40,60 < 80	Both 0.0000
Duration	4 < 24	0.0012
Pressure	70 < 100	0.0000

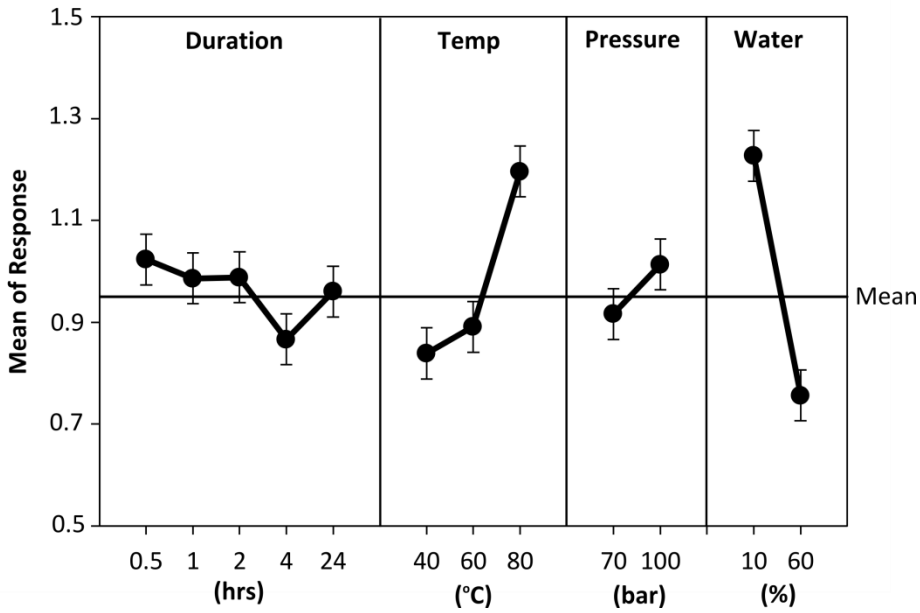

Figure 6.20 – *Main effects plot for the factors: duration, temperature, pressure and water.*

Interaction plots are shown for the interaction between the duration and temperature and the duration and water content (Figure 6.21). Other interaction plots were not considered due to their low importance in the model (low ω^2), and the lack of normality and equal variances of the dataset. Larger amounts of carbonate were formed within phase 1 at the higher temperatures and low reaction durations, however, when the reaction was extended to 4 hours, the carbonation within phase 1 decreased, compared with the consistent phase 1 to phase 2 ratio as duration increased at lower temperatures. The water content showed a similar interaction with duration, by remaining a steady ratio between phase 1:phase 2 at 60 % water, but a greater concentration of carbonate within phase 1 was observed using 10 % water at the lower durations, which then drops when the reaction is extended to 4 hours.

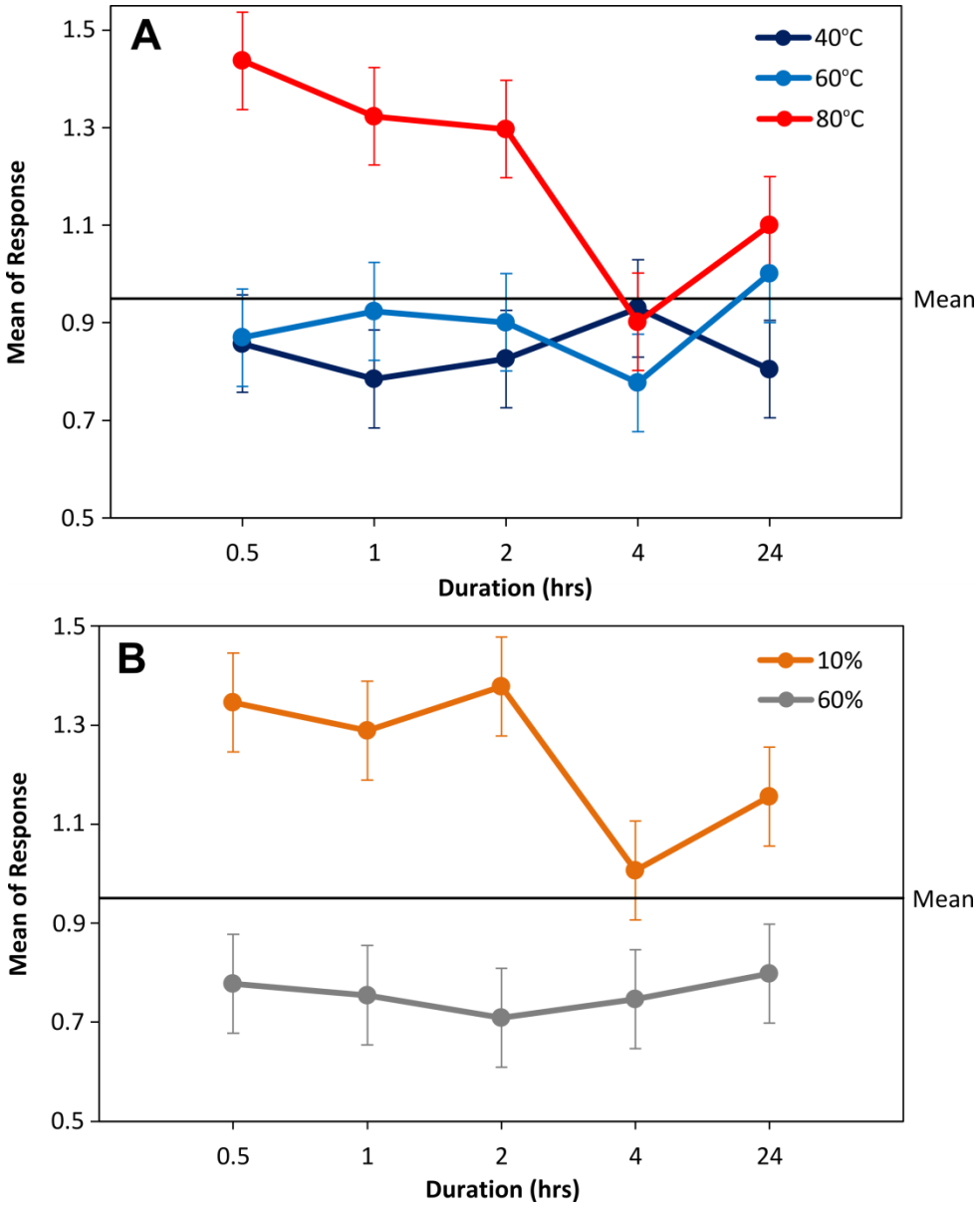

Figure 6.21 – *Interaction plots for A) duration and temperature and B) duration and water content.*

Three models have been produced and analysed using data provided from the analysis of spent oil shale that has undergone carbonation at high pressures and temperatures. The results will be discussed in terms of kinetics and the extent of carbonation to identify probable reaction mechanisms and opportunities for optimisation.

6.4 Discussion

The use of a factorial designed carbonation experiment alongside ANOVA statistical methods enabled the analysis of the effect of different factors and interaction effects, on the extent of carbonation. The confirmation of normality, equal variances and independence ensured the suitability of data for analysis, and in addition, the use of a dataset of 180 samples, including replicates, reduced errors associated with the results and allowed for factor effects to be distinguished with high levels of confidence. Compared to the analysis of standard error associated with carbonation values, such as in Chapter 5, a factorial design enabled the use of a robust method of statistical analysis and therefore made it possible to assess significance and magnitude - a first in a study of this kind on accelerated carbonation that is already known to be dependent on multiple variables. The relationship between these variables and the carbonation mechanism was investigated further based upon the experimental design and subsequent analysis.

Results showed that using a 2-level design, all the factors were significant in contributing to carbonation (Table 6.5), with the duration the most effective of these factors (Figure 6.4), where carbonation was increased when longer reaction times were used, indicating the kinetic control on the carbonation (Anthony et al., 2000). The interaction between the duration and temperature produced similar results with the interaction of the duration with pressure, indicating that the effect of temperature and pressure led to similar carbonation results (Figure 6.6). However, a strong 3-way interaction between the duration, temperature and pressure (Figure 6.7), showed that at 40 °C and 70 bar, most carbonation was achieved within 1 hour, with carbonation significantly decreasing if extended to 24 hours, whereas at 100 bar, the most carbonation occurred within 24 hours, regardless of the temperature. This difference was also indicated in the cube plot (Figure 6.8), which showed that for carbonation reactions extended to 24 hours; higher pressures, temperatures and water content was required for greater carbonation, yet for reactions occurring within one hour, the greatest carbonation was achieved at lower temperatures and pressures. This can be summarised as:

High T & P	>	Low T & P	>>	High T & P
24 hours		1 – 24 hours		1 hour

Results from the 2-level design were complex and indicated favourable conditions at the lowest forcing conditions (low temperatures, pressures and durations), suggesting that higher pressures and temperatures may be inhibiting carbonation in some way, perhaps by pore blocking or surface coating mechanisms. Therefore, the extension of a 2-level design to a full general linear model (GLM) was conducted to further improve the model and increase the significance of results. The resultant R^2 value was found to decrease, from 86 to 68 % (Table 6.7), due to increased errors from the experimental and analytical procedures, as the experiment was extended to analyse almost 4 times the number of samples as the 2-level design. Because the new model took into account more variables using a greater dataset, this led to the reduction in the standard error in the model and greater precision, while the inclusion of more factors, 2-way and 3-way interactions improved the overall sensitivity of the design and reduced the error on main factors, despite the low significance of some of these variables in the model itself. In addition, the effect of the duration and temperature were investigated in more detail, due to their significance and importance in the 2-level design.

By considering the results from the full factorial design, the influence of each factor on carbonation was investigated, taking into account the main factor's effects and interactions. By increasing the levels tested for the temperature and duration, to 3-levels and 5-levels respectively, the pressure and water content were insignificant and marginally significant, respectively, and each contributed to < 1 % of the model (Table 6.7). However, interaction effects between the pressure and water content with the duration and the temperature were determined to be significant, increasing the importance of the pressure and water variables within the GLM and on the amount of carbonation that can be achieved. The contribution from the main effects and interactions associated with the duration and temperature decreased (Figure 6.9), yet even so results suggest that these factors play a large role in the amount of carbonation that can be achieved and the kinetics of the reaction. The significance of all factors tested was in agreement with Ecke (2003) who discovered that the pressure, duration, temperature and water content were all important for the carbonation of MSWI, and also with Miller et al. (2013) for the carbonation of wollastonite using supercritical conditions.

The most important and simplest factor to interpret was the duration, where carbonation experiments at 4 hours and 24 hours achieved greater amounts of new carbonate than those at 30 minutes, 1 hour and 2 hours (Figure 6.10). This indicates that carbonation is completed

within 4 hours of the reaction, and extending the reaction to 24 hours does not significantly increase the amount of carbonate formed. Nevertheless, significant carbonation compared to the control was achieved within 30 minutes, indicating that carbonation does occur very quickly, in agreement with other research where carbonation was achieved on a timescale of minutes (Huijgen et al., 2005).

The difference between carbonating at 70 bar and 100 bar was not significant in this model, where CO_2 was supplied at sufficiently high pressure to infiltrate spent oil shale, to produce thick precipitated layers, compared to atmospheric pressures that favour precipitation at the surface of material (Cultrone et al., 2005). However, interaction mechanisms were observed between the pressure and temperature (Figure 6.12). When carbonating at the higher pressures, more carbonation was achieved at the higher temperature as well, otherwise, lower temperatures and pressures showed greater carbonation. This may be due to the availability of CO_2 acting to limit the carbonation. At the lower temperatures, more CO_2 is soluble in water and available for carbonation reactions, however, as the temperature increases, the solubility of CO_2 decreases, therefore an increase in pressure is required to compensate for the reduced solubility of CO_2 (Huijgen et al., 2006). In addition, the interaction between the duration and the pressure (Figure 6.11) indicated that for longer reactions, greater amounts of carbonation were achieved at higher pressures in 4 hours, yet there was little difference between carbonating at 70 bar or 100 bar in 24 hour reactions, indicating that the higher pressure speeds up the reaction by increasing the supply of CO_2 to active sites, but does not increase the extent of reaction (Domingo et al., 2006). At the lower durations, the reaction was likely to be incomplete and therefore higher pressures were not required and strong interaction effects were observed.

Similar to the pressure, the difference between carbonating at 40 °C or 80 °C was not identified to be a significant factor for carbonation. However, carbonating at 60 °C achieved the least carbonation from all the experiments studied (Figure 6.10); alone and when interacting with other factors. It may be that at 80 °C, the kinetics of the reaction is more favourable towards carbonation, whereas at 40 °C the solubility of CO_2 is more favourable (Fernandez Bertos et al., 2004). The interaction of temperature with duration (Figure 6.11) affected both the kinetics and extent of reaction, yet showed more significant differences at the lower durations (30 minutes to 2 hours) when the reaction was incomplete. During this pre-equilibrium region, the least carbonate was produced at 40 °C and 30 minutes, with an increased rate of reaction by using higher temperatures, that is perhaps diffusion controlled. The subsequent decline in carbonation when spent oil shale was reacted for one hour at 80 °C,

but an increase in carbonation at 40 °C, suggests that the availability of CO_2 was affecting the amount of carbonation when the reaction was given more time to proceed. Further carbonation at longer durations showed other driving forces to be affecting the formation of carbonate minerals. Higher temperatures of 80 °C produced more carbonate at the longer reaction times, in disagreement with others, where higher temperatures limited the overall carbonation in waste materials at lower pressures (Li et al., 2007; Rendek et al., 2006). Higher temperatures may favour diffusion of CO_2, if supercritical conditions are used; however inhibiting mechanisms may also play a part in the reaction mechanism.

The effect of the temperature and pressure on carbonation between 30 minutes to 1 hour was significantly different between reactions at 40 °C and 70 bar, compared to reactions at 80 °C and 100 bar (Figure 6.13). Carbonation decreased at the higher pressures and temperatures, compared to increasing at the lower pressures and temperatures, which may be due to incomplete carbonation at the lower durations, or inhibitory mechanisms. Reactions at 80 °C and 70 bar, compared to 40 °C and 100 bar, did not interact with each other at longer reaction durations, both showing an increase in carbonation from 2 to 24 hours, indicating diffusion-controlled slower reaction kinetics at play, resulting in the formation of greater amounts of carbonate overall within 24 hours.

The discovery of the dependence of newly formed carbonate on the water content (Figure 6.15) led to further analysis of the region of carbonate decomposition from thermogravimetric analysis, leading to the identification of two phases of carbonate decomposition (Figure 6.16). The first, less stable, phase 1 was decomposed at lower temperatures, from 550-750 °C; and the second phase 2, decomposed at higher temperatures up to 950 °C. Statistical analysis of the ratio of phase 1:phase 2 (Ph1:Ph2) was completed, producing a model explaining 97 % of the data (Table 6.10), due to the incorporation of significant factors, covariates and interactions. Although the date of TGA analysis was found to be a significant factor, it only contributed to 6.8 % of the model, showing that it allowed for the identification of other variables without itself affecting the main results. Instead, Ph1:Ph2 was found to be mainly dependent on the total carbonation, the duration, temperature and water content, where the percentage of water used in carbonation experiments was a distinguishing factor for the formation of different carbonate phases (Figure 6.17 and Figure 6.20). Further work on the characterisation of the two separate phases was completed in Chapter 7.

Greater amounts of water were shown to increase carbonation as the reaction time increased (Figure 6.11), with the exception of increasing the duration from 4 hours to 24 hours, which

showed little difference in carbonation, due to equilibrium being reached within 4 hours. Greater carbonation with more water at the longer durations could be a result of increased access to active sites, however too much water at the lower durations can prevent carbonation, by increasing the time it takes for ions to diffuse to reactive sites. Also, greater amounts of carbonation using 60 % water were linked to the formation of phase 2 carbonate, regardless of the length of the reaction (Figure 6.21). Greater variation in the amount of carbonation was also observed using 60 % water compared to 10 % water, with the onset of increased carbonation occurring first at lower temperatures (Figure 6.14), which may be due to the greater solubility of CO_2 coupled with access to reactive surfaces; before the higher temperatures which kinetically favour carbonation, yet with reduced CO_2 solubility.

Greater phase 1 carbonate was formed at the higher temperatures and with 10 % water especially at lower reaction durations, but was then reduced when the reaction was extended to 4 hours (Figure 6.21). With only 10 % water, total carbonation appears to be limited, with little difference between reactions at different durations, therefore showing an inhibitory effect, by not providing enough water for the dissolution of cations and carbonate that will enable precipitation (Cultrone et al., 2005). Limited water also prevents the formation of stable carbonate initially (Figure 6.21), but allows for dissolution and re-precipitation when reacted for longer periods of time, from 4 to 24 hours. In addition, more water is required at higher temperatures, indicating that the amount of water, and therefore the diffusion of ions becomes rate determining as the reaction becomes faster and also as the reaction progresses to longer durations (Sarvaramini et al., 2014; Cultrone et al., 2005).

The temperature and the water content were the most significant factors controlling the type of phase formed (Table 6.10), and the increased formation of phase 1 at higher temperatures and using less water could be due to the acceleration of the reaction. The precipitation of carbonate could occur too quickly, or could be reduced, favouring metastable forms of carbonate mineral or amorphous calcium carbonate (ACC) (Thiery et al., 2007). The increased rate of carbonation could decrease carbonation due to coating of reactive spent oil shale surfaces and reduction in permeability by pore blocking (Zhao et al., 2010; Daval et al., 2009). Further work could be carried out in-situ – by the use of atomic force microscopy, which has been developed for use at high pressures and could be used to look at the structural changes occurring during carbonation (Lea et al., 2011). Pore volumes in cement was shown to decrease by up to 26 % by carbonation (Fernandez Bertos et al., 2004), while an uneven distribution of carbonate minerals was reported on the surface of wollastonite minerals, that can prevent further carbonation by inhibiting diffusion of Ca^{2+} away from the surface and CO_3^{2-}

to the surface (Miller et al., 2013). However, higher pressures and concentrations of CO_2 favouring the formation of heterogeneous surfaces, are able to promote further carbonation (Xu et al., 1998).

Overall, the average carbonation, achieved from the factorial design to optimise CO_2 sequestration within spent oil shale, was 4.03 wt % CO_2 (Section 6.3.1.2). This value corresponds to 54.5 % of the theoretical amount, greater than the value previously obtained in Chapter 5 (46 %). The fact that carbonation was not significantly increased to reach closer to 100 % of the theoretical value suggests that reactive surfaces and space for the precipitation of carbonate minerals is limited as the reaction progresses (Alvarez et al., 2005), where maximum conversions of 60 to 70 % have been reported with FBC ash due to pore blocking (Anthony et al., 2000). Therefore, greater pressures and temperatures are required to increase the supply of CO_2, and also increase the rate of diffusion, dissolution and re-precipitation mechanisms, forcing CO_2 further through the material to access more reactive surfaces (Fernandez Bertos et al., 2004). The maximum carbonation reached within the statistical model, was 5.02 wt %, or 68.5 % of the theoretical value, when carbonated using greater forcing, using 60 % water, at 80 °C, 100 bar and for 4 hours. This is in agreement with the hypothesis that reacting spent oil shale for 4 hours enables the reaction to be completed. At the same conditions, 5.88 wt % CO_2 were also sequestered, which was 81.1 % of the theoretical value; however, this result was treated as an outlier in the model. The least carbonation, within the model, was only 36.7 % of the theoretical, when reacted at 70 bar, 60 °C and for 2 hours, an unfavourable temperature for carbonation and not enough time for complete reaction of the available calcium ions. Significant carbonation was still consequential when spent oil shale was reacted at lower temperatures and pressures, at subcritical conditions, where reactions peaked at the lower durations, due to being diffusion controlled. This resulted in more stable carbonate being formed, and may be preferential for implementation of economically more feasible carbonation reactions.

To identify the types of carbonate formed during reactions at high pressures and temperatures, further work was completed and discussed in Chapter 7, by the use of Fourier transform infrared (FTIR) spectroscopy. In addition, optimum conditions for carbonation were identified and specifically tailored for the retorting and combustion mechanisms for Jordanian oil shale, with aims to process oil shale to produce the least CO_2 emissions, the most oil recovery, and the ideal physical properties for use of the spent oil shale as a by-product.

6.5 Conclusions

A comprehensive factorial design and general linear model using results from ANOVA was accomplished, confirming the significance of the duration, temperature, pressure and water content on the extent of accelerated carbonation that could be achieved in spent oil shale. In particular, the duration controlled the total amount of carbonation when not inhibited by other factors, with completion of the reaction within 4 hours. Other controls on carbonation were the amount of CO_2 available for reaction and the diffusion rate, dominated by the pressure, temperature and water content, with greater variation in results at the lower durations when carbonation had not reached the maximum potential.

Maximum carbonation was reached within 4 hours, at 69 % of the theoretical value when reacted under supercritical conditions with 60 % water. Higher temperatures and pressures favoured the formation of greater amounts of carbonation, however, to be economically more feasible, significant carbonation was still achieved by reacting at 40 °C, 70 bar, within 1 hour.

The carbonation mechanism occurred very quickly, forming carbonate minerals within 30 minutes. The type of carbonate formed was split into two phases: phase 1 being decomposed between 550-770 °C, and phase 2 decomposing between 770-950 °C. Phase 1, of lower stability, was favoured at lower reaction durations when reactions were diffusion limited using less water, and it is likely that faster reactions favour the formation of a more metastable carbonate, that could block pores and prevent further carbonation. This is investigated further in Chapter 7. By increasing the duration of the reaction and using 60 % water, greater amounts of carbonate of greater stability were favoured, after the reaction has progressed through dissolution and recrystallization mechanisms that are especially dominant at higher pressures.

Multiple controls on the carbonation of spent oil shale were evident during this optimisation study, with inhibition by pore blocking or surface coating apparent, and reactions controlled by kinetics and CO_2 supply. The use of supercritical conditions was required to enhance carbonation; therefore further work on the cost-effectiveness of the accelerated carbonation reaction will be outlined in Chapter 7.

Chapter 7: Optimisation of oil shale processing

7.1 Introduction

Initial carbonation experiments have been carried out on Jordanian spent oil shale, determining that 5.02 wt % of CO_2 could be sequestered when reacted for 4 hours using 60 % water, under supercritical conditions of 80 °C and 100 bar. Carbonation occurred quickly and was also achieved at subcritical conditions (< 80 °C, 70 bar), leading to the question as to whether higher pressures and temperatures, that are more costly, are required if the technology is implemented to reduce CO_2 emissions produced during retorting of oil shale.

In addition to considering the amount of carbonation that can be achieved by accelerated sequestration reactions, the retorting process itself has a large control over the amount of CO_2 that is released into the atmosphere, by the decomposition of carbonate minerals within the oil shale, and by combustion of the organic matter remaining in the retorted oil shale. The mechanism for retorting oil shale is complex, consisting of a pyrolysis step, where the oil shale is heated in the absence of oxygen and oil is removed; followed by combustion, where the oil shale is heated at higher temperatures with oxygen to burn residual carbon (Brandt, 2009). This retorting mechanism was summarised previously in Figure 3.3. The processing conditions cause the physical properties of the oil shale to change on heating, and the amount of CO_2 that is released into the atmosphere as a result of retorting and combustion is likely to be high, and is discussed in more detail in Chapter 8. Due to the high levels of CO_2 emissions, improvements are suggested as how to reduce CO_2 emissions further, by not only carbonation but by modifying the processing conditions. In addition, separate to the modification of the retorting and combustion mechanisms that are a part of the Alberta Tacuik Process (ATP), decarbonation procedures have also been tested, with the aim to reduce the amount of carbonate minerals that are broken down during combustion and therefore reduce CO_2 emissions in this way. Decarbonation processes act to heat the oil shale further, to temperatures of 600-750 °C, after retorting and in the absence of oxygen (Odut, 2012). Carbonate minerals are decomposed, and it is thought the increased partial pressure of CO_2 acts to prevent further decomposition of carbonate minerals, thereby reducing CO_2 emissions (Fadaei et al., 2012).

A reduction in CO_2 emissions is not the primary objective for oil shale retorting, however, with other important factors taking precedence, including the amount of oil that can be obtained from the oil shale, and the suitability of spent oil shale to be used as a by-product as an

additive in the production of cement. The oil recovery and use of spent oil shale as a by-product, are both dependent on the structural and chemical properties of the source material, and can therefore be controlled along with CO_2 emissions by modifying the processing conditions. Therefore, this chapter aims to investigate controls on the CO_2 emissions produced at different stages of the retorting process, to reduce CO_2 emissions as much as possible without detrimental effect on the oil recovery or use of spent oil shale as a by-product in the cement industry. To do so, the importance of carbonating at high vs. low pressures was also considered.

Further experimental work and analysis has been completed to assess how changes to the processing conditions may affect the CO_2 emissions produced from oil shale. A factorial design was produced, so as to be able to analyse the effect of multiple factors on the amount of CO_2 released. Factors were produced by breaking down the retorting process, and looking at samples of oil shale, oil shale that has been retorted (pyrolysed) at various temperatures, retorted oil shale that has been decarbonated at various temperatures before combustion, and retorted oil shale that has been combusted at various temperatures (Figure 7.1). In addition, carbonation reactions were carried out on each of the samples prior to analysis. As in previous chapters, quantitative thermogravimetric analysis and analysis of variance were used so as to be able to validate results obtained from processing and carbonating, using the carbonate content as the response.

Further mineral identification and characterisation of various samples was conducted using X-ray diffraction (XRD) and Fourier transform infra-red spectroscopy (FTIR), to investigate the link between the carbonation reaction and the carbonate product in more detail, while the oil recovery and physical properties of the spent oil shale were also analysed.

7.2 Methodology

7.2.1 Sampling and factorial design

Samples processed using different conditions were provided by Jordan Energy and Mining, Monash University and UMATAC (Table 7.1). Oil shale was provided by JEML and oil shale retorted at 400 °C was provided by Monash University. UMATAC provided the following samples: oil shale retorted at 500 °C; oil shale retorted and then decarbonated from 600-750 °C followed by combustion at 600 °C; as well as oil shale retorted and combusted from 600-750 °C. Samples were prepared for analysis and carbonation experiments by grinding to a

constant particle size of < 1 mm using an agate pestle and mortar, before drying in the oven at 105 °C to remove any moisture. Samples of J-OS, MON and UMA-1 were also combusted at 600 °C for 1 hour, in Durham, and were referred to as J-OS Comb, MON Comb, and UMA-1 Comb, respectively.

Table 7.1 – *Processing conditions used to obtain the different oil shale and spent oil shale samples.*

Samples	Provider	Temperature (°C)		
		Pyrolysis	Decarb	Combustion
J-OS	JEML	-	-	-
MON	Monash University	400	-	-
UMA-1	Umatac	500	-	-
J-OS Comb	JEML & Durham	-	-	600
MON Comb	Monash & Durham	400	-	600
UMA-1 Comb	Umatac & Durham	500	-	600
UMA-2	Umatac	500	-	680
UMA-3	Umatac	500	-	725
UMA-4	Umatac	500	-	750
UMA-5	Umatac	500	600	600
UMA-6A	Umatac	500	680	600
UMA-6B	Umatac	500	680	600
UMA-6C	Umatac	500	680	600
UMA-7	Umatac	500	725	600
UMA-8	Umatac	500	750	600

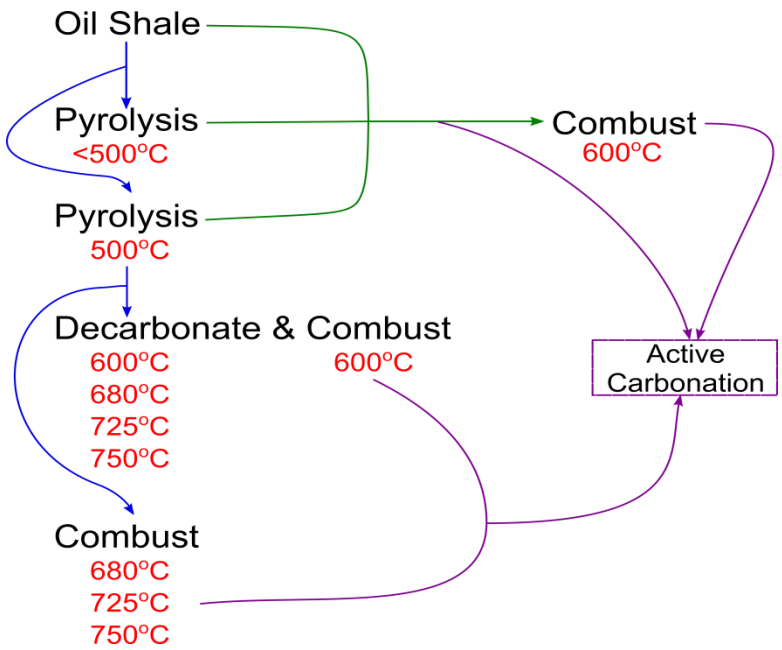

Figure 7.1 – *Flow diagram of the processing mechanisms tested with oil shale, including additional combustion and carbonation experiments.*

A partial factorial design was produced to test the effect of pyrolysis, combustion and carbonation on the resultant carbonate content, as there were too many variables to feasibly perform a full factorial design. The following variables were used to test the effect on the carbonation response: the temperature of pyrolysis, the temperature of decarbonation, the temperature of combustion, and carbonation experiments at low or high forcing conditions. The variables were chosen so that they vary while other variables remain constant, for example, as the temperature of decarbonation varied, the pyrolysis temperature and combustion temperature remained constant. As the temperature of combustion varied, the pyrolysis temperature remained constant and there was no decarbonation. As the temperature of pyrolysis varied, there was no decarbonation, and either there was no combustion, or the combustion temperature remained constant. The factors used in the models, as well as the number of factor levels, their assigned values, and expected response are provided in Table 7.2.

Table 7.2 - *Factors tested in the general linear models, their assigned values, and expected response on the carbonate content within processed oil shale.*

Factors	# of levels	level values	Response
Carbonation	3	Control, low forcing, high forcing	Increase carbonate content as react at high P&T (low and high forcing)
Pyrolysis temp	3	Control, 400 °C, 500 °C	Minimal effect on carbonate
Decarb temp	4	600, 680, 725, 750 (°C)	Decrease carbonate as increase temperature
Combustion temp	4	600, 680, 725, 750 (°C)	Decrease carbonate as increase temperature
Temperature	4	600, 680, 725, 750 (°C)	Decrease carbonate as increase temperature
'Decarb?'	2	Yes, no	Increase carbonate as decarb (Y), compared to combustion (N).

Note that, the variables 'carbonation' and 'decarb?' are dimensionless categorical variables in the model. The carbonation controls were samples that underwent heating without accelerated carbonation. Other samples of the same type were then subjected to different

carbonation mechanisms: low forcing and high forcing. The variable, 'decarb?', was used to identify samples that had been decarbonated at various temperatures before combustion at 600 °C (yes); or combusted at various temperatures, and therefore not decarbonated (no).

7.2.2 Experimental design and analysis

Each sample was analysed by XRD and TGA techniques, before and after carbonation experiments, to identify the changes in carbonate content and mineralogy due to processing, and due to accelerated CO_2 sequestration. The full experimental design is outlined in Figure 7.2. Samples were carbonated separately under high and low forcing conditions, where high forcing experiments were conducted for 4 hours, 80 °C, 100 bar and low forcing experiments at 1 hour, 40 °C, 70 bar, using 50 % water on all samples, with the method as described in Chapter 6. Replicate carbonation experiments were performed for each sample.

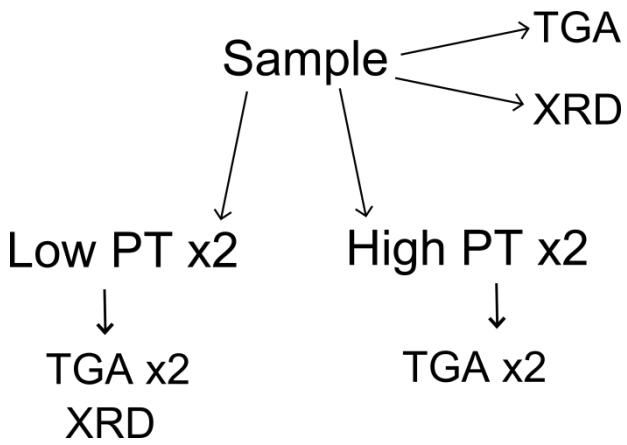

Figure 7.2 – *Experimental design, where low PT = carbonation at 40 °C, 70 bar, 1 hour and high PT = carbonation at 80 °C, 100 bar and 4 hours.*

Quantitative thermogravimetric analysis was used to determine how much carbonate was present in unreacted (controls) and reacted samples, at low and high forcing conditions, as described in Chapter 6, with weight loss attributed to carbonate decomposition between 600-950 °C. For samples of oil shale containing organic matter, the values for carbonate were corrected based on the loss of organic matter between 300-600 °C (Jaber et al., 2000). In addition, the weight loss derivative profiles were used to identify regions of differing carbonate composition.

X-ray diffraction methods were used as qualitative analysis, in the detection of the mineralogy of samples, before and after carbonation, as outlined in Chapter 2 and Appendix A. Additional analysis was provided by Fourier transform infra-red spectroscopy (FTIR) used to compliment XRD methods to determine the mineralogy of unreacted and reacted samples. FTIR analysis

(details in Appendix A) works by analysing the vibrational excitation of bonds, and therefore can be used to detect both crystalline and amorphous mineral matter within oil shales (Wang et al., 2009). Absorption bands are produced due to asymmetric or symmetric stretching, bending or rocking motions within bonds (Harwood et al., 1997). The position of the absorption band is based upon the strength of the bond, and is also related to the symmetry within the crystal structure. Any disorder within crystals will cause bands to shift (Schroeder, 2002).

7.2.3 Statistical analysis

Statistical analysis was performed using Minitab 14, and ANOVA was used with a general linear model (GLM) to determine significant factors that play a role in determining the overall carbonate content, the carbonate within phase 1, or carbonate within phase 2. As described in Chapter 6, main effects and interactions were determined at the 95 % confidence level, and *post-hoc* testing was used for the pairwise comparisons. The importance of each factor and interaction was displayed using the % variance (ω^2) and the main effects and interaction plots were produced in terms of the least squares means and standard error of this.

Analysis of variance (ANOVA) was initially used on the full dataset, using a GLM. Further models were produced by splitting the data, so that each factor could be analysed separately, to investigate the significance of each individual factor in more detail. In addition, XRD and TGA results were used to aid with conclusions about structural changes. The data were separated to analyse the effect of: the retorting temperature; the overall temperature of processing, by decarbonation or combustion; the combustion temperature; the effect of factors at separate carbonation conditions; followed by further phase analysis (Table 7.3).

Table 7.3 – *Factors tested in the GLMs produced by ANOVA, indicating the number of data points (N) and whether the data was normal.*

Model	Carbonation	Retorting temp	Decarb temp	Combustion temp	Normal data?	N
Full model	X	X	X	X	No	76
Retorting temp	X	X	-	-	Yes	15
Processing temp	X	-	Separated the 'temp' and 'decarb?'		No	50
Combustion temp	X	-	-	X	Yes	20
Carbonation	Separated	X	X	X	No	16
Phase 1	X	X	X	X	Yes	76
Phase 2	X	X	X	X	No	76

While the datasets were independent and showed equal variances using Levene's test, 50 % of the experimental models failed the normality test, based on the Anderson-Darling test. Due to the nature of the experimental design, the data could not be improved by log transformation or the removal of outliers. However, non-normality was accounted for in 3 of the 4 models that failed normality tests, based on: the number of samples, the skewness of the dataset, and the residuals. Firstly, the F-test, which identifies the ratio between variances, is often robust towards non-normality if the dataset is large, for example with > 50 data points (Schmider et al., 2010; Tiku, 1971). The robustness is more true for samples that are not significantly skewed, which was observed in the full dataset where the skewness factor was < 0.25 (Carver, 2004). In addition, the residuals (the distance from the fitted model values), were normal and did not show any trends when plotted against the fitted values, and therefore did not overestimate or underestimate values produced by the model. For the full model, the model based on the processing temperature, and the model used for phase 2 carbonate; these remained to be analysed by ANOVA due to the increased sensitivity with a larger numbers of samples. However, non-parametric analysis, was used to analyse the effect of factors on carbonation, where a smaller dataset was used (N < 20). Analysis by Kruskal Wallis was used, which tests the difference in the medians rather than the variances, and does not depend on normality. The null hypothesis was analysed and data with significantly different results, at 95 % confidence, was expressed by the corresponding P-value of < 0.05.

7.3 Results

7.3.1 Initial analysis

Thermogravimetric analysis was used to calculate the amount of carbonate in each of the samples, displayed in Figure 7.3 using coloured bars for the different processing steps and lines to indicate carbonation at low and high forcing. The samples with the most carbonate were the oil shale, J-OS, and oil shale samples retorted at 400 °C and 500 °C, MON and UMA-1 (blue bars); despite the differing retorting temperatures. These samples were combusted at 600 °C (green bars) and the carbonate content dropped significantly, also allowing carbonation to proceed (lines) and therefore replacing some of the carbonate that was lost by combustion. Samples were decarbonated at 600 °C, 680 °C, 725 °C and 750 °C, followed by combustion at 600 °C, UMA-5 to UMA-8 (purple bars). Finally, by increasing the combustion temperature from 680 to 750 °C, UMA-2 to UMA-4 (orange bars), carbonate content further decreased, and

the difference between carbonating samples at low forcing conditions (red line) and high forcing (maroon line) was realised.

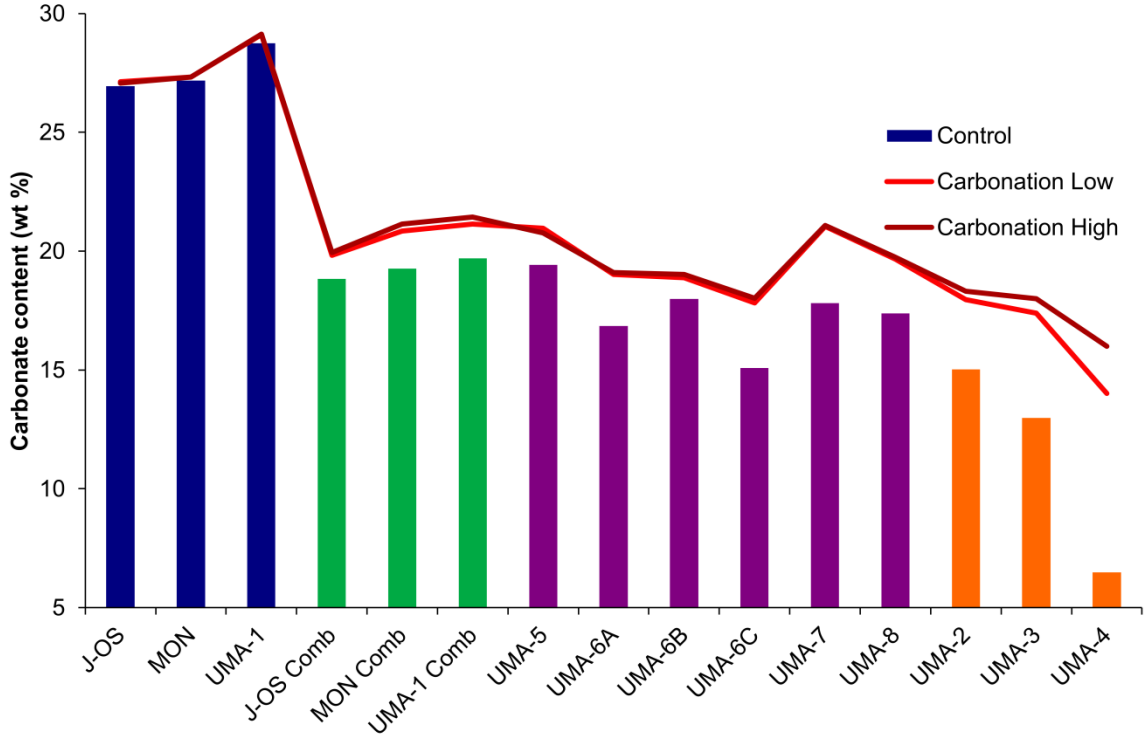

Figure 7.3 – *Carbonate concentration, in wt %, within all tested samples shown on the bar chart. Blue bars = retorted oil shale; green bars = retorted and combusted; purple bars = retorted, decarbonated at variable temperatures, and combusted; orange bars = retorted and combusted at variable temperatures. Lines indicate how much carbonate was added when reacted at high pressures and temperatures at low forcing (red line) and high forcing (maroon line).*

The significance of each of the variables was further tested by the use of statistical analysis, to determine the importance of each factor in controlling the carbonate content.

7.3.1.1 Full model

A general linear model using the full dataset based on 76 data points, was produced by ANOVA to analyse the control of the 4 factors: carbonation, pyrolysis, decarbonation, and combustion, on the amount of carbonate within samples (Table 7.4). The maximum carbonate content was 29.43 wt % CO_2, that occurred when retorted at 500 °C and carbonated at high forcing. The minimum carbonate content was 6.47 wt % CO_2, when retorted at 500 °C followed by combustion at 750 °C.

Table 7.4 – *General linear model produced by ANOVA, showing for each factor and interaction the degrees of freedom (DF), the probability (significant if P < 0.05), and the % variance (ω^2).*

Source	DF	P	ω^2
Carbonation	2	0.000	2.75 %
Pyrolysis	2	0.000	22.07 %
Decarbonation	4	0.000	2.16 %
Combustion	4	0.000	68.08 %
Carbonation*Combustion	8	0.000	3.61 %
R^2	99.1 %		
N	76		
S	0.489269		

The model explained 99.1 % of the variance in the dataset, while all factors tested was determined to be significant. The combustion and pyrolysis temperature were the most important of these factors, contributing to 68.1 and 22.1 % of the variance respectively. The interaction between carbonation and the combustion temperature was also determined to be significant, yet this interaction along with the variables, decarbonation and carbonation, were of low importance in the model (< 5 %). The factors and interactions in order of importance were: combustion, pyrolysis, carbonation, decarbonation and carbonation*combustion. *Post-hoc* testing was used to the determine the effect of each significant variable on the amount of carbonate, with the differences indicated in Table 7.5 and shown in the main effects plot in Figure 7.4. The results showed that combusting at lower temperatures resulted in more carbonate, and samples that were retorted at higher temperatures also had higher concentrations of carbonate. Also, samples that did not undergo decarbonation had greater amounts of carbonate, and samples that were carbonated at higher forcing had higher concentrations of carbonate compared to samples that were carbonated at lower forcing.

Table 7.5 – *Post-hoc testing results for each main factor effect, placed in order of importance for the GLM model.*

	Conditions	P-value
Combustion (°C)	600 > 680 > 725 > 750	0.000; 0.0336; 0.000
Pyrolysis (°C)	0 < 400 < 500	0.0229; 0.0001
Carbonation	Control < low < high	0.0000; 0.0040
Decarbonation (°C)	0 > 680, 725, 750	0.000, 0.184, 0.000
	680 < 750 < 600, 725	0.021; 0.006; 0.0033

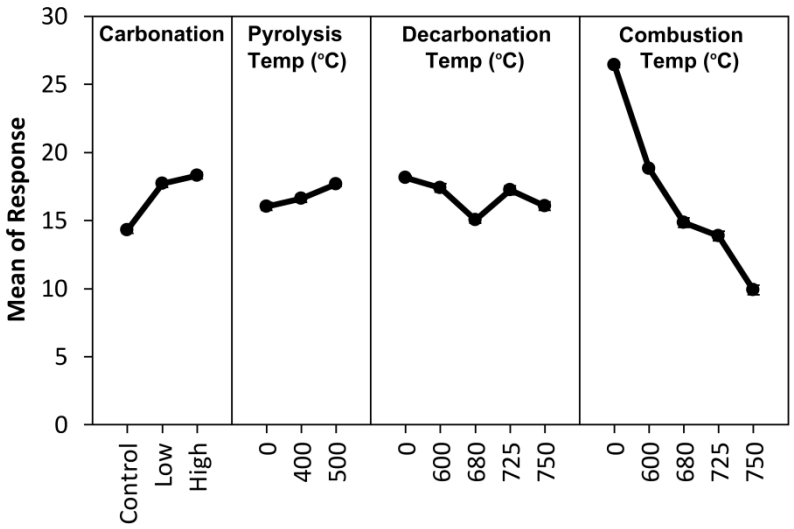

Figure 7.4 – *Main effects plot for the factors carbonation, pyrolysis, decarbonation and combustion temperature.*

The single interaction identified was between combustion and carbonation. Figure 7.5 shows the carbonate response due to an increase in combustion temperature at different carbonation conditions, where an increase in the temperature of combustion led to a decrease in the carbonate content, and an increase in the carbonation potential. At the highest temperatures (725 °C and 750 °C), differences were observed between carbonating at low forcing and high forcing, where carbonating at 100 bar, 80 °C for 4 hours resulted in more carbonate being formed. No carbonation was observed when samples were not combusted.

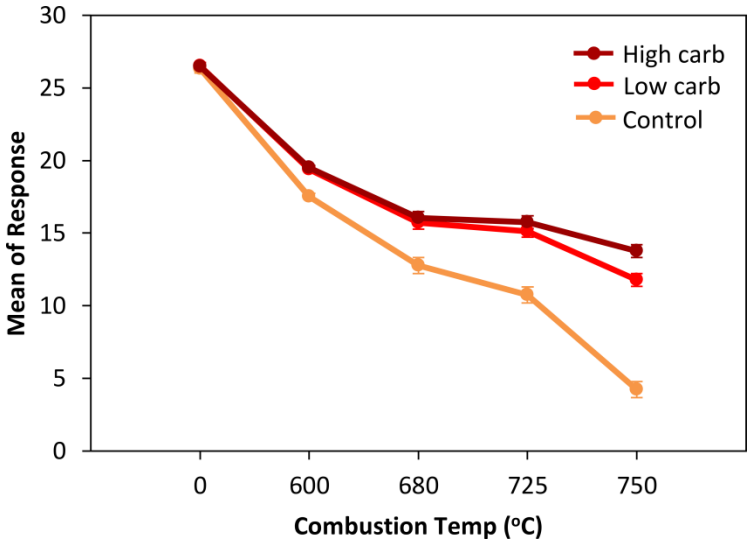

Figure 7.5 – *Interaction plot for combustion*carbonation*

Overall, the carbonate response was mainly affected by the retorting temperature and combustion temperature. Further models were produced by focusing on individual factors to investigate their statistical significance in more detail, and XRD and TGA results were used to identify structural changes.

7.3.2 Analysis of individual variables

7.3.2.1 Pyrolysis temperature

The effect of pyrolysis and carbonation on the carbonate content within spent oil shale is summarised in Figure 7.6, showing the change in carbonate content as oil shale and retorted oil shale (blue bars) were: carbonated (dashed line), combusted (green bars) or combusted and carbonated (lower dashed line). Samples contained more carbonate when only retorted; however, these samples did not show any carbonation, which is in agreement with the results from the interaction between carbonation and combustion, as produced by the full model. As samples were combusted, the carbonate content decreased, and carbonation was able to occur.

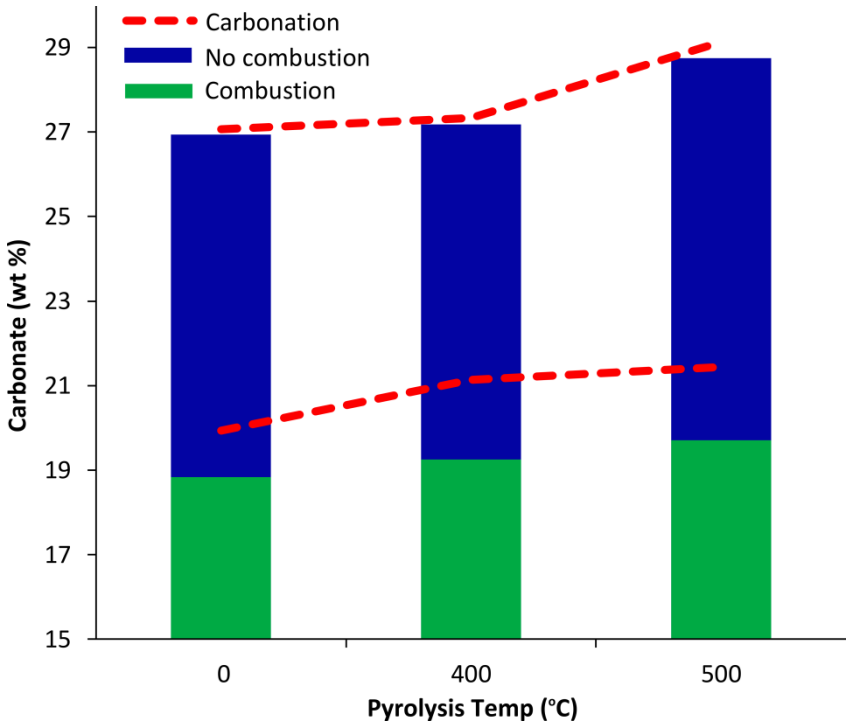

Figure 7.6 – *Bar chart of the carbonate content within samples of: oil shale, oil shale retorted at 400 °C and oil shale retorted at 500 °C. Lower bar charts represent samples that were combusted, and upper bar charts represent samples that were not combusted. Dashed lines represent active carbonation on each of the 6 samples presented.*

X-ray diffraction (XRD) analysis was conducted on the oil shale and retorted oil shale samples: J-OS, MON and UMA-1. Minerals detected in oil shale include: calcite and quartz at high concentrations, apatite, dolomite, cristobalite, feldspar, kaolinite and goethite. Smaller amounts of smectite/illite, hematite, gypsum and lime were also identified. Results showed some variation between the samples, and a reduction in cristobalite and clay minerals was observed as samples were retorted (Figure 7.7). Despite UMA-1 being retorted at higher temperatures than MON, it was UMA-1 that contained dolomite, with none observed in MON.

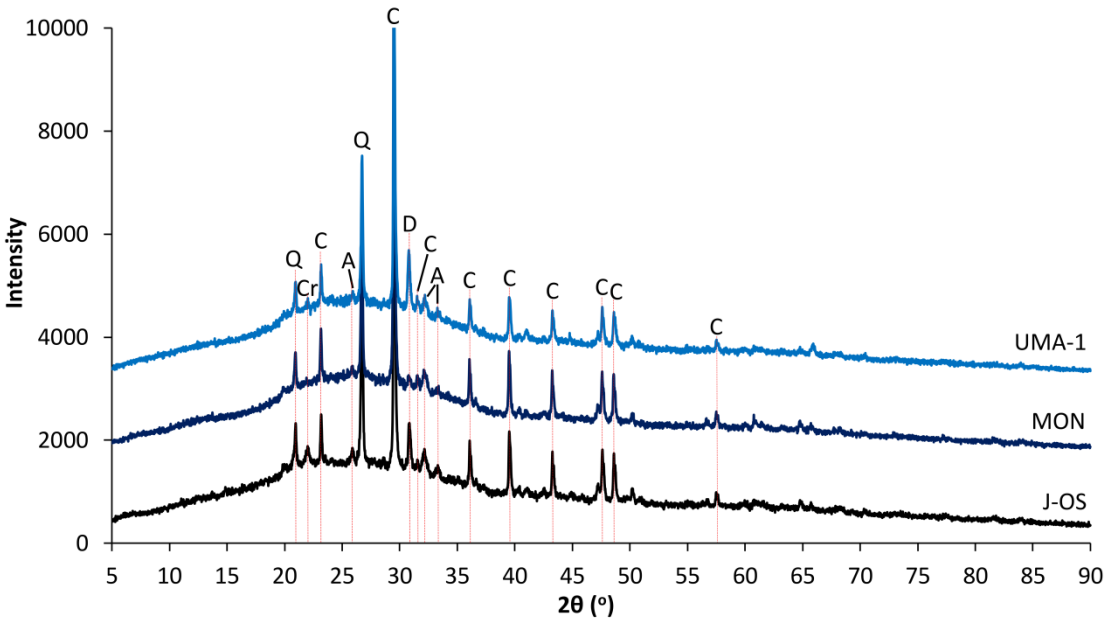

Figure 7.7 – *X-ray diffraction patterns for oil shale (J-OS), oil shale retorted at 400 °C (MON) and oil shale retorted at 500 °C (UMA-1). Minerals identified include calcite (C), quartz (Q), dolomite (D), apatite (A) and cristobalite (Cr).*

The occurrence of dolomite corresponded to the TGA derivative curves, where a shoulder was identified at ~800 °C, attributed to loss of CO_2 from dolomite (Figure 7.8). This was confirmed by the testing of a dolomite standard that showed two stages of weight loss for the decomposition (Equation 7.1).

$$CaMg(CO_3)_2 \rightarrow MgO + CaCO_3 + CO_2 \rightarrow CaO + CO_2 \qquad \text{Eq. 7.1}$$

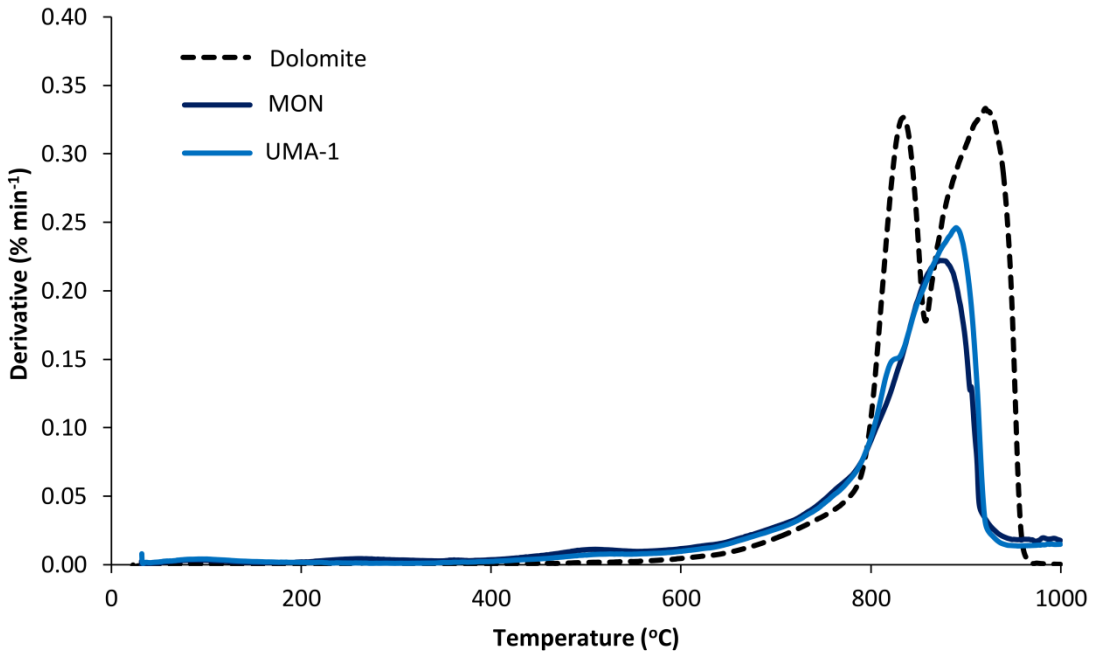

Figure 7.8 – *Thermogravimetric weight loss derivative profiles for retorted samples MON and UMA-1, compared to a dolomite standard, shown by the dashed line.*

A general linear model (Table 7.6) was produced based on a smaller number of data points (N=15), to determine the effect of the pyrolysis temperature, on combusted samples that allowed for carbonation. The minimum carbonate content (18.84 wt % CO_2) was detected within combusted oil shale that was not carbonated, however maximum carbonate (21.45 wt % CO_2) was measured in oil shale retorted at 500 °C, combusted and carbonated at high forcing.

Table 7.6 - *General linear model produced by ANOVA looking at the effect of pyrolysis on the carbonate content, showing for each factor and interaction the degrees of freedom (DF), the probability (significant if P < 0.05), and the % variance (ω^2).*

Source	DF	P	ω^2
Carbonation	2	0.000	46.89 %
Pyrolysis	2	0.000	41.09 %
Carbonation*Pyrolysis	4	0.002	1.95 %
R^2	99.78 %		
N	15		
S	0.0608008		

Results from the GLM explained 99.8 % of the variance in the dataset, and carbonation and pyrolysis were both significant factors, of similar high importance in the model and a difference of ω^2 of 5.8 %. The interaction between carbonation*pyrolysis was also identified, yet the importance of this was low (< 5 %). *Post-hoc* analysis showed both factors to have a positive effect on the carbonate content (Table 7.7; Figure 7.9). Accelerated carbonation caused the carbonate content to increase, and carbonation at the highest temperatures and pressures caused the amount of carbonate to increase further. Additionally, increasing the retorting temperature caused the carbonate content to increase.

Table 7.7 - *Post-hoc testing results for each main factor effect, placed in order of importance.*

	Conditions	**P-value**
Carbonation	Control < low < high	0.0000; 0.0012
Pyrolysis (°C)	0 < 400 < 500	0.0000; 0.0003

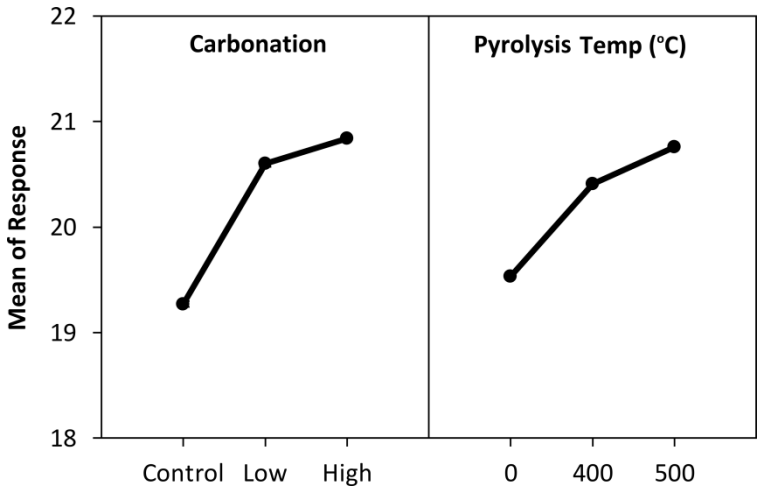

Figure 7.9 – *Main effects plot for the factors carbonation and pyrolysis temperature.*

Despite the low contribution from the interaction between carbonation and pyrolysis towards the model, a slight increase in carbonation when using higher pressures and temperatures could be realised when samples were also retorted (at either 400 °C or 500 °C) (Figure 7.10).

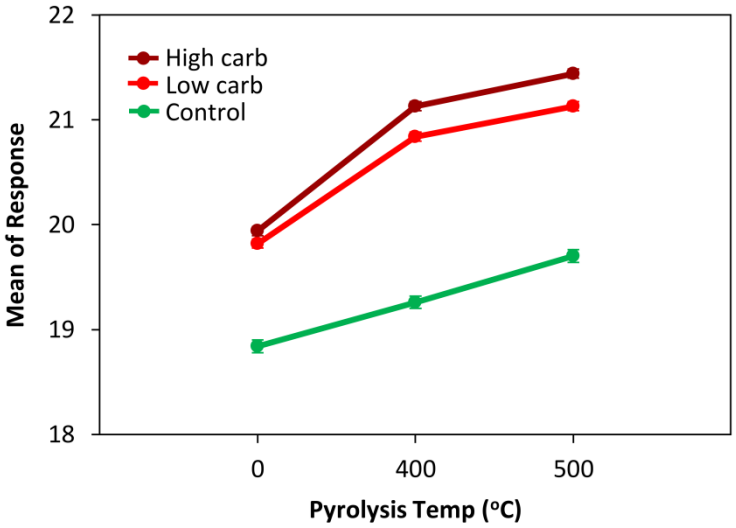

Figure 7.10 – *Interaction plot for pyrolysis*carbonation.*

7.3.2.2 Processing temperature

Figure 7.11 illustrates the difference between samples that were decarbonated and combusted, compared to samples that were combusted without prior decarbonation, showing greater variation in the carbonate content when combusted, yet fairly constant and high carbonate values when decarbonated.

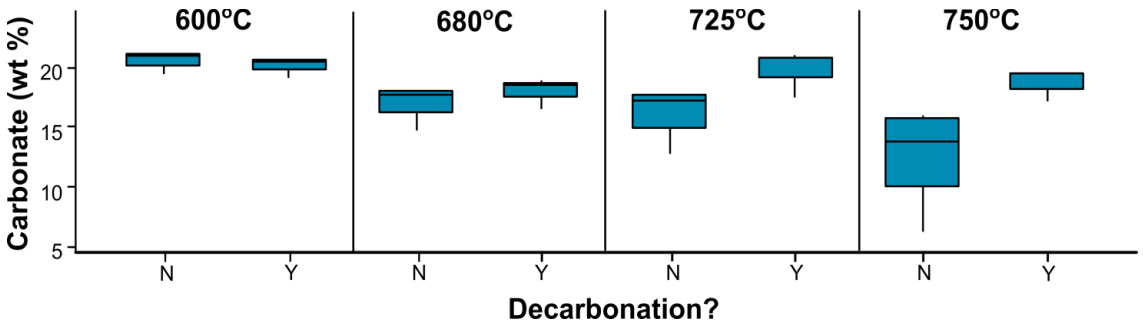

Figure 7.11 – *Boxplot of the carbonate content within oil shale that has been heated from 600 to 750 °C, by decarbonation and combustion, or combustion alone.*

Samples UMA-6A, 6B, and 6C, were decarbonated at 680 °C and combusted at 600 °C. They were analysed by XRD and TGA techniques, with results shown in Figure 7.12 and Table 7.8, respectively. The XRD patterns of decarbonated oil shales showed a reduction in calcite, clay, and feldspar and an increase in anhydrite, compared to samples that were only retorted. Dolomite was found to vary in concentration between samples, with high concentrations

observed in UMA-6A, but being absent in UMA-6C. Thermogravimetric analysis partially corresponded with the XRD results, with greater overall carbonate concentrations in UMA-6A compared to UMA-6C, however it is likely that UMA-6B contained the highest concentration of calcium carbonate out of the three samples of UMA-6A, UMA-6B and UMA-6C. The amount of carbonation that occurred was inversely proportional to the original carbonate content, with carbonation occurring in decreasing order from UMA-6C → UMA-6A → UMA-6B.

Table 7.8 – *Weight loss from TGA, within phase 1 (600-770 °C) and phase 2 (770-950 °C) for samples UMA-6 and UMA-6 high.*

	Phase 1	Phase 2	Sum		Phase 1	Phase 2	Sum	*DIFF*
6A	3.59	13.26	16.85	**6A-high**	5.16	13.94	19.1	***2.25***
6B	3.83	14.16	17.99	**6B-high**	4.68	14.31	18.99	***1***
6C	2.52	12.57	15.09	**6C-high**	5.49	12.56	18.05	***2.96***

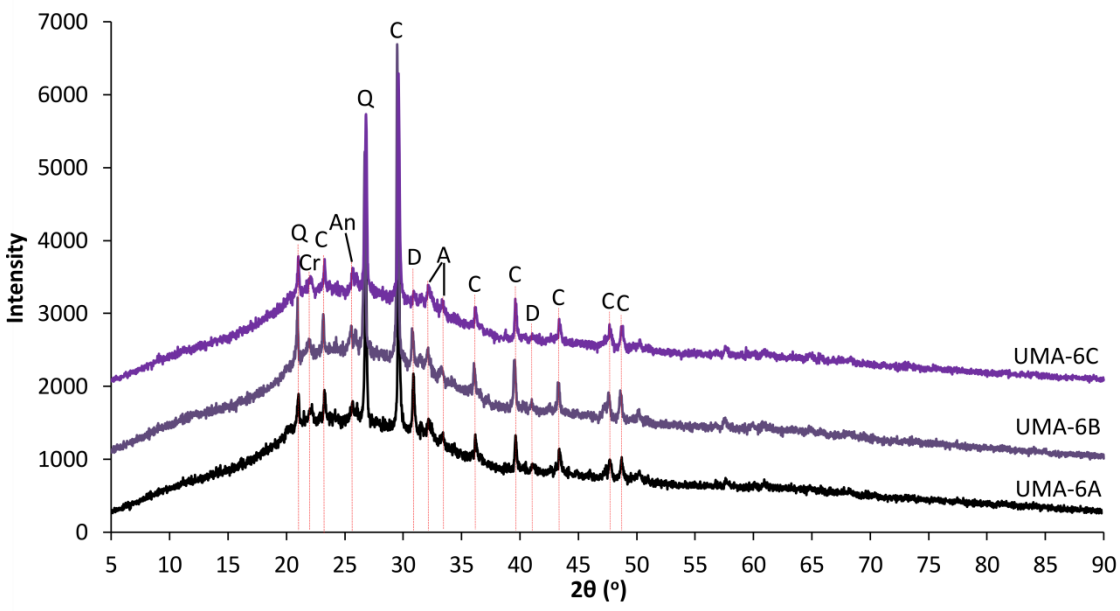

Figure 7.12 – *X-ray diffraction patterns for decarbonated samples UMA-6A, UMA-6B and UMA-6C. Minerals identified include calcite (C), quartz (Q), dolomite (D), apatite (A), anhydrite (An) and cristobalite (Cr).*

Because of the complex effects on carbonate content as a result of varied decarbonation temperature, a general linear model was produced based upon the overall processing temperature, and a separate variable to determine whether samples were decarbonated or combusted during this heating process. A dataset of 50 data points was used to produce a general linear model using ANOVA (Table 7.9). Maximum carbonate was detected at 21.45 wt % CO_2 for oil shale retorted at 500 °C, combusted at 600 °C and carbonated at high forcing. Minimum carbonate (6.47 wt % CO_2) occurred when oil shale was retorted at 500 °C and combusted at 750 °C, and in both cases samples were not decarbonated.

Table 7.9 - *General linear model produced by ANOVA, showing for each factor and interaction the degrees of freedom (DF), the probability (significant if P < 0.05), and the % variance (ω^2).*

Source	DF	P	ω^2
Carbonation	2	0.000	22 %
'Decarb?'	1	0.000	13.94 %
Temperature	3	0.000	32.2 %
Carbonation*'Decarb?'	2	0.000	3.17 %
Carbonation*Temperature	6	0.000	3.74 %
'Decarb?'*Temperature	3	0.000	20.36 %
Carbonation*'Decarb?'*Temperature	6	0.001	0.23 %
R^2	97.84 %		
N	50		
S	0.539661		

The model explained 98 % of the variance within the dataset and all the factors tested were significant. Interactions between all the factors were also identified, including carbonation*'decarb?', carbonation*temperature, 'decarb?'*temperature and the 3-way interaction carbonation*'decarb?'*temperature. Variables in order of importance were: temperature, carbonation, 'decarb?'*temperature, 'decarb?'. Also significant was the interaction between carbonation and 'decarb?'; and carbonation and temperature, however the importance of these were low (< 5 %). In addition, the 3-way interaction showed ω^2 < 0.5 % and was therefore not analysed further. *Post-hoc* testing showed that decarbonation led to greater amounts of carbonate and carbonation at low or high forcing provided greater concentrations of carbonate compared to samples that did not undergo accelerated carbonation (Table 7.10; Figure 7.14). The difference between the carbonate content when

heated at 680 °C and 725 °C was insignificant in this model, due to the complex decarbonation effects, but a decreasing trend in carbonate was still apparent for the complete series of 600-750 °C.

Table 7.10 – *Post-hoc testing results for each main factor effect, placed in order of importance.*

	Conditions	**P-value**
Temperature (°C)	600 > 680, 725 > 750	0.0000; 0.0000
Carbonation	Control < low, high	0.0000
'Decarb?'	Y > N	0.0000

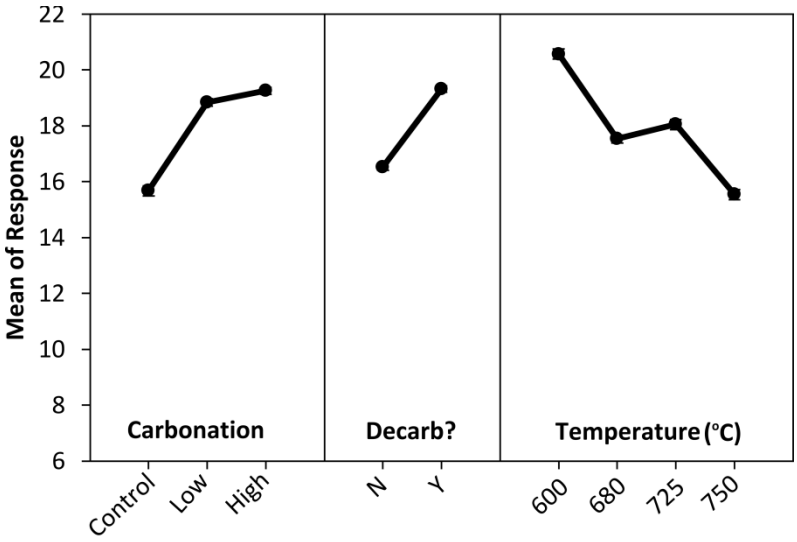

Figure 7.13 – *Main effects plot for the factors carbonation, 'decarb?', and temperature.*

The interaction between carbonation and 'decarb?' (Figure 7.14A), showed that greater amounts of carbonate were retained when samples were decarbonated compared to combusted, yet greater carbonation was possible when samples were combusted rather than decarbonated. The temperature of decarbonation or combustion was the most important factor in the model, and the interaction of temperature in Figure 7.14B, showed that as samples were combusted at increasing temperatures, carbonate content decreased, but as samples were decarbonated, carbonate content remained high with no trend apparent. On comparison of the overall temperature with carbonation (Figure 7.14C), the carbonation potential increased as the temperature increased, with only a slight difference between carbonating at low and high pressures apparent. *Post-hoc* testing revealed no significant difference between carbonating at high forcing or low forcing in this model, and carbonation was only able to proceed as samples were decarbonated or combusted.

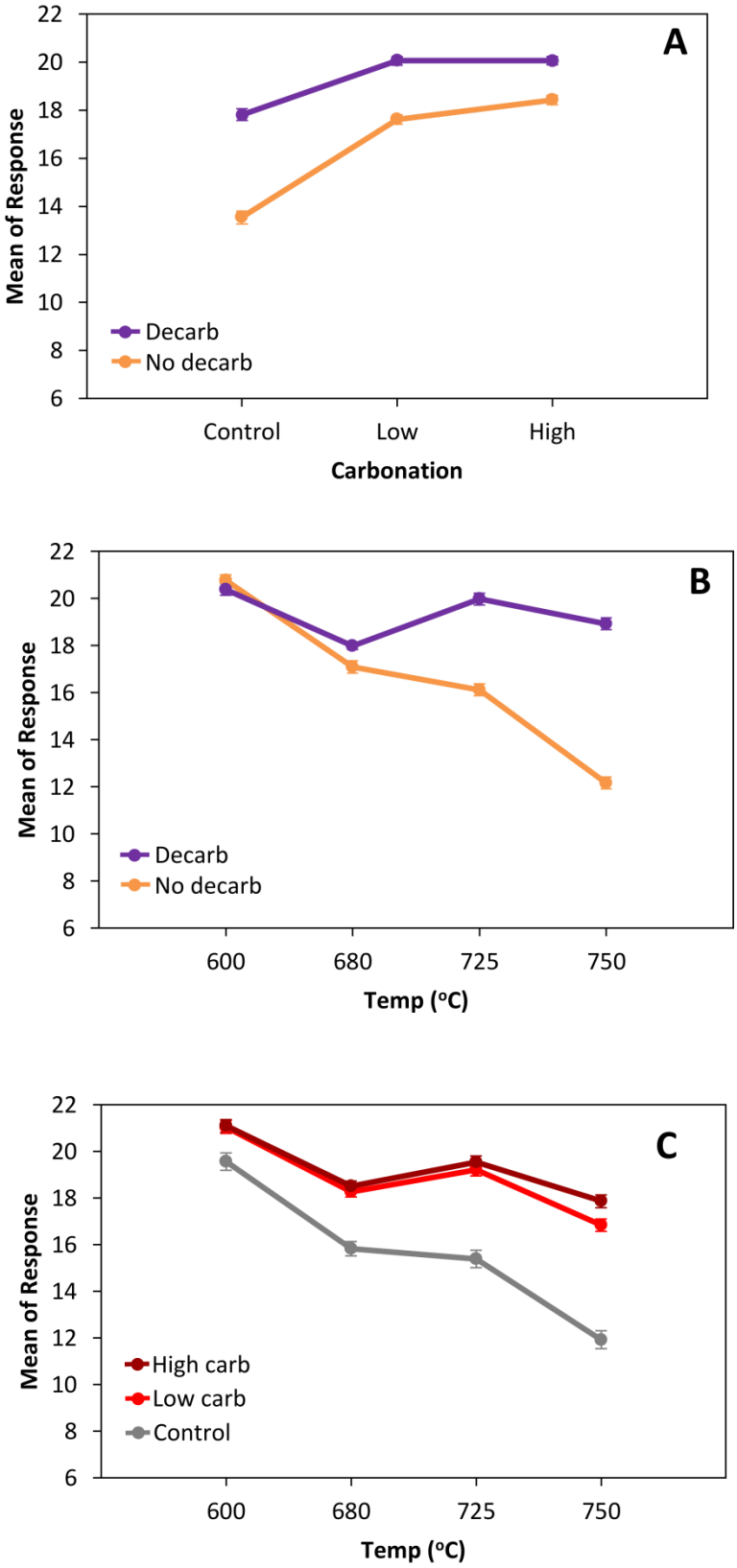

Figure 7.14 – *Interaction plot for A) carbonation*'decarb?'; B) temp*'decarb?'; and C) temp*carb.*

7.3.2.3 Combustion temperature

Analysis of variance for both the full model, and reduced model based upon the overall temperature of processing, showed the importance of the combustion temperature in determining the overall carbonate content. Analysis by XRD indicated the decrease in calcium carbonate and magnesium carbonate, as the combustion temperature increased. As well as this, retorted oil shale underwent various reactions and structural changes on combustion, leading to a different mineralogical structure, as discussed previously in Chapter 3. The XRD patterns of oil shale combusted from 600 °C to 750 °C, showed a reduction in calcite, dolomite, clay, and feldspar, the appearance of high temperature apatite (Knyazev et al., 2012), and the formation of anhydrite, as well as amorphous high temperature phases, likely to be aluminate and silicate phases (Figure 7.15). No ettringite was observed within combusted samples, as ettringite forms from the weathering and hydration of sulphate minerals such as anhydrite. As samples were combusted at increasing temperatures, further minerals were identified, including periclase and portlandite. In addition trace amounts of magnetite, lime, gehlenite and grossite were detected at high temperatures.

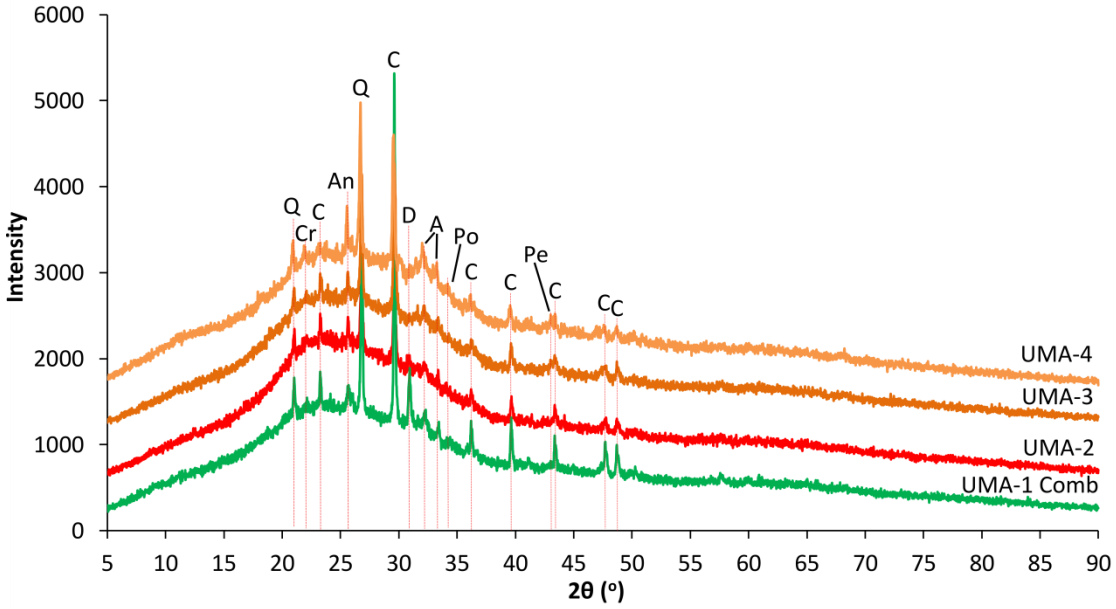

Figure 7.15 – *X-ray diffraction patterns for combusted samples UMA-1 Comb, UMA-2, UMA-3 and UMA-4, combusted at 600 °C, 680 °C, 725 °C and 750 °C respectively. Minerals identified include: calcite (C), quartz (Q), anhydrite (An), apatite (A), dolomite (D), portlandite (Po), periclase (Pe) and cristobalite (Cr).*

Thermogravimetric analysis confirmed the presence of portlandite in UMA-4 with a small weight loss step at ~450 °C corresponding to the loss of water from $Ca(OH)_2$. In addition, the

weight loss profiles from TGA also showed decreasing concentrations of carbonate as the temperature of combustion increased (Figure 7.16).

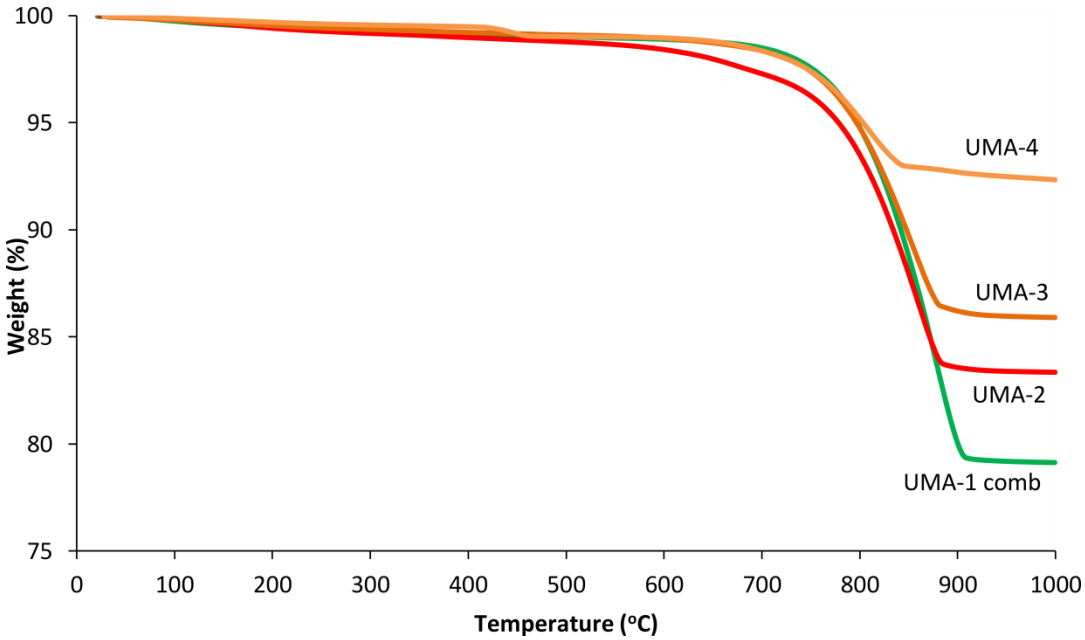

Figure 7.16 – *Thermogravimetric weight loss patterns for UMA-1 Comb, UMA-2, UMA-3 and UMA-4.*

Data also displayed an increasing range of carbonate concentrations as the combustion temperature increased (Figure 7.17). In addition, thermogravimetric analysis identified different phases of weight loss that increased as the temperature increased, being explored in more detail in Section 7.3.3.

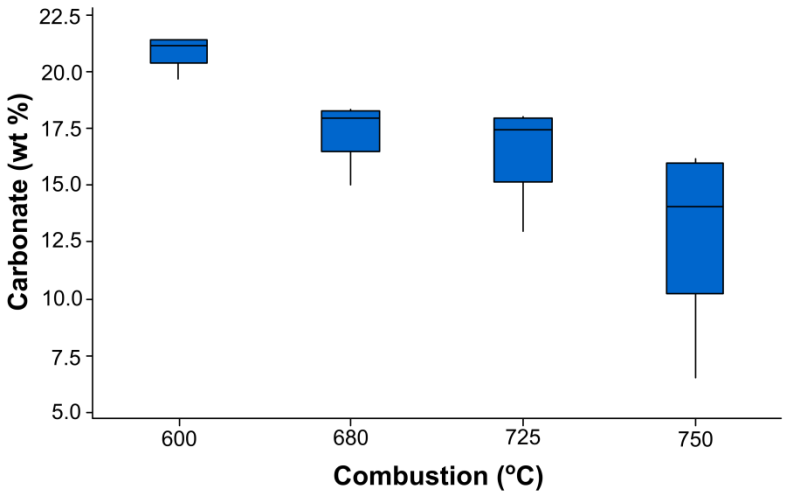

Figure 7.17 – *Bar chart showing carbonate content with increasing combustion temperature.*

Focussing on the combustion temperature, when samples were retorted at 500 °C, 20 data points were used to produce a general linear model (Table 7.11). The minimum and maximum amount of carbonate was as indicated in the previous model (6.47 and 21.45 wt % CO_2 respectively).

Table 7.11 - *General linear model produced by ANOVA looking at the effect of combustion on the carbonate content, showing for each factor and interaction the degrees of freedom (DF), the probability (significant if P < 0.05), and the % variance (ω^2).*

Source	DF	P	ω^2
Carbonation	2	0.000	27.92 %
Combustion	3	0.000	61.87 %
Carbonation*Combustion	6	0.000	9.66 %
R^2	99.96 %		
N	20		
S	0.110494		

The variances within the dataset were modelled well, with an R^2 value of 99.96 %. Both the combustion temperature and the carbonation forcing conditions were significant in determining the carbonate content within samples, as well as the interaction between these two variables. The variables in order of importance were: combustion, carbonation, and carbonation*combustion, with the contribution from the combustion temperature (> 60 %) much greater than the carbonation and carbonation*combustion combined (< 40 %). *Post-hoc* testing (Table 7.12; Figure 7.18) confirmed the significance of carbonation in increasing the carbonate content within combusted samples, especially at higher pressures and temperatures, with the most carbonate being formed when carbonated at 100 bar and 80 °C for 4 hours.

Table 7.12 – *Post-hoc testing results for each main factor effect, placed in order of importance.*

	Conditions	P-value
Combustion (°C)	600 > 680 > 725 > 750	0.0000
Carbonation	Control < low < high	0.0000

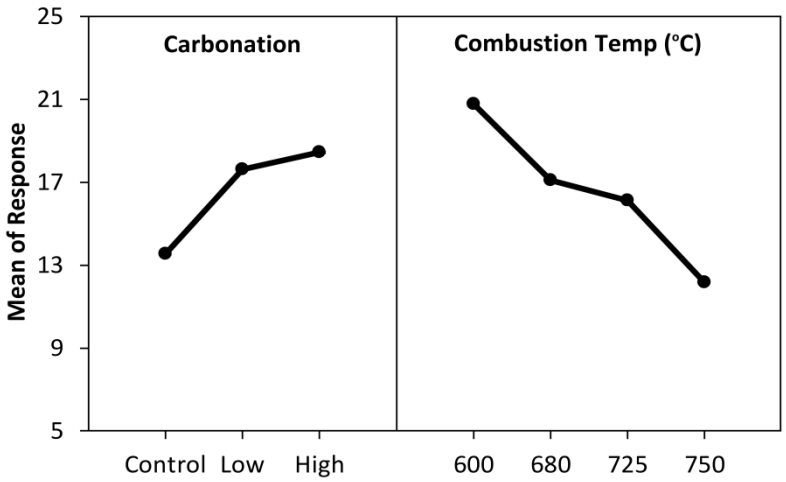

Figure 7.18 – *Main effects plot for the factors carbonation and combustion temperature.*

The interaction plot of carbonation*combustion (Figure 7.19) is similar to the same interaction that was observed in the full model (Figure 7.5), except the use of a control is absent in this current reduced model. The focus on the combustion temperature caused an increase in the importance of the carbonation variable in this model compared to the full model (increased from 2.8 % to 27.9 %), as well as the interaction carbonation*combustion (increased from 3.6 % to 9.7 % of the model).

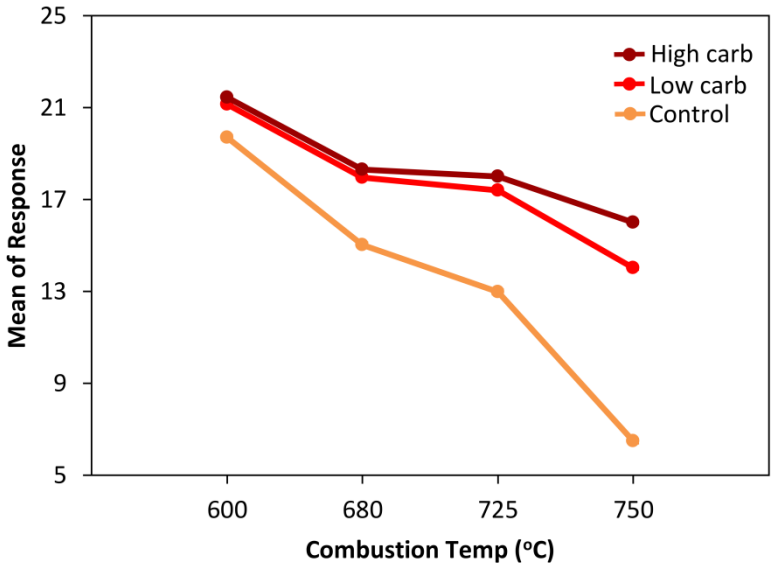

Figure 7.19 – *Interaction plot for combustion*carbonation.*

7.3.2.4 Carbonation

Even though the amount of carbonate within samples decreased overall as the combustion temperature increased, the amount of carbonation that occurred increased as the carbonate content decreased. This can also be expressed by splitting the data to focus on the samples that were carbonated at low forcing, high forcing, and samples that did not undergo carbonation (control) (Figure 7.20).

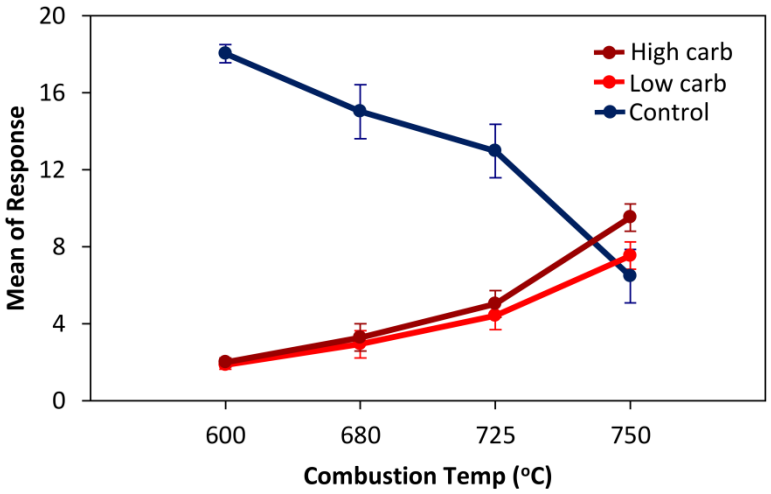

Figure 7.20 – *The response (carbonate content, wt %) when samples were combusted from 600 to 750 °C, and the new carbonate added when carbonated at low forcing and high forcing.*

Non-parametric analysis was used, due to the small number of samples in these separated models (N=16). The Kruskal-Wallis test showed that the carbonate content was unaffected by pyrolysis and decarbonation, with the combustion temperature the only significant factor towards the amount of carbonate that was formed by carbonation at elevated pressures and temperatures. Table 7.13 shows the P-value for each of the variables used in the model for the control samples, the samples carbonated at low forcing, and samples carbonated at high forcing, with combustion the only variable with a P-value < 0.05, that is significant by the standards of this study.

Table 7.13 – *P-value for the significance of pyrolysis, decarbonation, and combustion temperature on the carbonate content within the 3 separate models for: control samples, samples carbonated at low forcing, and samples carbonated at high forcing.*

Factor	Control	Low	High
Pyrolysis	0.184	0.11	0.102
Decarbonation	0.775	0.791	0.863
Combustion	0.028	0.033	0.028

All the models produced showed R^2 > 97.5 %, explaining the majority of variances within the data based on the significant factors displayed in each model. The importance of each factor and interaction, in each of the 6 models is displayed in Table 7.14. Of the 6 general linear models, interactions were not largely observed to be important, and the combustion temperature and conditions used for carbonation were observed to be the most important factors overall.

Table 7.14 – *Factors of importance within the different models, where: P = pyrolysis temperature, Co = combustion temperature, C = carbonation, D? = decarb or combust, T = temperature, D = decarbonation temperature.*

Model	N	R^2	Importance	
			> 10 %	> 20 %
Full	76	99.1		P, Co
Retorting	15	99.8		C, P
Processing	50	97.8	D?	C, T, D?*T
Combust	20	99.96		C, Co
Phase 1	76	98	D, C*Co	C, Co
Phase 2	76	99.2		P, Co

7.3.3 Further phase analysis

Two phases of carbonate decomposition were identified in Chapter 6; therefore further analysis of these phases was conducted based upon the temperature of processing and subsequent carbonation mechanisms. Figure 7.21 shows the variation in carbonate loss from two regions of weight loss, by using the derivative of the curve. Increasing temperatures of combustion led to decreasing carbonate content from 770-950 °C (phase 2), yet increasing carbonate content from 600-770 °C (phase 1). Also of note is the shoulder that appeared in 'UMA-1 High', but was missing from other samples, likely to be attributed to dolomite or Mg-carbonate. The position of the peak maximum on the derivative curve, for both phase 1 and phase 2, shifted to higher temperatures as the concentration increased, a typical characteristic of thermal decomposition curves (Todor, 1976).

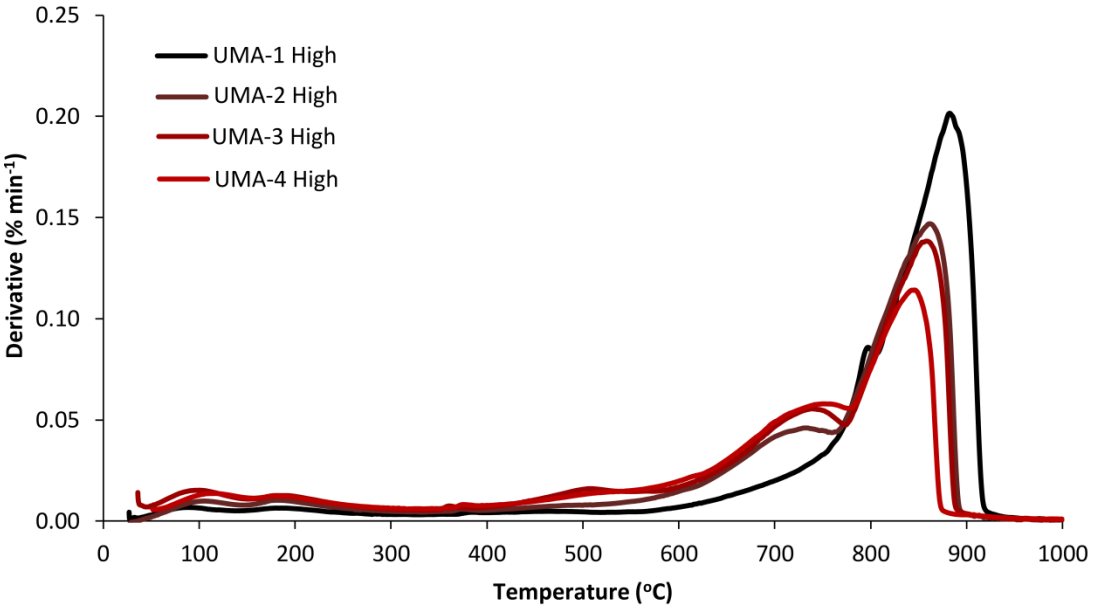

Figure 7.21 – *Thermogravimetric weight loss derivative profiles for combusted and carbonated samples UMA-1 High, UMA-2 High, UMA-3 High and UMA-4 High.*

By splitting the carbonate concentration, into the two regions of decomposition where phase 1 = 600-770 °C and phase 2 = 770-950 °C, models were produced to test the effect of variables on the amount of carbonate within phase 1 and phase 2. The first model was produced for phase 1, based on 76 data points (Table 7.15). Minimum phase 1 carbonate was 1.92 wt % CO_2, when retorted at 400 °C and combusted at 600 °C, however maximum phase 1 carbonate was achieved when retorted at 500 °C, combusted at 750 °C then carbonated at low forcing.

Table 7.15 - *General linear model produced by ANOVA for Phase 1, showing for each factor and interaction the degrees of freedom (DF), the probability (significant if P < 0.05), and the % variance (ω^2).*

Source	DF	P	ω^2
Carbonation	2	0.000	27.73 %
Pyrolysis	2	0.001	1.87 %
Decarbonation	4	0.000	13.94 %
Combustion	4	0.000	34.87 %
Carbonation*Decarbonation	8	0.000	1.32 %
Carbonation*Combustion	8	0.000	16.98 %
R^2	97.96 %		
N	76		
S	0.231934		

Results from the general linear model provided explanation for 98 % of variances within the dataset, with all factors significant in determining the amount of carbonate within phase 1. Interactions were also significant, between carbonation and the decarbonation or combustion temperature. The variables in order of importance were: combustion, carbonation, carbonation*combustion, and decarbonation. These variables were followed by pyrolysis and carbonation*decarbonation, which were both of weak importance, with $\omega^2 < 2$ %. The variables that included carbonation showed the largest percentage variance, and therefore importance, compared to the full model (46 % compared to 6.4 %) indicating the large role it takes in producing phase 1 carbonate. *Post-hoc* testing results (Table 7.16) showed that greater phase 1 carbonate was discovered when samples were carbonated, and when samples were combusted at temperatures > 600 °C. Also, greater phase 1 carbonate was detected when samples of oil shale were not pyrolysed and not combusted.

Table 7.16 – *Post-hoc testing results for each main factor effect, placed in order of importance.*

	Conditions	**P-value**
Combustion (°C)	600 < 0, 680, 725, 750	0.0000
Carbonation	Control < low, high	0.0000
Decarbonation (°C)	0, 600, 750 < 680, 725	0.0000; 0.0108
Pyrolysis (°C)	0 > 500	0.0007

The second model was produced for phase 2 (Table 7.17), and the results were again based upon 76 data points, revealing a high value of regression for the ANOVA. The minimum value for carbonate within phase 2 was 4.23 wt % CO_2, when retorted at 500 °C and combusted at 750 °C. The greatest amount of carbonate within phase 2 was 24.9 wt % CO_2, when retorted at 500 °C and carbonated at high forcing.

Table 7.17 - *General linear model produced by ANOVA for Phase 2, showing for each factor and interaction the degrees of freedom (DF), the probability (significant if P < 0.05), and the % variance (ω^2).*

Source	DF	P	ω^2
Carbonation	2	0.000	0 %
Pyrolysis	2	0.000	24.01 %
Decarbonation	4	0.000	4.47 %
Combustion	4	0.000	69.61 %
Carbonation*Combustion	8	0.000	0.74 %
R^2	99.15 %		
N	76		
S	0.486029		

The R^2 value explained 99 % of the variances within the data and the same factors were determined to be important in determining the carbonate within phase 2, as from the ANOVA of phase 1, with the exception of the interaction between carbonation*decarbonation, that was not significant. The contribution from each of the factors also changed significantly, with increased importance due to the retorting and combustion temperature, now 24 % and 70 % respectively, increased from 2 % and 35 % from phase 1 carbonate. The decarbonation temperature dropped in importance to contribute to < 5 % of the model, and despite the significance of carbonation as a factor, both the factor and the interaction between carbonation*combustion, were of low importance, < 1 % combined that was significantly less than 46 % contribution of carbonation towards phase 1 carbonate. *Post-hoc* results are provided in Table 7.18, highlighting the importance of the combustion temperature, with greater carbonate content found in phase 2 when combusted at lower temperatures, and also when pyrolysed at higher temperatures. The difference between carbonating at high conditions compared to low conditions was also relevant, with similarities of the phase 2 model, to the full model.

Table 7.18 – *Post-hoc testing results for each main factor effect, placed in order of importance.*

	Conditions	P-value
Combustion (°C)	0 > 600 > 680 > 725 > 750	0.0000; 0.0000; 0.0016; 0.0000
Pyrolysis (°C)	0 < 400 < 500	0.0016; 0.0000
Decarbonation (°C)	0 > 600 > 725, 750 > 680	0.0233; 0.0007, 0.0000; 0.0000
Carbonation	Control < low < high	0.0028; 0.0202

The interaction between the temperature of decarbonation, and the temperature of combustion, when carbonated at high forcing conditions, is illustrated for phase 1 and phase 2 in Figure 7.22. The axis for the 'mean of response', that is equal to the carbonate content in wt %, were different between Figure 7.22 A and B, due to the significantly less carbonate that was found at temperatures < 770 °C. When carbonated at high forcing, high combustion temperatures and decarbonation temperatures were required for greater phase 1 carbonate content, yet the opposite was true for phase 2, with lower combustion temperatures favouring higher carbonate concentrations.

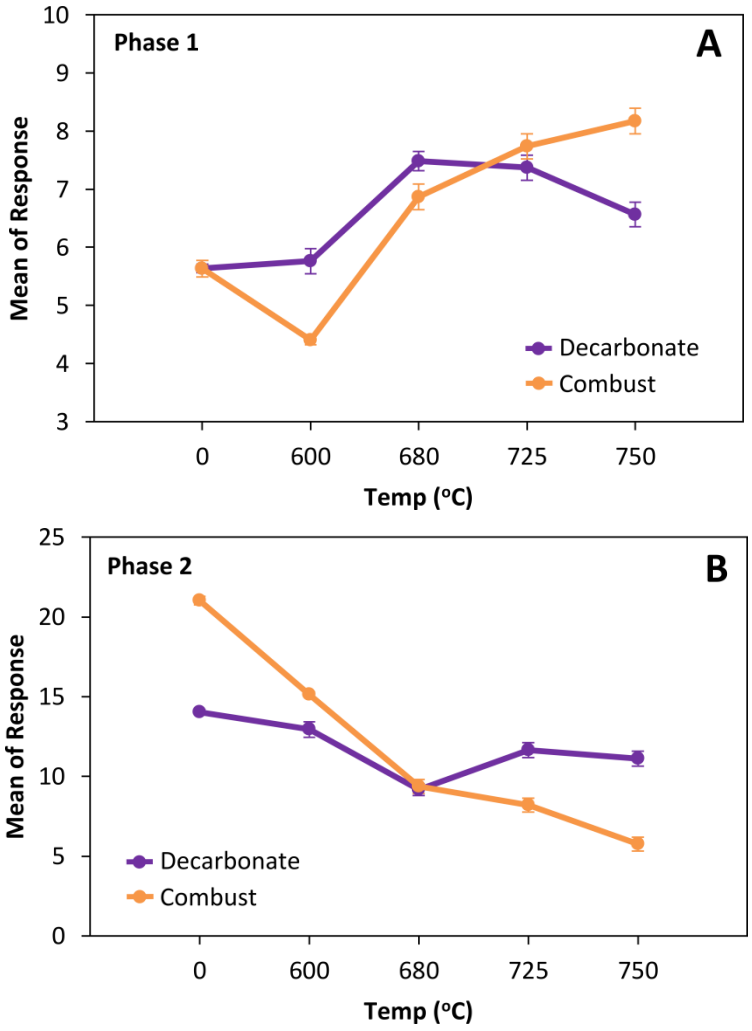

Figure 7.22 – *Interaction plot for temperature of decarbonation and combustion, for A) phase 1 and B) phase 2.*

7.3.4 Carbonate minerals

To examine the type of carbonate that was formed in spent oil shale by accelerated carbonation mechanisms, firstly, the carbonate minerals produced by the carbonation of pure minerals reactive towards carbonation were determined, by using the calcium hydroxide mineral, portlandite [$Ca(OH)_2$], and the calcium silicate mineral, wollastonite [$CaSiO_3$]. Portlandite, formed from the hydration of CaO, and calcium silicate minerals, are both present in spent oil shale that underwent combustion at high temperatures. Wollastonite and portlandite samples were carbonated, and the change in mineralogy was analysed by both XRD and FTIR analysis.

Portlandite showed some natural calcite from the XRD pattern of the sample that was not reacted, however on reaction at high pressures, both portlandite and calcite were detected at high concentrations (Figure 7.23). For wollastonite, again trace amounts of calcite were detected in the unreacted sample and when reacted with CO_2 at high pressures, increased concentrations of calcite were detected, however in addition, aragonite and amorphous material, possibly silica, was observed (Figure 7.24).

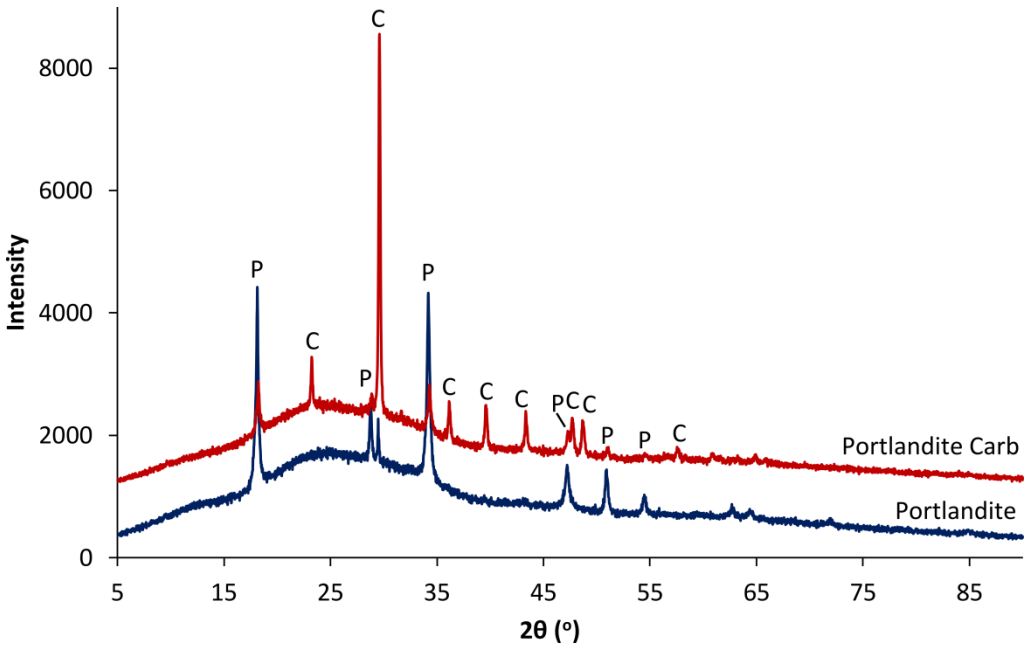

Figure 7.23 – *X-ray diffraction patterns of portlandite and carbonated portlandite, with minerals labelled including calcite (C) and portlandite (P).*

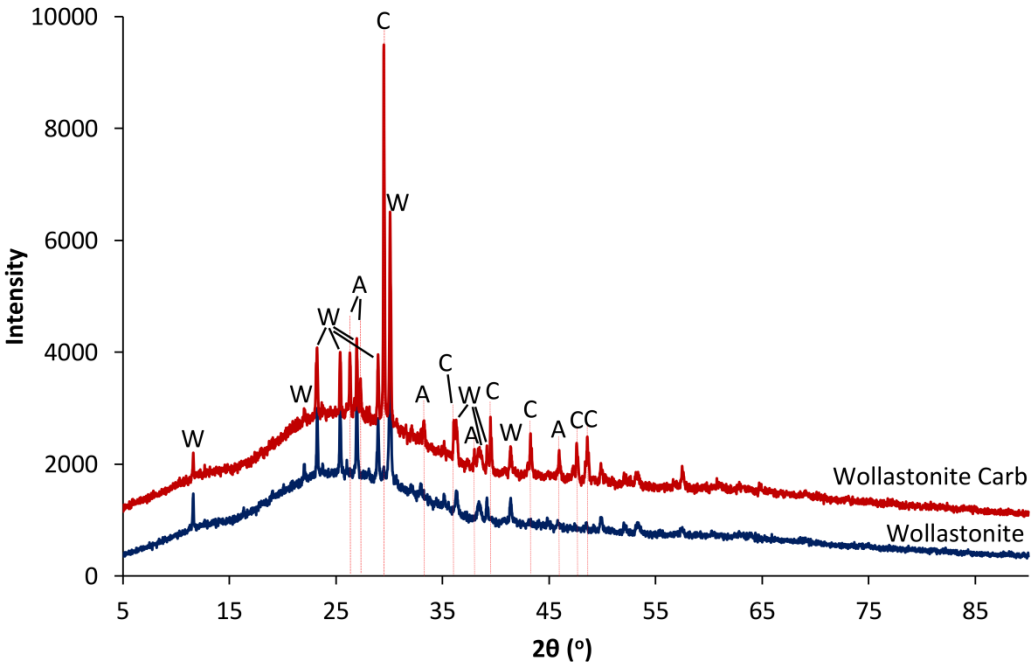

Figure 7.24 – *X-ray diffraction patterns of wollastonite and carbonated wollastonite, with minerals identified including wollastonite (W), calcite (C), and aragonite (A).*

Fourier transform infra-red spectroscopy was used to confirm the presence or absence of certain functional groups within solid materials and aided with the identification of carbonate minerals. Firstly, absorption bands from controls, including calcite, aragonite, portlandite and wollastonite were tabulated according to their frequency and assigned mineral group (Table 7.19), corresponding to literature values.

Table 7.19 – *Assignments for FTIR analysis of calcite, aragonite, portlandite and wollastonite, in wavenumber (cm^{-1}). Literature assignments were: [1] = Fernandez-Carrasco et al., (2012); [2] = Miller et al. (2013) [3] = Kalinkina et al. (2001); Smidt et al. (2008).*

FTIR band assignment:	Mineral	Calcite	Aragonite	$Ca(OH)_2$	Wollastonite
OH	Hydroxide	-	-	3640	-
CO_3^-	Carbonate[1]	1400, sh1430	1430, 1480	1420, 1480	vw
Si-O	Wollastonite[2]	-	-	-	1060
Si-O	Silica[3]	-	-	-	1020
CO_3^-	Carbonate	870	850	870	900
CO_3^-	Carbonate	710	680, 690	w	710, 680
Si-O	Wollastonite	-	-	-	640

On analysis by FTIR, peaks corresponding to calcite were picked up at high intensities from carbonated portlandite (Figure 7.25), with peaks at 1400-1500, 870, 710 and 670 cm^{-1} (Fernandez-Carrasco, 2012). Carbonated wollastonite, on the other hand, showed a reduction in silicate peaks, at 1020, 900 and 650 cm^{-1}, while an increase in intensity of carbonate peaks at 1400-1550, 880, 860, 710 and 680 cm^{-1} (Figure 7.26). Of note, is the broadening of the carbonate out-of-plane bending mode compared to that of carbonated portlandite, as well as the increase in peaks at lower wavenumbers, that correspond to aragonite as well as calcite.

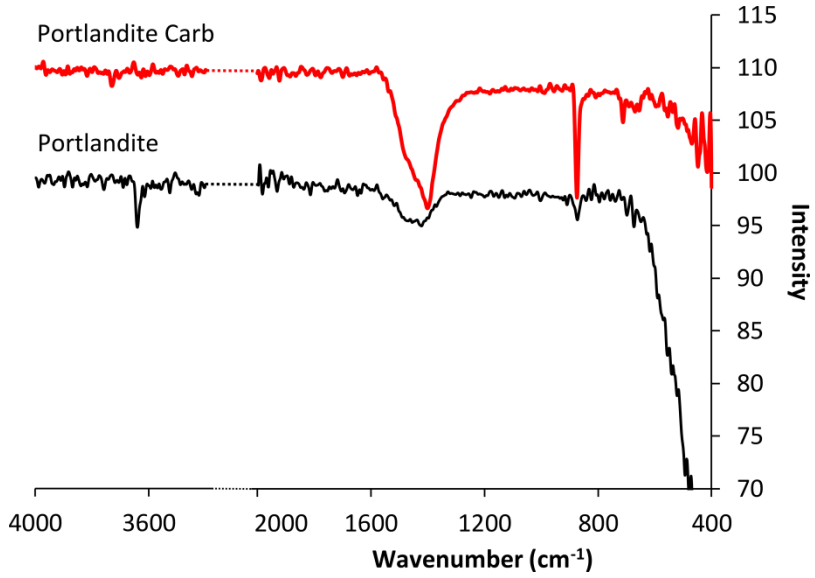

Figure 7.25 – *Spectra from FTIR analysis of portlandite and carbonated portlandite.*

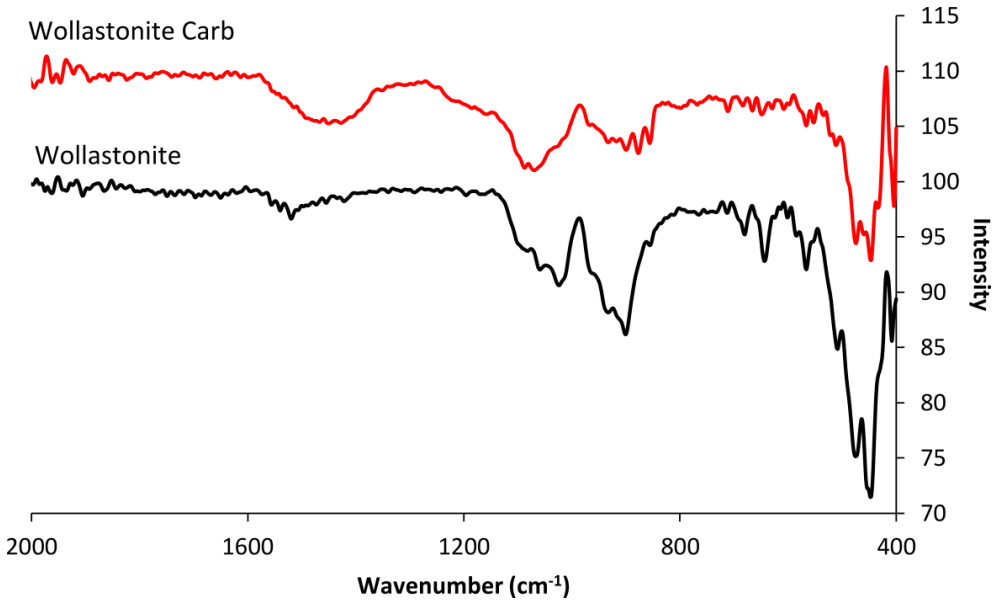

Figure 7.26 – *Spectra from FTIR analysis for wollastonite and carbonated wollastonite.*

Analysis of combusted and carbonated spent oil shale samples clearly show structural changes that occur as the combustion temperature is increased from 600 to 750 °C, and as samples are carbonated at low and high forcing. On combusting, a weak peak at 740 cm^{-1} in the sample combusted at lower temperatures was detected, which could correspond to dolomite or vaterite (Fernandez-Carrasco, 2012). At higher temperatures of combustion, less calcite was remaining in the sample, leading to a weaker and broader peak at ~1420 cm^{-1} and the absence of a peak at 710 cm^{-1}. In addition, there was the appearance of two new peaks, a strong broad peak at ~910 cm^{-1} and a weaker peak at 640 cm^{-1}, related to a silicate mineral structure, similar to wollastonite (Lanas et al., 2004).

The main difference between UMA-4 and the carbonated samples is the disappearance of the silicate band at ~910 cm^{-1}. Stronger carbonate peaks at ~1400 cm^{-1} that are broader than calcite alone, indicate disorder or multiple carbonate structures, and UMA-4 Low shows a broader band in this area of the spectrum compared to UMA-4 High (Kalinkin et al., 2004). The presence of a shoulder at 850 cm^{-1} suggests the presence of calcite or aragonite. The weaker peaks at 710 and 740 cm^{-1} also suggest the presence of carbonate minerals (Sdiri et al., 2010). Details of the mineral assignments are provided in Table 7.20 and peaks < 600 cm^{-1} are attributed to apatite, anhydrite and other metal oxides or silicates.

Table 7.20 - *Assignments from FTIR analysis of carbonated portlandite, carbonated wollastonite, oil shale combusted at 600 °C and 750 °C and carbonated spent oil shale, in wavenumber (cm^{-1}). Literature assignments were: [1] = Fernandez-Carrasco et al., (2012); Kalinkin et al. (2004), [2] = Thompson et al. (2012), [3] = Lanas et al. (2004).*

FTIR	Mineral	$Ca(OH)_2$ Carb	Woll Carb	J-OS Comb	UMA-4	UMA-4 High
CO_3^-	Carbonate[1]	1400 - 1500	1400 - 1550	1410	1400 - 1500	1400 - 1520
Si-O	Quartz[2]	-	1060	1080	1080	1080
Si-O	Silicate (eg. C_2S)[3]	-	sh1020, 900 w	-	910, 940	-
CO_3^-	Calcite/aragonite[1]	870	880, 860	870, sh850	870, sh850	870, sh850
Si-O	Quartz[2]	-	-	800, 780	795, sh770	795, sh770
CO_3^-	Vaterite/dolomite[1]	-	-	740 w	vw	vw
	Calcite/aragonite[1]	710, 670	710, 680	710, 680	710w, 680	710w, 690
Si-O	Silicate (eg. woll)	-	650 w	-	640	650

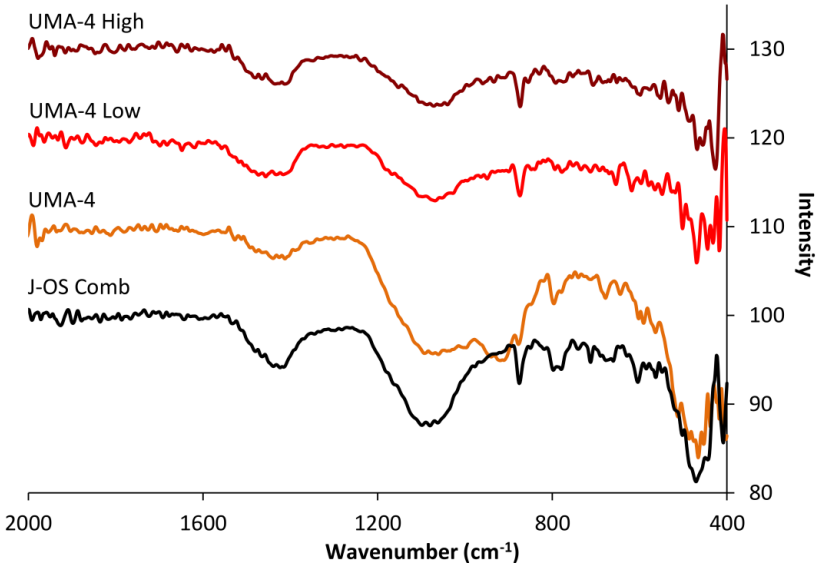

Figure 7.27 – *Spectra from FTIR analysis for combusted samples J-OS Comb and UMA-4, as well as carbonated samples UMA-4 Low, and UMA-4 High.*

Looking at the X-ray diffraction pattern for UMA-4 and UMA-4 carbonated samples, UMA-4 showed the presence of portlandite, periclase and also silicate from a weak reflection at 30.2° 2θ. Within the carbonated samples, portlandite and periclase reflections were missing, yet an increase in calcite was observed, and reflections from aragonite, and possibly vaterite or magnesite. The broadening at the base of the calcite peak at ~30° 2θ, highlighted in Figure 7.28, was also picked up in the carbonated samples, which may be due to disorder due to the carbonation of silicate minerals.

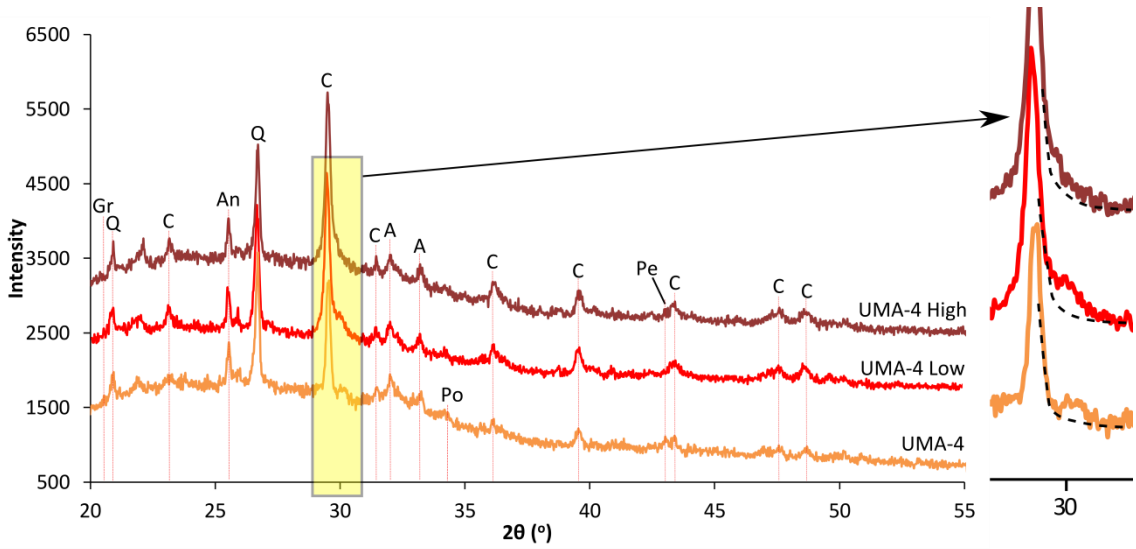

Figure 7.28 – *X-ray diffraction patterns for UMA-4, UMA-4 Low and UMA-4 High. Identified minerals include calcite (C), quartz (Q), apatite (A), portlandite (Po), periclase (Pe) and grossite (Gr). The highlighted area was expanded to the right of the diffraction patterns and the dotted line follows the path of a natural calcite reflection.*

7.4 Discussion

7.4.1 Statistical analysis

The use of a full model enabled the analysis of the whole dataset. With the full model of the whole dataset, the pyrolysis and combustion temperature were observed to be important in controlling the carbonate content (Table 7.4). The other factors, carbonation and decarbonation, were significant, but their effects were masked, therefore smaller models were used to look at individual factors in more detail.

7.4.1.1 Pyrolysis

Retorted samples, that did not undergo combustion, showed similar carbonate contents and minimal carbonate loss on retorting, because temperatures did not reach the zone of carbonate decomposition. Because the decomposition of carbonate minerals provides reactive Ca or Mg containing minerals for accelerated carbonation, the retorted samples showed no potential for carbonation, as indicated by the interaction plot between carbonation*combustion in the full model (Figure 7.5).

Higher concentrations of carbonate were observed in samples that were retorted at 500 °C, however the reason for this is likely to be linked to the mineralogy of samples, and in particular varied dolomite contents were observed (Figure 7.7). Once samples were combusted, a small amount of carbonation could be achieved when reacted at pressure and temperature, an average of 1.5 wt % CO_2, and both the carbonation and the retorting temperature were of equal importance on the resultant carbonate value (Table 7.6). As the retorting temperature increased, on samples that were also combusted, the carbonate content was also seen to increase (Figure 7.6). The heterogeneity between the retorted samples may influence the concentration of carbonate within the combusted samples, due to processing in different locations and by different methods. For example, dolomite decomposes at lower temperatures and was found at greater concentrations within UMA-1, therefore the greater loss of CO_2 from UMA-1, compared with MON, could be explained when combusted at 600 °C.

Greater carbonation was achieved in retorted samples, when carbonated at 100 bar and 80 °C for 4 hours, than when carbonated at 70 bar and 40 °C for 1 hour (Figure 7.9). This is in agreement with results from Chapter 6, and is discussed in more detail in Section 7.4.3. Furthermore, the carbonation potential was shown to be affected by the retorting temperature in ANOVA models; with greater carbonation, when pyrolysed at higher temperatures (Figure 7.10). Because more carbonation was achieved when samples were

retorted prior to combustion, it is likely that the removal of organic matter promoted carbonation. This may be due to organic matter coating reactive minerals, and inhibiting carbonation, or due to structurally opening up pores to provide space for carbonate mineral precipitation. On looking at the regions where carbonation occurs from retorted and combusted samples, J-OS Comb only shows an increase in carbonate in phase 1, whereas for MON Comb and UMA-1 Comb, an increase in carbonation in phase 2 occurred as the temperature of retorting increased (Figure 7.29). The increase in carbonation in phase 2 again may be related to the structural properties of the oil shale, with increased reactive surfaces when retorted, allowing for carbonation of more stable carbonate minerals over longer periods of time.

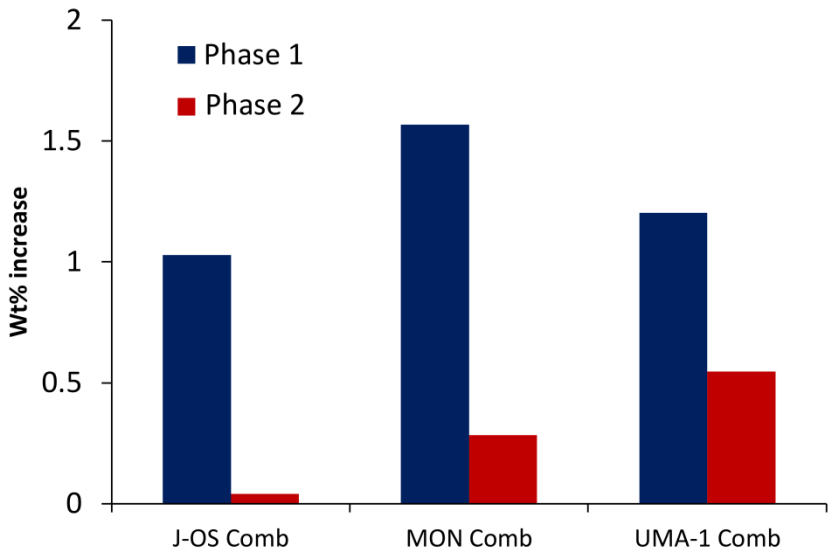

Figure 7.29 - *Percentage of new carbonate within phase 1 and phase 2, formed at high forcing, within samples processed at increasing retorting temperatures followed by combustion at 600 °C.*

7.4.1.2 Decarbonation

By heating retorted oil shale, in an atmosphere void of oxygen, organic carbon is not completely removed by oxidation, and therefore the production of CO_2 is from the decomposition of carbonate minerals alone. It then follows, that the combusted samples should show greater concentrations of carbonate, compared with those samples decarbonated at the same temperature, as organic matter acts to dilute the overall carbonate concentration within decarbonated samples. However, this was not observed, and the analysis of the processing temperature identified the greater importance of the combustion process, compared with the decarbonation process, on the carbonate content of samples (Figure 7.14). Decarbonated samples did not show the same extent of decomposition of carbonate as

combusted samples processed at the same temperatures. In addition, re-carbonation was not achieved to the same extent as samples combusted at the same temperatures, due to the lack of reactive minerals for reaction. It is possible that resultant high partial pressures of CO_2 within the decarbonation chamber, or a lack of a flowing atmosphere during decarbonation, could result in re-precipitation of carbonate minerals (Fadaei et al., 2012), and decarbonation processes were tested on oil shales, as a method to reduce the CO_2 emissions (Odut, 2012).

As discussed in previous chapters, the use of TGA as a quantitative technique to measure the carbonate content within samples of spent oil shale was determined to be reliable producing very little error. The majority of error is likely to come from heterogeneity within the samples themselves. Samples UMA-6A, 6B, and 6C, were all processed at 680 °C in the absence of O_2, before being combusted at 600 °C. This would be expected to remove similar amounts of CO_2, considering samples were subjected to the same conditions of processing. However, XRD and TGA results indicated that samples tested were heterogeneous (Table 7.8 and Figure 7.12), showing variation of ~3 wt %, and indicating differing amounts of dolomite and calcite within samples.

The mineralogy of all the decarbonated samples was most similar to the oil shale combusted at 600 °C (UMA-1 Comb), rather than samples combusted at higher temperatures (Figure 7.15). No N_2 was used in decarbonation of UMA-5, and UMA-8 was decarbonated for 2 hours compared with 2.5 hours for the other samples. However, taking this into consideration the decarbonation trend observed is difficult to interpret. An increase in carbonation did occur as the carbonate minerals decomposed, further supporting an indication of heterogeneity and variation in the original carbonate concentration due to variations in processing conditions, or complex and inconsistent decarbonation mechanisms. For example, the carbonation of UMA-7 was greater than that for UMA-6, even though UMA-7 had more initial carbonate. This indicates that UMA-7 may have started off with more carbonate before processing, in comparison with UMA-6. In addition, carbonation may have naturally formed before accelerated carbonation mechanisms (Thompson et al., 2012). The significance of decarbonation is complex, and more samples would be needed for further evaluation of these results. By decarbonation processes: rather than decrease the amount of carbonate, carbonate content is higher than those combusted at the same temperature. It may be that higher partial pressures of CO_2 are produced during the decarbonation process, preventing further decomposition of carbonate minerals and resulting in higher concentrations.

7.4.1.3 Combustion

As the combustion temperature increased, the decomposition of carbonate minerals, predominantly dolomite and calcite also increased. This was indicated by a reduction in calcite and dolomite reflections from XRD (Figure 7.15), and from a reduction in carbonate weight loss by TGA (Figure 7.16). In particular, the loss of the shoulder at 800 °C from the TGA derivative profile, that was present in UMA-1 Comb, indicated the loss of dolomite. The combustion of oil shale also resulted in the formation of new mineral phases. New mineral phases detected within the spent oil shale were: anhydrite that acts as an inhibitor to carbonation; and periclase and portlandite - both minerals reactive towards carbonation. Due to the relatively low concentrations of the Mg/Ca oxides and hydroxides, it is likely that calcium silicates and calcium aluminates were also formed, which are then able to react further by accelerated carbonation (Fernández-Carrasco et al., 2008). These minerals can be difficult to detect by XRD methods due to their commonly amorphous nature when formed at high temperatures (Motlep et al., 2007). However, trace amounts of gehlenite [$Ca_2Al(AlSiO_7)$] and grossite [$CaAl_4O_7$] were detected within spent oil shale material from XRD analysis.

Further structural analysis was completed using FTIR analysis, confirming the presence of calcium silicate minerals in samples combusted at 750 °C (Figure 7.27), with the appearance of reflections at 910, 940 cm^{-1} due to C_3S or C_2S type silicates (Lanas et al., 2004). Metastable silicate phases are commonly formed when solids are heated for short periods of time at high temperatures (Trindade et al., 2009), and amorphous silicate was identified by the broadening of the Si-O stretching band from 1000-1200 cm^{-1} (Miller et al., 2013).

The combustion temperature was determined to be the most significant variable in defining the amount of carbonate within samples of processed oil shale. As the temperature of combustion increased, the carbonate content significantly decreased (Figure 7.18) due to greater calcination as heating moves further into the zone of carbonate decomposition that occurs between 600-950 °C (Fadaei et al., 2012). Furthermore, combustion was a prerequisite for carbonation reactions to succeed (Figure 7.20), which is why the importance of the carbonation factor comes to light in the combustion model, with an increase in importance of carbonation by a factor of 10, when comparing the full model with the combustion model (Table 7.4 and 7.11).

As the combustion temperature increased, the amount of carbonate within samples decreased. Therefore, the potential for re-carbonation increased, due to the increase in reactive material, and therefore the increased range of carbonate values was also observed.

When combusted at 750 °C, the most carbonate was lost, resulting in 6.47 wt % CO_2 within the remaining carbonate. However, as this sample was carbonated, at 100 bar, 80 °C, and 4 hours, carbonate was increased to 16 wt % CO_2, or 75 % of the maximum carbonate possible after pyrolysis and combustion. This maximum carbonate was 21.44 wt % CO_2, when retorted at 500 °C, combusted at 600 °C and carbonated at 100 bar, 80 °C and 4 hours. Despite the increased carbonation at higher temperatures, there was less carbonate overall and samples of spent oil shale were not able to re-carbonate to 100 % of the expected value. This may be a result of increased pore space, but a reduction in reactive surface area is often observed in sintered samples of CaO (Alvarez et al., 2005), and less reactive surfaces may lead to less overall carbonation.

In addition, due to an increase in carbonation as the combustion temperature increased, the difference between carbonating at low and high pressures became prominent, but only when combusted at temperatures > 680 °C and not when decarbonated (Figure 7.14). This may be linked to the removal of organic matter. In addition, the carbonation*combustion interaction increased in importance from 3.6-9.6 % of the combustion model from the full model (Table 7.11). The Kruskal-Wallis test, which is an analogue of ANOVA, showed that the new carbonate formed, when carbonated at low forcing or high forcing, was unaffected by pyrolysis and decarbonation temperatures (Table 7.13), but was affected by combustion, further confirming the importance of this interaction between carbonation and combustion.

7.4.2 Phase analysis

Phase analysis was conducted to further confirm and identify the formation of carbonate minerals by accelerated carbonation methods. New carbonate minerals formed as a result of carbonation reactions on combusted samples were categorized as phase 1 and phase 2 carbonate minerals, being split into the two regions of decomposition, dependent on the processing temperature and carbonation processes. Phase 1 carbonates were decomposed between 600-770 °C from TGA, while phase 2 carbonates were decomposed between 770-950 °C. As samples were combusted, weight loss occurred in both phase 1 and phase 2, although decomposition was dominant in phase 2 which contains the majority of carbonate minerals (Figure 7.21). Only low concentrations of phase 1 carbonate were observed within unreacted samples, and carbonate in phase 1 increased, as samples were carbonated (Figure 7.30). The position of the derivative peak maximum shifted to higher temperatures (Figure 7.21) as the concentration of phase 1 increased, due to an increase in the temperature

gradient within the solid material leading to higher temperatures of decomposition (Jaber et al., 2000).

The importance of carbonation, and the interaction of carbonation with combustion, was strong for the phase 1 carbonate model, contributing to 45 % of the observed trends in the data (Table 7.15). Combustion was also an important factor, and the maximum carbonation within phase 1 was achieved in samples that had lost the most carbonate from combustion. However, carbonation was not determined to be an important factor in the formation of phase 2 carbonate, with the pyrolysis and combustion temperature dominant in the model, similar to the full model focused on the overall carbonate content. The conditions required for maximum and minimum carbonate content within phase 2 were also the same for the maximum and minimum overall carbonate. These models therefore indicate that combustion was the main control on carbonate within phase 2, and recarbonation predominantly occurred in phase 1. However, the exception to this occurred in samples combusted at 750 °C, where carbonation at high forcing occurred in both phases 1 and 2, with 4.73 wt % CO_2 in phase 2 (Figure 7.30), yet less carbonation in phase 2 at low forcing (2.83 wt %).

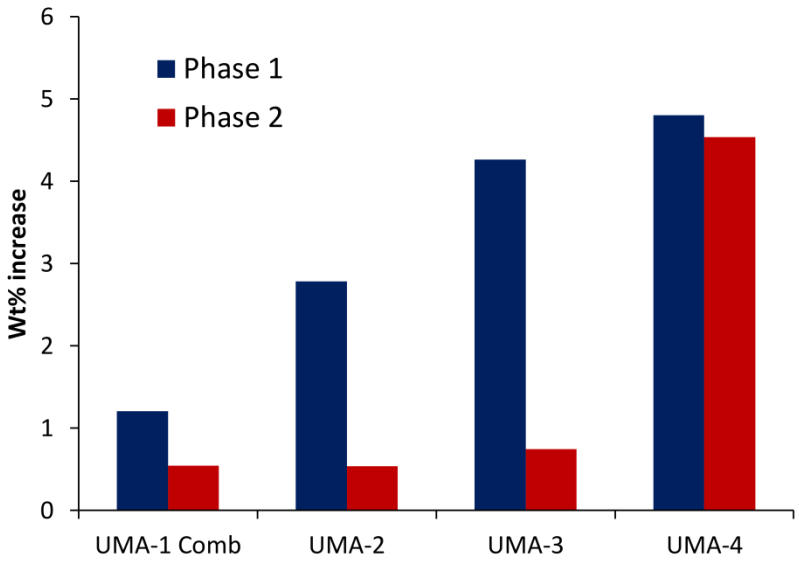

Figure 7.30 – *Percentage of new carbonate within phase 1 and phase 2, formed at high forcing, within samples processed at increasing combustion temperatures.*

The observation of carbonation within phase 2 of the oil shale combusted at 750 °C is similar to results observed in Chapter 6, with carbonation occurring in both phases when oil shale was combusted at high temperatures. The results implicate that phase 2 carbonation was inhibited when combusted at the lower temperatures. This inhibition at the lower temperatures may be due to the coating of reactive minerals with residual carbon, and may be related to why

phase 2 carbonate increased as samples of oil shale were retorted at higher temperatures. Alternatively, an increase in pore space may allow for precipitation of calcite, compared with metastable and disordered forms that may be preferentially precipitated in limited pore space. The difference between phase 1 and phase 2 was therefore analysed further, by chemical analysis.

The XRD and FTIR patterns for the reaction products from carbonated portlandite and wollastonite were compared to the spectra produced from carbonated spent oil shale samples. These analytical techniques were used to distinguish between the polymorphs of carbonate, formed within spent oil shale.

7.4.2.1 Mg-carbonates

Dolomite minerals were identified within phase 2 decomposition from the thermogravimetric weight loss curve, with dolomite minerals identified as a shoulder in this latter decomposition region (Trindade et al., 2009). By TGA, dolomite was identified within UMA-1-Comb (Figure 7.8), that was combusted at 600 °C, however dolomite disappeared when combusted at the higher temperatures, also corresponding with XRD analysis. The presence of periclase within these combusted samples is a result of the decomposition of dolomite, however, when samples were carbonated, dolomite was not reformed (Figure 7.15).

Dolomite and magnesite precipitation is very slow at room temperature, due to kinetic barriers caused by the hydration of Mg (Saldi et al., 2009). However, dolomite and magnesite can be formed at high pressures and temperatures (Althoff, 1977). Otherwise, metastable forms of Mg-carbonate may be formed, such as nesquehonite, hydromagensite and dypingite (Zhao et al., 2010). It is possible that magnesite is formed in the carbonated spent oil shale, by reprecipitation of the metastable phases, or direct precipitation at higher pressures (Felmy et al., 2012), however, due to the low concentrations this cannot be confirmed by the use of XRD or FTIR. A high magnesian calcite, where Mg is incorporated randomly within the calcite mineral structure, rather than ordered within dolomite, is another possibility. The reflection for Mg-calcite may lie between the dominant reflections for calcite and dolomite in the XRD pattern (Figure 7.28), due to increasing disorder, and therefore an increase in the relative d-spacing (Zhang et al., 2010).

7.4.2.2 Ca-carbonates

The reflection at 33° 2θ that is postulated to be from magnesite, could also be from vaterite, a metastable polymorph of calcite. Other types of calcium carbonate include metastable

aragonite and amorphous calcium carbonate (ACC) (Thiery et al., 2007). Aragonite and calcite decomposition by TGA occurs at similar temperatures, making them difficult to distinguish, but XRD analysis produces distinct reflections for aragonite so that it can be separated from calcite. This was observed in the XRD pattern of the carbonated wollastonite (Figure 7.24), where both calcite and aragonite were formed. However, portlandite carbonation (Figure 7.23) resulted in the formation of calcite only (Villain et al., 2007). This initial observation indicates that the carbonation of silicate minerals, compared with hydroxide, results in the formation of a metastable reaction product, and as a result of calcium silicate carbonation, weight loss occurs from 500-770 °C (Villain et al., 2007). The lower temperature of decomposition could be due to defects in the crystal structure that causes the mineral to be less thermally stable (Sdiri et al., 2010).

The carbonation of portlandite and wollastonite was also observed by the use of FTIR analysis (Figure 7.25 and 7.26). Both samples indicated some extent of natural carbonation, commonly observed due to their reactive nature with CO_2 (Cultrone et al., 2005;Huijgen et al., 2006), and calcium silicate hydrates are also observed to naturally carbonate in the environment (Milodowski et al., 2011). Portlandite carbonation was simple, with a decrease in bands corresponding to portlandite at 3640 cm^{-1}, and increase in carbonate bands at 1400-1500 cm^{-1}, 870 cm^{-1}, and 710 cm^{-1} that are caused by: asymmetric stretching, out-of-plane bending, and in-plane bending modes, respectively (Sdiri et al., 2010). Wollastonite absorption bands were observed between 900-1100 cm^{-1}, due to symmetric and asymmetric stretching of Si-O bonds (Miller et al., 2013). On carbonation, the peaks between 900-1000 cm^{-1} was reduced and carbonate bands were identified between 1400-1550 cm^{-1} (Table 7.19 and 7.29). The peak at ~1020 cm^{-1} was reduced and broadened, indicating the formation of amorphous silica from the carbonation reaction (Smidt et al., 2008; Kalinkina et al., 2001).

Extending the FTIR analysis to spent oil shale samples, the assignments became more complex, due to the occurrence of more minerals, at lower concentrations. As previously identified, high temperature silicates were observed in the FTIR spectra of UMA-4, from bands between 900-1000 cm^{-1}, similar to that of wollastonite (Figure 7.27). These silicates are unlikely to be hydrous, as the use of FTIR did not detect strong characteristic bands at > 3000 cm^{-1} from hydroxyl groups, indicating that the mineral phases were mostly anhydrous. The disappearance of the silicate band in the carbonated sample, further encourages the hypothesis that silicate is formed after combustion, which is then able to be carbonated at high pressures and temperatures. The band between 1400-1600 cm^{-1} increased in intensity due to the formation of new carbonate (Kalinkin et al., 2004). The broadening, and splitting of

the band is due to metastable and disordered carbonates, such as ACC or vaterite. This band is caused by the asymmetric stretch of the carbonate ion, so splitting indicates a lack of symmetry within the carbonate mineral (Thompson et al., 2012).

The band at 1410 cm^{-1} has been assigned as calcite, and the shoulder at 1460 cm^{-1} to ACC. Shifting of this shoulder to 1475 cm^{-1} is attributed to increasing amounts of ACC (Miller et al., 2013), and both UMA-4-Low and UMA-4-High have shoulders at this frequency. However, UMA-4-High contains a stronger calcite reflection, corresponding with the phase analysis, where 4.7 wt % of phase 2 carbonate was formed at high forcing (Figure 7.30), compared to only 2.8 wt % by low forcing. Both samples produced similar amounts of phase 1 carbonate, 4.7 wt % at low forcing, and 4.8 wt % at high forcing. Vaterite is favoured at high pressures, low temperatures and alkaline conditions, whereas calcite forms at low pressures and neutral conditions (Cizer et al., 2012; Domingo et al., 2006). Amorphous calcium carbonate is commonly formed in supersaturated solutions, based on Otswald's law of stages, and is a precursor to calcite or aragonite (Clarkson et al., 1992; Addadi et al., 1987). The characteristic band for ACC is at ~1074 cm^{-1} (Schroeder, 2002), however this overlaps with the Si-O stretching mode (Cizer et al., 2012). Furthermore, amorphous calcium carbonate cannot be identified using XRD analysis, however, shoulders on the calcite reflection, at 30^{o} 2θ (Figure 7.28), may be due to the formation of a disordered carbonate, or carbonate formed from the reaction of silicate.

On further analysis of the weight loss of carbonated and combusted spent oil shale samples, from TGA analysis, the total weight loss was constant and independent of the combustion temperature (Equation 7.2; Figure 7.31), at 23 to 24 wt %. The total weight loss was attributed to original carbonate remaining after combustion, new carbonate formed from accelerated carbonation reactions, and other minerals formed after carbonation that decomposed at temperatures < 600 °C by TGA.

$$Total\ (wt\ \%) = Original\ carbonate + New\ carbonate + Other \qquad \text{Eq. 7.2}$$

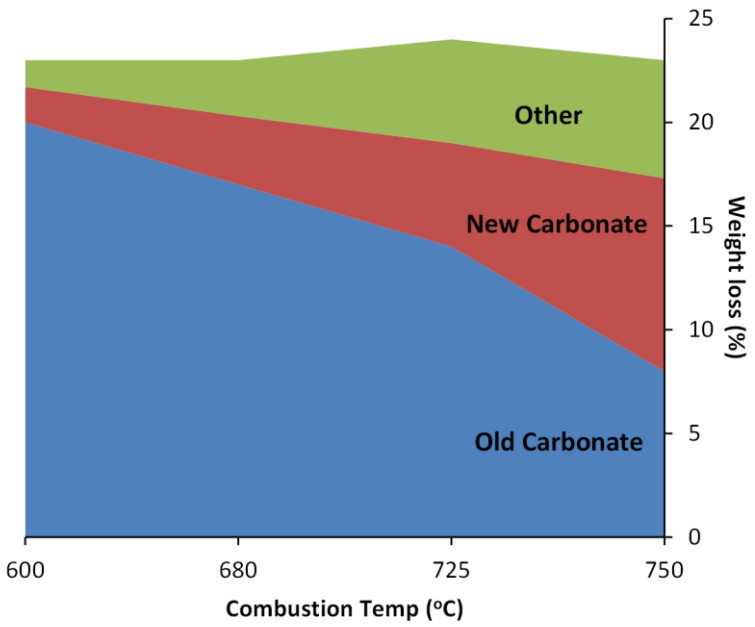

Figure 7.31 – *The total percentage weight loss from TGA, for old carbonate, new carbonate and other phases, as the combustion temperature increased.*

A greater degree of splitting of the carbonate band in FTIR spectra corresponds to lower temperature weight loss from TGA (Kalinkin et al., 2004), and therefore indicates that perhaps a greater concentration of carbonate is being formed than envisaged originally. The splitting suggests that carbonate is disordered or poorly formed, which may explain why lower temperature decomposition occurs from TGA and weight loss at temperatures < 600 °C increased as samples were carbonated.

New mineral phases such as anhydrite and wollastonite do not thermally decompose at low temperatures. The ACC decomposes in this temperature region by decarboxylation mechanisms, being thermally less stable than other forms of carbonate (Brecevic et al., 1989), however, weight loss could also be from loss of water due to dehydration of Mg-carbonate minerals, or hydrated silicate or aluminate minerals, such as CSH or CAH (Lanas et al., 2004). The use of TGA-MS would be able to clarify the types of mineral decomposing at lower temperatures, and can be used to identify ACC (Miller et al., 2013). This could provide opportunities for further work.

7.4.3 Optimum processing conditions

Altering the retorting, decarbonation and combustion temperature, can have an effect on the CO_2 emissions, the oil yield, and the use of spent oil shale as a by-product. For example, increasing the retorting and combustion temperature will:

- increase the amount of CO_2 that is emitted;
- increase the oil yield;
- produce spent oil shale that is beneficial for use in the cement industry;
- produce excess energy that can be exported as electricity.

The peak pyrolysis temperature, determines the oil yield, and how much cracking occurs (Jaber et al., 2000). Studies by Han et al, (2009) has looked at the effect of the retorting temperature, as well as duration, and particle size on the composition and extent of oil recovered. The amount of oil obtained increases, as the temperature is increased. However this does require a greater amount of energy input, as well as detrimental cracking/coking of the oil at higher temperatures. It was determined that the optimum temperature, for retorting of Chinese oil shale from Huadian, to be between 460-490 °C (Han, 2009), compared with 550 °C, for retorting of Jordanian oil shale (Jaber et al., 2000). Alongside this, an increase in duration also causes increased yield at the lower temperatures, suggesting that retorting at lower temperatures could be feasible if retained in the retort for a longer duration (Han, 2009).

Maximum oil yield produced at the higher retorting temperatures, also corresponded with maximum carbonation and therefore reduction in CO_2 emissions, when retorted at 500 °C, combusted, and then carbonated at supercritical pressures and temperatures (Figure 7.10). However, other economic considerations also should be taken into account: if heated at higher temperatures, oil shale needs to be ground sufficiently to be thoroughly heated (Shawabkeh et al., 2013); alternatively, if oil shale is retorted at lower temperatures of ~400 °C, this can be cheaper to operate whilst generating sufficient oil yields, but would need to spend more time in the retorting chamber (Fei et al., 2012).

Decarbonation mechanisms or combustion at temperatures < 680 °C, could also allow for a reduction in CO_2 emissions, and as calcium carbonate decomposition is endothermic, this could have a positive effect on the heat balance within the combustion (Fadaei et al., 2012). However, combustion at 600 °C is not beneficial for allowing spent oil shale to be used as a by-product in the cement industry, as to be used as an additive in cement production, spent oil shale needs to be combusted at high temperatures, to produce high concentrations of lime and portlandite. In addition, the burning of residual carbon is required to produce heat for the whole retorting process (Brandt, 2009) and may produce excess energy that can be exported as electricity (See Chapter 8). Carbonation is limited when oil shale is combusted at lower temperatures, therefore it is questionable as to whether it is feasible to carbonate, if only 1.5 wt % CO_2 is added as a result.

The very maximum carbonation, achieved by optimisation experiments (Chapter 6), was 5.9 wt %, when samples were reacted at 80 °C, 100 bar, 4 hours and using 60 % water. This is compared to a theoretical value of 7.7 wt % based on the available Ca and Mg oxide and silicate content. The maximum carbonation for samples that underwent varied processing mechanisms was 9.5 wt %, or 73 % of the theoretical value of 14.4 wt %, for oil shale retorted at 500 °C, combusted at 750 °C and carbonated at 80 °C, 100 bar, 4 hours, and 50 % water. The extent of carbonation was similar for both samples of spent oil shale, combusted at 750 °C that achieved maximum carbonation, with both showing the formation of high concentrations of calcite, within phase 2, with values at 59 % and 51 % for spent oil shale analysed in chapter 6 and chapter 7, respectively.

Inhibition of phase 2 carbonate was established by carbonating at high temperatures and with low water (10 %), as identified from optimisation studies (Table 7.17). However, inhibition was also extended to samples that were combusted at temperatures < 750 °C, and also to some extent, oil shale combusted at 750 °C and carbonated at low forcing, forming 2.83 wt % CO_2 in phase 2, compared with 4.73 wt % CO_2 from high forcing. An increase in calcium silicate phases, at the higher combustion temperatures, favours the formation of metastable carbonate, such as aragonite and ACC (Villain et al., 2007), and in addition carbonation of amorphous silicates is observed to result in a carbonate phase associated with the amorphous silicate, rather than as a separate precipitate (Thompson et al., 2012). This may explain why carbonate within phase 1 is formed, however, does not correspond with an increase in phase 2 carbonate at the higher combustion temperatures. Instead, loss of organic matter, or an increase in the porosity, may allow for the precipitation of stable carbonates, where the reactive surfaces are accessed on carbonating at supercritical conditions and sufficient reaction durations.

7.5 Conclusions

A partial factorial design, combined with analysis of variance, indicated that the carbonate content within spent oil shale samples was dependent on the temperature of retorting, decarbonation and combustion, as well as accelerated carbonation processes. The ideal retorting temperature is 500 °C, as this allowed for increased carbonation, and produces the greatest oil yield (Jaber et al., 2000). Decarbonation mechanisms were determined to be complex and inconsistent; therefore future work is required to interpret the benefits of implementing this in the retort design.

The combustion temperature was the most important factor on the carbonate content of spent oil shale. Combustion of oil shale was required to allow for carbonation, which was ~2 wt % CO_2 when combusted at 600 °C and then increased to ~10 wt % when combusted at 750 °C. Although the most CO_2 can be re-sequestered within spent oil shale at high temperatures of combustion, the largest emissions are produced as a result of carbonate decomposition.

Supercritical conditions and longer reaction durations (4 hours, 100 bar, 80 °C) allowed for greater amounts of carbonation, when combusted at temperatures > 680 °C, as limited porosity/active surfaces were likely to inhibit carbonation regardless of the reaction conditions. Furthermore, stable calcite was favoured with sufficient access to active surfaces, when carbonated under supercritical conditions and for longer durations, further supporting conclusions from Chapter 6, that carbonation of calcite is controlled by diffusion kinetics and CO_2 supply.

Within carbonated spent oil shale, disordered and metastable forms of carbonate were detected, likely to include ACC, vaterite and aragonite, due to the carbonation of high temperature Ca-silicate minerals formed during combustion processes. These disordered carbonate phases are less thermally stable than calcite minerals; however, still offer a permanent method to store CO_2 within carbonate minerals.

There is potential for the reduction of CO_2 emissions from oil shale processing, based on a reduction in the combustion temperature, or by accelerated carbonation; while the greatest oil yield is recommended at 500 °C pyrolysis temperature. The industrial context of the relationships between the processes will be investigated in more detail in Chapter 8, to suggest a mechanism for optimal retorting of Jordanian oil shale. This incorporates the production of offsets: from the use of spent oil shale in the cement industry, and from the production of electricity exports.

Chapter 8: Conclusions

8.1 Conclusions

The objective of this thesis was to investigate methods to minimise the impact of oil shale processing in Jordan, and the 6 experimental chapters in this thesis explored the characteristics and potential of using spent oil shale for this purpose. The thesis can be divided into 3 sections, where the first section (Chapters 1, 2 and 3) investigates the characteristics of oil shale and spent oil shale, identifying methods for the spent oil shale to be used as a by-product and setting the scene for subsequent research. Secondly (Chapter 4), the environmental stability of Lothian spent oil shale was studied, acting as an analogue to Jordanian spent oil shale. Finally, (Chapters 5, 6 and 7) industrial applications were researched in more detail, focusing on the optimisation of accelerated carbonation mechanisms, along with suggestions for modifications of the oil shale processing design.

8.1.1 Setting the scene

It was observed that there is a need for increased production of oil from unconventional sources, to meet increase in global energy demand (EIA, 2013). In particular oil shale contains proven resources of 2.5 to 3.2 trillion barrels of oil, worldwide (Dyni, 2006). Significant inter-deposit variation of oil shale was apparent on analysis of 15 global oil shale deposits that varied in age from Estonian Ordovician marine oil shale, to Tertiary Lacustrine deposits found in Asia and North America. The mineralogy of oil shale determines the mechanism for processing and waste disposal; therefore the oil shales were classified into four groups: marine, muddy marine, lacustrine and saline lacustrine. The classifications were based on their chemical composition, which was controlled by the depositional environment.

Oil shales that require particularly harsh processing conditions were the marine and saline lacustrine deposits, which were: depleted in clay minerals, that can optimise oil recovery and reduce coking reactions (Hu et al., 2014; Patterson, 1994); and enriched in carbonate minerals, that increase the heat requirements for retorting and produce increased CO_2 emissions from the decomposition of carbonate minerals (Sohns et al., 1951). Jordanian oil shale (J-OS) was found to contain ~60 % calcite and dolomite, and additionally, J-OS, like other marine deposits, showed enrichment in heavy metals that may be of environmental risk. Nonetheless, J-OS is suitable for oil extraction, with deposits suitable for surface mining and high concentrations of organic matter (Alali et al., 2006). Therefore, further work was accomplished to identify

methods to reduce the impact of oil shale processing, while retaining an environmentally stable material.

8.1.2 Protecting the environment

In terms of the environmental stability of Jordanian spent oil shale (J-SOS), weathered material was concentrated in heavy metals by ~15 to 20 % compared to J-OS, indicating that elements are retained within spent oil shale after retorting processes. Due to the alkaline nature of the spent oil shale, elements are likely to be retained within the residual fractions (Essington, 1991), such as Ca-silicates that were identified within J-SOS. However, long-term weathering was not considered.

In particular, Lothian spent oil shale was determined to be enriched in trace elements, within clay and organic fractions, that may be susceptible to release into the environment by weathering. Therefore, environmental mobility studies were conducted on the bings, subjected to weathering for > 50 years. Using sequential extraction studies, to divide spent oil shale and associated soil into five rock fractions, the majority of trace elements of environmental significance were found to be retained within residual fractions in spent oil shale, with > 90 % of elements partitioned within the immobile fractions at all the sites, and > 85 % within the residual fraction at 3 of the 5 sites. Heating of the oil shale, led to the formation of aluminosilicates, that were able to adsorb trace metals and the spent oil shale remained environmentally stable. Soil, in the bing environments, was formed partially from the mechanical breakdown of spent oil shale. An enrichment of trace elements within the soil samples, and partitioning predominantly in residual fractions, confirmed the lack of mobility of trace elements during weathering processes.

Results indicate that J-SOS is likely to also be stable by long term weathering, however because of the complex controls on the mobility of trace elements in spent oil shale deposits, Jordanian oil shale, along with other oil shales should be assessed on an individual basis.

8.1.3 Industrial applications

8.1.3.1 CO_2 sequestration

The optimisation of J-OS processing was considered and CO_2 sequestration was identified as a technique to reduce CO_2 emissions, by the capture and long-term storage within spent oil shale. The use of spent oil shale was highlighted due to the high concentration of Ca/Mg oxide, hydroxide and silicate minerals, where the theoretical carbonation was calculated to be

7.7 wt % CO_2. Reactions were undertaken using supercritical CO_2, hydrated spent oil shale, and a factorial design, and analysis of variance (ANOVA) methods were used to optimise for carbonation, while also considering the impact of processing mechanisms. Water was required for carbonation, however, water supply in Jordan is limited and needs to be carefully monitored and reduced as much as possible (Jaber et al., 1997c). Therefore, carbonation mechanisms trialled in laboratory experiments used minimal water, and ≥ 50 % was determined to be sufficient for carbonation to allow for complete dissolution of reactive ions, 20 times less than Estonian researchers in the same field performing carbonation on spent oil shale slurry (Uibu et al., 2009).

Combustion of retorted oil shale was required for carbonation, and the sequestration of CO_2 within spent oil shale was possible even at low temperatures of combustion, from 600 °C. Greater carbonation was achieved at higher temperatures of combustion, due to the increased abundance of reactive minerals and greater carbonation was also achieved at high temperatures of pyrolysis, indicating that the removal of organic matter promotes the precipitation of carbonate minerals, with increased access to reactive surfaces. Carbonation was primarily achieved in metastable or disordered forms, such as amorphous calcium carbonate (ACC), precipitated by the carbonation of silicate minerals; where metastable carbonate products were favoured at high temperatures and short reaction durations, inhibiting further carbonation by pore blocking or surface coating. However, longer reaction durations increased the precipitation of stable carbonate, and calcite was especially favoured within spent oil shale that was retorted at 500 °C and combusted at 750 °C, followed by carbonation at supercritical conditions (100 bar, 80 °C) due to precipitation being controlled by diffusion to reactive mineral surfaces and CO_2 supply.

The loss of CO_2 is not only a result of carbonate decomposition, but also from the combustion of residual carbon, upgrading of oil, and power production (Melo, 2012). Nevertheless, estimates for the reduction in CO_2 emissions by accelerated carbonation was made, based on an evaluation of the total CO_2 emissions where:

- The total CO_2 emissions as a result of oil shale retorting by the ATP process, without CO_2 sequestration, is estimated to be 280-300 kg CO_2/bbl.
- Maximum carbonation, as determined by bench experiments, was 5 wt % CO_2, when carbonated at supercritical conditions for 4 hours, at 100 bar, 80 °C, with 60 % water, which was 69 % of the theoretical value.

- Assuming that all of the J-SOS is used to sequester CO_2, without producing extra emissions itself, CO_2 emissions have the potential to be reduced by 29 kg CO_2/bbl.

In terms of costs, there are benefits to using spent oil shale compared to other methods of CO_2 sequestration by mineralisation techniques, with implications to the economic feasibility of carbon capture within spent oil shale:

- Alkaline waste material, such as spent oil shale, has increased reactivity in comparison to silicate feedstocks (Huijgen et al., 2005), therefore thermal or chemical processing is not required before carbonation. Thermal processing alone could add $100/tonne CO_2 (Jacobs et al., 2011).

- Carbon dioxide is produced at the source of spent oil shale production, therefore compression and transportation of CO_2, that can be very costly, is not required. It is estimated that $50-60/tonne CO_2 is required for the capture and transport of CO_2 alone (Hitch et al., 2012), the cost for J-SOS may be lower considering also that transportation is not required. In addition, only 12 % of the CO_2 within emissions need be captured, if 50 % of the spent oil shale is subjected to accelerated carbonation mechanisms.

- Mining and crushing of oil shale is already incorporated into the cost of retorting, and therefore would not be required for spent oil shale carbonation. The use of supercritical CO_2 would also negate the need for extensive grinding, another large cost associated with mineralisation methods, with costs upwards of $25/tonne CO_2 (Renforth, 2012).

- Water is already supplied for the cooling of spent oil shale, and can also be used within carbonation mechanisms.

- Excess heat that would be used in the production of electricity for exports can be used instead for production of subcritical or supercritical CO_2.

8.1.3.2 Process optimisation

A process has been identified where a 10.4 % reduction in emissions could be achieved by accelerated carbonation using 50 % water, for 4 hours, at 100 bar and 80 °C. The greatest carbonation within spent oil shale was obtained when it had been retorted and combusted at high temperatures. However, when considering the optimal combustion temperature for the reduction in CO_2 emissions, other considerations need to be assessed, such as the increase in

CO_2 emissions at higher processing temperatures. Furthermore, the use of spent oil shale in the cement industry could provide additional revenue, as well as the sale of electricity (up to 30MW) to the Jordanian grid. The offset CO_2 emissions, therefore could reduce the carbon intensity of retorting oil shale further, however, these offsets are only applicable when processed at higher temperatures. The advantages and disadvantages of processing at various temperatures are outlined in Table 8.1, and the emissions associated with each combustion temperature and mitigation mechanism are estimated in Figure 8.1.

Table 8.1 – *Advantages and disadvantages to processing of oil shale at differing temperatures of combustion.*

Combustion temp	Advantages	Disadvantages
600 °C	• Least CO_2 emissions	• Not for cement use • Does not produce enough heat required for retorting • No electricity exports • Minimal carbonation
680 °C	• More carbonation	• Not for cement use • May not produce enough heat • No electricity offsets
725 °C	• More carbonation • Used in cement production • Partial power exports?	• More CO_2 emissions
750 °C	• Most suitable for cement • Most power exports • Most carbonation	• Highest CO_2 emissions

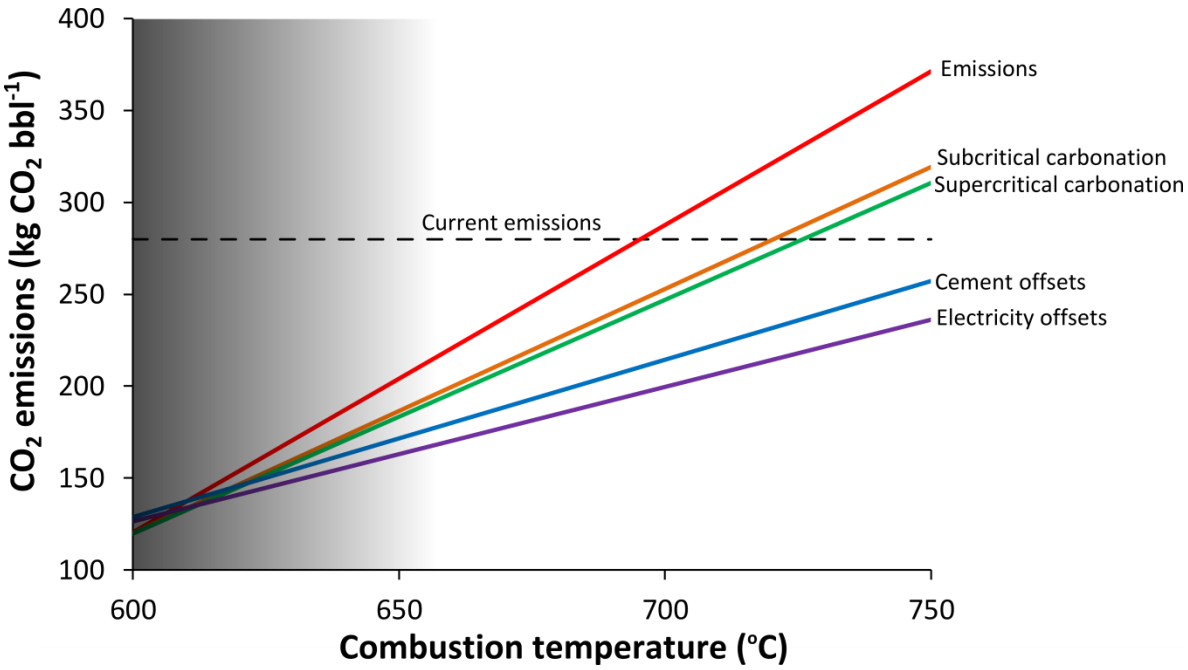

Figure 8.1 – *Estimated CO_2 emissions, based on oil shale that was combusted for 2 hours at 600 to 750 °C, with carbonation and offsets. Current emissions are represented by the dashed line, and the highlighted area represents insufficient temperatures to provide heat for the retorting of oil shale.*

The emissions were calculated based on the following assumptions:

- Carbon dioxide emissions are 280 kg CO_2/bbl and 4000 bbl/day is produced.
- To be used in the cement industry, spent oil shale must contain a high concentration of reactive minerals, similar to those required for accelerated carbonation, and therefore carbonated material cannot be used. A value of 5 % of total spent oil shale produced was used in cement production, based on 10 % being used in cement operations that produce 1 million tonnes/year, such as the Northern Cement Company (NCC), in Jordan (NCC, 2014).
- Carbonation was assumed to be suitable for scale-up processes, and calculations were made based on the remaining 95 % of spent oil shale being used to sequester CO_2. This is for demonstration purposes and the tonnage used is likely to be < 5000 tonnes SOS/day.
- Excess heat when oil shale was combusted at 750 °C, can be exported as electricity at 30MW. The wattage was scaled down for each of the lower combustion temperatures, according to the proportion of carbon burnt. At lower temperatures, the amount of power produced will be considerably less, but it is unknown how this will affect the heat requirements within the retort, or the excess power produced.

- Emissions from carbonate decomposition were calculated to be 26 % of the total emissions, when combusted at 750 °C by the ATP. This was assumed to be the same for other temperatures of combustion, so as to scale up/down emissions based on their original carbonate composition.

In terms of feasibility, a full cost-benefit analysis would be required to determine the ideal processing mechanisms for a reduction in CO_2 emissions, coupled with the production of by-products and oil recovery. However, the following can be suggested based on the information provided:

- Low combustion temperatures (600 °C) may not provide enough heat to retort oil shale.
- When spent oil shale is combusted at temperatures < 680 °C, no offsets can be gained, as spent oil shale is not sufficiently calcined for use in cement manufacture, and there may be no excess heat for electricity exports.
- At combustion temperatures > 725 °C, cement and electricity offsets may be gained, with the greatest electricity export and accelerated carbonation at 750 °C.
- The difference in carbonating at greater pressures and reaction durations is relevant at 750 °C, with > 25 % increase in carbonate content through carbonation at 100 bar, 80 °C and 4 hours. Supercritical CO_2 is also recommended for use on J-SOS of large particle size.
- If carbon credits were valued at \$80/tonne CO_2 (EASAC, 2007), it is possible that revenue could be produced, if the gain from carbon credits outweighs the gain from electricity exports (Figure 8.2).

The cost of using supercritical CO_2 to actively sequester CO_2 within J-SOS is greater than using passive weathering or enhanced carbonation methods. However, the use of supercritical conditions means that spent oil shale could be used without further grinding. Pre-processing methods are estimated to cost ~\$80-\$100/tonne of CO_2 (Jacobs et al., 2011), therefore meaning that supercritical carbonation could generate cost-savings: it is estimated that the cost of compressing CO_2 (at 150 bar and 40 °C) to be transported by pipeline, is in the region of \$10/tonne CO_2 (Zhang et al., 2006), whereas the cost to both capture and transport CO_2 is estimated at \$50/tonne CO_2 ((Hitch and Dipple, 2012).

Assuming that the cost to sequester CO_2 within spent oil shale is \$50/tonne CO_2 and 200 tonnes of CO_2 are captured per day, the cost for active sequestration is \$10,000/day. A scenario was used to identify at what point the capture of CO_2 within spent oil shale is uneconomic, based on the amount of carbonation achieved and varying costs of carbon credits. Figure 8.2 shows the different scenarios, where the purple dashed line corresponds to total CO_2 emissions reduced due to sequestration of CO_2 within spent oil shale, and the solid coloured lines are the different prices for carbon credits based on the reduction in emissions. Based on the estimated cost of CO_2 sequestration, it is only viable when it reaches 80 % of the theoretical carbonation at \$60/tonne of CO_2, or at ~60 % when carbon credits are priced at \$80/tonne. Current costs of carbon credits are lower than these values, however they are expected to rise, with one estimate placing the value of carbon credits at \$200/tonne by 2027 (Hitch and Dipple, 2012).

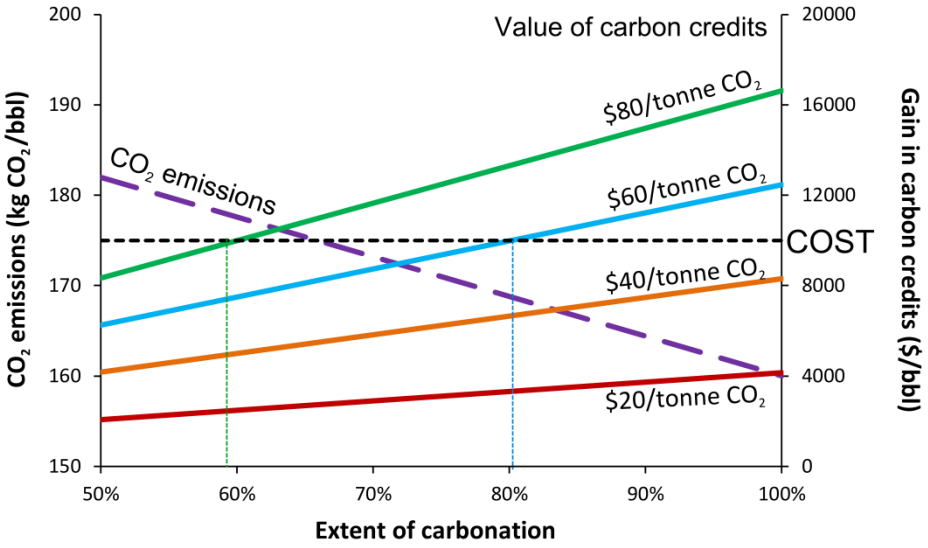

Figure 8.2 – *The cost benefits of carbon credits (\$20-\$80/tonne CO_2) is assessed against the total cost of active CO_2 sequestration (\$10,000/day, black dashed line) and the extent of carbonation required to be cost-effective. This is shown against the resultant reserve-to-tank CO_2 emissions after CO_2 sequestration and offsets (purple dashed line).*

The potential for reduction in emissions, based on previous considerations is displayed in Figure 8.3. The reduction of emissions from oil shale is shown in sequential steps that could be implemented to optimise the retorting process in terms of CO_2 emissions, by:

1. Reducing the temperature of combustion to 600 °C, without any offsets;
2. Combusting at 750 °C, but using spent oil shale in cement manufacture;
3. Electricity offsets, based on 30MW of power;

4. Passive weathering, incorporating 95 % of spent oil shale and assuming 8 % of sequestration compared to active processes (Uibu et al., 2009);

5. Active sequestration, assuming a reduction in electricity offsets due to 10 % of electricity used in the capture of CO_2 and carbonation procedures.

Production emissions for oil shale are displayed with emissions values for other common unconventional and conventional processing methods, identifying the opportunity to reduce emission to be comparable to that of tertiary oil recovery.

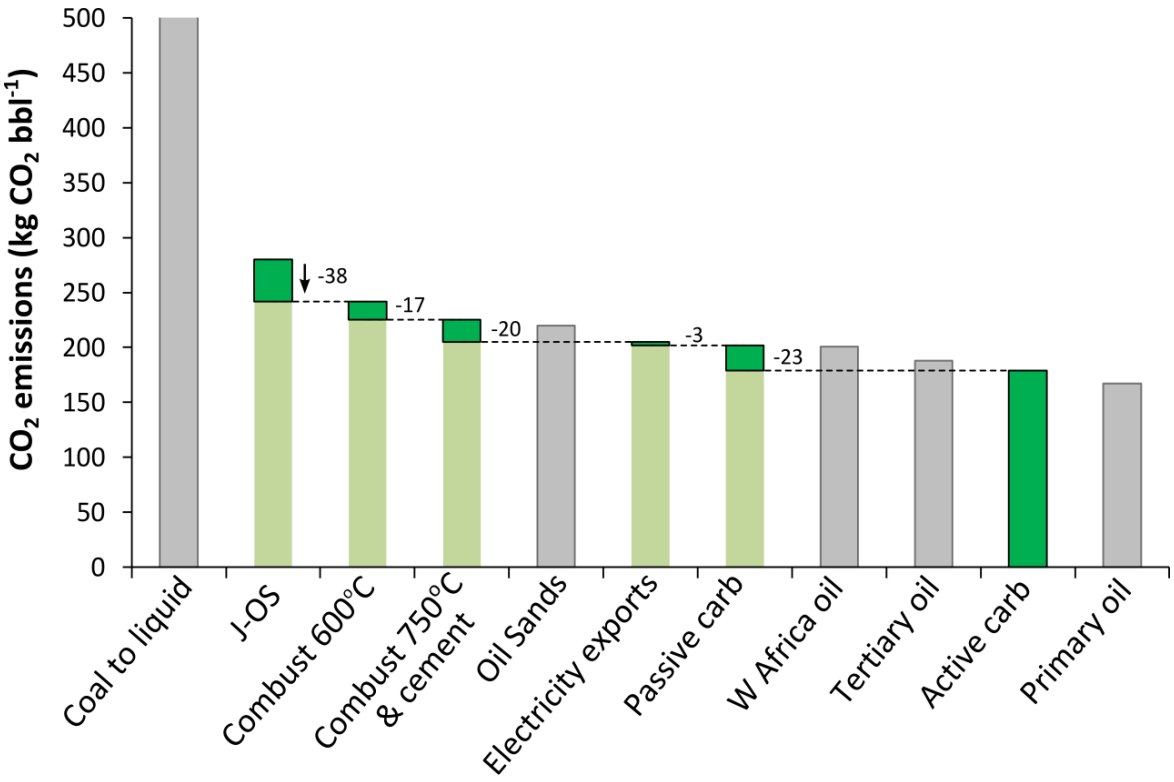

Figure 8.3 – *CO_2 production emissions from conventional and unconventional methods, as displayed by the grey bars. The green bars show the potential for a reduction in CO_2 emissions of Jordanian oil shale processing.*

In addition to carbon offsets produced using: excess energy to provide electricity, and using spent oil shale in the cement industry; JEML and UMATAC have further developed the ATP process, so that is extremely energy efficient and produces large oil yields. The process uses excess heat from the combustion process, to preheat and retort oil shale entering the chamber, while minimising water usage (Brandt, 2009). However, other offsets not currently in consideration by JEML could also be implemented into the plant design, including: the use of renewable technology, afforestation techniques, or soil sequestration by restorative methods.

The planting of forests in particular is perceived as a cost effective way to reduce and offset CO_2 emissions, and costs are estimated at < \$50/tonne of CO_2 sequestered within the plant biomass (Richards & Stokes, 2004). Alternatively, the sequestration of CO_2 within soil is perceived as another bridging solution to the reduction of CO_2 emissions, with the potential to sequester 0.2-0.4 billion tonnes of carbon/year in desert regions and could act to reduce erosion and improve soil characteristics, although challenges do exist in Jordan with the harsh arid climate and reduced resources (Lal, 2004).

A project in Jordan, that has received financial backing and is in development, is the Sahara Forest Project (saharaforestproject, 2014). This incorporates: renewable energy by photovoltaic technology, desalination of water from the Gulf of Aqaba, production of biofuels, development of agriculture, and forestation that acts to draw down CO_2 from the atmosphere. Future plans are to develop this project over 4,000 hectares, in the Middle East, where it is projected that 50,000 tonnes of CO_2/year could be sequestered: in comparison to emissions from the retorting and combustion of oil shale, this is 12 % of total emissions. If a similar project was to be employed by JEML, this could account for a further reduction in emissions by 34 kg CO_2/bbl. These techniques, if applied and maintained correctly, could further reduce emissions, and combined with active sequestration methods, total CO_2 emissions could be less than those produced during conventional oil recovery methods (Figure 8.3).

8.2 Limitations and future work

8.2.1 Environmental studies

The heterogeneity within spent oil shale deposits was apparent and mixing between overburden and spent oil shale was also encountered. Therefore, increased sampling at deposits, including the sampling of bings at depth, may also allow for conclusions to be made on the drainage mechanisms and weathering processes occurring throughout the deposits (Motlep et al., 2010). A future comprehensive and factorial sampling design, accompanied with analysis of fewer extracts, could allow for results of statistical significance and a principal component analysis may be used to determine main controls on the weathering in the Lothian bing environment (Worrall and Pearson, 2001).

Inductively coupled plasma mass spectrometry (ICP-MS) was used to analyse the concentration of a suite of elements within sequential extracts from five different rock phases, from samples of rock, soil and waste. Due to the high concentration of total dissolved solids

within the reagents used in the sequential extraction process, dilution factors were large (up to 1/1000 dilution), to minimise the effect of interference within the instrument. Resultant low concentrations of elements of interest were often below the detection limit, especially within the exchangeable and carbonate fractions and for light elements such as Fe and Ni. The use of different extraction reagents, and ICP-OES as the analytical method using duplicates, could allow for more accurate analysis of sequential extracts, also including the analysis of major elements in addition to trace elements.

Jordanian spent oil shale is enriched in heavy metals, likely to be retained within residual fractions of the rock that are not susceptible to release by weathering. However, future work is also required to ensure the environmental stability, once deposited and weathered over long periods of time. The use of carbonation as a method to reduce CO_2 emissions, may also act to improve the stability of deposits, and combined CO_2 sequestration with environmental remediation, using waste materials with high concentrations of heavy metals, has been considered by several authors. In spent oil shale, alkaline minerals were detected such as portlandite and ettringite. The reaction of CO_2 with spent oil shale may act to reduce the mobility of inorganic compounds (Reddy et al., 1994). A reduction in the mobility of elements is a result of the decrease in porosity, the partitioning of elements within the non-carbonated silicate material, as well as a reduction in pH from the neutralisation reaction by forming carbonates (Fernandez Bertos et al., 2004). In other waste materials, such as MSWI ash, carbonation led to a reduction of lead and zinc leaching (Li et al., 2007; Bertos et al., 2004; Ecke, 2003). In addition the mobility of Cu was reduced by 50 % (Meima et al., 2002), while Pb was stabilised within MSWI in a separate carbonation study (Jiang et al., 2009). As well as reducing the leaching of toxic metals, MSWI ash can be used in construction once treated by natural carbonation, by the carbonation of high temperature amorphous phases (Rendek et al., 2006; Ecke, 2003). Lothian spent oil shale, has been removed from the bings to be used in construction of roads in the area (Harvie, 2005), and Jordanian spent oil shale may also be suitable for a similar purpose.

8.2.2 CO_2 sequestration

Limitations with the calculation of the theoretical and actual extent of CO_2 sequestration were encountered. The theoretical carbonation, estimated at 7.7 wt % CO_2, was a low estimate due to the assumption that all sulphate, phosphate, and existing carbonate minerals are bound to the Ca/Mg cations within the spent oil shale. By removing sulphur during retorting processes, this could prevent the formation of sulphate minerals that inhibit carbonation, thereby

increasing the theoretical and actual carbonation. Alternatively, the use of adjuvants, or thermal processing methods prior to carbonation, could also allow for increased reduction in CO_2 emissions and is recommended for future work to optimise carbonation further to approach 100 % of the theoretical carbonation.

The actual extent of carbonation, was calculated based on thermogravimetric methods, where carbonate was assumed to decompose > 600 °C, in a stoichiometric 1:1 ratio of cation:anion. However, amorphous/metastable carbonates may decompose at temperatures < 600 °C, and it is therefore likely that the amount of carbonation is underestimated by current quantitative TGA methods. Therefore, the use of TGA-MS may allow for detection of greater amounts of carbonate that could result in carbonation occurring closer to 100 % of the theoretical value.

8.2.3 Optimisation processes

To enable carbonation of spent oil shale at source, on an industrial scale, further studies need to be performed, investigating the requirement of supercritical conditions with samples of spent oil shale that have not been ground to a fine powder. While the use of quantitative thermogravimetric methods did suffer from setbacks during the course of continual analysis over several months, it does offer a comprehensive and statistically significant method to determine the change in carbonate content by CO_2 sequestration of spent oil shale. However, when analysing samples that were processed at different temperatures, the concentration of carbonate may be underestimated or overestimated, due to differing amounts of residual carbon within the rock. Therefore, analysis of the total CO_2 emissions, not just from the decomposition of carbonate minerals, may be beneficial for future work and comparison studies.

Also of note is the heterogeneity of samples and variation of processing mechanisms observed in samples processed by UMATAC and Monash University, compared with J-SOS produced by JEML. This means that results should be interpreted with some degree of uncertainty. The calculations based on these results may involve a significant amount of error and therefore are just used as a basis for future work on the applicability of carbonation and improvements to the ATP processing of Jordanian oil shale.

8.2.4 Global oil shales

The use of CO_2 sequestration techniques with oil shale from other global deposits could be viable, depending on their chemical composition and suitability for carbonation. In particular, other marine deposits, such as those from Israel and Morocco, could be carbonated, while

deposits from Estonia have already been identified as potential storage points for the sequestration of CO_2 (Uibu et al., 2009).

With regards to processing methods, it is likely that carbonate poor deposits are beneficial in terms of heating requirements and reducing CO_2 emissions, such as those from China and Mongolia. The environmental mobility of heavy metals, enriched within deposits, would require further research focused on individual deposits, but the limited mobility within Lothian deposits suggests that other clay rich deposits may act in a similar way.

Deposits from the Green River formation, and Thailand, are likely to offer the most environmentally stable waste material due to low concentrations of heavy metals compared to other oil shales, and high concentrations of carbonate minerals that retain elements within Ca-silicates formed during high temperature processing. With a high potential for accelerated carbonation, these lacustrine oil shales deposited in saline conditions are suggested for further work on accelerated carbonation within waste materials such as spent oil shale, and greater concentrations of Mg-containing minerals would result in a greater drawdown of CO_2 per unit volume of waste, than for Ca-containing minerals (Huijgen, 2003).

Oil shale samples were not considered to be economically viable for the extraction of heavy metals, as by-products alongside oil recovery. However, due to intra-deposit variation, further studies are required on the heterogeneity, both vertically and laterally, for the evaluation of individual deposits.

8.3 Concluding remarks

- A comprehensive characterisation study was completed on 15 global oil shales, which were categorised according to similarities in mineralogy and chemical composition. Jordanian oil shale was most similar in composition to Estonian, Israeli and Moroccan oil shales: other marine deposits.

- Lothian spent oil shale deposits were environmentally stable with respect to the leaching of trace elements of environmental significance. Trace elements resided predominantly within residual fractions of the spent oil shale and immobile fractions within associated soils. The composition and processing techniques used on the oil shale were identified to be controlling factors in the mobility of trace elements, and Jordanian spent oil shale is predicted to also be stable with respect to the mobility of trace elements.

- Jordanian spent oil shale was suitable for CO_2 sequestration, and carbonation experiments were carried out using supercritical CO_2. Supercritical conditions were chosen so that energy intensive pre-processing of spent oil shale is not required, and as electricity produced during the Alberta Tacuik Process can be used in the active carbonation process.

- By establishing a factorial experimental design and using quantitative thermogravimetric analysis to measure the amount of CO_2 sequestered within spent oil shale after carbonation, the reaction was optimised and statistically significant factors identified. In particular, carbonation at supercritical conditions, for > 4 hours, yielded the maximum carbonate content.

- Optimisation experiments sequestered an average of 4 wt % CO_2, or an extent of reaction of 55 %. In industrial terms this corresponds to a reduction in emissions of 24 kg CO_2/bbl. Maximum sequestration was achieved when spent oil shale was carbonated for 4 hours, at 100 bar, 80 °C, and 60 % water, reaching 69 % extent of reaction, and a potential reduction in emission of 29 kg CO_2/bbl.

- An increased understanding of the type of carbonate precipitated during the carbonation experiments was achieved, with both calcite and disordered/metastable forms of carbonate precipitated, of differing thermal stability. Both types of carbonate mineral offer a permanent solution to the sequestration of CO_2, and increased carbonation was realised as spent oil shale was combusted at increasing temperatures.

- A new study on the optimisation of retorting and combustion conditions was completed and processing conditions are likely to yield the greatest oil recovery by retorting oil shale at 500 °C, combusting oil shale at 750 °C, reducing CO_2 emissions by active sequestration and other offsets.

- The sequestration of CO_2 within Jordanian spent oil shale has been demonstrated, with opportunities to reduce CO_2 emissions produced by the Alberta Tacuik Process by 10 %. This technique has the potential to be used on other marine/saline lacustrine spent oil shale deposits, and could offer great potential for mitigating CO_2 emissions associated with oil shale production.

- Other offsetting methods combined with active sequestration, such as the use of spent oil shale in the cement industry, and electricity exports, could reduce reserve-to-tank

emissions by 36 %, with feasibility increased as carbon credit prices increase >$80/tonne CO_2.

- The development of a global industrial technique, for the carbonation of spent oil shale has been identified for future work, to identify a cost-effective method of reducing CO_2 emissions without environmental impacts.

Appendices

Appendix A – Detailed methodology

The detailed methodology for sample preparation and use of analytical techniques is provided in the following appendix. A general description of the methodology in the context of each research question is covered in the methodology section of individual chapters.

A.1 Sample preparation and storage

For whole rock, mineralogical and thermal analysis, rock samples of particle size < 2 cm, were powdered to < 0.5 mm grain size, by the use of an agate pestle and mortar. For samples not already processed, weathered surfaces were removed using a hammer, and the samples were crushed to smaller pieces (< 2 cm) using a hammer and plastic bags to avoid contamination of samples. Ground rock samples were then dried at 105 °C for 12 hours, before being stored in polypropylene vials in a desiccator cabinet over silica.

A.2 X-ray diffraction (XRD)

Samples analysed by XRD methods were sieved to < 0.2 mm, and were evenly distributed onto a glass XRD slide, thinly coated with a layer of petroleum jelly. Excess powder was removed, and the slide was placed onto the sample holder of the Bruker D8 Advance instrument. Diffraction patterns were obtained by using CuKα radiation (λ=1.5406 Å) and a nickel filter to remove any CuKβ radiation. A scanning rate of 3°/min was employed, at 40 kV, 200 mA, and a step size of 0.02° from 5-90° 2θ. A slit size of 20 mm was used, along with a knife edge and constant sample rotation. Data was exported into EVA software for further analysis.

A.3 X-ray fluorescence (XRF)

X-ray fluorescence analysis was achieved by Nick Marsh in the Department of Geology, University of Leicester. Powdered samples of 5 g size were added to a 10 ml glass vial, dried at 105 °C for 12 hours, and stored in a dessicator with a plastic snap top used on the vials. The weight loss during ignition (LOI) was determined by adding each sample to an alumina crucible, and heating in a muffle furnace at 950 °C for 1 hour. The weight of the crucible, as well as the weight of the combined crucible and sample, before and after analysis, was recorded.

Around 2 g of dried flux, was added to a Pt/Au crucible, and placed in a gas burner for 5 minutes. After cooling, the weight loss was determined. Dried flux (3 g plus the determined weight loss) was then added to a Pt/Au crucible, and 0.6 g of ignited sample was added and

mixed together. The crucible was placed in a gas burner, and the rock was fused. The fusion bead was produced by adding the liquid to a casting dish, and the samples were stored in a dessicator prior to analysis. XRF analysis was achieved using the PANalytical Axios Advanced XRF Spectrometer along with rock standards and blanks, and results were re-calculated to include LOI.

A.4 Inductively coupled plasma mass spectrometry (ICP-MS)

A standard method was used in the preparation and analysis of oil shales and Jordanian spent oil shale (Chapter 2 and 3), in addition to spent oil shale, rock, soil and vegetation samples collected from Scotland (Chapter 4), by inductively coupled plasma mass spectrometry (ICP-MS) (Ottley et al., 2003). Samples and international reference materials (W-2, BHVO-1, AGV-1, BEN, NBS 688), of 100 mg size, were transferred to teflon vials, alongside 4 blank vials and 4 duplicates for one of the samples. The addition of 1 ml HNO_3 and 4 ml HF followed, and the sample set was refluxed at 150 °C using a hotplate for 48 hours, before being removed and allowed to cool. The vial caps were carefully removed, and vials were placed back on the hotplate to allow for the evaporation of the acid, and removal of fluoride ions as SiF_4. When only a few µl of the acid mixture remained in the vials, samples were removed from the hotplate and allowed to cool. A further 1 ml of HNO_3 was added to each vial, and the acid was evaporated to leave a moist residue. This step was repeated, to ensure the complete dissolution of residual mineral matter, and vials were allowed to cool before the addition of 2.5 ml HNO_3 and ~10 ml MQ water. Samples were refluxed overnight, cooled, then transferred to a 50 ml sterilin, with the washings from the sample vial, then 1 ml of Re/Rh internal standard was added and solutions were diluted to 50 ml, resulting in a HNO_3 concentration of ~3.5 %.

Prior to analysis, an Eppendorf pipette was used to transfer 1 ml of each sample into test tubes, using 2 solutions of diluent (pre-prepared ~3.5 % HNO_3) to ensure no contamination from the pipetting procedure. A ten-fold dilution, by the addition of 10 ml of diluent, was carried out and solutions were mixed before being placed in the sample rack for analysis using a Perking Elmer Sciex 6000 ICP-MS. Blanks were analysed first, followed by standards and samples, with the analysis of one blank, one standard, and one replicate every 6+ samples. Once all the samples were analysed, the standards and blanks were analysed again to finish the analysis.

For quantitative analysis, regular checks were undertaken to ensure the instrument was performing correctly and that the samples were prepared appropriately. This was done by

analysing: the standard error on instrumental repeats; the concentration of elements within blanks, standards, duplicates and replicates; instrumental drift correction; and variation between isotopes. The use of international reference materials enabled the calibration of the instrument, by the production of calibration curves to ensure that the concentration of solutions was at the right level for detection in the instrument, and therefore to accurately analyse the desired elemental suite. In addition, calibration curves were used to identify problems with any of the elemental isotopes used by ICP-MS. An internal standard was used to identify errors caused by inadequate sample preparation, or to correct for instrumental signal drift that occurs throughout analysis due to sensitivity changes within the instrument or by suspended particles blocking the nebuliser. A mixture of Re and Rh was chosen for use as an internal standard, because these elements produce detectable and distinct peaks, they are found at low concentrations within the analysed material, and are chemically similar to the elements that were analysed; thereby reducing interference from matrix effects (Gill, 1997).

Blanks, standards and replicates were analysed multiple times throughout the analysis to further ensure the results obtained were accurate and reliable. Blanks were used to ensure that no contamination of samples occurred, either through sample preparation or through the instrument. Replicates were used during the analysis as an additional check for instrumental drift and contamination, whereas duplicates provided information on the heterogeneity of samples and errors associated with the preparation and dissolution process. Finally, following the confirmation of data validity, the concentrations of elements detected were corrected using the dilution factor (x5000) and were then converted into concentrations within the rock, in mg/kg.

In Chapter 4, solutions from the sequential extraction process, for fractions 1 to 4 (exchangeable, carbonate, Fe-Mn oxides, and organic), were analysed using ICP-MS analysis. Firstly, external standards were prepared. This was done by diluting stock solutions of the following elements: Mg, Al, K, Ca, Sc, Ti, V, Cr, Mn, Fe, Co, Ni, Cu, Zn, Ga, Rb, Sr, Y, Zr, Nb, Cs, Ba, La, Ce, Pr, Nd, Sm, Eu, Gd, Tb, Dy, Ho, Er, Tm, Yb, Lu, Hf, Ta, Pb, Th and U. Stock solutions of individual elements contained 1000 mg/l, with the exception of Mg, Al, Ca and Fe where stock solution concentrations were 10000 mg/l. Elements were then grouped, according to estimated concentrations within each extract solution, based on previous trial and error using a small selection of sample extracts, and whole rock/residual concentrations previously analysed. A solution for each group of elements was then prepared, by pipetting 20 µl of each elemental stock solution, and diluting to 20 ml using acid diluent. Standard A was then prepared by the addition of each grouped solution, by varying dilution factors, to result in

concentrations given in Table E.1 in Appendix E. For example, 20 ul of the grouped solution containing Sc, 40 ul of the grouped solution containing Ti, 0.4 ml of the grouped solution containing Mn, and 4 ml of the grouped solution containing Mg, was added to a vial and was topped up to 40 ml using diluent, to prepare the appropriate concentration of standard A for analysis with extracts from fraction 1 of the sequential extraction procedure. Subsequent standard solutions were then produced by the dilution of Standard A, where: Standard A = 100 %; Standard B = 50 %; Standard C = 10 %; Standard D = 5 %; Standard E = 1 % and Standard F = 0 % (blank). Samples and standards were diluted prior to analysis, with dilution factors 1/500 for extracts from fractions 1, 2 and 4, however for analysis of fraction 3 (Fe-Mn oxides), a greater dilution factors was used (1/1000) due to a greater concentration of TDS. These dilution steps resulted in a total dilution of 1/4027 and 1/8053, respectively, for the complete sequential extraction and analysis.

A.5 Thermogravimetric analysis (TGA)

Ground samples of 200 mg size were transferred to a platinum crucible, and were heated using a high mass thermogravimetric analysis 1200 iSeries analyser, from 25-1000 °C, at a rate of 20 °C/min, under a N_2 atmosphere (flow 20 cc/min). The weight loss was recorded at 1 °C intervals, then the data were analysed using Infinity Pro Software before being exported for further analysis. The use of samples of high mass is useful in limiting errors due to heterogeneity, while care was taken to ensure the correct operation of the TGA by the analysis of calcium oxalate standards, and 2-3 replicates of samples.

In Chapter 7, further standards were analysed using TGA, and were then compared back to the weight loss profile for samples. These samples included aragonite, dolomite, Mg-rich limestone, calcite, wollastonite and portlandite.

A.6 Optical microscopy (OM)

Images of thin sections of Jordanian oil shale were taken using a Nikon Eclipse 50iPOL binocular polarising microscope, up to 10x magnification, and a computer-controlled camera to view and save the images.

A.7 Scanning electron microscopy and energy dispersive spectroscopy (SEM-EDS)

Images of oil shale particles were produced using a Hitachi TM 1000 tabletop scanning electron microscope with energy dispersive spectroscopy (SEM-EDS), using a voltage of 15 kV. A 1 cm piece of rock, with a flat base, was placed onto a carbon strip on a sample mount, using tweezers. The mount was adjusted so that there was a 2-3 mm gap between the rock and the

ceiling of the vacuum chamber. The mount was placed in the chamber, and air was evacuated before images were produced at magnification between 700x – 7000x, and resolution of 30 nm. Microanalysis was performed using the attached SwiftED-TM EDS system, used to identify elements within minerals from the SEM images.

A.8 Fourier transform infrared (FTIR) spectroscopy

Reflectance spectra from FTIR analysis were recorded using a Perkin-Elmer Paragon FTIR spectrometer in the range 4000-400 cm^{-1}, resolution 8 cm^{-1} and the accumulation of 64 scans. First a background scan was performed, by leaving the IR window clear and standing back from the instrument during the process to prevent the appearance of CO_2 bands in the spectra. Once complete, a small amount (< 5 mg) of powdered sample was placed on the IR window, so that it is completely covered, and is screwed into place using the accessory piece. The sample scan is obtained; the background scan is subtracted from this to produce a resultant sample spectrum which is then exported for further analysis. In Chapter 7, standards were analysed using FTIR to identify and tabulate key absorption bands. The standards included: aragonite, dolomite, Mg-rich limestone, calcite, wollastonite and portlandite, in addition to carbonated portlandite and carbonated wollastonite.

Appendix B – Mineral formulae

Table B.1 - *Mineral formulae and XRD peak labels for XRD analysis in Chapter 2.*

Reflection	Mineral Name	Standard Mineral Formula
Al	Analcime	$NaAlSi_2O_6.H_2O$
An	Anhydrite	$CaSO_4$
Ak	Ankerite	$Ca(Fe,Mg,Mn)(CO_3)_2$
A	Apatite (X=monodentate anion)	$Ca_5(PO_4)_3X$
C	Calcite	$CaCO_3$
Ch	Chlorite	$(Mg,Fe)_6(Si,Al)_4O_{10}(OH)_8$
Cr	Cristobalite	SiO_2
Da	Dawsonite	$NaAlCO_3(OH)_2$
D	Dolomite	$CaMg(CO_3)_2$
Pl	Plagioclase feldspar	$NaAlSi_3O_8 – CaAl_2Si_2O_8$
F	K-feldspar	$KAlSi_3O_8$
Ge	Gehlenite	$Ca_2Al_2SiO_7$
Go	Goethite	$FeO(OH)$
G	Gypsum	$CaSO_4.2H_2O$
H	Hematite	Fe_2O_3
I	Illite (and muscovite)	$KAl_2(Si_3Al)O_{10}(OH)_2$
J	Jarosite	$KFe_3(OH)_6(SO_4)_2$
K	Kaolinite	$Al_2Si_2O_5(OH)_4$
M	Magnetite	Fe_3O_4
S	Montmorillonite (smectite)	$(Na)Mg_{0.5}AlMgSi_4O_{10}(OH)_2.H_2O$
P	Pyrite	FeS_2
Q	Quartz	SiO_2
Si	Siderite	$FeCO_3$

Appendix C – X-ray diffraction patterns

X-ray diffraction patterns for the oil shale samples analysed in Chapter 2.

Lothian

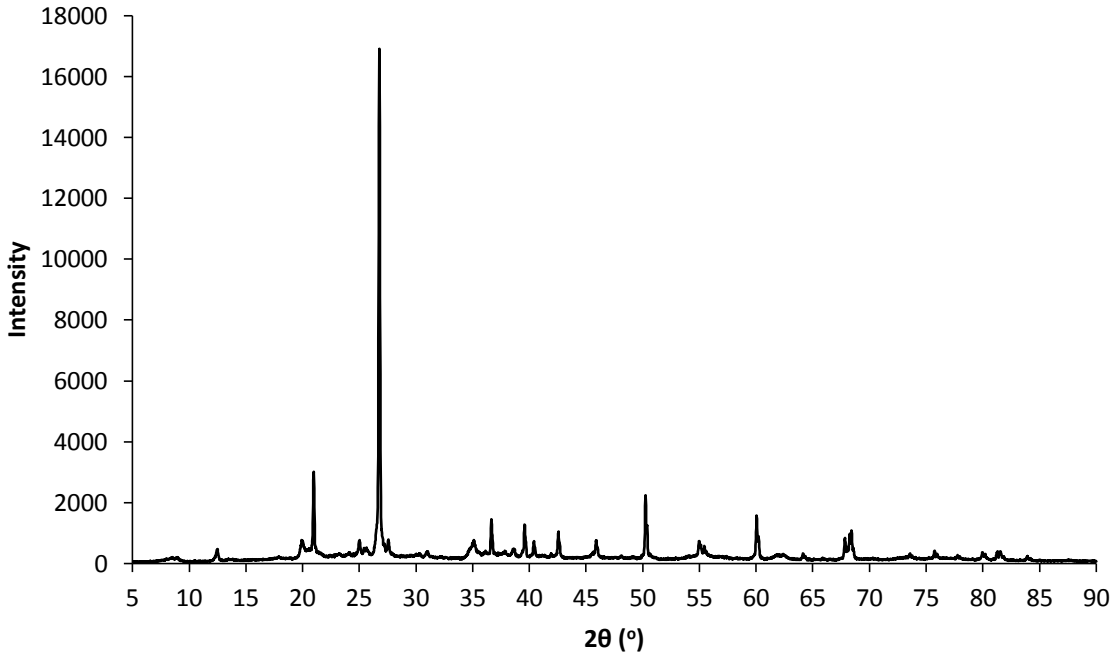

Figure C.1 – *XRD pattern of Lothian oil shale.*

Estonia

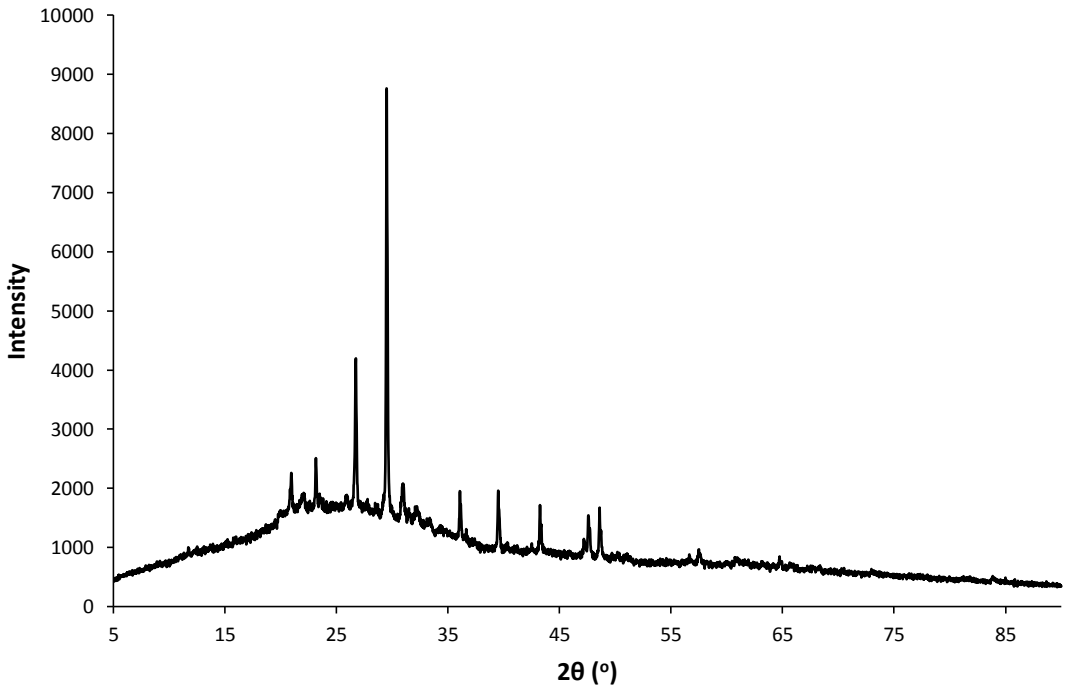

Figure C.2 – *XRD pattern of Estonian oil shale.*

Morocco

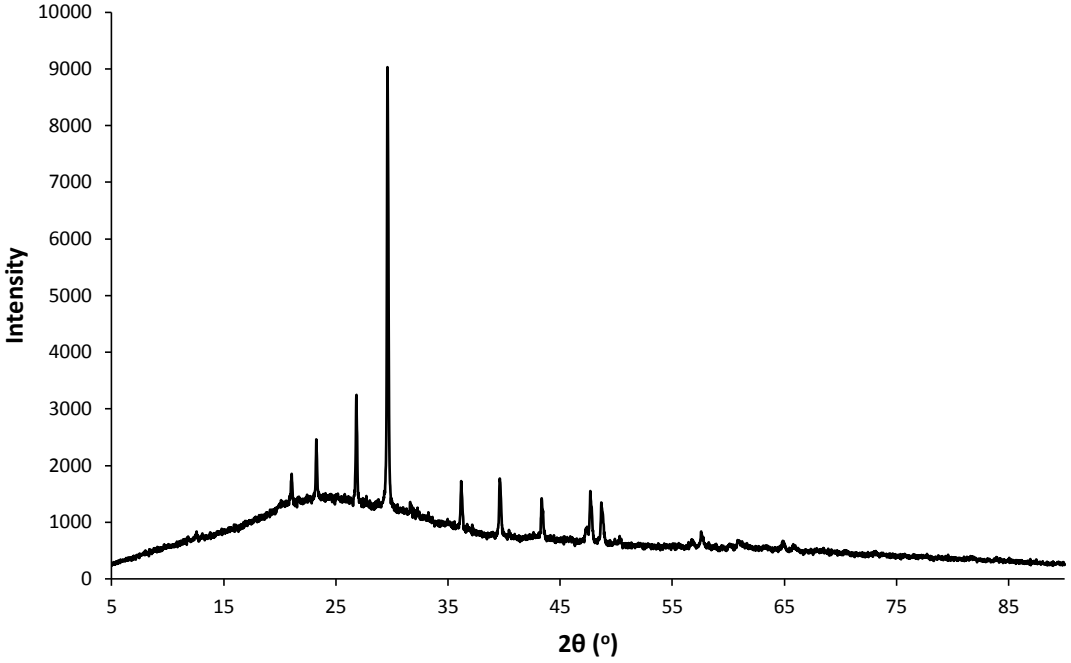

Figure C.3 – *XRD pattern of Moroccan oil shale.*

Israel

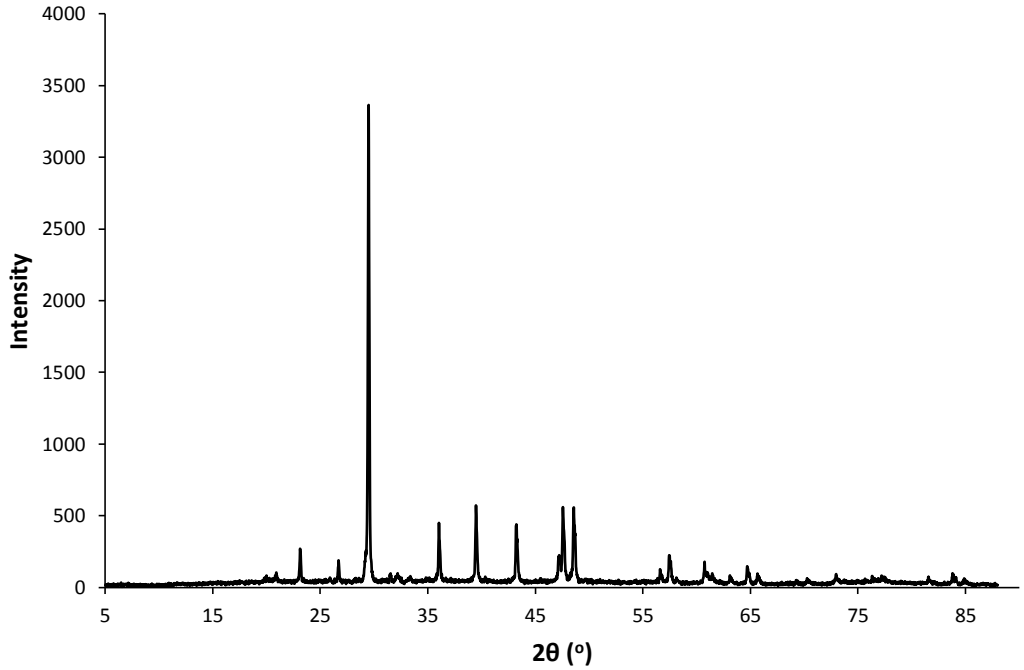

Figure C.4 – *XRD pattern of Israeli oil shale.*

Jordan

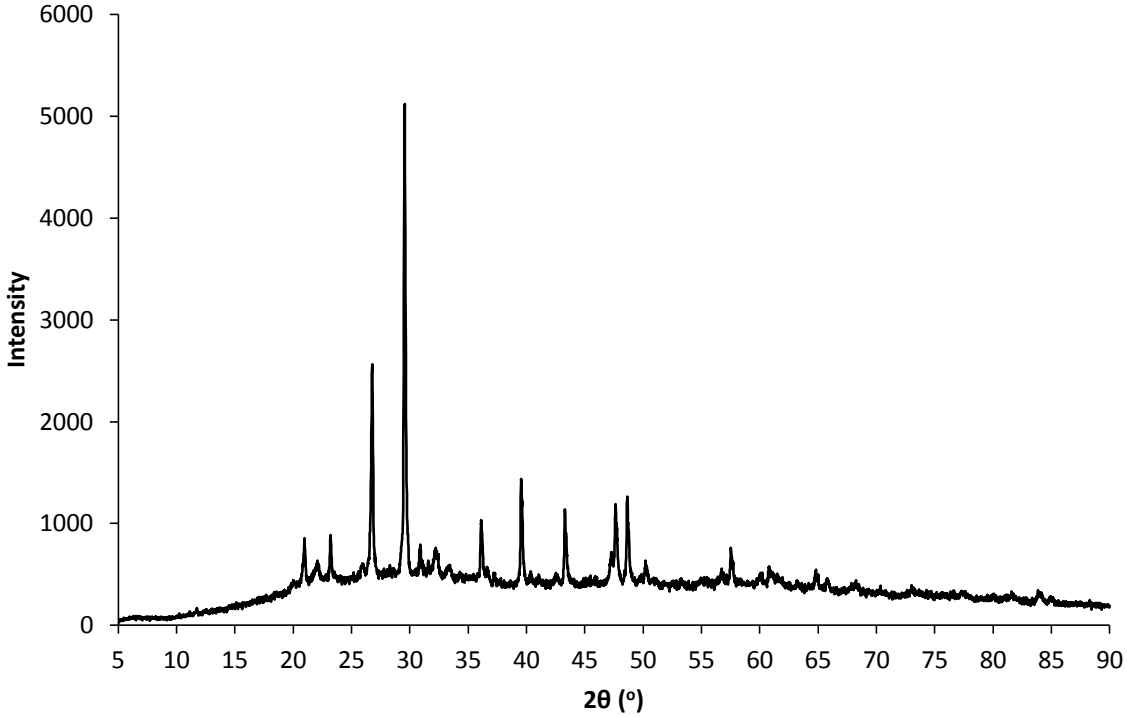

Figure C.5 – *XRD pattern of Jordanian oil shale.*

Mongolia

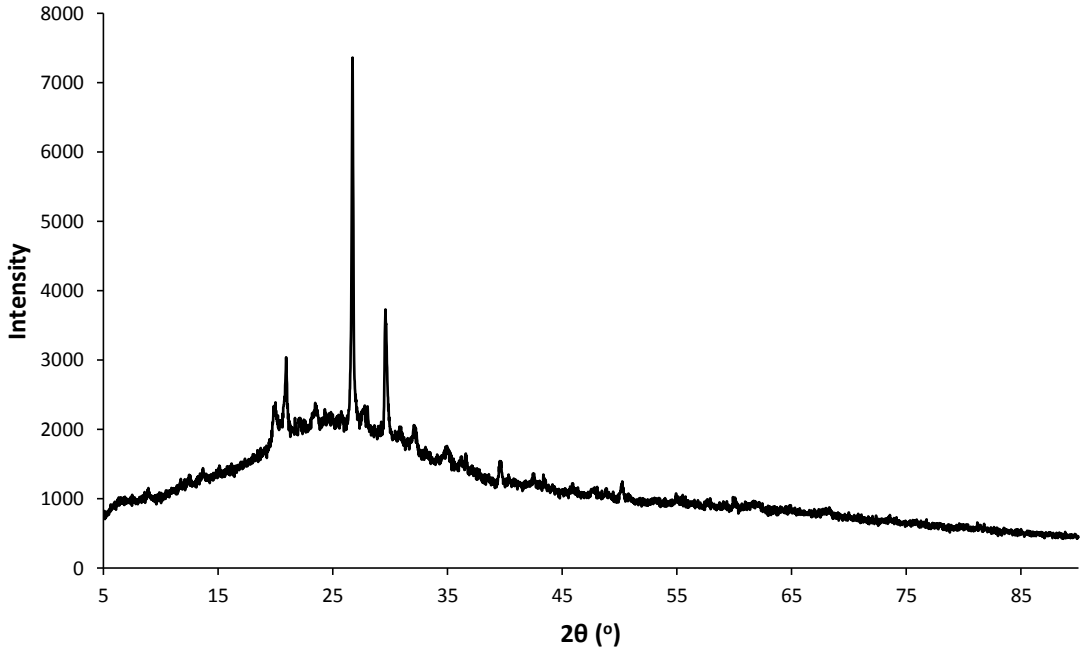

Figure C.6 – *XRD pattern of Mongolian oil shale.*

Harbin

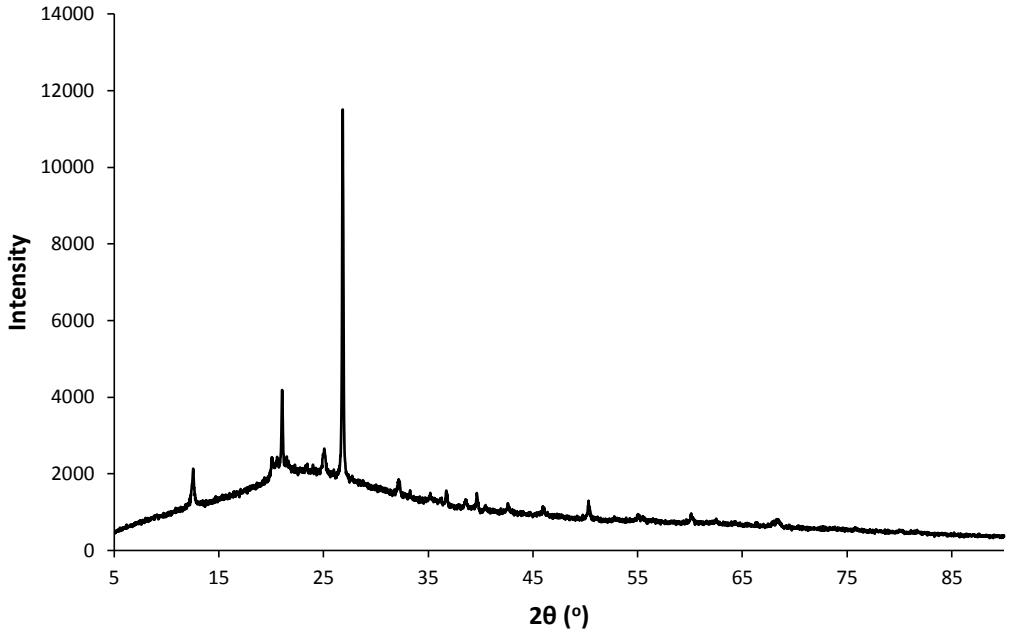

Figure C.7 – *XRD pattern of Harbin oil shale.*

Fushun

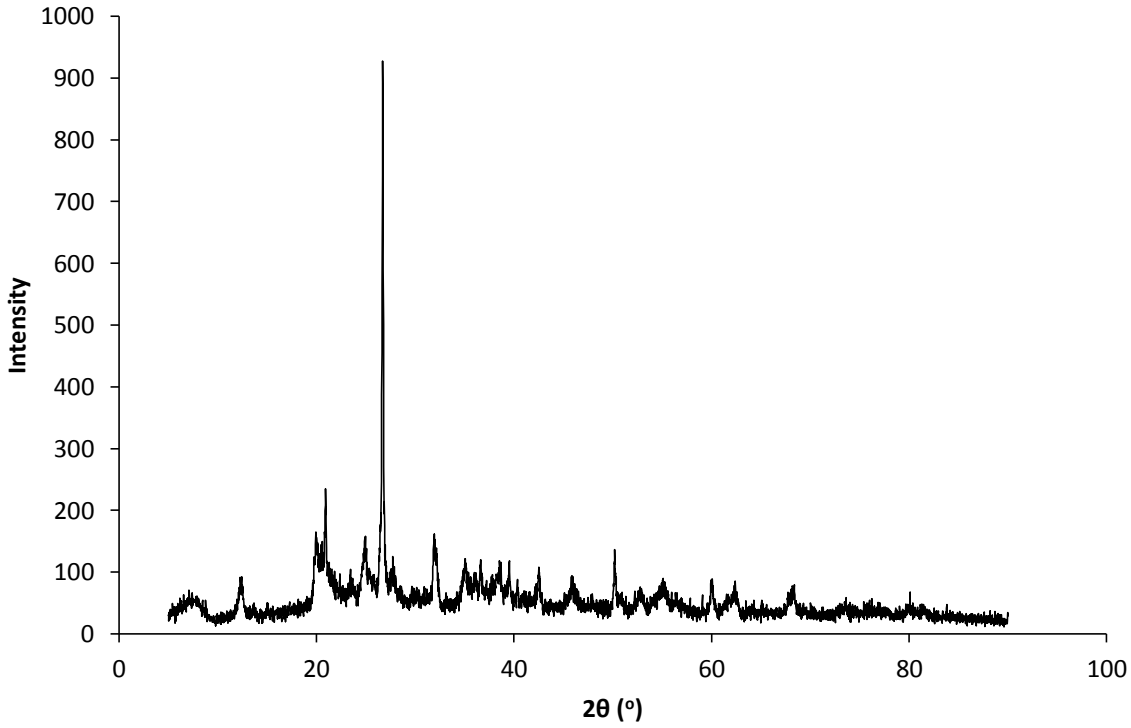

Figure C.8 – *XRD pattern of Fushun oil shale.*

Thailand

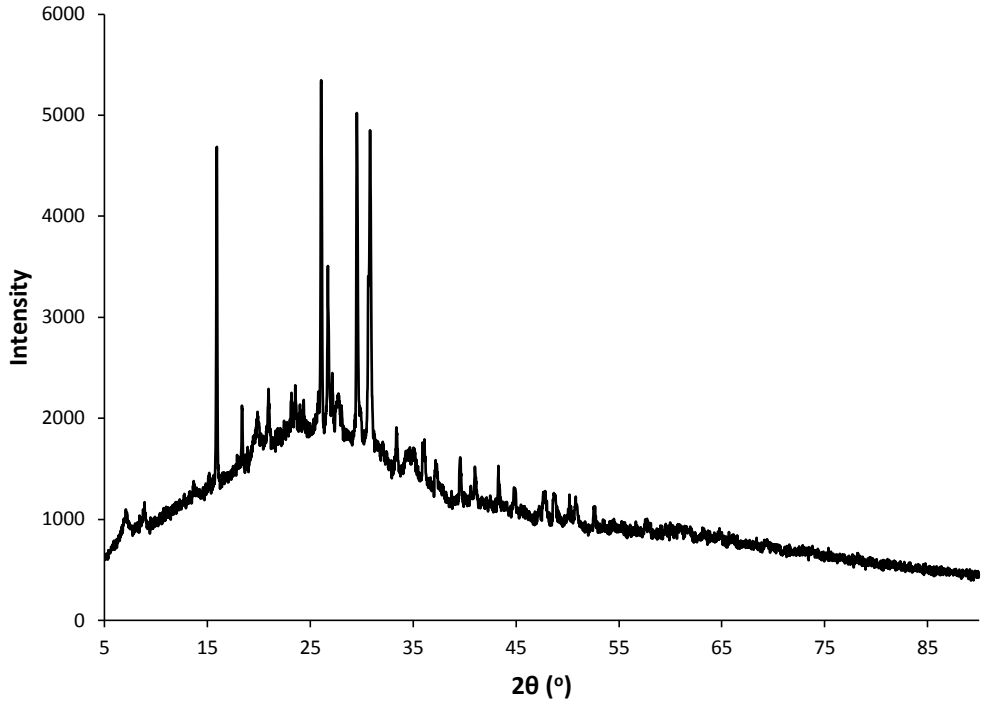

Figure C.9 – *XRD pattern of Thailand oil shale.*

Australia

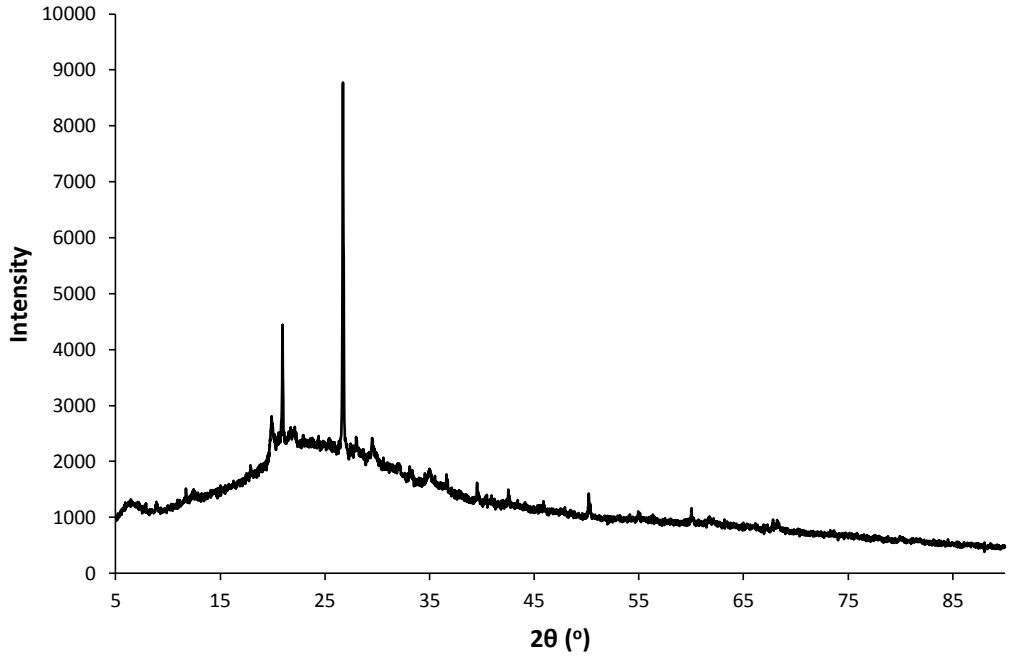

Figure C.10 – *XRD pattern of Australian oil shale.*

Saskatchewan

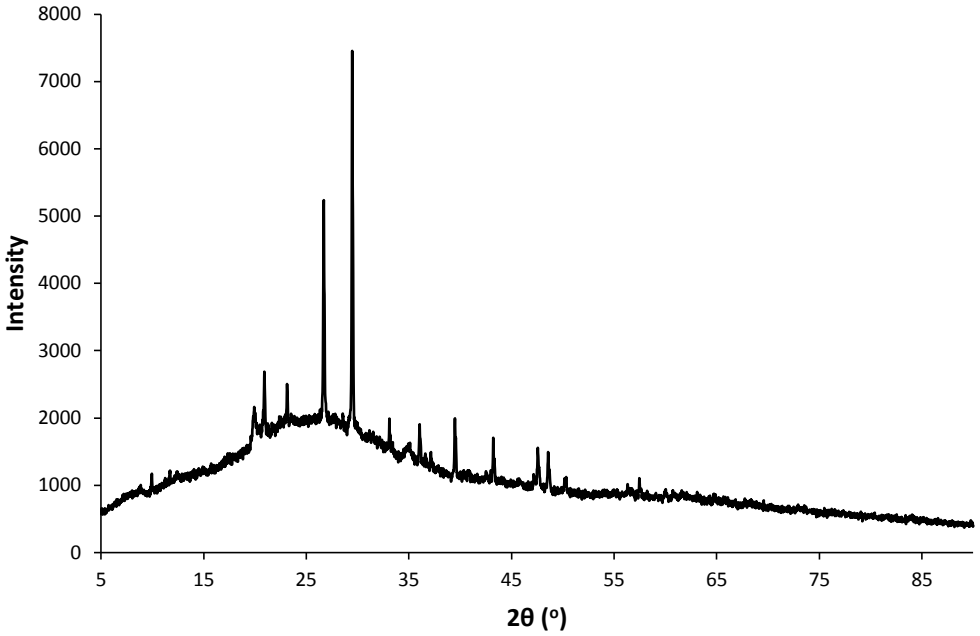

Figure C.11 – *XRD pattern of Saskatchewan oil shale.*

New Brunswick

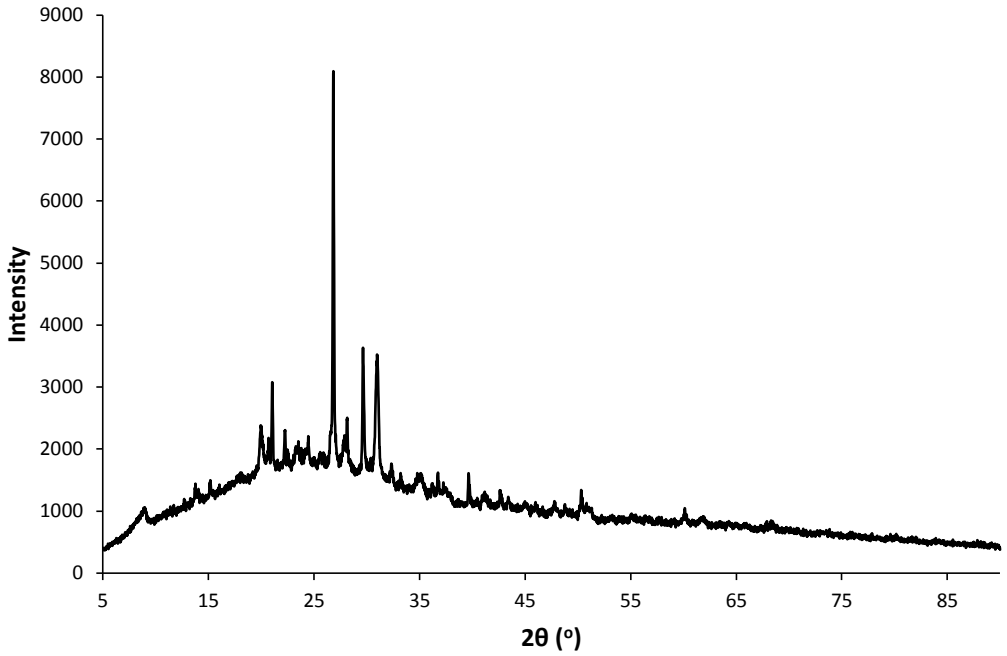

Figure C.12 – *XRD pattern of New Brunswick oil shale.*

Wyoming

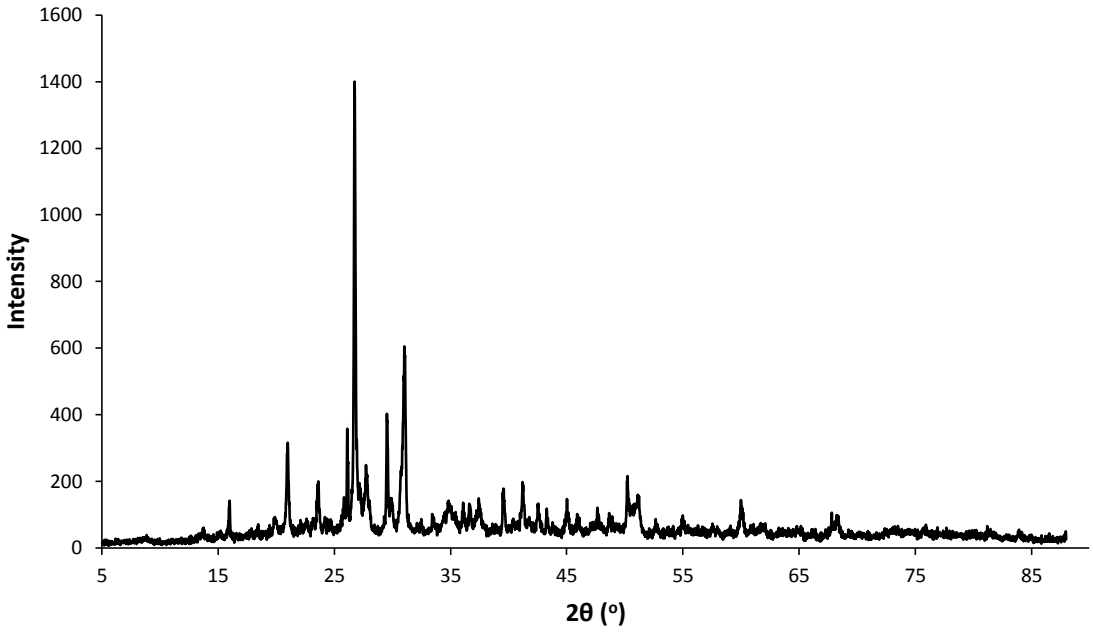

Figure C.13 – *XRD pattern of Wyoming oil shale.*

Colorado

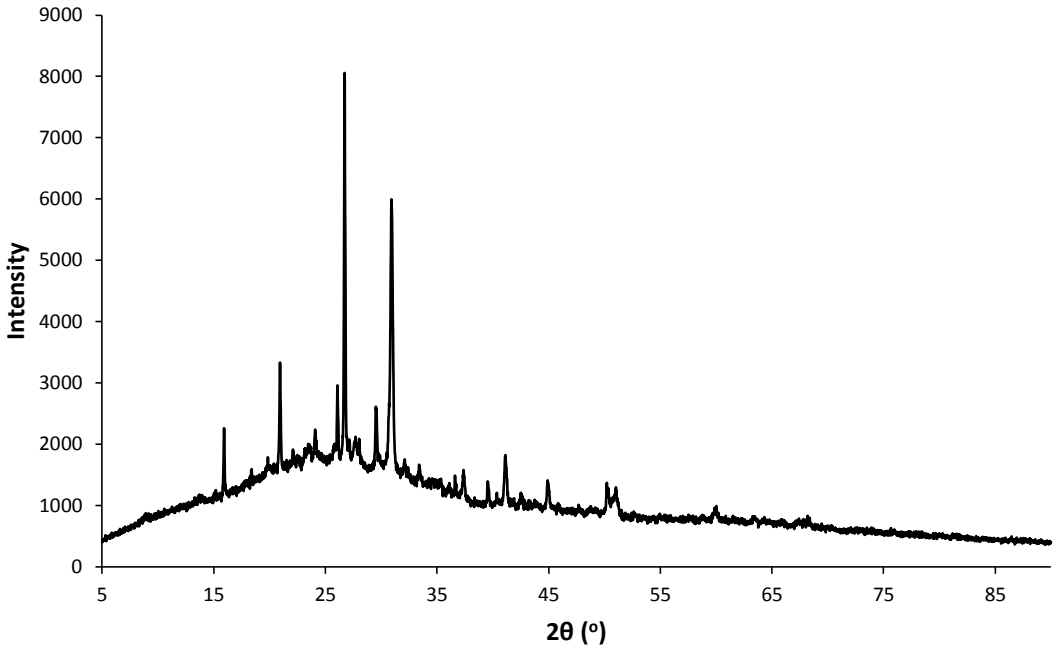

Figure C.14 – *XRD pattern of Colorado oil shale.*

Utah

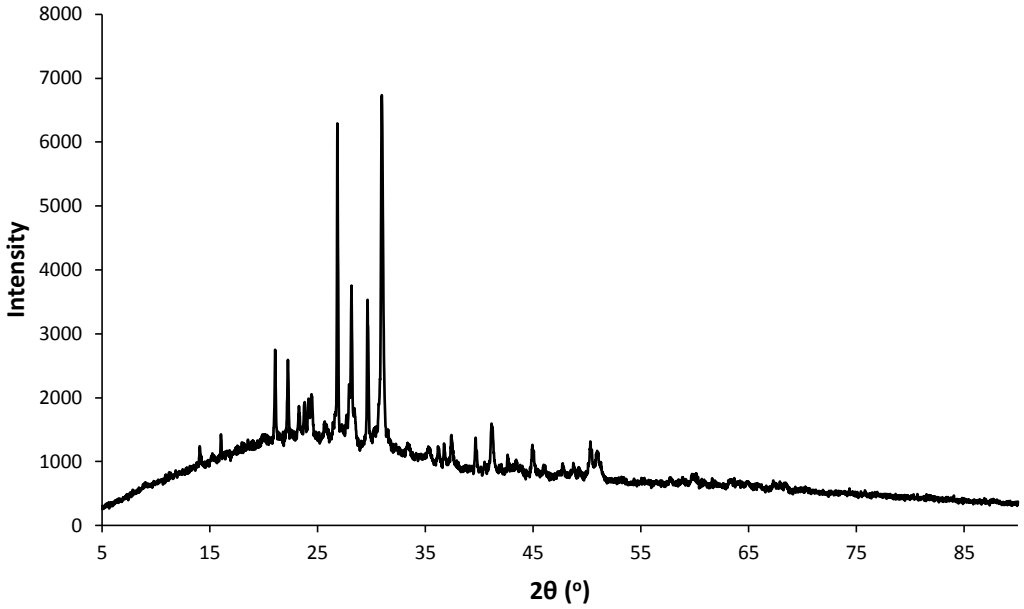

Figure C.15 – *XRD pattern of Utah oil shale.*

Appendix D – Data tables

Table D.1 – *Recorded trace elemental concentrations (A) and the associated standard deviation (B) in mg/kg for the oil shales and concentrations for UCC, NASC, PAAS and chondrite from the literature as specified in the chapter text. Any concentrations below the detection limit (bdl), were recorded when the concentration - 3*sd - 3*blank sd <0. Error is not recorded for the standards.*

Table A	Lothian	Estonia	Morocco	Israel	Jordan	Mongolia	Harbin	Fushun	Thailand	Australia	Saskatchewan	New Brunswick	Wyoming	Colorado	Utah	UCC	NASC	PAAS	Chondrite
Sc	bdl	bdl	bdl	bdl	bdl	bdl	bdl	15.97	bdl	8.07	bdl	7.92	bdl	bdl	5.02	13.60	14.90	16.00	
Ti	6383.60	1050.15	758.24	809.19	672.23	2366.43	1927.07	6287.70	1741.25	2458.14	2203.99	2764.43	2007.99	1131.07	1098.70	2456	4200	6000	
V	100.20	152.20	549.10	66.30	161.70	71.29	44.13	116.90	73.95	77.92	529.70	90.70	99.48	72.00	83.50	107	130	140	
Cr	83.52	370.45	52.99	242.10	420.41	bdl	bdl	86.46	bdl	13.39	40.69	11.25	9.25	bdl	bdl	83	125	100	
Mn	79.77	59.63	37.17	52.66	24.20	1585.31	204.46	621.89	336.11	736.51	192.84	578.52	313.66	195.16	220.72	600	465	852	
Co	5.76	5.27	6.60	7.22	4.07	10.28	11.17	20.50	20.38	12.17	14.74	14.05	8.73	9.77	9.66	17	26	20	
Ni	bdl	95.82	124.00	115.00	bdl	bdl	bdl	bdl	67.70	bdl	64.56	bdl	bdl	bdl	bdl	44	58	60	
Cu	22.34	78.40	57.72	66.85	83.59	22.85	15.19	45.01	50.38	33.28	66.50	38.71	44.01	33.92	36.45	25	-	50	
Zn	132.20	354.10	281.10	195.90	543.13	90.46	33.99	77.43	49.33	68.77	184.30	50.98	53.24	47.17	34.01	71	-	85	
Ga	21.84	5.77	3.19	4.07	3.57	15.63	11.71	23.12	14.21	12.85	13.23	13.21	12.21	6.73	6.63	17	-	20	
Rb	116.00	26.41	18.87	9.87	11.22	87.97	34.99	59.65	155.20	63.37	75.10	70.49	99.00	78.86	52.48	112	125	160	
Sr	371.40	825.00	856.00	1214.00	768.28	425.00	119.80	122.10	264.20	184.40	235.90	613.40	533.30	792.80	754.20	350	142	200	
Y	25.03	26.91	16.70	34.63	21.48	22.43	22.66	22.34	14.52	20.25	26.75	18.02	13.33	11.44	9.32	22	27	27	
Zr	229.30	35.06	32.77	27.25	25.20	115.30	37.24	175.80	30.21	83.01	86.34	77.41	61.90	29.59	28.79	190	200	210	
Nb	23.27	4.00	2.59	2.62	2.52	8.20	6.23	21.37	11.40	5.97	12.12	7.73	9.23	4.78	5.20	12.00	13.00	15.60	
Cs	5.67	1.49	1.21	0.70	0.63	7.89	2.43	4.74	16.77	4.84	5.07	5.59	6.20	3.30	3.47	4.60	5.16	6.00	

Ba	553.30	132.20	116.40	44.51	54.23	295.50	133.00	393.80	270.50	252.00	570.10	372.70	491.60	376.50	366.40	550	636	650	
La	40.74	13.57	10.47	13.86	8.58	30.22	33.29	41.04	24.14	14.50	27.72	17.02	23.55	13.62	13.55	30.00	32.00	38.20	0.24
Ce	82.92	19.09	12.59	14.26	10.63	60.12	68.24	78.01	43.88	29.59	47.60	35.19	44.00	25.42	26.79	64	73	80	0.61
Pr	8.70	2.46	1.67	2.32	1.49	6.27	7.03	8.27	4.52	3.42	5.59	3.92	4.78	2.74	2.82	7.10	7.90	8.90	0.09
Nd	37.94	11.66	7.81	11.59	7.21	27.55	29.99	36.28	18.86	16.36	25.15	18.14	20.46	11.87	11.94	26.00	33.00	33.90	0.46
Sm	6.65	2.26	1.44	2.28	1.39	4.92	5.22	6.34	3.46	3.49	4.67	3.59	3.51	2.04	2.11	4.50	5.70	5.60	0.15
Eu	1.42	0.51	0.35	0.54	0.33	0.91	0.95	1.58	0.61	0.82	1.06	0.86	0.82	0.53	0.53	0.88	1.24	1.10	0.06
Gd	6.01	2.51	1.69	2.79	1.63	4.87	5.23	6.26	3.47	3.52	4.90	3.57	3.54	2.04	2.14	3.80	5.20	4.70	0.20
Tb	0.77	0.37	0.25	0.43	0.25	0.67	0.70	0.78	0.48	0.54	0.68	0.53	0.46	0.28	0.29	0.64	0.85	0.77	0.04
Dy	4.16	2.42	1.60	2.89	1.64	3.68	3.87	4.12	2.50	3.18	3.87	3.08	2.39	1.62	1.54	3.50	5.80	4.68	0.25
Ho	0.86	0.56	0.36	0.70	0.39	0.73	0.75	0.76	0.46	0.66	0.80	0.62	0.45	0.37	0.31	0.80	1.04	1.00	0.05
Er	2.52	1.66	1.04	2.06	1.19	2.04	2.11	2.06	1.26	1.87	2.21	1.73	1.20	1.18	0.83	2.30	3.40	2.90	0.16
Tm	0.44	0.29	0.17	0.35	0.20	0.35	0.36	0.33	0.22	0.33	0.38	0.30	0.20	0.22	0.14	0.33	0.50	0.40	0.02
Yb	2.77	1.70	0.97	2.10	1.24	2.18	2.23	1.91	1.25	1.95	2.23	1.82	1.11	1.45	0.84	2.20	3.06	2.80	0.16
Lu	0.45	0.31	0.16	0.36	0.22	0.36	0.35	0.30	0.20	0.31	0.36	0.30	0.19	0.24	0.14	0.32	0.46	0.43	0.02
Hf	5.96	0.88	0.87	0.71	0.54	3.04	1.15	4.50	0.89	2.39	2.22	2.15	1.85	0.87	0.83	5.80	6.30	5.00	
Ta	1.61	bdl	bdl	bdl	bdl	0.60	0.45	1.20	1.23	0.44	0.79	0.53	0.64	bdl	bdl	1.00	1.12	1.28	
Pb	19.36	7.23	8.53	4.88	4.30	34.52	26.68	16.80	55.06	11.96	17.24	16.35	20.10	22.39	24.40	17.00	-	20.00	
Th	12.84	3.19	1.90	1.72	1.40	12.71	10.35	8.59	13.74	6.29	8.06	5.64	5.43	6.69	4.40	10.70	12.30	14.60	
U	3.84	24.44	7.89	15.06	21.57	7.10	2.51	1.90	18.56	2.18	19.84	3.85	4.55	8.34	4.37	2.80	2.66	3.10	
Sr/Ba	0.67	6.24	7.35	27.27	14.17	1.44	0.90	0.31	0.98	0.73	0.41	1.65	1.08	2.11	2.06	0.64	0.22	0.31	
LREE/HREE	15.41	7.14	7.94	5.36	6.09	13.50	14.45	17.33	15.54	8.10	11.09	9.83	16.80	10.85	14.66	13.51	10.46	13.28	2.55

Table B	Lothian	Estonia	Morocco	Israel	Jordan	Mongolia	Harbin	Fushun	Thailand	Australia	Saskatchewan	New Brunswick	Wyoming	Colorado	Utah
Sc	0.75	0.83	0.52	0.00	0.40	0.62	0.43	0.60	0.75	0.47	0.55	0.77	0.50	0.59	0.00
Ti	24.58	17.38	5.39	23.98	11.39	7.79	13.19	56.94	8.99	5.99	4.80	23.38	4.80	12.59	22.78
V	0.49	0.97	2.71	1.32	0.96	0.93	0.40	2.09	0.47	0.95	2.64	1.64	1.43	0.06	0.50
Cr	2.18	4.94	1.49	5.17	8.31	1.85	1.33	1.63	1.94	0.64	1.85	3.03	0.35	1.44	0.88
Mn	1.55	1.55	1.55	0.00	1.16	11.62	1.55	3.87	3.10	6.97	0.77	3.10	10.07	4.65	3.10
Co	0.17	0.24	0.16	0.01	0.16	0.05	0.14	0.16	0.04	0.05	0.10	0.21	0.15	0.18	0.01
Ni	16.92	11.03	11.06	2.99	8.13	9.29	2.92	7.27	5.44	5.53	11.72	8.49	7.28	9.13	3.57
Cu	0.17	1.35	0.55	0.70	1.13	0.53	0.23	0.57	0.76	0.26	0.09	1.40	0.08	0.28	0.05
Zn	1.16	3.11	2.63	2.07	3.59	2.38	1.31	2.38	1.96	1.17	0.80	1.01	0.23	2.27	1.16
Ga	0.13	0.24	0.08	0.10	0.10	0.14	0.01	0.25	0.08	0.29	0.29	0.13	0.30	0.03	0.06
Rb	0.45	0.28	0.10	0.34	0.06	1.78	0.01	1.00	1.91	0.58	0.13	1.24	4.23	0.22	0.83
Sr	5.50	1.43	0.59	16.25	7.23	9.60	0.31	1.14	0.13	2.12	1.97	1.96	15.45	5.52	13.47
Y	0.32	0.15	0.24	0.38	0.16	0.01	0.20	0.38	0.18	0.74	0.05	0.25	0.01	0.03	0.06
Zr	2.36	0.54	0.36	0.33	0.42	1.59	0.31	3.82	0.37	1.23	0.80	1.09	0.52	0.27	0.05
Nb	0.01	0.01	0.08	0.02	0.04	0.10	0.01	0.07	0.05	0.09	0.08	0.04	0.22	0.01	0.10
Cs	0.05	0.04	0.02	0.02	0.02	0.05	0.01	0.06	0.04	0.04	0.08	0.00	0.03	0.01	0.03
Ba	11.10	0.41	1.14	0.40	0.48	2.41	1.91	0.39	2.58	0.50	1.89	8.26	10.36	7.74	1.56
La	0.90	0.23	0.09	0.30	0.06	0.23	0.57	0.38	0.30	0.44	0.45	0.29	0.38	0.50	0.27
Ce	3.60	0.14	0.12	0.01	0.20	1.43	2.08	0.11	0.47	0.27	0.11	1.01	0.91	0.74	0.24
Pr	0.27	0.03	0.00	0.04	0.01	0.04	0.22	0.14	0.09	0.04	0.07	0.14	0.13	0.11	0.01
Nd	1.62	0.22	0.32	0.21	0.10	0.49	0.55	0.04	0.33	0.23	0.29	0.35	0.79	0.34	0.07
Sm	0.23	0.02	0.03	0.03	0.05	0.06	0.19	0.09	0.04	0.11	0.03	0.07	0.06	0.06	0.05

Eu	0.03	0.00	0.00	0.02	0.00	0.01	0.01	0.04	0.02	0.03	0.02	0.01	0.04	0.01	0.02
Gd	0.13	0.06	0.02	0.03	0.04	0.05	0.12	0.02	0.07	0.01	0.00	0.06	0.07	0.05	0.03
Tb	0.02	0.00	0.01	0.00	0.00	0.00	0.00	0.01	0.01	0.02	0.00	0.01	0.01	0.01	0.00
Dy	0.04	0.02	0.03	0.02	0.01	0.08	0.11	0.07	0.04	0.06	0.02	0.03	0.02	0.02	0.02
Ho	0.01	0.01	0.01	0.01	0.01	0.00	0.02	0.04	0.01	0.01	0.02	0.01	0.00	0.01	0.00
Er	0.04	0.04	0.05	0.02	0.01	0.03	0.06	0.03	0.02	0.08	0.02	0.04	0.05	0.02	0.01
Tm	0.00	0.01	0.01	0.01	0.01	0.00	0.02	0.00	0.00	0.00	0.01	0.01	0.01	0.01	0.01
Yb	0.07	0.04	0.02	0.02	0.03	0.03	0.03	0.03	0.02	0.03	0.01	0.05	0.01	0.02	0.01
Lu	0.01	0.00	0.01	0.02	0.01	0.01	0.01	0.01	0.00	0.00	0.01	0.01	0.00	0.00	0.00
Hf	0.06	0.01	0.02	0.02	0.02	0.09	0.04	0.10	0.03	0.09	0.09	0.03	0.05	0.01	0.03
Ta	0.01	0.06	0.07	0.07	0.07	0.07	0.06	0.07	0.06	0.06	0.07	0.05	0.05	0.06	0.07
Pb	0.24	0.10	0.21	0.26	0.14	0.80	0.59	0.50	0.85	0.12	0.24	0.07	0.21	0.27	0.34
Th	0.04	0.07	0.03	0.02	0.03	0.39	0.04	0.18	0.06	0.09	0.03	0.04	0.12	0.06	0.01
U	0.03	0.12	0.13	0.08	0.29	0.17	0.02	0.00	0.12	0.02	0.06	0.03	0.10	0.18	0.01

Appendix E

Table E.1 – *Concentrations of elements (µg/kg) within Standard A, prepared for each extraction step.*

Step:	Fraction 1	Fraction 2	Fraction 3	Fraction 4
Dilution:	1/500	1/500	1/1000	1/500
Mg	100	100	100	100
Al	100	100	100	100
K	100	100	100	100
Ca	100	100	100	100
Sc	0.5	0.5	1	1
Ti	1	1	10	20
V	1	1	10	10
Cr	1	1	1	1
Mn	10	20	100	100
Fe	100	100	100	100
Co	1	1	10	1
Ni	1	1	10	10
Cu	1	1	10	10
Zn	1	1	10	10
Ga	0.5	0.5	1	0.5
Rb	1	1	10	1
Sr	10	20	10	20
Y	1	1	1	10
Zr	1	1	1	1
Nb	0.5	0.5	0.5	0.5
Cs	0.5	0.5	0.5	0.5
Ba	10	20	1	20
La	1	1	1	10
Ce	1	1	1	10
Pr	0.5	0.5	1	1
Nd	1	1	1	10
Sm	0.5	0.5	1	1
Eu	0.5	0.5	0.5	0.5
Gd	0.5	0.5	0.5	1
Tb	0.5	0.5	0.5	0.5
Dy	0.5	0.5	0.5	1
Ho	0.5	0.5	0.5	0.5
Er	0.5	0.5	0.5	0.5
Tm	0.5	0.5	0.5	0.5
Yb	0.5	0.5	0.5	0.5
Lu	0.5	0.5	0.5	0.5
Hf	1	1	1	1
Ta	0.5	0.5	0.5	0.5
Pb	1	1	10	10
Th	1	1	10	10
U	0.5	0.5	10	10

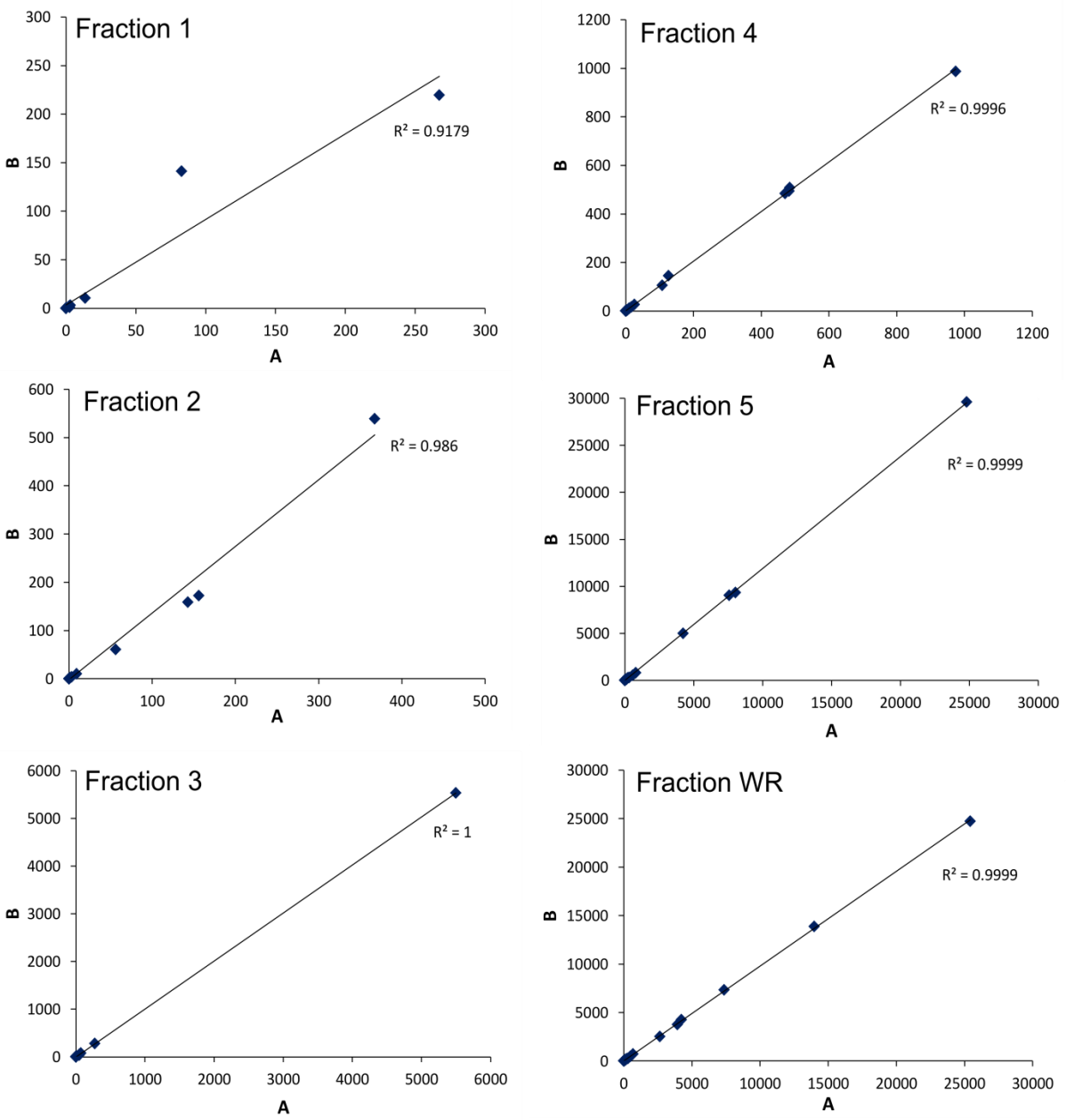

Figure E.1 – *Correlation curves of elemental concentrations in mg/l within replicates (A&B) of spent oil shale from site 1, for each fraction analysed.*

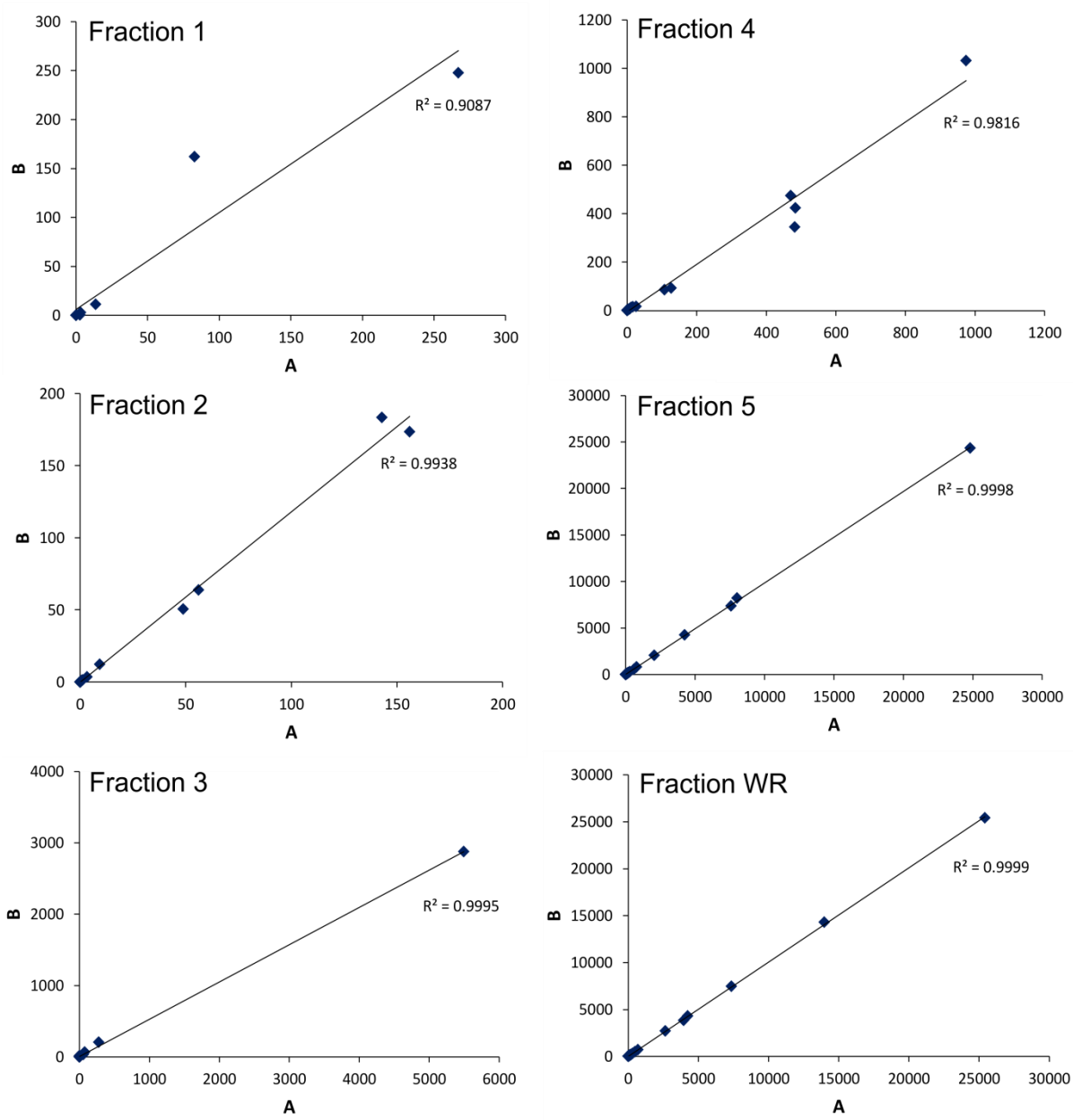

Figure E.2 - *Correlation curves of elemental concentrations in mg/l within duplicates (A&B) of spent oil shale from site 1, for each fraction analysed.*

Table E.2 – *Trace elemental concentrations from fraction 1, in mg/kg, from ICP-MS analysis. Concentrations below the detection limit (bdl) were recorded when: concentration – 3*sd – 3*blank sd < 0.*

	1A	1Arpt	16A	35A	2A	3A	4A	5A	6A	7A	8A	9A	10A	11A	12A	13A	14A	17A
Mg	13.8	10.49	11.17	12.37	76.14	41.92	17.74	10.04	316.1	184.3	36.18	271.2	135.8	142.6	521.1	56.1	294	227.4
Al	2.093	2.055	bdl	bdl	6.572	3.939	6.282	bdl	bdl	1.27	bdl	bdl	bdl	0.636	bdl	0.715	bdl	bdl
K	82.75	141.3	162.1	183.1	104.5	168.1	104.7	112.3	183.5	442.9	170.9	482	671.6	523.5	537.2	293.6	669.2	263.5
Ca	267.2	219.4	247.9	263.8	757.8	219.3	230	211	3048	2850	106.3	1442	1479	2081	3869	264.5	3993	1498
Sc	0.146	0.128	0.157	0.146	0.154	0.166	0.173	0.178	0.182	0.18	0.151	0.153	0.159	0.172	0.175	0.185	0.173	0.17
Ti	bdl	bdl	bdl	0.081	bdl	bdl	bdl	bdl	bdl	bdl	bdl	bdl	bdl	0.163	bdl	0.094	bdl	bdl
V	0.286	0.289	0.281	0.322	0.343	0.121	0.091	0.335	0.053	0.116	0.224	0.524	0.739	0.034	0.034	0.031	0.017	0.03
Cr	0.034	0.041	0.051	0.051	0.03	0.032	0.034	0.032	0.035	0.045	0.036	0.037	0.041	0.04	0.047	0.043	0.046	0.048
Mn	bdl	bdl	bdl	bdl	1.211	0.171	0.175	bdl	bdl	0.076	0.097	0.211	0.157	2.016	0.179	1.65	4.002	19.59
Fe	bdl	bdl	bdl	bdl	bdl	bdl	bdl	bdl	bdl	bdl	bdl	bdl	bdl	bdl	bdl	30.38	28.34	62.09
Co	bdl	bdl	bdl	bdl	bdl	bdl	bdl	bdl	bdl	bdl	bdl	bdl	bdl	bdl	bdl	bdl	bdl	bdl
Ni	0.004	bdl	bdl	bdl	0.005	bdl	bdl	bdl	bdl	bdl	bdl	bdl	0.003	0.014	0.012	0.01	0.031	0.004
Cu	bdl	bdl	bdl	bdl	bdl	bdl	bdl	bdl	0.213	bdl	bdl	bdl	bdl	bdl	bdl	bdl	bdl	bdl
Zn	2.728	1.104	0.382	1.179	0.956	0.302	1.449	1.12	3.026	2.544	0.331	1.304	1.203	2.914	2.568	1.499	0.419	6.265
Ga	bdl	bdl	bdl	bdl	0.02	0.003	bdl	bdl	bdl	0.008	bdl	0.006	bdl	0.003	bdl	bdl	bdl	bdl
Rb	bdl	bdl	bdl	bdl	bdl	bdl	bdl	bdl	bdl	bdl	bdl	bdl	bdl	bdl	bdl	bdl	bdl	bdl
Sr	bdl	bdl	bdl	bdl	1.699	0.922	3.449	2.199	23.9	27.96	0.41	37.29	45.46	17.98	37.13	4.635	32.18	5.823
Y	0.008	bdl	bdl	bdl	0.01	0.014	0.02	0.008	bdl	bdl	bdl	0.025	0.01	0.007	0.071	0.041	bdl	0.073
Zr	bdl	bdl	bdl	bdl	bdl	bdl	bdl	bdl	bdl	bdl	bdl	bdl	bdl	bdl	bdl	bdl	bdl	bdl
Nb	bdl	bdl	bdl	bdl	bdl	bdl	bdl	bdl	bdl	bdl	bdl	bdl	bdl	bdl	bdl	bdl	bdl	bdl
Cs	0.028	0.028	0.022	0.025	0.013	0.028	0.019	0.012	0.013	0.028	0.019	0.045	0.072	0.049	0.006	0.056	0.099	bdl
Ba	3.136	3.034	2.988	3.498	4.022	5.649	4.013	3.003	8.762	19.63	8.911	34.55	34.03	13.45	32.12	13.55	8.303	24.93
La	bdl	bdl	bdl	bdl	0.004	bdl	0.013	0.007	bdl	0.01	bdl	0.107	0.003	bdl	0.058	0.04	bdl	0.052
Ce	bdl	bdl	bdl	bdl	bdl	bdl	bdl	bdl	bdl	bdl	bdl	0.087	bdl	bdl	bdl	0.016	bdl	bdl
Pr	bdl	0.002	0.002	bdl	0.003	bdl	0.007	0.003	bdl	0.003	0.003	0.025	0.004	bdl	0.013	0.014	0.003	0.019
Nd	bdl	0.007	bdl	bdl	0.019	0.007	0.03	0.019	bdl	0.013	0.014	0.118	0.013	0.012	0.066	0.073	0.018	0.101
Sm	0.003	0.002	bdl	bdl	0.003	bdl	0.009	0.003	bdl	0.003	0.004	0.02	0.004	0.004	0.015	0.018	0.004	0.025
Eu	0.006	0.006	0.003	0.003	bdl	0.005	0.006	0.004	0.003	0.006	0.005	0.009	0.004	bdl	0.008	0.007	0.004	0.005
Gd	bdl	bdl	bdl	bdl	bdl	bdl	bdl	bdl	bdl	bdl	bdl	bdl	bdl	bdl	bdl	bdl	bdl	bdl
Tb	bdl	bdl	bdl	bdl	bdl	bdl	bdl	bdl	bdl	bdl	bdl	bdl	bdl	bdl	bdl	bdl	bdl	bdl
Dy	bdl	bdl	bdl	bdl	bdl	bdl	bdl	bdl	bdl	bdl	bdl	bdl	bdl	bdl	bdl	bdl	bdl	0.008
Ho	bdl	0.002	bdl	bdl	0.002	bdl	bdl	bdl	bdl	0.002	0.002	bdl	bdl	0.002	bdl	0.004	bdl	bdl
Er	bdl	bdl	bdl	bdl	bdl	bdl	bdl	bdl	bdl	bdl	bdl	bdl	bdl	bdl	bdl	bdl	bdl	bdl
Tm	0.003	bdl	bdl	bdl	bdl	bdl	bdl	bdl	bdl	bdl	bdl	bdl	bdl	bdl	bdl	bdl	bdl	bdl
Yb	bdl	bdl	bdl	bdl	bdl	bdl	bdl	bdl	bdl	bdl	bdl	bdl	bdl	bdl	bdl	bdl	bdl	bdl
Lu	bdl	bdl	bdl	bdl	bdl	bdl	bdl	bdl	bdl	bdl	bdl	bdl	bdl	bdl	bdl	bdl	bdl	bdl
Hf	bdl	bdl	bdl	bdl	bdl	bdl	bdl	bdl	bdl	bdl	bdl	bdl	bdl	bdl	bdl	bdl	bdl	bdl
Ta	bdl	bdl	bdl	bdl	bdl	bdl	bdl	bdl	bdl	bdl	bdl	bdl	bdl	bdl	bdl	bdl	bdl	bdl
Pb	bdl	bdl	bdl	bdl	bdl	bdl	bdl	bdl	bdl	bdl	bdl	bdl	bdl	bdl	bdl	bdl	bdl	bdl
Th	bdl	bdl	bdl	bdl	bdl	bdl	bdl	bdl	bdl	bdl	bdl	bdl	bdl	bdl	bdl	bdl	bdl	bdl
U	0.003	0.002	bdl	0.003	0.012	bdl	0.004	bdl	0.016	0.004	0.003	0.011	0.006	0.018	0.008	0.001	0.021	0.022

	18A	19A	20A	21A	22A	23A	24A	25A	26A	26Arpt	27A	36A	28A	29A	30A	31A	32A	33A
Mg	620.5	315.3	321.6	195.8	236.9	304.6	357.2	234.2	197.9	270.4	335.8	358.9	309.2	213.9	198.1	234.7	265.4	310.2
Al	13.78	22.46	2.707	30.29	bdl	bdl	4.111	bdl	6.008	3.469	10.98	9.185	0.373	5.299	bdl	18.26	6.221	11.87
K	736.5	546.8	587.9	698.5	604.4	846.8	937.8	573	648.3	958.7	865.3	983.4	561.3	1847	2662	1364	1306	1504
Ca	3711	1417	1988	851.6	2855	2892	2597	1143	732.5	981.3	952.7	982.2	1429	1033	599.6	807.3	1094	679.7
Sc	0.188	0.211	0.184	0.242	0.214	0.199	0.196	0.236	bdl	0.128	0.088	0.153	0.068	0.105	0.119	0.129	0.142	0.152
Ti	bdl	bdl	bdl	bdl	bdl	bdl	bdl	bdl	bdl	bdl	bdl	0.163	bdl	0.132	bdl	bdl	0.055	bdl
V	0.095	0.073	0.064	0.05	0.058	0.033	0.058	0.023	0.031	0.038	0.046	0.046	0.032	0.052	0.032	0.031	0.036	0.038
Cr	0.05	0.05	0.056	0.06	0.066	0.062	0.062	0.073	0.015	0.029	0.024	0.03	0.02	0.03	0.026	0.026	0.029	0.027
Mn	8.973	9.62	3.084	2.423	2.444	2.36	7.192	10.31	4.288	5.827	10.6	9.383	bdl	4.244	28.55	5.835	6.503	6.334
Fe	bdl	70.31	bdl	103.1	99.46	bdl	132.2	151.8	bdl	bdl	bdl	bdl	bdl	bdl	bdl	bdl	bdl	bdl
Co	bdl	bdl	bdl	bdl	bdl	bdl	bdl	bdl	0.081	bdl	0.238	bdl	bdl	bdl	bdl	bdl	bdl	bdl
Ni	0.006	0.008	bdl	0.011	bdl	bdl	bdl	bdl	0.014	0.01	0.021	0.017	0.012	0.016	0.022	0.022	0.045	0.028
Cu	bdl	bdl	bdl	bdl	bdl	bdl	bdl	bdl	bdl	bdl	0.199	bdl	0.019	0.209	0.162	bdl	0.145	0.172
Zn	15.1	6.326	5.939	6.254	5.976	6.02	5.927	6.157	0.811	0.864	2.098	2.972	0.523	1.394	3.065	9.016	1.58	1.916
Ga	bdl	bdl	bdl	0.009	bdl	bdl	bdl	bdl	0.015	0.012	0.019	0.013	0.012	0.019	0.013	0.019	0.015	0.016
Rb	bdl	bdl	bdl	bdl	bdl	bdl	bdl	bdl	bdl	bdl	bdl	bdl	bdl	bdl	bdl	bdl	bdl	bdl
Sr	23.38	6.064	16.01	3.723	17.4	18.16	18.45	11.57	1.765	3.726	3.832	3.952	14.87	3.885	0.093	1.297	6.068	4.345
Y	0.045	0.07	0.056	0.089	0.014	0.015	0.022	0.066	bdl	bdl	0.035	0.018	bdl	0.014	bdl	0.053	bdl	0.045
Zr	bdl	0.014	bdl	0.039	bdl	bdl	bdl	bdl	bdl	bdl	bdl	bdl	bdl	bdl	bdl	bdl	bdl	bdl
Nb	bdl	bdl	bdl	bdl	bdl	bdl	bdl	bdl	bdl	bdl	bdl	bdl	bdl	bdl	bdl	bdl	bdl	bdl
Cs	0.063	0.077	0.064	0.093	0.006	0.012	0.024	0.027	0.008	0.01	0.019	0.014	0.006	0.009	0.004	0.006	0.01	0.007
Ba	22.41	4.164	24.12	3.96	17.83	12.77	13.8	26.44	4.252	5.331	4.425	4.226	1.461	3.295	4.047	3.465	3.048	7.8
La	0.064	0.051	0.054	0.044	0.012	0.009	0.023	0.053	bdl	0.002	0.034	0.019	bdl	0.005	bdl	0.085	bdl	0.035
Ce	bdl	bdl	bdl	bdl	bdl	bdl	bdl	bdl	bdl	bdl	0.009	bdl	bdl	bdl	bdl	0.054	bdl	bdl
Pr	0.016	0.022	0.018	0.024	0.006	0.004	0.008	0.019	0.002	0.002	0.01	0.006	bdl	0.004	bdl	0.021	bdl	0.012
Nd	0.08	0.121	0.095	0.13	0.038	0.024	0.047	0.112	bdl	0.011	0.049	0.03	bdl	0.02	bdl	0.102	bdl	0.057
Sm	0.016	0.027	0.02	0.038	0.008	0.005	0.012	0.026	0.003	0.003	0.011	0.007	bdl	0.005	bdl	0.022	0.003	0.014
Eu	0.002	0.006	0.002	0.009	bdl	bdl	bdl	0.004	bdl	bdl	0.003	bdl	bdl	bdl	bdl	0.004	bdl	0.003
Gd	bdl	bdl	bdl	bdl	bdl	bdl	bdl	bdl	bdl	bdl	bdl	bdl	bdl	bdl	bdl	bdl	bdl	bdl
Tb	bdl	bdl	bdl	bdl	bdl	bdl	bdl	bdl	bdl	bdl	bdl	bdl	bdl	bdl	bdl	bdl	bdl	bdl
Dy	0.002	0.007	bdl	0.015	bdl	bdl	bdl	0.009	bdl	bdl	bdl	bdl	bdl	bdl	bdl	0.004	bdl	bdl
Ho	0.002	bdl	0.002	0.004	bdl	bdl	bdl	0.002	bdl	bdl	bdl	0.002	0.002	bdl	bdl	0.003	bdl	0.003
Er	bdl	bdl	bdl	bdl	bdl	bdl	bdl	bdl	bdl	bdl	bdl	bdl	bdl	bdl	bdl	bdl	bdl	bdl
Tm	bdl	bdl	bdl	bdl	bdl	bdl	bdl	bdl	0.013	bdl	0.016	bdl	0.005	0.004	bdl	bdl	0.002	bdl
Yb	bdl	bdl	bdl	bdl	bdl	bdl	bdl	bdl	bdl	bdl	bdl	bdl	bdl	bdl	bdl	bdl	bdl	bdl
Lu	bdl	bdl	bdl	bdl	bdl	bdl	bdl	bdl	0.029	bdl	0.044	bdl	bdl	bdl	bdl	bdl	bdl	bdl
Hf	bdl	bdl	bdl	bdl	bdl	bdl	bdl	bdl	bdl	bdl	bdl	bdl	bdl	bdl	bdl	bdl	bdl	bdl
Ta	bdl	bdl	bdl	bdl	bdl	bdl	bdl	bdl	bdl	bdl	bdl	bdl	bdl	bdl	bdl	bdl	bdl	bdl
Pb	bdl	bdl	bdl	bdl	bdl	bdl	bdl	bdl	bdl	bdl	bdl	bdl	bdl	bdl	bdl	bdl	bdl	bdl
Th	bdl	bdl	bdl	bdl	bdl	bdl	bdl	bdl	bdl	bdl	bdl	bdl	bdl	bdl	bdl	bdl	bdl	bdl
U	0.008	0.015	0.011	0.033	0.006	0.002	0.002	0.012	0.002	bdl	0.006	0.002	bdl	0.003	0.001	bdl	0.002	0.005

Table E.3 – *The standard deviation from fraction 1, in mg/kg, from ICP-MS analysis. Concentrations below the detection limit (bdl) were recorded when: concentration – 3*sd – 3*blank sd < 0.*

	1A	1Arpt	16A	35A	2A	3A	4A	5A	6A	7A	8A	9A	10A	11A	12A	13A	14A	17A
Mg	0.2	0.3	0.2	0.3	0.5	0.3	1	0.09	5	3	0.6	2	1	1	2	1	1	1
Al	0.5	0.08	bdl	bdl	0.1	0.9	0.3	bdl	bdl	0.02	bdl	bdl	bdl	0.1	bdl	0.03	bdl	bdl
K	4	2	6	7	1	6	2	6	4	6	3	0.3	20	6	9	7	10	7
Ca	10	3	3	0.7	6	7	10	10	10	0.3	7	40	3	1	50	8	30	30
Sc	0.03	0.03	0.03	0.03	0.02	0.03	0.04	0.03	0.02	0.02	0.02	0.01	0.02	0.01	0.03	0.01	0.01	0.02
Ti	bdl	bdl	bdl	0.01	bdl	bdl	bdl	bdl	bdl	bdl	bdl	bdl	bdl	0.01	bdl	0.007	bdl	bdl
V	0.01	0.002	0.0008	0.01	0.003	0.003	0.007	0.007	0.006	0.005	0.0008	0.004	0.004	0.002	0.006	0.0008	0.001	0.0004
Cr	0.001	0.002	0.003	0.006	0.003	0.002	0.002	0.002	0.003	0.004	0.002	0.003	0.001	0.005	0.003	0.002	0.003	0.004
Mn	bdl	bdl	bdl	bdl	0.01	0.02	0.002	bdl	bdl	0.008	0.003	0.006	0.004	0.04	0.003	0.002	0.02	0.1
Fe	bdl	bdl	bdl	bdl	bdl	bdl	bdl	bdl	bdl	bdl	bdl	bdl	bdl	bdl	bdl	3	4	10
Co	bdl	bdl	bdl	bdl	bdl	bdl	bdl	bdl	bdl	bdl	bdl	bdl	bdl	bdl	bdl	bdl	bdl	bdl
Ni	bdl	bdl	bdl	bdl	0.0004	bdl	bdl	bdl	bdl	bdl	bdl	bdl	bdl	0.001	0.001	0.0004	0.002	0.0004
Cu	bdl	bdl	bdl	bdl	bdl	bdl	bdl	bdl	0.02	bdl	bdl	bdl	bdl	bdl	bdl	bdl	bdl	bdl
Zn	0.06	0.03	0.01	0.06	0.02	0.006	0.05	0.05	0.01	0.02	0.02	0.02	0.03	0.02	0.1	0.08	0.04	0.1
Ga	bdl	bdl	bdl	bdl	0.004	0.0004	bdl	bdl	bdl	0.002	bdl	0.0004	bdl	bdl	bdl	bdl	bdl	bdl
Rb	bdl	bdl	bdl	bdl	bdl	bdl	bdl	bdl	bdl	bdl	bdl	bdl	bdl	bdl	bdl	bdl	bdl	bdl
Sr	bdl	bdl	bdl	bdl	0.06	0.02	0.04	0.03	0.05	0.3	0.06	0.08	0.02	0.1	0.2	0.04	0.3	0.08
Y	0.001	bdl	bdl	bdl	bdl	0.0004	0.001	0.0004	bdl	bdl	bdl	0.0008	0.002	0.001	0.002	0.002	bdl	0.001
Zr	bdl	bdl	bdl	bdl	bdl	bdl	bdl	bdl	bdl	bdl	bdl	bdl	bdl	bdl	bdl	bdl	bdl	bdl
Nb	bdl	bdl	bdl	bdl	bdl	bdl	bdl	bdl	bdl	bdl	bdl	bdl	bdl	bdl	bdl	bdl	bdl	bdl
Cs	0.001	0.0008	0.0004	0.0004	0.0004	0.0004	0.002	0.0004	0.001	bdl	0.0004	0.002	0.003	0.002	0.001	0.001	0.0004	bdl
Ba	0.06	0.004	0.1	0.02	0.01	0.1	0.07	0.1	0.09	0.06	0.1	0.3	0.2	0.09	0.2	0.1	0.06	0.08
La	bdl	bdl	bdl	bdl	bdl	bdl	bdl	0.002	bdl	0.0004	bdl	bdl	0.0008	bdl	0.0004	0.0004	bdl	0.001
Ce	bdl	bdl	bdl	bdl	bdl	bdl	bdl	bdl	bdl	bdl	bdl	0.001	bdl	bdl	bdl	0.0008	bdl	bdl
Pr	bdl	bdl	bdl	bdl	bdl	bdl	0.0008	bdl	bdl	bdl	bdl	0.0004	0.0004	bdl	bdl	0.0004	0.0004	0.0004
Nd	bdl	0.0008	bdl	bdl	0.001	bdl	0.002	0.001	bdl	0.0008	0.0008	bdl	0.002	0.0004	0.0008	0.002	0.002	0.008
Sm	0.0004	0.0006	bdl	bdl	0.0002	bdl	0.003	0.0004	bdl	0.0008	0.001	0.0004	0.0006	0.0004	0.001	0.001	0.0008	0.0008
Eu	0.0004	0.001	0.0008	0.0008	bdl	0.0004	bdl	0.0004	0.0008	0.0004	bdl	0.0008	0.0008	bdl	0.0008	0.0008	bdl	0.0004
Gd	bdl	bdl	bdl	bdl	bdl	bdl	bdl	bdl	bdl	bdl	bdl	bdl	bdl	bdl	bdl	bdl	bdl	bdl
Tb	bdl	bdl	bdl	bdl	bdl	bdl	bdl	bdl	bdl	bdl	bdl	bdl	bdl	bdl	bdl	bdl	bdl	bdl
Dy	bdl	bdl	bdl	bdl	bdl	bdl	bdl	bdl	bdl	bdl	bdl	bdl	bdl	bdl	bdl	bdl	bdl	0.0006
Ho	bdl	bdl	bdl	bdl	bdl	bdl	bdl	bdl	bdl	bdl	bdl	bdl	bdl	bdl	bdl	0.0008	bdl	bdl
Er	bdl	bdl	bdl	bdl	bdl	bdl	bdl	bdl	bdl	bdl	bdl	bdl	bdl	bdl	bdl	bdl	bdl	bdl
Tm	bdl	bdl	bdl	bdl	bdl	bdl	bdl	bdl	bdl	bdl	bdl	bdl	bdl	bdl	bdl	bdl	bdl	bdl
Yb	bdl	bdl	bdl	bdl	bdl	bdl	bdl	bdl	bdl	bdl	bdl	bdl	bdl	bdl	bdl	bdl	bdl	bdl
Lu	bdl	bdl	bdl	bdl	bdl	bdl	bdl	bdl	bdl	bdl	bdl	bdl	bdl	bdl	bdl	bdl	bdl	bdl
Hf	bdl	bdl	bdl	bdl	bdl	bdl	bdl	bdl	bdl	bdl	bdl	bdl	bdl	bdl	bdl	bdl	bdl	bdl
Ta	bdl	bdl	bdl	bdl	bdl	bdl	bdl	bdl	bdl	bdl	bdl	bdl	bdl	bdl	bdl	bdl	bdl	bdl
Pb	bdl	bdl	bdl	bdl	bdl	bdl	bdl	bdl	bdl	bdl	bdl	bdl	bdl	bdl	bdl	bdl	bdl	bdl
Th	bdl	bdl	bdl	bdl	bdl	bdl	bdl	bdl	bdl	bdl	bdl	bdl	bdl	bdl	bdl	bdl	bdl	bdl
U	0.0004	bdl	bdl	0.0004	0.0008	bdl	0.0008	bdl	0.002	0.0008	bdl	0.0004	0.0008	0.0004	0.0008	bdl	0.001	0.0008

	18A	19A	20A	21A	22A	23A	24A	25A	26A	26Arpt	27A	36A	28A	29A	30A	31A	32A	33A
Mg	5	2	10	3	3	8	2	6	2	5	5	3	3	0.5	1	3	3	3
Al	0.003	0.2	0.4	0.5	bdl	bdl	0.08	bdl	0.2	0.2	0.4	0.3	0.003	0.02	bdl	0.1	0.07	0.07
K	20	20	40	30	30	40	40	30	5	20	20	20	6	10	20	30	20	3
Ca	20	20	50	8	70	10	6	10	20	10	0.8	6	20	10	0.2	1	10	7
Sc	0.03	0.02	0.04	0.03	0.02	0.02	0.03	0.04	bdl	0.01	0.01	0.02	0.008	0.009	0.02	0.004	0.01	0.01
Ti	bdl	bdl	bdl	bdl	bdl	bdl	bdl	bdl	bdl	bdl	bdl	0.03	bdl	0.006	bdl	bdl	0.02	bdl
V	0.0004	0.02	0.003	0.001	0.002	bdl	0.002	0.001	bdl	0.004	0.002	0.0008	0.003	0.005	0.006	0.0008	0.001	bdl
Cr	0.003	0.0004	0.003	0.002	0.003	0.006	0.004	0.006	0.003	0.004	0.002	0.003	0.002	0.004	0.002	0.003	0.003	0.003
Mn	0.06	0.02	0.08	0.02	0.001	0.04	0.1	0.05	0.04	0.05	0.1	0.1	bdl	0.01	0.2	0.01	0.02	0.08
Fe	bdl	7	bdl	20	20	bdl	30	40	bdl	bdl	bdl	bdl	bdl	bdl	bdl	bdl	bdl	bdl
Co	bdl	bdl	bdl	bdl	bdl	bdl	bdl	bdl	0.007	bdl	0.005	bdl	bdl	bdl	bdl	bdl	bdl	bdl
Ni	0.0004	0.001	bdl	0.001	bdl	bdl	bdl	bdl	0.002	0.0004	0.0008	0.002	0.002	0.002	0.0004	0.0008	0.002	0.001
Cu	bdl	bdl	bdl	bdl	bdl	bdl	bdl	bdl	bdl	bdl	0.008	bdl	0.001	0.008	0.004	bdl	0.02	0.002
Zn	0.03	0.06	0.03	0.08	0.2	0.008	0.06	0.06	0.04	0.02	0.07	0.008	0.03	0.07	0.02	0.2	0.03	0.05
Ga	bdl	bdl	bdl	0.002	bdl	bdl	bdl	bdl	0.002	0.002	0.0008	0.0004	0.0004	0.005	0.003	0.001	0.004	0.0008
Rb	bdl	bdl	bdl	bdl	bdl	bdl	bdl	bdl	bdl	bdl	bdl	bdl	bdl	bdl	bdl	bdl	bdl	bdl
Sr	0.09	0.03	0.2	0.1	0.1	0.2	0.1	0.07	0.008	0.1	0.1	0.1	0.2	0.04	0.006	0.07	0.02	0.09
Y	0.005	0.0008	0.002	0.0008	0.0008	0.001	0.002	0.0008	bdl	bdl	0.0008	bdl	bdl	0.001	bdl	0.0008	bdl	0.001
Zr	bdl	0.0008	bdl	0.006	bdl	bdl	bdl	bdl	bdl	bdl	bdl	bdl	bdl	bdl	bdl	bdl	bdl	bdl
Nb	bdl	bdl	bdl	bdl	bdl	bdl	bdl	bdl	bdl	bdl	bdl	bdl	bdl	bdl	bdl	bdl	bdl	bdl
Cs	0.002	0.003	bdl	0.001	0.001	0.0008	0.002	0.001	0.0008	0.0004	0.0008	0.001	0.0008	0.0008	0.0004	bdl	0.0004	0.0004
Ba	0.1	0.03	0.1	0.04	0.2	0.008	0.1	0.3	0.02	0.05	0.03	0.1	0.02	0.07	0.02	0.06	0.004	0.2
La	0.0004	bdl	0.002	0.005	0.002	bdl	0.002	0.0004	bdl	bdl	0.0008	0.001	bdl	bdl	bdl	bdl	bdl	0.002
Ce	bdl	bdl	bdl	bdl	bdl	bdl	bdl	bdl	bdl	bdl	0.0004	bdl	bdl	bdl	bdl	0.002	bdl	bdl
Pr	bdl	0.0004	0.0008	0.0008	0.0004	bdl	0.001	0.001	bdl	bdl	0.0008	bdl	bdl	bdl	bdl	bdl	bdl	bdl
Nd	0.004	0.002	0.008	0.002	0.003	0.003	0.005	0.004	bdl	0.0008	0.004	0.006	bdl	0.004	bdl	0.002	bdl	0.0004
Sm	0.002	0.003	0.001	0.002	0.001	0.002	0.002	0.0002	0.0006	0.0004	0.0006	0.0006	bdl	0.0008	bdl	0.001	0.0002	0.0006
Eu	0.0004	0.0008	bdl	0.0004	bdl	bdl	bdl	bdl	bdl	bdl	bdl	bdl	bdl	bdl	bdl	0.0008	bdl	0.0004
Gd	bdl	bdl	bdl	bdl	bdl	bdl	bdl	bdl	bdl	bdl	bdl	bdl	bdl	bdl	bdl	bdl	bdl	bdl
Tb	bdl	bdl	bdl	bdl	bdl	bdl	bdl	bdl	bdl	bdl	bdl	bdl	bdl	bdl	bdl	bdl	bdl	bdl
Dy	0.0002	0.001	bdl	0.002	bdl	bdl	bdl	0.002	bdl	bdl	bdl	bdl	bdl	bdl	bdl	0.0002	bdl	bdl
Ho	bdl	bdl	bdl	0.0004	bdl	bdl	bdl	bdl	bdl	bdl	bdl	bdl	bdl	bdl	bdl	0.0004	bdl	0.0004
Er	bdl	bdl	bdl	bdl	bdl	bdl	bdl	bdl	bdl	bdl	bdl	bdl	bdl	bdl	bdl	bdl	bdl	bdl
Tm	bdl	bdl	bdl	bdl	bdl	bdl	bdl	bdl	0.0008	bdl	0.0004	bdl	bdl	bdl	bdl	bdl	0.0004	bdl
Yb	bdl	bdl	bdl	bdl	bdl	bdl	bdl	bdl	bdl	bdl	bdl	bdl	bdl	bdl	bdl	bdl	bdl	bdl
Lu	bdl	bdl	bdl	bdl	bdl	bdl	bdl	bdl	bdl	bdl	bdl	bdl	bdl	bdl	bdl	bdl	bdl	bdl
Hf	bdl	bdl	bdl	bdl	bdl	bdl	bdl	bdl	bdl	bdl	bdl	bdl	bdl	bdl	bdl	bdl	bdl	bdl
Ta	bdl	bdl	bdl	bdl	bdl	bdl	bdl	bdl	bdl	bdl	bdl	bdl	bdl	bdl	bdl	bdl	bdl	bdl
Pb	bdl	bdl	bdl	bdl	bdl	bdl	bdl	bdl	bdl	bdl	bdl	bdl	bdl	bdl	bdl	bdl	bdl	bdl
Th	bdl	bdl	bdl	bdl	bdl	bdl	bdl	bdl	bdl	bdl	bdl	bdl	bdl	bdl	bdl	bdl	bdl	bdl
U	0.0008	0.002	0.001	0.002	0.0004	bdl	bdl	0.001	0.0004	bdl	0.0004	0.0004	bdl	0.0004	bdl	bdl	0.0004	bdl

Table E.4 – *Trace elemental concentrations from fraction 2, in mg/kg, from ICP-MS analysis. Concentrations below the detection limit (bdl) were recorded when: concentration – 3*sd – 3*blank sd < 0.*

	1A	1Arpt	16A	35A	2A	3A	4A	5A	6A	7A	8A	9A	10A	11A	12A	13A	14A	17A
Mg	9.377	10.35	12.25	15.8	33.96	10.19	10.44	13.85	387	551.3	8.794	102.6	70.29	103.5	187	29.15	183.4	62.52
Al	56.17	60.36	63.78	70.06	76.22	85.16	61	39.42	148.9	2527	133.8	404.3	436.9	596.3	416.4	570.2	356.1	99.06
K	142.9	158.6	183.4	202	122	187.5	157.8	135.1	148.1	286.3	214.5	317.5	564.5	310.3	318.8	211.6	410.3	150.4
Ca	156	172.2	173.4	241	268.3	225.6	69.52	155.3	11880	12830	152.9	575.2	556.7	1190	1279	158.9	3334	718
Sc	0.142	0.15	0.188	0.194	0.107	0.302	0.117	0.108	0.493	2.002	0.176	0.685	0.625	0.315	0.483	0.75	0.27	0.213
Ti	0.211	0.268	0.301	0.329	0.106	bdl	0.391	0.647	bdl	2.003	0.344	bdl	bdl	0.194	bdl	bdl	bdl	bdl
V	0.271	0.294	0.295	0.38	0.374	0.24	0.149	0.467	0.058	1.898	0.519	0.815	2	0.07	0.04	0.01	0.019	0.234
Cr	0.616	0.66	0.82	0.872	0.613	0.486	0.637	0.665	0.689	3.993	0.759	0.995	0.936	0.931	0.853	0.839	0.93	1.259
Mn	0.571	0.613	0.678	0.77	3.883	2.687	2.832	0.629	31.09	48.2	1.077	5.062	5.871	35.37	7.828	8.271	45.42	106.1
Fe	bdl	24.13	48.16	52.48	bdl	bdl	30.91	bdl	35.19	592.3	37.31	54.05	168.2	347.8	79.25	193	160.3	110.1
Co	0.045	0.06	0.037	0.03	0.089	0.038	0.297	0.057	0.069	0.389	0.099	0.168	0.106	2.184	0.545	0.285	0.36	0.633
Ni	0.011	bdl	bdl	bdl	0.129	0.023	0.382	0.059	0.375	1.046	0.08	0.4	1.886	3.605	1.645	0.707	3.872	0.654
Cu	48.8	bdl	50.49	bdl	53.68	38.26	48.04	49.49	46.15	47.15	49.17	47.39	44.41	48.84	47.03	51.06	56.78	52.75
Zn	0.852	bdl	bdl	1.088	0.954	0.497	bdl	1.391	bdl	3.632	5.323	7.232	1.078	6.189	3.8	1.738	3.12	4.727
Ga	0.009	0.011	0.012	0.014	0.035	0.052	0.021	0.014	0.042	0.543	0.029	0.297	0.031	0.035	0.039	0.051	bdl	0.029
Rb	0.453	0.505	0.475	0.505	0.279	0.66	0.333	0.309	0.673	1.218	0.66	1.344	2.192	1.112	0.881	1.135	1.653	0.32
Sr	1.284	1.44	1.423	1.571	2.962	2.089	1.381	1.063	34.59	102.6	2.048	20.02	29.28	16.79	17.27	4.578	36.71	5.428
Y	0.304	0.318	0.35	0.384	0.606	3.369	0.35	0.285	1.401	3.393	0.566	2.534	0.859	0.484	1.493	0.848	0.129	0.552
Zr	bdl	bdl	bdl	bdl	0.025	0.025	bdl	0.009	bdl	0.056	0.014	0.137	0.037	0.02	0.023	0.014	0.033	0.193
Nb	bdl	0.004	bdl	bdl	bdl	bdl	bdl	bdl	0.003	0.002	0.007	0.007	0.007	0.006	0.006	0.006	0.006	bdl
Cs	0.015	0.015	0.014	0.017	bdl	0.016	bdl	bdl	bdl	0.017	0.015	0.026	0.062	0.023	bdl	0.036	0.07	bdl
Ba	3.282	3.448	3.627	3.892	8.295	6.161	3.074	1.338	22.13	57.18	8.094	46.35	59.59	36.58	38.5	21.51	18.55	30.99
La	0.23	0.241	0.251	0.279	0.585	0.911	0.463	0.343	1.296	6.998	0.455	5.5	0.558	0.233	0.71	0.814	0.079	0.376
Ce	0.402	0.425	0.434	0.472	1.158	1.588	0.798	0.669	1.164	8.287	1.049	9.741	0.721	0.363	1.114	1.239	0.148	0.85
Pr	0.057	0.06	0.062	0.07	0.149	0.261	0.111	0.078	0.248	1.367	0.143	1.332	0.134	0.057	0.167	0.17	0.024	0.11
Nd	0.268	0.291	0.308	0.337	0.68	1.368	0.49	0.347	1.142	5.396	0.676	5.674	0.659	0.337	0.843	0.841	0.148	0.579
Sm	0.062	0.068	0.069	0.073	0.137	0.408	0.099	0.068	0.241	0.997	0.159	1.086	0.163	0.097	0.214	0.199	0.039	0.145
Eu	0.017	0.018	0.017	0.019	0.03	0.124	0.048	0.036	0.076	0.256	0.049	0.244	0.053	0.022	0.063	0.053	0.011	0.042
Gd	0.126	0.136	0.106	0.11	0.175	0.618	0.15	0.12	0.348	0.975	0.254	0.996	0.277	0.219	0.377	0.327	0.125	0.208
Tb	bdl	0.013	0.035	0.011	bdl	0.06	bdl	bdl	0.021	0.113	0.11	0.193	0.117	0.103	0.13	0.126	0.095	0.117
Dy	0.061	0.062	0.068	0.074	0.107	0.585	0.068	0.056	0.222	0.676	0.13	0.548	0.157	0.096	0.259	0.195	0.026	0.111
Ho	0.009	0.011	0.011	0.012	0.019	0.116	0.01	0.008	0.042	0.122	0.02	0.096	0.029	0.017	0.053	0.037	0.003	0.018
Er	0.04	0.046	0.042	0.042	0.067	0.333	0.041	0.039	0.123	0.319	0.076	0.272	0.099	0.065	0.167	0.123	0.029	0.058
Tm	0.004	0.006	0.004	0.003	0.007	0.041	0.004	0.004	0.015	0.039	0.012	0.038	0.015	0.011	0.023	0.018	0.006	0.009
Yb	0.09	0.116	0.068	0.062	0.108	0.307	0.094	0.099	0.162	0.303	0.163	0.327	0.179	0.152	0.227	0.203	0.127	0.098
Lu	0.016	0.02	0.01	0.009	0.017	0.047	0.016	0.017	0.029	0.047	0.031	0.056	0.033	0.029	0.041	0.038	0.026	0.018
Hf	bdl	bdl	bdl	bdl	bdl	bdl	bdl	bdl	bdl	bdl	bdl	bdl	bdl	bdl	bdl	bdl	bdl	bdl
Ta	bdl	bdl	bdl	bdl	bdl	bdl	bdl	bdl	bdl	bdl	bdl	bdl	bdl	bdl	bdl	bdl	bdl	bdl
Pb	0.161	0.202	0.16	0.149	0.728	0.181	0.17	0.17	0.155	0.315	0.351	0.577	0.626	0.351	0.456	0.456	0.306	3.406
Th	0.122	0.146	0.108	0.109	0.133	0.19	0.135	0.138	0.145	0.637	0.246	0.517	0.203	0.181	0.188	0.219	0.17	0.139
U	0.016	0.016	0.017	0.018	0.051	0.027	0.012	0.006	0.152	0.051	0.043	0.157	0.091	0.097	0.102	0.066	0.21	0.223

	18A	19A	20A	21A	22A	23A	24A	25A	26A	26Arpt	27A	36A	28A	29A	30A	31A	32A	33A
Mg	226.9	98.71	102	66.08	123.7	212.1	129.3	63.77	153.1	186.4	245.7	256.3	164.5	164.5	112.7	172.1	238.6	210.1
Al	377.6	660.4	652.7	895.1	124.4	465.5	286.7	577.4	29.17	39.62	27.9	34.31	1.268	39.82	8.913	127.7	29.75	64.89
K	298.3	304.5	288.3	382.9	231.2	391.6	412.3	286.6	436.5	561.7	558.7	583.3	313.1	587.9	546.6	560.9	541.2	585.7
Ca	2033	675.3	816.2	510.8	1192	1656	1362	503.9	1493	2271	1349	1559	1910	1923	811.9	1216	1855	1187
Sc	0.265	0.333	0.386	0.49	0.24	0.327	0.247	0.451	0.286	0.3	0.338	0.328	0.228	0.262	0.225	0.336	0.23	0.304
Ti	0.587	0.533	bdl	0.639	0.133	0.136	bdl	0.198	bdl	bdl	bdl	0.475	bdl	bdl	bdl	bdl	bdl	bdl
V	0.406	0.202	0.337	0.145	0.238	0.089	0.186	0.076	0.111	0.137	0.3	0.256	bdl	0.286	0.129	0.083	bdl	0.32
Cr	0.964	1.006	0.963	1.106	0.975	1.059	0.963	1.19	2.341	3.068	3.079	3.133	2.016	2.738	2.334	2.428	2.772	2.885
Mn	114.4	102.5	19.22	13.19	51.22	49.89	80.69	54.88	18.41	21.06	71.19	70.41	4.637	17.85	106.3	26.19	29.01	68.53
Fe	102.1	109.3	216.5	209.7	65.62	192.7	88.65	185	bdl	bdl	bdl	bdl	bdl	bdl	bdl	bdl	bdl	bdl
Co	0.93	1.036	0.351	0.335	0.631	0.678	0.638	0.489	0.161	0.326	0.266	0.272	0.161	0.276	0.26	0.67	0.39	0.578
Ni	0.637	0.856	0.603	0.969	0.683	0.805	0.511	1.026	1.115	0.254	1.353	0.272	0.781	0.773	0.672	0.791	2.293	0.642
Cu	50.17	51.9	46.51	45.5	48.08	48.56	52.43	57.78	213.6	bdl	273.2	271.4	199.6	243.6	202.1	222.5	245.2	236
Zn	9.499	8.279	3.543	3.207	5.38	1.905	7.578	2.178	11.38	33.66	17.63	23.88	7.161	11.67	16.45	26.78	20.4	12.38
Ga	0.038	0.049	0.052	0.051	0.045	0.024	0.029	0.054	bdl	bdl	bdl	bdl	bdl	bdl	bdl	bdl	bdl	bdl
Rb	1.009	1.344	1.357	1.735	0.377	0.856	0.973	0.91	1.971	1.119	2.209	1.16	1.858	2.019	2.023	2.736	2.042	2.555
Sr	17.92	6.169	11.34	6.27	10.84	15.52	14.04	8.959	9.908	12.15	9.745	9.231	21.78	13.91	5.75	9.618	15.98	13.8
Y	0.506	0.625	0.774	0.592	0.737	0.394	0.436	0.997	0.066	0.131	0.322	0.296	0.058	0.272	0.072	0.429	0.119	0.449
Zr	0.131	0.241	0.168	0.414	0.089	0.067	0.055	0.152	bdl	bdl	bdl	bdl	bdl	bdl	bdl	bdl	bdl	bdl
Nb	0.004	0.004	bdl	0.007	bdl	bdl	bdl	bdl	bdl	0.03	bdl	bdl	0.034	0.022	0.014	0.038	0.024	0.042
Cs	0.014	0.029	0.026	0.048	bdl	bdl	0.012	0.005	bdl	bdl	bdl	bdl	bdl	bdl	bdl	bdl	bdl	bdl
Ba	30.48	4.345	32.25	5.428	22.79	22.17	19.15	30.72	13.99	16.41	11.38	10.91	3.342	20.35	10.91	16.3	23.51	27.74
La	0.422	0.357	0.544	0.256	0.709	0.29	0.317	0.566	0.077	0.103	0.195	0.175	bdl	0.322	0.044	0.326	0.085	0.26
Ce	0.677	0.854	0.693	0.688	1.354	0.443	0.631	1.168	0.197	0.242	0.485	0.423	0.131	0.707	0.187	0.803	0.257	0.735
Pr	0.111	0.132	0.153	0.118	0.196	0.076	0.091	0.185	0.01	0.012	0.054	0.04	bdl	0.07	0.004	0.081	0.012	0.07
Nd	0.542	0.71	0.776	0.682	0.974	0.4	0.481	1.009	0.101	0.115	0.36	0.288	bdl	0.397	0.077	0.445	0.121	0.483
Sm	0.124	0.174	0.183	0.19	0.222	0.096	0.116	0.254	bdl	0.014	0.074	0.051	bdl	0.07	bdl	0.099	0.018	0.099
Eu	0.034	0.046	0.05	0.048	0.054	0.025	0.03	0.072	0.046	bdl	0.06	bdl	0.036	0.044	0.03	0.054	0.034	0.062
Gd	0.177	0.225	0.245	0.225	0.26	0.146	0.161	0.318	0.036	0.451	0.119	0.322	0.501	0.379	0.268	0.699	0.349	0.544
Tb	0.07	0.06	0.056	0.045	0.04	0.035	0.033	0.073	0.471	bdl	0.519	bdl	0.499	0.33	0.302	0.338	0.347	0.525
Dy	0.094	0.129	0.146	0.134	0.149	0.071	0.086	0.192	bdl	bdl	0.062	0.045	bdl	0.043	bdl	0.07	bdl	0.081
Ho	0.015	0.019	0.024	0.022	0.025	0.012	0.012	0.033	bdl	bdl	0.004	bdl	bdl	bdl	bdl	bdl	bdl	0.006
Er	0.051	0.059	0.07	0.064	0.069	0.04	0.04	0.089	bdl	0.092	0.038	0.074	0.128	0.099	0.06	0.168	0.081	0.14
Tm	0.012	0.008	0.01	0.008	0.008	0.006	0.006	0.012	0.004	0.01	0.008	0.004	0.006	0.014	0.016	0.036	0.02	0.024
Yb	0.085	0.078	0.086	0.08	0.078	0.068	0.066	0.099	0.045	0.613	0.064	0.363	0.756	0.485	0.382	0.877	0.5	0.641
Lu	0.014	0.012	0.014	0.013	0.012	0.011	0.01	0.016	0.008	0.113	0.012	0.062	0.165	0.097	0.077	0.181	0.099	0.135
Hf	bdl	bdl	bdl	0.009	bdl	bdl	bdl	bdl	bdl	bdl	bdl	bdl	bdl	bdl	bdl	bdl	bdl	bdl
Ta	bdl	bdl	bdl	bdl	bdl	bdl	bdl	bdl	bdl	bdl	bdl	bdl	bdl	bdl	bdl	bdl	bdl	bdl
Pb	4.361	2.327	1.254	0.999	0.94	0.303	0.504	0.733	2.014	2.317	2.666	2.268	1.17	1.811	1.844	2.135	1.936	2.825
Th	0.136	0.138	0.169	0.197	0.126	0.103	0.096	0.187	1.693	0.489	1.784	0.427	1.768	1.309	1.367	1.582	1.469	1.512
U	0.114	0.114	0.114	0.172	0.176	0.045	0.067	0.105	bdl	bdl	0.014	0.008	bdl	0.024	bdl	0.026	0.002	0.018

Table E.5 – *The standard deviation from fraction 2, in mg/kg, from ICP-MS analysis. Concentrations below the detection limit (bdl) were recorded when: concentration – 3*sd – 3*blank sd < 0.*

	1A	1Arpt	16A	35A	2A	3A	4A	5A	6A	7A	8A	9A	10A	11A	12A	13A	14A	17A
Mg	0.2	0.08	0.07	0.3	0.2	0.08	0.1	0.3	5	6	0.2	0.5	0.6	1	1	0.2	0.7	0.3
Al	0.6	0.1	0.3	0.3	0.4	0.9	0.3	0.08	1	6	1	1	4	8	3	0.6	1	0.04
K	4	0.3	2	2	0.6	0.7	2	2	2	2	5	3	5	2	3	0.4	2	0.9
Ca	5	3	2	6	3	3	1	3	50	30	4	3	9	6	7	2	20	10
Sc	0.002	0.005	0.008	0.0008	0.0004	0.005	0.003	bdl	0.0004	0.008	0.007	0.006	0.001	0.004	0.01	0.01	0.007	0.0004
Ti	0.01	0.02	0.02	0.02	0.01	bdl	0.1	0.04	bdl	0.04	0.06	bdl	bdl	0.008	bdl	bdl	bdl	bdl
V	0.002	0.006	bdl	0.004	0.001	0.0004	0.001	0.002	0.003	0.02	0.005	bdl	0.01	0.006	0.002	0.001	0.004	0.005
Cr	0.02	0.04	0.04	0.05	0.04	0.04	0.02	0.01	0.006	0.08	0.04	0.03	0.02	0.03	0.04	0.04	0.05	0.03
Mn	0.006	0.008	0.01	0.02	0.06	0.06	0.02	0.006	0.08	0.1	0.009	0.08	0.08	0.09	0.2	0.2	0.2	1
Fe	bdl	4	3	3	bdl	bdl	3	bdl	1	5	3	1	4	5	2	2	4	2
Co	0.0008	0.006	0.003	0.002	0.005	0.0004	0.003	0.002	0.0004	0.006	0.006	0.0008	0.0008	0.0004	0.009	0.004	0.002	0.002
Ni	0.001	bdl	bdl	bdl	0.02	0.005	0.006	0.004	0.01	0.03	0.0008	0.004	0.05	0.006	0.004	0.01	0.07	0.008
Cu	4	bdl	5	bdl	4	3	4	4	2	6	5	5	5	5	4	6	6	5
Zn	0.05	bdl	bdl	0.02	0.002	0.002	bdl	0.02	bdl	0.02	0.02	0.09	0.006	0.2	0.04	0.1	0.02	0.08
Ga	0.0008	0.001	bdl	0.002	0.0008	0.002	0.0008	0.0004	0.002	0.003	0.001	0.003	0.003	0.001	0.002	0.0004	bdl	0.0004
Rb	0.006	0.004	0.004	0.001	0.001	0.01	0.0008	0.0008	0.008	0.02	0.01	0.0008	0.03	0.006	0.02	0.02	0.02	0.0004
Sr	0.004	0.009	0.01	0.007	0.006	0.002	0.009	0.008	0.1	2	0.03	0.05	0.3	0.3	0.1	0.04	0.4	0.05
Y	0.0004	0.002	0.008	0.003	0.01	0.01	0.004	0.002	0.005	0.05	0.007	0.007	0.01	0.005	0.004	0.01	0.004	0.009
Zr	bdl	bdl	bdl	bdl	0.003	0.001	bdl	0.0004	bdl	0.004	0.002	0.008	0.002	0.0004	0.001	0.0008	0.0004	0.003
Nb	bdl	0.0004	bdl	bdl	bdl	bdl	bdl	bdl	bdl	bdl	0.0004	0.0008	0.001	bdl	0.0004	0.0008	bdl	bdl
Cs	0.0004	bdl	0.0004	0.0008	bdl	0.002	bdl	bdl	bdl	0.0004	0.002	0.001	0.0004	0.0004	bdl	0.0008	bdl	bdl
Ba	0.01	0.03	0.06	0.01	0.06	0.02	0.006	0.007	0.2	1	0.07	0.4	0.5	0.4	0.1	0.2	0.2	0.1
La	0.003	0.002	0.003	0.005	0.009	0.01	0.009	0.002	0.01	0.08	0.0008	0.08	0.01	0.001	0.004	0.003	0.0004	0.007
Ce	0.004	0.003	0.006	0.006	0.01	0.02	0.005	0.01	0.0008	0.02	0.01	0.09	0.004	0.007	0.006	0.003	0.001	0.03
Pr	0.0004	0.0008	0.0004	0.0004	0.004	0.003	0.002	0.002	0.003	0.008	0.0008	0.008	0.0004	bdl	0.003	0.0004	0.002	0.002
Nd	0.0008	0.002	0.007	0.01	0.01	0.02	0.007	0.001	0.02	0.006	0.003	0.06	0.01	0.01	0.001	0.006	0.009	0.02
Sm	0.003	0.003	0.003	0.002	0.002	0.002	0.002	0.002	0.009	0.01	0.004	0.02	0.003	0.005	0.004	0.001	0.0008	0.003
Eu	0.0008	0.0004	bdl	0.0004	0.001	0.004	bdl	0.002	0.0004	0.005	0.001	0.0008	0.0004	0.0004	0.003	0.002	0.0008	0.0004
Gd	0.005	0.001	0.002	0.002	0.004	0.004	0.002	0.004	0.008	0.003	0.003	0.0004	0.009	0.008	0.01	0.005	0.002	0.003
Tb	bdl	0.003	0.002	0.002	bdl	bdl	bdl	bdl	0.001	0.0004	0.002	0.002	0.001	0.003	0.002	0.003	0.002	0.004
Dy	0.002	0.001	0.0008	0.003	0.003	0.005	0.003	0.001	0.007	0.01	0.0006	0.005	0.0006	0.001	0.006	0.002	0.002	0.005
Ho	0.0008	0.0004	bdl	0.0004	bdl	0.0004	bdl	0.0004	0.0004	0.0004	0.001	0.0008	0.002	0.0008	0.0008	0.0004	bdl	0.0004
Er	0.001	0.002	0.0004	0.0004	0.0004	0.0006	0.002	0.0008	0.003	0.002	0.001	0.008	0.002	0.002	0.002	0.002	0.001	0.001
Tm	0.0004	bdl	0.0004	0.0004	0.0004	0.002	0.0004	bdl	0.0004	0.0008	0.0004	bdl	bdl	0.0008	0.0004	0.0004	0.0008	bdl
Yb	0.002	0.002	0.002	0.001	0.003	0.004	0.0008	0.003	0.002	0.005	0.003	0.002	0.001	0.003	0.003	0.001	0.002	0.002
Lu	0.0004	bdl	0.0004	0.0004	bdl	bdl	0.001	0.0004	0.0004	0.0004	0.0004	0.0008	0.0008	0.0008	0.0004	0.001	0.0004	0.0004
Hf	bdl	bdl	bdl	bdl	bdl	bdl	bdl	bdl	bdl	bdl	bdl	bdl	bdl	bdl	bdl	bdl	bdl	bdl
Ta	bdl	bdl	bdl	bdl	bdl	bdl	bdl	bdl	bdl	bdl	bdl	bdl	bdl	bdl	bdl	bdl	bdl	bdl
Pb	0.004	0.005	0.007	0.004	0.007	0.004	0.003	0.004	0.003	0.003	0.01	0.05	0.008	0.002	0.007	0.008	0.005	0.02
Th	0.001	bdl	0.002	0.004	0.003	0.002	0.0004	0.002	0.002	0.003	bdl	0.01	0.004	0.006	0.002	0.004	0.005	0.0004
U	0.0004	bdl	0.0008	0.0004	0.002	0.0004	0.0004	bdl	0.002	0.001	0.0008	0.0008	0.003	bdl	0.005	0.0004	0.003	0.006

	18A	19A	20A	21A	22A	23A	24A	25A	26A	26Arpt	27A	36A	28A	29A	30A	31A	32A	33A
Mg	3	1	0.8	0.5	0.6	0.9	0.5	0.2	3	3	2	2	1	1	0.9	0.7	3	5
Al	0.5	10	3	10	0.3	2	10	0.7	2	1	0.6	0.5	0.2	0.1	0.4	0.7	0.3	0.4
K	2	0.8	0.6	0.07	0.6	3	0.8	0.5	20	30	10	2	20	3	0.7	3	1	40
Ca	40	3	7	4	6	10	3	0.8	40	30	7	20	30	40	30	30	10	20
Sc	0.006	0.005	0.009	0.01	bdl	0.004	0.008	0.004	0.002	0.01	0.008	bdl	0.01	0.01	0.03	0.02	0.04	0.04
Ti	0.07	0.02	bdl	0.06	0.005	0.003	bdl	0.03	bdl	bdl	bdl	0.07	bdl	bdl	bdl	bdl	bdl	bdl
V	0.005	0.004	0.004	0.0004	0.002	0.003	0.002	0.001	0.002	0.004	0.02	0.008	bdl	bdl	bdl	0.02	bdl	0.04
Cr	0.06	0.03	0.05	0.05	0.02	0.05	0.01	0.06	0.3	0.2	0.09	0.2	0.3	0.2	0.07	0.2	0.1	0.2
Mn	0.08	0.5	0.2	0.1	0.4	0.3	0.2	0.2	0.3	0.2	0.4	0.4	0.03	0.1	0.6	0.4	0.01	1
Fe	6	3	3	3	5	2	5	7	bdl	bdl	bdl	bdl	bdl	bdl	bdl	bdl	bdl	bdl
Co	0.0004	0.01	0.005	0.005	0.02	0.003	0.002	0.006	0.004	0.02	0.004	0.006	0.004	bdl	0.03	0.02	0.02	0.004
Ni	0.01	0.0008	0.003	0.02	0.03	0.01	0.02	0.008	0.06	0.004	0.2	bdl	0.04	0.1	0.002	0.06	0.07	0.04
Cu	5	5	5	5	5	6	6	7	30	bdl	20	20	20	20	20	20	20	10
Zn	0.1	0.02	0.07	0.01	0.1	0.07	0.02	0.07	0.2	1	0.5	0.6	0.4	0.05	0.01	0.8	0.2	0.4
Ga	0.002	0.0008	0.004	0.0008	bdl	0.003	0.0004	bdl	bdl	bdl	bdl	bdl	bdl	bdl	bdl	bdl	bdl	bdl
Rb	0.02	0.007	0.01	0.03	0.0008	0.01	0.01	0.002	0.08	0.02	0.01	0.01	0.03	0.02	0.01	0.006	0.02	0.1
Sr	0.02	0.02	0.1	0.03	0.04	0.2	0.04	0.02	0.2	0.2	0.05	0.02	0.5	0.2	0.03	0.03	0.03	0.3
Y	0.006	0.004	0.001	0.01	0.01	0.001	0.002	0.0004	0.006	0.002	0.004	0.01	0.002	0.002	0.002	bdl	0.004	0.02
Zr	0.003	0.004	0.003	0.01	0.003	0.004	0.004	0.002	bdl	bdl	bdl	bdl	bdl	bdl	bdl	bdl	bdl	bdl
Nb	0.0008	0.0004	bdl	0.0008	bdl	bdl	bdl	bdl	bdl	bdl	bdl	bdl	bdl	0.004	0.002	0.008	0.002	0.002
Cs	bdl	0.0008	0.001	bdl	bdl	bdl	bdl	bdl	bdl	bdl	bdl	bdl	bdl	bdl	bdl	bdl	bdl	bdl
Ba	0.06	0.07	0.1	0.006	0.4	0.1	0.2	0.3	0.1	0.2	0.1	0.03	0.04	0.2	0.09	0.4	0.2	0.6
La	0.003	0.0004	0.009	0.001	0.008	0.002	0.004	0.01	0.004	0.006	0.002	0.008	bdl	0.008	bdl	bdl	0.002	0.004
Ce	0.003	0.004	0.0008	0.004	0.002	0.002	0.006	0.01	0.004	0.002	bdl	0.02	0.006	0.002	bdl	0.02	0.008	0.02
Pr	0.0008	0.001	0.002	0.002	0.002	0.0008	0.002	0.002	0.002	bdl	bdl	bdl	bdl	bdl	bdl	0.002	bdl	0.002
Nd	0.001	0.008	0.01	0.02	0.01	0.002	0.007	0.01	0.01	0.01	0.006	0.02	bdl	0.006	0.004	0.02	0.01	0.02
Sm	0.006	0.004	0.004	0.004	0.006	0.003	0.0008	0.004	bdl	0.004	0.005	0.003	bdl	0.01	bdl	0.004	0.004	0.01
Eu	0.004	0.002	0.0008	0.0008	0.0008	0.003	0.0004	0.002	bdl	bdl	bdl	bdl	0.004	0.002	0.004	0.004	bdl	0.004
Gd	0.008	0.006	0.007	0.002	0.005	0.002	0.01	0.01	0.002	0.03	0.004	0.004	0.01	0.02	0.002	0.002	0.02	0.004
Tb	0.002	0.004	0.004	0.002	0.003	0.002	0.002	0.0008	bdl	bdl	0.004	bdl	0.01	0.002	0.002	0.008	0.02	0.02
Dy	0.001	0.001	0.006	0.002	0.003	0.003	0.002	0.001	bdl	bdl	0.006	0.002	bdl	0.005	bdl	0.003	bdl	0.007
Ho	0.0004	0.0004	0.0008	0.0004	0.0004	0.0004	0.0004	0.001	bdl	bdl	bdl	bdl	bdl	bdl	bdl	bdl	bdl	bdl
Er	0.0008	0.0006	0.002	0.005	0.003	0.002	0.0004	0.004	bdl	0.004	0.002	0.006	0.006	0.007	0.004	0.006	0.004	0.005
Tm	bdl	0.0008	bdl	0.0004	bdl	0.0008	0.0004	0.0008	bdl	0.002	0.002	bdl	bdl	0.004	0.002	bdl	0.002	0.002
Yb	0.0008	0.001	0.001	0.003	0.002	0.002	0.004	0.0004	0.001	0.008	0.005	0.006	0.005	0.008	0.008	0.008	0.002	0.03
Lu	0.0004	bdl	bdl	bdl	bdl	0.0008	bdl	0.001	0.002	bdl	0.002	0.002	0.006	0.002	0.002	0.006	bdl	0.006
Hf	bdl	bdl	bdl	0.001	bdl	bdl	bdl	bdl	bdl	bdl	bdl	bdl	bdl	bdl	bdl	bdl	bdl	bdl
Ta	bdl	bdl	bdl	bdl	bdl	bdl	bdl	bdl	bdl	bdl	bdl	bdl	bdl	bdl	bdl	bdl	bdl	bdl
Pb	0.05	0.008	0.007	0.04	0.02	0.003	0.006	0.01	0.04	0.03	0.04	0.02	0.05	0.04	0.04	0.04	0.03	0.04
Th	0.0004	0.0008	0.002	0.004	0.002	0.003	0.003	0.008	0.03	0.01	0.02	0.004	0.008	0.04	0.01	0.04	0.04	0.06
U	0.001	0.0004	0.001	0.002	0.0004	0.0008	0.0008	0.0004	bdl	bdl	0.002	bdl	bdl	0.004	bdl	0.002	bdl	bdl

Table E.6 - *Trace elemental concentrations from fraction 3, in mg/kg, from ICP-MS analysis. Concentrations below the detection limit (bdl) were recorded when: concentration – 3*sd – 3*blank sd < 0.*

	1A	1Arpt	16A	35A	2A	3A	4A	5A	6A	7A	8A	9A	10A	11A	12A	13A	14A	17A
Mg	74.4	76	66	35.4	125	106	53.7	49.5	1260	875	34.3	325	77.1	729	393	106	1030	35.1
Al	276	278	203	95	246	563	146	98.7	892	3050	651	917	1760	1800	1220	2520	3850	1400
K	48.9	32.6	35.3	39.9	bdl	127	26.2	bdl	51.6	118	50.3	105	330	97	176	38.3	168	bdl
Ca	33.2	bdl	bdl	bdl	194	42.4	bdl	bdl	1240	2910	bdl	102	98	313	339	bdl	1210	105
Sc	0.95	0.69	bdl	bdl	0.41	1.45	bdl	bdl	4.65	4.12	bdl	4.96	1.71	2.29	4.4	1.56	3.36	1.75
Ti	54.3	53.3	30.4	4.28	37.7	38.1	15.1	22.2	7.6	4.33	34.8	5.71	31.4	4.74	2.69	12.4	12.5	47.9
V	3.17	3.07	2.4	1.75	3.44	8.87	2.8	2.25	21.9	17.2	10.7	29.3	45.7	8.95	15.6	8.21	13.5	15.8
Cr	3.37	3.25	1.85	bdl	1.75	4.89	bdl	0.86	1.33	5.14	3.17	13.1	3.89	1.04	2.22	bdl	1.83	3.82
Mn	8.34	8.44	5.72	2.09	37.1	56.1	8.65	9.1	1410	281	16.1	770	130	174	94	83.4	541	111
Fe	5500	5530	2880	134	3840	14500	2470	1600	29200	12300	7510	25300	13600	13100	29100	13600	34900	10400
Co	0.59	0.59	0.36	0.04	1.15	0.82	1.03	0.23	1.98	6.89	0.91	4.75	4.38	7.93	8.17	2.32	4.99	2.07
Ni	2.48	2.38	1.57	bdl	3.33	4.88	3.54	bdl	3.53	24.3	3.27	8.55	18.6	16.8	12	5.2	22.4	2.48
Cu	3.13	bdl	bdl	bdl	bdl	bdl	bdl	2.02	2.25	bdl	bdl	bdl	2.15	bdl	25.3	4.92	4.58	6.89
Zn	bdl	bdl	bdl	bdl	bdl	bdl	bdl	bdl	bdl	23	bdl	6.43	bdl	2.75	33.2	bdl	bdl	bdl
Ga	0.31	0.3	0.2	0.08	0.56	0.66	0.16	0.11	0.81	2.07	0.48	1.47	0.84	1.54	0.84	1.3	1.76	1.22
Rb	0.22	0.21	0.23	0.21	0.11	0.58	0.16	0.11	0.45	0.92	0.26	0.76	1.67	0.54	0.58	0.54	0.86	0.1
Sr	0.8	0.83	0.86	0.8	2.67	1.32	1.27	0.24	11.2	53.6	2.47	9.38	10.4	8.43	9.39	1.9	20.8	1.7
Y	0.52	3.35	13.3	13.1	1.84	3.35	0.68	0.37	2.51	4.13	6.52	22.2	9.81	16.4	30.5	19.8	17.3	16.6
Zr	1.1	1.23	0.88	0.44	1.36	1.38	0.74	0.74	3.73	1.64	1.27	4.03	3.53	1.54	2.87	1.25	3.95	2.71
Nb	0.43	0.43	0.26	bdl	0.23	0.34	bdl	0.22	bdl	bdl	0.3	bdl	0.21	bdl	bdl	bdl	0.77	bdl
Cs	0.02	0.02	0.02	0.02	0.01	0.03	0.01	0.01	0.01	0.02	0.02	0.03	0.07	0.03	0	0.03	0.06	bdl
Ba	0.32	bdl	0.57	0.5	bdl	0.33	bdl	0.4	5.81	11.8	2.25	14.9	20.9	11.5	1.86	bdl	0.72	bdl
La	0.46	0.44	0.48	0.53	2.29	1.54	0.81	0.22	3.77	6.3	0.96	14.2	1.74	3.08	4.35	2.45	4.43	3.82
Ce	1.11	1.1	1.19	1.24	5.12	3.5	1.47	0.54	11	13.4	2.59	29.6	4.18	6.36	7.95	5.06	12.2	9.24
Pr	0.14	0.14	0.16	0.18	0.65	0.47	0.21	0.06	0.73	1.43	0.37	3.56	0.56	0.75	1.1	0.68	1.58	1.22
Nd	0.6	0.59	0.75	0.81	2.55	2.08	0.88	0.23	2.76	5.49	1.66	13.6	2.6	3.36	4.71	2.93	6.8	5.27
Sm	0.16	0.16	0.19	0.23	0.51	0.56	0.19	0.05	0.52	1.08	0.42	2.55	0.65	0.83	1.23	0.74	1.57	1.2
Eu	0.05	0.05	0.06	0.07	0.13	0.17	0.1	0.02	0.16	0.28	0.12	0.56	0.18	0.18	0.36	0.18	0.39	0.33
Gd	0.15	0.22	0.32	0.34	0.41	0.61	0.2	0.08	0.54	0.97	0.46	2.12	0.75	0.99	1.53	0.89	1.52	1.2
Tb	bdl	0.02	0.04	0.05	0.04	0.08	bdl	bdl	0.07	0.13	0.07	0.33	0.1	0.16	0.3	0.15	0.23	0.19
Dy	0.13	0.13	0.16	0.18	0.37	0.67	0.13	0.05	0.45	0.82	0.32	1.38	0.66	0.96	1.62	0.74	1.18	0.92
Ho	0.02	0.02	0.03	0.03	0.07	0.12	0.02	0.01	0.09	0.15	0.06	0.23	0.11	0.19	0.33	0.14	0.2	0.16
Er	0.06	0.05	0.07	0.07	0.19	0.36	0.06	0.03	0.23	0.39	0.14	0.65	0.32	0.54	0.99	0.41	0.54	0.43
Tm	0	0.09	0.4	0.39	0.02	0.05	0.01	0.01	0.04	0.06	0.18	0.62	0.26	0.44	0.82	0.59	0.47	0.45
Yb	0.04	0.04	0.07	0.07	0.17	0.31	0.04	0.02	0.19	0.31	0.11	0.65	0.27	0.52	0.96	0.5	0.51	0.35
Lu	bdl	0.01	0.01	0.01	0.02	0.04	0	0	0.03	0.05	0.02	0.09	0.04	0.08	0.14	0.07	0.07	0.05
Hf	bdl	bdl	bdl	bdl	bdl	bdl	bdl	bdl	bdl	bdl	bdl	bdl	bdl	bdl	bdl	bdl	bdl	bdl
Ta	bdl	bdl	bdl	bdl	bdl	bdl	bdl	bdl	bdl	bdl	bdl	bdl	bdl	bdl	bdl	bdl	bdl	bdl
Pb	0.22	0.17	0.21	0.15	1.3	0.12	bdl	bdl	0.2	0.29	0.35	0.84	bdl	bdl	1.1	0.21	0.19	14.5
Th	0.2	0.24	0.27	0.27	0.48	0.57	0.16	0.07	0.46	1.37	0.53	2.5	0.57	0.79	1.03	0.75	3.15	1.04
U	0.04	0.04	0.03	0.02	0.07	0.06	0.02	bdl	0.19	0.11	0.08	0.21	0.23	0.21	0.21	0.14	0.68	0.28

	18A	19A	20A	21A	22A	23A	24A	25A	26A	26Arpt	27A	36A	28A	29A	30A	31A	32A	33A
Mg	438	383	614	516	322	606	321	280	38.6	36.8	71.4	38.4	27.2	69.5	21.7	108	55.7	67.9
Al	3530	3180	2470	4000	1050	1730	1820	1680	97.2	85.2	240	141	bdl	177	39.2	933	151	375
K	86.6	348	109	513	74.9	148	116	72.8	200	bdl	256	bdl	bdl	158	bdl	177	bdl	bdl
Ca	722	193	291	228	389	540	419	96.1	914	700	456	259	2370	684	bdl	341	693	562
Sc	1.83	1.72	2.17	3.36	1.61	2.07	1.07	1.7	2	bdl	2.19	bdl	bdl	bdl	bdl	bdl	bdl	bdl
Ti	17.4	36.6	15.1	87	24.8	7.04	7.01	12.5	bdl	bdl	bdl	bdl	6.23	bdl	bdl	bdl	bdl	bdl
V	16	17.9	18.4	25.9	18.8	10.1	8.78	10.5	0.83	bdl	2.36	1.23	bdl	2.68	bdl	2.25	0.65	2.7
Cr	2.34	3.24	2.2	4.9	2.6	1.57	1.67	1.95	bdl	bdl	bdl	bdl	bdl	bdl	bdl	bdl	bdl	bdl
Mn	153	194	182	179	145	281	144	276	9.16	8.31	27.3	17.4	1.33	18.2	23.2	38.4	13.6	44.1
Fe	9040	12100	11400	20200	8950	14800	8290	11400	387	335	904	361	bdl	993	bdl	2810	585	1950
Co	3.85	3.81	4.45	3.44	2.93	5.34	3.09	4.14	0.25	0.2	0.51	0.23	bdl	0.41	bdl	1.2	0.37	1
Ni	7.69	7.31	8.67	7.32	4.26	8.73	7.11	6.27	bdl	bdl	bdl	bdl	bdl	bdl	bdl	bdl	10	bdl
Cu	8.3	10.1	6.17	20.2	9.57	4.51	3.46	14	bdl	bdl	bdl	bdl	bdl	bdl	bdl	bdl	7.39	10
Zn	2.92	6.17	9.06	bdl	bdl	21.1	11.6	14.8	bdl	bdl	bdl	bdl	bdl	bdl	bdl	bdl	bdl	69.2
Ga	1.93	1.95	1.89	2.88	1.03	1.1	1.03	1.15	0.11	0.11	0.21	bdl	bdl	0.18	bdl	0.42	0.11	0.26
Rb	0.7	1.37	0.85	2.52	0.17	0.45	0.39	0.32	0.5	bdl	0.72	bdl	0.4	0.54	0.47	0.98	bdl	0.72
Sr	11.6	17.2	9	22.8	7.57	11.5	9.68	5.88	4.11	3.27	5.09	2.67	17.3	4.84	0.71	3.75	5.69	6.26
Y	17.4	16.4	17.8	18.1	6.16	6.59	6.86	8.87	2.51	10.5	2.35	11.4	1.84	3.08	2.47	4.75	3.28	5.25
Zr	2.21	2.73	2.52	4.69	2.33	1.96	1.5	2.03	0.49	bdl	bdl	bdl	bdl	0.85	0.69	1.43	0.86	1.52
Nb	0.25	0.43	0.26	0.99	bdl	bdl	bdl	bdl	bdl	bdl	bdl	bdl	bdl	bdl	bdl	bdl	bdl	bdl
Cs	0.03	0.05	0.04	0.08	bdl	0.01	0.01	0.01	bdl	bdl	0.02	0.02	bdl	bdl	bdl	0.02	0.01	0.02
Ba	14.1	0.28	bdl	bdl	bdl	7.47	bdl	14.2	4.3	4.15	2.36	3.47	bdl	1.84	2.95	2.23	8.54	1.49
La	5.23	3.48	5.24	4.88	5.5	4.92	3.29	4.18	0.47	0.43	0.98	0.64	0.03	1.32	0.2	2.43	0.5	1.42
Ce	11.4	8.08	11.1	11.5	12.1	9.97	7.55	9.37	0.97	0.9	2.14	1.37	0.05	2.7	0.43	5.22	1.13	3.39
Pr	1.42	1.11	1.44	1.66	1.54	1.21	1.02	1.22	0.11	0.11	0.29	0.18	0.01	0.35	0.05	0.68	0.15	0.42
Nd	5.96	4.94	5.89	7.26	6.32	4.82	4.4	5.17	0.49	0.46	1.15	0.73	bdl	1.4	0.22	2.87	0.61	1.73
Sm	1.28	1.11	1.29	1.71	1.32	0.98	0.98	1.16	0.12	0.11	0.24	0.17	bdl	0.29	0.04	0.62	0.14	0.36
Eu	0.32	0.27	0.31	0.41	0.31	0.27	0.25	0.3	0.03	0.02	0.06	0.04	0	0.07	0.02	0.15	0.03	0.09
Gd	1.3	1.06	1.3	1.54	1.12	0.96	0.97	1.15	bdl	0.36	0.27	0.42	bdl	0.36	0.17	0.69	0.27	0.52
Tb	0.19	0.17	0.2	0.23	0.16	0.2	0.2	0.23	bdl	bdl	bdl	bdl	bdl	0.13	bdl	0.21	bdl	0.22
Dy	1.01	0.78	1	1.19	0.87	0.81	0.78	0.88	0.09	0.07	0.17	0.12	bdl	0.2	0.04	0.42	0.11	0.31
Ho	0.17	0.13	0.18	0.2	0.15	0.15	0.13	0.16	bdl	bdl	bdl	bdl	bdl	bdl	bdl	0.07	bdl	0.05
Er	0.46	0.35	0.49	0.53	0.41	0.39	0.36	0.41	bdl	bdl	0.09	0.05	bdl	0.09	bdl	0.18	bdl	0.13
Tm	0.46	0.44	0.47	0.47	0.11	0.14	0.15	0.2	0.07	0.32	0.06	0.36	0.06	0.08	0.08	0.12	0.09	0.15
Yb	0.39	0.31	0.42	0.46	0.33	0.34	0.3	0.34	0.04	bdl	0.07	0.05	bdl	0.07	bdl	0.14	0.05	0.11
Lu	0.05	0.04	0.05	0.06	0.05	0.05	0.04	0.05	bdl	bdl	bdl	bdl	bdl	bdl	bdl	0.02	bdl	0.01
Hf	bdl	bdl	bdl	bdl	bdl	bdl	bdl	bdl	bdl	bdl	bdl	bdl	bdl	bdl	bdl	bdl	bdl	bdl
Ta	bdl	bdl	bdl	bdl	bdl	bdl	bdl	bdl	bdl	bdl	bdl	bdl	bdl	bdl	bdl	bdl	bdl	bdl
Pb	16.4	46.8	4.1	20.3	5.34	0.95	1.2	2.56	1.72	1.62	5.01	2.83	bdl	1.47	1.06	1.81	1.23	3.68
Th	1.04	1.25	1.28	2.26	1.43	1	0.87	1.19	0.2	0.18	0.27	0.2	0.1	0.4	0.2	0.73	0.28	0.65
U	0.21	0.19	0.17	0.36	0.21	0.11	0.14	0.13	0.02	0	0.04	0.03	bdl	0.06	0.02	0.05	bdl	0.04

Table E.7 - *The standard deviation from fraction 3, in mg/kg, from ICP-MS analysis. Concentrations below the detection limit (bdl) were recorded when: concentration – 3*sd – 3*blank sd < 0.*

	1A	1Arpt	16A	35A	2A	3A	4A	5A	6A	7A	8A	9A	10A	11A	12A	13A	14A	17A
Mg	0.5	0.5	0.5	0.5	0.4	3	0.4	0.3	20	10	0.8	3	0.4	40	9	3	20	0.4
Al	0.9	0.9	1	2	2	80	1	0.8	0.4	80	3	8	10	10	0.8	80	30	20
K	7	4	5	4	bdl	4	6	bdl	8	9	8	6	6	7	5	4	7	bdl
Ca	7	bdl	bdl	bdl	30	6	bdl	bdl	20	90	bdl	10	8	20	10	bdl	20	20
Sc	0.06	0.04	bdl	bdl	0.03	0.09	bdl	bdl	0.06	0.07	bdl	0.06	0.09	0.02	0.1	0.03	0.06	0.07
Ti	1	0.5	0.3	0.4	0.6	0.7	0.4	0.7	0.1	0.3	2	0.5	0.2	0.7	0.6	0.2	0.4	2
V	0.03	0.03	0.04	0.03	0.04	0.08	0.03	0.02	0.3	0.4	0.06	0.1	0.4	0.09	0.02	0.1	0.3	0.2
Cr	0.1	0.07	0.1	bdl	0.08	0.07	bdl	0.1	0.07	0.1	0.1	0.1	0.1	0.1	0.1	bdl	0.1	0.1
Mn	0.03	0.06	0.1	0.04	0.7	2	0.1	0.09	10	1	0.1	3	0.2	0.3	0.7	0.1	10	0.5
Fe	50	60	20	20	30	200	10	20	100	200	200	500	100	60	200	60	700	100
Co	0.009	0.01	0.005	0.003	0.009	0.004	0.02	0.01	0.02	0.2	0.03	0.01	0.04	0.003	0.02	0.005	0.06	0.01
Ni	0.07	0.07	0.07	bdl	0.2	0.1	0.2	bdl	0.2	0.2	0.1	0.2	0.3	0.1	0.2	0.2	0.3	0.1
Cu	0.1	bdl	bdl	bdl	bdl	bdl	bdl	0.1	0.3	bdl	bdl	bdl	0.1	bdl	0.5	0.1	0.09	0.2
Zn	bdl	bdl	bdl	bdl	bdl	bdl	bdl	bdl	bdl	0.9	bdl	2	bdl	0.6	0.9	bdl	bdl	bdl
Ga	0.02	0.02	0.005	0.005	0.01	0.006	0.009	0.002	0.03	0.03	0.02	0.003	0.02	0.03	0.004	0.003	0.03	0.01
Rb	0.01	0.04	0.01	0.01	0.02	0.04	0.01	0.03	0.02	0.01	0.03	0.02	0.01	0.03	0.02	0.04	0.03	0.03
Sr	0.008	0.02	0.02	0.03	0.04	0.05	0.02	0.009	0.03	0.008	0.03	0.06	0.04	0.06	0.1	0.03	0.4	0.07
Y	0.007	0.02	0.02	0.3	0.01	0.1	0.01	0.003	0.05	0.03	0.08	0.06	0.05	0.04	0.1	0.2	0.3	0.2
Zr	0.02	0.02	0.02	0.01	0.02	0.01	0.04	0.04	0.07	0.07	0.04	0.03	0.07	0.01	0.06	0.03	0.1	0.08
Nb	0.03	0.03	0.04	bdl	0.05	0.04	bdl	0.02	bdl	bdl	0.04	bdl	0.05	bdl	bdl	bdl	0.02	bdl
Cs	0.003	0.001	0.001	0.0003	0.001	0.004	0.0003	0.002	0.0003	0.003	0.002	0.001	0.002	0.0003	0.001	0.003	0.002	bdl
Ba	0.06	bdl	0.08	0.03	bdl	0.03	bdl	0.02	0.08	0.05	0.02	0.2	0.06	0.05	0.06	bdl	0.03	bdl
La	0.002	0.001	0.005	0.005	0.009	0.02	0.03	0.004	0.03	0.03	0.008	0.1	0.002	0.001	0.03	0.02	0.05	0.02
Ce	0.007	0.01	0.03	0.01	0.03	0.03	0.04	0.0006	0.1	0.07	0.02	0.2	0.02	0.004	0.1	0.004	0.08	0.1
Pr	0.002	0.002	0.005	0.003	0.002	0.006	0.0008	0.002	0.002	0.002	0.006	0.03	bdl	0.01	0.01	0.006	0.007	0.01
Nd	0.01	0.004	0.01	0.03	0.03	0.01	0.003	0.002	0.05	0.09	0.02	0.2	0.03	0.06	0.004	0.06	0.01	0.1
Sm	0.009	0.002	0.005	0.01	0.009	0.01	0.01	0.005	0.004	0.007	0.01	0.05	0.02	0.02	0.03	0.02	0.02	0.04
Eu	bdl	bdl	bdl	0.004	bdl	0.002	0.003	0.002	bdl	0.002	0.005	0.005	0.0008	0.0008	0.004	0.003	0.006	0.0008
Gd	0.01	0.03	0.01	0.01	0.004	0.003	0.02	0.006	0.003	0.006	0.01	0.02	0.03	0.02	0.02	0.02	0.01	0.03
Tb	bdl	0.002	0.003	0.002	0.004	0.007	bdl	bdl	0.005	0.003	0.005	0.004	0.004	0.003	0.003	0.007	0.02	0.003
Dy	0.004	0.004	0.004	0.003	0.005	0.01	0.01	0.003	0.004	0.02	0.008	0.02	0.009	0.004	0.01	0.01	0.009	0.03
Ho	0.0003	0.002	0.001	0.001	0.003	0.0003	0.001	0.0003	0.006	0.002	0.003	0.0003	0.001	0.002	0.002	0.005	0.001	0.003
Er	0.003	0.005	0.007	0.003	0.003	0.006	0.005	0.002	0.01	0.01	0.005	0.02	0.01	0.009	0.03	0.007	0.007	0.009
Tm	0.0009	0.003	0.01	0.007	0.00005	0.002	0.00005	0.002	0.002	0.004	0.0009	0.01	0.0009	0.004	0.005	0.005	0.009	0.002
Yb	0.003	0.001	0.003	0.002	0.003	0.01	0.007	0.002	0.009	0.01	0.006	0.02	0.006	0.03	0.007	0.008	0.01	0.005
Lu	bdl	0.001	0.001	0.0003	0.0003	0.0003	0.001	0.0003	0.001	0.001	0.0003	0.001	0.0003	0.003	0.001	0.001	0.003	0.003
Hf	bdl	bdl	bdl	bdl	bdl	bdl	bdl	bdl	bdl	bdl	bdl	bdl	bdl	bdl	bdl	bdl	bdl	bdl
Ta	bdl	bdl	bdl	bdl	bdl	bdl	bdl	bdl	bdl	bdl	bdl	bdl	bdl	bdl	bdl	bdl	bdl	bdl
Pb	0.01	0.01	0.02	0.01	0.03	0.02	bdl	bdl	0.01	0.01	0.02	0.04	bdl	bdl	0.03	0.02	0.02	0.1
Th	0.003	0.009	0.003	0.01	0.009	0.01	0.006	0.004	0.01	0.005	0.007	0.005	0.01	0.004	0.03	0.004	0.05	0.009
U	0.002	0.0008	0.0008	bdl	0.002	0.002	0.002	bdl	0.005	0.003	bdl	0.008	0.0008	0.002	0.002	0.003	0.008	0.004

	18A	19A	20A	21A	22A	23A	24A	25A	26A	26Arpt	27A	36A	28A	29A	30A	31A	32A	33A
Mg	6	4	5	4	8	5	2	1	0.6	2	1	1	0.4	0.9	0.4	2	3	1
Al	80	40	10	70	30	40	6	7	0.7	1	6	4	bdl	2	2	20	1	0.9
K	4	80	5	10	10	6	10	4	20	bdl	20	bdl	bdl	20	bdl	40	bdl	bdl
Ca	10	6	20	8	10	20	20	10	50	40	50	50	70	80	bdl	50	50	40
Sc	0.04	0.04	0.03	0.04	0.05	0.03	0.1	0.1	0.2	bdl	0.2	bdl	bdl	bdl	bdl	bdl	bdl	bdl
Ti	0.3	0.4	0.3	0.8	0.5	0.3	0.7	0.3	bdl	bdl	bdl	bdl	1	bdl	bdl	bdl	bdl	bdl
V	0.07	0.08	0.2	0.02	0.05	0.03	0.02	0.08	0.1	bdl	0.2	0.09	bdl	0.1	bdl	0.2	0.2	0.2
Cr	0.09	0.09	0.09	0.2	0.08	0.07	0.2	0.1	bdl	bdl	bdl	bdl	bdl	bdl	bdl	bdl	bdl	bdl
Mn	1	0.6	2	2	3	7	0.04	4	0.3	0.2	0.3	0.2	0.05	0.4	0.08	0.1	0.2	0.3
Fe	100	80	100	400	400	300	80	100	60	50	60	50	bdl	60	bdl	70	70	80
Co	0.03	0.01	0.01	0.005	0.06	0.04	0.03	0.02	0.02	0.02	0.04	0.05	bdl	0.01	bdl	0.09	0.01	0.04
Ni	0.09	0.2	0.2	0.1	0.2	0.2	0.09	0.1	bdl	bdl	bdl	bdl	bdl	bdl	bdl	bdl	0.8	bdl
Cu	0.1	0.3	0.3	0.6	0.7	0.2	0.09	0.09	bdl	bdl	bdl	bdl	bdl	bdl	bdl	bdl	1	1
Zn	0.7	0.9	1	bdl	bdl	0.7	2	0.6	bdl	bdl	bdl	bdl	bdl	bdl	bdl	bdl	bdl	2
Ga	0.07	0.006	0.02	0.006	0.05	0.01	0.03	0.006	0.02	0.02	0.01	bdl	bdl	0.01	bdl	0.008	0.008	0.04
Rb	0.03	0.01	0.02	0.03	0.02	0.02	0.03	0.01	0.09	bdl	0.2	bdl	0.07	0.07	0.1	0.09	bdl	0.09
Sr	0.04	0.1	0.07	0.04	0.1	0.04	0.01	0.05	0.2	0.2	0.1	0.2	0.04	0.1	0.09	0.1	0.2	0.2
Y	0.1	0.03	0.2	0.08	0.2	0.02	0.006	0.06	0.04	0.2	0.04	0.3	0.02	0.08	0.02	0.1	0.07	0.2
Zr	0.03	0.07	0.05	0.02	0.02	0.06	0.05	0.03	0.1	bdl	bdl	bdl	bdl	0.08	0.1	0.1	0.08	0.1
Nb	0.03	0.04	0.03	0.05	bdl	bdl	bdl	bdl	bdl	bdl	bdl	bdl	bdl	bdl	bdl	bdl	bdl	bdl
Cs	0.001	0.003	0.002	0.002	bdl	0.001	0.002	0.0003	bdl	bdl	0.001	0.005	bdl	bdl	bdl	0.005	0.001	0.005
Ba	0.08	0.01	bdl	bdl	bdl	0.1	bdl	0.3	0.2	0.2	0.2	0.1	bdl	0.1	0.2	0.2	0.1	0.08
La	0.07	0.03	0.06	0.06	0.04	0.008	0.05	0.02	0.007	0.007	0.01	0.01	0.003	0.01	0.02	0.04	0.02	0.05
Ce	0.03	0.01	0.1	0.04	0.05	0.06	0.05	0.09	0.01	0.01	0.03	0.03	0.007	0.04	0.01	0.02	0.02	0.01
Pr	0.02	0.0008	0.02	0.005	0.01	0.002	0.02	0.006	0.004	bdl	0.004	0.004	bdl	0.004	0.004	0.004	0.004	0.008
Nd	0.05	0.02	0.07	0.1	0.05	0.03	0.04	0.04	0.03	0.06	0.07	0.03	bdl	0.05	0.05	0.05	0.02	0.09
Sm	0.03	0.03	0.04	0.02	0.02	0.005	0.03	0.01	0.02	0.01	0.01	0.02	bdl	0.02	0.007	0.03	0.003	0.03
Eu	0.0008	0.008	0.004	0.005	0.01	0.003	0.01	0.002	bdl	bdl	0.004	bdl	bdl	0.004	bdl	bdl	0.004	0.008
Gd	0.02	0.02	0.007	0.04	0.003	0.02	0.01	0.01	bdl	0.05	0.03	0.03	bdl	0.01	0.02	0.05	0.05	0.01
Tb	0.003	0.003	0.007	0.005	0.006	0.003	0.01	0.01	bdl	bdl	bdl	bdl	bdl	0.01	bdl	0.02	bdl	0.01
Dy	0.02	0.006	0.03	0.02	0.02	0.008	0.03	0.02	0.02	0.01	0.01	0.03	bdl	0.02	0.01	0.02	0.02	0.02
Ho	0.002	0.003	0.006	0.003	0.003	0.002	0.0003	0.007	bdl	bdl	bdl	bdl	bdl	bdl	bdl	0.005	bdl	0.001
Er	0.008	0.006	0.02	0.008	0.02	0.006	0.007	0.01	bdl	bdl	0.02	0.009	bdl	0.007	bdl	0.01	bdl	0.009
Tm	0.008	0.01	0.008	0.002	0.006	0.00005	0.005	0.005	0.008	0.02	0.0003	0.01	0.008	0.004	0.004	0.004	0.008	0.008
Yb	0.01	0.003	0.01	0.01	0.007	0.005	0.006	0.006	0.005	bdl	0.01	0.01	bdl	0.01	bdl	0.005	0.009	0.01
Lu	0.0003	0.002	0.004	0.002	0.001	0.0003	0.001	0.0003	bdl	bdl	bdl	bdl	bdl	bdl	bdl	0.002	bdl	0.002
Hf	bdl	bdl	bdl	bdl	bdl	bdl	bdl	bdl	bdl	bdl	bdl	bdl	bdl	bdl	bdl	bdl	bdl	bdl
Ta	bdl	bdl	bdl	bdl	bdl	bdl	bdl	bdl	bdl	bdl	bdl	bdl	bdl	bdl	bdl	bdl	bdl	bdl
Pb	0.2	0.6	0.08	0.2	0.03	0.02	0.03	0.03	0.1	0.05	0.07	0.2	bdl	0.08	0.08	0.1	0.06	0.06
Th	0.01	0.007	0.02	0.01	0.003	0.01	0.009	0.02	0.03	0.009	0.03	0.01	0.01	0.03	0.02	0.01	0.03	0.04
U	bdl	0.004	0.004	0.01	bdl	bdl	0.003	0.0008	bdl	bdl	0.004	0.004	bdl	0.004	bdl	0.008	bdl	0.008

Table E.8 - *Trace elemental concentrations from fraction 4, in mg/kg, from ICP-MS analysis. Concentrations below the detection limit (bdl) were recorded when: concentration – 3*sd – 3*blank sd < 0.*

	1A	1Arpt	16A	35A	2A	3A	4A	5A	6A	7A	8A	9A	10A	11A	12A	13A	17A
Mg	482	494	344	288	442	161	49.5	167	3620	1730	29	198	137	395	143	142	158
Al	470	485	474	558	2110	523	349	154	4590	18600	460	3470	4380	5990	5660	7770	1750
K	108	105	85.5	102	78.7	206	88.6	82.6	235	882	141	310	782	302	427	258	46.3
Ca	974	986	1030	1180	1820	234	1090	113	15100	13800	1130	242	858	991	519	268	361
Sc	0.78	0.65	0.44	0.44	0.58	0.26	0.49	bdl	3.41	6.52	bdl	0.86	1.46	1.29	1.25	1.1	bdl
Ti	26.1	25.9	16.6	12.8	10.6	28.2	7.29	8.95	52.5	157	34.1	20.6	68.4	33.4	15	39.4	184
V	1.78	1.81	1.62	2.03	1.42	1.05	0.51	0.63	5.02	19.6	2.56	4.64	10.5	2.72	1.93	1.79	4.18
Cr	bdl	0.27	bdl	bdl	bdl	bdl	bdl	bdl	1.64	12.4	0.29	1.47	0.58	0.96	1.08	0.32	4.21
Mn	2.65	2.74	2.35	2.44	23.9	6.12	2.68	1.68	264	106	5	28.2	8.41	34.7	9.26	12.3	18.7
Fe	127	145	91.8	73.8	143	169	494	59.6	2640	3670	147	327	742	2070	988	1540	924
Co	0.1	0.09	0.03	bdl	0.49	0.07	0.79	0.09	2.07	2.2	0.29	0.61	0.59	2.68	1.37	1.63	0.92
Ni	0.49	0.46	0.25	0.18	1.7	0.63	2.76	0.58	5.73	5.5	0.65	1.93	2.45	22	13.5	17.7	2.11
Cu	0.64	0.71	0.61	0.48	2.75	0.51	11.6	6.29	0.97	6.32	0.27	1.12	3.63	57.6	5.71	38.9	2.68
Zn	bdl	0.51	1.08	1.15	0.72	bdl	bdl	2.81	6.7	13.4	1.09	8.94	1.29	6.62	13.3	2.27	12.8
Ga	0.4	0.41	0.39	0.43	0.46	0.1	0.35	0.03	1.26	2.29	0.28	0.67	0.44	0.62	0.42	0.3	0.31
Rb	0.16	0.13	bdl	0.12	bdl	0.73	bdl	bdl	3.05	15.5	0.36	4.88	9.14	4.27	6.05	3.71	0.15
Sr	10.9	11	11.4	13.9	13.6	4.03	12.7	1.21	111	157	15.1	8.86	12.7	18.6	11	5.92	2.58
Y	4.67	4.45	4.58	5.6	bdl	bdl	6.39	bdl	12.3	4.18	2.75	1.19	3.21	3.42	1.04	bdl	bdl
Zr	0.15	0.14	0.08	0.05	0.19	0.13	0.46	0.11	1.31	3.07	0.11	0.46	0.52	2.06	2.44	2.33	1.18
Nb	0.18	0.18	0.13	0.15	0.07	0.07	0.05	0.09	0.11	0.39	0.18	0.06	0.16	0.13	0.06	0.1	0.38
Cs	0.05	0.04	0.03	0.04	0.02	0.08	0.03	0.02	0.21	1.54	0.06	0.52	0.82	0.6	0.26	0.44	0.03
Ba	9.11	9.15	9.13	11.2	5.91	6.35	4.2	3.63	83	33	10.3	23	50.7	51.9	38.6	23.4	18.4
La	7.08	7.11	6.52	6.95	2.92	1.1	6.65	0.34	25.1	13.3	3.98	11.1	5.06	8.52	3.66	2.58	2.12
Ce	16.7	16.4	15.4	16.8	6.04	2.71	12.4	0.8	52.1	27	11.9	21.1	12.3	13.9	8	4.59	4.27
Pr	2.45	2.5	2.31	2.54	0.8	0.41	2.63	0.13	7.21	3.82	1.67	2.72	1.79	2.04	1.34	0.68	0.6
Nd	10.8	11.1	10.2	11.3	3.03	1.86	11.9	0.6	28.6	15.2	7.53	9.98	7.98	8.58	6.19	2.83	2.46
Sm	2.95	2.96	2.79	3.13	0.66	0.53	3.25	0.19	6.18	3.41	2.11	2.06	2.18	2.22	1.76	0.73	0.57
Eu	0.75	0.74	0.71	0.81	0.16	0.11	0.84	0.03	1.63	0.71	0.55	0.44	0.55	0.44	0.45	0.15	0.11
Gd	2.9	2.87	2.69	3.08	0.4	0.35	3.31	bdl	5.95	2.81	2	1.56	2.11	2.16	1.62	0.52	0.31
Tb	0.4	0.37	0.37	0.43	0.08	0.08	0.48	0.03	0.82	0.39	0.3	0.23	0.35	0.27	0.21	0.07	0.03
Dy	2.19	2.17	2.11	2.42	0.48	0.4	2.63	0.17	4	1.91	1.59	1.03	1.68	1.7	1.22	0.6	0.4
Ho	0.33	0.34	0.33	0.39	0.07	0.05	0.41	0.04	0.65	0.36	0.29	0.18	0.3	0.28	0.18	0.09	0.06
Er	0.66	0.63	0.63	0.77	0.08	bdl	0.92	bdl	1.37	0.6	0.45	0.28	0.54	0.59	0.25	0.09	bdl
Tm	bdl	bdl	bdl	bdl	bdl	bdl	bdl	bdl	bdl	bdl	bdl	bdl	bdl	bdl	bdl	bdl	bdl
Yb	0.32	0.31	0.31	0.39	0.13	0.03	0.52	bdl	0.73	0.4	0.27	0.23	0.36	0.45	0.18	0.13	0.04
Lu	0.02	0.01	0.01	0.02	bdl	bdl	0.04	bdl	0.08	0.03	0.01	bdl	0.03	0.03	bdl	bdl	bdl
Hf	bdl	bdl	bdl	bdl	bdl	bdl	bdl	bdl	bdl	bdl	bdl	bdl	bdl	bdl	bdl	bdl	bdl
Ta	bdl	bdl	bdl	bdl	bdl	bdl	bdl	bdl	bdl	bdl	bdl	bdl	bdl	bdl	bdl	bdl	0.01
Pb	0.42	0.43	0.33	0.37	3.87	1.08	0.08	bdl	10.4	3.44	0.44	2.71	6.87	2.25	9.9	1.58	24.5
Th	0.91	0.87	0.67	0.72	bdl	bdl	0.34	bdl	0.97	3.84	0.08	0.27	0.13	0.97	0.4	0.06	bdl
U	0.17	0.18	0.17	0.19	0.09	0.02	0.2	0.01	0.36	0.3	0.25	0.1	0.3	0.23	0.11	0.09	0.11

	18A	19A	20A	21A	22A	23A	24A	25A	26A	26Arpt	27A	36A	28A	29A	30A	31A	32A	33A
Mg	547	317	554	390	480	895	443	328	43.4	41	82.2	59.3	4.69	104	32.5	225	50.1	87.1
Al	6650	5850	6970	5910	2860	7250	5950	5000	398	418	879	647	12.5	774	121	2430	475	1120
K	328	331	363	476	231	536	402	228	bdl	bdl	78.9	bdl	bdl	57.9	bdl	157	49.5	bdl
Ca	2310	1740	2580	1330	2040	3260	2140	2200	389	197	210	113	2890	446	201	472	186	470
Sc	0.49	0.36	1.21	1.23	0.66	1.77	0.57	1.12	bdl	bdl	bdl	bdl	bdl	bdl	bdl	bdl	bdl	bdl
Ti	86.1	99.6	75.6	127	106	56.9	77.1	41.3	8.71	9.62	18.7	13.4	bdl	27.5	13.6	25.8	11.5	23.3
V	8.29	6.58	5.05	5.72	4.33	5.28	5.62	3.22	0.78	0.76	1.68	1.25	0.83	1.89	0.45	2.89	1.18	1.59
Cr	3.38	2.87	1.99	3.13	1.89	3.98	2.03	2.16	bdl	bdl	bdl	bdl	bdl	2.51	bdl	1.82	bdl	1.13
Mn	30	27.9	29	27.4	26.1	74.2	46.1	45.8	11.5	11.8	17	19.8	0.28	17.4	11.8	20.6	19.7	34
Fe	1770	1540	1570	2060	817	3660	1740	1350	bdl	182	291	205	bdl	258	140	1110	264	471
Co	2.32	1.38	1.77	1.47	0.93	3.44	1.84	1.64	bdl	bdl	0.28	bdl	bdl	0.24	0.14	0.56	bdl	0.22
Ni	9.94	7.57	9.78	14.4	3.77	19.9	8.39	10.5	0.73	0.52	1.22	0.54	bdl	0.9	0.41	3.5	5.88	1.34
Cu	13	9.43	12.7	17.3	3.01	14.3	8.15	5.91	1.26	bdl	1.08	bdl	bdl	1.83	bdl	1.4	1.3	1.35
Zn	24	14.1	12.3	10.7	9.81	19.3	21	9.3	6.27	bdl	bdl	bdl	bdl	bdl	bdl	7.6	2.91	13.4
Ga	0.9	0.67	0.93	0.68	0.55	1.05	0.81	0.56	0.05	bdl	0.11	0.07	bdl	0.12	bdl	0.27	0.06	0.13
Rb	4.16	4.08	5.73	6.38	2.05	5.56	3.28	2.61	bdl	bdl	0.42	bdl	bdl	bdl	bdl	bdl	bdl	bdl
Sr	31.2	33.5	35.6	30.7	26.8	38.7	30.9	22.5	3.32	1.49	4.4	2.09	25.8	6.65	1.65	4	2.3	2.52
Y	2.21	3.28	3.32	1.49	2.21	3.03	2.03	3.59	bdl	bdl	bdl	bdl	bdl	bdl	bdl	bdl	bdl	bdl
Zr	2.02	2.18	2.1	4.23	1.57	3.41	2.74	1.66	0.27	0.21	bdl	0.21	bdl	0.38	0.19	0.62	bdl	0.38
Nb	0.49	0.52	0.38	0.66	0.33	0.22	0.39	0.16	bdl	bdl	0.09	bdl	bdl	0.07	bdl	0.07	bdl	bdl
Cs	0.51	0.58	0.6	1.04	0.17	0.45	0.35	0.24	bdl	bdl	0.04	0.03	bdl	0.04	bdl	0.12	bdl	0.04
Ba	35.2	38.4	51.7	69	30.5	52.2	35.6	42.4	5.24	4.41	7.83	6.41	2.4	8.89	2.47	9	6.51	10.1
La	6.77	5.66	9.06	5.3	6.82	9.38	7.15	7.64	0.25	0.2	0.43	0.26	bdl	0.71	0.09	1.29	0.27	0.64
Ce	14.8	12.4	19.1	10.9	13.5	19.9	16.7	15.6	0.52	0.32	0.89	0.47	bdl	1.5	0.19	2.61	0.52	1.35
Pr	2.09	1.83	2.75	1.66	1.92	2.84	2.38	2.24	0.07	0.06	0.11	0.08	bdl	0.2	0.03	0.37	0.08	0.18
Nd	8.62	7.9	11.3	6.96	7.86	11.8	9.9	9.23	0.26	0.25	0.43	0.34	bdl	0.86	0.1	1.61	0.37	0.8
Sm	2.11	2.01	2.74	1.71	1.93	2.78	2.38	2.3	0.07	0.06	0.11	0.09	bdl	0.22	bdl	0.34	0.08	0.18
Eu	0.46	0.5	0.59	0.41	0.42	0.64	0.54	0.57	bdl	bdl	bdl	bdl	bdl	0.06	bdl	bdl	bdl	bdl
Gd	1.92	1.99	2.46	1.45	1.75	2.47	2.12	2.15	1.38	bdl	1.16	bdl	1.33	1.74	1.22	bdl	bdl	bdl
Tb	0.24	0.26	0.32	0.19	0.23	0.31	0.27	0.29	0.08	bdl	0.19	bdl	0.12	0.14	0.6	bdl	0.33	0.46
Dy	1.37	1.56	1.76	1.19	1.37	1.71	1.48	1.63	0.07	bdl	0.1	bdl	0.04	0.2	bdl	0.2	bdl	0.12
Ho	0.21	0.24	0.27	0.19	0.21	0.26	0.22	0.26	bdl	bdl	bdl	bdl	bdl	bdl	bdl	0.35	bdl	bdl
Er	0.35	0.42	0.48	0.31	0.38	0.44	0.38	0.5	bdl	bdl	bdl	bdl	bdl	bdl	bdl	bdl	bdl	bdl
Tm	bdl	bdl	bdl	bdl	bdl	bdl	bdl	bdl	bdl	bdl	bdl	bdl	bdl	bdl	bdl	bdl	bdl	bdl
Yb	0.21	0.25	0.28	0.23	0.24	0.28	0.26	0.31	bdl	bdl	bdl	bdl	bdl	bdl	bdl	bdl	bdl	bdl
Lu	bdl	bdl	0.01	bdl	bdl	0.01	bdl	0.02	bdl	bdl	bdl	bdl	bdl	bdl	bdl	bdl	bdl	bdl
Hf	bdl	bdl	bdl	bdl	bdl	bdl	bdl	bdl	0.71	bdl	0.57	bdl	0.74	0.78	0.62	bdl	bdl	bdl
Ta	0.01	0.01	bdl	0.01	0	bdl	0	bdl	bdl	bdl	bdl	bdl	bdl	bdl	bdl	bdl	bdl	bdl
Pb	26.9	57.2	15.9	66.2	11.2	8.56	4.19	9.59	1.27	0.48	3.3	1.53	bdl	1.32	0.92	1.43	0.56	2.12
Th	0.22	bdl	1.23	0.32	0.41	1.8	0.37	0.48	bdl	bdl	bdl	bdl	bdl	bdl	bdl	bdl	bdl	bdl
U	0.28	0.21	0.31	0.27	0.27	0.21	0.19	0.2	bdl	bdl	bdl	bdl	bdl	0.05	0.01	bdl	bdl	bdl

Table E.9 - *The standard deviation from fraction 4, in mg/kg, from ICP-MS analysis. Concentrations below the detection limit (bdl) were recorded when: concentration – 3*sd – 3*blank sd < 0.*

	1A	1Arpt	16A	35A	2A	3A	4A	5A	6A	7A	8A	9A	10A	11A	12A	13A	17A
Mg	4	10	5	2	10	2	2	5	8	8	0.3	3	1	3	1	3	0.7
Al	2	9	8	6	30	10	7	4	9	80	0.2	60	5	90	60	200	40
K	3	7	4	3	5	5	5	4	3	2	4	9	3	3	7	10	7
Ca	6	20	10	20	6	9	30	10	10	100	6	8	5	10	10	10	10
Sc	0.06	0.1	0.03	0.05	0.05	0.05	0.09	bdl	0.05	0.1	bdl	0.06	0.04	0.05	0.06	0.03	bdl
Ti	0.2	1	0.4	0.05	0.3	0.5	0.3	0.6	0.2	0.7	0.3	0.7	0.1	0.1	1	0.3	2
V	0.02	0.04	0.009	0.03	0.01	0.03	0.008	0.003	0.06	0.05	0.02	0.05	0.07	0.004	0.008	0.009	0.04
Cr	bdl	0.06	bdl	bdl	bdl	bdl	bdl	bdl	0.1	0.1	0.04	0.07	0.05	0.06	0.05	0.05	0.1
Mn	0.08	0.06	0.08	0.06	0.05	0.09	0.04	0.04	4	0.05	0.009	0.2	0.03	0.4	0.1	0.2	0.5
Fe	9	20	10	9	10	10	7	10	40	20	7	10	20	20	20	20	40
Co	0.004	0.009	0.005	bdl	0.02	0.005	0.01	0.01	0.03	0.03	0.02	0.007	0.03	0.04	0.01	0.03	0.03
Ni	0.03	0.02	0.02	0.01	0.05	0.02	0.02	0.02	0.1	0.09	0.01	0.07	0.03	0.2	0.07	0.09	0.05
Cu	0.06	0.06	0.1	0.06	0.1	0.03	0.04	0.4	0.03	0.04	0.03	0.05	0.05	0.2	0.04	0.2	0.08
Zn	bdl	0.08	0.07	0.08	0.08	bdl	bdl	0.1	0.2	0.4	0.1	0.07	0.09	0.09	0.06	0.08	0.1
Ga	0.01	0.003	0.006	0.0002	0.005	0.003	0.002	0.003	0.003	0.01	0.007	0.005	0.004	0.01	0.007	0.008	0.01
Rb	0.007	0.03	bdl	0.02	bdl	0.04	bdl	bdl	0.1	0.04	0.02	0.02	0.02	0.07	0.2	0.06	0.03
Sr	0.04	0.1	0.05	0.02	0.1	0.01	0.03	0.04	2	0.03	0.3	0.01	0.1	0.09	0.3	0.05	0.1
Y	0.05	0.1	0.1	0.06	bdl	bdl	0.1	bdl	0.05	0.05	0.07	0.09	0.07	0.07	0.06	bdl	bdl
Zr	0.005	0.0009	0.004	0.0009	0.003	0.0005	0.005	0.002	0.04	0.05	0.002	0.005	0.008	0.02	0.02	0.03	0.05
Nb	0.004	0.003	0.008	0.003	0.003	0.003	0.004	0.007	0.002	0.002	0.002	0.0007	0.01	0.001	0.007	0.002	0.01
Cs	0.001	0.002	0.001	0.004	0.0008	0.001	0.001	0.001	0.002	0.03	0.0008	0.008	0.003	0.004	0.01	0.006	0.002
Ba	0.3	0.1	0.07	0.1	0.09	0.06	0.04	0.05	1	0.8	0.04	0.4	1	1	0.06	0.8	0.06
La	0.002	0.1	0.009	0.1	0.01	0.01	0.04	0.005	0.1	0.1	0.04	0.3	0.1	0.09	0.08	0.07	0.04
Ce	0.006	0.2	0.2	0.1	0.1	0.04	0.1	0.01	0.4	0.6	0.2	0.06	0.2	0.3	0.08	0.1	0.03
Pr	0.02	0.02	0.006	0.0008	0.003	0.007	0.02	0.002	0.1	0.05	0.03	0.01	0.03	0.06	0.02	0.01	0.002
Nd	0.03	0.2	0.06	0.1	0.06	0.06	0.2	0.004	0.4	0.008	0.2	0.05	0.08	0.2	0.04	0.1	0.04
Sm	0.05	0.02	0.05	0.01	0.01	0.02	0.02	0.007	0.1	0.05	0.06	0.02	0.03	0.05	0.02	0.01	0.02
Eu	0.007	0.01	0.02	0.006	0.002	0.007	0.005	0.002	0.01	0.01	0.01	0.02	0.002	0.02	0.01	0.01	0.003
Gd	0.08	0.02	0.04	0.07	0.05	0.02	0.08	bdl	0.1	0.04	0.02	0.04	0.02	0.08	0.03	0.03	0.02
Tb	0.009	0.005	0.008	0.008	0.004	0.01	0.02	0.005	0.008	0.006	0.01	0.007	0.004	0.007	0.008	0.006	0.005
Dy	0.02	0.01	0.02	0.03	0.007	0.02	0.08	0.008	0.03	0.02	0.02	0.02	0.02	0.05	0.009	0.02	0.007
Ho	0.004	0.003	0.002	0.006	0.002	0.003	0.02	0.004	0.01	0.01	0.004	0.006	0.002	0.006	0.003	0.004	0.003
Er	0.01	0.02	0.01	0.01	0.01	bdl	0.01	bdl	0.02	0.02	0.01	0.01	0.02	0.04	0.01	0.009	bdl
Tm	bdl	bdl	bdl	bdl	bdl	bdl	bdl	bdl	bdl	bdl	bdl	bdl	bdl	bdl	bdl	bdl	bdl
Yb	0.007	0.01	0.02	0.008	0.006	0.006	0.03	bdl	0.01	0.01	0.004	0.005	0.009	0.006	0.01	0.004	0.005
Lu	0.003	0.003	0.002	0.004	bdl	bdl	0.002	bdl	0.004	0.003	0.003	bdl	0.002	0.004	bdl	bdl	bdl
Hf	bdl	bdl	bdl	bdl	bdl	bdl	bdl	bdl	bdl	bdl	bdl	bdl	bdl	bdl	bdl	bdl	bdl
Ta	bdl	bdl	bdl	bdl	bdl	bdl	bdl	bdl	bdl	bdl	bdl	bdl	bdl	bdl	bdl	bdl	0.001
Pb	0.01	0.01	0.03	0.02	0.04	0.03	0.01	bdl	0.2	0.04	0.01	0.04	0.2	0.03	0.02	0.03	0.5
Th	0.03	0.01	0.02	0.01	bdl	bdl	0.01	bdl	0.02	0.06	0.008	0.01	0.006	0.04	0.008	0.006	bdl
U	0.003	0.005	0.006	0.008	0.002	0.001	0.004	0.002	0.007	0.004	0.002	0.002	0.002	0.008	0.004	0.004	0.0007

	18A	19A	20A	21A	22A	23A	24A	25A	26A	26Arpt	27A	36A	28A	29A	30A	31A	32A	33A
Mg	20	7	4	4	20	7	5	2	0.9	0.7	2	0.8	1	2	2	3	0.8	2
Al	200	200	80	80	50	90	100	90	5	8	10	1	2	10	5	4	0.9	20
K	10	20	10	10	20	2	2	2	bdl	bdl	20	bdl	bdl	10	bdl	10	10	bdl
Ca	30	20	60	20	6	10	10	30	70	50	40	30	70	50	40	80	40	30
Sc	0.03	0.05	0.04	0.06	0.04	0.05	0.05	0.06	bdl	bdl	bdl	bdl	bdl	bdl	bdl	bdl	bdl	bdl
Ti	2	3	1	2	1	0.3	2	0.9	0.3	0.3	1	1	bdl	3	0.8	2	1	0.3
V	0.04	0.2	0.02	0.1	0.005	0.007	0.04	0.007	0.04	0.06	0.03	0.01	0.05	0.04	0.02	0.03	0.06	0.05
Cr	0.06	0.08	0.06	0.08	0.05	0.08	0.05	0.04	bdl	bdl	bdl	bdl	bdl	0.2	bdl	0.3	bdl	0.2
Mn	0.04	0.5	0.1	0.4	0.3	0.2	0.5	0.3	0.1	0.2	0.05	0.2	0.05	0.09	0.1	0.4	0.1	0.1
Fe	20	40	20	40	20	20	20	20	bdl	40	50	50	bdl	30	40	50	50	50
Co	0.02	0.05	0.05	0.05	0.02	0.006	0.01	0.03	bdl	bdl	0.03	bdl	bdl	0.03	0.02	0.03	bdl	0.04
Ni	0.04	0.2	0.08	0.5	0.07	0.1	0.06	0.2	0.2	0.04	0.08	0.1	bdl	0.1	0.04	0.1	0.2	0.2
Cu	0.1	0.2	0.3	0.6	0.03	0.2	0.05	0.1	0.3	bdl	0.1	bdl	bdl	0.3	bdl	0.2	0.1	0.3
Zn	0.07	0.3	0.2	0.1	0.3	0.4	0.2	0.3	0.3	bdl	bdl	bdl	bdl	bdl	bdl	0.3	0.3	0.4
Ga	0.01	0.006	0.02	0.02	0.02	0.02	0.02	0.003	0.001	bdl	0.009	0.01	bdl	0.01	bdl	0.009	0.007	0.003
Rb	0.01	0.08	0.09	0.008	0.007	0.05	0.09	0.01	bdl	bdl	0.03	bdl	bdl	bdl	bdl	bdl	bdl	bdl
Sr	0.1	0.3	0.2	0.09	0.5	0.6	0.07	0.1	0.05	0.1	0.1	0.04	0.4	0.1	0.1	0.1	0.06	0.06
Y	0.04	0.07	0.04	0.03	0.09	0.08	0.09	0.07	bdl	bdl	bdl	bdl	bdl	bdl	bdl	bdl	bdl	bdl
Zr	0.01	0.2	0.03	0.07	0.004	0.06	0.001	0.04	0.02	0.04	bdl	0.03	bdl	0.02	0.007	0.03	bdl	0.007
Nb	0.006	0.0007	0.005	0.01	0.004	0.001	0.006	0.002	bdl	bdl	0.01	bdl	bdl	0.01	bdl	0.006	bdl	bdl
Cs	0.001	0.01	0.01	0.0008	0.0008	0.002	0.001	0.003	bdl	bdl	0.004	0.006	bdl	0.004	bdl	0.006	bdl	0.002
Ba	0.3	0.2	0.7	0.4	0.04	0.2	0.8	0.2	0.4	0.3	0.2	0.1	0.1	0.6	0.6	0.2	0.3	0.4
La	0.07	0.003	0.1	0.03	0.004	0.08	0.2	0.07	0.02	0.005	0.009	0.01	bdl	0.04	0.02	0.02	0.005	0.02
Ce	0.06	0.04	0.2	0.06	0.02	0.1	0.3	0.4	0.01	0.01	0.02	0.01	bdl	0.03	0.01	0.1	0.02	0.03
Pr	0.02	0.03	0.03	0.003	0.002	0.02	0.04	0.03	0.006	0.006	0.008	0.004	bdl	0.004	0.004	0.02	0.004	0.002
Nd	0.06	0.06	0.04	0.03	0.06	0.05	0.2	0.09	0.01	0.01	0.01	0.04	bdl	0.05	0.02	0.02	0.009	0.03
Sm	0.04	0.007	0.03	0.03	0.03	0.05	0.04	0.1	0.008	0.009	0.02	0.01	bdl	0.02	bdl	0.03	0.003	0.01
Eu	0.002	0.004	0.002	0.006	0.005	0.004	0.02	0.004	bdl	bdl	bdl	bdl	bdl	0.01	bdl	bdl	bdl	bdl
Gd	0.02	0.03	0.06	0.04	0.07	0.03	0.02	0.03	0.1	bdl	0.09	bdl	0.2	0.1	0.2	bdl	bdl	bdl
Tb	0.01	0.008	0.009	0.004	0.005	0.007	0.01	0.01	0.02	bdl	0.02	bdl	0.02	0.02	0.03	bdl	0.02	0.03
Dy	0.04	0.02	0.05	0.01	0.03	0.03	0.03	0.02	0.01	bdl	0.02	bdl	0.009	0.02	bdl	0.02	bdl	0.02
Ho	0.004	0.008	0.0007	0.005	0.003	0.008	0.007	0.003	bdl	bdl	bdl	bdl	bdl	bdl	bdl	0.01	bdl	bdl
Er	0.01	0.02	0.03	0.01	0.01	0.02	0.02	0.008	bdl	bdl	bdl	bdl	bdl	bdl	bdl	bdl	bdl	bdl
Tm	bdl	bdl	bdl	bdl	bdl	bdl	bdl	bdl	bdl	bdl	bdl	bdl	bdl	bdl	bdl	bdl	bdl	bdl
Yb	0.01	0.01	0.009	0.01	0.006	0.008	0.007	0.007	bdl	bdl	bdl	bdl	bdl	bdl	bdl	bdl	bdl	bdl
Lu	bdl	bdl	0.002	bdl	bdl	0.002	bdl	0.002	bdl	bdl	bdl	bdl	bdl	bdl	bdl	bdl	bdl	bdl
Hf	bdl	bdl	bdl	bdl	bdl	bdl	bdl	bdl	0.05	bdl	0.07	bdl	0.03	0.06	0.1	bdl	bdl	bdl
Ta	0.002	0.001	bdl	0.002	bdl	bdl	0.0007	bdl	bdl	bdl	bdl	bdl	bdl	bdl	bdl	bdl	bdl	bdl
Pb	0.2	0.7	0.2	0.6	0.06	0.1	0.03	0.1	0.06	0.04	0.08	0.08	bdl	0.1	0.09	0.08	0.05	0.05
Th	0.03	bdl	0.02	0.02	0.004	0.008	0.006	0.02	bdl	bdl	bdl	bdl	bdl	bdl	bdl	bdl	bdl	bdl
U	0.004	0.002	0.004	0.004	0.0007	0.0003	0.008	0.005	bdl	bdl	bdl	bdl	bdl	0.006	0.002	bdl	bdl	bdl

Table E.10 - *Trace elemental concentrations from fraction 5, in mg/kg, from ICP-MS analysis. Concentrations below the detection limit (bdl) were recorded when: concentration – 3*sd – 3*blank sd < 0.*

	1A	16A	2A	3A	4A	5A	6A	7A	8A	9A	10A	11A	12A	13A	17A	18A
Mg	2240	2070	4270	2370	1750	1490	7260	1960	2090	1110	1570	1790	1900	1780	564	1870
Al	29600	24300	19600	22200	23500	29600	10700	18600	23300	24900	23900	23900	26200	22500	6030	20500
K	5000	4250	4240	4310	4710	4530	1970	4250	3540	4210	3450	4220	4320	3270	1450	3720
Ca	813	825	7560	450	591	555	287	1320	316	331	274	471	146	222	508	1350
Sc	21.7	19.7	21.2	21.1	21.5	20.8	10.6	12.2	18.8	18.1	21.9	16.9	17.7	17.4	3.11	17.2
Ti	9020	7360	5090	5940	6280	10500	3440	6680	9130	7570	9360	6650	8880	7830	3590	6900
V	190	179	158	137	174	195	80.4	134	133	178	225	192	187	164	39.9	161
Cr	145	137	157	150	166	142	80.9	136	127	159	145	158	142	129	50.1	145
Mn	149	143	1240	589	203	404	2550	434	278	527	210	280	79.8	335	130	424
Fe	9350	8210	14800	14600	6990	8420	56100	5660	7230	6800	8610	5680	9980	6110	2780	11000
Co	33.5	29.7	32.1	28.7	27.4	30	17	25.8	30.5	24.9	54.7	17.7	11.6	20.1	5.27	25.1
Ni	125	116	125	123	118	107	62.9	106	102	122	156	75.8	74	63.8	21.7	108
Cu	77.7	64.8	41.9	50.3	51.9	66.2	24.7	37.2	50.2	53.6	61.2	30.2	29.8	16.7	7.78	48.8
Zn	144	150	65.3	125	112	126	39.5	61.4	132	95.9	165	95.5	65.8	84.6	25.1	159
Ga	34.4	33.3	39.6	29.6	29.7	34.8	13.5	25.4	32.7	31.6	33.5	32.6	30.4	31.8	7.4	28.8
Rb	129	135	145	146	158	113	71.7	151	113	140	114	129	123	97.1	29.5	122
Sr	270	298	267	129	213	209	32.8	151	209	132	113	194	91.7	154	78.2	202
Y	35.8	35.9	24.8	31	34.7	39.1	8.89	18.5	29.8	27.9	38.8	30.5	27.5	31.2	13.5	28.7
Zr	230	212	143	177	239	282	113	176	222	206	250	206	204	207	194	208
Nb	32.2	30.4	19.2	23.1	35.3	42.3	12.4	24.5	37.1	29.3	36.4	27.7	29.9	32	11.2	29
Cs	10.9	10.6	9.61	10.2	15.8	9.21	5.57	12.6	7.45	11.8	8.42	9.69	9.66	6.78	1.21	8.92
Ba	523	567	482	431	496	413	193	448	428	504	760	458	286	331	253	451
La	49.9	52.5	32.9	42.4	41	53.9	7.77	14.4	43.4	19.2	48.9	44.9	41.1	44	19	35.9
Ce	94.9	95.5	61.7	82.6	81.9	110	13.9	30.7	82.9	39.6	88.3	86.1	81.1	87.8	37.4	66.9
Pr	12.5	12.6	8.47	10.7	10.2	14	1.7	3.45	10.5	4.99	12.3	11.4	10.4	11.4	4.74	8.54
Nd	46.3	46.7	32.9	39.9	38.3	52.4	6.02	12.2	39	18.4	45.4	43	37.5	43.5	17.9	31.2
Sm	8.06	8.38	6.15	7.22	6.92	10	1.07	2.13	6.82	3.47	8.24	7.45	6.33	7.9	3.13	5.43
Eu	1.92	1.98	1.43	1.67	1.52	2.39	0.27	0.52	1.62	0.84	1.98	1.89	1.5	1.93	0.54	1.33
Gd	6.85	7.35	5.56	6.31	6.12	8.53	1.03	2.03	5.78	3.43	7.06	6.08	5.06	6.5	2.7	4.79
Tb	1.01	1.07	0.8	0.93	0.95	1.32	0.17	0.36	0.86	0.63	1.06	0.88	0.78	0.96	0.39	0.74
Dy	5.85	6.09	4.4	5.24	5.61	7.2	1.2	2.57	5.06	4.26	6.25	4.92	4.39	5.4	2.22	4.5
Ho	1.21	1.25	0.88	1.07	1.2	1.42	0.29	0.62	1.07	0.96	1.31	1	0.91	1.09	0.46	0.97
Er	3.33	3.39	2.32	2.91	3.42	3.75	0.95	1.96	2.96	2.76	3.62	2.74	2.54	2.86	1.3	2.77
Tm	0.61	0.55	0.36	0.47	0.56	0.64	0.17	0.34	0.49	0.45	0.58	0.43	0.44	0.45	0.21	0.45
Yb	3.34	3.45	2.3	3.01	3.63	3.7	1.22	2.35	3.11	2.88	3.65	2.73	2.49	2.82	1.47	2.95
Lu	0.53	0.54	0.37	0.48	0.58	0.57	0.21	0.38	0.49	0.46	0.57	0.43	0.39	0.44	0.24	0.47
Hf	5.67	5.41	3.68	4.4	5.81	7.14	2.35	4.39	5.6	5.34	5.99	5.04	5.02	5.2	5.18	5.06
Ta	2.16	2.11	1.28	1.61	2.06	2.9	0.81	1.68	2.5	2	2.46	1.89	2.06	2.19	0.76	2.04
Pb	27.2	28.4	0.97	18.9	3.01	13.1	8.34	18.2	24.3	24.5	75.5	25.5	9.66	18.4	9.58	38.7
Th	12.9	12.6	9.76	12	13.1	14.5	4.7	8.02	11.5	11.3	12.2	11.6	11.4	11.8	5.87	10
U	4.79	4.57	4.08	2.83	3.89	4.11	1.41	2.7	3.82	2.89	5.37	4.39	2.84	3.49	1.59	3.67

	19A	20A	21A	22A	23A	24A	25A	26A	27A	36A	28A	29A	30A	31A	32A	33A
Mg	2030	2180	2020	1190	2000	1620	1330	82.7	307	227	302	313	52.8	683	121	329
Al	24600	24300	23300	13200	18800	18700	17200	958	2800	2110	3670	3810	635	7600	1610	5480
K	4150	4230	4130	2840	3780	3130	3180	159	466	354	694	724	99.3	1420	242	914
Ca	1100	1230	640	952	1120	887	676	27	203	144	150	161	bdl	157	24.4	79.6
Sc	20.8	18.8	19.6	9.42	15.5	15.5	13.7	bdl	2.42	bdl	2.46	2.35	bdl	5.99	bdl	3.52
Ti	6630	7780	6910	4780	6040	7300	5530	314	756	569	1190	1230	295	2440	622	1690
V	212	178	203	99.8	133	129	131	7.02	24.3	17.6	24.7	25.6	3.97	49.8	10.5	32.9
Cr	157	152	146	89.1	131	116	116	15.5	23.6	17.4	31.6	32.5	5.42	53.9	10.6	47.3
Mn	606	490	549	313	458	599	674	21.7	92.9	72.8	72	74.3	17.8	136	40.3	110
Fe	13900	12200	14500	5940	8380	9490	9980	489	1810	1310	1710	1790	296	3210	768	2650
Co	24.4	25.4	23	14.4	15.1	22.7	18.2	bdl	3.23	2.46	4.04	4.14	bdl	5.9	1.73	4.83
Ni	103	109	83.5	59	72.4	83.2	75.2	37.9	12	8.33	16.6	15.3	bdl	33.7	4.33	70.1
Cu	52	49.7	42.2	24.9	26.2	33	31.5	2.05	6.05	4.55	6.41	6.47	bdl	9.91	1.83	6.98
Zn	142	142	113	63.4	72.7	99.6	94.6	7.65	19.1	12.9	24.9	20.9	5.53	30.3	9.26	25.6
Ga	30.6	32.2	28.1	17.8	24.6	25.2	23	1.17	3.66	2.6	4.51	4.62	0.74	9.05	1.88	6.36
Rb	116	134	107	85.4	133	94.3	104	4.19	14.1	9.85	18.7	19	2.26	43.8	6.09	24.9
Sr	183	205	154	193	127	175	132	6.59	25.9	18.3	29.9	30.8	3.85	31.8	10.8	22.5
Y	29	29.9	26.9	19.5	20	23.5	22.6	1.09	3.29	2.45	4.35	4.54	0.98	7.22	1.72	6.2
Zr	202	232	203	171	161	204	154	9.09	26.3	18.5	35.2	38.2	10.2	64	15.7	47.8
Nb	27.9	33.4	28.7	19.6	23.3	32.1	20.8	1.19	3.29	2.45	4.82	4.85	0.94	8.79	2.37	5.74
Cs	10.1	9.49	9.38	5.74	10	7.14	7.46	0.33	1.14	0.81	1.45	1.48	0.13	3.74	0.47	1.79
Ba	506	466	480	363	399	394	471	20.1	64	45.7	70.5	73.2	13	118	27.2	105
La	42.2	38.4	38.8	24.6	26.2	31.1	29.3	1.48	4.64	3.53	5.5	5.47	1.35	8.52	2.45	8.5
Ce	78.2	71.3	73.6	47.3	50.8	58.4	55.9	2.64	8.32	6.35	10.7	10.6	2.68	17.3	4.67	17
Pr	9.67	9.11	8.9	6.09	6.2	7.31	7.11	0.33	1.07	0.8	1.37	1.36	0.33	2.02	0.58	2.06
Nd	33.6	33.3	30	22.6	22.4	27	26.2	1.16	3.81	2.86	4.85	4.88	1.19	7.05	2.07	7.14
Sm	5.84	5.74	5.41	4.01	3.82	4.78	4.56	0.21	0.63	0.48	0.83	0.83	0.22	1.21	0.36	1.22
Eu	1.38	1.44	1.28	0.95	0.92	1.22	1.08	0.05	0.16	0.12	0.2	0.2	0.04	0.29	0.09	0.28
Gd	4.92	5.13	4.37	3.52	3.26	4.09	3.98	0.17	0.53	0.39	0.69	0.69	0.17	1.01	0.3	0.99
Tb	0.77	0.78	0.75	0.54	0.52	0.64	0.6	0.01	0.07	0.06	0.1	0.1	0.02	0.17	0.04	0.16
Dy	4.52	4.68	4.3	3.22	3.23	3.88	3.61	0.18	0.52	0.39	0.7	0.71	0.17	1.12	0.27	0.99
Ho	1	1.03	0.95	0.67	0.69	0.82	0.76	0.04	0.11	0.08	0.15	0.15	0.03	0.25	0.06	0.22
Er	2.85	2.93	2.88	1.91	2.03	2.32	2.19	0.11	0.32	0.24	0.45	0.44	0.1	0.73	0.17	0.63
Tm	0.51	0.48	0.5	0.32	0.34	0.38	0.36	0.02	0.06	0.05	0.08	0.08	0.02	0.14	0.03	0.11
Yb	3.02	3.18	3.09	2.08	2.25	2.45	2.39	0.12	0.34	0.27	0.47	0.48	0.1	0.8	0.19	0.67
Lu	0.47	0.5	0.48	0.34	0.36	0.38	0.38	0.02	0.06	0.04	0.07	0.08	0.02	0.13	0.03	0.11
Hf	4.85	5.69	5.04	4.56	4.02	4.93	4.03	0.23	0.64	0.46	0.89	0.96	0.28	1.57	0.39	1.23
Ta	1.92	2.28	2.11	1.36	1.61	2.17	1.44	0.08	0.22	0.17	0.34	0.34	0.06	0.6	0.16	0.4
Pb	398	30.5	275	16.4	16	20.6	48.1	1.46	15.3	10.6	3.8	3.8	0.66	5.83	1.71	10.9
Th	11.6	10.9	11.5	7.15	9.09	9.41	8.97	0.37	1.29	0.99	1.64	1.63	0.42	3.04	0.72	2.4
U	4.26	3.93	3.9	2.43	2.58	2.75	2.77	0.15	0.49	0.37	0.59	0.57	0.11	0.92	0.23	0.77

Table E.11 - *The standard deviation from fraction 5, in mg/kg, from ICP-MS analysis. Concentrations below the detection limit (bdl) were recorded when: concentration – 3*sd – 3*blank sd < 0.*

	1A	16A	2A	3A	4A	5A	6A	7A	8A	9A	10A	11A	12A	13A	17A	18A
Mg	60	50	70	20	10	70	50	30	20	20	30	40	10	10	5	50
Al	600	600	80	300	0.05	1000	10	100	80	10	900	300	200	100	200	200
K	60	100	10	70	60	100	6	60	60	80	0.2	90	10	3	10	100
Ca	20	10	40	9	2	20	2	60	0.6	5	8	3	2	2	8	30
Sc	0.2	0.5	0.2	0.1	0.007	0.2	0.1	0.2	0.07	0.6	0.7	0.005	0.1	0.1	0.06	0.2
Ti	70	9	1	40	70	100	70	100	50	100	300	200	40	40	20	100
V	1	0.8	0.7	0.2	0.4	3	0.9	5	0.1	8	9	4	1	1	0.2	2
Cr	0.7	1	4	2	2	3	0.7	0.4	3	0.7	3	1	3	1	0.08	1
Mn	2	0.8	40	3	2	20	30	9	5	7	5	0.8	2	0.8	2	7
Fe	100	100	200	100	100	500	300	40	100	50	100	80	200	70	60	70
Co	0.9	0.3	0.09	0.3	0.2	1	0.2	0.4	0.3	0.4	0.1	0.2	0.2	0.01	0.04	0.2
Ni	2	2	2	1	0.4	2	1	0.9	2	0.9	1	2	0.5	0.6	0.1	2
Cu	0.2	0.6	0.2	0.5	0.5	0.1	0.5	0.5	0.2	0.7	0.5	0.7	0.2	0.2	0.1	0.6
Zn	0.1	1	0.9	0.3	0.9	1	0.8	2	1	0.9	0.6	2	0.3	2	0.6	2
Ga	0.4	0.2	0.02	0.1	0.2	0.1	0.1	0.6	0.6	0.8	0.4	0.2	0.4	0.1	0.2	0.3
Rb	1	0.6	8	7	0.1	2	1	0.4	1	2	3	1	3	0.4	0.6	2
Sr	0.4	2	1	0.2	3	8	0.9	3	1	0.2	2	2	2	1	1	0.4
Y	0.04	0.1	0.2	0.09	0.06	2	0.2	0.3	0.3	0.06	1	0.1	0.3	0.4	0.1	0.3
Zr	2	2	0.9	0.3	0.9	10	3	2	1	2	0.2	1	0.4	4	1	4
Nb	0.6	0.03	0.2	0.3	0.5	0.9	0.07	0.2	0.6	0.3	0.4	0.2	0.004	0.5	0.2	0.5
Cs	0.2	0.09	0.07	0.3	0.1	0.04	0.02	0.01	0.07	0.03	0.08	0.1	0.2	0.01	0.006	0.1
Ba	30	5	7	10	1	20	2	0.1	9	2	2	6	9	5	1	2
La	3	0.09	0.2	0.04	0.2	2	0.02	0.02	0.2	0.02	0.5	0.2	0.07	0.5	0.06	0.1
Ce	5	3	0.08	0.7	1	0.6	0.2	0.1	0.7	0.4	1	0.4	0.3	0.3	0.03	1
Pr	0.5	0.0003	0.05	0.03	0.002	0.04	0.005	0.05	0.06	0.04	0.05	0.007	0.1	0.1	0.08	0.04
Nd	3	0.1	0.2	0.2	0.04	2	0.07	0.08	0.3	0.01	0.2	0.4	0.8	2	0.1	0.6
Sm	0.6	0.08	0.07	0.2	0.08	0.2	0.02	0.02	0.03	0.04	0.03	0.02	0.06	0.07	0.02	0.07
Eu	0.04	0.04	0.005	0.004	0.008	0.02	0.002	0.005	0.03	0.002	0.003	0.01	0.01	0.02	0.002	0.003
Gd	0.6	0.2	0.03	0.05	0.06	0.6	0.006	0.03	0.03	0.03	0.08	0.07	0.03	0.08	0.01	0.06
Tb	0.07	0.02	0.009	0.01	0.008	0.02	0.0008	0.003	0.005	0.007	0.01	0.01	0.005	0.005	0.0009	0.007
Dy	0.2	0.05	0.07	0.01	0.02	0.2	0.008	0.02	0.05	0.05	0.1	0.05	0.04	0.03	0.04	0.07
Ho	0.08	0.004	0.001	0.009	0.0009	0.07	0.006	0.003	0.01	0.002	0.02	0.007	0.01	0.005	0.01	0.03
Er	0.1	0.04	0.01	0.02	0.03	0.05	0.02	0.002	0.03	0.02	0.04	0.02	0.03	0.01	0.02	0.07
Tm	0.03	0.009	0.0007	0.006	0.0008	0.03	0.003	0.0002	0.006	0.001	0.002	0.001	0.01	0.008	0.006	0.005
Yb	0.2	0.05	0.01	0.02	0.008	0.09	0.01	0.001	0.01	0.02	0.02	0.01	0.02	0.02	0.01	0.01
Lu	0.01	0.004	0.007	0.005	0.0002	0.001	0.002	0.006	0.003	0.0002	0.002	0.003	0.007	0.004	0.0008	0.01
Hf	0.4	0.005	0.02	0.06	0.03	0.3	0.04	0.02	0.01	0.02	0.06	0.08	0.1	0.03	0.009	0.1
Ta	0.08	0.009	0.003	0.03	0.003	0.03	0.002	0.002	0.002	0.02	0.002	0.01	0.03	0.004	0.004	0.04
Pb	2	0.07	0.02	0.03	0.03	0.5	0.1	0.09	0.2	0.2	0.6	0.09	0.2	0.2	0.2	0.6
Th	0.5	0.2	0.02	0.04	0.07	0.2	0.1	0.02	0.08	0.06	0.07	0.2	0.07	0.07	0.001	0.3
U	0.1	0.008	0.04	0.008	0.04	0.02	0.01	0.01	0.03	0.02	0.03	0.03	0.06	0.02	0.02	0.08

	19A	20A	21A	22A	23A	24A	25A	26A	27A	36A	28A	29A	30A	31A	32A	33A
Mg	40	50	80	60	10	10	7	0.4	3	7	3	10	0.3	4	1	3
Al	400	800	800	400	600	300	60	7	9	80	9	90	2	100	10	10
K	100	100	200	30	100	20	20	0.4	2	10	1	20	0.2	3	2	0.05
Ca	20	30	20	6	4	20	10	0.5	0.6	5	6	3	bdl	2	0.9	0.6
Sc	0.4	0.3	0.4	0.3	0.1	0.4	0.04	bdl	0.04	bdl	0.06	0.09	bdl	0.03	bdl	0.03
Ti	100	200	100	100	80	40	30	3	20	10	3	20	8	40	0.6	10
V	3	3	2	1	0.3	0.2	0.9	0.2	0.3	0.4	0.2	0.3	0.1	0.01	0.04	0.7
Cr	3	3	1	1	1	0.4	2	0.5	0.2	0.7	0.4	0.8	0.09	0.3	0.2	1
Mn	10	10	10	bdl	3	7	4	bdl	0.8	2	2	2	bdl	2	bdl	3
Fe	200	100	400	50	40	40	60	4	4	40	40	30	3	40	2	50
Co	0.4	0.1	0.5	0.1	0.1	0.1	0.1	bdl	0.01	0.06	0.09	0.1	bdl	0.01	0.03	0.003
Ni	2	2	2	0.3	0.5	0.3	0.06	0.02	0.1	0.2	0.1	0.02	bdl	0.1	0.03	0.6
Cu	0.8	0.7	0.6	0.2	0.1	0.6	0.3	0.06	0.08	0.07	0.09	0.2	bdl	0.09	0.05	0.1
Zn	2	3	0.7	0.6	0.4	0.9	0.8	0.09	0.02	0.4	0.5	0.5	0.3	0.2	0.3	0.5
Ga	0.5	1	0.01	0.08	0.04	0.4	0.3	0.008	0.1	0.01	0.07	0.04	0.006	0.2	0.05	0.1
Rb	3	3	0.2	1	2	0.1	2	0.05	0.3	0.2	0.2	0.2	0.02	0.6	0.02	0.6
Sr	4	5	2	3	2	2	3	0.04	0.1	0.5	0.7	0.7	0.04	0.7	0.1	0.07
Y	0.6	1	0.7	0.3	0.1	0.04	0.4	0.04	0.01	0.06	0.2	0.2	0.01	0.1	0.01	0.02
Zr	3	6	5	10	0.08	5	0.2	0.3	0.09	0.5	0.2	0.8	0.006	0.4	0.2	0.01
Nb	0.4	0.6	0.9	0.4	0.04	0.02	0.08	0.04	0.01	0.03	0.06	0.06	0.0004	0.06	0.008	0.06
Cs	0.2	0.07	0.1	0.2	0.04	0.01	0.03	0.003	0.02	0.006	0.0004	0.01	0.0004	0.009	0.002	0.07
Ba	10	10	20	10	4	4	7	0.4	0.5	1	3	1	0.02	2	0.1	0.9
La	0.1	0.9	2	0.4	0.05	0.2	0.1	0.05	0.1	0.06	0.3	0.07	0.009	0.2	0.02	0.3
Ce	0.6	2	3	0.9	0.7	0.02	0.7	0.07	0.2	0.03	0.5	0.02	0.003	0.3	0.1	0.6
Pr	0.1	0.2	0.1	0.1	0.06	0.06	0.08	0.01	0.0003	0.003	0.05	0.02	0.004	0.05	0.0008	0.04
Nd	0.3	0.5	1	0.6	0.07	0.2	0.1	0.002	0.09	0.04	0.3	0.1	0.02	0.2	0.03	0.1
Sm	0.1	0.07	0.3	0.05	0.03	0.06	0.05	0.008	0.02	0.03	0.04	0.03	0.009	0.02	0.006	0.07
Eu	0.01	0.02	0.003	0.02	0.004	0.01	0.01	0.002	0.0008	0.004	0.01	0.004	0.0002	0.004	0.002	bdl
Gd	0.04	0.08	0.3	0.1	0.004	0.03	0.01	0.004	0.03	0.003	0.05	0.01	0.007	0.04	0.002	0.02
Tb	0.006	0.02	0.02	0.02	0.004	0.004	0.01	0.003	0.0008	0.002	0.003	0.0007	0.003	0.0009	0.0008	0.004
Dy	0.03	0.08	0.1	0.07	0.03	0.05	0.04	0.003	0.008	0.005	0.01	0.01	0.008	0.02	0.006	0.02
Ho	0.02	0.01	0.06	0.007	0.009	0.006	0.02	0.004	0.0008	0.001	0.006	0.002	0.0001	0.002	0.0001	0.02
Er	0.02	0.006	0.07	0.04	0.01	0.003	0.02	0.001	0.002	0.006	0.003	0.005	0.005	0.02	0.002	0.03
Tm	0.007	0.006	0.03	0.002	0.008	0.001	0.003	0.001	0.001	0.002	0.004	0.001	0.001	0.002	0.0007	0.001
Yb	0.01	0.1	0.1	0.02	0.01	0.03	0.02	0.007	0.001	0.01	0.02	0.008	0.003	0.01	0.007	0.03
Lu	0.005	0.009	0.002	0.001	0.0004	0.01	0.002	0.0002	0.001	0.002	0.003	0.001	0.0009	0.009	0.001	0.003
Hf	0.1	0.1	0.2	0.08	0.004	0.04	0.03	0.01	0.02	0.008	0.06	0.01	0.005	0.02	0.005	0.04
Ta	0.005	0.05	0.04	0.006	0.02	0.008	0.0003	0.002	0.002	0.0006	0.01	0.006	0.001	0.004	0.0009	0.02
Pb	2	0.6	10	0.3	0.2	0.1	0.3	0.07	0.4	0.3	0.1	0.08	0.01	0.1	0.03	0.4
Th	0.05	0.1	0.3	0.1	0.02	0.01	0.04	0.002	0.01	0.006	0.04	0.005	0.004	0.01	0.01	0.09
U	0.04	0.06	0.04	0.08	0.04	0.01	0.03	0.0003	0.002	0.004	0.03	0.02	0.002	0.004	0.01	0.01

Table E.12 - *Trace elemental concentrations from whole rock, in mg/kg, from ICP-MS analysis. Concentrations below the detection limit (bdl) were recorded when: concentration – 3*sd – 3*blank sd<0.*

	1A	1Arpt	1Arpt2	2A	3A	4A	5A	6A	7A	8A	9A	10A	11A	12A	13A
Mg	2520	2610	2690	4630	2510	1900	1510	6880	2350	2210	1290	1680	2050	1910	1710
Al	24700	25300	26600	22400	25300	27000	28700	10700	21800	27500	27600	26800	27000	24900	24700
K	4260	4400	4600	4440	4730	5190	4510	1790	3980	3980	4350	4020	4280	4150	3230
Ca	3770	3840	4060	9260	767	1030	563	7290	9300	673	821	824	1370	1240	369
Sc	22.8	22.6	23.5	24.5	26.7	25.7	20.4	17	20.6	22.2	25.4	25.6	20.6	21.9	20.6
Ti	7320	7280	7520	5700	6910	7280	10600	3040	6080	10500	7890	10200	6770	7400	8210
V	171	170	177	180	166	202	200	95.7	156	157	217	307	204	185	173
Cr	143	141	145	164	165	180	143	66.2	139	137	175	153	147	132	120
Mn	709	716	750	1320	740	252	382	4070	827	334	1440	363	555	165	410
Fe	13900	14000	14600	16100	20300	8620	8820	58500	8800	10000	13100	12900	9390	15300	9260
Co	31.6	31.5	32.2	35.2	32.4	32.3	30.4	18.6	32.1	35.4	30.7	61	31.3	20.4	23.1
Ni	120	120	123	137	137	141	108	45.6	135	116	150	212	130	98.5	77.6
Cu	73.2	74.3	75.4	51.5	65.8	77.8	73.3	22.3	41.8	62.9	61.2	78.6	90.6	53.8	56.2
Zn	122	122	125	62	115	105	125	42.4	80.3	125	116	145	106	100	76.8
Ga	31.2	31.1	32	37.7	30.6	30.7	35.4	12.8	25.5	33.7	31.6	33.9	31.8	29	30.2
Rb	123	121	124	140	149	167	111	64.6	145	114	146	121	124	121	92.5
Sr	265	262	277	301	142	243	213	198	439	232	194	184	247	135	157
Y	40.8	41.1	42.2	30.4	41.8	51.9	40.2	30	30.3	39.6	38.8	46.7	43.1	37.2	33.4
Zr	214	211	218	138	172	249	285	103	142	233	203	251	181	189	196
Nb	29.2	29.3	29.6	18.6	24.4	36.6	43	11	20.7	38.7	28.1	35.8	26	27.2	29.6
Cs	9.42	9.32	9.56	9.29	10.5	15.9	7.93	5.06	11.5	7.57	11.6	8.27	9.4	9.02	6.62
Ba	468	467	478	462	423	470	418	273	607	426	549	805	503	366	335
La	46.6	47.4	47.8	38.7	46.7	52.3	53.8	34.5	37.7	50.2	49	53.5	53.7	44	43.6
Ce	91.8	94	94.5	72.6	92.4	107	108	70.2	72.6	101	98.2	107	100	87.4	87.4
Pr	12.6	12.8	12.8	8.52	10.2	12.2	14.3	7.8	8.01	11.3	10.9	12.4	11.7	11.7	9.8
Nd	47.7	48.5	48	38.4	46.8	57.8	53.5	36.7	36.6	50.4	48.4	56.1	52.2	43.5	44
Sm	8.95	9.24	9.32	7.22	8.94	11.6	10.1	7.23	6.91	9.97	8.88	10.7	10	8.29	8.28
Eu	2.29	2.35	2.35	1.75	2.17	2.79	2.5	1.95	1.63	2.46	1.99	2.63	2.42	2.05	2.01
Gd	7.98	8.52	8.51	6.62	8.25	11.1	8.64	7.16	6.36	8.92	7.55	9.61	9.05	7.33	7.2
Tb	1.23	1.28	1.28	0.95	1.24	1.65	1.31	0.99	0.93	1.31	1.15	1.46	1.32	1.14	1.07
Dy	6.92	7.01	7.18	5.18	7.12	9.16	7.24	5.16	5.29	7.33	6.63	8.2	7.22	6.4	5.93
Ho	1.34	1.39	1.4	1.03	1.42	1.77	1.43	0.95	1.05	1.42	1.36	1.62	1.41	1.28	1.18
Er	3.65	3.69	3.72	2.67	3.8	4.61	3.73	2.28	2.8	3.75	3.67	4.27	3.66	3.42	3.12
Tm	0.63	0.63	0.63	0.44	0.63	0.74	0.64	0.35	0.46	0.61	0.62	0.69	0.6	0.59	0.51
Yb	3.44	3.49	3.5	2.59	3.69	4.27	3.63	1.97	2.79	3.53	3.67	3.96	3.42	3.26	2.99
Lu	0.55	0.53	0.55	0.41	0.57	0.66	0.56	0.32	0.44	0.56	0.56	0.63	0.54	0.5	0.47
Hf	5.12	5.16	5.11	3.55	4.33	5.68	6.97	2.12	3.77	5.69	5.01	5.8	4.58	4.67	4.74
Ta	1.96	1.97	2	1.25	1.61	2.05	2.82	0.69	1.39	2.53	1.88	2.33	1.71	1.86	1.96
Pb	18.6	19.5	19.7	6.28	20.1	3.44	12.6	14.9	19.3	24.5	26.7	81	24.8	18.5	17.5
Th	12.4	12.8	12.9	10.2	12.9	14.1	14.1	5.45	11.6	12.5	13.5	12.6	12.3	11.9	11.1
U	4	4.11	4.07	4.23	2.9	4.36	4.12	1.81	2.64	4.17	3.16	5.7	4.5	2.95	3.3

	14A	16A	17A	18A	19A	20A	21A	22A	23A	24A	25A	26A	27A	29A	31A
Mg	2360	2700	840	1630	1720	2210	1760	1920	2530	1900	1700	399	630	568	789
Al	22100	25400	10600	17900	19900	25000	20500	19500	23900	22500	23300	868	2100	3300	5640
K	3730	4280	1700	2890	3270	4060	3490	3820	4410	3460	3790	1220	1250	2770	2610
Ca	2580	3840	896	2750	1610	2220	1180	2480	2690	2160	1740	1590	1060	1920	1050
Sc	21.8	22.3	8.48	15.6	18.8	21.7	20.9	16.1	22.1	19.4	20.6	bdl	bdl	2.16	4.66
Ti	5900	7470	5030	5130	5010	7470	5630	6500	6970	8200	6640	252	533	1020	1690
V	178	176	83.4	145	185	188	194	149	165	153	168	7.39	20.5	26.3	39.2
Cr	131	145	80.7	108	128	140	129	112	145	118	138	6.23	29.2	27.6	33.9
Mn	2070	691	409	603	853	696	664	643	916	854	1220	92.9	225	143	200
Fe	23100	14300	6700	10300	14000	14300	15300	10100	13200	12000	15100	524	1300	1770	2850
Co	22.9	32.2	11.8	24.7	24.4	30	22.2	22.6	24.9	29.6	28	bdl	bdl	4.3	6.51
Ni	81.2	128	35.8	97.6	96.2	126	89.8	68.4	108	104	114	2.99	86.3	16.2	24.9
Cu	43.8	76	26.1	62.9	78.4	73.6	67.3	46.1	50.5	50.8	57.5	7.34	4.92	13.8	15.5
Zn	117	118	72.8	153	151	136	117	103	101	124	118	26.5	30.4	31.9	42.6
Ga	25.4	30.5	12.9	22.4	29.6	29.9	27.1	23.6	27.6	27.5	27.3	1.12	2.88	4.18	7.12
Rb	105	126	38.5	85.7	94.7	121	97.8	106	143	96.7	119	8.91	17	20.8	36
Sr	210	312	90.4	210	182	259	181	258	202	248	184	43.5	55.1	73.7	47.9
Y	30.6	41.7	21.9	30.9	30.4	38.3	35.2	35.1	32.1	32.7	40.2	1.56	3.84	5.67	8.07
Zr	177	211	196	146	156	209	173	198	170	194	177	7.6	17.1	31	42.3
Nb	25.1	30	14.5	21.1	21.8	29.6	24.4	23.9	24.1	32.5	22.7	1.01	2.47	3.95	5.96
Cs	8.62	9.3	2.03	6.56	8.38	8.88	8.79	6.91	10.7	7.21	8.37	0.34	0.89	1.26	2.7
Ba	477	494	304	390	447	530	478	472	469	430	579	59.3	86.6	104	121
La	33.8	49.5	24.6	35.7	38.7	46.7	39.9	41.5	40.2	40.6	45.9	1.99	5.12	6.75	9.54
Ce	68	94.5	50.6	69.4	77	90.1	78.2	81.4	79.5	82.6	90.7	3.67	9.77	13.5	20
Pr	8.86	10.8	5.46	7.72	10.1	10	10.4	9.01	8.67	9.11	10.1	0.49	1.25	1.84	2.61
Nd	32.8	48.5	24.8	35	36	45.4	38.2	40.9	38.9	41.4	46	1.87	4.59	6.98	9.5
Sm	6.17	9.3	4.7	6.69	6.96	8.75	7.33	7.76	7.37	8.06	8.77	0.36	0.88	1.3	1.85
Eu	1.52	2.31	1.08	1.64	1.7	2.12	1.86	1.81	1.76	2.02	2.18	0.09	0.22	0.32	0.46
Gd	5.62	8.75	4.28	6.31	5.95	8.1	6.52	7.19	6.57	7.33	8.27	0.33	0.86	1.15	1.64
Tb	0.87	1.27	0.64	0.94	0.97	1.18	1.04	1.06	0.99	1.08	1.2	0.05	0.11	0.17	0.26
Dy	5.17	7.02	3.59	5.17	5.27	6.56	5.86	5.95	5.52	5.91	6.66	0.27	0.66	0.96	1.46
Ho	1.07	1.38	0.72	1.03	1.03	1.3	1.16	1.19	1.11	1.15	1.29	0.05	0.15	0.19	0.28
Er	3.01	3.64	1.94	2.69	2.9	3.46	3.25	3.17	2.93	3.01	3.38	0.14	0.35	0.5	0.77
Tm	0.54	0.59	0.33	0.44	0.48	0.57	0.55	0.52	0.48	0.49	0.54	0.02	0.07	0.08	0.13
Yb	3.13	3.4	2	2.56	2.81	3.32	3.09	3.11	2.88	2.87	3.23	0.13	0.35	0.48	0.74
Lu	0.5	0.53	0.33	0.4	0.45	0.52	0.49	0.49	0.45	0.44	0.51	0.02	0.05	0.08	0.12
Hf	4.26	5.06	5.45	3.54	3.85	5	4.11	5.09	4.27	4.74	4.47	0.19	0.45	0.75	1.08
Ta	1.57	1.96	0.97	1.37	1.54	1.95	1.67	1.6	1.66	2.13	1.51	0.07	0.17	0.26	0.42
Pb	21.3	20.4	54.1	74.8	467	47.9	347	37.7	24.7	24.6	61.9	5.38	18.8	6.5	7.69
Th	10.4	12.3	6.46	8.59	10.7	11.9	11.3	10.4	11.8	10.5	11.5	0.44	1.27	1.78	2.8
U	3.25	3.98	2.19	3	3.72	3.81	3.93	3.3	2.93	2.92	3.35	0.15	0.44	0.62	0.73

Table E.13 - *The standard deviation from whole rock, in mg/kg, from ICP-MS analysis. Concentrations below the detection limit (bdl) were recorded when: concentration – 3*sd – 3*blank sd < 0.*

	1A	1Arpt	1Arpt2	2A	3A	4A	5A	6A	7A	8A	9A	10A	11A	12A	13A
Mg	30	90	100	90	20	30	9	40	30	40	5	30	20	40	20
Al	200	900	1000	500	200	200	200	200	200	600	100	200	40	300	40
K	20	100	100	60	20	50	60	30	7	30	30	100	100	50	30
Ca	50	100	80	100	20	8	3	90	20	20	1	4	9	5	8
Sc	0.1	0.6	0.4	0.3	0.5	0.5	0.2	0.08	0.3	0.02	0.5	0.3	0.03	0.01	0.07
Ti	70	100	100	10	80	30	300	40	90	60	40	10	100	20	70
V	1	2	5	0.08	2	0.7	4	0.7	1	2	2	0.4	1	0.7	0.8
Cr	0.6	4	6	2	1	2	1	0.4	0.3	0.4	0.3	2	2	2	2
Mn	7	20	40	3	8	5	40	70	0.8	2	bdl	9	3	2	8
Fe	200	500	700	100	300	100	20	500	50	50	100	200	90	300	100
Co	1	0.6	0.9	0.3	0.06	0.4	0.04	0.02	0.1	0.3	0.5	0.2	0.02	0.03	0.1
Ni	1	1	2	0.2	2	2	0.7	0.5	0.4	1	0.8	1	0.4	0.6	1
Cu	0.4	0.5	1	0.2	0.2	0.6	2	0.1	0.9	0.7	0.2	0.5	0.1	0.2	1
Zn	0.8	0.1	2	0.9	0.2	3	3	0.01	1	0.01	2	2	2	0.1	0.2
Ga	0.4	0.6	0.5	0.6	0.4	0.1	0.8	0.002	0.2	0.2	0.4	0.2	0.6	0.3	0.2
Rb	4	2	3	3	1	1	3	0.7	0.8	0.2	2	3	0.7	0.5	1
Sr	10	7	9	5	0.7	4	2	0.9	8	0.9	2	0.4	3	1	3
Y	2	0.8	1	0.1	0.3	0.2	0.1	0.5	0.1	0.1	0.3	0.4	0.03	0.01	0.4
Zr	8	7	2	2	1	0.6	1	2	0.9	0.3	0.3	4	0.2	0.2	0.6
Nb	1	0.7	0.1	0.2	0.3	0.5	0.4	0.05	0.05	0.08	0.2	0.09	0.1	0.05	0.07
Cs	0.1	0.1	0.3	0.2	0.004	0.04	0.06	0.05	0.09	0.008	0.09	0.02	0.06	0.02	0.001
Ba	2	10	20	2	2	0.3	2	3	1	3	6	10	6	7	2
La	1	0.7	0.7	0.1	0.1	0.1	0.5	0.3	0.04	0.2	0.2	0.3	0.3	0.7	0.3
Ce	2	0.3	0.3	0.6	0.3	0.7	2	0.2	0.5	2	0.3	2	0.3	0.2	0.3
Pr	0.3	0.1	0.05	0.1	0.03	0.03	0.5	0.1	0.04	0.01	0.06	0.1	0.001	0.2	0.2
Nd	1	2	0.7	0.3	0.03	0.2	0.02	0.3	0.04	0.9	0.4	0.3	0.1	1	0.006
Sm	0.2	0.2	0.1	0.1	0.06	0.04	0.07	0.1	0.04	0.05	0.07	0.2	0.08	0.1	0.02
Eu	0.03	0.02	0.04	0.02	0.03	0.02	0.1	0.03	0.005	0.03	0.008	0.02	0.03	0.06	0.05
Gd	0.09	0.2	0.1	0.03	0.03	0.005	0.09	0.1	0.09	0.004	0.04	0.09	0.03	0.09	0.1
Tb	0.03	0.02	0.04	0.01	0.02	0.001	0.02	0.004	0.006	0.02	0.01	0.003	0.02	0.01	0.02
Dy	0.1	0.1	0.1	0.04	0.06	0.06	0.1	0.02	0.03	0.04	0.05	0.1	0.01	0.2	0.06
Ho	0.03	0.01	0.008	0.006	0.005	0.02	0.009	0.0009	0.003	0.008	0.03	0.003	0.009	0.002	0.01
Er	0.07	0.02	0.09	0.02	0.03	0.06	0.09	0.01	0.002	0.02	0.03	0.03	0.04	0.03	0.02
Tm	0.02	0.02	0.02	0.0003	bdl	0.009	0.0003	0.001	0.004	0.003	0.01	0.01	0.007	0.02	0.008
Yb	0.03	0.07	0.05	0.03	0.05	0.03	0.06	0.01	0.01	0.02	0.02	0.02	0.007	0.05	0.02
Lu	0.007	0.01	0.003	0.006	0.006	0.007	0.01	0.001	0.006	0.005	0.006	0.02	0.0007	0.003	0.005
Hf	0.2	0.1	0.08	0.04	0.07	0.02	0.04	0.02	0.08	0.02	0.08	0.07	0.02	0.06	0.009
Ta	0.006	0.01	0.006	0.02	0.03	0.007	0.005	0.01	0.02	0.05	0.02	0.03	0.02	0.01	0.01
Pb	0.6	0.09	0.3	0.1	0.2	0.01	0.06	0.1	0.06	0.2	0.2	0.3	0.1	0.4	0.1
Th	0.2	0.02	0.05	0.0003	0.1	0.07	0.3	0.08	0.04	0.07	0.1	0.05	0.03	0.1	0.02
U	0.05	0.1	0.08	0.02	0.003	0.008	0.02	0.04	0.003	0.001	0.04	0.007	0.04	0.06	0.004

	14A	16A	17A	18A	19A	20A	21A	22A	23A	24A	25A	26A	27A	29A	31A
Mg	30	30	6	30	40	40	20	20	40	30	30	9	20	20	20
Al	300	700	70	400	400	500	300	200	800	40	1000	20	40	90	70
K	80	70	4	50	50	1	100	10	60	20	200	20	40	70	40
Ca	40	10	20	50	20	10	20	0.8	90	20	10	20	40	40	10
Sc	0.06	0.2	0.09	0.02	0.1	0.1	0.1	0.2	0.5	0.09	0.4	bdl	bdl	0.07	0.09
Ti	7	40	20	40	50	80	30	100	10	70	50	4	10	20	30
V	0.4	0.3	0.9	0.04	1	0.7	0.04	0.5	3	1	0.9	0.2	0.2	0.6	0.8
Cr	0.3	2	1	1	1	0.8	1	0.9	3	2	2	0.2	0.8	0.5	0.5
Mn	20	2	3	2	9	10	2	8	8	2	8	2	8	2	6
Fe	300	200	60	80	200	100	60	100	200	100	200	8	100	20	70
Co	0.2	0.4	0.06	0.2	0.5	0.4	0.4	0.2	0.5	0.4	0.4	bdl	bdl	0.08	0.08
Ni	0.3	0.2	0.2	3	2	1	1	0.6	3	0.5	2	0.02	3	0.2	0.2
Cu	0.3	2	0.06	1	0.8	0.7	0.7	2	2	1	1	0.09	0.8	0.2	0.1
Zn	0.6	2	1	2	2	2	0.4	1	2	0.8	2	0.3	0.6	1	1
Ga	0.2	0.2	0.07	0.1	0.1	0.2	0.3	0.3	0.2	0.2	0.6	0.04	0.06	0.1	0.2
Rb	2	1	0.3	0.4	0.003	0.06	0.1	0.5	4	3	0.1	0.3	0.1	0.5	0.6
Sr	2	2	0.4	3	2	0.6	0.8	3	7	5	0.7	1	0.4	3	0.4
Y	0.08	0.4	0.07	0.3	0.3	0.2	0.2	0.7	0.9	0.5	0.3	0.03	0.06	0.2	0.2
Zr	1	0.5	2	0.8	3	1	1	1	5	2	1	0.09	0.03	0.5	0.6
Nb	0.2	0.6	0.006	0.2	0.4	0.1	0.1	0.08	0.4	1	0.002	0.02	0.06	0.07	0.003
Cs	0.2	0.1	0.01	0.04	0.1	0.05	0.1	0.03	0.1	0.1	0.1	0.002	0.02	0.02	0.06
Ba	2	0.4	0.5	1	10	10	4	2	2	7	10	0.7	3	2	2
La	0.5	0.04	0.3	0.2	2	0.4	0.7	0.3	0.6	0.8	0.6	0.04	0.1	0.2	0.1
Ce	0.9	0.5	0.3	0.2	3	1	2	0.1	0.7	2	0.5	0.1	0.05	0.2	0.03
Pr	0.09	0.1	0.08	0.1	0.1	0.1	0.06	0.1	0.2	0.1	0.009	0.009	0.02	0.02	0.07
Nd	0.5	0.6	0.2	0.1	1	0.4	0.03	0.6	0.6	0.5	0.5	0.07	0.4	0.1	0.1
Sm	0.1	0.1	0.03	0.01	0.2	0.05	0.3	0.02	0.2	0.2	0.2	0.008	0.02	0.03	0.005
Eu	0.02	0.03	0.007	0.02	0.03	0.04	0.0004	0.03	0.02	0.03	0.04	0.003	0.004	0.02	0.002
Gd	0.02	0.1	0.005	0.05	0.3	0.1	0.2	0.06	0.06	0.2	0.05	0.03	0.003	0.03	0.05
Tb	0.03	0.009	0.01	0.01	0.05	0.003	0.03	0.01	0.04	0.03	0.01	0.006	0.03	0.008	0.004
Dy	0.1	0.07	0.06	0.04	0.1	0.04	0.03	0.06	0.08	0.1	0.06	0.008	0.03	0.02	0.03
Ho	0.02	0.003	0.006	0.01	0.06	0.007	0.04	0.003	0.02	0.02	0.01	0.001	0.02	0.001	0.0001
Er	0.05	0.02	0.02	0.02	0.08	0.06	0.02	0.02	0.05	0.05	0.08	0.003	0.02	0.01	0.02
Tm	0.005	0.01	0.003	0.0003	0.01	0.0006	0.004	0.005	0.003	0.003	0.007	0.0007	0.005	0.0004	0.006
Yb	0.01	0.03	0.01	0.03	0.07	0.06	0.07	0.02	0.02	0.08	0.05	0.01	0.03	0.009	0.01
Lu	0.01	0.007	0.003	0.004	0.006	0.007	0.01	0.002	bdl	0.005	0.004	0.0005	bdl	0.001	0.003
Hf	0.04	0.02	0.07	0.02	0.1	0.06	0.08	0.04	0.1	0.06	0.009	0.01	0.02	0.03	0.03
Ta	0.004	0.02	0.001	0.02	0.01	0.01	0.03	0.01	0.02	0.02	0.02	0.003	0.01	0.001	0.0006
Pb	0.4	0.3	0.1	0.5	10	0.6	5	0.2	0.4	0.4	0.4	0.09	0.4	0.1	0.06
Th	0.2	0.2	0.03	0.001	0.2	0.2	0.2	0.03	0.2	0.2	0.2	0.01	0.03	0.02	0.03
U	0.07	0.0007	0.02	0.02	0.05	0.07	0.03	0.03	0.05	0.04	0.07	0.001	0.0007	0.03	0.002

References

A

Abed, A. M., Arouri, K., Amiereh, B. S., Al-Hawari, Z., (2009) Characterization and Genesis of Some Jordanian Oil Shales. *Dirasat Pure Sciences*, **36**(1): 7-17.

Addadi, L., Moradian, J., Shay, E., Maroudas, N. G., Weiner, S., (1987) A chemical-model for the cooperation of sulfates and carboxylates in calcite crystal nucleation – relevance to biomineralization. *Proceedings of the National Academy of Sciences of the United States of America*, **84**(9): 2732-2736.

Al-Otoom, A. Y., Shawabkeh, R. A., Al-Harahsheh, A. M., Shawaqfeh, A. T., (2005) The chemistry of minerals obtained from the combustion of Jordanian oil shale. *Energy*, **30**(5): 611-619.

Alali, J., Abu Salah, A., Al Omari, W.,Yasin, S. M., (2006) Oil Shale in Jordan. Natural Resources Authority of Jordan, 26.

Albarède, F., (2003) Geochemistry: An Introduction. Cambridge University Press. 248.

Aleksandrov, J., (2009) 85 Years of Oil Shale Processing in Estonia. *Oil Shale*, **26**(4): 540-542.

Alexander, G., Maroto-Valer, M. M., Gafarova-Aksoy, P., (2007) Evaluation of reaction variables in the dissolution of serpentine for mineral carbonation. *Fuel*, **86**(1-2): 273-281.

Allix, P., Burnham, A., Fowler, T., Herron, M., Kleinberg, R., Symington, B., (2010) Coaxing Oil from Shale. In: *Oilfield Review.* Winter 2010/2011, **22(**4). Schlumberger, Houston, US, pp. 4-15.

Althoff, P. L., (1977) Structural refinements of dolomite and a magnesian calcite and implications for dolomite formation in marine-environment. *American Mineralogist*, **62**(7-8): 772-783.

Alvarez, D., Abanades, J. C., (2005) Pore-size and shape effects on the recarbonation performance of calcium oxide submitted to repeated calcination/recarbonation cycles. *Energy & Fuels*, **19**(1): 270-278.

Anthony, E. J., Jia, L., Woods, J., Roque, W., Burwell, S., (2000) Pacification of high calcic residues using carbon dioxide. *Waste Management*, **20**(1): 1-13.

Aradottir, E. S. P., Sigurdardottir, H., Sigfusson, B., Gunnlaugsson, E., (2011) CarbFix: a CCS pilot project imitating and accelerating natural CO_2 sequestration. *Greenhouse Gases-Science and Technology*, **1**(2): 105-118.

Assima, G. P., Larachi, F., Beaudoin, G., Molson, J., (2013a) Dynamics of carbon dioxide uptake in chrysotile mining residues - Effect of mineralogy and liquid saturation. *International Journal of Greenhouse Gas Control*, **12**: 124-135.

Assima, G. P., Larachi, F., Molson, J., Beaudoin, G., (2013b) Accurate and direct quantification of native brucite in serpentine ores-New methodology and implications for CO_2 sequestration by mining residues. *Thermochimica Acta*, **566**: 281-291.

B

Barth, M. G., McDonough, W. F.,Rudnick, R. L., (2000) Tracking the budget of Nb and Ta in the continental crust. *Chemical Geology*, **165**(3-4): 197-213.

Bateman, K., Rochelle, C., Lacinska, A., Wagner, D., (2011) CO_2-porewater-rock reactions - Large-scale column experiment (Big Rig II). *10th International Conference on Greenhouse Gas Control Technologies*, **4**: 4937-4944.

Belazi, A. U., Davidson, C. M., Keating, G. E., Littlejohn, D., (1995) Determination of heavy-metals in sediments from the Cumbrian coast, NW England, UK. *Journal of Analytical Atomic Spectrometry*, **10**(3): 233-240.

Benson, S. M., Cole, D. R., (2008) CO_2 Sequestration in Deep Sedimentary Formations. *Elements*, **4**(5): 325-331.

Bertos, M. F., Li, X., Simons, S. J. R., Hills, C. D., Carey, P. J., (2004) Investigation of accelerated carbonation for the stabilisation of MSW incinerator ashes and the sequestration of CO_2. *Green Chemistry*, **6**(8): 428-436.

Bhargava, S., Awaja, F., Subasinghe, N. D., (2005) Characterisation of some Australian oil shale using thermal, X-ray and IR techniques. *Fuel*, **84**(6): 707-715.

Birdwell, J.E., (2012) Review of rare earth element concentrations in oil shales of the Eocene Green River Formation: U.S. Geological Survey Open-File Report 2012–1016, 20.

Bobicki, E. R., Liu, Q. X., Xu, Z. H., Zeng, H. B., (2012) Carbon capture and storage using alkaline industrial wastes. *Progress in Energy and Combustion Science*, **38**(2): 302-320.

Boggs, S., (2009) Petrology of Sedimentary Rocks. Cambridge University Press.

BP, (2013) BP Statistical Review of World Energy: June 2013. 62nd Edition. BP, London, 48.

Brandt, A. R., (2008) Converting Oil Shale to Liquid Fuels: Energy Inputs and Greenhouse Gas Emissions of the Shell in Situ Conversion Process. *Environmental Science & Technology*, **42**: 7489-7495.

Brandt, A. R., (2009) Converting Oil Shale to Liquid Fuels with the Alberta Taciuk Processor: Energy Inputs and Greenhouse Gas Emissions. *Energy & Fuels*, **23**: 6253-6258.

Brecevic, L., Nielsen, A. E., (1989) Solubility of amorphous calcium-carbonate. *Journal of Crystal Growth*, **98**(3): 504-510.

Breit, G. N., Wanty, R. B., (1991) Vanadium accumulation in carbonaceous rocks – a review of geochemical controls during deposition and diagenesis. *Chemical Geology*, **91**(2): 83-97.

Brown, E., (2001) Introduction to Thermal Analysis: Techniques and Applications. Springer. 264.

Bsieso, M. S., (2003) Jordan's experience in oil shale studies employing different technologies. *Oil Shale*, **20**(3): 360-370.

Busch, A., Alles, S., Gensterblum, Y., Prinz, D., Dewhurst, D. N., Raven, M. D., Stanjek, H., Krooss, B. M., (2008) Carbon dioxide storage potential of shales. *International Journal of Greenhouse Gas Control*, **2**(3): 297-308.

C

Cardenas-Escudero, C., Morales-Florez, V., Perez-Lopez, R., Santos, A., Esquivias, L., (2011) Procedure to use phosphogypsum industrial waste for mineral CO_2 sequestration. *Journal of Hazardous Materials*, **196**: 431-435.

Carruthers, R. G., Caldwell, W., Steuart, D. R., (1912) The oil shales of the Lothians. *Memoirs of the Geological Survey, Scotland*. Geological Survey of Great Britain. H.M.S.O., Edinburgh.

Carver, R. H., (2004) Doing Data Analysis With Minitab 14. Brooks/Cole, Thomson Learning. 356.

Chen, Z. Y., O'Connor, W. K., Gerdemann, S. J., (2006) Chemistry of aqueous mineral carbonation for carbon sequestration and explanation of experimental results. *Environmental Progress*, **25**(2): 161-166.

Chen, C., Wang, S., Cui, R., Zheng, Y., Gu, S., (2007) Study on Geochemical Characteristics and Genesis of Dalianhe Oil Shale in Heilongjiang Province, Paper presented at Proceedings of the 27th Oil Shale Symposium, October 15-17 2007, Colorado School of Mines, Golden CO.

Choudhury, H., Cary, R., (2001) Concise International Chemical Assessment Document 33; Barium and Barium Compounds. World Health Organisation, Geneva.

Cizer, O., Rodriguez-Navarro, C., Ruiz-Agudo, E., Elsen, J., Van Gemert, D., Van Balen, K., (2012) Phase and morphology evolution of calcium carbonate precipitated by carbonation of hydrated lime. *Journal of Materials Science*, **47**(16): 6151-6165.

Clarkson, J. R., Price, T. J., Adams, C. J., (1992) Role of metastable phases in the spontaneous precipitation of calcium-carbonate. *Journal of the Chemical Society-Faraday Transactions*, **88**(2): 243-249.

Climatemps (2014) Average climate and temperature data. [Online, accessed 23rd November 2014] www.climatemps.com

Cornell, R. M., (1993) Adsorption of cesium on minerals: A review, *Journal of Radioanalytical and Nuclear Chemistry,* **171**: 483-500.

Cultrone, G., Sebastian, E., Huertas, M. O., (2005) Forced and natural carbonation of lime-based mortars with and without additives: Mineralogical and textural changes. *Cement and Concrete Research*, **35**(12): 2278-2289.

D

Dale, L. S., Fardy, J. J., (1984) Trace-element partitioning during the retorting of some Australian oil shales. *Environmental Science & Technology*, **18**(11): 887-889.

Dammer, A. R., Killen, J. C., Biglarbigi, K., Crawford, P. M., Johnson, H., (2007) Secure Fuels from Domestic Resources: The Continuing Evolution of America's Oil Shale and Tar Sands Industries. Fourth Edition: September 2010. U.S. Department of Energy, Washington, DC, 95.

Das, K., (1989) Solvent and supercritical fluid extraction of oil shale: A literature survey. Technical Note, U.S. Department of Energy.

Daval, D., Martinez, I., Corvisier, J., Findling, N., Goffe, B., Guyot, F., (2009) Carbonation of Ca-bearing silicates, the case of wollastonite: Experimental investigations and kinetic modeling. *Chemical Geology*, **265**(1-2): 63-78.

Dehen, W., (2010) Entering a New Age of Electricity. In: *World Energy Insight 2010: Official Publication of the World Energy Council to mark the 21st World Energy Congress.* World Energy Council, First Magazine, London, UK, pp. 28-29.

Diamond, L. W., Akinfiev, N. N., (2003) Solubility of CO_2 in water from -1.5 to 100 degrees C and from 0.1 to 100 MPa: evaluation of literature data and thermodynamic modelling. *Fluid Phase Equilibria*, **208**(1-2): 265-290.

Dietzel, M., Usdowski, E., Hoefs, J., (1992) Chemical and C-13/C-12-isotope and O-18/O-16-isotope evolution of alkaline drainage waters and the precipiation of calcite. *Applied Geochemistry*, **7**(2): 177-184.

Domingo, C., Loste, E., Gomez-Morales, J., Garcia-Carmona, J., Fraile, J., (2006) Calcite precipitation by a high-pressure CO_2 carbonation route. *Journal of Supercritical Fluids*, **36**(3): 202-215.

Dyni, J. R., (2006) Geology and Resources of Some World Oil-Shale Deposits: U.S. Geological Survey Scientific Investigations Report 2005-5294, 42.

E

Ecke, H., (2003) Sequestration of metals in carbonated municipal solid waste incineration (MSWI) fly ash. *Waste Management*, **23**(7): 631-640.

Ellis, R., (2011) Oil Shale: A Fuel Lifeline. Oil Shale Information Centre.

Energy Institute, (2010) Good Plant Design and Operation for Onshore Carbon Capture Installations and Onshore Pipelines: A Recommended Practice Guidance Document. Energy Institute, UK, 125.

Essington, M. E., (1989) Trace-element mineral transformations associated with hydration and recarbonation of retorted oil-shale. *Environmental Geology and Water Sciences*, **13**(1): 59-66.

Essington, M. E., (1991) Laboratory weathering of combusted oil-shale. *Journal of Environmental Quality*, **20**(4): 794-801.

European Academies Science Advisory Council (EASAC), (2007) A Study on the EU Oil Shale Industry – viewed in the Light of the Estonian Experience: A Report by EASAC to the Committee on Industry, Research and Energy of the European Parliament. EASAC, 65.

F

Fadaei, H., Sennoune, M., Salvador, S., Lapene, A., Debenest, G., (2012) Modelling of non-consolidated oil shale semi-coke forward combustion: Influence of carbon and calcium carbonate contents. *Fuel*, **95**(1): 197-205.

Fei, Y., Marshall, M., Jackson, W. R., Gorbaty, M. L., Amer, M. W., Cassidy, P. J., Chaffee, A. L., (2012) Evaluation of several methods of extraction of oil from a Jordanian oil shale. *Fuel*, **92**(1): 281-287.

Felmy, A. R., Qafoku, O., Arey, B. W., Hu, J. Z., Hu, M., Schaef, H. T., Ilton, E. S., Hess, N. J., Pearce, C. I., Feng, J., Rosso, K. M., (2012) Reaction of water-saturated supercritical CO_2 with forsterite: Evidence for magnesite formation at low temperatures. *Geochimica Et Cosmochimica Acta*, **91**: 271-282.

Fernández-Carrasco, L., Rius, J., Miravitlles, C., (2008) Supercritical carbonation of calcium aluminate cement. *Cement and Concrete Research*, **38**(8–9): 1033-1037.

Fernández-Carrasco, L., Torrens-Martín, D., Morales, L. M., Martínez-Ramírez, S., (2012) Infrared Spectroscopy in the Analysis of Building and Construction Materials, Infrared Spectroscopy - Materials Science, Engineering and Technology, Prof. Theophanides Theophile (Ed.), InTech.

Fernandez Bertos, M., Simons, S. J. R., Hills, C. D., Carey, P. J., (2004) A review of accelerated carbonation technology in the treatment of cement-based materials and sequestration of CO_2. *Journal of Hazardous Materials*, **112**(3): 193-205.

Figueroa, J. D., Fout, T., Plasynski, S., McIlvried, H., Srivastava, R. D., (2008) Advances in CO_2 capture technology - The US Department of Energy's Carbon Sequestration Program. *International Journal of Greenhouse Gas Control*, **2**(1): 9-20.

Filgueiras, A. V., Lavilla, I., Bendicho, C., (2002) Chemical sequential extraction for metal partitioning in environmental solid samples. *Journal of Environmental Monitoring*, **4**(6): 823-857.

Fischer, P. A., (2005) Hopes for shale oil are revived. *World Oil*, **226**(8): 69-74.

Fleurance, S., Cuney, M., Malartre, F., Reyx, J., (2013) Origin of the extreme polymetallic enrichment (Cd, Cr, Mo, Ni, U, V, Zn) of the Late Cretaceous-Early Tertiary Belqa Group, central Jordan. *Palaeogeography Palaeoclimatology Palaeoecology*, **369**: 201-219.

Frei, C., (2010) The World Energy Council: Meeting Global Energy Challenges. In: *World Energy Insight 2010: Official Publication of the World Energy Council to mark the 21st World Energy Congress.* World Energy Council, First Magazine, London, UK, pp. 6-9.

Fu, X. G., Wang, J., Zeng, Y. H., Tan, F. W., Feng, X. L., (2010) REE geochemistry of marine oil shale from the Changshe Mountain area, northern Tibet, China. *International Journal of Coal Geology*, **81**(3): 191-199.

G

Gadonneix, P., (2010) Managing the Energy Transition to a Sustainable Future. In: *World Energy Insight 2010: Official Publication of the World Energy Council to mark the 21st World Energy Congress.* World Energy Council, First Magazine, London, UK, pp. 4-5.

Gaus, I., Azaroual, M., Czernichowski-Lauriol, I., (2005) Reactive transport modelling of the impact of CO_2 injection on the clayey cap rock at Sleipner (North Sea). *Chemical Geology*, **217**(3-4): 319-337.

Gerdemann, S. J., O'Connor, W. K., Dahlin, D. C., Penner, L. R., Rush, H., (2007) Ex situ aqueous mineral carbonation. *Environmental Science & Technology*, **41**(7): 2587-2593.

Gibbins, J., Chalmers, H., (2008) Carbon capture and storage. *Energy Policy*, **36**(12): 4317-4322.

Gill, R., (1997) Modern analytical geochemistry : an introduction to quantitative chemical analysis for earth, environmental and materials scientists. *Geochemistry series*. Longman, Harlow, 329.

Gislason, S. R., Wolff-Boenisch, D., Stefansson, A., Oelkers, E. H., Gunnlaugsson, E., Sigurdardottir, H., Sigfusson, B., Broecker, W. S., Matter, J. M., Stute, M., Axelsson, G., Fridriksson, T., (2010) Mineral sequestration of carbon dioxide in basalt: A pre-injection overview of the CarbFix project. *International Journal of Greenhouse Gas Control*, **4**(3): 537-545.

Gromet, L. P., Dymek, R. F., Haskin, L. A., Korotev, R. L., (1984) The North-American shale composite – It's compilation, major and trace-element characteristics. *Geochimica Et Cosmochimica Acta*, **48**(12): 2469-2482.

Gunning, P. J., Hills, C. D., Carey, P. J., (2010) Accelerated carbonation treatment of industrial wastes. *Waste Management*, **30**(6): 1081-1090.

H

Hall, C., Barnes, P., Billimore, A. D., Jupe, A. C., Turrillas, X., (1996) Thermal decomposition of ettringite $Ca_6(Al(OH)_6)_2(SO_4)_3.26H_2O$. *Journal of the Chemical Society-Faraday Transactions*, **92**(12): 2125-2129.

Hanni, R., (1996) Energy and valuable material by-product from firing Estonian oil shale. *Waste Management*, **16**(1-3): 97-99.

Harber, A. J.,Forth, R. A., (2001) The contamination of former iron and steel works sites. *Environmental Geology*, **40**(3): 324-330.

Harrison, A. L., Power, I. M., Dipple, G. M., (2013) Accelerated Carbonation of Brucite in Mine Tailings for Carbon Sequestration. *Environmental Science & Technology*, **47**(1): 126-134.

Hartmann, J., Kempe, S., (2008) What is the maximum potential for CO_2 sequestration by "stimulated" weathering on the global scale? *Naturwissenschaften*, **95**(12): 1159-1164.

Harvie, B., (2005) West Lothian Biodiversity Action Plan: Oil Shale Bings, West Lothian Local Biodiveristy Action Plan partnership, West Lothian Council, Linlithgow, Scotland, 40.

Harvie, B. A., (2010) Historical review paper the shale-oil industry in Scotland 1858-1962. I: Geology and history. *Oil Shale*, **27**(4): 354-358.

Harvie, B. A., (2011) Historical review paper the shale-oil industry in Scotland 1858-1962. II: Oil-shale quality, resources and technological advances. *Oil Shale*, **28**(1): 78-84.

Harwood, L. M., Claridge, T. D. W., (1997) Introduction to organic spectroscopy. *Oxford chemistry primers*. Oxford University Press, Oxford, 91.

Hauff, P. L., Foord, E. E., Rosenblum, S., Hakki, W., (1983) Hashemite, $Ba(Cr,S)O_4$, a new mineral from Jordan. *American Mineralogist*, **68**(11-1): 1223-1225.

Hepple, R. P., Benson, S. M., (2005) Geologic storage of carbon dioxide as a climate change mitigation strategy: performance requirements and the implications of surface seepage. *Environmental Geology*, **47**(4): 576-585.

Hill, R. J., Lewan, M. D., (2006) Evaluating oil-shale byproducts of environmental concern by hydrous pyrolysis, Poster presented at the Proceedings of the 26th Oil Shale Symposium, October 16-20 2006,Colorado School of Mines, Golden, CO.

Hitch, M., Dipple, G. M., (2012) Economic feasibility and sensitivity analysis of integrating industrial-scale mineral carbonation into mining operations. *Minerals Engineering*, **39**: 268-275.

Horowitz, A. J., Demas, C. R., Fitzgerald, K. K., Miller, T. L., Rickert, D. A., (1994) U.S. Geological Survey Protocol for the collection and processing of surface-water samples for the subsequent determination of inorganic constituents in filtered water: Open-File Report 94-539, U.S. Geological Survey, Virginia, U.S., 63.

Hovelmann, J., Austrheim, H., Jamtveit, B., (2012a) Microstructure and porosity evolution during experimental carbonation of a natural peridotite. *Chemical Geology*, **334**: 254-265.

Hovelmann, J., Putnis, C. V., Ruiz-Agudo, E.,Austrheim, H., (2012b) Direct Nanoscale Observations of CO_2 Sequestration during Brucite $Mg(OH)_2$ Dissolution. *Environmental Science & Technology*, **46**(9): 5253-5260.

Hu, M. J., Cheng, Z. Q., Zhang, M. Y., Liu, M. Z., Song, L. H., Zhang, Y. Q., Li, J. F., (2014) Effect of Calcite, Kaolinite, Gypsum, and Montmorillonite on Huadian Oil Shale Kerogen Pyrolysis. *Energy & Fuels*, **28**(3): 1860-1867.

Huijgen, W. J. J., Comans, R. N. J. (2003) Carbon dioxide sequestration by mineral carbonation: Literature review. ECN, 52.

Huijgen, W. J. J., Witkamp, G. J., Comans, R. N. J., (2005) Mineral CO_2 sequestration by steel slag carbonation. *Environmental Science & Technology*, **39**(24): 9676-9682.

Huijgen, W. J. J., Witkamp, G. J., Comans, R. N. J., (2006) Mechanisms of aqueous wollastonite carbonation as a possible CO_2 sequestration process. *Chemical Engineering Science*, **61**(13): 4242-4251.

Hutton, A. C., (1987) Petrographic classification of oil shales. *International Journal of Coal Geology*, **8**(3): 203-231.

I

Ibrahim, K. M., Jaber, J. O., (2007) Geochemistry and environmental impacts of retorted oil shale from Jordan. *Environmental Geology*, **52**(5): 979-984.

Inorganic Crystal Structure Database (ICSD), (2014) National chemical database service, royal society of chemistry [online] Available at: www.cds.rsc.org

International Energy Agency (IEA), (2010) World Energy Outlook 2010: Executive Summary. International Energy Agency, Paris, France, 18.

International Energy Agency (IEA), (2013) World Energy Outlook 2013: Executive Summary. International Energy Agency, Paris, France, 12.

J

Jaber, J. O., Probert, S. D., (1997a) Exploitation of Jordanian oil-shales. *Applied Energy*, **58**(2-3): 161-175.

Jaber, J. O., Probert, S. D., (2000) Non-isothermal thermogravimetry and decomposition kinetics of two Jordanian oil shales under different processing conditions. *Fuel Processing Technology*, **63**(1): 57-70.

Jaber, J. O., Probert, S. D., Badr, O., (1997b) Energy and environmental issues for Jordan. *Applied Energy*, **57**(1): 45-101.

Jaber, J. O., Probert, S. D., Badr, O., (1997c) Water scarcity: A fundamental crisis for Jordan. *Applied Energy*, **57**(2-3): 103-127.

Jaber, J. O., Mohsen, M. S., Probert, S. D., Alees, M., (2001) Future electricity-demands and greenhouse-gas emissions in Jordan. *Applied Energy*, **69**(1): 1-18.

Jaber, J. O., Sladek, T. A., Mernitz, S., Tarawneh, T. M.,(2009) Future Policies and Strategies for Oil Shale Development in Jordan. Jordan Journal of Mechanical and Industrial Engineering, **2(**1): 31-44.

Jackson, P. M., (2009) The Future of Global Oil Supply: Understanding the Building Blocks. Cambridge Energy Research Associates (CERA), Cambridge, MA, US, 16.

Jacobs, A. D., Hitch, M., (2011) Experimental mineral carbonation: approaches to accelerate CO_2 sequestration in mine waste materials. *International Journal of Mining Reclamation and Environment*, **25**(4): 321-331.

Jeong, K. M., Patzer, J. F., (1983) Indigenous mineral matter effects in pyrolysis of Green River oil-shale. *Acs Symposium Series*, **230**: 529-542.

Jiang, J. G., Chen, M. Z., Zhang, Y., Xu, X., (2009) Pb stabilization in fresh fly ash from municipal solid waste incinerator using accelerated carbonation technology. *Journal of Hazardous Materials*, **161**(2-3): 1046-1051.

Jo, H., Jang, Y. N., Jo, H. Y., (2012) Influence of NaCl on mineral carbonation of CO_2 using cement material in aqueous solutions. *Chemical Engineering Science*, **80**: 232-241.

Johns, W. D., (1979) Clay mineral catalysis and petroleum generation. *Annual review of Earth and Planetary sciences,* **7** (1): 183-198.

Johnson, C. L., Greene, T. J., Zinniker, D. A., Moldowan, J. M., Hendrix, M. S., Carroll, A. R., (2003) Geochemical characteristics and correlation of oil and nonmarine source rocks from Mongolia. *Aapg Bulletin*, **87**(5): 817-846.

Johnson, R. C., Mercier, T. J., Brownfield, M. E., Pantea, M. P., Self, J. G., (2010) An Assessment of In-Place Oil Shale Resources in the Green River Formation, Piceance Basin, Colorado: US Geological Survey Digital Data Series DDS-69-Y, 187.

Johnson, R. C., Mercier, T. J., Brownfield, M. E., Self, J. G., (2010) Assessment of In-Place Oil Shale Resources in the Eocene Green River Formation, Uinta Basin, Utah and Colorado: US Geological Survey Digital Data Series DDS-69-BB, 153.

Jordan Energy and Mining (JEML), (2009) [Online] Available at: www.jeml.co.uk [Accessed January 2014].

Jordan Energy and Mining (JEML), (2012) Jordan Energy and Mining Limited Annual Review 2011/2012. 32

K

Kalinkin, A. M., Kalinkina, E. V., Politov, A. A., Makarov, V. N., Boldyrev, V. V., (2004) Mechanochemical interaction of Ca silicate and aluminosilicate minerals with carbon dioxide. *Journal of Materials Science*, **39**(16-17): 5393-5398.

Kalinkina, E. V., Kalinkin, A. M., Forsling, W., Makarov, V. N., (2001) Sorption of atmospheric carbon dioxide and structural changes of Ca and Mg silicate minerals during grinding - II. Enstatite, akermanite and wollastonite. *International Journal of Mineral Processing*, **61**(4): 289-299.

Karabakan, A., Yurum, Y., (1998) Effect of the mineral matrix in the reactions of oil shales: 1. Pyrolysis reactions of Turkish Goynuk and US Green River oil shales. *Fuel*, **77**(12): 1303-1309.

Kashem, M. A., Singh, B. R., Kondo, T., Huq, S. M. I., Kawai, S., (2007) Comparison of extractability of Cd, Cu, Pb and Zn with sequential extraction in contaminated and non-contaminated soils. *International Journal of Environmental Science and Technology*, **4**(2): 169-176.

Kashirskii, V., Koval, A., (2007) Oil shales - An alternative source of fuel and raw materials. *Oil Shale*, **24**(4): 497-498.

Kearney, C., (2010) The Great Disconnect on Energy Policy. In: *World Energy Insight 2010: Official Publication of the World Energy Council to mark the 21st World Energy Congress.* World Energy Council, First Magazine, London, UK, pp. 30-31.

Kelly, K. E., Silcox, G. D., Sarofim, A. F., Pershing, D. W., (2011) An evaluation of ex situ, industrial-scale, aqueous CO_2 mineralization. *International Journal of Greenhouse Gas Control*, **5**(6): 1587-1595.

Khoury, H. N., Al-Zoubi, A. S., (2014) Origin and characteristics of Cr-smectite from Suweileh area, Jordan. *Applied Clay Science*, **90**: 43-52.

Klein, F., McCollom, T. M., (2013) From serpentinization to carbonation: New insights from a CO_2 injection experiment. *Earth and Planetary Science Letters*, **379**: 137-145.

Knyazev, A. V., Chernorukov, N. G., Bulanov, E. N., (2012) Apatite-structured compounds: Synthesis and high-temperature investigation. *Materials Chemistry and Physics*, **132**(2-3): 773-781.

Kolonic, S., Damste, J. S. S., Bottcher, M. E., Kuypers, M. M. M., Kuhnt, W., Beckmann, B., Scheeder, G., Wagner, T., (2002) Geochemical characterization of Cenomanian/Turonian black shales from the Tarfaya Basin (SW Morocco) - Relationships between palaeoenvironmental conditions and early sulphurization of sedimentary organic matter. *Journal of Petroleum Geology*, **25**(3): 325-350.

Korbol, R., Kaddour, A., (1995) Sleipner-vest CO_2 disposal – injection of removed CO_2 into the Utsira formation. *Energy Conversion and Management*, **36**(6-9): 509-512.

Krol, A. A., Bell, P. R. F., Greenfield, P. F., Dunstan, M. J., (1986) Ion-exchange properties of retorted Rundle oil-shale. *Water Research*, **20**(10): 1299-1306.

Kumar, R., Bansal, V., Badhe, R. M., Madhira, I. S. S., Sugumaran, V., Ahmed, S., Christopher, J., Patel, M. B., Basu, B., (2013) Characterization of Indian origin oil shale using advanced analytical techniques. *Fuel*, **113**: 610-616.

Kuusik, R., Uibu, M., Kirsimae, K., (2005) Characterization of oil shale ashes formed at industrial-scale CFBC boilers. *Oil Shale*, **22**(4): 407-419.

Kuzyakov, Y., Domanski, G., (2000) Carbon input by plants into the soil. Review. *Journal of Plant Nutrition and Soil Science-Zeitschrift Fur Pflanzenernahrung Und Bodenkunde*, **163**(4): 421-431.

L

Lackner, K. S., Wendt, C. H., Butt, D. P., Joyce, E. L., Sharp, D. H., (1995) Carbon-dioxide disposal in carbonate minerals. *Energy*, **20**(11): 1153-1170.

Lackner, K. S., Butt, D. P., Wendt, C. H., (1997) Progress on binding CO_2 in mineral substrates. *Energy Conversion and Management*, **38**: S259-S264.

Lackner, K. S., (2002) Carbonate chemistry for sequestering fossil carbon. *Annual Review of Energy and the Environment*, **27**: 193-232.

Lal, R., (2004) Soil carbon sequestration to mitigate climate change, *Geoderma,* **123**: 1-22.

Lanas, J., Bernal, J. L. P., Bello, M. A., Galindo, J. I. A., (2004) Mechanical properties of natural hydraulic lime-based mortars. *Cement and Concrete Research*, **34**(12): 2191-2201.

Lea, A. S., Higgins, S. R., Knauss, K. G., Rosso, K. M., (2011) A high-pressure atomic force microscope for imaging in supercrticial carbon dioxide, *Review of scientific instruments,* **82**, 7.

Legodi, M. A., de Waal, D., (2007) The preparation of magnetite, goethite, hematite and maghemite of pigment quality from mill scale iron waste. *Dyes and Pigments*, **74**(1): 161-168.

Leventhal, J. S., (1991) Comparison of organic geochemistry and metal enrichment in 2 black shales – Cambrian alum shale of Sweden and Devonian chattanooga shale of United-States. *Mineralium Deposita*, **26**(2): 104-112.

Lewan, M. D.,Maynard, J. B., (1982) Factors controlling enrichment of vanadium and nickel in the bitumen of organic sedimentary-rocks. *Geochimica Et Cosmochimica Acta*, **46**(12): 2547-2560.

Li, X. M., Bertos, M. F., Hills, C. D., Carey, P. J., Simon, S., (2007) Accelerated carbonation of municipal solid waste incineration fly ashes. *Waste Management*, **27**(9): 1200-1206.

Liive, S., (2010) Oil Shale – the Unconventional which will become Conventional. In: *World Energy Insight 2010: Official Publication of the World Energy Council to mark the 21st World Energy Congress.* World Energy Council, First Magazine, London, UK, pp. 24-27.

Lindner, A. W., (1983) Geology and geochemistry of some Queensland tertiary oil shales. *Acs Symposium Series*, **230**: 97-118.

Lipin, B. R., MacKay, G. A., (1989) Geochemistry and Mineralogy of Rare Earth Elements. Mineralogical Society of America. 348.

M

Macauley, G., (1981) Geology of the Oil Shale Deposits of Canada: Open File Report OFR-754. Geological Survey of Canada, Calgary, Alberta, 164.

Mackenzie, F., (1996) The natural heritage interest of bings (waste tips) in Scotland, Information and Advisory note number 50, Scottish Natural Heritage, 10.

Mayes, W. M., Younger, P. L., Aumonier, J., (2006) Buffering of alkaline steel slag leachate across a natural wetland. *Environmental Science & Technology*, **40**(4): 1237-1243.

Mazotti, M., (2005) Mineral carbonation and industrial uses of carbon dioxide. Chapter 7. IPCC special report on carbon dioxide capture and sotrage. Intergovernmental Panel on Climate Change.

McDonough, W. F., Sun, S. S., (1995) The composition of the Earth. *Chemical Geology*, **120**(3-4): 223-253.

McKee, B., (2010) The Outlook for Carbon Capture and Storage. In: *World Energy Insight 2010: Official Publication of the World Energy Council to mark the 21st World Energy Congress.* World Energy Council, First Magazine, London, UK, 41.

McLennan, S. M., (1989) Rare-earth elements in sedimentary rocks – influence of provenance and sedimentary processes. *Geochemistry and Mineralogy of Rare Earth Elements*, **21**. Mineralogical Soc America, Washington, 169-200.

McLennan, S. M., (2001) Relationships between the trace element composition of sedimentary rocks and upper continental crust. *Geochemistry Geophysics Geosystems*, **2**(4).

Meima, J. A., van der Weijden, R. D., Eighmy, T. T., Comans, R. N. J., (2002) Carbonation processes in municipal solid waste incinerator bottom ash and their effect on the leaching of copper and molybdenum. *Applied Geochemistry*, **17**(12): 1503-1513.

Metz, B., Davidson, O. R., Bosch, P. R., Dave, R., Meyer, L. A. (Eds.), (2007) Contribution of Working Group III to the Fourth Assessment Report of the Intergovernmental Panel on Climate Change, Cambridge University Press, Cambridge, United Kingdom and New York, NY, USA, 863.

Metz, B., Davidson, O. R., Coninck, H., Loos, M., Meyer, L. A. (Eds.), (2005) Carbon Dioxide Capture and Storage. IPCC Special Report Prepared by Working Group III of the Intergovernmental Panel on Climate Change, Cambridge University Press, New York, NY, USA, 443.

Miller, Q. R. S., Thompson, C. J., Loring, J. S., Windisch, C. F., Bowden, M. E., Hoyt, D. W., Hu, J. Z., Arey, B. W., Rosso, K. M., Schaef, H. T., (2013) Insights into silicate carbonation processes in water-bearing supercritical CO_2 fluids. *International Journal of Greenhouse Gas Control*, **15**: 104-118.

Milodowski, A. E., Rochelle, C. A., Lacinska, A., Wagner, D., (2011) A natural analogue study of CO_2-cement interaction: Carbonation of calcium silicate hydrate-bearing rocks from

Northern Ireland. In: Gale, J., Hendriks, C.,Turkenberg, W. (Eds.), 10th International Conference on Greenhouse Gas Control Technologies. Energy Procedia. Elsevier Science Bv, Amsterdam, 5235-5242.

Mingos, D. M. P., (1998) Essential Trends in Inorganic Chemistry. Oxford University Press. 392.

Minster, T., (2013) Oil Shale Occurrences in Israel: Geological Updated Information – 2013. Geological Survey of Israel (GSI), Jerusalem, Israel, 75.

Montes-Hernandez, G., Perez-Lopez, R., Renard, F., Nieto, J. M., Charlet, L., (2009) Mineral sequestration of CO_2 by aqueous carbonation of coal combustion fly-ash. *Journal of Hazardous Materials*, **161**(2-3): 1347-1354.

Moomaw, W., Burgherr, P., Heath, G., Lenzen, M., Nyboer, J., Verbruggen, A., (2011) Anexx II: Methodology. In: *IPCC Special Report on Renewable Energy Sources and Climate Change Mitigation.* Cambridge University Press, Cambridge, UK and New York, US, 28.

Moore, D. M., Reynolds, R. C., (1997) X-ray Diffraction and the Identification and Analysis of Clay Minerals. Oxford University Press. 378.

Morales-Florez, V., Santos, A., Lemus, A., Esquivias, L., (2011) Artificial weathering pools of calcium-rich industrial waste for CO_2 sequestration. *Chemical Engineering Journal*, **166**(1): 132-137.

Moskalyk, R. R., Alfantazi, A. M., (2003) Processing of vanadium: a review. *Minerals Engineering*, **16**(9): 793-805.

Motlep, R., Kirsimae, K., Talviste, P., Puura, E., Jurgenson, J., (2007) Mineral composition of Estonian oil shale semi-coke sediments. *Oil Shale*, **24**(3): 405-422.

Motlep, R., Sild, T., Puura, E.,Kirsimae, K., (2010) Composition, diagenetic transformation and alkalinity potential of oil shale ash sediments. *Journal of Hazardous Materials*, **184**(1-3): 567-573.

Muhammad, A. F., El Salmawy, M. S., Abdelaala, A. M., Sameah, S., (2011) El-Nakheil oil shale: material characterization and effect of acid leaching. *Oil Shale*, **28**(4): 528-547.

Myneni, S. C. B., Traina, S. J., Logan, T. J., (1998) Ettringite solubility and geochemistry of the $Ca(OH)_2$-$Al_2(SO_4)_3$-H_2O system at 1 atm pressure and 298 K. *Chemical Geology*, **148**(1-2): 1-19.

N

Navarro, R., Guzman, J., Saucedo, I., Revilla, J., Guibal, E., (2007) Vanadium recovery from oil fly ash by leaching, precipitation and solvent extraction processes. *Waste Management*, **27**(3): 425-438.

O

O'Connor, W. K., Dahlin, D. C., Turner, P. C., Walters, R., (1999) Carbon Dioxide Sequestration by Ex-Situ Mineral Carbonation, Paper presented at the Proceedings of the Second Annual Dixy Lee Ray Memorial Symposium, American Society of Mechanical Engineers, August 29 - September 2 1999, Washington D.C.

Odut, S., (2012) The Alberta Tacuik Process (ATP) for Jordan: Comprehensive Feasibility Study and Scale-Up. Presented at the Jordan International Oil Shale Symposium, May 2012.

Oelkers, E. H., Gislason, S. R., Matter, J., (2008) Mineral Carbonation of CO_2. *Elements*, **4**(5): 333-337.

Olejnik, S., Algina, J., (2003) Generalized eta and omega squared statistics: Measures of effect size for some common research designs. *Psychological Methods*, **8**(4): 434-447.

Orupold, K., Habicht, J., Tenno, T., (2008) Leaching behaviour of oil shale semicoke: Compliance with the waste acceptance criteria for landfills. *Oil Shale*, **25**(2): 267-275.

Oskierski, H. C., Dlugogorski, B. Z., Jacobsen, G., (2013) Sequestration of atmospheric CO_2 in chrysotile mine tailings of the Woodsreef Asbestos Mine, Australia: Quantitative mineralogy, isotopic fingerprinting and carbonation rates. *Chemical Geology*, **358**: 156-169.

Ottley, C. J., Pearson, D. G., Irvine, G. J., (2003) A routine method for the dissolution of geological samples for the analysis of REE and trace elements via ICP-MS. *Plasma Source Mass Spectrometry: Applications and Emerging Technologies*. Royal Soc Chemistry, Cambridge, 221-230.

P

Pachauri, R. K., Reisinger, A., (Eds.), (2007) Contribution of Working Groups I, II and III to the Fourth Assessment Report of the Intergovernmental Panel on Climate Change, IPCC, Geneva, Switzerland, 104.

Parliamentary Office of Science and Technology (POST), (2006) Carbon Footprint of Electricity Generation: October 2006, (268) POST, London, 4.

Parnell, J., (1988) Lacustrine petroleum source rocks in the Dinantian Oil Shale Group, Scotland: a review. From: Fleet, A. J., Kelts, K., and Talbot, M. R. (eds), 1988, *Lacustrine Petroleum Source Rocks, Geological Society Special Publication*, (40): 235–246.

Patterson, J. H., (1994) A review of the effects of minerals in processing of Australian oil shales. *Fuel*, **73**(3): 321-327.

Pimentel, P. M., Oliveira, R., Melo, D. M. A., Anjos, M. J., Melo, M. A. F.,Gonzalez, G., (2010) Characterization of retorted shale for use in heavy metal removal. *Applied Clay Science*, **48**(3): 375-378.

Potter, P. E., Maynard, J. B., Pryor, W. A., (1980) Sedimentology of shale: study guide and reference source. Springer-Verlag. 310.

Power, I. M., Wilson, S. A., Dipple, G. M., (2013) Serpentinite Carbonation for CO_2 Sequestration. *Elements*, **9**(2): 115-121.

Preston, C., Monea, M., Jazrawi, W., Brown, K., Whittaker, S., White, D., Law, D., Chalaturnyk, R., Rostron, B., (2005) IEA GHG Weyburn CO_2 monitoring and storage project. *Fuel Processing Technology*, **86**(14–15): 1547-1568.

Prigiobbe, V., Hanchen, M., Werner, M., Baciocchi, R., Mazzotti, M., (2009) Mineral carbonation process for CO_2 sequestration. *Greenhouse Gas Control Technologies 9*, **1**(1): 4885-4890.

Pufahl, P. K., Grimm, K. A., Abed, A. M., Sadaqah, R. M. Y., (2003) Upper Cretaceous (Campanian) phosphorites in Jordan: implications for the formation of a south Tethyan phosphorite giant. *Sedimentary Geology*, **161**(3-4): 175-205.

Q

Qiu, Y.-W., Yu, K.-F., Zhang, G., Wang, W.-X., (2011) Accumulation and partitioning of seven trace metals in mangroves and sediment cores from three estuarine wetlands of Hainan Island, China. *Journal of Hazardous Materials*, **190**(1-3): 631-638.

R

Rajeshwar, K., (1983) Thermal-analysis of coals, oil shales and oil sands. *Thermochimica Acta*, **63**(1): 97-112.

Rajeshwar, K., Jones, D. B., DuBow, J. B., (1981) Characterization of oil shales by differential scanning calorimetry. *Analytical Chemistry*, **53**(1): 121-122.

Rajeshwar, K., Nottenburg, R., Dubow, J., (1979) Thermophysical properties of oil shales. *Journal of Materials Science*, **14**(9): 2025-2052.

Rauret, G., Lopez-Sanchez, J. F., Sahuquillo, A., Rubio, R., Davidson, C., Ure, A., Quevauviller, P., (1999) Improvement of the BCR three step sequential extraction procedure prior to the certification of new sediment and soil reference materials. *Journal of Environmental Monitoring*, **1**(1): 57-61.

Reddy, K. J., Gloss, S. P., Wang, L., (1994) Reaction of CO_2 with alkaline solid-wastes to reduce contaminant mobility. *Water Research*, **28**(6): 1377-1382.

Reeder, R. J., (1983) Carbonates: mineralogy and chemistry. Mineralogical Society of America. 399.

Reinsalu, E., Valgma, I., (2007) Oil shale resources for oil production. *Oil Shale*, **24**(1): 9-14.

Rendek, E., Ducom, G., Germain, P., (2006) Carbon dioxide sequestration in municipal solid waste incinerator (MSWI) bottom ash. *Journal of Hazardous Materials*, **128**(1): 73-79.

Renforth, P., (2012) The potential of enhanced weathering in the UK. *International Journal of Greenhouse Gas Control*, **10**: 229-243.

Renforth, P., Kruger, T., (2013) Coupling Mineral Carbonation and Ocean Liming. *Energy & Fuels*, **27**(8): 4199-4207.

Renforth, P., Manning, D. A. C., Lopez-Capel, E., (2009) Carbonate precipitation in artificial soils as a sink for atmospheric carbon dioxide. *Applied Geochemistry*, **24**(9): 1757-1764.

Richards, K. R., and Stokes, C., (2004) A review of forest carbon sequestration cost studies: a dozen years of research, *Climatic Change,* **63**: 1-48.

Russell, P. L., (1990) Oil shales of the world: their origin, occurrence and exploitation. Pergamon, Oxford, ix, 753.

S

Saether, O. M., Banks, D., Kirso, U., Bityukova, L., Sorlie, J. E., (2004) The chemistry and mineralogy of waste from retorting and combustion of oil shale. In: Giere, R., and Stille, P. (eds) 2004, *Energy, Waste, and the Environment: a geochemical perspective.* The Geological Society, London, Special Publications, (236): 263-284.

Saharaforestproject (2014) Sahara Forest Project, Jordan [online] www.saharaforestproject.com [Accessed 26th November 2014]

Saldi, G. D., Jordan, G., Schott, J., Oelkers, E. H., (2009) Magnesite growth rates as a function of temperature and saturation state. *Geochimica Et Cosmochimica Acta*, **73**(19): 5646-5657.

Sanna, A., Dri, M., Hall, M. R., Maroto-Valer, M., (2012) Waste materials for carbon capture and storage by mineralisation (CCSM) - A UK perspective. *Applied Energy*, **99**: 545-554.

Sarvaramini, A., Assima, G. P., Beaudoin, G., Larachi, F., (2014) Biomass torrefaction and CO_2 capture using mining wastes - A new approach for reducing greenhouse gas emissions of co-firing plants. *Fuel*, **115**: 749-757.

Scanlon, D. M., (1980) The Midland Valley of Scotland and Ireland: Petroleum Geology. Aberdeen University.

Schmider, E., Ziegler, M., Danay, E., Beyer, L., Buhner, M., (2010) Is It Really Robust? Reinvestigating the Robustness of ANOVA Against Violations of the Normal Distribution Assumption. *Methodology-European Journal of Research Methods for the Behavioral and Social Sciences*, **6**(4): 147-151.

Schrag, D. P., (2007) Preparing to capture carbon. *Science*, **315**(5813): 812-813.

Schramke, J. A., (1992) Neutralization of alkaline coal fly-ash leachates by $CO_{2(g)}$. *Applied Geochemistry*, **7**(5): 481-492.

Schroeder, P. A., (2002) Infrared spectroscopy in clay science. The clay minerals society, Colorado, **181**: 181-202.

Scottish Oils, (1938) The Scottish Shale Oil Industry. Scottish Oils and Shell-Mex Ltd.
Sdiri, A., Higashi, T., Hatta, T., Jamoussi, F., Tase, N., (2010) Mineralogical and spectroscopic characterization, and potential environmental use of limestone from the Abiod formation, Tunisia. *Environmental Earth Sciences*, **61**(6): 1275-1287.
Seifritz, W., (1990) CO_2 disposal by means of silicates. *Nature*, **345**(6275): 486-486.
Shawabkeh, K., (1991) The Geology of the Adir Area Map Sheet No. 3152-II, Bulletin 18. NRA, Amman, 32.
Shawabkeh, A. Q., Al-Naafa, M. A., (2013) Shale hold time for optimum oil shale retorting inside a batch-loaded fluidized-bed reactor. *Oil Shale*, **30**(2): 173-183.
Shendrikar, A. D., Faudel, G. B., (1978) Distribution of trace-metals during oil-shale retorting. *Environmental Science & Technology*, **12**(3): 332-334.
Shirav, M., Zimmels, Y., (1988) The pathway of trace-elements during oil-shale combustion – a clue to their availability for leaching processes. *Environmental Geology and Water Sciences*, **11**(1): 55-64.
Shriver, D., Atkins, P., Overton, T., Rourke, J., (2009) Inorganic Chemistry. W. H. Freeman. 824.
Siirde, A., (2008) Oil shale - Global solution or part of the problem? *Oil Shale*, **25**(2): 201-202.
Smidt, E., Meissi, K., Schwanninger, M., Lechner, P., (2008) Classification of waste materials using Fourier transform infrared spectroscopy and soft independent modeling of class analogy. *Waste Management*, **28**(10): 1699-1710.
Smith, J. W., (1983) The chemistry which created Green River formation oil-shale. *Abstracts of Papers of the American Chemical Society*, **185**(MAR): 50.
Sohns, H. W., Mitchell, L. E., Cox, R. J., Barnet, W. I., Murphy, W. I. R., (1951) Heat requirements for retorting oil shale. *Industrial and Engineering Chemistry*, **43**(1): 33-36.
Song, M. N., Zhang, D. K., (2009) An experimental investigation into the oxidation of four pyritic shales from Western Australia. *Minerals Engineering*, **22**(6): 550-559.
Stanfield, K. E., (1949) Method of Assaying Oil Shale by a Modified Fischer Retort: Revision of R. I. 3977., Washington D. C., 13.
Stanmore, B. R., Gilot, P., (2005) Review-calcination and carbonation of limestone during thermal cycling for CO_2 sequestration. *Fuel Processing Technology*, **86**(16): 1707-1743.
Sumner, M. E., (2000) Handbook of soil science. CRC Press. 2148.
Sundquist, E. T., (1980) Oil shales and carbon-dioxide. *Science*, **208**(4445): 740-741.
Surface, J. A., Skemer, P., Hayes, S. E., Conradi, M. S., (2013) In Situ Measurement of Magnesium Carbonate Formation from CO_2 Using Static High-Pressure and -Temperature C-13 NMR. *Environmental Science & Technology*, **47**(1): 119-125.
Suwannathong, A., Khummongkol, D., (2007) Oil Shale Resource in Mae Sot Basin, Thailand. Presented at the 27th Oil Shale Symposium, Colorado School of Mines, 15-17 October, 2007.

T

Tai, C. Y., Chen, W. R., Shih, S. M., (2006) Factors affecting wollastonite carbonation under CO_2 supercritical conditions. *Aiche Journal*, **52**(1): 292-299.
Tans, P., (2014) Recent Monthly Average Mauna Loa CO_2. NOAA Earth System Research Laboratory (NOAA/ESRL). [Online, accessed on 6th April, 2014] www.esrl.noaa.gov/gmd/ccgg/trends/
Taylor, J. R., (1997) An Introduction to Error Analysis: The Study of Uncertainties in Physical Measurements. University Science Books. 327.
Taylor, S. R., McLennan, S. M., (1985) The Continental Crust. Wiley. 328.
Taylor, S. R., McLennan, S. M., (1995) The geochemical evolution of the continental-crust. *Reviews of Geophysics*, **33**(2): 241-265.

Teramura, S., Isu, N., Inagaki, K., (2000) New building material from waste concrete by carbonation. *Journal of Materials in Civil Engineering*, **12**(4): 288-293.

Tessier, A., Campbell, P. G. C., Bisson, M., (1979) Sequential extraction procedure for the speciation of particulate trace-metals. *Analytical Chemistry*, **51**(7): 844-851.

Thiery, M., Villain, G., Dangla, P., Platret, G., (2007) Investigation of the carbonation front shape on cementitious materials: Effects of the chemical kinetics. *Cement and Concrete Research*, **37**(7): 1047-1058.

Thompson, S. P., Day, S. J., Parker, J. E., Evans, A., Tang, C. C., (2012) Fine-grained amorphous calcium silicate $CaSiO_3$ from vacuum dried sol-gel - Production, characterisation and thermal behaviour. *Journal of Non-Crystalline Solids*, **358**(5): 885-892.

Thompson, L. G.,Thomson, W. J., (1983) A comparison of mineral reactions for 2 Colorado oil-shale samples. *Abstracts of Papers of the American Chemical Society*, **185**(MAR): 74.

Tiku, M. L., (1971) Power Function of the F-Test Under Non-Normal Situations. *Journal of the American Statistical Association*, **66**(336): 913-916.

Todor, D. N., (1976) Thermal Analysis of Minerals. Abacus Press, Tunbridge Wells, Kent, 256.

Trikkel, A., Kuusik, R., Martins, A., Pihu, T., Stencel, J. M., (2008) Utilization of Estonian oil shale semicoke. *Fuel Processing Technology*, **89**(8): 756-763.

Trindade, M. J., Dias, M. I., Coroado, J., Rocha, F., (2009) Mineralogical transformations of calcareous rich clays with firing: A comparative study between calcite and dolomite rich clays from Algarve, Portugal. *Applied Clay Science*, **42**(3-4): 345-355.

Tuttle, M. L. W., Breit, G. N., Goldhaber, M. B., (2009) Weathering of the New Albany Shale, Kentucky: II. Redistribution of minor and trace elements. *Applied Geochemistry*, **24**(8): 1565-1578.

U

Uibu, M., Kuusik, R., Andreas, L., Kirsimae, K., (2011) The CO_2-binding by Ca-Mg-silicates in direct aqueous carbonation of oil shale ash and steel slag. *10th International Conference on Greenhouse Gas Control Technologies*, **4**: 925-932.

Uibu, M., Uus, M., Kuusik, R., (2009) CO_2 mineral sequestration in oil-shale wastes from Estonian power production. *Journal of Environmental Management*, **90**(2): 1253-1260.

Ure, A., Davidson, C., (2002) Chemical Speciation in the Environment. Wiley. 480.

U.S. Energy Information Administration (EIA), (2010) International Energy Outlook 2010. U.S. Department of Energy, Washington, DC, 338.

U.S. Energy Information Administration (EIA), (2013) International Energy Outlook 2013. U.S. Department of Energy, Washington, DC, 312.

V

Vangkilde-Pedersen, T., Anthonsen, K. L., Smith, N., Kirk, K., Neele, F., Van der Meer, B., Le Gallo, Y., Bossie-Codreanu, D., Wojcicki, A., Le Nindre, Y.-M., Hendriks, C., Dalhoff, F., Christensen, P. N., (2009) Assessing European capacity for geological storage of carbon dioxide–the EU GeoCapacity project. *Energy Procedia*, **1**(1): 2663-2670.

Vassilev, S. V., Vassileva, C. G., (1996) Occurrence, abundance and origin of minerals in coals and coal ashes. *Fuel Processing Technology*, **48**(2): 85-106.

Veski, R., (2005) The volumes of spent oil shale from Estonian oil-shale processing units in 1921-2002. *Oil Shale*, **22**(3): 345-357.

Villain, G., Thiery, M., Platret, G., (2007) Measurement methods of carbonation profiles in concrete: Thermogravimetry, chemical analysis and gammadensimetry. *Cement and Concrete Research*, **37**(8): 1182-1192.

W

Wang, D. M., Xu, Y. M., He, D. M., Guan, J., Zhang, O. M., (2009) Investigation of mineral composition of oil shale. *Asia-Pacific Journal of Chemical Engineering*, **4**(5): 691-697.

Weltje, G. J., and Tjallingii, R., (2008) Calibration of XRF core scanners for quantitative geochemical logging of sediment cores: Theory and application, *Earth and Planetary Science Letters,* **274**: 423-438.

Westlothian council, (2014) West Lothian Council - West Lothian. [online] Available at: http://www.westlothian.gov.uk/ [Accessed 6 Aug. 2014].

World Energy Council (WEC), (2007) Survey of Energy Resources: 2007. World Energy Council, London, UK, 600.

World Energy Council (WEC), (2010) Survey of Energy Resources: 2010. World Energy Council, London, UK, 618.

World Energy Council (WEC), (2013) World Energy Resources: 2013 Survey. World Energy Council, London, UK, 468.

White, C. M., Smith, D. H., Jones, K. L., Goodman, A. L., Jikich, S. A., LaCount, R. B., DuBose, S. B., Ozdemir, E., Morsi, B. I.,Schroeder, K. T., (2005) Sequestration of carbon dioxide in coal with enhanced coalbed methane recovery - A review. *Energy & Fuels*, **19**(3): 659-724.

Wigley, T. M. L., (2006) A combined mitigation/geoengineering approach to climate stabilization. *Science*, **314**(5798): 452-454.

Worrall, F., Pearson, D. G., (2001) Water-rock interaction in an acidic mine discharge as indicated by rare earth element patterns. *Geochimica Et Cosmochimica Acta*, **65**(18): 3027-3040.

X

Xu, B. A., Giles, D. E., Ritchie, I. M., (1998) Reactions of lime with carbonate-containing solutions. *Hydrometallurgy*, **48**(2): 205-224.

Xu, T. F., Apps, J. A., Pruess, K., (2005) Mineral sequestration of carbon dioxide in a sandstone-shale system. *Chemical Geology*, **217**(3-4): 295-318.

Y

Yamamoto, M., Bat-erdene, D., Ulziikhishig, P., Watanabe, Y., Imai, N., Kajiwara, Y., Takeda, N., Nakajima, T., (1998) Organic Geochemistry and Palynology of Lower Cretaceous Zuunbayan Oil Shales, Mongolia. Bulletin of the Geological Survey of Japan, **49(6)**, pp.257-274.

Yoffe, O., Nathan, Y., Wolfarth, A., Cohen, S., Shoval, S., (2002) The chemistry and mineralogy of the Negev oil shale ashes. *Fuel*, **81**(9): 1101-1117.

Z

Zakir, H. M., Shikazono, N., (2006) Comparison of three sequential extraction schemes for heavy metal fractionation in sediment samples. *Geochimica Et Cosmochimica Acta*, **70**(18): A730-A730.

Zhang, Z. X., Wang, G. X., Massarotto, P., Rudolph, V., (2006) Optimisation of pipeline transport for CO_2 sequestration, *Energy Conversion and Management*, **47**: 702-715.

Zhang, F. F., Xu, H. F., Konishi, H., Roden, E. E., (2010) A relationship between d(104) value and composition in the calcite-disordered dolomite solid-solution series. *American Mineralogist*, **95**(11-12): 1650-1656.

Zhang, F. S., Yamasaki, S., Kimura, K., (2001) Rare earth element content in various waste ashes and the potential risk to Japanese soils. *Environment International*, **27**(5): 393-398.

Zhao, L., Sang, L. Q., Chen, J., Ji, J. F., Teng, H. H., (2010) Aqueous Carbonation of Natural Brucite: Relevance to CO_2 Sequestration. *Environmental Science & Technology*, **44**(1): 406-411.